

**Sedimentary sequences and microbial
mats of Iberian saline lakes as tools for the
investigation of modern and sub-recent
environmental processes**

A thesis submitted to the University of Manchester for the degree of

Doctor of Philosophy

in the Faculty of Science and Engineering, School of Natural
Sciences and Department of Earth and Environmental Sciences

2023

Connor J.C. Doyle

Department of Earth and Environmental Sciences

Contents

Abstract	4
Declaration.....	5
Copyright Statement.....	6
Publications	7
Acknowledgements	8
Dedication.....	9
Chapter 1 - Introduction.....	10
1.1 Background.....	10
1.2 The Importance of Saline Lakes, Microbialites & Microbe-Mineral Interactions.....	12
1.3 Current Issues, Research Questions and Scope of Thesis.....	18
Chapter 2 – Literature Review	27
2.1 Introduction.....	29
2.2 Saline Lacustrine Systems.....	33
2.3 Sedimentary Features of Saline Lakes	40
2.4 Microbial Mats – Processes and Controls.....	52
2.5 Review of Previous work on Study Sites.....	70
2.5 Conclusions	73
Chapter 3 – Regional Setting and Methodological Approach.....	100
3.1 Introduction.....	100
3.2 Saline lakes and microbial mats in the Iberian Peninsula.....	100
3.3 Site Justification and Overview.....	101
3.4 Methodological Approach.....	114
Chapter 4 – Facies variability and depositional settings of Laguna Salada de Chiprana, Northeast Spain	143
4.1 Introduction.....	145
4.2 Study Area.....	146
4.3 Methods.....	151
4.4 Results	157
4.5 Discussion	178
4.6 Conclusions	191
Chapter 5 - Spatio-temporal variations in the geochemistry of hypersaline lakes: Laguna Salada de Chiprana, NE Spain	200
5.1 Introduction.....	203
5.2 Study Area.....	205

5.3 Material and Methods	208
5.4 Results	215
5.5 Discussion	226
5.6 Conclusions	243
Chapter 6 – Mineralogical Assemblages and Hydrochemical Modelling of Laguna Salada de Chiprana, Northeast Spain.....	259
6.1 Introduction.....	261
6.2 Study Area.....	263
6.3 Material and Methods	266
6.4 Results	271
6.5 Discussion	304
6.6 Conclusions	313
Chapter 7 - Development of modern and sub-recent lacustrine microbialites in southwestern Europe: Insights into environmental and depositional controls using X- Ray CT and petrography	324
7.1 Introduction.....	326
7.2 Materials and Methods.....	328
7.3 Results	334
7.4 Discussion	380
7.5 Conclusions	395
Chapter 8 – Synthesis	409
8.1 Saline lakes as palaeoenvironmental archives	410
8.2 Microbialite morphological and geochemical characteristics	416
8.3 Summary and Future Work	420
Appendix 1 – Samples	427
Appendix 2 – Sedimentology	434
Appendix 3 – Other Material	466

Appendices 4 and 5, containing geochemical and petrographical data, respectively, have been provided on a USB drive.

Abstract

This thesis aimed to provide deeper insights the effectiveness of hypersaline lacustrine settings and microbial mats as palaeoenvironmental archives, while attempting to further understand the spatial complexities of the depositional and sub-depositional settings of saline lakes and characteristics of microbial mats within them. To achieve this, key objectives included the sedimentological, geochemical and hydrological analysis of sediments from Laguna Salada de Chiprana and other lacustrine settings throughout the Iberian Peninsula, combined with analysis of the macro and micro-morphology and geochemistry of microbial mats. The first chapter presents a high-resolution sedimentological dataset of Lake Chiprana and describes and interprets facies variations throughout the last three to four centuries in order to establish the spatio-temporal variability in the depositional settings of the lake. This is succeeded by a μ XRF-based dataset presented in the second data chapter, which provides insights into the key intrinsic and extrinsic geochemical processes acting upon Lake Chiprana throughout the lake. Finally, the third data chapter presents a study of the mineralogical and hydrochemical aspects of the lake in order to provide supporting evidence as to the palaeoenvironmental changes identified in the sedimentary sequence and to determine the hydrochemical evolution of the lake under different environmental domains. In addition, the petrography, morphology and biogeochemistry of microbial mats and microbialites occurring both within Laguna Salada de Chiprana and three other Iberian lakes were studied extensively in the fourth and fifth data chapters. In the fourth chapter, computerised tomographical scans and petrographical analyses were employed to determine the mesoscale and microscale structures associated with mats from each of the lakes, This allowed for the characterisation of the morphology and texture of mat structures and the pertinent processes responsible for their formation, lending deeper insights into the small-scale processes and environments of deposition that contributed to their development.

Declaration

The University of Manchester
PhD by published work Candidate Declaration

Candidate Name: Connor Doyle

Faculty: Science and Engineering

Thesis Title: Sedimentary sequences and microbial mats of Iberian saline lakes as tools for the investigation of modern and sub-recent environmental processes

I declare that no portion of the work referred to in the thesis has been submitted in support of an application for another degree or qualification of this or any other university or other institute of learning.

Total Words (Not including appendices): 87486

Total words (Not including references): 68352

Copyright Statement

- i. The author of this thesis (including any appendices and/or schedules to this thesis) owns certain copyright or related rights in it (the “Copyright”) and s/he has given the University of Manchester certain rights to use such Copyright, including for administrative purposes.
- ii. Copies of this thesis, either in full or in extracts and whether in hard or electronic copy, may be made only in accordance with the Copyright, Designs and Patents Act 1988 (as amended) and regulations issued under it or, where appropriate, in accordance with licensing agreements which the University has from time to time. This page must form part of any such copies made.
- iii. The ownership of certain Copyright, patents, designs, trademarks and other intellectual property (the “Intellectual Property”) and any reproductions of copyright works in the thesis, for example graphs and tables (“Reproductions”), which may be described in this thesis, may not be owned by the author and may be owned by third parties. Such Intellectual Property and Reproductions cannot and must not be made available for use without the prior written permission of the owner(s) of the relevant Intellectual Property and/or Reproductions.
- iv. Further information on the conditions under which disclosure, publication and commercialisation of this thesis, the Copyright and any Intellectual Property and/or Reproductions described in it may take place is available in the University IP Policy (see <http://documents.manchester.ac.uk/DocuInfo.aspx?DocID=2442> 0), in any relevant Thesis restriction declarations deposited in the University Library, the University Library’s regulations (see <http://www.library.manchester.ac.uk/about/regulations/>) and in the University’s policy on Presentation of Theses.

Status of Publications

Chapter 4 (Paper 1) – Facies Variability and Depositional Settings of Laguna Salada de Chiprana, an Iberian Hypersaline Lake

Connor Doyle, Stefan Schroeder, Juan Pablo Corella, Blas Valero-Garces

This chapter has been published in the journal *Sedimentology*.

Chapter 5 (Paper 2) – Spatio-Temporal Variations in the Geochemistry of Laguna Salada de Chiprana, NE Spain

Connor Doyle, Stefan Schroeder, Juan Pablo Corella, Blas Valero-Garces

This chapter has been published in the journal *Geosciences*.

Chapter 6 (Paper 3) - Mineralogical Assemblages and Hydrochemical Modelling of Laguna Salada de Chiprana, Northeast Spain

Connor Doyle, Stefan Schroeder, Juan Pablo Corella, Fernando Gazquez, Ana Moreno, Blas Valero-Garces

Chapter 7 (Paper 4) - Development of modern and sub-recent lacustrine microbial mats in southwestern Europe: Insights into environmental controls

Connor Doyle, Stefan Schroeder, Juan Pablo Corella, Mario Morellon, Celia Martin-Puertas, Julia Behnsen, Blas Valero-Garces

Acknowledgements

The production of this thesis throughout the last difficult few years would absolutely have been impossible without the supervisory team that have assisted me throughout the journey of the PhD. Firstly, my primary supervisor, Stefan Schroeder, has provided a constant source of support and assistance, and I am immensely grateful to the many discussions we have had over email, in-person, and for the most part, online! You are undoubtedly a leader in the field of sedimentology and your expertise in unravelling complex sedimentological sequences has been unrivalled when interpreting the weird and wonderful world of saline lakes.

Secondly, to my co-supervisors Juan Pablo Corella Aznar and Blas Lorenzo Valero-Garces. Your combined knowledge in lacustrine sedimentology is unparalleled; whether it be the interpretation of a complex geochemical dataset, or how to operate a pneumatic boat for the collection of your sediment cores; there can be no comparison to your willingness and patience in each and every scenario. Your help and assistance have made this PhD possible during a time when labwork and data collection were nigh on impossible.

In the Department of Earth and Environmental Sciences, I have immense gratitude to John Waters, Jon Fellowes, Lewis Hughes, Abby Ragazzon-Smith and Lee Paul. They provided a constant source of assistance in the operation and training of the use of complex technical equipment ranging from X-ray diffractometers to digestion microwaves. I also thank my colleagues in the NERC DTP, particularly Rhys and Jake, who have been great friends and colleagues throughout the past several years.

The team based at the Geography labs in the School of Environment of Education at the University of Manchester are also a critical acknowledgement that have made this PhD possible. John Moore, Thomas Bishop and Jonathan Yarwood have been a constant source of friendship, support and great laughs during my time spent in

the labs, and I thank each of them enormously for their help and assistance in keeping the cores cold, introducing me to new and complex techniques, and working through some tough datasets.

In the Henry Moseley X-Ray Institute, my sincere thanks go to Julia Behnsen, Tristan Lowe and Amin Garbout. They have all been instrumental in the collection and processing of complex computerised tomographical data that have been hugely novel and interesting throughout this project.

I also thank colleagues and collaborators at the Pyrenean Institute of Ecology and the University of Almeria. Ines, Elena, Hannah, Jorge, Marcel, Fernando and many others have provided unprecedented amounts of help during times when labwork was impossible, and I thank each and every one of them for their constant support.

Finally, and most importantly, I have the utmost gratitude for my family and for my partner, Eve. Your constant patience and support throughout the project and the pandemic, listening to my ramblings about saline lakes and microbial mats, and just generally keeping me sane throughout the time spent in lockdown are all so appreciated. I absolutely could not have done it without any of you, and especially not without the love and support provided by my mother, Dawn, my unofficial mother-in-law, Celia, and the care and partnership provided by you, Eve.

Dedication

This thesis is dedicated to the father figures in my life. Firstly to my father Jimmy, who passed away unexpectedly in 2013. Secondly, to my grandfathers James and Harry, who both passed away during the course of this project in 2019 and 2021. I know all of you would have enjoyed reading this thesis, even if you weren't sure what most of it meant! Finally, I also dedicate to it Paul and David – you have been father figures in the times when it really mattered.

Chapter 1 - Introduction

1.1 Background

1.1.1 Saline Lakes

Saline lakes are scientifically and economically valuable settings that are distributed worldwide (Figure 1.1) and which demonstrate a diverse range of physiochemical and biological attributes (Zadereev *et al.*, 2020). They undergo environmental variations at a wide variety of scales (Williams, 2002), and are often considered highly important archives of geochemical information throughout the globe (Naftz *et al.*, 2008). Furthermore, many saline lakes also contain a wide spectrum of unique ecological sub-environments (Brock & Hammer, 1987), and due to the harsh environmental conditions associated with them, are often seen to nullify the development of complex biological life (Stenger-Kovács *et al.*, 2014). Most saline lakes have been associated with “endorheic” basins where hydrological outputs such as evapotranspiration are highly intense and predominate over hydrological inputs (Deocampo & Jones, 2013). As such, many examples are associated with arid to semi-arid regions throughout the globe (Last & Last, 2012) such as the Iberian Peninsula (Comin & Alonso, 1988). Saline lakes in this region and also around the globe contain sedimentary sequences which display significant variability both spatially and temporally (Hardie *et al.*, 1978; Schröder *et al.*, 2018), and they are often host to unique sedimentary deposits known as microbial mats (Bauld, 1981; Guerrero, 1992). These mats are highly complex and are known to exhibit a range of interactions with the sediments associated with them (Dupraz *et al.*, 2004; Visscher & Stolz, 2005), developing strong biogeochemical gradients (Visscher & Stolz, 2005; Prieto-Barajas *et al.*, 2018), forming and dissolving minerals (Dupraz *et al.*, 2009), and generating small-scale facies variability (Bourillot *et al.*, 2020). As such, both saline lakes and microbial mats can be studied to gain unique insights into the wide range of processes occurring within lacustrine settings.

Increasing amounts of work have begun to consider the plausibility of saline lakes and microbial mats in understanding palaeoenvironmental and biogeochemical processes (Schröder *et al.*, 2018; Bourillot *et al.*, 2020). However, though some work has been undertaken (Valero-Garcés & Kelts, 1995), there are currently no general facies models associated with saline-hypersaline lakes, and understanding the processes leading to facies variability within these systems remains challenging (Brock & Hammer, 1987) (see chapter 2). A range of sedimentary structures associated with saline lakes have been described in the literature (Eugster & Hardie, 1978; Valero-Garcés & Kelts, 1995; Schröder *et al.*, 2018), and it is well known that they can be influenced by a range of climatic, hydrological and biological factors (Verleyen *et al.*, 2010). Therefore, a considerable effort is required to improve how saline lacustrine facies, including microbial mats, can be used for the reconstruction of palaeoenvironments and the investigation of microbe-sediment interactions.

1.1.2 Microbes and Microbial Mats

Microbial life has maintained a role in the evolution of the Earth throughout the last 3.5 billion years (Schopf *et al.*, 2007; Tice *et al.*, 2011), and microbes fundamentally have maintained a significant role in the regulation of many different global cycles throughout this time (Visscher & Stolz, 2005; Prieto-Barajas *et al.*, 2018). Many microbial-geosphere interactions are also known to occur within a diverse range of environments (Keller & Zengler, 2004), including hypersaline and saline-alkaline lacustrine systems (Dupraz *et al.*, 2004; Polerecky *et al.*, 2007; Wright, 2012), the marine realm (Kirchman, 2016; Collins *et al.*, 2020) and also extensively in terrestrial settings (Wu *et al.*, 2009; Voser *et al.*, 2022). Microbial processes are perhaps most unique when occurring within microbial mats; defined as multi-layered biofilms with distinct functional groups of microbes (Franks & Stolz, 2009; Prieto-Barajas *et al.*, 2018). These mats, often strongly associated with many saline lakes (Guerrero, 1992), are biologically intricate structures generated by microbes and their interactions with the environment they colonise within (Vasconcelos *et al.*, 2006; Dupraz *et al.*, 2009). Typically, these mats occur as micrometre to centimetre or even

metre-scale ecosystems (van Gemerden, 1993; Visscher & Stolz, 2005), and contain laminae comprising distinct groups of microbes that are interlaminated with detrital material and endogenic minerals (Riding, 2011; Prieto-Barajas *et al.*, 2018). Different functional groups of microbes associated with such mats are responsible for metabolic processes (Visscher & Stolz, 2005) such as photosynthesis (Merz, 1992), methanogenesis (Cadena *et al.*, 2018), sulphate reduction (Hao, 2003) and sulphide oxidation (Gibson, 1980).

1.2 The Importance of Saline Lakes, Microbialites & Microbe-Mineral Interactions

1.2.1 Significance of Saline Lakes

Saline lakes are generally recognised as important locales that serve a spectrum of economic, industrial and ecological and scientific uses (Brock & Hammer, 1987). From an applied perspective, work by Jellison *et al.* (2008) has perhaps highlighted their economic and industrial uses most extensively, while a vast plethora of other works have extensively detailed the applied functions of various individual saline lake environments. For example, Bioeconomics (2012) have reported on the applications of Great Salt Lake to the State of Utah, and described the lake as providing services for the extraction of mineral deposits such as salt and potash, its use for recreational activities, waste assimilation, and other important services. Other notable examples of economically significant saline lake environments include Lake Urmia, Iran, which is used for agricultural activities (Schulz *et al.*, 2020), while many Chinese salt lakes are used for mineral resources (Kong *et al.*, 2017). For example, saline lakes are well documented as large resources of lithium, with the largest lithium resource globally being situated in Salar de Atacama, Chile (Cubillos *et al.*, 2018).

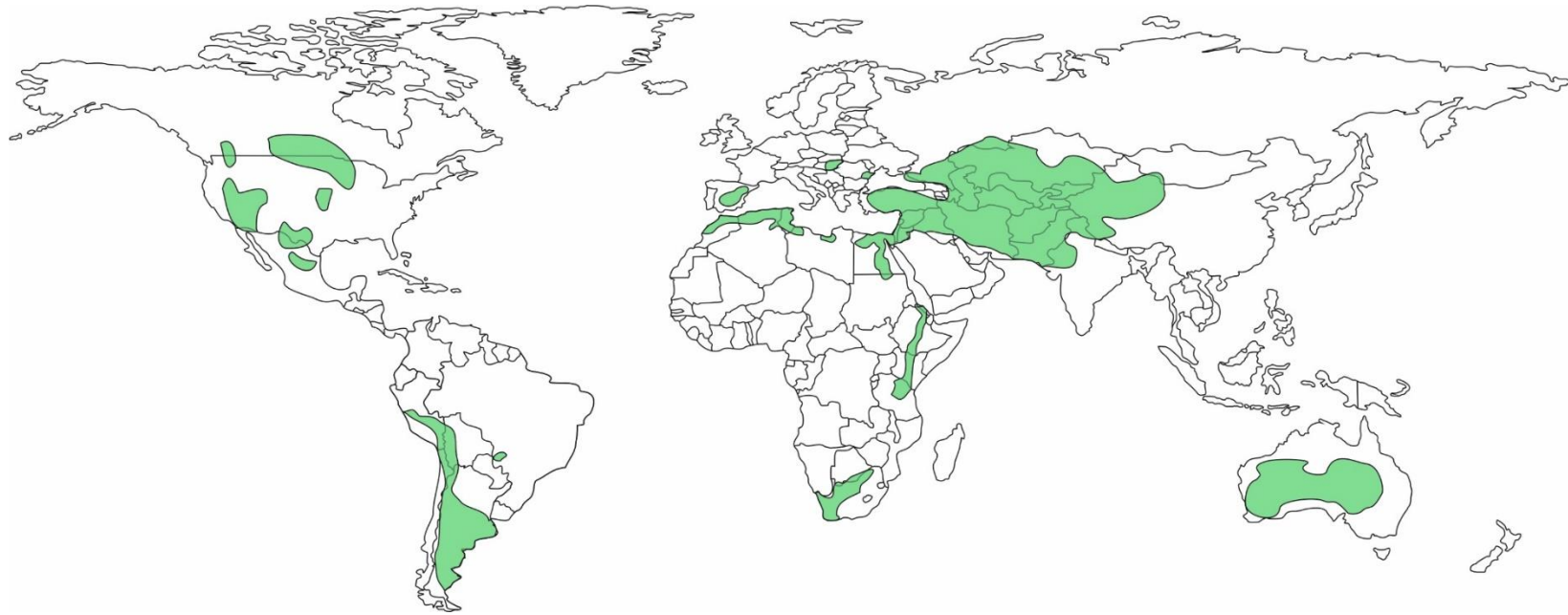


Figure 1.1 – Approximate distribution of saline lakes around the globe. Adapted from Williams (2002) and Finlayson (2016).

A vast plethora of studies have also shown that many saline lakes can record environmental and anthropogenic changes on varied temporal scales (Last & Schweyen, 1983; Valero-Garcés & Kelts, 1995; Valero-Garcés *et al.*, 2000; Last & Ginn, 2005; Medley *et al.*, 2007). This has been highlighted in particular by studies focusing upon Saskatchewan saline lakes (Rawson & Moore, 1944; Hammer, 1978; Bowman & Sachs, 2008), where variations in the physicochemical characteristics of the lakes coupled with the influence of climatic and geological factors lead to the generation of distinctive lacustrine settings throughout the region (Last & Ginn, 2005). In brief, saline lakes are becoming increasingly recognised as valuable palaeoenvironmental repositories with which climatic and environmental change can be understood (Gasse *et al.*, 1997; Deocampo *et al.*, 2009).

1.2.2 Significance of Microbial Mats and Microbialites

The varied biological processes associated with microbial mats occurring within a wide spectrum of environments merits an increased understanding of their intrinsic characteristics and subsequently their interactions with their environment (Dupraz *et al.*, 2009). From a scientific perspective, microbes are well known to be established in processes such as the cycling of atmospheric gases (Kertesz & Mirleau, 2004; Clokie, 2008; Saini *et al.*, 2011). In the geological sciences, the mineral products they are associated with are critical for understanding their role in processes of mineral formation, dissolution and alteration (Bazylinski *et al.*, 2007; Dupraz *et al.*, 2009) and the evolution of such mineral products in response to diagenetic processes (Tan *et al.*, 2018). The ongoing examination and investigation of modern processes will be vital for consolidating our knowledge of the role microbe-mineral interactions have played not only in the present but also throughout geologic time.



Figure 1.2 - Location of several unique and important microbial mats around the globe (see Table 1.1 for further details). Microbial mats and biofilms are ultimately present in many different environments, but unique and well developed examples have been discovered in these locations that have been the subject of intense study concerning their biogeochemical properties.

Table 1.1 - Table displaying key examples of saline lakes around the globe where unique and important microbial mat ecosystems are present and are known to be representative of important microbe-mineral interactions.

Abbreviations: CYN - Cyanobacteria, AHB - Aerobic heterotrophic bacteria, SRB - Sulphate-reducing bacteria, CSB - Colourless sulphur bacteria, PSY - Psychrophilic bacteria, PRO - Proteobacteria, CHL - Chloroflexi, BCT - Bacteroidetes, MET - Methanogens, PSB - Purple sulphur bacteria.

No.	Site	Location	Physicochemical Properties	Key Microbial Functional Groups	Reference(s)
1	Laguna Salada de Chiprana	Ebro Basin, Northeast Spain	Hypersaline lake with evaporite and carbonate precipitates	CYN, AHB, CSB and SRB.	(Jonkers <i>et al.</i> , 2003)
2	Laguna de Las Eras	Duero Basin, Central Spain	Alkaline lake	CYN, AHB, CSB and SRB.	(Sanz-Montero <i>et al.</i> , 2019)
3	Lake Clifton	Australia	Saline coastal lake	CYN, AHB, PSB and SRB	(Moore <i>et al.</i> , 1984)
4	Pyramid Lake	USA	Saline lake/flat	CYN, PSB	(Arp <i>et al.</i> , 1999)
5	Atacama Desert	Chile	Salt flats with evaporite precipitates	CYN, PRO, BCT	(Rasuk <i>et al.</i> , 2016)
6	Storr's Lake	San Salvador Island, Bahamas	Evaporitic hypersaline lake/lagoon	Varied	(Paul <i>et al.</i> , 2016)
7	Shark Bay	Western Australia	Evaporitic hypersaline lagoon/pool	PRO, CHL	(Awramik & Riding, 1988; Papineau <i>et al.</i> , 2005)

8	Great Salt Lake	USA	Saline lake	CYN, CHL	(Bouton <i>et al.</i> , 2016; Pace <i>et al.</i> , 2016)
9	Eleuthera Island	Bahamas	Hypersaline lagoon	CYN, CHL	(Dupraz <i>et al.</i> , 2004)
10	Lagoa Vermelha	Southern Brazil	Shallow hypersaline lagoon	CYN, AHB, PSB, SRB	(Vasconcelos <i>et al.</i> , 2006; Spadafora <i>et al.</i> , 2010)
11	East African Lakes	East African Rift	Lacustrine to hydrochemical	Varied	(Casanova, 1994)
12	Abu Dhabi Coasts	UAE	Marine/coastal	Varied	(Bontognali, 2010)

In contrast, from an applied perspective, microbial mats have been widely recognised for their role in both depositional processes (Bourillot *et al.*, 2020) and in diagenetic reactions (Rezende *et al.*, 2013), leading to the development of a wide spectrum of complex deposits (Grey & Awramik, 2020). As such, they have gained substantial attention when considering their potential roles in unconventional hydrocarbon reservoirs (Lipinski *et al.*, 2013; Rezende *et al.*, 2013; Mohriak, 2015; Rezende & Pope, 2015). Work on these reservoirs with regards to diagenetic processes (Pace *et al.*, 2016), the interplay of biotic and abiotic processes (Wright & Barnett, 2015) and the contribution of microbes to porosity and permeability (Rezende *et al.*, 2013) is still needed, particularly in the case of key examples such as the pre-salt reservoirs of the Santos and Campos Basins of Brazil (Carminatti *et al.*, 2008) and in Angola (Laurent *et al.*, 2016).

1.3 Current Issues, Research Questions and Scope of Thesis

1.3.1 Research Questions

Research concerning saline lakes and the development of microbial mats in both contemporary and ancient saline lacustrine settings has expanded rapidly within the past few decades. However, problems remain in our understanding of how saline lakes function, how they can act as palaeoenvironmental archives, and how we can link contemporary microbial mat formation and processes with ancient microbialites and microbial sediments (Dupraz *et al.*, 2004; Riding, 2011). As such, key questions related to these problems include:

- ***Problem 1 – What information can be extracted from modern saline lakes to determine (palaeo)environmental processes both spatially and temporally, and subsequently, can saline lacustrine sedimentary sequences be reliably utilised for high-resolution palaeoenvironmental reconstructions?***

- ***Problem 2 - How do microbialite morphological and geochemical characteristics vary through space and time in different saline lacustrine settings?***
- ***Problem 3 - What are the effects of environmental and geochemical conditions on microbial mats in the present and the recent past?***

Questions also remain unanswered regarding the effects of extrinsic forcing mechanisms that act on saline lakes and microbial mats and the implications they have for these environments and their deposits. In particular, the effects of anthropogenic perturbations and climatic change upon microbial mat formation have received limited attention from the scientific community, particularly with regards to how changing land use and agricultural activities can affect water level change in saline lacustrine systems and the knock-on effect this has upon microbial mats (Camacho & De Wit, 2003). Ultimately, further investigations of saline lake environments and microbialite morphology and geochemistry are required for a deeper understanding of saline lake dynamics and processes, microbial mat and microbialite development, and the use of both saline lakes and microbialites as palaeoenvironmental archives (Schröder *et al.*, 2018). Thus, the overarching aim of the project is to improve the understanding of saline lake sedimentology, facies and geochemical variability, while also further defining the sedimentological, mineralogical and geochemical characteristics of microbial mats associated with these systems.

1.3.2 Aims & Objectives

As a result of the questions and issues stated previously, this thesis has several defined aims and objectives which have been developed in order to build upon these issues and contribute to knowledge of saline lakes and associated microbial mats and microbialites. They are:

1. ***Aim 1 - Assess spatio-temporal variability and subsequently palaeoenvironmental characteristics reflected in the sedimentology,***

geochemistry and hydrochemistry of Lake Chiprana, a hypersaline lake in Northeast Spain.

- 2. Aim 2 - Integrate a detailed assessment of variations in the petrography and morphology of modern and sub-recent microbial mats from the same setting and from comparable lacustrine settings in the Iberian peninsula to provide further detail into potential environmental signatures associated with saline lakes in the Iberian Peninsula.***

The first aim links primarily to problem 1, and was developed in order to understand both spatio-temporal variations in saline lacustrine sedimentology while assessing the validity of these settings as palaeoenvironmental archives. The second aim broaches problems 2 and 3, and hopes to contribute to our understanding of these issues by using both high-resolution morphological and petrographic analyses coupled with strong supporting investigations of the environments these microbial mats and microbialites are associated with. In turn, the choice of Lake Chiprana was primarily due to the unique sub-environments associated with the lake as well as the development of microbial mats within the present day which act as potential analogues for sub-recent microbialite structures, the lake's permanent nature, and the need for development upon and integration with previous studies. The goals are subsequently to further understand the use of facies, geochemical signatures, and changes in mineralogy and hydrochemistry in this setting for use as palaeoenvironmental indicators. This will contribute to the development of proxies such as hydrology, sedimentology, geochemistry and limnological conditions that can potentially be applied in other hypersaline lakes globally where microbial mats develop. Understanding key environmental shifts from a range of sedimentological and geochemical characteristics in addition to the use of distinctive morphological and petrographic features of microbialites as potential indicators of intrinsic limnological conditions will allow for the development of new insights into palaeoenvironmental and anthropogenic change. As such, the objectives of the thesis are to:

- **Objective 1 – Undertake a detailed sedimentological and geochemical study of hypersaline Lake Chiprana in order to determine the validity and reliability of such settings as potential high-resolution environmental archives.**
- **Objective 2 – Characterise and compare key microbial fabrics and textures associated occurring in modern, sub-recent and fossil Iberian saline lakes, and determine what environmental conditions they were developing within.**
- **Objective 3 - Assess variations in microbial mat development and limnology within comparative lacustrine environments to understand the effect of environmental fluctuations on microbial mats and their formation in saline-lacustrine settings.**

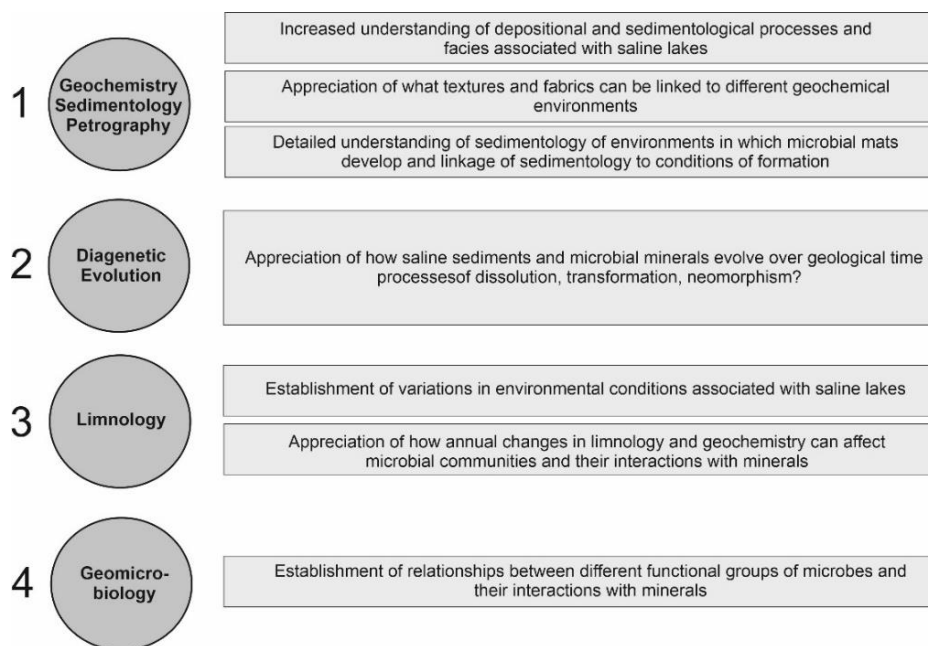


Figure 1.3 – Primary hypotheses of the project and their predicted impact and outcomes.

References

- Arp, G., Thiel, V., Reimer, A., Michaelis, W. and Reitner, J.** (1999) Biofilm exopolymers control microbialite formation at thermal springs discharging into the alkaline Pyramid Lake, Nevada, USA. *Sediment. Geol.*, **126**, 159–176.
- Awramik, S.M. and Riding, R.** (1988) Role of algal eukaryotes in subtidal columnar stromatolite formation. *Proc. Natl. Acad. Sci.*, **85**, 1327–1329.
- Bauld, J.** (1981) 8. Occurrence of benthic microbial mats in saline lakes. *Hydrobiologia*, **81–82**, 87–111.
- Bazylinski, D.A., Frankel, R.B. and Konhauser, K.O.** (2007) Modes of biomineralization of magnetite by microbes. *Geomicrobiol. J.*, **24**, 465–475.
- Bioeconomics** (2012) Economic significance of the Great Salt Lake to the State of Utah. 50.
- Bourillot, R., Vennin, E., Dupraz, C., Pace, A., Foubert, A., Rouchy, J.M., Patrier, P., Blanc, P., Bernard, D., Lesseur, J. and Visscher, P.T.** (2020) The record of environmental and microbial signatures in ancient microbialites: The terminal carbonate complex from the neogene basins of southeastern Spain. *Minerals*, **10**, 1–50.
- Bouton, A., Vennin, E., Mulder, T., Pace, A., Bourillot, R., Thomazo, C., Brayard, A., Goslar, T., Buoncristiani, J.F., Désaubliaux, G. and Visscher, P.T.** (2016) Enhanced development of lacustrine microbialites on gravity flow deposits, Great Salt Lake, Utah, USA. *Sediment. Geol.*, **341**, 1–12.
- Bowman, J.S. and Sachs, J.P.** (2008) Chemical and physical properties of some saline lakes in Alberta and Saskatchewan. *Saline Systems*. doi: 10.1186/1746-1448-4-3
- Brock, M.A. and Hammer, U.T.** (1987) *Saline Lake Ecosystems of the World.*, 1st edn. Springer, Dordrecht, 580 pp.
- Cadena, S., García-Maldonado, J.Q., López-Lozano, N.E. and Cervantes, F.J.** (2018) Methanogenic and Sulfate-Reducing Activities in a Hypersaline Microbial Mat and Associated Microbial Diversity. *Microb. Ecol.*, **75**, 930–940.
- Camacho, A. and De Wit, R.** (2003) Effect of nitrogen and phosphorus additions on a benthic microbial mat from a hypersaline lake. *Aquat. Microb. Ecol.*, **32**, 261–273.
- Carminatti, M., Dr, B., Wolff, B. and Gamboa, L.** (2008) New Exploratory Frontiers In Brazil. *19th World Pet. Congr.*, 11.
- Casanova, J.** (1994) Stromatolites from the East African Rift: A Synopsis. In: *Phanerozoic Stromatolites II*, 193–226.
- Clokic, M.** (2008) Microbes and oxygen. *Microbiol. Today*, **35**, 116–119.
- Collins, S., Boyd, P.W. and Doblin, M.A.** (2020) Evolution, Microbes, and Changing Ocean Conditions. *Ann. Rev. Mar. Sci.*, **12**, 181–208.
- Comin, F.A. and Alonso, M.** (1988) Spanish salt lakes: Their chemistry and biota. *Hydrobiologia*, **158**, 237–245.
- Connon, S.A., Lester, E.D., Shafaat, H.S., Obenhuber, D.C. and Ponce, A.** (2007) Bacterial diversity in hyperarid atacama desert soils. *J. Geophys. Res. Biogeosciences*, **112**, 1–9.
- Cubillos, C.F., Aguilar, P., Grágeda, M. and Dorador, C.** (2018) Microbial Communities From the World's Largest Lithium Reserve, Salar de Atacama,

Chile: Life at High LiCl Concentrations. *J. Geophys. Res. Biogeosciences*, **123**, 3668–3681.

- Deocampo, D.M., Cuadros, J., Wing-Dudek, T., Olives, J. and Amouric, M.** (2009) Saline lake diagenesis as revealed by coupled mineralogy and geochemistry of multiple ultrfine clay phases: Pliocene Olduvai Gorge, Tanzania. *Am. J. Sci.*, **309**, 834–868.
- Deocampo, D.M. and Jones, B.F.** (2013) Geochemistry of Saline Lakes. In: *Treatise on Geochemistry: Second Edition*, 2nd edn. (Ed. K. Turekian and H. Holland), Elsevier, 7, 437–469.
- Dupraz, C., Reid, R.P., Braissant, O., Decho, A.W., Norman, R.S. and Visscher, P.T.** (2009) Processes of carbonate precipitation in modern microbial mats. *Earth-Science Rev.*, **96**, 141–162.
- Dupraz, C., Visscher, P.T., Baumgartner, L.K. and Reid, R.P.** (2004) Microbe-mineral interactions: Early carbonate precipitation in a hypersaline lake (Eleuthera Island, Bahamas). *Sedimentology*, **51**, 745–765.
- Eugster, H. and Hardie, L.** (1978) Saline Lakes. In: *Lakes: Chemistry, Geology, Physics* (Ed. A. Lerman), Springer, New York, NY, 237–293.
- Finlayson, C.M.** (2016) Salt Lakes. In: *The Wetland Book*, 1–12.
- Franks, J. and Stolz, J.F.** (2009) Flat laminated microbial mat communities. *Earth-Science Rev.*, **96**, 163–172.
- Gasse, F., Barker, P., Gell, P.A., Fritz, S.C. and Chalié, F.** (1997) Diatom-inferred salinity in palaeolakes: An indirect tracer of climate change. *Quat. Sci. Rev.*, **16**, 547–563.
- Gibson, D.T.** (1980) Microbial Metabolism. In: *Handbook of Environmental Chemistry*, 2, 161–192.
- Grey, K. and Awramik, S.M.** (2020) Handbook for the study and description of microbialites, Bulletin 1. *Geological Survey of Western Australia*, 1-278 pp.
- Guerrero, M.C.** (1992) Microbial mats in the inland saline lakes of Spain. *Limnetica*, **8**, 197–204.
- Hammer, U.T.** (1978) The Saline Lakes of Saskatchewan I. Background and Rationale for Saline Lakes Research. *Int. Rev. der gesamten Hydrobiol. und Hydrogr.*, **63**, 173–177.
- Hao, O.J.** (2003) Sulphate-reducing bacteria. In: *Handbook of Water and Wastewater Microbiology*, 459–469.
- Hardie, L.A., Smoot, J.P. and Eugster, H.P.** (1978) Saline Lakes and their Deposits: A Sedimentological Approach. In: *Modern and Ancient Lake Sediments*, 7–41.
- Jellison, R., Williams, W.D., Timms, B., Alcocer, J. and Aladin, N. V.** (2008) Salt lakes: Values, threats and future. In: *Aquatic Ecosystems: Trends and Global Prospects*, 94–110.
- Jonkers, H.M., Ludwig, R., De Wit, R., Pringault, O., Muyzer, G., Niemann, H., Finke, N. and De Beer, D.** (2003) Structural and functional analysis of a microbial mat ecosystem from a unique permanent hypersaline inland lake: “La Salada de Chiprana” (NE Spain). *FEMS Microbiol. Ecol.*, **44**, 175–189.
- Keller, M. and Zengler, K.** (2004) Tapping into microbial diversity. *Nat. Rev. Microbiol.*, **2**, 141–150.
- Kertesz, M.A. and Mirleau, P.** (2004) The role of soil microbes in plant sulphur nutrition. In: *Journal of Experimental Botany*, 55, 1939–1945.

- Kirchman, D.L.** (2016) Growth Rates of Microbes in the Oceans. *Ann. Rev. Mar. Sci.*, **8**, 285–309.
- Kong, R., Xue, F., Wang, J., Zhai, H. and Zhao, L.** (2017) Research on Mineral Resources and Environment of Salt Lakes in Qinghai Province based on System Dynamics Theory. *Resour. Policy*, **52**, 19–28.
- Last, F.M. and Last, W.M.** (2012) Lacustrine carbonates of the northern Great Plains of Canada. *Sediment. Geol.* **277–278**:1–31.
- Last, W.M. and Ginn, F.M.** (2005) Saline systems of the Great Plains of western Canada: an overview of the limnogeology and paleolimnology. *Saline Systems*, **1**, 1–38.
- Last, W.M. and Schweyen, T.H.** (1983) Sedimentology and geochemistry of saline lakes of the Great Plains. *Hydrobiologia*, **105**, 245–263.
- Laurent, G.C., Edoardo, P., Ian, S.R., Peacock, D.C.P., Roger, S., Ragnar, P., Hercinda, F. and Vladimir, M.** (2016) Origin and diagenetic evolution of gypsum and microbialitic carbonates in the Late Sag of the Namibe Basin (SW Angola). *Sediment. Geol.*, **342**, 133–153.
- Lipinski, C.J., Franseen, E.K. and Goldstein, R.H.** (2013) Reservoir analog model for oolite-microbialite sequences, Miocene terminal carbonate complex, Spain. *Am. Assoc. Pet. Geol. Bull.*, **97**, 2035–2057.
- Medley, P., Tibert, N.E., Patterson, W.P., Curran, H.A., Greer, L. and Colin, J.P.** (2007) Paleosalinity history of middle Holocene lagoonal and lacustrine deposits in the Enriquillo Valley, Dominican Republic based on pore morphometrics and isotope geochemistry of Ostracoda. *Micropaleontology*, **53**, 409–419.
- Merz, M.U.E.** (1992) The biology of carbonate precipitation by cyanobacteria. *Facies*, **26**, 81–101.
- Mohriak, W.** (2015) Pre-Salt Carbonate Reservoirs in the South Atlantic and World-wide Analogs.
- Moore, L., Knott, B. and Stanley, N.** (1984) The stromatolites of Lake Clifton, Western Australia - living structures representing the origins of life. *Search*, **14**, 309–314.
- Naftz, D., Angerth, C., Kenney, T., Waddell, B., Darnall, N., Silva, S., Perschon, C. and Whitehead, J.** (2008) Anthropogenic influences on the input and biogeochemical cycling of nutrients and mercury in Great Salt Lake, Utah, USA. *Appl. Geochemistry*, **23**, 1731–1744.
- Pace, A., Bourillot, R., Bouton, A., Vennin, E., Galaup, S., Bundeleva, I., Patrier, P., Dupraz, C., Thomazo, C., Sansjofre, P., Yokoyama, Y., Franceschi, M., Anguy, Y., Pigot, L., Virgone, A. and Visscher, P.T.** (2016) Microbial and diagenetic steps leading to the mineralisation of Great Salt Lake microbialites. *Sci. Rep.*, **6**, 1–12.
- Papineau, D., Walker, J.J., Mojzsis, S.J. and Pace, N.R.** (2005) Composition and structure of microbial communities from stromatolites of Hamelin Pool in Shark Bay, Western Australia. *Appl. Environ. Microbiol.*, **71**, 4822–4832.
- Paul, V.G., Wronkiewicz, D.J., Mormile, M.R. and Foster, J.S.** (2016) Mineralogy and microbial diversity of the microbialites in the Hypersaline Storr's Lake, the Bahamas. *Astrobiology*, **16**, 282–300.
- Polerecky, L., Bachar, A., Schoon, R., Grinstein, M., Jørgensen, B.B., De Beer, D. and Jonkers, H.M.** (2007) Contribution of Chloroflexus respiration to oxygen cycling in a hypersaline microbial mat from Lake Chiprana, Spain. *Environ. Microbiol.*, **9**, 2007–2024.

- Prieto-Barajas, C.M., Valencia-Cantero, E. and Santoyo, G.** (2018) Microbial mat ecosystems: Structure types, functional diversity, and biotechnological application. *Electron. J. Biotechnol.* **31**:48–56.
- Rasuk, M.C., Fernández, A.B., Kurth, D., Contreras, M., Novoa, F., Poiré, D. and Farías, M.E.** (2016) Bacterial Diversity in Microbial Mats and Sediments from the Atacama Desert. *Microb. Ecol.*, **71**, 44–56.
- Rawson, D.S. and Moore, J.E.** (1944) the Saline Lakes of Saskatchewan. *Can. J. Res.*, **22d**, 141–201.
- Rezende, M.F. and Pope, M.C.** (2015) Importance of depositional texture in pore characterization of subsalt microbialite carbonates, offshore Brazil. *Geol. Soc. Spec. Publ.*, **418**, 193–207.
- Rezende, M.F., Tonietto, S.N. and Pope, M.C.** (2013) Three-dimensional pore connectivity evaluation in a Holocene and Jurassic microbialite buildup. *Am. Assoc. Pet. Geol. Bull.*, **97**, 2085–2101.
- Riding, R.** (2011) Microbialites, stromatolites, and thrombolites. In: *Encyclopedia of Earth Sciences Series*, 635–654.
- Saini, R., Kapoor, R., Kumar, R., Siddiqi, T.O. and Kumar, A.** (2011) CO₂ utilizing microbes - A comprehensive review. *Biotechnol. Adv.*, **29**, 949–960.
- Sanz-Montero, M.E., Cabestrero, Ó. and Sánchez-Román, M.** (2019) Microbial Mg-rich carbonates in an extreme alkaline lake (Las Eras, Central Spain). *Front. Microbiol.*, **10**, 1–15.
- Schopf, J.W., Kudryavtsev, A.B., Czaja, A.D. and Tripathi, A.B.** (2007) Evidence of Archean life: Stromatolites and microfossils. *Precambrian Res.*, **158**, 141–155.
- Schröder, T., van 't Hoff, J., Ortiz, J.E., de Torres Pérez-Hidalgo, T.J., López-Sáez, J.A., Melles, M., Holzhausen, A., Wennrich, V., Viehberg, F. and Reicherter, K.** (2018) Shallow hypersaline lakes as paleoclimate archives: A case study from the Laguna Salada, Málaga province, southern Spain. *Quat. Int.*, **485**, 76–88.
- Schulz, S., Darehshouri, S., Hassanzadeh, E., Tajrishy, M. and Schüth, C.** (2020) Climate change or irrigated agriculture – what drives the water level decline of Lake Urmia. *Sci. Rep.*, **10**, 1–10.
- Spadafora, A., Perri, E., Mckenzie, J.A. and Vasconcelos, C.Óg.** (2010) Microbial biomineralization processes forming modern Ca:Mg carbonate stromatolites. *Sedimentology*, **57**, 27–40.
- Stenger-Kovács, C., Lengyel, E., Buczkó, K., Tóth, F.M., Crossetti, L.O., Pellingner, A., Doma, Z.Z. and Padisák, J.** (2014) Vanishing world: Alkaline, saline lakes in Central Europe and their diatom assemblages. *Inl. Waters*, **4**, 383–396.
- Tan, Q., Shi, Z., Hu, X.Q., Wang, Y., Tian, Y.M. and Wang, C.C.** (2018) Diagenesis of microbialites in the lower Cambrian Qingxudong Formation, South China: Implications for the origin of porosity in deep microbial carbonates. *J. Nat. Gas Sci. Eng.*, **51**, 166–182.
- Tice, M.M., Thornton, D.C.O., Pope, M.C., Olszewski, T.D. and Gong, J.** (2011) Archean microbial mat communities. *Annu. Rev. Earth Planet. Sci.*, **39**, 297–319.
- Valero-Garcés, B.L. and Kelts, K.R.** (1995) A sedimentary facies model for perennial and meromictic saline lakes: Holocene Medicine Lake Basin, South Dakota, USA. *J. Paleolimnol.*, **14**, 123–149.

- Valero-Garcés, B.L., Navas, A., Machin, J., Stevenson, T., Davis, B., Valero-Garcés, B.L., Navas, A., Machin, J., Stevenson, T., Davis, B., Valero-Garcés, B.L., Navas, A., Machin, J., Stevenson, T. and Davis, B.** (2000) Responses of a Saline Lake Ecosystem in a Semiarid Region to Irrigation and Climate Variability. *AMBIO A J. Hum. Environ.*, **29**, 344–350.
- van Gemerden, H.** (1993) Microbial mats: A joint venture. *Mar. Geol.*, **113**, 3–25.
- Vasconcelos, C., Warthmann, R., McKenzie, J.A., Visscher, P.T., Bittermann, A.G. and van Lith, Y.** (2006) Lithifying microbial mats in Lagoa Vermelha, Brazil: Modern Precambrian relics? *Sediment. Geol.*, **185**, 175–183.
- Verleyen, E., Sabbe, K., Hodgson, D.A., Grubisic, S., Taton, A., Cousin, S., Wilmotte, A., De Wever, A., Van Der Gucht, K. and Vyverman, W.** (2010) Structuring effects of climate-related environmental factors on Antarctic microbial mat communities. *Aquat. Microb. Ecol.*, **59**, 11–24.
- Visscher, P.T. and Stolz, J.F.** (2005) Microbial mats as bioreactors: Populations, processes, and products. *Palaeogeogr. Palaeoclimatol. Palaeoecol.*, **219**, 87–100.
- Voser, T.M., Campbell, M.D. and Carroll, A.R.** (2022) How different are marine microbial natural products compared to their terrestrial counterparts? *Nat. Prod. Rep.*, **39**, 7–19.
- Williams, W.D.** (2002) Environmental threats to salt lakes and the likely status of inland saline ecosystems in 2025. *Environ. Conserv.*, **29**, 154–167.
- Wright, V.P.** (2012) Lacustrine carbonates in rift settings: the interaction of volcanic and microbial processes on carbonate deposition. *Geol. Soc. London, Spec. Publ.*, 39–47.
- Wright, V.P. and Barnett, A.J.** (2015) An abiotic model for the development of textures in some South Atlantic early Cretaceous lacustrine carbonates. *Geol. Soc. Spec. Publ.*, **418**, 209–219.
- Wu, C.H., Bernard, S.M., Andersen, G.L. and Chen, W.** (2009) Developing microbe-plant interactions for applications in plant-growth promotion and disease control, production of useful compounds, remediation and carbon sequestration. *Microb. Biotechnol.*, **2**, 428–440.
- Zadereev, E., Lipka, O., Karimov, B., Krylenko, M., Elias, V., Pinto, I.S., Alizade, V., Anker, Y., Feest, A., Kuznetsova, D., Mader, A., Salimov, R. and Fischer, M.** (2020) Overview of past, current, and future ecosystem and biodiversity trends of inland saline lakes of Europe and Central Asia. *Inl. Waters*, **10**, 438–452.

Chapter 2 - Literature Review

Abstract

Numerous saline and hypersaline lakes exist throughout the globe, exhibiting a diverse range of hydrological conditions, sedimentary sequences, and containing potential high-resolution palaeoenvironmental records that can be used to investigate changes in environmental processes throughout the recent geological past. Many saline lakes have been studied in detail throughout the past few decades, and their significance as ecological, environmental, and economical repositories is becoming widely realised. They are also host to a wide spectrum of flora and fauna, and are capable of generating highly unique depositional environments and sedimentological features. Perhaps some of the most unique deposits are found in the form of microbial mats. These mats, defined as biosedimentary structures consisting of different functional groups of microbes, develop as a result of a complex series of biological activities occurring within the mats and abiotic processes acting upon them. The importance of such deposits stems from their ability to respond to shifts in environmental conditions rapidly, lending them to be potential excellent indicators of palaeoenvironmental change throughout the geological record. In this review, the importance and degree of previous work undertaken upon saline lakes and microbial mats and their characteristics is discussed. Also discussed are the dissolution, formation and alteration of mineral products by microbial mats, and what sedimentary products may be produced as a result.

2.1 Introduction

Saline lacustrine systems are geographically widespread around the globe and are ecologically, economically and geologically important environmental systems. They are found in substantial numbers throughout areas such as the Iberian Peninsula (Alonso, 1998), parts of the Americas (Last & Ginn, 2005), and the African continent (Philip & Mosha, 2012). In the present day, the importance of many saline lakes stems from their role in the economic exploitation of resources (Bioeconomics, 2012), for their ability to provide habitats for various fauna and flora (Jellison *et al.*, 2008), and due to the insights they can potentially provide into complex depositional, hydrological and geochemical processes (Valero-Garcés & Kelts, 1995; Schröder *et al.*, 2018). Though saline lakes are widespread and often of interest to both the industrial and scientific communities, their representation within the literature has only recently begun to take hold. In the past decade alone, substantial advances in our understanding of these unique depositional systems have been made (Brock & Hammer, 1987; Deocampo & Jones, 2013). In the present day, a wide variety of studies have emerged which have begun to characterise these unique environments (Figure 2.1) in greater detail (Jellison *et al.*, 2008; Finlayson, 2016).

Saline lakes are also hosts to unique sedimentary deposits known as microbial mats, defined as horizontally stratified communities of microbes (Prieto-Barajas *et al.*, 2018), and often considered to be multi-layered, complex examples of biofilms (Guerrero, 1992; Rich & Maier, 2015). These mats are laminated biological ecosystems that have existed on Earth for over 3 billion years (Franks & Stolz, 2009). They consist of a spectrum of different functional groups of bacteria and other microorganisms (Prieto-Barajas *et al.*, 2018). They also exhibit sharp chemical gradients (Jorgensen *et al.*, 1983), and are recognised by many studies to play an important role in the many biogeochemical cycles in many of the Earth's environments (Herman & Kump, 2005) (Table 2.1). Microbial mats, sediments produced by microbes, are furthermore known as the earliest forms of life, with several examples being dated to 3.4-3.5Ga (Clarke & Stoker, 2013). Through geological time,

stromatolites have also been shown to be responsible for significant contributions to the evolution of the Earth's biosphere (Riding, 2000), potentially even being responsible for major geological episodes such as the Great Oxygenation Event circa 2.4Ga (Fischer *et al.*, 2016). Subsequently, they represent unique ecosystems that can be used for investigating geological and biological processes (Seckbach, 2016), potential extra-terrestrial life (Davies *et al.*, 2016), and microbial interactions with minerals (Dupraz *et al.*, 2004).

Overall, there are still challenges when attempting to utilise saline lakes as palaeoenvironmental archives, when linking modern day microbial mat formation and processes with ancient microbe-mineral interactions (Dupraz *et al.*, 2004; Riding, 2011a), and when determining the interplay between these two phenomena. Further investigations of saline lakes are required for a greater understanding of their hydrological, geochemical and sedimentological processes and their use as potential palaeoenvironmental archives (Hammer, 1986; Schröder *et al.*, 2018). Further investigations of the effect of environmental and human factors acting on saline lakes and microbial mats and the implications they have for mat development and preservation (Riding, 2000; Bouton *et al.*, 2016) are also needed. For example, the effects of anthropogenic activities upon saline lake characteristics and microbial mat formation have received somewhat limited attention, particularly with regards to the effects of evolving agricultural activities and managed water level change in saline lacustrine systems (Camacho & De Wit, 2003) where many microbial mat ecosystems develop (Guerrero, 1992).

2.1.1 - Scope of Review

This review will consider the current understanding of both saline lakes and microbial mats as tools to understand palaeoenvironmental changes throughout the geological

Table 2.1 – Table illustrating the key microbial activities associated with various elements. Microbes undertake a wide variety of metabolic processes that contribute to the biogeochemical cycling of various elements, and these processes vary according to the functional group of microbes undertaking such cycling. As a result of the metabolic activities of microbes, different mineral precipitates may form, and various other mineral products may undergo diagenesis and dissolution. Table modified from Gadd (2010).

<i>Element(s)</i>	Microbial Processes	Mineral Interactions
<i>Carbon, Oxygen</i>	<ul style="list-style-type: none"> • Uptake and degradation of organic and inorganic compounds. • Photosynthesis. • Methanogenesis. • CO₂ fixation and production. 	<ul style="list-style-type: none"> • Carbonate formation. • Carbonate dissolution.
<i>Nitrogen</i>	<ul style="list-style-type: none"> • Nitrogen fixation. • Nitrification and denitrification. • Ammonia fermentation. 	<ul style="list-style-type: none"> • Carbonate formation.
<i>Sulphur</i>	<ul style="list-style-type: none"> • Degradation of sulphuric organic compounds. • Uptake of organic and inorganic sulphuric compounds. • Oxidation and reduction of sulphuric compounds. 	<ul style="list-style-type: none"> • Dissolution of sulphur-containing minerals. • Formation of sulphides and sulphates.

<i>Manganese</i>	<ul style="list-style-type: none"> • Mn(IV) reduction. • Mn(II) oxidation. 	<ul style="list-style-type: none"> • Accumulation of Mn oxides. • Mn biomineralisation.
<i>Phosphorus</i>	<ul style="list-style-type: none"> • Decomposition of phosphatic compounds. • Transformation of organic phosphorus. • Phosphorus transfer to plants. 	<ul style="list-style-type: none"> • Dissolution of phosphates and phosphorus containing minerals. • Formation of secondary phosphate minerals.
<i>Iron</i>	<ul style="list-style-type: none"> • Fe(III) reduction to Fe(II). • Fe(II) oxidation to Fe(III). 	<ul style="list-style-type: none"> • Biological weathering of Fe containing minerals. • Biological mineralisation of ferrous and ferric precipitates. • Dissolution of Fe by siderophores.

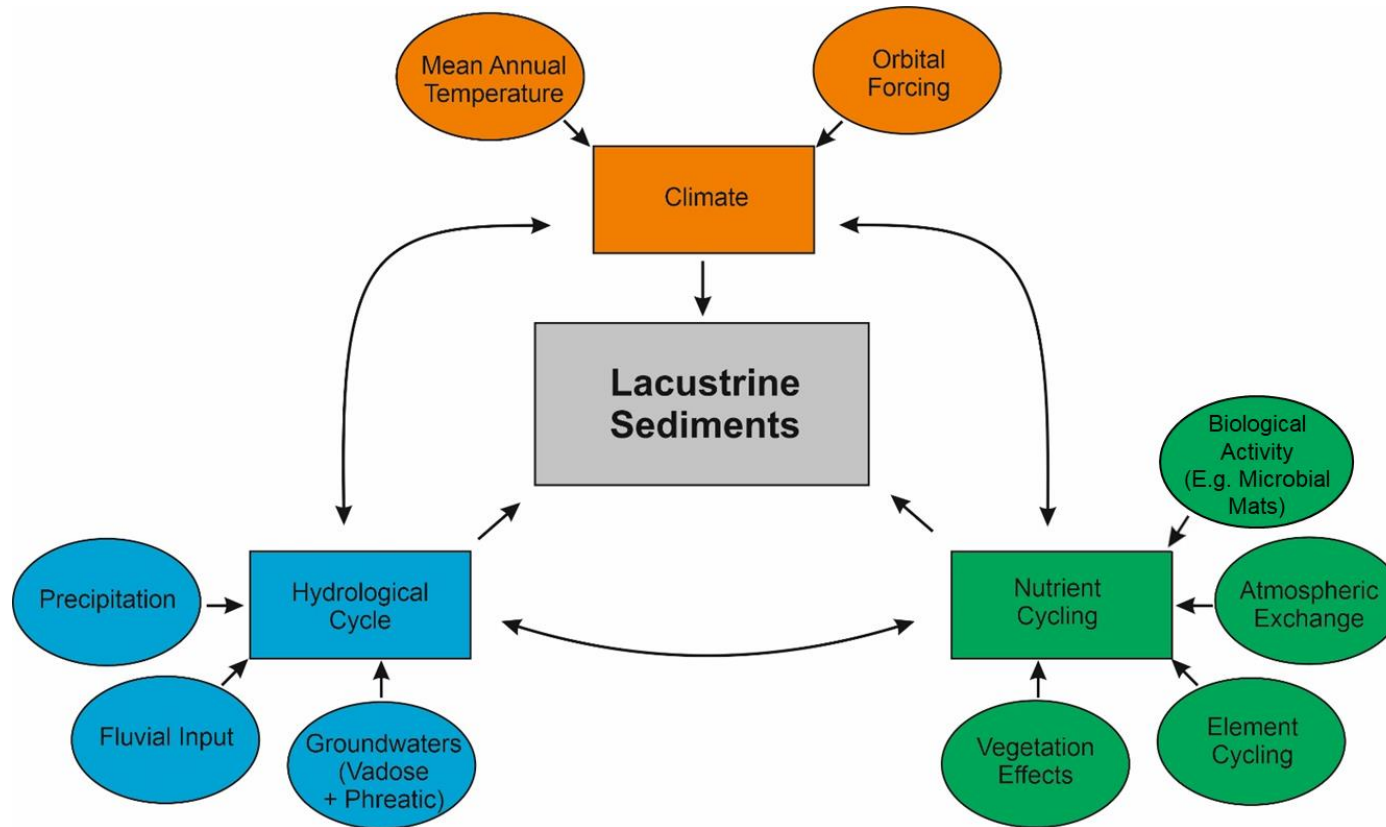


Figure 2.1 - Summarised diagram illustrating the key components and processes occurring within saline lakes and their effects on sedimentology. Partially modified from Zolitschka (2013).

past and will also consider current knowledge regarding microbial processes and microbial mat formation. For saline lakes, the current understanding of their hydrological, geochemical and sedimentological features will be assessed, and their use as palaeoenvironmental archives will be discussed. In the case of microbial mats, their key processes will be discussed, and the products they produce analysed. Altogether, this will form the basis for a review of the current state of understanding of saline lakes and microbial mats and how contemporary processes occurring within these systems can be linked with ancient sedimentological and mineralogical products associated with saline lakes and microbial mats.

2.2 Saline Lacustrine Systems

2.2.1 Distribution

2.2.1.1 Global occurrence

Saline lakes are distributed worldwide, and their origin and distribution is controlled by a unique mixture of climatic and hydrogeological factors (Kelts, 1988). In the present, saline lakes are found occurring in the greatest concentrations within Central Asia (Williams, 2002), East and North Africa (Philip & Mosha, 2012), and throughout the Americas (Ittis, 1993; Piovano *et al.*, 2002; Last & Ginn, 2005; Jones *et al.*, 2009). Many saline lakes are also broadly classified in terms of their distribution as seawater-derived and not seawater-derived according to Zandereev (2018), with the former originating from seawater, and the latter typically being associated with intercontinental formation. In most cases where saline lakes form continentally, they are strongly associated with the distribution of endorheic, “closed” basins (Eugster & Hardie, 1978; Hammer, 1986). According to Yapiyev *et al.* (2017) such conditions require evaporation to exceed sources of inflow, and are primarily met in endorheic basins due to strong evaporative processes over significant timescales. It is thus hypothesised by Deocampo and Jones (2013b) that the strongest distribution of closed basins and thus saline lakes is in areas of continental uplift, within extensional basins, and throughout many intermontane basins. Key examples of such basins and the concentration of saline lakes within which have

received extensive attention, as further highlighted by Deocampo and Jones (2013b), include the extensional basin of the East African Rift (Philip & Mosha, 2012), the compressional settings of the Atacama and Chilean Altiplano (Marazuela *et al.*, 2019), and the topographical depression associated with the Dead Sea (Calder & Neal, 1984; ten Brink, 1998).

2.2.1.2 Examples of saline lake distribution and genesis

Overall, a wide range of factors are necessary for the genesis of saline lakes around the globe (Brock & Hammer, 1987), and there are numerous case studies that investigate the key factors which are responsible for their conception. In the case of the Northern Great Plains of Canada for example, a vast number of saline lakes have been identified and described (Last & Schweyen, 1983). The significant distribution of such environments throughout this area is postulated by Last and Ginn (2005) to have arisen as a result of glacial activity and subsequent deglaciation generating distinct geomorphological depressions throughout the landscape. Subsequently, they stipulate that the presence of saline groundwater (Last, 2002), fluctuating sub-humid to sub-arid climatic conditions (Carroll *et al.*, 2018) and salt input from evaporitic and carbonate-rich bedrock (Last, 1992) are often demonstrated within these studies and other modelling-based approaches (Nield *et al.*, 2008; Tweed *et al.*, 2011) to be a key factor for the saline nature of many of these lacustrine systems.

In the case of the East African Rift, saline lake genesis is suggested to have arisen from the extensional tectonic processes, unique geomorphology and strong distribution of volcanic bedrock associated with this region (Schagerl & Renaut, 2016). In many cases along the East African Rift, such saline lakes are stipulated in review by Schagerl (2016) and by Bergner *et al.* (2009) using Argon/Argon and Carbon-14 isotopes to be controlled by a mixture of tectonics, high evaporation and variable inflow from groundwater, run-off, and hydrothermal springs, leading to a spectrum of examples including playas such as Lake Magadi (Getenet *et al.*, 2020), ephemeral lakes such as Lake Elmentaita (Oduor & Schagerl, 2007), and permanent

waterbodies such as Lake Bogoria (Jirsa *et al.*, 2013; Schagerl & Renaut, 2016). In any case, the limnological characteristics of these environments are often individually unique, and they are host to a broad spectrum of ecological communities (Grant & Jones, 2016; Kavembe *et al.*, 2016; Mengistou, 2016), geochemical conditions (Deocampo & Renaut, 2016; De Cort *et al.*, 2019), and economic resources (Kasedde, 2013).

2.2.2 Limnological Characteristics

The generation and distribution of many saline lakes is ultimately controlled by a complex set of processes and underlying factors (Hardie *et al.*, 1978; Deocampo & Jones, 2013), and the subsequent characteristics of saline lakes are the result of an interplay of such factors (Last, 2013). Understanding the contribution of such factors to the variations in saline lake characteristics is a key topic of investigation in the research of these systems (Hammer, 1986). Overall, saline lakes are complex ecological, geochemical and depositional systems, and this section aims to discuss what is currently understood about their limnological features.

2.2.2.1 Geochemistry and Hydrology

2.2.2.1.1 Overview

According to Deocampo and Jones (2013), there are three fundamental hydrologic conditions that must be met in order for saline lakes to form and remain permanent. These conditions begin with the stipulation that the outflow from the lake must be restricted enough such that there is either a complete absence of water leaving the lake or so little that the hydrological system remains closed (Hammer, 1986). In tandem, it is also stipulated that evaporation must be greater than the degree of inflow to the system, but this inflow must also remain ample enough in order to maintain the main waterbody of the lake. The fulfilment of such conditions is regulated by a wide range of factors, and it must also be considered that variations in both volume and surface area can lead to varying degrees of permanence and ephemerality within saline lakes, ultimately leading to the highly variable

Table 2.2 – Characteristics of key saline lakes found around the globe. Adapted and updated where possible from Hammer (1986a).

Country	Lake	Volume km ³	Surface Area km ²	Average Depth m	Max Depth m	Reference
Kyrgyzstan	Issyk-Kul	1378	6232	278	668	(Wang <i>et al.</i> , 2021)
Turkey	Lake Van	607	3764	171	451	(Ozguven & Demir Yetis, 2020)
Israel-Jordan	Dead Sea	132	630	199	298	(Bookman, 2020)
Kazakhstan	Balkhash	106	18210	5.7	26	(Sala <i>et al.</i> , 2020)
China	Qinghai	119.6	4473	21	32.8	(Zaixing & Chao, 2021)
Tajikistan	Karakul	26.6	380	50.6	242	(Mischke <i>et al.</i> , 2010)
Australia	Eyre (North)	27.7	9690	1.5-4	5.7	(Fu <i>et al.</i> , 2017)
Iran	Urmia	2.5	5200	0.4	16	(Nhu <i>et al.</i> , 2020)
U.S.A	Pyramid Lake	25-55	450-900	60	109	(Adams & Rhodes, 2019)
U.S.A	Great Salt Lake	11.8	2638	4.9	~7.5	(Baskin <i>et al.</i> , 2022)
Tibet-India	Panggong Tso	~15-20	700	30	100	(Dortch <i>et al.</i> , 2011)
U.S.A	Salton Sea	7.4	889	3.9	13	(USGS, 2021)
U.S.A	Mono Lake	3.66	~170	17	48	(Mono Lake Committee, 2019)
Mongolia	Orog Nuur	~0.5	146	3	~5m	(Walther <i>et al.</i> , 2016)
U.S.A	Walker Lake	2.5	100	-	21	(Petryshyn <i>et al.</i> , 2016)
Peru	Poopo	-	-	-	-	(Bengtsson, 2012)
Dominican Republic	Enriquillo	~4-5	352.00	6.1	52	(Wright <i>et al.</i> , 2015)
Australia	Corangamite	1.509	251.00	6	6	(Williams, 1995)
U.S.A	Owens	-	-	-	-	(Reheis, 1997)
Canada	Manito Lake	0.185	78	3.8	~20	(Last <i>et al.</i> , 2012)
U.S.A	Abert	0.000072	6.66	~5	3.4	(Moore, 2016)
Iran	Niriz-Nargiz	0.605	1210	0.5	1.1	(Brock & Hammer, 1987)
Canada	Redberry	0.506	54.4	9.3	18	(Brock & Hammer, 1987)
Canada	Little Quill	0.471	181	2.6	4.3	(Brock & Hammer, 1987)
Canada	Big Quill	0.461	307	1.5	2.6	(Brock & Hammer, 1987)

geochemical and hydrological conditions associated with these ecosystems (Brock & Hammer, 1987).

2.2.2.2 Physical and Geochemical Attributes

Saline lakes also display a wide range of physical characteristics, including size and surface area, volume, temperature and morphology (Hammer, 1986). Most saline lakes are typically distributed in the semi-arid/arid and sub-tropical latitudes (Hammer, 1986; Jellison *et al.*, 2008). Furthermore, though a significant distribution of saline lakes are stipulated by Hammer (1986a) to occur at altitudes between 400m and 1500m a.s.l (Last, 2013), many examples have also been discovered outside such altitudes. For example, the Dead Sea is situated at an altitude of approximately 430m below sea level (ten Brink, 1998), while Namtso Lake in Tibet occurs at approximately 4720m above sea level (Zheng *et al.*, 2022). Saline lakes are also known to vary significantly in surface area and volume (Brock & Hammer, 1987), with many examples present globally that display volumes and surface area in varying ratios (Table 2.2).

According to Hammer (1986a) and Deocampo and Jones (2013), the concentration and abundance of major ions within saline lakes and subsequently geochemical characteristics (e.g. Figure 2.2) such as pH, redox, productivity and carbon dioxide concentrations are influenced by several factors, and often, the variation of such factors can be highly interlinked. The extensive review of saline lake geochemistry by Deocampo and Jones (2013) indicates that the pH of many saline lakes can vary significantly, with factors such as high Ca-Mg concentrations leading to neutral pH values, while high Si and alkali carbonate concentrations lead to alkaline pH values (Bowen & Benison, 2009; Deocampo & Jones, 2013). They further stipulate that the effects of biological processes can amplify characteristics such as P_{CO_2} , which further effects the pH of the lakewaters (Duarte *et al.*, 2008; Deocampo & Jones, 2013).

Overall, saline lakes display highly variable geochemical and hydrochemical characteristics, and the pioneering study by Hardie and Eugster (1970)

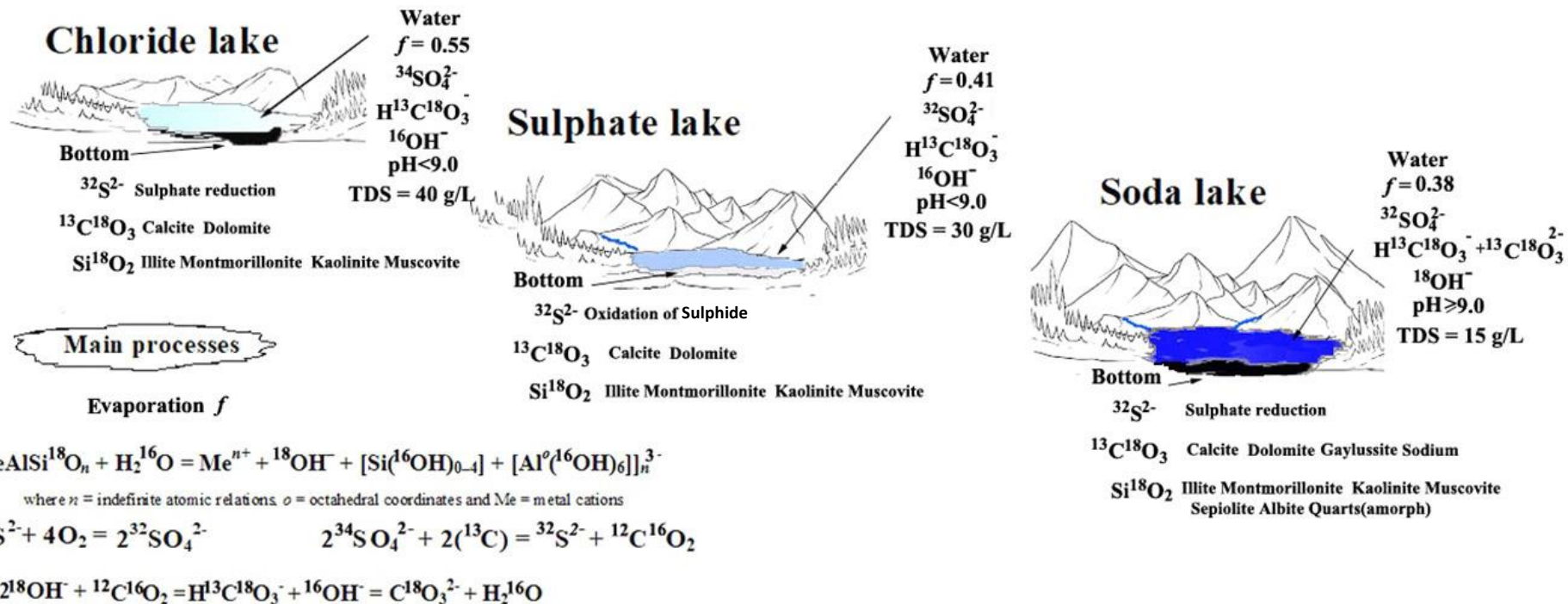


Figure 2.2 – Types of saline lakes in the case of the Transbaikalia area, Russia with controlling factors illustrated. Reproduced from Borzenko (2021). Copyright 2021 Elsevier. Reproduced with permission from Elsevier.

defined a spectrum of different “types” of brines associated with saline lakes that are controlled by the abundance of the different anions and cations occurring within the lake water. Such cations and anions typically include Na^+ , K^+ , Mg^{2+} , Cl^- , Ca^{2+} , SO_4^{2-} , HCO_3^- , and CO_3^{2-} , and typically, based on the study by Hardie and Eugster (1970), there are four main types of brines that can be classified according to the dominant ions. The first is a type “I” brine, which is represented by $\text{Na-CO}_3\text{-SO}_4\text{-Cl}$ (Hardie & Eugster, 1970), with key examples of such brines being identified in lakes such as Mono Lake, U.S.A (Jellison *et al.*, 1999) and Lake Magadi in Kenya (Hardie & Eugster, 1970; Eugster, 1980). The second brine type (type “II”) is composed of $\text{NaCl-Na}_2\text{SO}_4$, and has been identified in examples such as Sambhar Lake, India (Susarla *et al.*, 1991) and in the case of various brines in Saline Valley, U.S.A (Hardie, 1968; Hardie & Eugster, 1970). The third brine (type “III”) is associated with Na-Mg-Ca-Cl (Hardie & Eugster, 1970), and has recently been related to cases of subsurface brines in sedimentary basins throughout Siberia (Novikov *et al.*, 2018). Finally, the fourth brine type (type “IV”) displays major ions $\text{Na-Mg-SO}_4\text{-Cl}$ (Hardie & Eugster, 1970), with many interesting examples being identified throughout the Iberian peninsula such as in Lake Chiprana in the Ebro Basin (De Wit *et al.*, 2013). The primary control on brine genesis is postulated to be related to underlying geological factors, with most lakes forming in areas of karstic collapse and high aeolian erosion within evaporitic basins dominated by gypsum, marl and limestones (Comin & Alonso, 1988). Further evolutionary trends in brine composition, mostly between sodium-chloride and magnesium-sulphate rich, are related primarily to local geological variations and changes in the climatic regime.

Generally, many studies have stipulated that the geochemical characteristics of saline lakes are primarily controlled by inflow associated with the lake (Hardie & Eugster, 1970; Eugster & Hardie, 1978; Last & Ginn, 2005; Deocampo & Jones, 2013). It is also widely agreed that the abundance of ionic components in many saline lakes is influenced by underlying geological formations as a result of inflow delivering material from these formations to the waterbody (Last, 2002; Yechieli &

Wood, 2002; Deocampo & Jones, 2013) and from the weathering of geological bedrock (Last, 2013). In the case of many of the saline lakes of the Great Plains of Northern America for example, the effects of bedrock geology upon lakewater geochemistry has been extensively studied and summarised mostly by Last and Ginn (2005). They exhibit that many lakes distributed throughout the Eastern Prairies region have significantly lower concentrations of Na, HCO₃, CO₃ and SO₄ than those found within south-west and West-Central Saskatchewan (Last, 1989) as a result of the composition of groundwater and the degree of evaporation and precipitation.

Though such geological controls are believed to be crucial for the initial character of saline lake water chemistry (Last, 2002), one must also consider the subsequent effect of water removal by evaporation on lake chemistry (Hardie & Eugster, 1970; Hardie *et al.*, 1978). Many saline lakes are fundamentally situated in semi-arid to arid climates where evaporation often exceeds hydrological input (Lowenstein *et al.*, 1985; Brock & Hammer, 1987), and variations in evaporation intensity are known to have significant effects on the hydrochemical (Yechieli & Wood, 2002), mineralogical (Hardie & Eugster, 1970) and sedimentological (Hardie *et al.*, 1978; Valero-Garcés & Kelts, 1995) characteristics of these environments. Generally, increasing evaporation leads to increasing concentrations of the primary ionic constituents of the water (Deocampo & Jones, 2013). Thus, as defined by Hardie and Eugster (1970) and Hardie *et al.* (1978), such evaporation leads to the evolution of the brines and lakewaters such that they follow a specific path of mineral precipitation (see section 3.1.2) as dictated by the chemical composition of the initial waters.

2.3 Sedimentary Features of Saline Lakes

2.3.1 Sedimentology and Mineralogy

2.3.1.1 Facies and Depositional Features

Saline lakes often contain sedimentary sequences and modern lake-bed sediments that vary not only over significant temporal scales, but also significantly throughout the spatial domain (Banner, 1982; Last & Schweyen, 1983). There are few well-

established facies and depositional models exist for saline lakes, but a plethora of studies have nonetheless identified a spectrum of sedimentological deposits associated with these systems. Ultimately, there are a broad spectrum of processes occurring within saline lakes on various scales as defined by Hammer (1986a)(see Table 2.3), and the variable scale and intensity of such processes leads to the generation of a wide variety of depositional features associated with saline lakes.

Perhaps the most extensive studies focusing upon and reviewing the sedimentology of saline lakes were those undertaken by Hardie et al. (1978) and later Hammer (1986a). Hardie et al. (1978) discuss the key processes leading to sedimentological variability in saline lakes (i.e. biology, chemistry, and hydrology), and defined a number of key sub-environments that can typically be identified in most saline lake environments (Table 2.4). They include:

- “Alluvial fans and sandflats”, many of which have been identified in various salt lakes throughout Death Valley, USA such as those within the Pleistocene and modern sediments of the Badwater Basin (Roberts *et al.*, 1994)
- “Dry mudflats”, which they define as being adjacent to the waterbody of the lake, with intermittent wetting and drying induced by lake drawdown leading to the deposition of silts and sands. Also described are mineral crusts that are deposited during periods of drawdown and dissolved into the lakewaters during flooding (Hardie & Eugster, 1970; Hardie *et al.*, 1978). Such salt crusts are described in a vast range of recent studies, ranging from examples throughout the saline lakes of the Chilean Altiplano (Risacher *et al.*, 2003) to those of the Iberian Peninsula (Cabestrero *et al.*, 2018a).
- The ephemeral and/or perennial saline lake itself, with the extent and ephemerality of this environment being dictated by the annual fluctuations in lake water level and the subaerial water table (Wurtsbaugh *et al.*, 2017)

Table 2.3 – Table modified from Last & Schweyen (1983) and later Hammer (1986a) illustrating the key depositional processes in different types of saline lakes in the Great Plains of Canada.

Processes	All Saline Lakes	Playa and Ephemeral Saline Lakes	Perennial Saline Lakes
<i>Physical</i>	Evaporative concentration Groundwater discharge into basin	Surface flooding and desiccation Evaporative pumping Aeolian transport, setup and deflation Freezing and thawing	Stratification/destratification of the water column Shoreline processes Turbidity flow Flocculation of fine-grained material Wind and sheetflow transport
		Precipitation of soluble salts and minerals Formation of salt crystal rafts Formation of salt spring deposits Intra-sedimentary growth of salt crystals Cyclic precipitation and dissolution Freeze-out precipitation Clay mineral authigenesis	Subaqueous precipitation and dissolution of salts Freeze-out precipitation
<i>Biological</i>	Photosynthesis Respiration Decomposition and biochemical alteration Perturbation by fauna		Production Decomposition and biochemical alteration

Table 2.4 – Summarised depositional sub-environments and features from the review undertaken by Hardie *et al.* (1978).

Depositional Subenvironment	Facies and Depositional Features	Associated Structures
<i>Alluvial Fan</i>	Gravelly wedges Braid channel deposits - coarse gravel bars with coarse sand and gravel Incised channel fills - narrow gravelly lenses Sieve deposits - Well sorted gravels Debris flows - Poorly sorted sandy deposits with varying amounts of mud Caliche formed by groundwater pumping	Massive Imbrication, planar horizontal lamination Fining upwards Sorting of gravels and pebbles Massive and potentially waning upwards Pore cements
<i>Sandflat</i>	Planar and wavy laminated sands Caliche formed by groundwater pumping	Planar lamination, ripples, dunes, cut-and-fill structures Pore cements, gypsum dehydration to anhydrite
<i>Dry Mudflat</i>	Polygonal mudcracks Thin saline crusts Sand patches	Irregular to wavy mudcracks, desiccation cracks Varying thickness, composition, laminae disruption Wind ripples, sand rills
<i>Ephemeral Saline Lake</i>	Thin beds of mudstone from suspension settling Microbial mats Chemical deposits	Lamination, varying thickness, rippling and microbial mats, mudcracking at exposed margins Laminae, organic matter Lamination, coupling with mud laminae
<i>Perennial Saline Lake</i>	Chemical deposits Microbial mats Massive to laminated mudstones and claystones	Lamination, highly variable composition, layer couplets, diagenetic recrystallisation Laminae, organic matter Lamination, grain size variations

<i>Windblown Dune Field</i>	Dunefield deposits, dune sand, aeolian sediments	Deflation pavements, caliche
<i>Perennial Stream Floodplain</i>	Meander and braid deposits	Planar lamination, cross-bedding
	Point-bar, scroll-bar, levee, crevasse-splay, flood-basin, ox-bow lake, braid-bar/channel deposits	Subaerial caliche and silcrete, flow structures and lamination
<i>Ephemeral Stream Floodplain</i>	Braid channel deposits and coarse braid bar deposits	Grain size fluctuations, planar lamination, wavy antidune bedding, megaripples, mudcracks, clay drapes, scour-and-fill
	Channel-fill conglomerates	Inclined bedding and lamination
	Trough cross-bedded and planar sands and gravels	Cross-bedding, lamination
	Fine grained laminated sand	Planar and wavy lamination, ripples
<i>Springs and spring-fed ponds</i>	Tufa and travertine deposits	Mound structures, coated grains, diagenetic cements, chemical laminae, fenestral fabrics
	Vegetative deposits and organic-rich layers	Laminae, organic matter, fossils
<i>Shoreline Features</i>	Spits, longshore bars, beaches and beach ridges	-
	Deltaic deposits	-
	Algal mounds and ooid sand shoals	-

Altogether, this study effectively and concisely reviews the key deposits and facies associated with many saline lakes, and many works following it have adopted a similar approach to characterising and classifying saline lake deposits.

Valero-Garcés and Kelts (1995) have generated a more in-depth model for the case of perennial, meromictic saline lakes (Figure 2.3). Key facies and depositional features defined in this work included “clastic littoral deposits, spring deposits, microbial mats, bench slope deposits, and pelagial clastic, chemical and organic deposits”. Broadly, they define such facies according to their primary lithology and structures, firstly describing coarse clastic facies, consisting of gravels, bioclastic and clastic sands, and silts to be associated with the littoral and shoreline setting from suspension settling, wave-reworking and storm events (Valero-Garcés & Kelts, 1995). In contrast, they determine muddy facies consisting of grey and intercalated muds with varying amounts of organic matter to be associated with the pelagial setting as a result of suspension settling. Thirdly, they indicate that precipitated facies such as aragonite and gypsum result from mineralisation within the water column, while travertine and concretionary gypsum are related to springs and reworked material delivered to the lake (Valero-Garcés & Kelts, 1995). Finally, organic facies including microbial mats and sapropelic muds are associated with pelagial deposition and settling of organic matter in this setting (Valero-Garcés & Kelts, 1995). Though this study describes in detail the characteristics of various saline lake deposits, they are in this case attributable primarily to examples of perennial, meromictic lakes as Medicine Lake is described as, and the true facies variability of many lacustrine systems is likely much more complex than one such example.

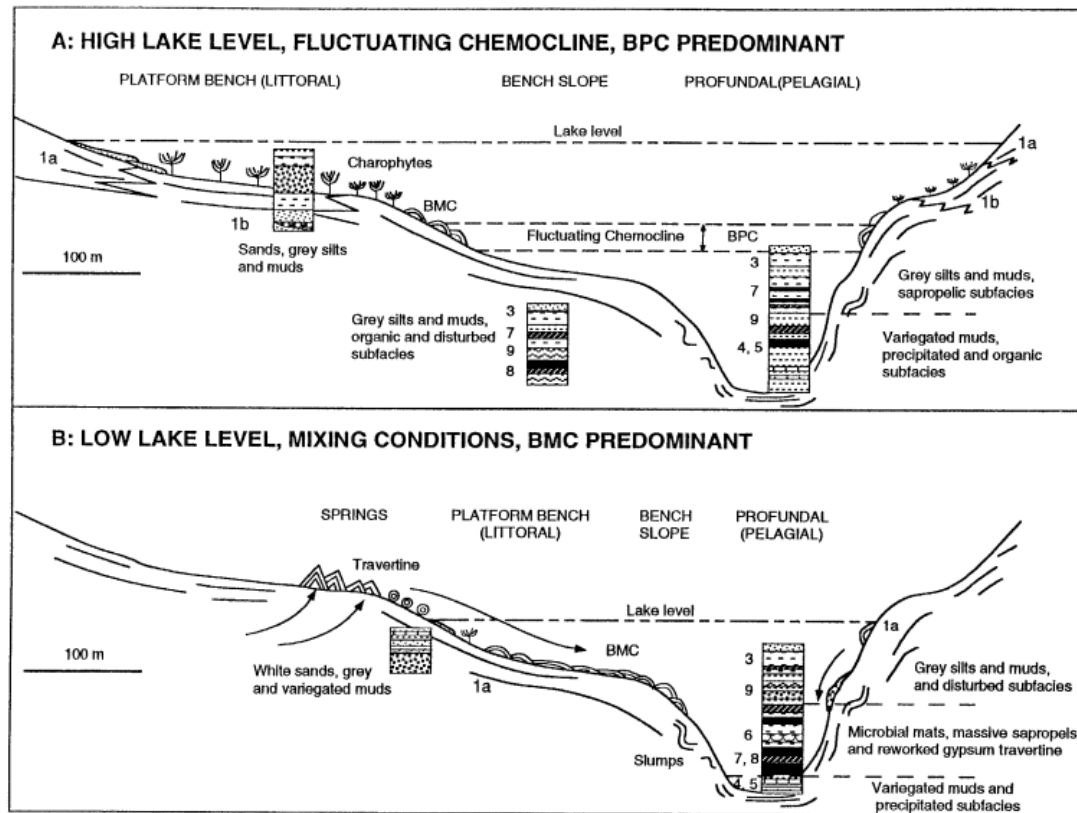


Figure 2.3 – Facies model generated by Valero-Garcés & Kelts (1995) for the case of Medicine Lake, Canada in application to the characterisation of perennial, meromictic saline lakes. Copyright 1995 Springer Nature, reproduced with permission of Springer Nature.

2.3.1.2 Mineral Phases

In addition to the range of facies and depositional characteristics associated with saline lakes, their mineralogy can also be highly variable. Table 2.5, modified from Deocampo and Jones (2013), describes the key mineralogical phases associated with many saline lakes that can precipitate throughout the lake (Hardie & Eugster, 1970). However, one must also consider that many mineral phases within saline lakes can also be derived from inflow to the lake (Last, 2002, 2013)(e.g. quartz, phyllosilicates, and other clay minerals), and that there are often diagenetic factors to consider (Yechieli & Ronen, 1997) which may further alter mineral phases associated with the lake (Mees *et al.*, 2011; Last, 2013). Typical phases associated with many saline lakes include a wide range of carbonates, calcium and magnesium sulphates, halides, and fluorides (Table 2.5)(Deocampo & Jones, 2013; Last, 2013). The brine types defined by Hardie & Eugster (1970) are an effective insight into the potential phases that will precipitate with increasing evaporative concentration and evolution of the lakewaters/brine, and the likely precipitation pathways that will be followed as a result of this increasing concentration (Deocampo & Jones, 2013) (Figure 2.4). Thus, with increasing evaporation and the precipitation of a defined assemblage of endogenic minerals, many studies typically postulate that the minerals identified in saline lake sediments can be used as an indicator of the degree of evaporation and subsequently the palaeosalinity of the lake throughout geological time (Hardie & Eugster, 1970; Last, 2002, 2013; McHenry *et al.*, 2020) The broad spectrum of mineral phases associated with saline lakes and saline lake sediments are thus widely acknowledged to represent a critical component in understanding the geochemistry and palaeoenvironmental changes associated with such systems (McHenry *et al.*, 2020).

Table 2.5 – Key minerals and phases associated with saline lakes. Adapted from Deocampo & Jones (2013). Copyright Elsevier 2014. Reproduced with permission of Elsevier.

Group	Phase	Formula	
Carbonates	Calcite	CaCO ₃	
	Aragonite	CaCO ₃	
	Dolomite	CaMg(CO ₃) ₂	
	Huntite	CaMg ₃ (CO ₃) ₄	
	Magnesite	MgCO ₃	
	Hydromagnesite	4(MgCO ₃)•Mg(OH) ₂ •4H ₂ O	
	Nesquehonite	MgCO ₃ •3H ₂ O	
	Pirssonite	CaCO ₃ •Na ₂ CO ₃ •2H ₂ O	
	Gaylussite	CaCO ₃ •Na ₂ CO ₃ •5H ₂ O	
	Trona	Na ₃ H(CO ₃) ₂ •2H ₂ O	
	Thermonatrite	Na ₂ CO ₃ •H ₂ O	
	Nahcolite	NaHCO ₃	
	Natron	Na ₂ CO ₃ •10H ₂ O	
	Sulphates	Gypsum	CaSO ₄ •2H ₂ O
		Anhydrite	CaSO ₄
Mirabilite		Na ₂ SO ₄ •10H ₂ O	
Thenardite		Na ₂ SO ₄	
Epsomite		MgSO ₄ •7H ₂ O	
Hexahydrate		MgSO ₄ •6H ₂ O	
Starkeyite		MgSO ₄ •4H ₂ O	
Kieserite		MgSO ₄ •H ₂ O	
Bloedite		Na ₂ Mg(SO ₄) ₂ •4H ₂ O	
Glauberite		Na ₂ SO ₄ •CaSO ₄	
Kainite		KCl•MgSO ₄ •3H ₂ O	
Schoenite		K ₂ SO ₄ •MgSO ₄ •6H ₂ O	
Leonite		K ₂ SO ₄ •MgSO ₄ •4H ₂ O	
Polyhalite		K ₂ SO ₄ •MgSO ₄ •2CaSO ₄ •2H ₂ O	
Burkeite		Na ₆ (SO ₄) ₂ CO ₃	
Chlorides	Halite	NaCl	
	Hydrohalite	NaCl•2H ₂ O	
	Sylvite	KCl	
	Antarctite	CaCl ₂ •6H ₂ O	
	Bischofite	MgCl ₂ •6H ₂ O	
	Tachyhydrite	CaMg ₂ Cl ₆ •12H ₂ O	
	Carnallite	KCl•MgCl ₂ •6H ₂ O	

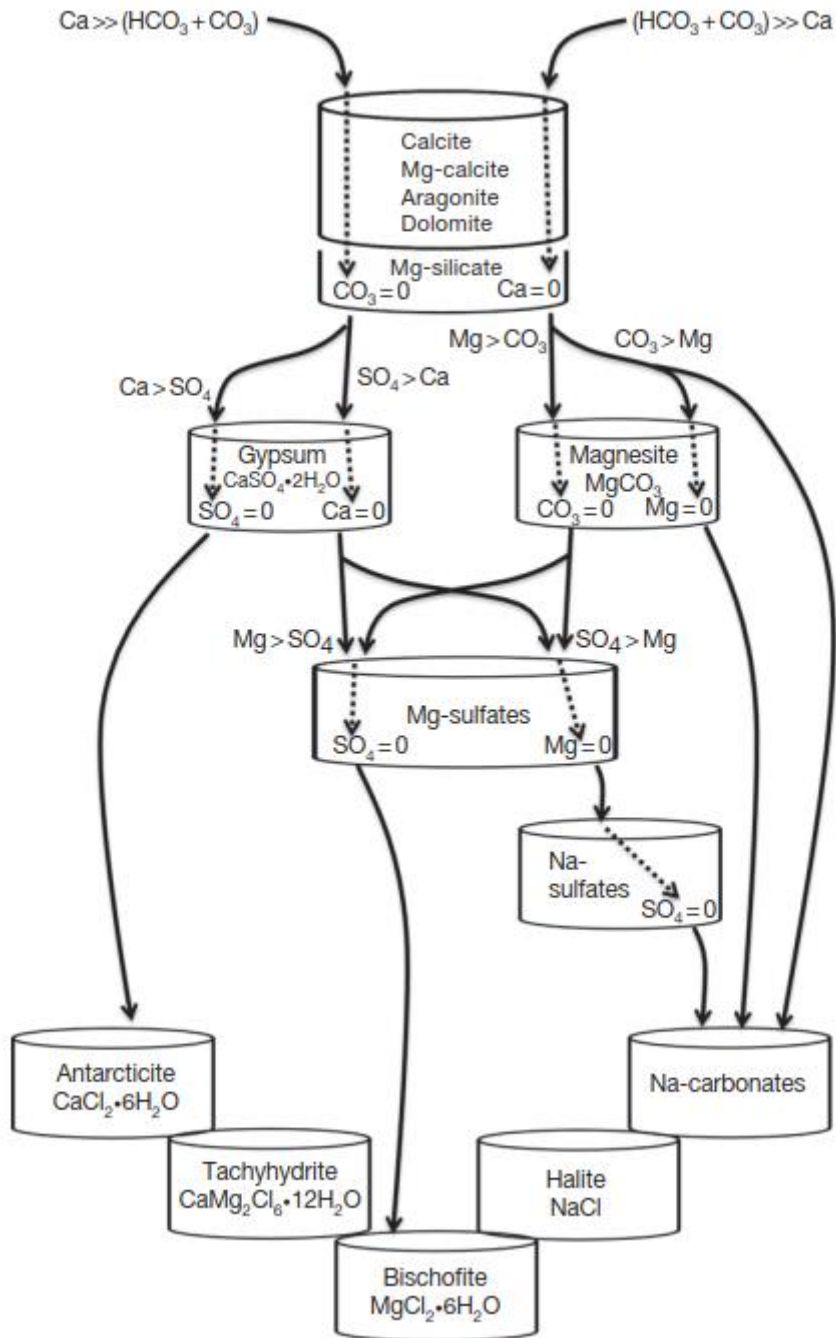


Figure 2.4 – Flow chart from Deocampo & Jones (2013) illustrating mineral precipitation pathways within closed-basin brines as a result of increasing evaporative concentration. Copyright Elsevier 2014. Reproduced with permission of Elsevier.

2.3.2 Relating Sedimentary Features to Environmental Processes and Application as Palaeoenvironmental Archives

The wide range of facies and minerals associated with saline lakes are indicative of an equally wide spectrum of environmental processes occurring within such systems (Hardie *et al.*, 1978). In the past, saline lakes were often overlooked as potential palaeoenvironmental archives due to the high variability associated with these systems (Last, 2013), particularly in the case of highly ephemeral saline lakes (Last & Schweyen, 1983) where erosive conditions may have been extensive in negating sediment deposition. In more recent years, increasing numbers of studies are emerging which have begun to exhibit the effectiveness of these systems as valid and reliable archives of environmental information. According to Hardie *et al.* (1978), shifts in facies and sedimentary structures are critical for understanding variations in lake levels and depositional subenvironments (Valero-Garcés & Kelts, 1995), mineralogical fluctuations can give insights into sediment sources (McHenry *et al.*, 2020) and hydrologic conditions (Pienitz *et al.*, 2000), while changes in biological communities including diatoms, chironomids and ostracods can indicate changes in lakewater chemistry and salinity (Evans, 1993).

It is widely agreed that alongside such records, saline lakes are also exceptional palaeolimnological repositories as they are often sensitive to both environmental and anthropogenic changes (Brock & Hammer, 1987; Evans, 1993; Deocampo & Jones, 2013; Last, 2013). Thus, while classic sedimentological, geochemical and biological analyses are now being widely undertaken in a range of saline lake sediments around the globe (Pienitz *et al.*, 2000; Schröder *et al.*, 2018), there are also emerging techniques being applied which complement such analyses in the high-resolution characterisation of these settings. For example, techniques involving the use of isotopes of hydration water of minerals such as gypsum, though long established (Sofer, 1978), have been recently applied to saline lake sequences to determine past variations in climatic factors (Gázquez *et al.*, 2015, 2017). For example, in the case

of Lago de Estanya in the Benabarre region of Northeast Spain, Gázquez *et al.* (2018) define triple oxygen isotopes for gypsum hydration water throughout the sedimentary sequence in order to resolve palaeo-humidity changes occurring in the region.

Overall, saline lake sediments are becoming increasingly recognised as reliable archives of palaeoenvironmental information (Last, 2002), especially in areas where other environmental and climatic records may be rare, such as throughout the Ebro Basin of Northeastern Spain (Hammer, 1986; Alonso, 1998). The characteristics of saline lake deposits ultimately reflect a complex interplay of geochemical, biological and physical processes (Hardie *et al.*, 1978), and many studies now adopt a multi-faceted and multi-proxy approach to unravel the environmental information contained within these unique depositional settings. Specifically, there are several well-known sedimentological facies and models associated with saline lakes that are linked directly or postulated to be related to specific controls. For example, variations in mineralogy and the interlamination of various minerals and other detritus is often directly linked to the degree of evaporation from the lake and/or the delivery of detrital input, while the onset of the development of unique facies such as microbial mats is linked to a complex set of biotic factors and ultimately harsh environmental conditions that allow for the mats to develop (typically in the form of heightened salinities). Elsewhere, other studies have linked erosive tabular beds with cross-stratification to flooding events and channelised geobodies present within saline lakes, while mudstone beds with lensoidal sands and efflorescent salt crusts to sediment trapping and salt dissolution occurring within saline mudflats adjacent to the lake (Simplicio *et al.*, 2017). Within saline lakes themselves, studies such as those by Benison *et al.* (2007) have postulated that varying grain sizes of detrital facies can be closely linked to the intensity of flood events, while drawdown and concentration by evaporation of the lakewaters leads to precipitation of minerals such as kaolinite where aluminium concentrations are particularly high. Finally, a more recent study by Semmani *et al.* (2022) has shown that cyclical development of

facies such as oolitic grainstones, mollusc packstones and laminated bindstones and gypsum-psuedomorphed limestone are hypothesised to be linked to transgressive and regressive cycles occurring throughout carbonate-rich saline lake environments as modelled after a succession from Butte louton. Overall, the development of new facies models and linkage of processes to rock record will allow for deeper insights into the complexity of these unique systems in the near future.

2.4 Microbial Mats – Processes and Controls

2.4.1 Concepts & Significance of Microbial Mats and Minerals

Relationships between microbes and the geosphere have been recognised since the advent of the first pioneering studies in the fields of biogeochemistry and geomicrobiology (Beerstecher, 1954). Since then, the phrase “microbe-mineral interactions” has been adapted to apply to a wide range of microbial processes that are related to mineral formation, dissolution and alteration (Dupraz *et al.*, 2004). Despite this, different microbe-mineral interactions have received varying amounts of attention, and different microbes are known to be capable of the production a spectrum of mineralogical products (Riding, 2011a). General evaluation of the literature body and recent reviews by Dong (2010) and Vaughan and Lloyd (2011) indicate for example that processes of carbonate precipitation and the products of different microbe-mineral interactions are becoming increasingly understood due to a multitude of both lab and field-based studies. In contrast, topics such as the microbial dissolution and diagenesis of and the effects of variable environmental controls on the physicochemical nature of microbial mats are generally less well understood (Bouton *et al.*, 2016). Nevertheless, many pioneering studies are emerging (Dasgupta *et al.*, 2021) that are correcting this imbalance and placing new focus upon the various roles microbes play in the role of mineral cycling, and broadly, a number of fundamental terms and concepts have emerged throughout the literature that are now applied in many such studies.

2.4.1.1 Biominerals & Organominerals

The terms “biomineral” and “organomineral” are fundamental nomenclature for many studies focusing upon microbe-mineral interactions, and have been discussed in a review by Dupraz *et al.* (2009)(Figure 2.5). Broadly, there are three processes that are known to promote the formation of biominerals and organominerals: biologically-controlled mineralisation, biologically-induced mineralisation, and biologically-influenced mineralisation (Dupraz *et al.*, 2009; Eymard *et al.*, 2020). Biologically-controlled mineralisation, according to Mann (2001) is a process recognised to involve a significant biological control (e.g. within shells) on the mineral products produced, with microbes using specific elements to produce the phase in question (Weiner & Addadi, 2011). In contrast, according to Dupraz *et al.* (2009), processes of biologically-induced and -influenced mineralisation do not involve such strict biological control. Biologically-induced mineralisation is stipulated by Dupraz *et al.* (2009) to occur as a result of organisms producing the conditions required for minerals to form within an environment. Finally, biologically-influenced mineralisation, as also first proposed also by Dupraz *et al.* (2009), represents a process that they stipulate in which changes in physicochemical variables induce the mineralisation of organic matrices produced by microbes. However, influence by microbes can also involve dissolution in many cases, as is discussed later in the chapter.

These processes are broadly considered by most studies to be the primary components of biomineralisation and organomineralisation (Dupraz *et al.*, 2009). In the study by Mann (2001), it was suggested that the term biomineralisation should include processes of biologically-controlled and biologically-influenced mineralisation. New terminology was recommended by Perry *et al.* (2007), who suggested that the nomenclature of “organomineral” should be used to refer to minerals produced without any clear evidence of “direct biological controls on mineral precipitation”. This process of organomineralisation has been suggested to involve the passive mineralisation of organic matter and substances (Perry *et al.*,

2007; Dupraz *et al.*, 2009) (such as the EPS matrix, see below) without any direct or indirect microbial intervention (Dupraz *et al.*, 2009), with this organic matter influencing the character of the phases that are produced (Trichet & Défarge, 1995).

2.4.1.2 Extracellular Polymeric Substances

Extracellular polymeric substances, typically abbreviated to EPS or the EPS matrix, are often recognised as a major part of many microbial mats (Dupraz & Visscher, 2005; Gázquez *et al.*, 2018). The EPS consists of proteins, DNA, lipids and polysaccharides (Flemming & Wingender, 2010; Prieto-Barajas *et al.*, 2018). In many cases, the EPS matrix has been shown to play a major part in controlling environmental parameters such as water chemistry and temperature (Flemming *et al.*, 2007). The matrix has also been shown to allow microbes to obtain nutrients from their environment and substrate as stated by Flemming & Wingender (2010). Finally, the EPS matrix has also been deemed a potential energy source for different functional groups of microbes which may degrade it to fuel their metabolism according to Dupraz *et al.* (2004). Overall, the EPS matrix has been increasingly shown in recent years to play a major role in microbe-mineral interactions.

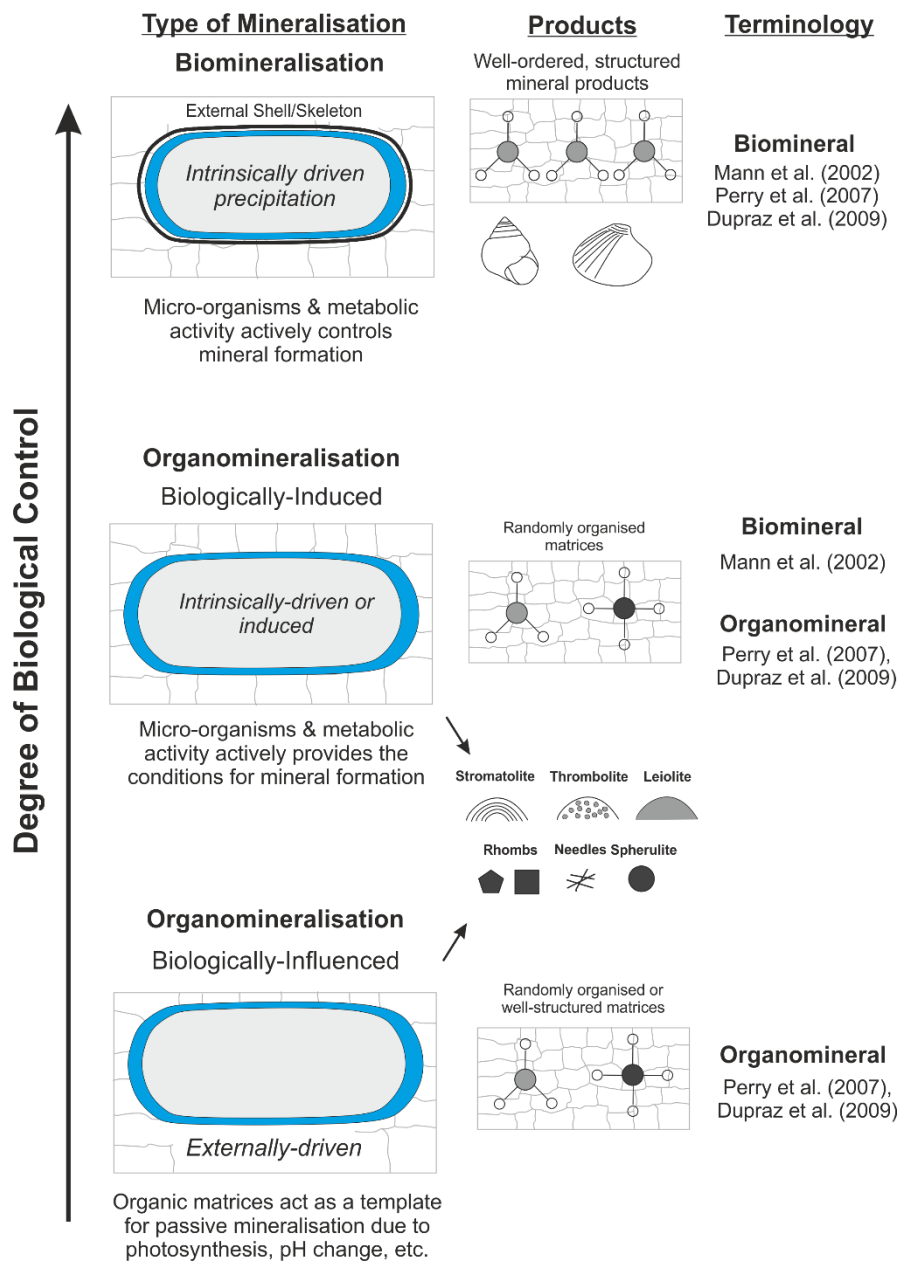


Figure 2.5 - Processes of biomineral and organomineral formation. Modified after Dupraz *et al.* (2009). Copyright Elsevier 2009. Reproduced with permission of Elsevier.

2.4.1.3 Microbialites

Perhaps some of the earliest and most fundamental nomenclature regarding microbial deposits is the term “microbialite” as introduced by Burne and Moore (1987) to characterise “organosedimentary deposits that have accreted as a result of a benthic microbial community trapping and binding detrital sediment and/or forming the locus of mineral precipitation”. Though the term microbialite has often been applied to many structures with layered, clotted and potential skeletal fabrics (Riding, 2011a) (Figure 2.6), the biogenicity of such deposits as initially proposed by Kalkowsky (1908) is not always clear and is highly debated in the literature. No unified agreement is present with regards to microbialite development and evolution (Awramik & Grey, 2005; Hickman-Lewis *et al.*, 2019), and there is no feature that has been uniformly attributed to biogenic processes associated with potential microbial structures. Though some specific microfabrics and textures have been attributed to biogenic processes (Riding, 2011b; a) it is widely known that non-biological processes can also affect microbialite characteristics (Sumner, 2000; Wright & Barnett, 2015; Bouton *et al.*, 2016). Overall, this represents a recurrent problem in the literature and when classifying microbialites in the geological record and will require a spectrum of work that will need to be undertaken upon an equally broad spectrum of modern and ancient microbial sediments if the issue is to be resolved (Bosak *et al.*, 2013).

2.4.2 Structure of Microbial Mats and Biofilms

Microbial ecosystems consist of various groups of microbes distributed within the EPS matrix (Bolhuis *et al.*, 2014; Prieto-Barajas *et al.*, 2018). The EPS develops into a laminated “film” consisting of microbes and other components, typically termed a biofilm (O’Toole *et al.*, 2000; Flemming & Wingender, 2010; Flemming *et al.*, 2016). It has been suggested that biofilms represent primitive microbial ecosystems (O’Toole *et al.*, 2000; De Beer & Stoodley, 2014), and it is well known that microbes can participate in the production of much

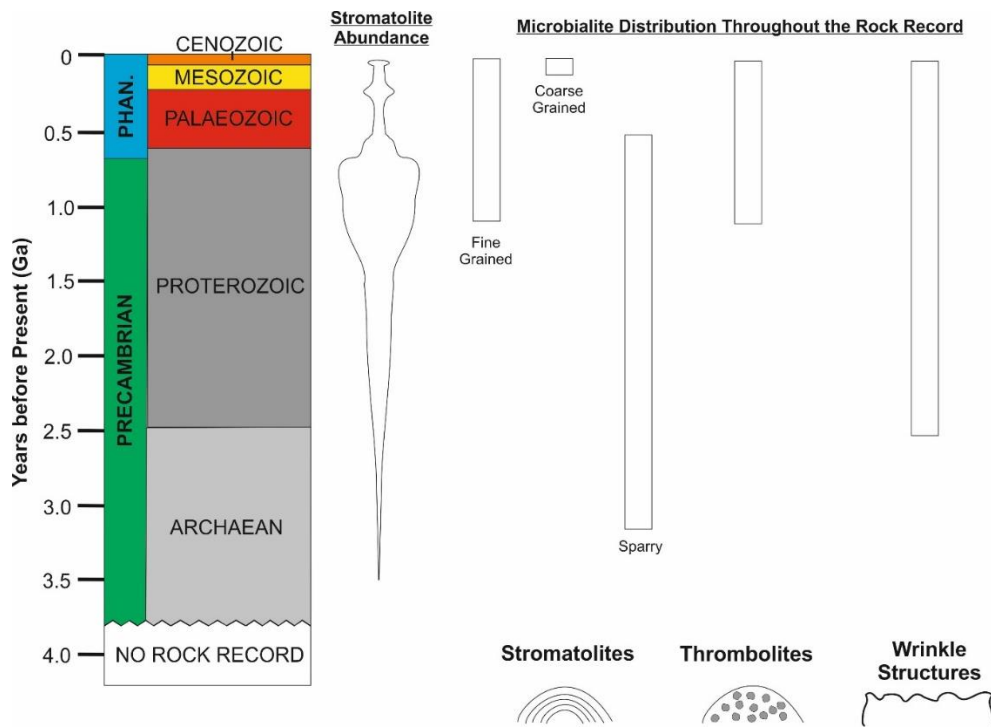


Figure 2.6 – Diagram exhibiting types of microbialites commonly found in the geological record. Stromatolites have been identified in many different studies with variable morphological habits, grain sizes and components (Riding, 2011a). Thrombolites or microbial sediments with clotted and often peloidal microfabrics have generally only been identified occurring up to ~1Ga (Riding, 2000). Wrinkle structures are described as mm-cm scale ridges or pits common sediments fossiliferous sediments, and have been more recently reviewed in detail by Mariotti et al (2014). Partially modified from Condie & Sloan (1997).

more complex structures. Though subject to a wide range of definitions, they are perhaps best defined by Cohen (1989) as “stratified microbial communities that develop in the environmental micro-gradients established at the interfaces of water and solid substrates, forming a laminated multilayer of biofilms that can alter the environmental micro-gradients in this interface as a result of their own communal metabolism”.

2.4.2.1 Microbial Mats - Structure & Processes

Microbial mats are known to contain a wide variety of groups of biological communities (Franks & Stolz, 2009; Prieto-Barajas *et al.*, 2018). Typically, groups of microbes with specific biological activities are termed “functional groups”, and occur in distinct laminae throughout a mat (Figure 2.7) (Baker & Banfield, 2003; Franks & Stolz, 2009; Prieto-Barajas *et al.*, 2018). In most microbial mats, typical groups of microbes include oxygenic cyanobacteria, aerobic heterotrophic bacteria, sulphate-reducing bacteria and sulphide-oxidising bacteria (van Gemerden, 1993; Visscher & Stolz, 2005; Prieto-Barajas *et al.*, 2018). In some cases however, other groups of micro-organisms such as methanogenic, non-sulphur and nitrifying bacteria have also been shown to be present (Orphan *et al.*, 2008). As a result, a wide spectrum of processes occur in many microbial mats such as photosynthesis, sulphate reduction and sulphide oxidation and methanogenesis. (Bolhuis *et al.*, 2014; Prieto-Barajas *et al.*, 2018).

Table 2.6 and Figure 2.7 depict several common processes that occur in a typical microbial mat (Visscher & Stolz, 2005; Prieto-Barajas *et al.*, 2018). Broadly, oxygenic cyanobacteria and anoxygenic phototrophs are known to use light as an energy source and utilise inorganic sources of carbon (Canfield & Des Marais, 1993; Prieto-Barajas *et al.*, 2018). Sulphate-reducing and sulphide oxidising bacteria respectively reduce sulphate or oxidise sulphide (Pfennig & Widdel, 1982; Barton & Hamilton, 2007). Aerobic and anaerobic heterotrophs derive their energy from carbon oxidation via respiration (Visscher & Stolz, 2005). Nitrogen fixing bacteria acquire energy by

fixing atmospheric dinitrogen (Severin *et al.*, 2010). Altogether, it is generally well understood that many microbial functional groups are associated with particular roles and vertical hierarchies within microbial mats (Visscher & Stolz, 2005; Prieto-Barajas *et al.*, 2018)(Figure 2.7).

The behaviour of different functional groups of microbes has also been recognised to vary dramatically between different microbial mats (Prieto-Barajas *et al.*, 2018). For example, Frund and Cohen (1992) and Visscher *et al.* (1992) identified populations of sulphate-reducing bacteria at the surface of mats as opposed to photoautotrophic cyanobacteria, and a study by Hoehler *et al.* (2002) illustrated that methanogenesis peaked at the surface of a microbial mat. Other studies concerning sulphate-reducing bacteria also illustrated that oxic environments are largely inhibitive to the growth of these bacteria (Krekeler *et al.*, 1998), but more recent works have illustrated the survival of sulphate-reducing bacteria in oxic conditions. In a study by Dolla *et al.* (2006) for example, it was illustrated that sulphate reducing bacteria had developed enzymatic systems for the elimination of oxygen in order to survive. Ultimately, examples of such discoveries bear great significance for understanding microbial mats. Functional groups of microbes interact with mineral products and environmental settings in a variety of manners (Dupraz *et al.*, 2009; Valdespino-Castillo *et al.*, 2018), and as such a broad variety of products, processes and diagenetic pathways have been identified and are currently still being investigated (Dupraz *et al.*, 2011).

Table 2.6 – Common functional groups of microbes occurring within microbial mats, their metabolism and the common reactions they undertake. Reproduced from Visscher & Stolz (2005). Copyright Elsevier 2005. Reproduced with permission of Elsevier.

Functional group	Daytime metabolic function	Nighttime metabolic function
Cyanobacteria	Carbon fixation (photosynthesis): $\text{CO}_2 + \text{H}_2\text{O} \rightarrow \text{CH}_2\text{O} + \text{O}_2$	Fermentation (including H_2 production), N_2 fixation, glycogen degradation
Aerobic heterotrophs	Carbon oxidation (respiration): $\text{CH}_2\text{O} + \text{O}_2 \rightarrow \text{CO}_2 + \text{H}_2\text{O}$	Fermentation, denitrification: $5\text{CH}_2\text{O} + 2\text{H}_2\text{O} \rightarrow \text{HCO}_3^- + \text{H}^+ + 4\text{CH}_3\text{O}$ and $5\text{CH}_2\text{O} + 4\text{NO}_3^- \rightarrow 5\text{HCO}_3^- + \text{H}^+ + 2\text{N}_2 + \text{H}_2\text{O}$
Sulfide oxidizers	Sulfide oxidation: $\text{H}_2\text{S} + 2\text{O}_2 \rightarrow \text{SO}_4^{2-} + 2\text{H}^+$ (sometimes coupled to carbon fixation)	Denitrification, fermentation: $5\text{HS}^- + 8\text{NO}_3^- \rightarrow 5\text{SO}_4^{2-} + 4\text{N}_2 + \text{H}_2\text{O} + 3\text{OH}^-$
Phototrophic sulfide oxidizers	Carbon fixation (anoxygenic photosynthesis coupled to sulfide oxidation): $2\text{CO}_2 + \text{H}_2\text{S} + 2\text{H}_2\text{O} \rightarrow 2\text{CH}_2\text{O} + \text{SO}_4^{2-} + 2\text{H}^+$	Fermentation, synthesis of Bchl <i>a</i> , degradation of glycogen
Anaerobic heterotrophs-sulfate reducers	Carbon oxidation (sulfate respiration): $2\text{CH}_2\text{O} + \text{SO}_4^{2-} \rightarrow 2\text{HCO}_3^- + 2\text{H}_2\text{S}$	Same as daytime
Anaerobic heterotrophs-methanogens	Carbonate respiration: $4\text{H}_2 + \text{CO}_2 \rightarrow \text{CH}_4 + 2\text{H}_2\text{O}$ and $2\text{CH}_2\text{O} \rightarrow \text{CH}_4 + \text{CO}_2$	Same as daytime

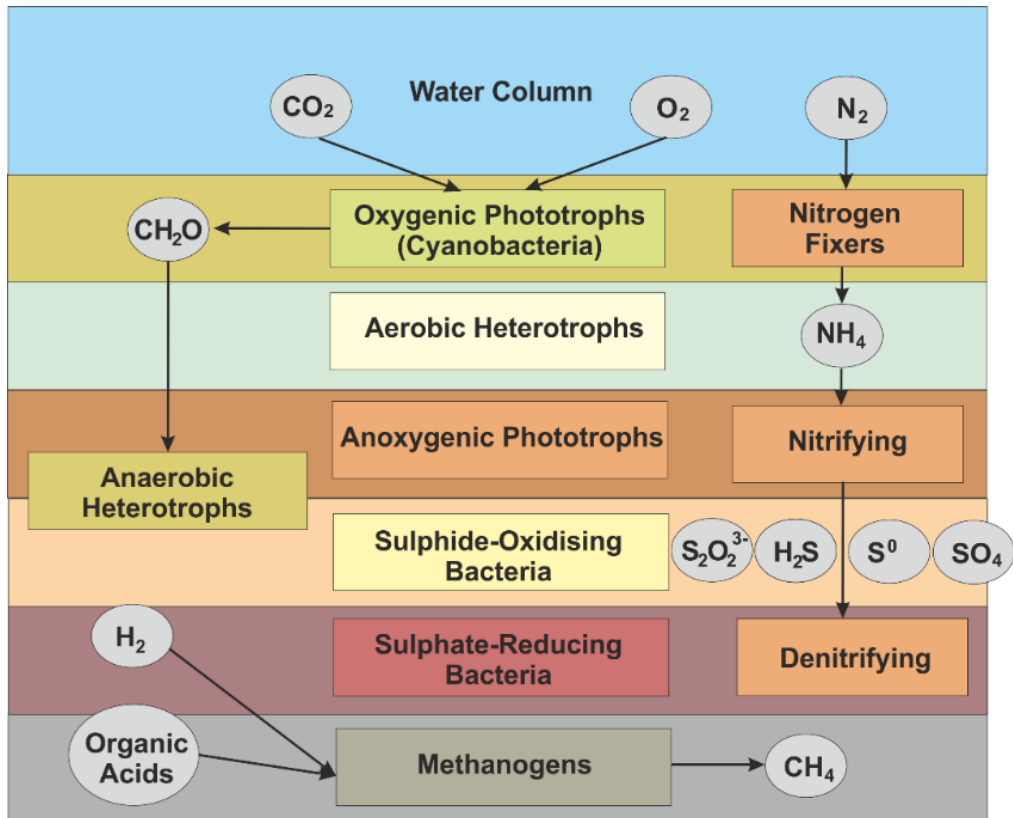


Figure 2.7 - Diagram illustrating common functional groups of micro-organisms occurring within microbial mats and the biological processes they undertake. After Prieto-Barajas *et al.* (2018). Copyright Elsevier 2018. Republished with permission of Elsevier, Creative Commons License.

2.4.3 Products of Microbe-Mineral Interactions

Perhaps the most widely recognised microbialites are the layered stromatolites, but as shown in Figure 2.8 below, there can be a significant amount of variation in the morphological and petrographic properties of all types of microbialites (Riding, 2011a). A wide range of definitions have subsequently emerged in the attempt to classify and categorise these deposits (Krumbein, 1983; Decho, 2000; Franks & Stolz, 2009). However, it must be made apparent that microbial mats are inherently recognised as complex ecosystems (Visscher & Stolz, 2005; Dupraz *et al.*, 2009; Prieto-Barajas *et al.*, 2018), and as such can be responsible for the generation of a complex range of sedimentological products (Moore & Burne, 1987).

2.4.3.1 Key Components of Microbial Sediments

Microbial mats and microbialites are broadly recognised to consist of several distinctive components, textures and fabrics (Gerdes *et al.*, 2000; Riding, 2011a). Reviews by Burne and Moore (1987) and Riding (2000) have discussed in detail the key constituents of these deposits, and have also attempted to introduce a standard classification, but this has proved difficult due to the complex controls acting on many of these deposits. Primary structural characteristics of many microbialites are shown in Figure 2.9. These components, as described by Riding (2000), include micrite, microspar and spar cements, allochthonous grains, trapped and bound material and pore space. Riding (2000) suggested that dense micrite, clotted fabrics, calcified cyanobacterial sheaths and peloids represent the primary micritic components, while microspar and spar tend to occur within cyanobacterial sheaths or as interstitial cements (Riding, 2000, 2011a; Guido *et al.*, 2022). Allochthonous trapped and bound grains are also recognised as a key component of many microbial deposits, and represent detrital material that is trapped in the EPS compounds of the mat (Riding, 2000, 2011a; Suarez-Gonzalez *et al.*, 2019). The occurrence of microbialites throughout the geological record is however extensive (Awramik, 1992; Riding, 2011a), and as such many microbialites display varying abundances of these components with distinctive morphology and chemical characteristics. Detailed

studies of the macro-, meso- and micro-structures of these deposits will undoubtedly allow for the development of a reliable categorisation of these deposits.

2.4.3.2 Types of Microbialites

Microbialites are generally divided into several types: stromatolites with a laminated fabric (Dupraz and Visscher, 2005; Riding, 2007), thrombolites with a clotted fabric (Shapiro, 2000; Mobberley *et al.*, 2013) and leiolites with a structureless or massive fabric (Riding, 1999; MEI, 2007). Though each of these microbialite types displays distinct characteristics, there are a wide variety of morphological sub-types that can also be (Figure 2.9). This has already been reviewed in detail by Riding (1991a, 2000) and more recently by Chen & Lee (2014). The key morphological types will be briefly discussed and complemented with new findings concerning the classification of these unique deposits.

2.4.3.2.1 Stromatolites

Stromatolites were first widely discussed by Kalkowsky (1908), and they are broadly defined as laminated microbial deposits exhibiting domal and columnal morphologies (Riding, 1999). Despite this, Awramik & Grey (2005) state that accurately defining biogenicity in many stromatolites is often difficult or obscured due to diagenesis, as well as the processes contributing to the generation of both biotic and abiotic laminated structures (Grotzinger & Rothman, 1996). Nonetheless, a spectrum of different varieties of stromatolites have been identified in a broad spectrum of works. As summarised by Riding (2000), examples include skeletal varieties consisting of calcified microbes (Wendt, 1993), agglutinated varieties consisting of bound particulate sediment (Tosti & Riding, 2017), and even freshwater tufa stromatolites (Edwards *et al.*, 2017). A review by Bosak *et al.* (2013) has stromatolite deposits in detail, including current knowledge of their growth mechanisms, biogenicity, and their occurrence throughout the geological record. From this review and many studies concerning stromatolites, it is apparent there are still many questions concerning these structures, such as their response to

environmental change, their morphological development, and their relationships to modern microbial mats.

2.4.3.2.2 Thrombolites

Thrombolites, initially defined by Aitken (1967), display typically clotted internal fabrics throughout their structure (Riding, 2011a). The construction of microbial frameworks which undergo repeated erosion and diagenesis are believed to be the primary processes responsible for thrombolite generation (Bosence & Gallois, 2022), and there are a number of varieties that have been identified. These include, according to Riding (2000, 2011a) calcified thrombolites consisting of calcified microbes, agglutinated thrombolites consisting of oolitic and bioclastic sediment, tufa thrombolites, and post-depositional thrombolites. There are also several experimental approaches which have been undertaken to understanding thrombolite genesis, mineralogy and development, with a study by Mobberley *et al.* (2015) providing insights into spatial variations in metabolic activity which may have led to the clotted textures associated with thrombolites.

2.4.3.2.3 Dendrolites & Leiolites

Dendrolites and leiolites represent two types of microbialites that have received much less attention in comparison to the stromatolites and thrombolites (Riding, 2011a). Both have been described in detail by (Riding, 1991b, 2000), but their description in the literature is scarce. Nonetheless, dendrolites are typically described as microbialites displaying branching and dendritic morphologies (Riding, 2000), and are believed to form when microbes generate a framework throughout the microbialite structures in order to form shrubs and branches (Suosaari *et al.*, 2018). On the other hand, leiolites are defined as microbialites displaying structureless macrofabrics (Riding, 2000). Like the dendrolites, these deposits are postulated by Dupraz *et al.* (2011) to be formed by accretion and calcification of bacterial colonies. Detailed investigations of these deposits will be required in order to understand how modern processes can be linked to ancient leiolites and

dendrolites and the processes responsible for their formation that occurred in the geological past.

2.4.4 - Microbial and Mineralogical Responses to Geochemical Fluctuations

Though products of microbe-mineral interactions are becoming increasingly well-defined, perhaps less well-defined are the responses of microbial mats to fluctuations in the geochemistry of the environment they are associated with (Casillas-Martinez *et al.*, 2005). This particular issue can be recognised when attempting to compare mineral products of microbes between different geochemical settings. There are no clear categorisations that aim to relate microbe-mineral interactions, biological processes and mineralogical phases associated with these mats with specific geochemical settings. Nonetheless, some emerging studies are addressing this issue which are discussed in this section.

A number of studies have indeed shown that environmental change can significantly affect microbial mats (Casillas-Martinez *et al.*, 2005; Allewalt *et al.*, 2006; Abed *et al.*, 2007; Steinman & Abbott, 2013). Environmental shifts have been shown to influence which functional groups of microbes are found in different microbial mats and thus which metabolic processes occur (Prieto-Barajas *et al.*, 2018; Reinold *et al.*, 2019). In addition, external environmental fluctuations can alter the geochemical characteristics of the setting in which mats are forming (Kelts & Talbot, 1990; Martín-Puertas *et al.*, 2011). For example, changes in the chemistry of saline lakes can induce compositional variations in mineralogical phases (Hardie & Eugster, 1970), and this can subsequently affect which minerals may precipitate within microbial mats (Casillas-Martinez *et al.*, 2005). Similarly, such studies also recognise that changing abundances of detritus within the mats can reflect varying amounts of detrital material being delivered to the system and thus being trapped within the mats (Casillas-Martinez *et al.*, 2005).

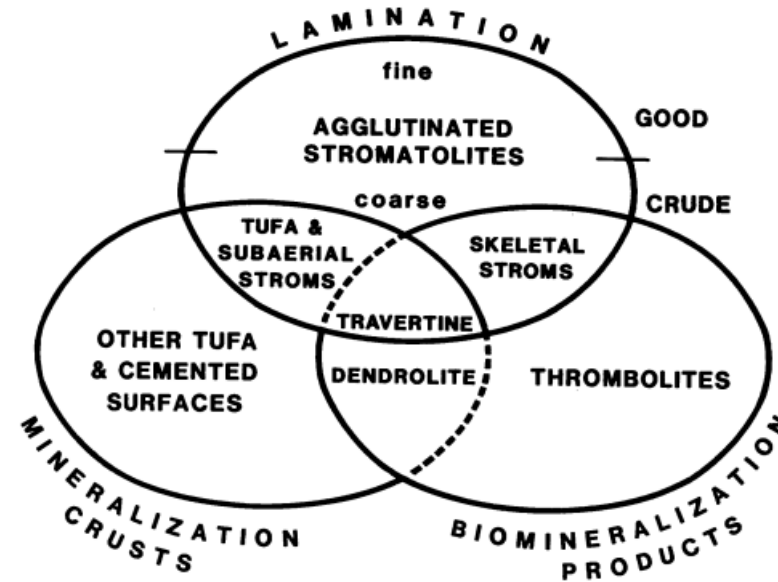
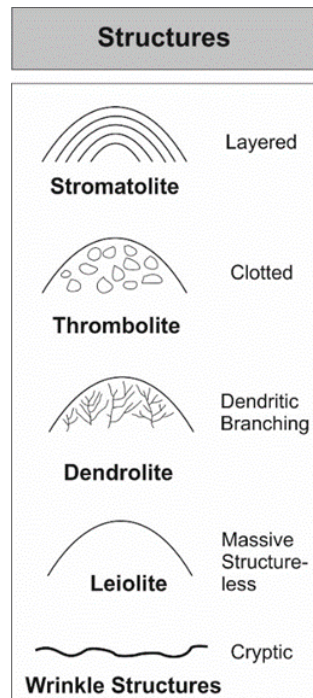


Figure 2.8 – Diagram illustrating key types of microbial structures found in the geological record. The depicted fabrics and textures are often interchangeable between stromatolites, thrombolites, dendrolites and leiolites (see Riding (2011)), and must be interpreted carefully in order to determine the precise biological and abiological processes acting during formation. Left partially modified from Dupraz *et al.* (2011), right diagram reproduced from Riding (1991a). Copyright Springer-Verlag 1991. Reproduced with permission of Springer-Verlag.

Work by Casillas-Martinez et al. (2005) has also explored the interactions of a microbial community with minerals occurring in a hypersaline microbial mat from Cabo Rojo, Puerto Rico. They showed that seasonal variations in environmental and limnological factors, namely precipitation and salinity, led to variations in the community composition of the mat. They indicate that the mineralogy the mats changed between dry and wet seasons, with community composition and metabolic activity leading to variations in the potential for the mat to trap and bind minerals and other detrital material (Casillas-Martinez *et al.*, 2005). This study therefore shows that environmental change can drive the biological processes associated with microbial mats and lead to fluctuations in the mineral phases found while increasing the potential for detrital material to be trapped and bound within a microbial mat (Casillas-Martinez *et al.*, 2005).

Since this study, several field- and lab-based studies have also emerged in this field. A laboratory-based study by Ahrendt et al. (2014) for example investigated the impact of fluctuations in CO₂ and subsequently pH on a lithifying microbial mat by incubating mats under controlled conditions. They demonstrated that increased concentrations of CO₂ had a negligible effect on the microbial community structure and the precipitation of carbonate, but caused enrichment of some strains of sulphate-reducing bacteria. Furthermore, a study by Cabestrero *et al.* (2018b) demonstrated the variability of microbial communities and their interactions with minerals through a hydrological cycle of the studied lakes. In this study and a succeeding study by Sanz-Montero et al. (2019b), it was exhibited that fluctuations in the water level of Laguna de Las Eras, an alkaline lake situated in Central Spain, caused shifts in the mineralogy of microbial mats. In the wet season, they demonstrated precipitation of hydrous phases of hydromagnesite, while in the dry season, Mg-rich and magnesite and dolomite were deposited instead (Cabestrero *et al.*, 2018b). Broadly, there are increasing numbers of studies focusing on the characterisation of variations in microbial mat mineralogy using both *in situ* (Gomez *et al.*, 2014; Eymard *et al.*, 2020; Baskin *et al.*, 2022; Della Porta *et al.*, 2022) and

experimental (Iniesto *et al.*, 2015; Newman *et al.*, 2017) approaches, and these previously discussed works are shedding light on the complex interplay that occurs between microbes, minerals and environmental change.

2.4.4.1 Relating Microbial Mats to Saline Lacustrine Systems

Though the development of microbial mats and associated microbialites has been acknowledged in a wide variety of settings, an abundance of these structures have primarily been documented in lacustrine environments with variable geochemical compositions. In particular, microbial processes and the development of microbialites and microbial carbonates occurring in non-marine hypersaline and alkaline lakes has been investigated by a spectrum of studies (Pinckney *et al.*, 1995; Jonkers *et al.*, 2003; Dupraz *et al.*, 2004, 2009; Villanueva *et al.*, 2007; Harris *et al.*, 2013; Cadena *et al.*, 2018). Such sites are abundant worldwide, and due to their extreme environmental conditions, microbial mats are able to proliferate and develop over long timescales. As such, the interactions between microbes, minerals and geochemistry in such sites are believed to play a “fundamental role in the precipitation, dissolution and alteration of minerals” (Paul *et al.*, 2016; Seckbach, 2016) and the long-term formation and development of microbialites (Dupraz *et al.*, 2004; Solari *et al.*, 2010; Chagas *et al.*, 2016).

Table 2.7 – Table showing several sites with variable geochemistry and the effects of geochemistry and wet and dry seasons, both between sites and within each site, on microbial community composition and mineralogy. (Casillas-Martinez *et al.*, 2005; Cabestrero *et al.*, 2018b; Sanz-Montero *et al.*, 2019)

Site	Chemistry	Community Composition	Mineralogy	Seasonal Variations		Reference(s)
				Wet	Dry	
Laguna de Las Eras, Central Spain	Alkaline	CYN	Hydromagnesite	↑ CYN	↑ Hydromagnesite	Cabestrero et al. (2018) Sanz-Montero et al. (2019)
		GNSB	Sulphates	↑ CO ₂	↑ PSB	
		SOB	Sulphates		↑ EPS production	
		PSB				
Altילו Chica, Central Spain	Saline	CYN	Aragonite	↑ Autotrophs	↑ Hydromagnesite	Cabestrero et al. (2018)
		GNSN	Calcite	↑ CO ₂	↑ PSB	
		PSB	Dolomite	↑ EPS production	↑ Sulphate	
		SRB				
Cabo Rojo, Puerto Rico	Hypersaline	CYN	Quartz	↑ Quartz	↑ Halite	Casillas-Martinez et al. (2005)
		ANOX	Halite	↑ EPS binding capacity	↓ Microbial Diversity	
		SOB				
		COI				

2.5 Review of Previous Work on Study Sites

2.5.1 Laguna Salada de Chiprana

The geology of the Chiprana region is distinguished by Oligo-Miocene marls and mudstones that are cross-cut by ribbon-shaped sandstone bodies (IGME, 2003). The interplay of these geological formations segments the lake, whereby the elongated sandstones form ridges that separate the lake into several basins (Vidondo *et al.*, 1993). The lake's hydrology is controlled by a Mediterranean climate with high evapotranspiration as the key hydrological output (1000-1500mm yr^{-1}), and low rainfall (~270mm yr^{-1}), groundwater input (~300mm yr^{-1}) and inflow from irrigation (~600mm yr^{-1}) that are delivered to the lake (Guerrero *et al.*, 1991; Jódar *et al.*, 2020). The lake water is also represented primarily by Na⁺, Mg²⁺, SO₄²⁻ and Cl⁻ ions, with the average salinity of the lake varying around approximately 40-80g/L (De Wit *et al.*, 2013). Seminal limnological characterisations of the lagoon by Guerrero *et al.* (1991), Vidondo *et al.* (1993), Diaz *et al.* (1998) and Valero-Garcés *et al.* (2000) have been previously undertaken and described the physicochemical characteristics of the site and the effects of climatic and anthropogenic perturbations on the overall trophic structure.

As a result of the limnological conditions, microbial mats, as described in later chapters, occur in abundance on the lake shores and in some cases, within the deeper sub-basins of the lacustrine system. A study by Jonkers *et al.* (2003) has provided a detailed description and analysis of the microbial mat community and the associated metabolic and biogeochemical activities that occur over a diel cycle, while Camacho and De Wit (2003) tested the responses of the microbial mat system to artificial phosphorus and nitrogen additions. More recently, De Wit *et al.* (2013) have evaluated the management steps that must be undertaken if the unique microbial communities in Laguna Salada de Chiprana are to be preserved. The community composition has largely remained stable over the last two decades based on a study undertaken in 2019 by Hickman-Lewis *et al.* (2019).

2.5.2 Lago de Estanya

According to Morellón *et al.* (2009a), the underlying geology is of Upper Triassic age and consists of marls and claystones, while Mid-Triassic Muschelkalk deposits form other topographical features such as hills and terraces throughout the area and basin. The hydrological setting is defined by input from groundwater, small creeks and inlets and from output by evaporation, leading to the development of Lake Estanya as a closed system (Morellón *et al.*, 2008, 2009b). The local climate is Mediterranean, and typically experiences an average range of temperatures between 4°C and 24°C, and an average annual rainfall of approximately 625mm (Vicente-Serrano *et al.*, 2010), with the summer drought typically lasting 2-3 months, though the lake remains filled during this time. The limnological characteristics of the lake are currently represented by brackish, sulphate and calcium-rich waters, with SO_4^{2-} , Ca^{2+} , Mg^{2+} , and Na^+ constituting the primary ions associated with these waters (Morellón *et al.*, 2011).

Microbial mats are not currently developing within Lago de Estanya, but have been identified in various sedimentological studies (Morellón *et al.*, 2008, 2009a) focusing on long cores retrieved from the site. Therein, microbial mats are shown developing in several intervals between 9.4 and 0.8ka, characteristically during periods in which the lake-waters fell and illustrated heightened salinities. A wide variety of studies utilising multi-proxy approaches have also been undertaken upon Lago de Estanya (Morellón *et al.*, 2009a; b, 2011; Vegas-Vilarrúbia *et al.*, 2013), with most of these studies focusing upon the palaeoenvironmental evolution of the site as represented in core sediments. These cores have been the subject of sedimentary facies analyses (Morellón *et al.*, 2009a), elemental and isotopic geochemistry (Morellón *et al.*, 2009b), and biological proxies such as diatoms, chironomids and pollen (Vegas-Vilarrúbia *et al.*, 2013). Coupled with chronological models generated from ^{14}C radiocarbon dating and ^{210}Pb and ^{137}Cs radiometric techniques (Riera *et al.*, 2004; Morellón *et al.*, 2009b), this has allowed for an understanding of environmental change throughout the region (Morellón *et al.*, 2011). As such, the development of

microbial mats throughout the Holocene within Lago de Estanya can be correlated to environmental, geochemical and hydrological fluctuations occurring throughout the same time period (Morellón *et al.*, 2008).

2.5.3 Laguna Zonar

The underlying geology of Lake Zonar is primarily characterised by Triassic carbonates, evaporites and mudstones (IGME, 2003; Martín-Puertas *et al.*, 2011). The climate is Mediterranean and governed by an average annual rainfall of approximately 530mm (Martín-Puertas *et al.*, 2008). The lake has a closed hydrological system that is governed by rainfall (~300-1100mmyr⁻¹) and several springs and creeks that drain to the lake as the primary hydrological inputs and high evaporation (~1700mmyr⁻¹) as the primary hydrological output (Valero-Garcés *et al.*, 2006; Martín-Puertas *et al.*, 2011). The limnological characteristics of the lake are currently represented by saline waters which predominantly consist of Na⁺, Cl⁻ and SO₄²⁻ ions (Martín-Puertas *et al.*, 2011).

Alike to Lago de Estanya, microbial mats are not currently developing within Laguna Zonar, but have been instead been identified in studies focusing on long core sediments by Martín-Puertas *et al.* (2008, 2009, 2011). These studies stipulate that microbial mats develop throughout the Medieval Climate Anomaly (0.8-1.3ka) and during the Early-Mid 20th century, during which lake-waters were lower and salinity increased. Several studies have utilised sedimentary facies analysis (Martín-Puertas *et al.*, 2008) geochemical variables and palaeolimnological indicators (Martín-Puertas *et al.*, 2011), and biological proxies including pollen, ostracods and diatoms (Valero-Garcés *et al.*, 2006). These data have allowed for the generation of high resolution palaeoenvironmental reconstructions for the last 4000 years (Martín-Puertas *et al.*, 2009)

2.5.4 Lago de Arreo

Lago de Arreo is a small saline lake located near Caicedo de Yuso in the Basque Country of Northern Spain. An Atlantic-Mediterranean climate governs the site, with an average annual temperature of 13°C and an average annual calculated rainfall of 670mm (Corella *et al.*, 2011). The lake is represented by an open hydrological system and receives input from ephemeral inlets and outlets, while evaporation rates are generally not significant (Morellón *et al.*, 2012). The lake is largely brackish, and is governed by an abundance of Ca²⁺, Mg²⁺, Na⁺, SO₄²⁻ and HCO₃⁻ ions (Corella *et al.*, 2011). Conspicuous microbial mats have not been observed developing in contemporary lake waters, but potential microbial fabrics have been identified preserved in core material previously characterised by Corella *et al.* (2013).

Several studies (Corella *et al.*, 2011, 2013, 2021) represent the literature body concerning the site. The studies have showed that the environmental record of Lago de Arreo was governed by significant interactions between climatic and anthropogenic throughout the last two and a half millennia (Corella *et al.*, 2011, 2013). They also illustrate that the sedimentological sequence consisted of five key environmental stages. The first stage, consisting of coarse alluvial sediments with high organic matter, is believed to correspond to the Iberian Roman Humid Period between 2.5 and ~1.4ka (Corella *et al.*, 2013). The second stage consists of carbonate rich facies and corresponds to high levels and moister climatic conditions between 1.4 and 1.1ka. The third stage, corresponding to the Medieval Climate Anomaly between 1.1 and 0.7ka, is characterised by increased salinity, lower lake level and more arid conditions (Corella *et al.*, 2021). This is followed by a shift to decreased lake salinity and generally more humid conditions in the Little Ice Age between 0.7 and 0.2ka. Finally, the fifth and final stage is characterised by a shift to more arid conditions from 0.2ka to the Modern day (Corella *et al.*, 2021).

2.6 - Conclusions

- Saline lakes are distributed globally and are characterised by a spectrum of environments with varying morphology, size, latitude and longitude, geochemistry, and depositional characteristics.

- Many saline lakes display distinctive limnological characteristics that are associated with key geochemical water/brine types and subsequently mineralogical phases.
- Saline lakes are also host to a wide range of depositional features, facies and minerals as a result of their diverse limnological characteristics, and due to their high sensitivity to external perturbations, many of these features are considered critical when using saline lakes as potential palaeolimnological archives.
- Microbial mats are host to a spectrum of biological activities, and they are important components of the various biogeochemical cycles that occur over different spatial and temporal scales.
- Microbes and microbial mats can contribute to the formation, dissolution and alteration of minerals, and are widely recognised to be key in the formation of biosedimentary deposits known as microbialites.
- Processes of mineral formation induced by microbes can be caused by biologically-controlled, -induced or -influenced precipitation, and the nucleation of such minerals can take place both within microbial cells and on the extracellular polymeric substance.
- Products of microbial interactions with minerals can produce a wide spectrum of structures ranging from the layered stromatolites to the aphanitic leolites, but discerning the biogenicity of many of these structures still remains a challenge.

References

- Abed, R.M.M., Kohls, K. and De Beer, D.** (2007) Effect of salinity changes on the bacterial diversity, photosynthesis and oxygen consumption of cyanobacterial mats from an intertidal flat of the Arabian Gulf. *Environ. Microbiol.*, **9**, 1384–1392.
- Adams, K.D. and Rhodes, E.J.** (2019) Late pleistocene to present lake-level fluctuations at pyramid and winnemucca lakes, Nevada, USA. *Quat. Res. (United States)*, **92**, 146–164.
- Ahrendt, S.R., Mobberley, J.M., Visscher, P.T., Koss, L.L. and Foster, J.S.** (2014) Effects of elevated carbon dioxide and salinity on the microbial diversity in lithifying microbial mats. *Minerals*, **4**, 145–169.
- Allewalt, J.P., Bateson, M.M., Revsbech, N.P., Slack, K. and Ward, D.M.** (2006) Effect of temperature and light on growth of and photosynthesis by *Synechococcus* isolates typical of those predominating in the Octopus Spring microbial mat community of Yellowstone National Park. *Appl. Environ. Microbiol.*, **72**, 544–550.
- Alonso, M.** (1998) The lagoons of Peninsular Spain. *Limnetica*, **15**, 1–176.
- Awramik, S.M.** (1992) The History and Significance of Stromatolites. In: *Early Organic Evolution*, 435–449.
- Awramik, S.M. and Grey, K.** (2005) Stromatolites: biogenicity, biosignatures, and bioconfusion. In: *Astrobiology and Planetary Missions*, 5906, 59060P.
- Baker, B.J. and Banfield, J.F.** (2003) Microbial communities in acid mine drainage. *FEMS Microbiol. Ecol.*, **44**, 139–152.
- Banner, F..** (1982) Salt Lakes. Proceedings of the International Symposium

on Athalassic (Inland) Salt Lakes, Adelaide, 1979. *W. Junk Publishers; Distributors for the U.S. and Canada, Kluwer Boston, The Hague; Boston: Hingham, MA, U.S.A*, 91-92 pp.

Barton, L.L. and Hamilton, A.W. (2007) Sulphate-reducing bacteria: Environmental and engineered systems. 1-538 pp.

Baskin, R.L., Della Porta, G. and Wright, V.P. (2022) Characteristics and controls on the distribution of sublittoral microbial bioherms in Great Salt Lake, Utah: Implications for understanding microbialite development. *Depos. Rec.*, **8**, 39–66.

Beerstecher, J. (1954) Petroleum microbiology: An introduction to microbiological petroleum engineering. *Science*, 1064 pp.

Bengtsson, L. (2012) Poopó Lake, Bolivia BT - Encyclopedia of Lakes and Reservoirs. In: (Ed. L. Bengtsson, R.W. Herschy, and R.W. Fairbridge), *Springer Netherlands*, Dordrecht, 616–618.

Benison, K.C., Bowen, B.B., Oboh-Ikuenobe, F.E., Jagniecki, E.A., LaClair, D.A., Story, S.L., Mormile, M.R. and Hong, B.Y. (2007) Sedimentology of acid saline lakes in southern Western Australia: Newly described processes and products of an extreme environment. *J. Sediment. Res.*, **77**, 366–388.

Bergner, A.G.N., Strecker, M.R., Trauth, M.H., Deino, A., Gasse, F., Blisniuk, P. and Dühnforth, M. (2009) Tectonic and climatic control on evolution of rift lakes in the Central Kenya Rift, East Africa. *Quat. Sci. Rev.*, **28**, 2804–2816.

Bioeconomics (2012) Economic significance of the Great Salt Lake to the State of Utah. 50.

Bolhuis, H., Cretoiu, M.S. and Stal, L.J. (2014) Molecular ecology of microbial mats. *FEMS Microbiol. Ecol.* 90:335–350.

Bookman, R. (2020) The Dead Sea and Its Deviation from Natural

Conditions. In: *Springer Water*, 1–33.

Borzenko, S. V. (2021) The main formation processes for different types of salt lakes: Evidence from isotopic composition with case studies of lakes in Transbaikalia, Russia. *Sci. Total Environ.*, **782**, 1–15.

Bosak, T., Knoll, A.H. and Petroff, A.P. (2013) The meaning of stromatolites. *Annu. Rev. Earth Planet. Sci.*, **41**, 21–44.

Bosence, D. and Gallois, A. (2022) How do thrombolites form? Multiphase construction of lacustrine microbialites, Purbeck Limestone Group, (Jurassic), Dorset, UK. *Sedimentology*, **69**, 914–953.

Bouton, A., Vennin, E., Pace, A., Bourillot, R., Dupraz, C., Thomazo, C., Brayard, A., Désaubliaux, G. and Visscher, P.T. (2016) External controls on the distribution, fabrics and mineralization of modern microbial mats in a coastal hypersaline lagoon, Cayo Coco (Cuba). *Sedimentology*, **63**, 972–1016.

Bowen, B.B. and Benison, K.C. (2009) Geochemical characteristics of naturally acid and alkaline saline lakes in southern Western Australia. *Appl. Geochemistry*, **24**, 268–284.

Brock, M.A. and Hammer, U.T. (1987) Saline Lake Ecosystems of the World., 1st edn. *Springer*, Dordrecht, 580 pp.

Cabestrero, Ó., del Buey, P. and Sanz-Montero, M.E. (2018a) Biosedimentary and geochemical constraints on the precipitation of mineral crusts in shallow sulphate lakes. *Sediment. Geol.*, **366**, 32–46.

Cabestrero, Sanz-Montero, M.E., Arregui, L., Serrano, S. and Visscher, P.T. (2018b) Seasonal Variability of Mineral Formation in Microbial Mats Subjected to Drying and Wetting Cycles in Alkaline and Hypersaline Sedimentary Environments. *Aquat. Geochemistry*, **24**, 79–105.

Cadena, S., García-Maldonado, J.Q., López-Lozano, N.E. and

- Cervantes, F.J.** (2018) Methanogenic and Sulfate-Reducing Activities in a Hypersaline Microbial Mat and Associated Microbial Diversity. *Microb. Ecol.*, **75**, 930–940.
- Calder, I.R. and Neal, C.** (1984) Evaporation from saline lakes: a combination equation approach. *Hydrol. Sci. Journal/Journal des Sci. Hydrol.*, **29**, 89–97.
- Camacho, A. and De Wit, R.** (2003) Effect of nitrogen and phosphorus additions on a benthic microbial mat from a hypersaline lake. *Aquat. Microb. Ecol.*, **32**, 261–273.
- Canfield, D.E. and Des Marais, D.J.** (1993) Biogeochemical cycles of carbon, sulfur, and free oxygen in a microbial mat. *Geochim. Cosmochim. Acta*, **57**, 3971–3984.
- Carroll, C., Parks, S.A., Dobrowski, S.Z. and Roberts, D.R.** (2018) Climatic, topographic, and anthropogenic factors determine connectivity between current and future climate analogs in North America. *Glob. Chang. Biol.*, **24**, 5318–5331.
- Casillas-Martinez, L., Gonzalez, M.L., Fuentes-Figueroa, Z., Castro, C.M., Nieves-Mendez, D., Hernandez, C., Ramirez, W., Sytsma, R.E., Perez-Jimenez, J. and Visscher, P.T.** (2005) Community structure, geochemical characteristics and mineralogy of a hypersaline microbial mat, Cabo Rojo, PR. *Geomicrobiol. J.*, **22**, 269–281.
- Chagas, A.A.P., Webb, G.E., Burne, R. V. and Southam, G.** (2016) Modern lacustrine microbialites: Towards a synthesis of aqueous and carbonate geochemistry and mineralogy. *Earth-Science Rev.*, **162**, 338–363.
- Chen, J. and Lee, J.H.** (2014) Current progress on the geological record of microbialites and microbial carbonates. *Acta Geol. Sin.*, **88**, 260–275.
- Clarke, J.D.A. and Stoker, C.R.** (2013) Searching for stromatolites: The

3.4Ga Strelley Pool Formation (Pilbara region, Western Australia) as a Mars analogue. *Icarus*, **224**, 413–423.

Cohen, Y. (1989) Photosynthesis in cyanobacterial mats and its relation to the sulfur cycle: a model for microbial sulfur interactions. In: *Microbial Mats, Physiological Ecology of Benthic Communities*,

Comin, F.A. and **Alonso, M.** (1988) Spanish salt lakes: Their chemistry and biota. *Hydrobiologia*, **158**, 237–245.

Condie, K.C. and **Sloan, R.E.** (1998) Origin and Evolution of Earth: Principles of Historical Geology. *Prentice Hall*, Upper Saddle River, NJ, 498 pp.

Corella, J.P., Amrani, A. El, Sigró, J., Morellón, M., Rico, E. and Valero-Garcés, B.L. (2011) Recent evolution of Lake Arreo, northern Spain: Influences of land use change and climate. *J. Paleolimnol.*, **46**, 469–485.

Corella, J.P., Benito, G., Monteoliva, A.P., Sigró, J., Calle, M., Valero-Garcés, B.L., Stefanova, V., Rico, E., Favre, A.C. and Wilhelm, B. (2021) A 1400-years flood frequency reconstruction for the Basque country (N Spain): Integrating geological, historical and instrumental datasets. *Quat. Sci. Rev.*, **262**, 1–15.

Corella, J.P., Stefanova, V., El Anjumi, A., Rico, E., Giralt, S., Moreno, A., Plata-Montero, A. and Valero-Garcés, B.L. (2013) A 2500-year multi-proxy reconstruction of climate change and human activities in northern Spain: The Lake Arreo record. *Palaeogeogr. Palaeoclimatol. Palaeoecol.*, **386**, 555–568.

Dasgupta, S., Peng, X. and Ta, K. (2021) Interaction between microbes, minerals, and fluids in deep-sea hydrothermal systems. *Minerals*, **11**, 1–15.

Davies, N.S., Liu, A.G., Gibling, M.R. and Miller, R.F. (2016) Resolving

MISS conceptions and misconceptions: A geological approach to sedimentary surface textures generated by microbial and abiotic processes. *Earth-Science Rev.*, **154**, 210–246.

De Beer, D. and Stoodley, P. (2014) Microbial biofilms. In: *The Prokaryotes: Applied Bacteriology and Biotechnology*, 343–372.

De Cort, G., Mees, F., Renaut, R.W., Sinnesael, M., Van der Meeren, T., Goderis, S., Keppens, E., Mbutia, A. and Verschuren, D. (2019) Late-Holocene sedimentation and sodium carbonate deposition in hypersaline, alkaline Nasikie Engida, southern Kenya Rift Valley. *J. Paleolimnol.*, **62**, 279–300.

De Wit, R., Guerrero, M.C., Legaz, A., Jonkers, H.M., Blocier, L., Gumiaux, C. and Gautret, P. (2013) Conservation of a permanent hypersaline lake: Management options evaluated from decadal variability of coleofasciculus chthonoplastes microbial mats. *Aquat. Conserv. Mar. Freshw. Ecosyst.*, **23**, 532–545.

Decho, A. (2000) Exopolymer microdomains as a structuring agent for heterogeneity within microbial biofilms. In: *Microbial sediments*, 9–15.

Della Porta, G., Hoppert, M., Hallmann, C., Schneider, D. and Reitner, J. (2022) The influence of microbial mats on travertine precipitation in active hydrothermal systems (Central Italy). *Depos. Rec.*, **8**, 165–209.

Deocampo, D.M. and Jones, B.F. (2013) Geochemistry of Saline Lakes. In: *Treatise on Geochemistry: Second Edition*, 2nd edn. (Ed. K. Turekian and H. Holland), *Elsevier*, **7**, 437–469.

Deocampo, D.M. and Renaut, R.W. (2016) Geochemistry of African Soda Lakes. In: *Soda Lakes of East Africa*, 77–93.

Diaz, P., Guerrero, M.C., Alcorlo, P., Baltanas, A., Florin, M. and Montes, C. (1998) Anthropogenic perturbations to the trophic structure in a permanent hypersaline shallow lake: La Salada de Chiprana

- (north-eastern Spain). *Int. J. Salt Lake Res.*, **7**, 187–210.
- Dolla, A., Fournier, M. and Dermoun, Z.** (2006) Oxygen defense in sulfate-reducing bacteria. *J. Biotechnol.*, **126**, 87–100.
- Dong, H.** (2010) Mineral-microbe interactions: A review. *Front. Earth Sci. China*, **4**, 127–147.
- Dortch, J.M., Owen, L.A., Caffee, M.W. and Kamp, U.** (2011) Catastrophic partial drainage of Pangong Tso, northern India and Tibet. *Geomorphology*, **125**, 109–121.
- Duarte, C.M., Prairie, Y.T., Montes, C., Cole, J.J., Striegl, R., Melack, J. and Downing, J.A.** (2008) CO₂ emissions from saline lakes: A global estimate of a surprisingly large flux. *J. Geophys. Res. Biogeosciences*, **113**, 1–7.
- Dupraz, C., Reid, R.P., Braissant, O., Decho, A.W., Norman, R.S. and Visscher, P.T.** (2009) Processes of carbonate precipitation in modern microbial mats. *Earth-Science Rev.*, **96**, 141–162.
- Dupraz, C., Reid, R.P. and Visscher, P.T.** (2011) Microbialites, modern. In: *Encyclopedia of Earth Sciences Series* (Ed. J. Reitner and V. Thiel), Springer Netherlands, Dordrecht, 617–635.
- Dupraz, C. and Visscher, P.T.** (2005) Microbial lithification in marine stromatolites and hypersaline mats. *Trends Microbiol.*, **13**, 429–438.
- Dupraz, C., Visscher, P.T., Baumgartner, L.K. and Reid, R.P.** (2004) Microbe-mineral interactions: Early carbonate precipitation in a hypersaline lake (Eleuthera Island, Bahamas). *Sedimentology*, **51**, 745–765.
- Edwards, M.J.K., Anderson, C.R., Perissinotto, R. and Rishworth, G.M.** (2017) Macro- and meso-fabric structures of peritidal tufa stromatolites along the Eastern Cape coast of South Africa. *Sediment. Geol.*, **359**, 62–75.

- Eugster, H.** and **Hardie, L.** (1978) Saline Lakes. In: *Lakes: Chemistry, Geology, Physics* (Ed. A. Lerman), Springer, New York, NY, 237–293.
- Eugster, H.P.** (1980) Chapter 15 - Lake Magadi, Kenya, and Its Precursors. In: *Hypersaline Brines and Evaporitic Environments* (Ed. A.B.T.-D. in S. Nissenbaum), Elsevier, 28, 195–232.
- Evans, M.S.** (1993) Paleolimnological studies of saline lakes. *J. Paleolimnol.*, **8**, 97–101.
- Eymard, I., Alvarez, M.D.P., Bilmes, A., Vasconcelos, C. and Ariztegui, D.** (2020) Tracking organomineralization processes from living microbial mats to fossil microbialites. *Minerals*, **10**, 1–20.
- Finlayson, C.M.** (2016) Salt Lakes. In: *The Wetland Book*, 1–12.
- Fischer, W.W., Hemp, J. and Valentine, J.S.** (2016) How did life survive Earth's great oxygenation? *Curr. Opin. Chem. Biol.*, **31**, 166–178.
- Flemming, H.C., Neu, T.R. and Wozniak, D.J.** (2007) The EPS matrix: The "House of Biofilm Cells." *J. Bacteriol.*, **189**, 7945–7947.
- Flemming, H.C. and Wingender, J.** (2010) The biofilm matrix. *Nat. Rev. Microbiol.*, **8**, 623–633.
- Flemming, H.C., Wingender, J., Szewzyk, U., Steinberg, P., Rice, S.A. and Kjelleberg, S.** (2016) Biofilms: An emergent form of bacterial life. *Nat. Rev. Microbiol.*, **14**, 563–575.
- Franks, J. and Stolz, J.F.** (2009) Flat laminated microbial mat communities. *Earth-Science Rev.*, **96**, 163–172.
- Frund, C. and Cohen, Y.** (1992) Diurnal cycles of sulfate reduction under oxic conditions in cyanobacterial mats. *Appl. Environ. Microbiol.*, **58**, 70–77.
- Fu, X., Cohen, T.J. and Arnold, L.J.** (2017) Extending the record of lacustrine phases beyond the last interglacial for Lake Eyre in central Australia using luminescence dating. *Quat. Sci. Rev.*, **162**, 88–110.

- Gadd, G.M.** (2010) Metals, minerals and microbes: Geomicrobiology and bioremediation. *Microbiology*, **156**, 609–643.
- Gázquez, F., Evans, N.P. and Hodell, D.A.** (2017) Precise and accurate isotope fractionation factors ($\alpha^{17}\text{O}$, $\alpha^{18}\text{O}$ and α^{D}) for water and $\text{CaSO}_4 \cdot 2\text{H}_2\text{O}$ (gypsum). *Geochim. Cosmochim. Acta*, **198**, 259–270.
- Gázquez, F., Mather, I., Rolfe, J., Evans, N.P., Herwartz, D., Staubwasser, M. and Hodell, D.A.** (2015) Simultaneous analysis of $^{17}\text{O}/^{16}\text{O}$, $^{18}\text{O}/^{16}\text{O}$ and $2\text{H}/1\text{H}$ of gypsum hydration water by cavity ring-down laser spectroscopy. *Rapid Commun. Mass Spectrom.*, **29**, 1997–2006.
- Gázquez, F., Morellón, M., Bauska, T., Herwartz, D., Surma, J., Moreno, A., Staubwasser, M., Valero-Garcés, B., Delgado-Huertas, A. and Hodell, D.A.** (2018) Triple oxygen and hydrogen isotopes of gypsum hydration water for quantitative paleo-humidity reconstruction. *Earth Planet. Sci. Lett.*, **481**, 177–188.
- Gerdes, G., Krumbein, W.E. and Noffke, N.** (2000) Evaporite Microbial Sediments. In: *Microbial Sediments*, 196–208.
- Getenet, M., García-Ruiz, J.M., Verdugo-Escamilla, C. and Guerra-Tschuschke, I.** (2020) Mineral vesicles and chemical gardens from carbonate-rich alkaline brines of lake magadi, Kenya. *Crystals*, **10**, 1–21.
- Gomez, F.J., Kah, L.C., Bartley, J.K. and Astini, R.A.** (2014) Microbialites in a high-altitude Andean lake: Multiple controls on carbonate precipitation and lamina accretion. *Palaios*, **29**, 233–249.
- Grant, W.D. and Jones, B.E.** (2016) Bacteria, archaea and viruses of Soda Lakes. In: *Soda Lakes of East Africa*, 97–147.
- Grotzinger, J.P. and Rothman, D.H.** (1996) An abiotic model for stromatolite morphogenesis. *Nature*, **383**, 423–425.

- Guerrero, M.C.** (1992) Microbial mats in the inland saline lakes of Spain. *Limnetica*, **8**, 197–204.
- Guerrero, M.C., Balsa, J., Pascual, M. and Martínez, B.** (1991) Caracterización limnológica de la Laguna Salada de Chiprana (Zaragoza, España) y sus comunidades de bacterias fototróficas. *Limnetica*, **7**, 83–96.
- Guido, A., Sposato, M., Palladino, G., Vescogni, A. and Miriello, D.** (2022) Biomineralization of primary carbonate cements: a new biosignature in the fossil record from the Anisian of Southern Italy. *Lethaia*, **55**, 1–21.
- Hammer, U.T.** (1986) Saline lakes: their distribution and characteristics. *Can. Plains Proc.*, **17**, 1–22.
- Hardie, L.. and Eugster, H..** (1970) Evolution of closed-basin brines. *Miner. Soc. Amer. Spec.*, **3**, 273–290.
- Hardie, L.A.** (1968) The origin of the Recent non-marine evaporite deposit of Saline Valley, Inyo County, California. *Geochim. Cosmochim. Acta*, **32**, 1279–1301.
- Hardie, L.A., Smoot, J.P. and Eugster, H.P.** (1978) Saline Lakes and their Deposits: A Sedimentological Approach. In: *Modern and Ancient Lake Sediments*, 7–41.
- Herman, E.K. and Kump, L.R.** (2005) Biogeochemistry of microbial mats under Precambrian environmental conditions: A modelling study. *Geobiology*, **3**, 77–92.
- Hickman-Lewis, K., Gautret, P., Arbaret, L., Sorieul, S., De Wit, R., Foucher, F., Cavalazzi, B. and Westall, F.** (2019) Mechanistic morphogenesis of organo-sedimentary structures growing under geochemically stressed conditions: Keystone to proving the biogenicity of some Archaean stromatolites? *Geosci.*, **9**, 1–31.

- Hoehler, T.M., Albert, D.B., Alperin, M.J., Bebout, B.M., Martens, C.S.**
and **Des Marais, D.J.** (2002) Comparative ecology of H₂ cycling in sedimentary and phototrophic ecosystems. *Antonie van Leeuwenhoek, Int. J. Gen. Mol. Microbiol.*, **81**, 575–585.
- IGME** (2003) Mapa Geologico de Espana, 1:50000, (serie MAGNA). Hoja 988. Puente-Genil.
- Iltis, A.** (1993) Recent limnological changes in a saline lake of the Bolivian Altiplano, Lake Poopo. *Int. J. Salt Lake Res.*, **2**, 17–28.
- Iniesto, M., Zeyen, N., López-Archilla, A.I., Bernard, S., Buscalioni, Á.D., Guerrero, M.C. and Benzerara, K.** (2015) Preservation in microbial mats: Mineralization by a talc-like phase of a fish embedded in a microbial sarcophagus. *Front Earth Sci.* doi: 10.3389/feart.2015.00051
- J. D. Aitken** (1967) Classification and Environmental Significance of Cryptalgal Limestones and Dolomites, with Illustrations from the Cambrian and Ordovician of Southwestern Alberta. *SEPM J. Sediment. Res.*, **Vol. 37**, 1163–1178.
- Jellison, R., Macintyre, S. and Millero, F.J.** (1999) Density and conductivity properties of Na-CO₃-Cl-SO₄ brine from Mono Lake, California, USA. *Int. J. Salt Lake Res.*, **8**, 41–53.
- Jellison, R., Williams, W.D., Timms, B., Alcocer, J. and Aladin, N. V.** (2008) Salt lakes: Values, threats and future. In: *Aquatic Ecosystems: Trends and Global Prospects*, 94–110.
- Jirsa, F., Gruber, M., Stojanovic, A., Omondi, S.O., Mader, D., Körner, W. and Schagerl, M.** (2013) Major and trace element geochemistry of Lake Bogoria and Lake Nakuru, Kenya, during extreme draught. *Chemie der Erde*, **73**, 275–282.
- Jódar, J., Rubio, F.M., Custodio, E., Martos-Rosillo, S., Pey, J.,**

- Herrera, C., Turu, V., Pérez-Bielsa, C., Ibarra, P. and Lambán, L.J.** (2020) Hydrogeochemical, isotopic and geophysical characterization of saline lake systems in semiarid regions: The Salada de Chiprana Lake, Northeastern Spain. *Sci. Total Environ.*, **728**, 1–48.
- Jones, B.F., Naftz, D.L., Spencer, R.J. and Oviatt, C.G.** (2009) Geochemical evolution of Great Salt Lake, Utah, USA. *Aquat. Geochemistry*, **15**, 95–121.
- Jonkers, H.M., Ludwig, R., De Wit, R., Pringault, O., Muyzer, G., Niemann, H., Finke, N. and De Beer, D.** (2003) Structural and functional analysis of a microbial mat ecosystem from a unique permanent hypersaline inland lake: “La Salada de Chiprana” (NE Spain). *FEMS Microbiol. Ecol.*, **44**, 175–189.
- Jorgensen, B.B., Revsbech, N.P. and Cohen, Y.** (1983) Photosynthesis and structure of benthic microbial mats: Microelectrode and SEM studies of four cyanobacterial communities. *Limnol. Oceanogr.*, **28**, 1075–1093.
- Kalkowsky, E.** (1908) Oolith und Stromatolith im norddeutschen Buntsandstein. *Zeitschrift der Dtsch. Geol. Gesellschaft*, **60**, 68–125.
- Kasedde, H.** (2013) Towards the Improvement of Salt Extraction from Lake Katwe Raw Materials in Uganda. KTH, Royal Institute of Technology
- Kavembe, G.D., Meyer, A. and Wood, C.M.** (2016) Fish populations in East African Saline Lakes. In: *Soda Lakes of East Africa*, 227–257.
- Kelts, K.** (1988) Environments of deposition of lacustrine petroleum source rocks: An introduction. *Geol. Soc. Spec. Publ.*, **40**, 3–26.
- Kelts, K. and Talbot, M.** (1990) Lacustrine Carbonates as Geochemical Archives of Environmental Change and Biotic/Abiotic Interactions. In: *Large Lakes*, 1st edn. (Ed. M. Tilzer and C. Serruya), *Brock/Springer*, 288–315.

- Kirk Harris, J., Gregory Caporaso, J., Walker, J.J., Spear, J.R., Gold, N.J., Robertson, C.E., Hugenholtz, P., Goodrich, J., McDonald, D., Knights, D., Marshall, P., Tufo, H., Knight, R. and Pace, N.R.** (2013) Phylogenetic stratigraphy in the Guerrero Negro hypersaline microbial mat. *ISME J.*, **7**, 50–60.
- Krekeler, D., Teske, A. and Cypionka, H.** (1998) Strategies of sulfate-reducing bacteria to escape oxygen stress in a cyanobacterial mat. *FEMS Microbiol. Ecol.*, **25**, 89–96.
- Krumbein, W.E.** (1983) Stromatolites—the challenge of a term in space and time. *Dev. Precambrian Geol.*, **7**, 385–423.
- Last, F.M.** (2013) Carbonate microbialite formation in a prairie saline lake in Saskatchewan, Canada: paleohydrologic and paleoenvironmental implications. University of Manitoba
- Last, F.M., Last, W.M. and Halden, N.M.** (2012) Modern and late Holocene dolomite formation: Manito Lake, Saskatchewan, Canada. *Sediment. Geol.*, **281**, 222–237.
- Last, W.M.** (2002) Geolimnology of salt lakes. *Geosci. J.*, **6**, 347–369.
- Last, W.M.** (1992) Chemical composition of saline and subsaline lakes of the northern Great Plains, western Canada. *Int J Salt Lake Res.* doi: 10.1007/BF02904362
- Last, W.M.** (1989) Continental brines and evaporites of the northern Great Plains of Canada. *Sediment. Geol.*, **64**, 207–221.
- Last, W.M. and Ginn, F.M.** (2005) Saline systems of the Great Plains of western Canada: an overview of the limnogeology and paleolimnology. *Saline Systems*, **1**, 1–38.
- Last, W.M. and Schweyen, T.H.** (1983) Sedimentology and geochemistry of saline lakes of the Great Plains. *Hydrobiologia*, **105**, 245–263.
- Lowenstein, T.K., Hadie, L.A. and Hardie, L.A.** (1985) Criteria for the

recognition of salt-pan evaporites. *Sedimentology*, **32**, 627–644.

Mann, S. (2001) *Biom mineralization Principles and Concepts in Bioinorganic Materials Chemistry*.

Marazuela, M.A., Vázquez-Suñé, E., Ayora, C., García-Gil, A. and Palma, T. (2019) Hydrodynamics of salt flat basins: The Salar de Atacama example. *Sci. Total Environ.*, **651**, 668–683.

Martín-Puertas, C., Valero-Garcés, B.L., Brauer, A., Mata, M.P., Delgado-Huertas, A. and Dulski, P. (2009) The Iberian-Roman Humid Period (2600-1600 cal yr BP) in the Zoñar Lake varve record (Andalucía, southern Spain). *Quat. Res.*, **71**, 108–120.

Martín-Puertas, C., Valero-Garcés, B.L., Mata, M.P., González-Sampériz, P., Bao, R., Moreno, A. and Stefanova, V. (2008) Arid and humid phases in southern Spain during the last 4000 years: The Zoñar Lake record, Córdoba. *Holocene*, **18**, 907–921.

Martín-Puertas, C., Valero-Garcés, B.L., Mata, M.P., Moreno, A., Giralt, S., Martínez-Ruiz, F. and Jiménez-Espejo, F. (2011) Geochemical processes in a Mediterranean Lake: A high-resolution study of the last 4,000 years in Zoñar Lake, southern Spain. *J. Paleolimnol.*, **46**, 405–421.

McHenry, L.J., Kodikara, G.R.L., Stanistreet, I.G., Stollhofen, H., Njau, J.K., Schick, K. and Toth, N. (2020) Lake conditions and detrital sources of Paleolake Olduvai, Tanzania, reconstructed using X-ray Diffraction analysis of cores. *Palaeogeogr. Palaeoclimatol. Palaeoecol.*, **556**, 1–24.

Mees, F., Castañeda, C. and Van Ranst, E. (2011) Sedimentary and diagenetic features in saline lake deposits of the Monegros region, northern Spain. *Catena*. doi: 10.1016/j.catena.2011.01.010

MEI, M. (2007) *Revised Classification of Microbial Carbonates*:

Complementing the Classification of Limestones. *Earth Sci. Front.*, **14**, 222–232.

Mengistou, S. (2016) Invertebrates of East African Soda Lakes. In: *Soda Lakes of East Africa*, 205–226.

Mischke, S., Rajabov, I., Mustaeva, N., Zhang, C., Herzs Schuh, U., Boomer, I., Brown, E.T., Andersen, N., Myrbo, A., Ito, E. and Schudack, M.E. (2010) Modern hydrology and late Holocene history of Lake Karakul, eastern Pamirs (Tajikistan): A reconnaissance study. *Palaeogeogr. Palaeoclimatol. Palaeoecol.*, **289**, 10–24.

Mobberley, J.M., Khodadad, C.L.M. and Foster, J.S. (2013) Metabolic potential of lithifying cyanobacteria-dominated thrombolitic mats. *Photosynth. Res.*, **118**, 125–140.

Mobberley, J.M., Khodadad, C.L.M., Visscher, P.T., Reid, R.P., Hagan, P. and Foster, J.S. (2015) Inner workings of thrombolites: Spatial gradients of metabolic activity as revealed by metatranscriptome profiling. *Sci Rep.* doi: 10.1038/srep12601

Mono Lake Committee (2019) About Mono Lake. In: About Mono Lake. <https://www.monolake.org>.

Moore, J.N. (2016) Recent desiccation of Western Great Basin Saline Lakes: Lessons from Lake Abert, Oregon, U.S.A. *Sci. Total Environ.*, **554–555**, 142–154.

Moore, L.S. and Burne, R. V. (1987) Microbialites: organosedimentary deposits of benthic microbial communities. *Palaios*, **2**, 241–254.

Morellón, M., Pérez-Sanz, A., Corella, J.P., Büntgen, U., Catalán, J., González-Sampériz, P., González-Trueba, J.J., López-Sáez, J.A., Moreno, A., Pla-Rabes, S., Saz-Sánchez, M.A., Scussolini, P., Serrano, E., Steinhilber, F., Stefanova, V., Vegas-Vilarrúbia, T. and Valero-Garcés, B. (2012) A multi-proxy perspective on millennium-

long climate variability in the Southern Pyrenees. *Clim. Past* 8:683–700.

Morellón, M., Valero-Garcés, B., Anselmetti, F., Ariztegui, D.,

Schnellmann, M., Moreno, A., Mata, P., Rico, M. and Corella, J.P.

(2009a) Late quaternary deposition and facies model for karstic Lake Estanya (North-eastern Spain). *Sedimentology*, **56**, 1505–1534.

Morellón, M., Valero-Garcés, B., González-Sampériz, P., Vegas-

Vilarrúbia, T., Rubio, E., Rieradevall, M., Delgado-Huertas, A.,

Mata, P., Romero, Ó., Engstrom, D.R., López-Vicente, M., Navas,

A. and Soto, J. (2011) Climate changes and human activities

recorded in the sediments of Lake Estanya (NE Spain) during the

Medieval Warm Period and Little Ice Age. *J. Paleolimnol.*, **46**, 423–452.

Morellón, M., Valero-Garcés, B., Moreno, A., González-Sampériz, P.,

Mata, P., Romero, O., Maestro, M. and Navas, A. (2008) Holocene

palaeohydrology and climate variability in northeastern Spain: The

sedimentary record of Lake Estanya (Pre-Pyrenean range). *Quat. Int.*,

181, 15–31.

Morellón, M., Valero-Garcés, B., Vegas-Vilarrúbia, T., González-

Sampériz, P., Romero, Ó., Delgado-Huertas, A., Mata, P., Moreno,

A., Rico, M. and Corella, J.P. (2009b) Lateglacial and Holocene

palaeohydrology in the western Mediterranean region: The Lake

Estanya record (NE Spain). *Quat. Sci. Rev.*, **28**, 2582–2599.

Newman, S.A., Klepac-Ceraj, V., Mariotti, G., Pruss, S.B., Watson, N.

and **Bosak, T.** (2017) Experimental fossilization of mat-forming

cyanobacteria in coarse-grained siliciclastic sediments. *Geobiology*.

doi: 10.1111/gbi.12229

Nhu, V.H., Mohammadi, A., Shahabi, H., Shirzadi, A., Al-Ansari, N.,

- Ahmad, B. Bin, Chen, W., Khodadadi, M., Ahmadi, M., Khosravi, K., Jaafari, A. and Nguyen, H.** (2020) Monitoring and assessment of water level fluctuations of the lake urmia and its environmental consequences using multitemporal landsat 7 etm+ images. *Int. J. Environ. Res. Public Health*, **17**, 1–18.
- Nield, D.A., Simmons, C.T., Kuznetsov, A. V. and Ward, J.D.** (2008) On the evolution of salt lakes: Episodic convection beneath an evaporating salt lake. *Water Resour. Res.*, **44**, 1–17.
- Novikov, D.A., Chernykh, A. V. and Dultsev, F.F.** (2018) Geochemistry of brines in Vendian deposits of the Siberian platform. In: *IOP Conference Series: Earth and Environmental Science*, 193,
- O’Toole, G., Kaplan, H.B. and Kolter, R.** (2000) Biofilm formation as microbial development. *Annu. Rev. Microbiol.*, **54**, 49–79.
- Oduor, S.O. and Schagerl, M.** (2007) Phytoplankton primary productivity characteristics in response to photosynthetically active radiation in three Kenyan Rift Valley saline-alkaline lakes. *J. Plankton Res.*, **29**, 1041–1050.
- Orphan, V.J., Jahnke, L.L., Embaye, T., Turk, K.A., Pernthaler, A., Summons, R.E. and Des Marais, D.J.** (2008) Characterization and spatial distribution of methanogens and methanogenic biosignatures in hypersaline microbial mats of Baja California. *Geobiology*, **6**, 376–393.
- Ozguven, A. and Demir Yetis, A.** (2020) “Assessment of Spatiotemporal Water Quality Variations, Impact Analysis and Trophic Status of Big Soda Lake Van, Turkey. *Water. Air. Soil Pollut.*, **231**, 1–17.
- Paul, V.G., Wronkiewicz, D.J., Mormile, M.R. and Foster, J.S.** (2016) Mineralogy and microbial diversity of the microbialites in the Hypersaline Storr’s Lake, the Bahamas. *Astrobiology*, **16**, 282–300.
- Perry, R.S., Mcloughlin, N., Lynne, B.Y., Sephton, M.A., Oliver, J.D.,**

- Perry, C.C., Campbell, K., Engel, M.H., Farmer, J.D., Brasier, M.D.** and **Staley, J.T.** (2007) Defining biominerals and organominerals: Direct and indirect indicators of life. *Sediment. Geol.*, **201**, 157–179.
- Petryshyn, V.A., Juarez Rivera, M., Agić, H., Frantz, C.M., Corsetti, F.A.** and **Tripathi, A.E.** (2016) Stromatolites in Walker Lake (Nevada, Great Basin, USA) record climate and lake level changes ~35,000 years ago. *Palaeogeogr. Palaeoclimatol. Palaeoecol.*, **451**, 140–151.
- Pfennig, N.** and **Widdel, F.** (1982) The bacteria of the sulphur cycle. *Philos. Trans. R. Soc. Lond. B. Biol. Sci.*, **298**, 433–441.
- Philip, J.Y.N.** and **Mosha, D.M.S.** (2012) Salt Lakes of the African Rift System: A Valuable Research Opportunity for Insight into Nature's Concentrated Multi-Electrolyte Science. *Tanzania J. Sci.*, **38**, 1–13.
- Pienitz, R., Smol, J.P., Last, W.M., Leavitt, P.R.** and **Cumming, B.F.** (2000) Multi-proxy Holocene palaeoclimatic record from a saline lake in the Canadian Subarctic. *Holocene*, **10**, 673–686.
- Pinckney, J., Paerl, H.W.** and **Bebout, B.M.** (1995) Salinity control of benthic microbial mat community production in a Bahamian hypersaline lagoon. *J. Exp. Mar. Bio. Ecol.*, **187**, 223–237.
- Piovano, E.L., Ariztegui, D.** and **Moreiras, S.D.** (2002) Recent environmental changes in Laguna Mar Chiquita (central Argentina): A sedimentary model for a highly variable saline lake. *Sedimentology*, **49**, 1371–1384.
- Prieto-Barajas, C.M., Valencia-Cantero, E.** and **Santoyo, G.** (2018) Microbial mat ecosystems: Structure types, functional diversity, and biotechnological application. *Electron. J. Biotechnol.* 31:48–56.
- Reheis, M.C.** (1997) Dust deposition downwind of Owens (dry) Lake, 1991–1994: Preliminary findings. *J. Geophys. Res. Atmos.*, **102**, 25999–26008.

- Reinold, M., Wong, H.L., MacLeod, F.I., Meltzer, J., Thompson, A. and Burns, B.P.** (2019) The vulnerability of microbial ecosystems in a changing climate: Potential impact in shark bay. *Life*, **9**, 1–12.
- Rich, V.I. and Maier, R.M.** (2015) Chapter 6 - Aquatic Environments. In: (Ed. I.L. Pepper, C.P. Gerba, and T.J.B.T.-E.M. (Third E. Gentry), *Academic Press*, San Diego, 111–138.
- Riding, R.** (1991a) Classification of Microbial Carbonates. In: *Calcareous Algae and Stromatolites* (Ed. R. Riding), *Springer Berlin Heidelberg*, Berlin, Heidelberg, 21–51.
- Riding, R.** (1991b) Classification of Microbial Carbonates. In: *Calcareous Algae and Stromatolites* (Ed. R. Riding), *Springer Berlin Heidelberg*, Berlin, Heidelberg, Heidelberg, 21–51.
- Riding, R.** (2000) Microbial carbonates: The geological record of calcified bacterial-algal mats and biofilms. *Sedimentology*, **47**, 179–214.
- Riding, R.** (2011a) Microbialites, stromatolites, and thrombolites. In: *Encyclopedia of Earth Sciences Series*, 635–654.
- Riding, R.** (2011b) The nature of stromatolites: 3,500 million years of history and a century of research. *Lect. Notes Earth Sci.*, **131**, 29–74.
- Riding, R.** (1999) The term stromatolite: Towards an essential definition. *Lethaia*, **32**, 321–330.
- Riera, S., Wansard, G. and Julià, R.** (2004) 2000-Year environmental history of a karstic lake in the Mediterranean Pre-Pyrenees: The Estanya lakes (Spain). *Catena*
- Risacher, F., Alonso, H. and Salazar, C.** (2003) The origin of brines and salts in Chilean salars: A hydrochemical review. *Earth-Science Rev.*, **63**, 249–293.
- Roberts, S.M., Spencer, R.J. and Lowenstein, T.K.** (1994) Late Pleistocene saline lacustrine sediments, Badwater Basin, Death

Valley, California. *SEPM Core Work.*, **19**, 61–103.

Sala, R., Deom, J.M., Aladin, N. V., Plotnikov, I.S. and Nurtazin, S.

(2020) Geological History and Present Conditions of Lake Balkhash.

In: *Springer Water*, 143–175.

Sanz-Montero, M.E., Cabestrero, Ó. and Sánchez-Román, M. (2019)

Microbial Mg-rich carbonates in an extreme alkaline lake (Las Eras,

Central Spain). *Front. Microbiol.*, **10**, 1–15.

Schagerl, M. (2016) Soda lakes of East Africa. 1-408 pp.

Schagerl, M. and Renaut, R.W. (2016) Dipping into the Soda Lakes of

East Africa. In: *Soda Lakes of East Africa*, 3–24.

Schröder, T., van 't Hoff, J., Ortiz, J.E., de Torres Pèrez-Hidalgo, T.J.,

López-Sáez, J.A., Melles, M., Holzhausen, A., Wennrich, V.,

Viehberg, F. and Reicherter, K. (2018) Shallow hypersaline lakes as

paleoclimate archives: A case study from the Laguna Salada, Málaga

province, southern Spain. *Quat. Int.*, **485**, 76–88.

Seckbach, J. (2016) Microbes with Sediments STROMATOLITES :

Interaction of Microbes with Sediments, 1st edn. *Springer*, Dordrecht,

746 pp.

Semmani, N., Fournier, F., Léonide, P., Feist, M., Boularand, S. and

Borgomano, J. (2022) Transgressive-regressive cycles in saline lake

margin oolites: paleogeographic implications (Priabonian, Vistrenque

basin, SE France). *BSGF - Earth Sci Bull.* doi: 10.1051/bsgf/2022012

Severin, I., Acinas, S.G. and Stal, L.J. (2010) Diversity of nitrogen-fixing

bacteria in cyanobacterial mats. *FEMS Microbiol. Ecol.*, **73**, 514–525.

Shapiro, R.S. (2000) A comment on the systematic confusion of

thrombolites. *Palaios*, **15**, 166–169.

Simplicio, G., Basilici, G., Fernandes, L.R.M. and Sgarbi, G.N.C. (2017)

Temporal evolution of a Playa Lake: the sedimentary record of Quiricó

and Très Barras Formation (Sanfranciscana Basin, south-eastern Brazil). *Terrae*, **13**, 3–14.

Sofer, Z. (1978) Isotopic composition of hydration water in gypsum.

Geochim. Cosmochim. Acta, **42**, 1141–1149.

Solari, M.A., Hervé, F., Le Roux, J.P., Airo, A. and Sial, A.N. (2010)

Paleoclimatic significance of lacustrine microbialites: A stable isotope case study of two lakes at Torres del Paine, southern Chile.

Palaeogeogr. Palaeoclimatol. Palaeoecol., **297**, 70–82.

Steinman, B.A. and Abbott, M.B. (2013) Isotopic and hydrologic

responses of small, closed lakes to climate variability: Hydroclimate reconstructions from lake sediment oxygen isotope records and mass balance models. *Geochim. Cosmochim. Acta*, **105**, 342–359.

Suarez-Gonzalez, P., Benito, M.I., Quijada, I.E., Mas, R. and Campos-

Soto, S. (2019) 'Trapping and binding': A review of the factors controlling the development of fossil agglutinated microbialites and their distribution in space and time. *Earth-Science Rev.* 194:182–215.

Sumner, D.Y. (2000) Microbial vs Environmental Influences on the

Morphology of Late Archean Fenestrate Microbialites. In: *Microbial Sediments*, 307–314.

Suosaari, E.P., Awramik, S.M., Reid, R.P., Stolz, J.F. and Grey, K.

(2018) Living dendrolitic microbial mats in hamelin pool, Shark Bay, Western Australia. *Geosci.*, **8**, 1–17.

Susarla, V.R.K.S., Parekh, J.M. and Chitnis, U. V. (1991) Recovery of

sodium chloride, sodium sulphate and sodium carbonate from Sambhar Lake brine-A theoretical study. *Proc. Indian Acad. Sci. - Chem. Sci.*, **103**, 9–16.

ten Brink, T. (1998) The dead sea, the lake and its setting. *Eos, Trans.*

Am. Geophys. Union, **79**, 239–239.

- Tosti, F. and Riding, R.** (2017) Fine-grained agglutinated elongate columnar stromatolites: Tieling Formation, ca 1420 Ma, North China. *Sedimentology*, **64**, 871–902.
- Trichet, J. and Défarge, C.** (1995) Non-biologically supported organomineralization. In: *Bulletin de l'Institut Océanographique de Monaco*, *Bulletin de l'Institut Océanographique de Monaco*, **14**, 203–236.
- Tweed, S., Grace, M., Leblanc, M., Cartwright, I. and Smithyman, D.** (2011) The individual response of saline lakes to a severe drought. *Sci. Total Environ.*, **409**, 3919–3933.
- USGS** (2021) USGS Water Data for USA, National Water Information System: Web Interface. In: USGS 10254005 Salt. SEA NR Westmorl. CA. <https://waterdata.usgs.gov/nwis>.
- Valdespino-Castillo, P.M., Hu, P., Merino-Ibarra, M., López-Gómez, L.M., Cerqueda-García, D., Zayas, R.G. De, Pi-Puig, T., Lestayo, J.A., Holman, H.Y. and Falcón, L.I.** (2018) Exploring biogeochemistry and microbial diversity of extant microbialites in Mexico and Cuba. *Front. Microbiol.*, **9**, 1–22.
- Valero-Garcés, B.L., González-Sampériz, P., Navas, A., Machín, J., Mata, P., Delgado-Huertas, A., Bao, R., Moreno, A., Carrión, J.S., Schwalb, A. and González-Barrios, A.** (2006) Human impact since medieval times and recent ecological restoration in a Mediterranean lake: The Laguna Zoñar, southern Spain. *J. Paleolimnol.*, **35**, 441–465.
- Valero-Garcés, B.L. and Kelts, K.R.** (1995) A sedimentary facies model for perennial and meromictic saline lakes: Holocene Medicine Lake Basin, South Dakota, USA. *J. Paleolimnol.*, **14**, 123–149.
- Valero-Garcés, B.L., Navas, A., Machin, J., Stevenson, T., Davis, B.,**

- Valero-Garcés, B.L., Navas, A., Machin, J., Stevenson, T., Davis, B., Valero-Garcés, B.L., Navas, A., Machin, J., Stevenson, T. and Davis, B.** (2000) Responses of a Saline Lake Ecosystem in a Semiarid Region to Irrigation and Climate Variability. *AMBIO A J. Hum. Environ.*, **29**, 344–350.
- van Gernerden, H.** (1993) Microbial mats: A joint venture. *Mar. Geol.*, **113**, 3–25.
- Vaughan, D.J. and Lloyd, J.R.** (2011) Mineral-organic-microbe interactions: Environmental impacts from molecular to macroscopic scales. *Comptes Rendus Geosci.*, **343**, 140–159.
- Vegas-Vilarrúbia, T., González-Sampériz, P., Morellón, M., Gil-Romera, G., Pérez-Sanz, A. and Valero-Garcés, B.** (2013) Diatom and vegetation responses to late glacial and early holocene climate changes at lake estanya (southern pyrenees, NE Spain). *Palaeogeogr. Palaeoclimatol. Palaeoecol.*, **392**, 335–349.
- Vicente-Serrano, S.M., Beguería, S., López-Moreno, J.I., García-Vera, M.A. and Stepanek, P.** (2010) A complete daily precipitation database for northeast Spain: Reconstruction, quality control, and homogeneity. *Int. J. Climatol.*, **30**, 1146–1163.
- Vidondo, B., Martínez, B., Montes, C. and Guerrero, M.C.** (1993) Physico-chemical characteristics of a permanent Spanish hypersaline lake: La Salada de Chiprana (NE Spain). *Hydrobiologia*, **267**, 113–125.
- Villanueva, L., Navarrete, A., Urmeneta, J., White, D.C. and Guerrero, R.** (2007) Analysis of diurnal and vertical microbial diversity of a hypersaline microbial mat. *Arch. Microbiol.*, **188**, 137–146.
- Visscher, P.T., Prins, R.A. and van Gernerden, H.** (1992) Rates of sulfate reduction and thiosulfate consumption in a marine microbial mat.

FEMS Microbiol. Lett., **86**, 283–294.

- Visscher, P.T.** and **Stolz, J.F.** (2005) Microbial mats as bioreactors: Populations, processes, and products. *Palaeogeogr. Palaeoclimatol. Palaeoecol.*, **219**, 87–100.
- Walther, M., Tserendorj, G.** and **Enkhjargal, O.** (2016) Environmental changes of Orog Nuur (Bayan Khongor Aimag , South Mongolia). Lake deposits , paleo- shorelines and vegetation history . - Biological Resources of Mongolia ; Halle .
- Wang, J., Wu, J., Zhan, S.** and **Zhou, J.** (2021) Records of hydrological change and environmental disasters in sediments from deep Lake Issyk-Kul. *Hydrol Process.* doi: 10.1002/hyp.14136
- Weiner, S.** and **Addadi, L.** (2011) Crystallization pathways in biomineralization. *Annu. Rev. Mater. Res.*, **41**, 21–40.
- Wendt, J.** (1993) Solenoporacean Stromatolites. *Palaios.* doi: 10.2307/3515224
- Williams, W.D.** (2002) Environmental threats to salt lakes and the likely status of inland saline ecosystems in 2025. *Environ. Conserv.*, **29**, 154–167.
- Williams, W.D.** (1995) Lake Corangamite, Australia, a permanent saline lake: Conservation and management issues. *Lakes Reserv. Res. Manag.*, **1**, 55–64.
- Wright, V.D., Hornbach, M.J., Mchugh, C.** and **Mann, P.** (2015) Factors Contributing to the 2005-Present, Rapid Rise in Lake Levels, Dominican Republic and Haiti (Hispaniola). *Nat. Resour.*, **06**, 465–481.
- Wright, V.P.** and **Barnett, A.J.** (2015) An abiotic model for the development of textures in some South Atlantic early Cretaceous lacustrine carbonates. *Geol. Soc. Spec. Publ.*, **418**, 209–219.
- Wurtsbaugh, W.A., Miller, C., Null, S.E., Justin De Rose, R., Wilcock,**

- P., Hahnenberger, M., Howe, F. and Moore, J.** (2017) Decline of the world's saline lakes. *Nat. Geosci.*, **10**, 816–821.
- Yapiyev, V., Sagintayev, Z., Inglezakis, V.J., Samarkhanov, K. and Verhoef, A.** (2017) Essentials of Endorheic Basins and Lakes: A Review in the Context of Current and Future Water Resource Management and Mitigation Activities in Central Asia. *Water* **9**:
- Yechieli, Y. and Ronen, D.** (1997) Early diagenesis of highly saline lake sediments after exposure. *Chem. Geol.*, **138**, 93–106.
- Yechieli, Y. and Wood, W.W.** (2002) Hydrogeologic processes in saline systems: Playas, sabkhas, and saline lakes. *Earth-Science Rev.*, **58**, 343–365.
- Zaixing, J. and Chao, L.** (2021) Modern Sedimentary Systems of Qinghai Lake. 513–548.
- Zheng, P.R., Li, C.H., Ye, C., Wang, H., Wei, W.W., Zheng, Y. and Zheng, X. yong** (2022) Characteristic and affecting factors of wetland herbs' distribution in the radiant belt toward land of lake–terrestrial ecotone in Tibet, China. *Environ Sci Eur.* doi: 10.1186/s12302-022-00593-4
- Zolitschka, B.** (2013) VARVED LAKE SEDIMENTS. In: (Ed. S.A. Elias and C.J.B.T.-E. of Q.S. (Second E. Mock), *Elsevier*, Amsterdam, 573–581.

Chapter 3 - Regional Setting & Methodological

Approach

3.1 Introduction

This chapter describes the regional, geological and geomorphological setting of the saline lakes and microbialites located throughout the Iberian Peninsula that were investigated in this study, and the methods used to study these settings and the microbial mats they contain.

3.2 Saline lakes and microbial mats in the Iberian Peninsula

In Europe, saline lakes are strongly distributed throughout much of the Iberian peninsula (Comin & Alonso, 1988; Kortekaas *et al.*, 2009). Many such lakes occurring in this area are associated with the arid to semi-arid basins that occupy the peninsula and occur in groups known as “endorheic centres” (Figure 3.1) (Vergés & Fernández, 2006). Many of the lagoons and lakes are however ephemeral and undergo significant drawdown and subsequently desiccate in the summer period or during times of drought (Páscoa *et al.*, 2017). In winter and spring, when precipitation increases, their water levels recover and they expand throughout their drainage basin (Comin & Alonso, 1988). This subsequently establishes significant temporal fluctuations in the water levels of many Iberian saline lacustrine systems (Schröder *et al.*, 2018) and therefore in the characteristics of many of these systems (Kortekaas *et al.*, 2009).

A wide spectrum of environmental factors acting upon Iberian saline lakes lead to the development of highly diverse microbiological communities within these environments (Guerrero, 1992; Kortekaas *et al.*, 2009). In some cases, such communities occur as inconspicuous groups of bacteria which are distributed throughout the lake-bed

(Martínez-Alonso *et al.*, 2008). In other cases, complex microbial mats with established functional groups of microbes develop (Guerrero *et al.*, 2002; Jonkers *et al.*, 2003). These mats have been described in a range of permanent and ephemeral saline, alkaline and hypersaline lakes and lagoons throughout much the peninsula (Guerrero and de Wit, 1992). Due to the highly variable physicochemical and environmental conditions which govern many Iberian saline lakes (Alonso, 1998) and subsequently the mats themselves, such lakes represent important settings where the characteristics of microbial mats and their responses to environmental and anthropogenic change can be studied (Alonso, 1998). Additionally, several saline and brackish lakes occurring throughout the peninsula also contain evidence of microbial mat development within their recent Holocene sedimentary records (Valero-Garcés & Moreno, 2011; Valero-Garcés *et al.*, 2014). Such examples of sub-recent and Holocene-age microbial mats and microbialites occurring within these settings provide strong potential for producing geochemical and climatic reconstructions (Bourillot *et al.*, 2020), whilst simultaneously acting as indicators of past biological processes (Tunis *et al.*, 2011).

In this project, several lacustrine sites containing unique sedimentary sequences and examples of both contemporary (1-10 yrs BP) and sub-recent (50-11,000 yrs BP) microbial mats/microbialites were investigated. Detailed analyses of the sedimentology of each site were undertaken (appendix 2). Comparisons of modern environmental processes with analogous fossil microbial structures preserved in Holocene-aged core material were also carried out. A range of geological, geochemical and limnological techniques were further undertaken as described throughout this chapter in order to improve the overall understanding of variations in lacustrine sedimentology and geochemistry and the potential for these systems to act as palaeoenvironmental repositories.

3.3 Site Justification and Overview

Four sites were investigated in this study (Figure 3.2) which contained variable sedimentological records and either actively developing or sub-recent microbial mats within these records. The sedimentological sequence of each lake was described or analysed from pre-existing investigations, and sites with developing mats were monitored for limnological variations. Actively developing and sub-recent Holocene-age mats were also investigated to determine the effects of environmental factors on microbial communities occurring in these settings.

Justification of the sites chosen for this study was undertaken based on both the understanding of the sites from a sedimentological and geochemical perspective and based on the presence and abundance of microbial mats in the saline inland lakes of the Iberian Peninsula (Guerrero and de Wit, 1992). In the case of sedimentology and geochemistry, Lake Chiprana was chosen due to the absence of any multi-core study undertaken on the lake and to improve upon previous single core studies carried out here (Valero-Garcés *et al.*, 2000). In the case of microbial mats, a spectrum of such structures have been discovered in many of these lakes, but they are not always conspicuous features of every lake setting. Sites for the study of microbial mats were subsequently chosen based on the water chemistry of each setting and the preservation of microbial structures both within the contemporary lake waters and within the sedimentological record. In the case of modern microbial mats, at Laguna Salada de Chiprana, despite heavy evaporative losses in summer months, the waters are permanent and as such harbour permanently developing communities of microbial mats. This was therefore subjected to a limnological study in order to determine the effects of annual variations in water geochemistry and climatic factors on microbial mat development. This will be done in order to investigate the short-term development of these mats and the effects of environmental fluctuations on the presence of microbial community composition, bulk geochemistry and the interactions that occur between microbes and mineral products.

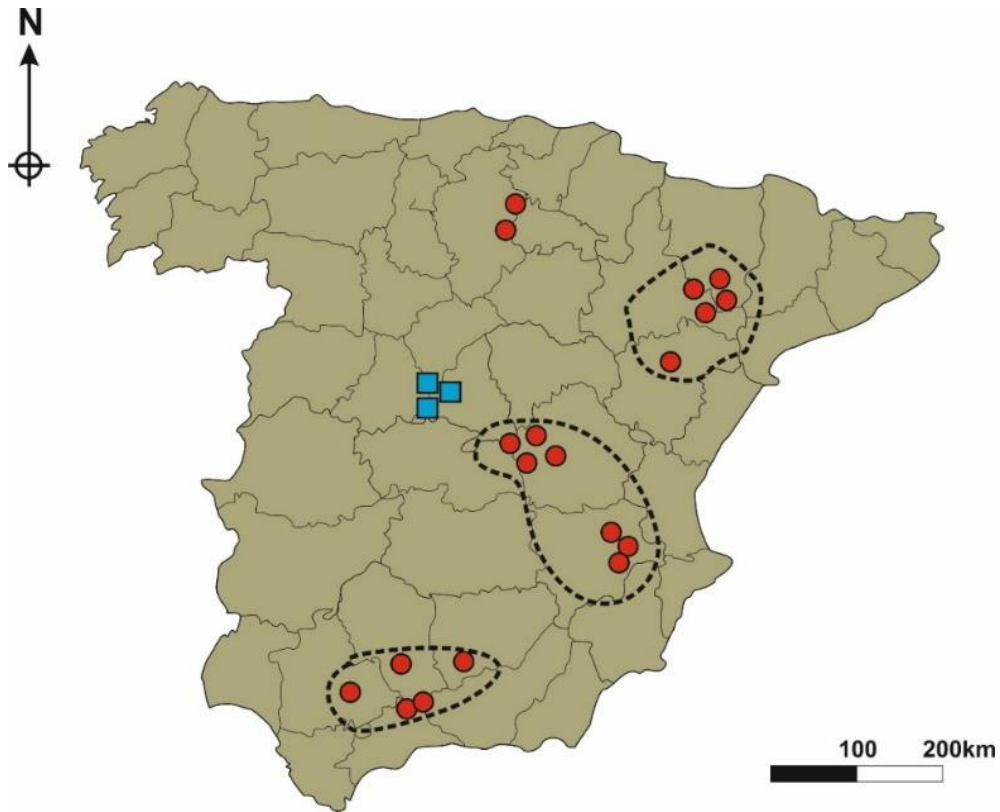


Figure 3.1 – Map displaying the location of various groups of saline and alkaline lakes occurring throughout the Iberian Peninsula. Red circles = Saline lakes, Blue squares = alkaline lakes, with the saline lakes being bounded by endorheic centres as indicated by the extent of the dashed lines. Saline and alkaline lakes are an inherent feature of the Iberian Peninsula and are present in many locations, but those highlighted here represent some of the primary lacustrine complexes with microbial mats developing within them. Modified from Guerrero and de Wit, (1992).

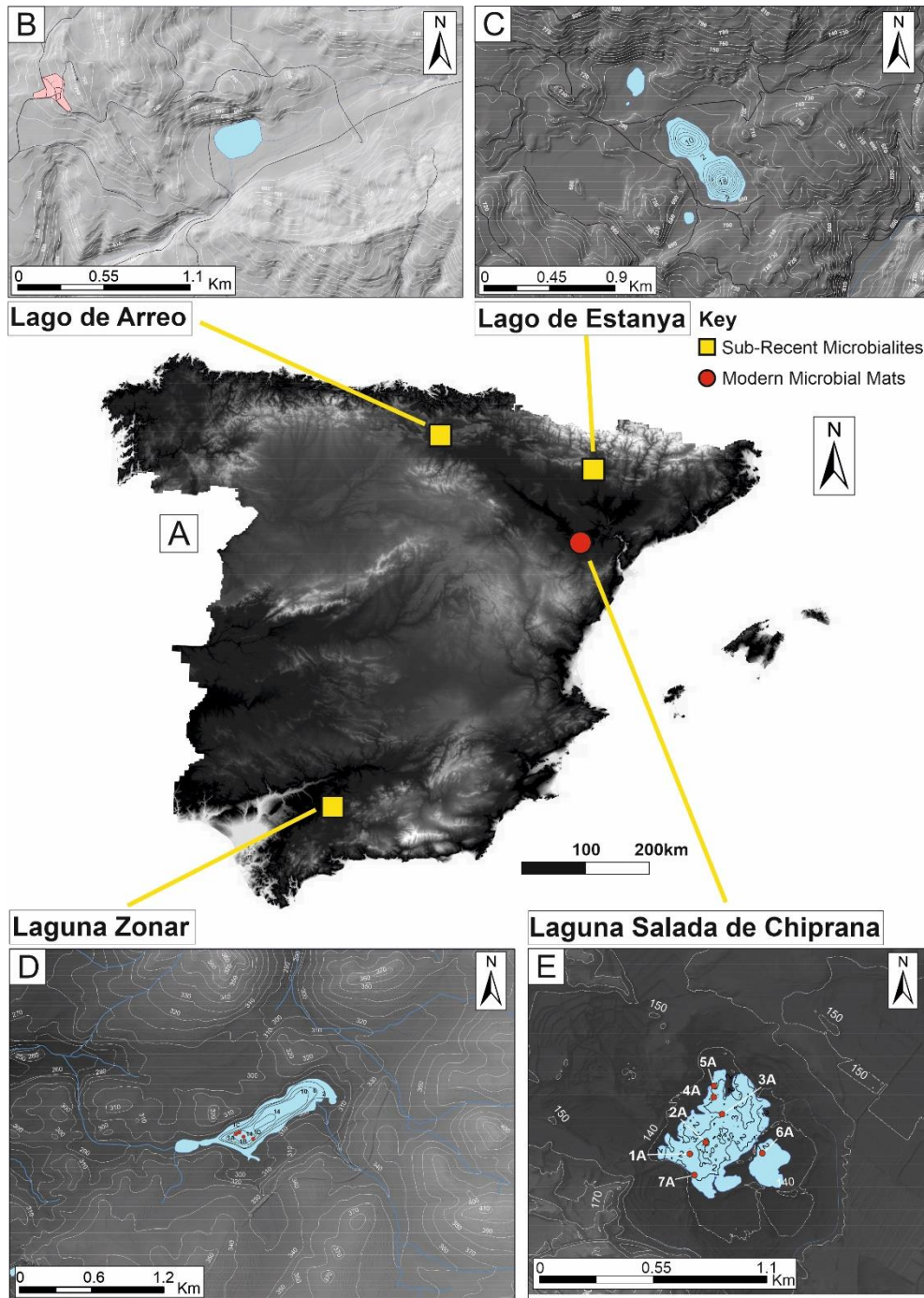


Figure 3.2 – Digital elevation model of the Iberian Peninsula with the sites containing actively developing microbial mats that will be investigated and discussed throughout this study. Data modelled from CNIG (<https://centrodedescargas.cnig.es/CentroDescargas/index.jsp#>).

Table 3.1 – Summary of the characteristics and location of the four lakes investigated in this project.

Site	Latitude	Longitude	Surface Area (km ²)	Hydrochemistry
Lago de Arreo	42°46'41.5"N	2°59'28.0"W	0.071	Subsaline, calcium/magnesium-rich
Lago de Estanya	42°01'43.3"N	0°31'43.3"E	0.144	Brackish, sulphate/calcium-rich
Laguna Salada de Chiprana	41°14'26.8"N	0°10'59.1"W	0.27km ²	Hypersaline, sulphate- rich
Laguna Zonar	37°28'57.7"N	4°41'29.7"W	0.381	Saline, chloride/sulphate-rich

3.3.1 Laguna Salada de Chiprana

Laguna Salada de Chiprana (41°14'30"N, 0°10'50"W) is a small, permanent saline-hypersaline lake complex situated in the endorheic Ebro Basin of Northeast Spain, close to the small municipality of Chiprana (Valero-Garces *et al.*, 2000; Doyle *et al.*, 2022)(see Figure 3.3). The lake is documented as the sole hypersaline lagoon found within Spain, and displays a maximum depth of ~5.6m recorded in 2000 (Valero-Garcés *et al.*, 2000; Doyle *et al.*, 2022), being situated approximately ~140m above sea level.

3.3.2 Lago de Estanya

Lago de Estanya (42°01'44.2"N 0°31'44.2"E) is a 2.45km² karstic lake situated approximately 670m above sea level in the Pre-Pyrenean Ranges of the Iberian Peninsula (Morellón *et al.*, 2009a; b), North-eastern Spain, near the small municipality of Estaña (Riera *et al.*, 2004). The lake structure is postulated to have developed as a result of the generation of karstic sinkholes associated with Upper Triassic evaporites and carbonates beneath the lake (IGME, 2003; Morellón *et al.*, 2009a), leading to the development of two segmented basins with depths of ~10 and ~20m (Morellón *et al.*, 2009a; b)(Figure 3.4).

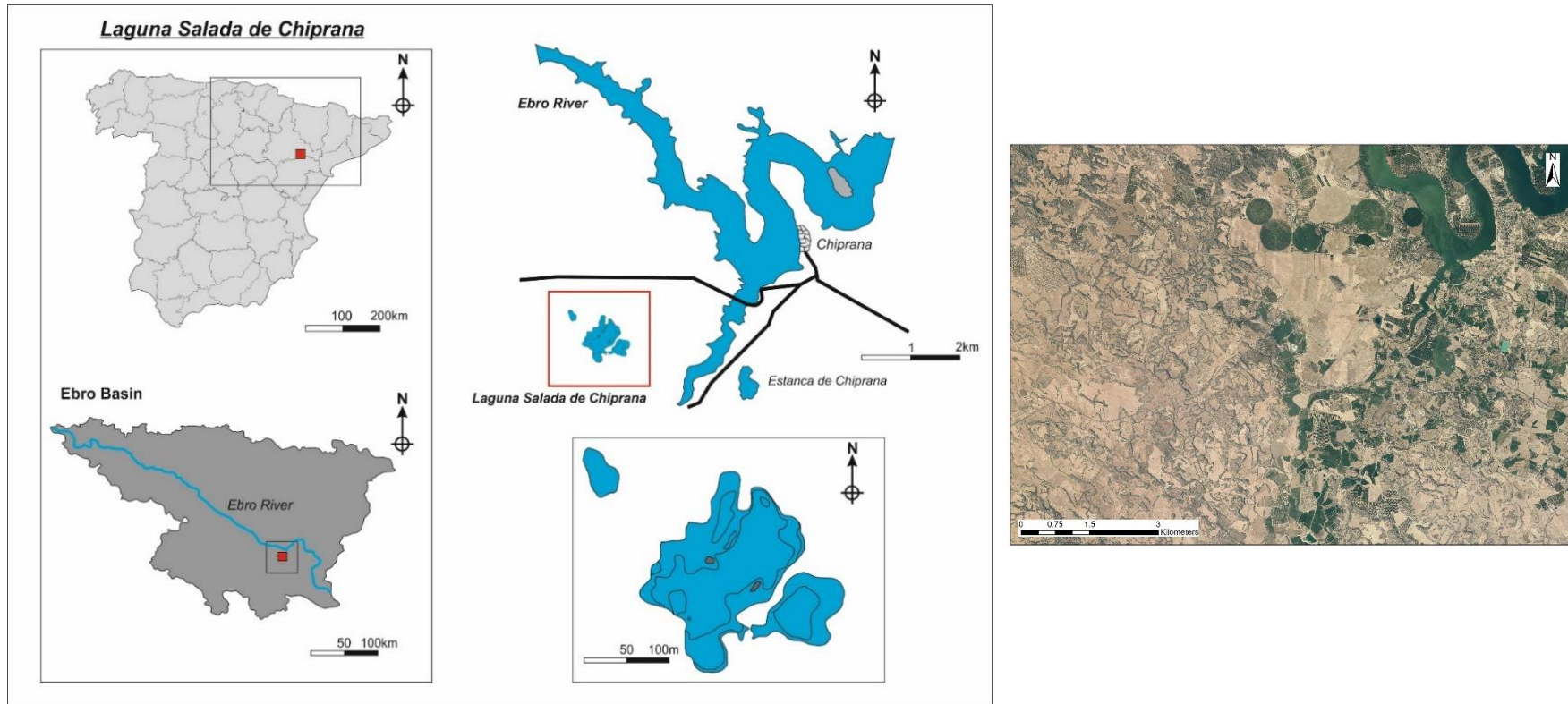


Figure 3.3 - Maps illustrating the location, morphology and bathymetry of Laguna Salada de Chiprana in the Ebro Basin, Northeast Spain with orthophoto satellite image. Data modelled from CNIG.

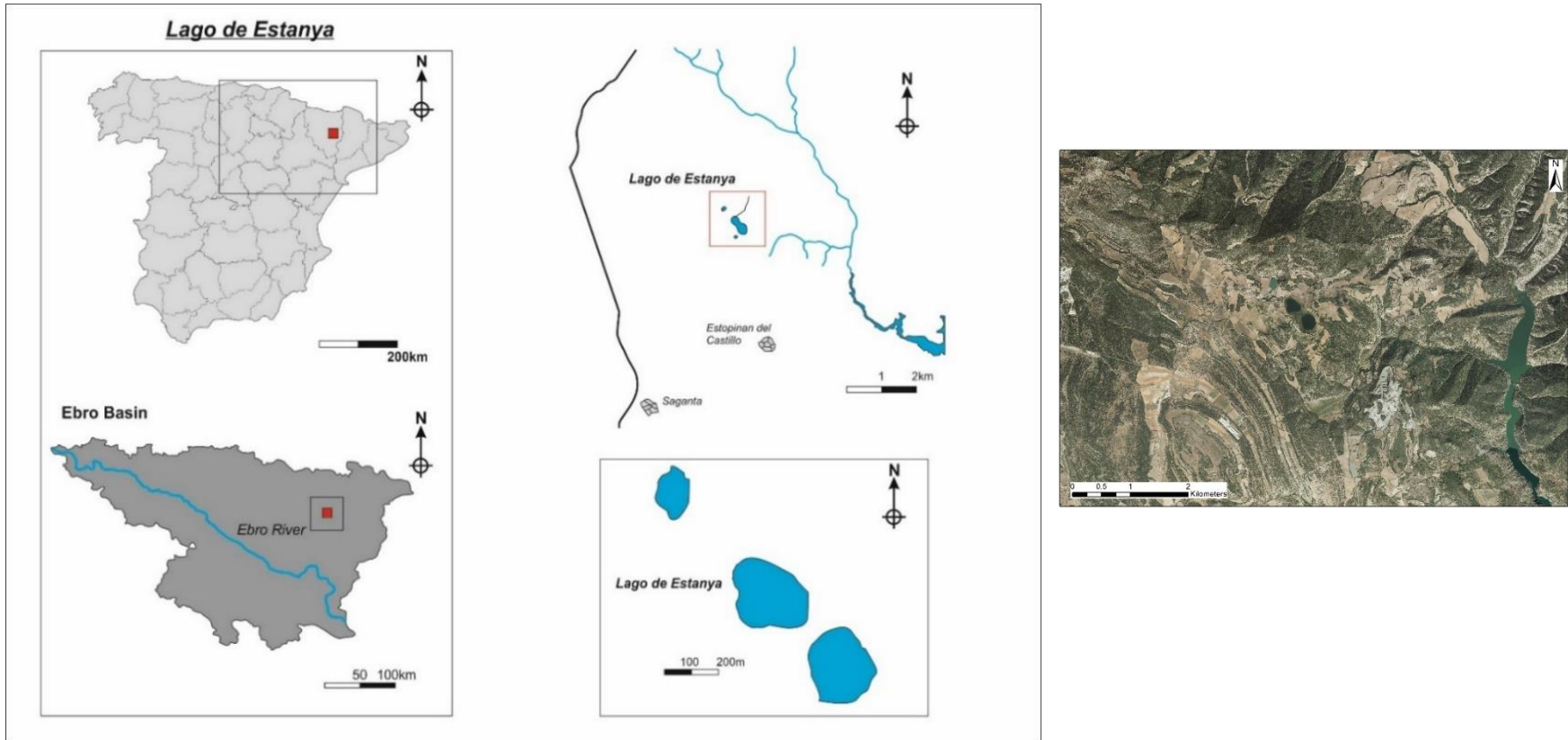


Figure 3.4 - Maps illustrating the location and morphology of Lago de Estanya in the Ebro Basin with accompanying orthophoto satellite image. The site is situated near the town of Estaña and is represented by two karstic sinkholes infilled by brackish lake-waters. Data modelled from CNIG.

3.3.3 Laguna Zonar

Laguna Zonar (37°29'00"N, 4°41'22"W) is a saline lake situated in the Córdoba province of Southern Spain at approximately 300 metres above sea level. The lake is a 0.37km², approximately 15m deep waterbody that developed in response to the dissolution and collapse of underlying karstic structures (Martín-Puertas *et al.*, 2011; Valero-Garcés *et al.*, 2014)..

3.3.4 Lago de Arreo

Lago de Arreo (42° 46' N, 2° 59' W;) is a small, 24 metre deep karstic lake situated in the western Ebro Basin in Northeast Spain at approximately 655 m above sea level (Figure 3.6) (Morellón *et al.*, 2012; Corella *et al.*, 2013). It overlies a mixed geology of intercalated Triassic clays, evaporites and gypsum formations with some volcanic rocks also being present in the area (Corella *et al.*, 2011a).

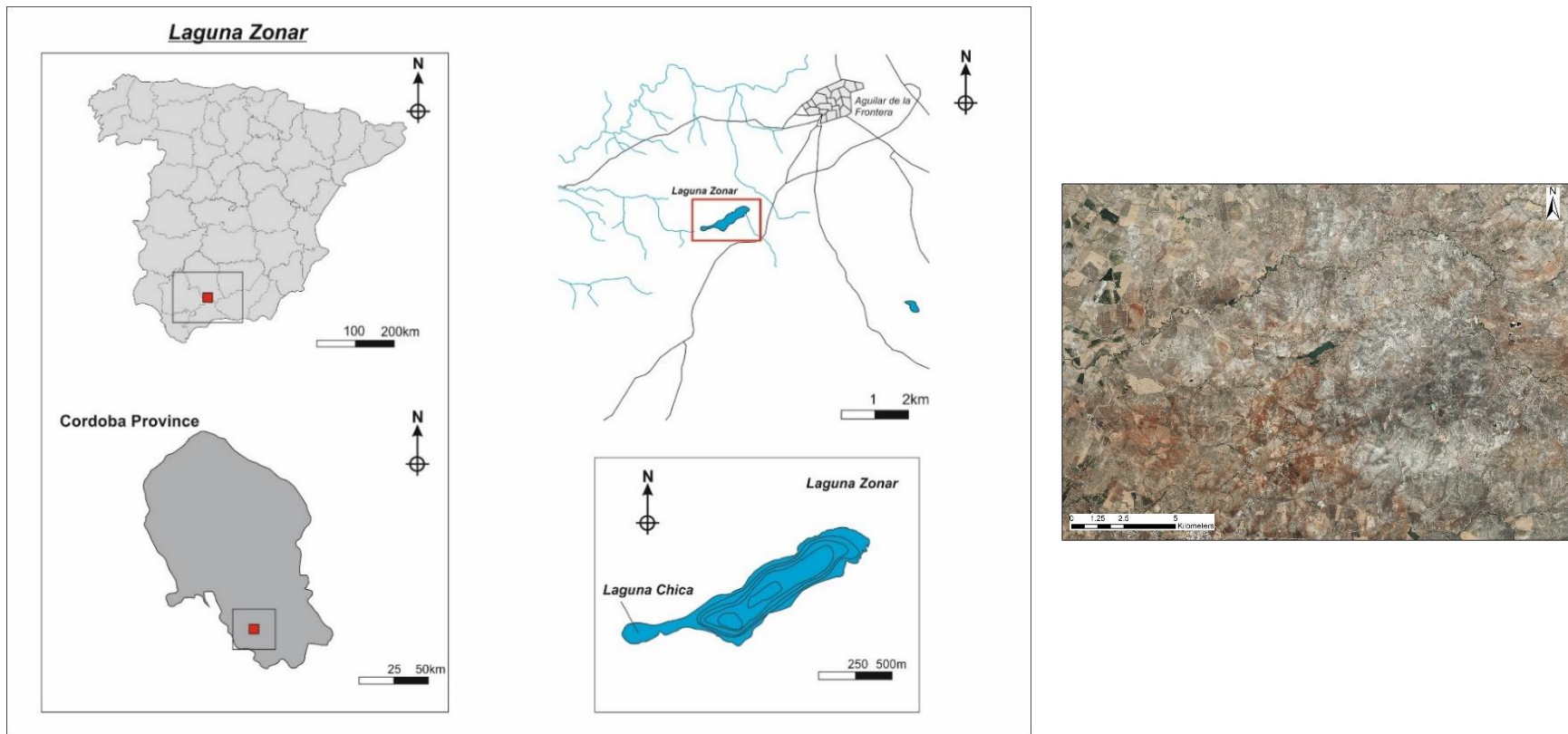


Figure 3.5 - Maps illustrating the location of Laguna Zonar in Cordoba, South Spain orthophoto satellite image. The lake is located approximately 3-4km from the small village of Aguilar de la Frontera, and is represented by a 0.37km² water body of saline chemistry. Data modelled from CNIG

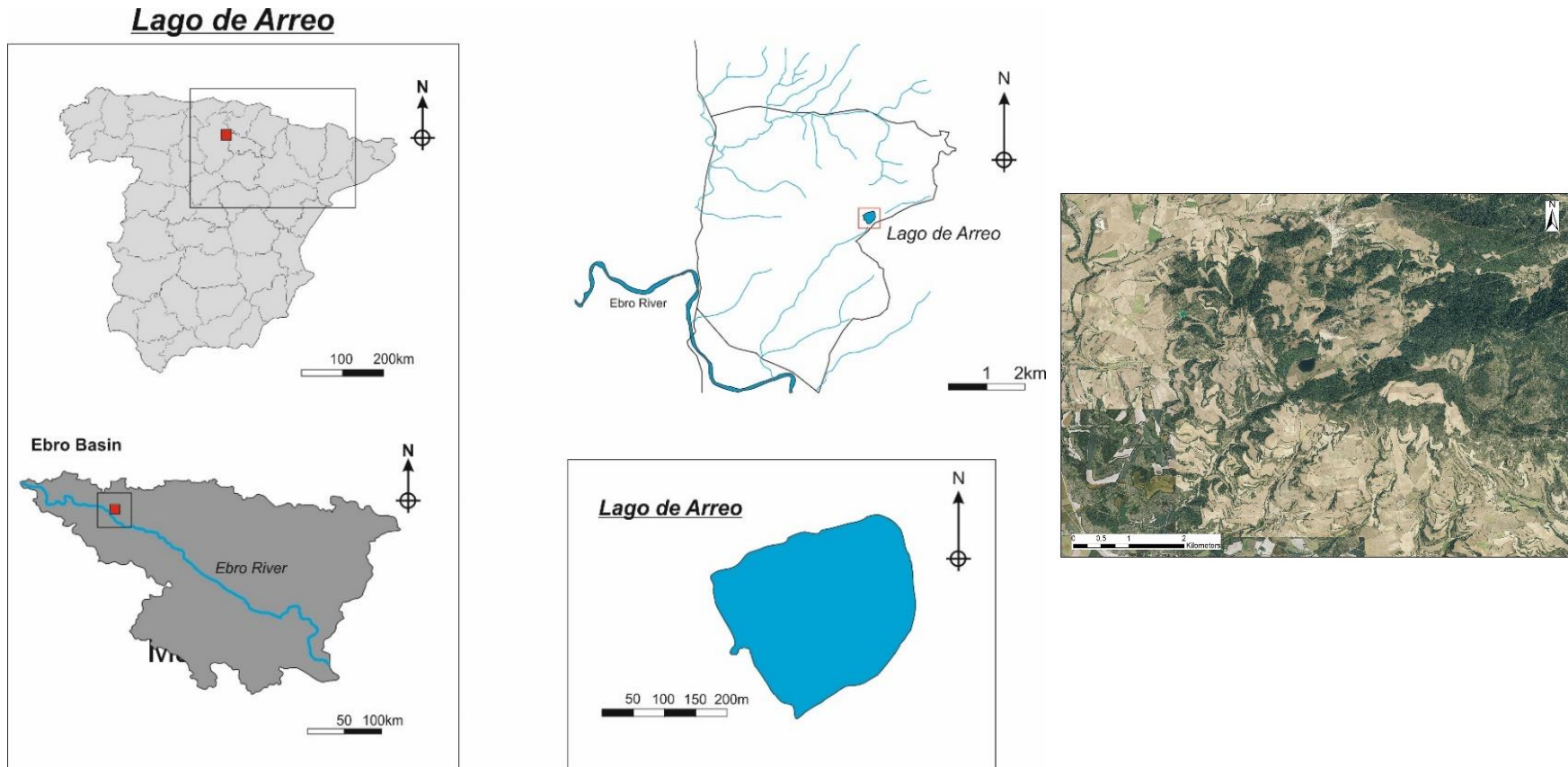


Figure 3.6 - Maps illustrating the location of Lago de Arreo in the Basque Country, Northern Spain with orthophoto satellite image. The lake is located 10km from the nearby town of Miranda de Ebro, and is currently brackish in composition. Microbial mats are not present in the contemporary lake waters, but potential microbialite formation has been documented in core sediments. Data modelled from CNIG.

3.4 Methodological Approach

3.4.1 Fieldwork, Sample Collection & Preparation

Fieldwork was undertaken over a three-year period to several of the sites investigated in this project and also to the Instituto Pirenaico de Ecologia to collect samples. Field visits were undertaken to Lake Chiprana and Lake Estanya in October 2018, March 2019, November 2019, and December 2021. However, field visits were not undertaken to Lake Arreo and Lake Zonar due to all relevant material being available at the Instituto Pirenaico de Ecologia.

Samples utilised for the project include whole sediment cores and subsamples, modern and actively developing microbial mats retrieved from the lake-bed and sub-fossil mats sampled from such sediment cores, and various sediment and water samples collected from the lakes. Short sediment cores measuring between 27 and 50cm in length were sampled from several areas of Lake Chiprana by dropping a UWITEC® gravity corer from a pneumatic boat (Doyle *et al.*, 2022). Six of the seven cores were taken in a NE-SW transect across the primary waterbody (Table 3.1), including sediments from both the littoral and profundal sub-environments, while the single remaining core was retrieved from the profundal setting in the smaller side lagoon of Lake Chiprana (Doyle *et al.*, 2022). Sub-samples from cores were taken every 0.5cm. Samples for thin section analysis were removed using a plastic slab and a wire cutter (see Figure 3.7), and half of the depth of the sediments in the core was removed such that material was left for further analysis. Several modern lakebed samples were also retrieved at a depth of approximately 30cm using a trowel from several sampling points around the lake.

These fresh sediment and microbial mat samples collected both from lake beds and core were however saturated with lake-water. The water saturation of the samples presented an obstacle in the preparation of thin sections, as this water required removal prior to

the sediments being cut into sections. To achieve this, a method to remove water from the sections by shock and freeze drying followed by subsequent impregnation of dried sediments with an epoxy resin (EpoFlo) (LacCore & CSDCO) was undertaken (see Corella *et al.*, 2011b) as detailed below. This technique involved the use of both shock- and freeze-drying of wet lake sediment slabs to remove moisture for subsequent impregnation by epoxy resin and is detailed in Figure 3.7. Liquid nitrogen was then poured into a Styrofoam cooler to a depth of 40-50cm, and sampled sediment slabs were lowered into the container using tongs and submerged for 5-10 minutes. Samples were removed from the container and transferred to a freeze for 3-5 days depending on the overall moisture content. Samples were finally removed from the freeze dryer and placed into their corresponding slabbing boxes to be transferred to a disposable aluminium tray used for vacuum and subsequent resin impregnation.

Table 3.1 – Locations of sediment cores investigated throughout this project. S = Surface, W = Water

Site	Core/Sample	Location	Water Depth (m)
Laguna Salada de Chiprana	CHI07-1A	N41.23957, W000.18393	~4m
Laguna Salada de Chiprana	CHI19-1A	N41.23937, W000.18482	3.7
Laguna Salada de Chiprana	CHI19-2A	N41.23989, W000.18378	3.6
Laguna Salada de Chiprana	CHI19-3A	N41.24120, W000.18270	3.5
Laguna Salada de Chiprana	CHI19-4A	N41.24202, W000.18318	1.2
Laguna Salada de Chiprana	CHI19-5A	N41.24255, W000.18315	1.2
Laguna Salada de Chiprana	CHI19-6A	N41.23929, W000.18026	2.7
Laguna Salada de Chiprana	CHI19-7A	N41.23836, W000.18456	1.4
Laguna Salada de Chiprana	S1/W1	41°14'21.0"N 0°11'08.8"W	0.3
Laguna Salada de Chiprana	S2/W2	41°14'22.7"N 0°11'09.4"W	0.2
Laguna Salada de Chiprana	S3/W3	41°14'22.8"N 0°10'50.8"W	0.3
Laguna Salada de Chiprana	S4/W4	41°14'23.5"N 0°10'50.4"W	0.2
Laguna Salada de Chiprana	S5/W5	41°14'24.0"N 0°10'49.7"W	0.2

Laguna Salada de Chiprana	W6	41°14'24.4"N 0°11'03.7"W	0.1-4
Lago de Arreo	CAI04-1A/1B-4	42°46'43.4"N 2°59'30.9"W	~24
Lago de Arreo	CAI04-1A/1B-5	42°46'43.4"N 2°59'30.9"W	~24
Lago de Arreo	CAI04-1A/1B-6	42°46'43.4"N 2°59'30.9"W	~24
Lago de Estanya	LEG04-1K-1A	42°01'39.3"N 0°31'47.4"E	~16
Lago de Estanya	LEG04-1K-3A	42°01'38.4"N 0°31'49.8"E	~16
Lago de Estanya	LEG04-1K-4A	42°01'49.1"N 0°31'40.1"E	~14-15
Laguna Zonar	ZON04-1A-1	37°28'52.8"N 4°41'40.5"W	~14
Laguna Zonar	ZON04-1C-1	37°28'52.7"N 4°41'40.7"W	~14

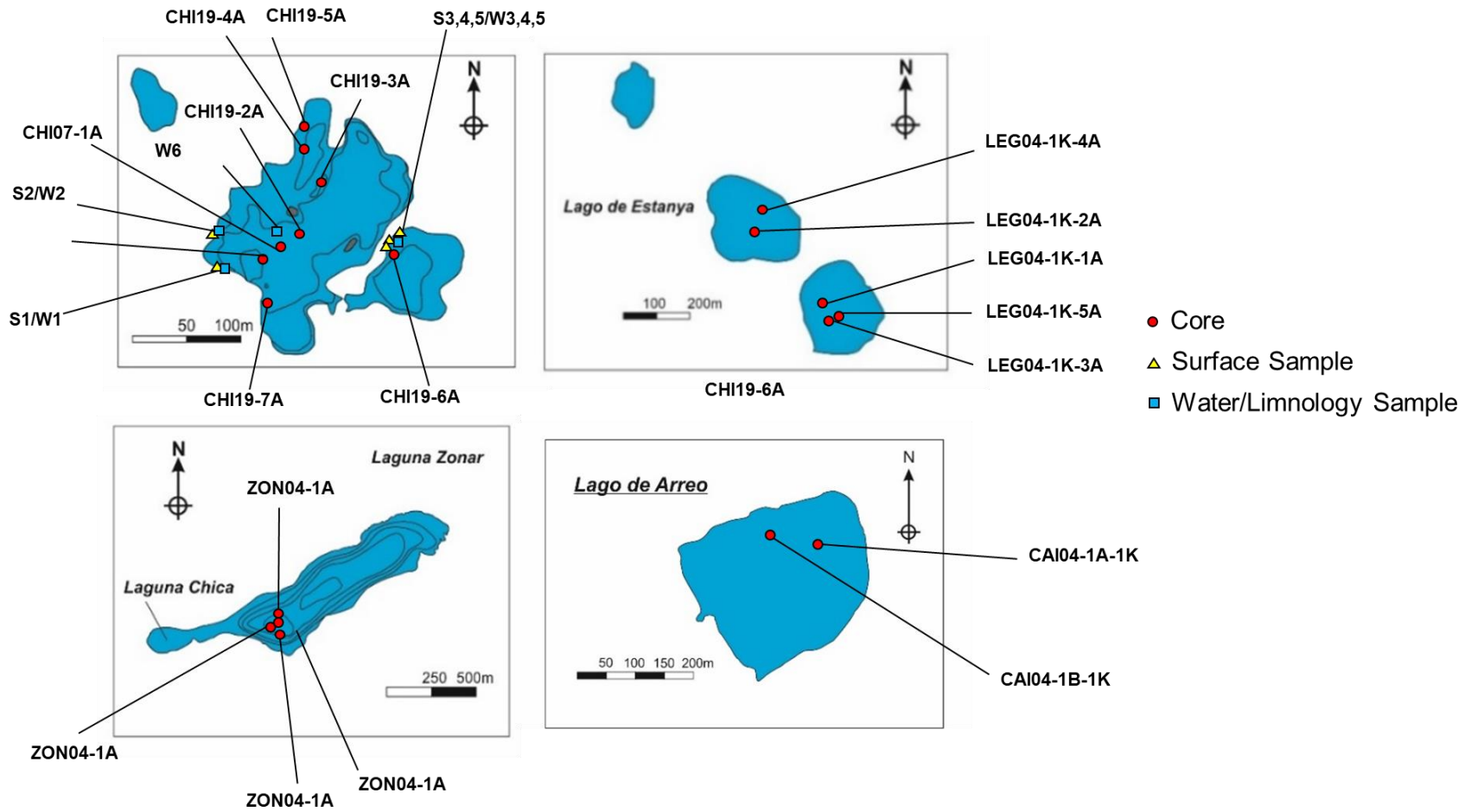


Figure 3.7 – Locations of samples and cores investigated in each of the lakes.

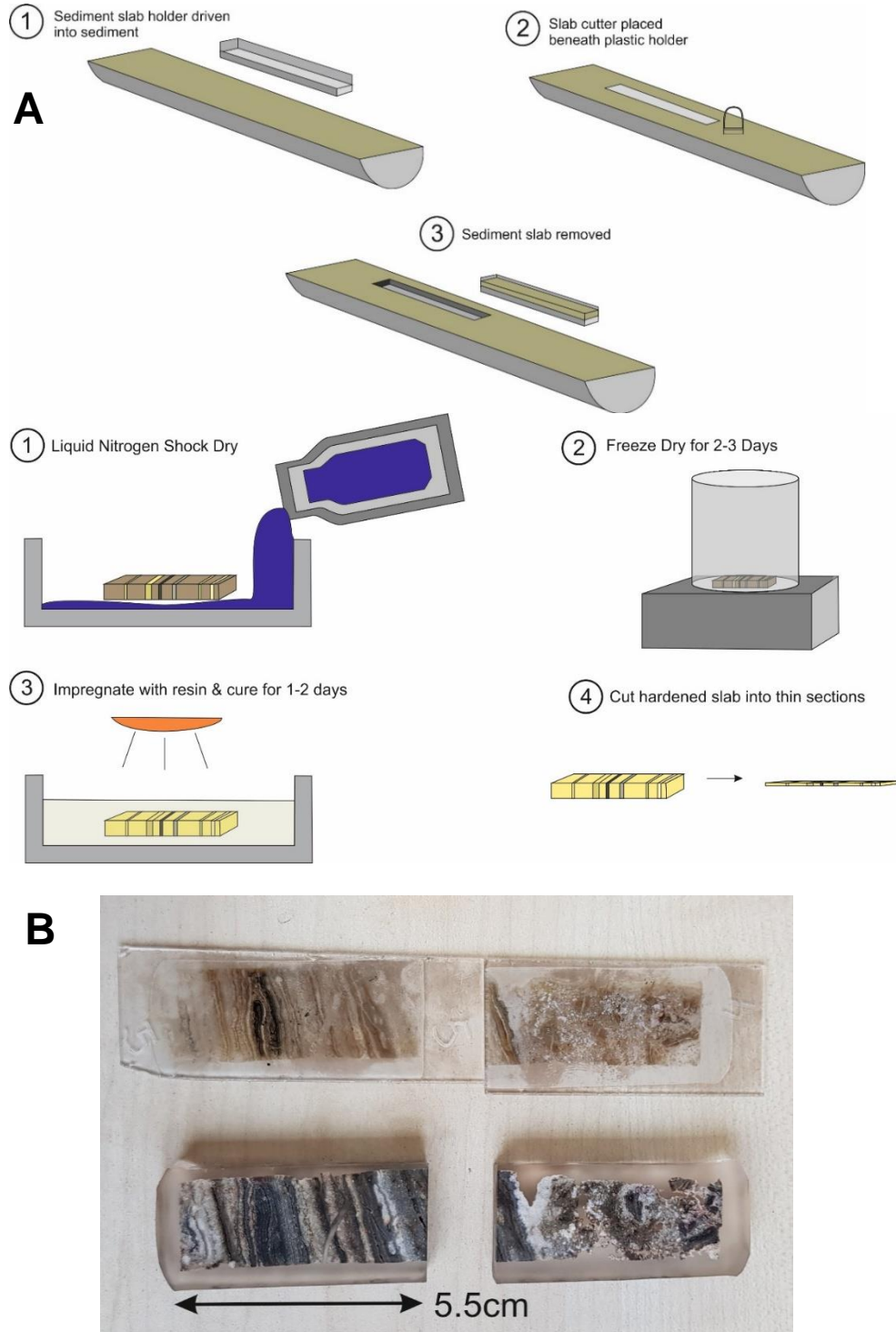


Figure 3.8 – A: Schematic diagram illustrating the process for the shock-freeze drying and epoxy resin impregnation of wet sediment slabs, with measurements for creating a batch of Epoxy Spurr Resin for impregnating freeze-dried thin section slabs. B: Photograph illustrating an epoxied sediment slab and accompanying thin section.

3.4.1.3 Epoxy/Spurr Resin Impregnation, Cutting & Lapping

The EpoFlo resin used was initially mixed following desiccation of the sediment slabs. Once mixed, the dried samples were placed in a disposable aluminium tray, covered with the mixed resin and placed into a desiccator or vacuum for several days and cured using heat lamps. Following total desiccation and resin hardening, the samples were removed and cut using a saw and lapped for thin section analysis.

3.4.2 Sedimentology and Petrography

3.4.2.1 Logging and Facies Analysis

Sediment cores from the four lakes were logged and described for their sedimentary characteristics, including analysis of sediment colour, approximate grain size of any visible grains, notable sedimentary structures, bed and laminae thickness, and visible variations in composition. Cores from lakes Arreo, Estanya and Zonar, collected in 2004 (see Table 3.1) were logged in accordance with previous studies on the cores (Martín-Puertas *et al.*, 2008; Morellón *et al.*, 2009a; Corella *et al.*, 2013). Facies analysis was further undertaken to develop sedimentological models and to determine downcore trends in facies associations where present. Sedimentary facies were described following naked-eye observations of the cores at the School of Geography, University of Manchester, and following analyses of smear slides, whereby wet sample is adhered to a slide with a cover slip and analysed via petrographic microscope, which were taken every centimetre from the cores (Schnurrenberger *et al.*, 2003; Doyle *et al.*, 2022). Cores were typically logged to the millimetre or less in order to generate high-resolution sedimentological profiles (see Appendix 2).

3.4.2.2 Petrographical Characterisation

Transmitted light, cathodoluminescence and scanning electron microscopic techniques were undertaken on thin sections sampled from core material retrieved from the four lakes. Optical photomicrographs were obtained using a Nikon Eclipse LV100NPOL microscope. Entire section scans were additionally obtained using a LV100NPOL microscope equipped with a SteppingStage mechanism and accompanying Petrog © 4.0 software. Sequential scanning of the sections was achieved by placing the sample on the stage and by using horizontal and vertical overlaps of approximately 15% between each image such that scans were continuous and connected.

In all thin sections, the distribution of carbonate, organic, siliciclastic and evaporitic material was further identified in cathodoluminescence photomicrographs obtained using a Meiji CITL Mk5 Optical Cathodoluminescence Microscope Stage operating at ~15kV. Finally, secondary electron and backscatter electron images were obtained using two SEM instruments: a FEI QUANTA 650 FEG ESEM equipped with a Bruker Instruments Quantax 70 EDS detector, and a HITACHI TM3000 tabletop SEM equipped with Bruker Xflash EDS detector. EDS and full section maps were also generated using the same FEI QUANTA 650 FEG ESEM using the image extension feature with a spot size of 6.0 and a voltage of 15kV.

3.4.2.3 CT Scanning

CT scanning of sediment cores and selected samples was undertaken to determine variations in facies and morphological characteristics of studied material. Scanning was undertaken at the Henry Moseley X-ray Imaging Facility, School of Materials, University of Manchester. Round core samples and rectangular sediment slabs were scanned using a Nikon High Flux 225Kv XTEK Bay. The core samples were mounted using a specifically designed sample holder which was mounted onto the stage (Hickman-Lewis *et al.*, 2017; Doyle *et al.*, 2022). Following this, a 1mm thick copper filter was placed over the tungsten X-ray source. Due to the large size of the cores, several scans of each core

were taken in a vertical orientation to accommodate the entire core sample. The instrument parameters were set at an accelerating voltage of 210 kV and 210 μ A current (Engelberg *et al.*, 2012). Sequential scans of 10cm x 12cm areas of larger samples were undertaken at regular intervals until the entirety of each sample was fully incorporated into the dataset. A 1mm thick copper filter was also placed over the tungsten X-ray source to reduce beam hardening (Engelberg *et al.*, 2012). The X-ray projections produced by the instrument were initially constructed in a 16-bit filetype in the AVIZO® Lite software package, and reduced to an 8-bit filetype in order to reduce the size of the dataset for workability. The dataset was also passed through a 2-step median filter to reduce noise. Voxel size and resolution typically ranged between 0.075 and 0.1mm.

3.4.3 Inorganic Geochemical & Mineralogical Analyses

3.4.3.1 ITRAX Core Scanning

Cores from Laguna Salada de Chiprana were initially split using a saw-cutter and imaged using a Cox Analytical Systems Itrax Core scanner at the School of Geography, University of Manchester (Doyle *et al.*, 2022), and later at the Large Lakes Observatory, Duluth, USA, also using an Itrax scanner. Cores were scanned to produce photographs, radiographs, and to obtain produce information about the intensities of major and minor elements (for example Al, Si, Fe, K, Ti, Ca, Mn and S(see chapter 5)). The system uses a synthetic glass standard to monitor the performance of the silicone drift detector and overall optical configuration. Confidence limits and calibration were tested using the method of XRF elemental transformation according to Weltje & Tjallingii (2008), whereby the data are subjected to a log-ratio transformation to provide estimates of sediment composition. All cores from Lake Chiprana were scanned at 1mm resolution at a tube voltage of 30kv and tube current of 30mA from a Mo-based tube (see chapter 5). Following this, select intervals with microbial mats were scanned at 0.2mm intervals using the same scanning parameters. Variable residence times between 15-30 seconds

were used due to fluctuating concentrations of different elements occurring within each core.

3.4.3.2 X-Ray Powder Diffraction Analyses

Bulk mineralogy was determined by X-ray diffraction using a Bruker D8 Advance diffractometer (Bruker Corporation, Billerica, Massachusetts, United States) with a Göbel Mirror and Lynxeye detector (Department of Earth and Environmental Sciences, University of Manchester) according to standard operating procedures provided by Dr. John Waters. The X-ray tube contains a copper source and generates CuK α 1 X-rays with a wavelength of 1.5406Å. ~0.1g of sample was ground with a pestle and mortar and mixed with ~1 ml of amyl acetate. Powdered and mixed samples were transferred to glass microscope slides and air dried. Samples were scanned from 5-70°2 θ , with a step size of 0.02° and a count time of 0.2s per step. XRD diffractograms were analysed with the Bruker DIFFRAC.EVA software using standards from the International Centre for Diffraction Data Database. Quartz was used as an internal standard to correct peak shift that is typically on the order of 10s of millidegrees. The instrument is routinely calibrated using a Bruker corundum standard. Quantitative analyses of XRD diffractograms was undertaken using DIFFRAC.TOPAS software in order to determine quantitative amounts of mineral phases. Error margins typically ranged from 0.1-2% according to wt% volume of each phase.

3.4.3.3 Loss On Ignition for Determination of Approximate TOC

Loss-on-ignition of dried sediment samples was also undertaken in order to provide insights into the approximate total organic carbon and carbonate content of the samples (Vereş, 2002; Doyle *et al.*, 2022). Freeze dried samples were heated in a CARBOLITE ELF11/14B furnace at incremental temperature steps of 550°C and 925°C for organic and carbonate content respectively. Samples were weighed before and after drying and

after each incremental temperature step, with the determination of loss on ignition (LOI) again using the methods described by Vereş (2002). These include drying sediment using either an oven or freeze-drier, and then combusting organic matter to ash and carbon dioxide at temperatures in a range between 500-550°C. Organic matter content is then proposed to be derived from the difference in weight of the sample after combustion. This is followed by combusting the sample at 925°C to 1000°C, allowing for an estimation of the amount of CO₂ released from carbonate minerals by multiplying weight loss between 500-550°C and 925-1000°C by 1.36. This ratio, according to Vereş (2002), defines the relationship between the molecular weights of CO₃ and CO₂.

3.4.3.4 ICP-MS/OES Analyses

For ICP-MS and ICP-OES analyses, freeze-dried samples were aliquoted and weighed to approximately 0.2g. 381 samples were used for the analyses with standard operating procedure provided by Dr. Jonathan Yarwood, and initial preparation of the samples involved digestion undertaken using an Aqua Regia (1 HNO₃ + 3 HCl) digestion method in a CEM MARS Xpress 6 Microwave digestion system. After the digestion, samples were filtered and diluted to a dilution ratio of 1:100 using deionised water. Sample aliquots were analysed using a Perkin Elmer Optima 8300 ICP-OES system and a PerkinElmer NexION 350D ICP-MS at the Department of Geography, School of Environment and Education, University of Manchester, and also at the Department of Earth and Environmental Sciences, University of Manchester. The ICP-OES and ICP-MS methodology used a 5-point linear calibration with a 99.999% minimum regression, with an internal Yttrium standard to correct for instrument drift and matrix interferences. ICP-OES results were initially quantified against this curve in mg/L, or ppm, at a limit of detection of 0.005mg/L. ICP-MS results were quantified against an internal standard in µg/L, or ppb to a detection limit of 0.005µg/L. Any figures below these detection limits were noted as being below the limit of detection (<LOD) including any quantities below zero, as the instrument cannot discern peaks from background noise below these levels.

All standards are certified, calibration curves have a 0.999 r^2 value, and replicates fall within 2.5% RSD.

3.4.3.5 Analysis of $\delta^{18}\text{O}$ and δD Gypsum Hydration Water

Methods presented here are following the standard operating procedure presented by Gázquez *et al.* (2022), and were undertaken at the University of Almeria. 1 gram of powdered gypsum sample was ground initially and separated using a 0.45mm sieve and distilled water to remove the clay fraction from the samples. The remaining sample powder was dried overnight in an oven at 40°C, subsequently being ground down and reheated again overnight at 40°C. Following this, powdered samples were dried at a temperature of 45 °C for 24 hours, and subsequently placed under vacuum to a pressure of $\sim 5 \times 10^{-3}$ mbar to remove adsorbed water. The isotopic analyses were undertaken using a Heat Induction Module (IM-CRDS, Picarro©) coupled to a Cavity Ring-Down Spectrometer (CRDS, Pi- carro© L2140i) located at the University of Almeria. Powdered samples were heated to final temperature of 250°C within the heat induction module, and the resultant water vapor was transferred CRDS analyser. This allowed for the measurement of $\delta^{18}\text{O}$ and $\delta^2\text{H}$ within the water vapor. The Gaussian peak generated from the analysis was interpreted by the Picarro software package like that described in Bauska *et al.* (2018). The results were standardised to the Vienna Standard Mean Ocean Water (V-SMOW), Standard Light Antarctic Precipitation (SLAP) and Greenland Ice Sheet Precipitation (GISP). Standardisation was achieved by analysing four gypsum standards prior to analysis of the samples, and these standards were calibrated against liquid water using the cryogenic extraction method defined by Gázquez *et al.* (2015). To account for instrument drift and repeatability, each sample was analysed 3–4 times consecutively. The mean analytical precision (1SD) of the 3–4 repetitions was 0.1‰ for $\delta^{18}\text{O}$ and 0.9‰ for $\delta^2\text{H}$. The drift of the CRDS instrument was monitored and corrected (if needed) by measuring one of the gypsum standards every 10–12 samples (Gázquez *et al.*, 2015).

3.4.3.6 Stable Isotopic Analyses

$\delta^{13}\text{C}_{\text{org}}$ isotopes of bulk organic matter and organic carbon were investigated to assess downcore variations in organic material and sources within the sediments. The technique was provided by Harald Strauss as also defined in Froidl (2021). In this case, organic carbon isotopes were measured on bulk rock samples at the Institut für Geologie und Paläontologie, Universität Munster, via sealed tube combustion. Following this, 7.5 to 35 mg of powdered sample was then decarbonated in a quartz tube using hydrochloric acid (25%). Deionised water was then used to rinse the samples until neutrality, and they were then dried at 40°C. The sample powder was also mixed homogeneously with CuO wire. Sealed tube combustion at 850°C for three hours was undertaken in order to liberate carbon dioxide from the samples, and was then purified cryogenically in a vacuum distillation line and collected in a Pyrex break-seal tube. Mass spectrometric measurements were performed on a ThermoScientific Delta V Advantage equipped with a dual inlet. USGS 24 (a graphite reference material) and an internal lab standard (a coal sample) were the standards used for the samples. Reproducibility was determined via replicate analyses of standard materials is better than 0.3 per mil (1 sigma).

3.4.4 Limnological & Hydrogeochemical Monitoring

3.4.4.1 On-Site Measurements

Several visits were undertaken to Laguna Salada de Chiprana in order to carry out limnological analyses of the site and to collect samples of microbial mats from different lacustrine sub-environments. Limnological analyses of the lake were undertaken using a YSI Exo1 Multiparameter multiprobe. The probe was suspended in the lakewaters for several minutes in order to take measurements of the water in the shoreline areas, and was suspended to the bottom depth of the lake from a pneumatic boat in order to

generate a vertical limnological profile. The Kor software package was used to calibrate to sensor, with three measurements being taken continuously at set intervals of several seconds. To calibrate the pH sensor, three calibration points were measured at pH 7, 10 and 4. For the conductivity sensor, a 1413 μS solution was used, and for the O₂ sensor, calibration was undertaken with water in equilibrium with the atmosphere (100% saturation). Standard measurements included:

- pH.
- Dissolved oxygen (% and mg/L).
- Temperature.
- Total dissolved solids (TDS).
- Conductivity ($\mu\text{S}/\text{cm}$).
- Salinity (PSU).

Rainfall and temperature data were also obtained both from monitors established in the region that are monitored by the regional government and from the KNMI Climate Explorer for the case of historical data throughout the 20th century.

3.4.4.2 Elemental Ionic Compositions

Concentrations of major and trace ions within the lakewaters were measured using ion chromatography and alkalinity titration. Analyses for major anions and cations were undertaken at the Instituto Pirenaico de Ecologia, and are defined here according to their standard operating procedure and as defined by Lambán *et al.* (2015). Samples were stored at 4°C in a dark cold-room and analysed within a week of being stored. The samples were first filtered through GF/F Whatman filters to remove particulate material, and were subsequently aliquoted into 4 x 12ml plastic tubes, each washed prior with 10% HCl. Eluents for cations and anions were comprised of 4.0 mmol/l tartaric acid + 0.75 mmol/l dipicolinic acid, and 3.2 mmol/l sodium carbonate + 1mmol/l sodium bicarbonate, respectively. Analysis of both cation and anion concentrations were

undertaken using Chemical Suppressed Ion Chromatography (APHA, 2018a) within a Metrohm 861 Advanced Compact IC. In the case of cations, analyses were undertaken in a Metrosep A Sup 2 polystyrene- divinylbenzene polymer column, while analyses were undertaken using a Metrosep C 2-250 silica gel with carboxyl groups column. New tubes with the samples were placed in the autosampler together with a tube containing the sampler check standard calibration. The method is programmed and the analysis is launched. The results are recorded in a chromatogram, the equipment software transforms the peak areas in concentrations (mg/l) according to the calibration performed.

In addition, samples, stored at 4°C in a dark cold room, were also analysed for alkalinity within several days as defined by IPE standard operating procedures. 100 mL of the sample was initially measured in a beaker, followed by adding 3 drops of phenolphthalein and stirring. This solution was then titrated in a Metrohm 798 MPT Titrino using Potentiometric Titration (APHA, 2018b), with 0.02N of sulfuric acid being added until the colour of the solution disappeared. Following this, 3 drops of mixed indicator were added to the sample. The sample was then titrated again with sulphuric acid until a pink tint was visible. The volume of acid remaining was then used for the calculation of total alkalinity. This allowed for insights into fluctuations in the concentration of major ions and elemental concentrations occurring throughout the lakes and to determine whether such fluctuations may influence the development of microbial mats occurring within the lakewaters.

3.4.4.3 Hydrochemical Modelling using PHREEQc

Geochemical modelling of lakewaters from Chiprana was undertaken using the PHREEQC Interactive Software Version 3.7.3 (Parkhurst, 1995; Parkhurst & Appelo, 2013). In this project, evaporative concentration and saturation indices of different phases were modelled using code supplied by the provided software manual (Parkhurst

& Appelo, 2013) and from the PhreeqC forums (<https://phreeqcusers.org/index.php>). The chemical characteristics of Lake Chiprana were inputted to the program, and this water was evaporated over a number of steps to increase or decrease elemental concentrations and saturation indices. Evaporation was modelled at a constant temperature of 25°C following guidelines supplied by Parkhurst & Appelo (2013). In all cases, the amount of water removed from the solution was undertaken by removing a set amount of moles of water in defined steps. The number of steps used was undertaken in order to define a continuous evaporation sequence and to determine a wide range of evaporation steps on overall water chemistry and following guidelines from the PhreeqC forums (<https://phreeqcusers.org/index.php>) to generate this model. It is assumed that there are approximately 55.55 moles of H₂O in one litre of water, and this value was used as a guideline for the % moles removed in each step. Analytes and variables used in the initial solution reactions included anions Cl⁻, Br⁻, SO₄²⁻ and cations Na⁺, K⁺, Ca²⁺, Mg²⁺ in addition to alkalinity and pH.

3.4.5 Other Analyses

3.4.5.1 Community Composition Analyses

Samples of the upper 5cm of sediment cores and fresh mat samples were collected with a sterilised trowel and then kept frozen at -20°C in sterilised 2L Nalgene bottles order to determine the biological composition and microbial community of the mats. To achieve this, methods defined by Christopher Boothman and Czinnerova *et al.* (2020) are described here. DNA was initially extracted from 0.2g of powdered sample by using a DNeasy PowerSoil Pro Kit (Qiagen, Manchester, U.K). Sequencing of PCR amplicons of 16S rRNA was conducted with the Illumina MiSeq platform (Illumina, San Diego, CA, USA), specifically targeting the V4 hyper variable region (forward primer, 515F, 5'-GTGYCAGCMGCCGCGGTAA-3'; reverse primer, 806R, 5'-GGACTACHVGGGTWTCTAAT-3') for 2 × 250-bp paired-end sequencing (Illumina).

The PCR amplification was performed using a Roche FastStart High Fidelity PCR System (Roche Diagnostics Ltd, Burgess Hill, UK) in 50µl reactions under a set of specific conditions. These conditions include:

- Initial denaturation at 95°C for 2 min,
- 36 cycles of 95°C for 30 s, 55°C for 30 s, 72°C for 1 min,
- Extension step of 5 min at 72°C.

The PCR products were then purified and normalised to ~20ng using a SequalPrep Normalization Kit (Fisher Scientific, Loughborough, UK), with amplicons from all samples being pooled in equimolar ratios. The run was performed using a 4.5pM sample library spiked with 4.5pM PhiX to a final concentration of 12% following the method of Schloss *et al.* (2013).

For QIIME2 analysis, methods defined by Christopher Boothman (pers. comm) and Straub *et al.* (2020) are defined. Firstly, sequences were imported into the QIIME2 q2cli v2021.044 software package. Sequences were trimmed with cutadapt, visually inspected with demux, and denoised with DADA25 in order to remove PhiX contamination, trim reads, correct errors, merge read pairs and remove PCR chimeras. Representative ASV sequences and their abundances were extracted by feature-table6. QIIME2 plugins were executed with DADA2 quality settings “- -p-trunc-len-f” of 230 and “- -p-trunc-len-r” of 220. Taxonomy was assigned using the Silva 1387 (99% identity clusters) database using the feature-classifier classify-sklearn function.”

3.4.5.2 Monitoring of Microbial Mats

In order to determine the effects of short-term anthropogenic and climatic perturbations on microbial mat formation and their subsequent interactions with mineral products on a high-resolution scale, monitoring of microbial mats was undertaken at La Salada de Chiprana intermittently over the course of the project where possible. This involved using a developed technique and device (see Figure 3.8) similar to those used by Drysdale &

Gillieson, (1997), Vázquez-Urbez *et al.*, (2010), and Arenas *et al.*, (2014) that was submerged and lowered onto the lake bed. Several limestone plates were developed and placed into the lake during a field visit in March 2019 (Figures 3.9-3.10). The limestone plates were developed at the University of Manchester by Lee Paul and consisted of Solnhofen limestone cut into 2cm thick rectangular (10-15cm x 5-10cm) shapes. These tablets were mounted and bolted onto a dense plastic base to prevent any movement in the lakewaters. To ensure stability, the tablets were dug into the level of the sediment on the lake floor in different locations, and their locations recorded using both GPS and 1.5-metre-long plastic poles driven into the sediment in close proximity to the tablets. However, due to the COVID-19 pandemic, the devices were unable to be retrieved regularly.

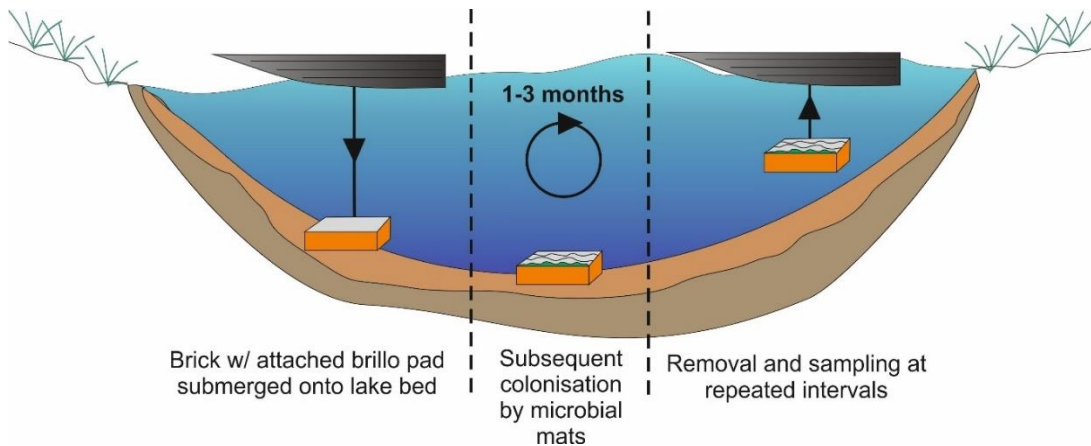


Figure 3.9 - Simplified diagram illustrating the proposed method to study in situ microbial mat development in lakes with actively growing mats. The device is lowered from a boat and securely placed onto the lakebed sediment. Subsequent colonisation by microbial mats should occur and following this the device will be sequentially removed from the lake sediment at regular intervals to retrieve samples in order to determine the effects of environmental change on mat development at high resolution temporal scales.



Figure 3.10 – Photograph showing a limestone slab ready to be installed in Laguna Salada de Chiprana during a field season in March 2019. Slabs were dug into the sediment at the interface with microbial mats and their position marked using a 1.5m measuring pole and GPS locations.

3.4.6 Transformation, Processing & Statistical Analysis of Geochemical Data

3.4.6.1 Processing and Statistical Analysis of Geochemical Datasets

There were a large number of elements outputted from the Itrax XRF scanners utilised throughout this study (see chapter 5). In addition, variations in characteristics such as organic content, water saturation, grain size and core topography had to be accounted for (Adlam, 2015; Woodward & Gadd, 2019). Thus, the dataset was quality controlled by removing data with a high mean standard error (MSE) and data with high argon (Ar) readings, the lattermost of which signify increased air in the core (Gebregiorgis *et al.*, 2020). Data were also transformed using the central-log-ratio calibration method defined by (Weltje & Tjallingii, 2008) in order to account for such effects using the ItraxR software package (Bishop, 2022). The geochemical datasets were then subjected to statistical analysis using the PAST4.0+ software package. The software contains various functions the analysis, manipulation, plotting and statistical treatment of data (Hammer *et al.*, 2001), and was primarily used in this study for bivariate Pearson correlative analyses and principal component analyses.

3.4.7 Summary of Methods

Table 3.2 below defines the methods carried out at each site in order to more clearly delineate which methods were applied in each lake.

Table 3.2 – Summary of methods applied to cores and sediment each setting. Green = Method applied, blue = data already available, Red = Not carried out due to constraints or inability to apply method. Numbers denote the number of samples/sampling points.

Method	Modern Microbial Mats	Core Sediments & Sub-Recent Microbial Mats			
	Laguna Salada de Chiprana	Laguna Salada de Chiprana	Lago de Estanya	Laguna Zonar	Lago de Arreo
Sedimentological/Facies Analysis	3 samples	9 cores	4 cores	4 cores	2 cores
Optical Microscopy	2 thin sections	31 thin sections	31 thin sections	11 thin sections	24 thin sections
Cathodoluminescence	2 thin sections	17 thin sections	17 thin sections	6 thin sections	12 thin sections
Scanning Electron Microscopy	2 thin sections	17 thin sections	17 thin sections	6 thin sections	12 thin sections
CT Scanning	7 cores	7 cores	5 samples	2 samples	3 samples
XRD	7 top core samples, 2 modern mats	281 samples			
XRF	7 top core samples	7 cores			
ICP-MS/OES	7 top core samples	266 samples			
TOC/LOI	7 top core samples	85 samples			
Radiocarbon Dating					
$\delta_{13}\text{C}_{\text{org}}$ Isotopes	7 top core samples	85 samples			
Community Composition Analyses	3 samples				

Table 3.3 – Summary of methods applied to water samples from each setting. Green = Method applied, blue = data already available, Red = Not carried out due to constraints or inability to apply method.

Method	Water Samples			
	Laguna Salada de Chiprana	Lago de Estanya	Laguna Zonar	Lago de Arreo
$\delta_{18}\text{O}/\delta\text{D}$ of Gypsum Water	33 samples			
Alkalinity Titration	4 samples			
Ionic Concentration	4 samples			
<i>In situ</i> Salinity	6 measurements			
<i>In situ</i> Temperature	6 measurements			
<i>In situ</i> Total Dissolved Solids	6 measurements			
<i>In situ</i> Dissolved Oxygen	6 measurements			

References

- Adlam, K.** (2015) THE VALUE OF THE GEOLOGICAL RECORD IN DETERMINING RATES AND DRIVERS OF COASTAL LAGOON SHORELINE DEVELOPMENT. University of Sydney
- Alonso, M.** (1998) The lagoons of Peninsular Spain . *Limnetica*, **15**, 1–176.
- Arenas, C., Vázquez-Urbez, M., Auqué, L., Sancho, C., Osácar, C. and Pardo, G.** (2014) Intrinsic and extrinsic controls of spatial and temporal variations in modern fluvial tufa sedimentation: A thirteen-year record from a semi-arid environment. *Sedimentology*, **61**, 90–132.
- Bauska, T.K., Walters, G., Gázquez, F. and Hodell, D.A.** (2018) Online Differential Thermal Isotope Analysis of Hydration Water in Minerals by Cavity Ringdown Laser Spectroscopy. *Anal. Chem.*, **90**, 752–759.
- Bishop, T.** (2022) Using Itrax Data in R. <https://tombishop1.github.io/itraxBook/>. Accessed 26 Aug 2022
- Bourillot, R., Vennin, E., Dupraz, C., Pace, A., Foubert, A., Rouchy, J.M., Patrier, P., Blanc, P., Bernard, D., Lesseur, J. and Visscher, P.T.** (2020) The record of environmental and microbial signatures in ancient microbialites: The terminal carbonate complex from the neogene basins of southeastern Spain. *Minerals*, **10**, 1–50.
- Comin, F.A. and Alonso, M.** (1988) Spanish salt lakes: Their chemistry and biota. *Hydrobiologia*, **158**, 237–245.
- Corella, J.P., Amrani, A. El, Sigró, J., Morellón, M., Rico, E. and Valero-Garcés, B.L.** (2011a) Recent evolution of Lake Arreo, northern Spain: Influences of land use change and climate. *J. Paleolimnol.*, **46**, 469–485.
- Corella, J.P., Moreno, A., Morellón, M., Rull, V., Giral, S., Rico, M.T., Pérez-Sanz, A. and Valero-Garcés, B.L.** (2011b) Climate and human impact on a meromictic lake during the last 6,000 years (Montcortès Lake, Central Pyrenees, Spain). *J. Paleolimnol.*, **46**, 351–367.

- Corella, J.P., Stefanova, V., El Anjoumi, A., Rico, E., Giral, S., Moreno, A., Plata-Montero, A. and Valero-Garcés, B.L.** (2013) A 2500-year multi-proxy reconstruction of climate change and human activities in northern Spain: The Lake Arreo record. *Palaeogeogr. Palaeoclimatol. Palaeoecol.*, **386**, 555–568.
- Czinnerova, M., Nguyen, N.H.A., Nemecek, J., Mackenzie, K., Boothman, C., Lloyd, J., Laszlo, T., Spanek, R., Cernik, M. and Sevcu, A.** (2020) In situ pilot application of nZVI embedded in activated carbon for remediation of chlorinated ethene-contaminated groundwater: effect on microbial communities. *Environ Sci Eur*. doi: 10.1186/s12302-020-00434-2
- Doyle, C., Schröder, S., Corella, J.P. and Valero Garces, B.** (2022) Facies variability and depositional settings of Laguna Salada de Chiprana, an Iberian hypersaline lake. *Sedimentology*, **69**, 2615–2641.
- Drysdale, R. and Gillieson, D.** (1997) Micro-erosion meter measurements of travertine deposition rates: a case study from Louie Creek, Northwest Queensland, Australia. *Earth Surf. Process. Landforms*, **22**, 1037–1051.
- Engelberg, D.L., Patrick, R.A.D., Wilson, C., McCrae, R. and Withers, P.J.** (2012) Three-dimensional imaging of inhomogeneous lithologies using X-ray computed tomography: characterization of drill core from the Borrowdale Volcanic Group. *Mineral. Mag.*, **76**, 2931–2938.
- Froidl, F.** (2021) Kinetics of petroleum generation from terrestrial organic matter: The examples of the lacustrine Berriasian Wealden Shales and Pennsylvanian hard coals, western Germany. Rheinisch -Westfälischen Technischen Hochschule Aachen
- Gázquez, F., Mather, I., Rolfe, J., Evans, N.P., Herwartz, D., Staubwasser, M. and Hodell, D.A.** (2015) Simultaneous analysis of 17O/16O, 18O/16O and 2H/1H of gypsum hydration water by cavity ring-down laser spectroscopy. *Rapid Commun. Mass Spectrom.*, **29**, 1997–2006.
- Gázquez, F., Monteserín, A., Obert, C., Fernández-Cortés, Á. and Calaforra, J.M.**

- (2022) The Absolute Age and Origin of the Giant Gypsum Geode of Pulpi (Almería, SE Spain). *Geosci.* doi: 10.3390/geosciences12040144
- Gebregiorgis, D., Giosan, L., Hathorne, E.C., Anand, P., Nilsson-Kerr, K., Plass, A., Lückge, A., Clemens, S.C. and Frank, M.** (2020) What Can We Learn From X-Ray Fluorescence Core Scanning Data? A Paleomonsoon Case Study. *Geochemistry, Geophys Geosystems.* doi: 10.1029/2019GC008414
- Guerrero, M.C.** (1992) Microbial mats in the inland saline lakes of Spain. *Limnetica*, **8**, 197–204.
- Guerrero, R., Piqueras, M. and Berlanga, M.** (2002) Microbial mats and the search for minimal ecosystems. *Int. Microbiol.*
- Hammer, Ø., Harper, D.A.T. and Ryan, P.D.** (2001) PAST: Paleontological statistics software package for education and data analysis. *Palaeontologia electronica.*
- Hickman-Lewis, K., Garwood, R.J., Withers, P.J. and Wacey, D.** (2017) X-ray microtomography as a tool for investigating the petrological context of Precambrian cellular remains. *Geol. Soc. Spec. Publ.*, **448**, 33–56.
- IGME** (2003) Mapa Geologico de Espana, 1:50000, (serie MAGNA). Hoja 988. Puente-Genil.
- Jonkers, H.M., Ludwig, R., De Wit, R., Pringault, O., Muyzer, G., Niemann, H., Finke, N. and De Beer, D.** (2003) Structural and functional analysis of a microbial mat ecosystem from a unique permanent hypersaline inland lake: “La Salada de Chiprana” (NE Spain). *FEMS Microbiol. Ecol.*, **44**, 175–189.
- Kortekaas, K.H., Vaya, J.-F.C. and Carrasco Vaya, J.-F.** (2009) Biodiversity of inland saltscapes of the Iberian Peninsula.
- Kozich, J.J., Westcott, S.L., Baxter, N.T., Highlander, S.K. and Schloss, P.D.** (2013) Development of a dual-index sequencing strategy and curation pipeline for analyzing amplicon sequence data on the miseq illumina sequencing platform. *Appl. Environ. Microbiol.* 79:5112–5120.
- LacCore** and **CSDCO** Subsample Preparation and Analysis.

<https://cse.umn.edu/csd/subsample-preparation-and-analysis>. Accessed 17 Jan 2023

Lambán, L.J., Jódar, J., Custodio, E., Soler, A., Sapriza, G. and Soto, R. (2015) Isotopic and hydrogeochemical characterization of high-altitude karst aquifers in complex geological settings. The Ordesa and Monte Perdido National Park (Northern Spain) case study. *Sci Total Environ.* doi: 10.1016/j.scitotenv.2014.11.030

Martín-Puertas, C., Valero-Garcés, B.L., Mata, M.P., González-Sampériz, P., Bao, R., Moreno, A. and Stefanova, V. (2008) Arid and humid phases in southern Spain during the last 4000 years: The Zoñar Lake record, Córdoba. *Holocene*, **18**, 907–921.

Martín-Puertas, C., Valero-Garcés, B.L., Mata, M.P., Moreno, A., Giralt, S., Martínez-Ruiz, F. and Jiménez-Espejo, F. (2011) Geochemical processes in a Mediterranean Lake: A high-resolution study of the last 4,000 years in Zoñar Lake, southern Spain. *J. Paleolimnol.*, **46**, 405–421.

Martínez-Alonso, M., Méndez-Álvarez, S., Ramírez-Moreno, S., González-Toril, E., Amils, R. and Gaju, N. (2008) Spatial heterogeneity of bacterial populations in monomictic Lake Estanya (Huesca, Spain). *Microb Ecol.* doi: 10.1007/s00248-007-9316-0

Morellón, M., Pérez-Sanz, A., Corella, J.P., Büntgen, U., Catalán, J., González-Sampériz, P., González-Trueba, J.J., López-Sáez, J.A., Moreno, A., Pla-Rabes, S., Saz-Sánchez, M.A., Scussolini, P., Serrano, E., Steinhilber, F., Stefanova, V., Vegas-Vilarrúbia, T. and Valero-Garcés, B. (2012) A multi-proxy perspective on millennium-long climate variability in the Southern Pyrenees. *Clim. Past* **8**:683–700.

Morellón, M., Valero-Garcés, B., Anselmetti, F., Ariztegui, D., Schnellmann, M., Moreno, A., Mata, P., Rico, M. and Corella, J.P. (2009a) Late quaternary deposition and facies model for karstic Lake Estanya (North-eastern Spain).

Sedimentology, **56**, 1505–1534.

Morellón, M., Valero-Garcés, B., Vegas-Vilarrúbia, T., González-Sampéris, P., Romero, Ó., Delgado-Huertas, A., Mata, P., Moreno, A., Rico, M. and Corella, J.P. (2009b) Lateglacial and Holocene palaeohydrology in the western Mediterranean region: The Lake Estanya record (NE Spain). *Quat. Sci. Rev.*, **28**, 2582–2599.

Parkhurst, D.L. (1995) User's guide to PHREEQC : a computer program for speciation, reaction-path, advective-transport, and inverse geochemical calculations. *Lakewood, Colo. : U.S. Dept. of the Interior, U.S. Geological Survey ; Denver, CO : Earth Science Information Center, Open-File Reports Section [distributor], 1995.*

Parkhurst, D.L. and Appelo, C.A.J. (2013) Description of input and examples for PHREEQC Version 3 — A computer program for speciation, batch-reaction, one-dimensional transport, and inverse geochemical calculations.

Páscoa, P., Gouveia, C.M., Russo, A. and Trigo, R.M. (2017) Drought trends in the Iberian Peninsula over the last 112 years. *Adv. Meteorol.*, **2017**, 1–15.

Riera, S., Wansard, G. and Julià, R. (2004) 2000-Year environmental history of a karstic lake in the Mediterranean Pre-Pyrenees: The Estanya lakes (Spain). *Catena*

Schnurrenberger, D., Russell, J. and Kelts, K. (2003) Classification of lacustrine sediments based on sedimentary components. *J. Paleolimnol.*, **29**, 141–154.

Schröder, T., van 't Hoff, J., Ortiz, J.E., de Torres Pèrez-Hidalgo, T.J., López-Sáez, J.A., Melles, M., Holzhausen, A., Wennrich, V., Viehberg, F. and Reicherter, K. (2018) Shallow hypersaline lakes as paleoclimate archives: A case study from the Laguna Salada, Málaga province, southern Spain. *Quat. Int.*, **485**, 76–88.

Straub, D., Blackwell, N., Langarica-Fuentes, A., Peltzer, A., Nahnsen, S. and Kleindienst, S. (2020) Interpretations of Environmental Microbial Community Studies Are Biased by the Selected 16S rRNA (Gene) Amplicon Sequencing Pipeline. *Front Microbiol.* doi: 10.3389/fmicb.2020.550420

- Tunis, G., Pugliese, N., Jurkovšek, B., Ogorelec, B., Drobne, K., Riccamboni, R. and Tewari, V.C.** (2011) Microbialites as Markers of Biotic and Abiotic Events in the Karst District, Slovenia and Italy. 251–272.
- Valero-Garcés, B., Morellón, M., Moreno, A., Corella, J.P., Martín-Puertas, C., Barreiro, F., Pérez, A., Giralt, S. and Mata-Campo, M.P.** (2014) Lacustrine carbonates of Iberian Karst Lakes: Sources, processes and depositional environments. *Sediment. Geol.* 299:1–29.
- Valero-Garcés, B.L. and Moreno, A.** (2011) Iberian lacustrine sediment records: Responses to past and recent global changes in the Mediterranean region. *J. Paleolimnol.*
- Valero-Garcés, B.L., Navas, A., Machin, J., Stevenson, T. and Davis, B.** (2000) Responses of a saline lake ecosystem in a semiarid region to irrigation and climate variability: The history of Salada Chiprana, central Ebro basin, Spain. *Ambio*, **29**, 344–350.
- Valero-Garcés, B.L., Navas, A., Machin, J., Stevenson, T., Davis, B., Valero-Garcés, B.L., Navas, A., Machin, J., Stevenson, T., Davis, B., Valero-Garcés, B.L., Navas, A., Machin, J., Stevenson, T. and Davis, B.** (2000) Responses of a Saline Lake Ecosystem in a Semiarid Region to Irrigation and Climate Variability. *AMBIO A J. Hum. Environ.*, **29**, 344–350.
- Vázquez-Urbez, M., Arenas, C., Sancho, C., Osácar, C., Auqué, L. and Pardo, G.** (2010) Factors controlling present-day tufa dynamics in the Monasterio de Piedra Natural Park (Iberian Range, Spain): Depositional environmental settings, sedimentation rates and hydrochemistry. *Int. J. Earth Sci.*, **99**, 1027–1049.
- Vereş, D.** (2002) A Comparative Study Between Loss on Ignition and Total Carbon Analysis on Mineralogenic Sediments. *Stud. Univ. Babeş-Bolyai, Geol.*, **47**, 171–182.
- Vergés, J. and Fernández, M.** (2006) Ranges and basins in the Iberian Peninsula: Their contribution to the present topography. *Geol. Soc. Mem.*, **32**, 223–234.

Weltje, G.J. and **Tjallingii, R.** (2008) Calibration of XRF core scanners for quantitative geochemical logging of sediment cores: Theory and application. *Earth Planet. Sci. Lett.*, **274**, 423–438.

Woodward, C.A. and **Gadd, P.S.** (2019) The potential power and pitfalls of using the X-ray fluorescence molybdenum incoherent: Coherent scattering ratio as a proxy for sediment organic content. *Quat. Int.*, **514**, 30–43.

Chapter 4 – Facies Variability and Depositional Settings of Laguna Salada de Chiprana, an Iberian Hypersaline Lake

Connor Doyle^a, Stefan Schröder^a, Juan Pablo Corella Aznar^b, Blas Valero Garces^c

a – Department of Earth and Environmental Sciences, University of Manchester, Manchester, UK

b – CIEMAT – Environmental Department (DMA), Avenida Complutense 40, E-28040 Madrid, Spain.

c – Instituto Pirenaico de Ecología, Consejo Superior de Investigaciones Científicas, Zaragoza, Spain

connor.doyle@postgrad.manchester.ac.uk

This chapter was accepted and published in *Sedimentology* on 5th May 2022.

Abstract

Hypersaline lakes are unique depositional environments that are highly sensitive to climatic changes and anthropogenic pressures. Strong physicochemical gradients and the interplay of physical, chemical and biological depositional processes coupled to variable preservation potential associated with these environments generate highly complex sedimentary sequences. This study aimed to investigate spatio-temporal variations throughout the last three centuries in the sedimentary sequence of Laguna Salada de Chiprana, a small, permanent hypersaline lake situated in Northeast Spain. Short sediment cores reveal a complex sedimentary sequence influenced by detrital, chemically-induced and biogenically-influenced depositional processes. Nine facies and subfacies associated with six sedimentological units represent six periods of environmental change beginning from approximately pre-1800 AD to the present day. They include a shallow, permanent saline lake that experienced brief periods of anoxia and drawdown between pre-1800 AD and ca 1850 AD. This was succeeded by increased lake levels and detrital input to the lake from ca 1850 to 1900 AD and a fall in lake levels and the establishment of microbial mats within bottom waters fluctuating between oxic and anoxic conditions from ca ~1900 to 1950 AD. From ca 1950/1960 AD, a minor increase in lake levels and colonization of the littoral and sub-littoral zones by macrophytic vegetation occurred; followed by falling lake levels and increasing salinity between 1960 and 1970 AD leading to widespread encrustation of macrophytes in the littoral zones by carbonate–evaporite precipitates. Finally, from ca 1970 AD to the present day, falling lake levels, elevated salinity and widespread colonisation of the lake by microbial mats characterise the sedimentary environments. Climate reconstructions and documentary evidence indicate that depositional evolution was mostly controlled by changes in farming practices and irrigation policies. Understanding Laguna Salada de Chiprana's depositional evolution contributes to future definitions of high-resolution palaeoenvironmental models, not only within the Iberian Peninsula but also in other locations where saline–hypersaline lakes act as a key source of palaeoenvironmental information.

Keywords

Lacustrine, Palaeolimnology, Hypersaline, Facies, Anthropocene

4.1 - Introduction

In recent decades, a wide range of studies have focused on the high-resolution sedimentological and geochemical characterisation of lacustrine sediments for the generation of palaeoenvironmental and depositional models which have allowed insights into climatic and environmental change (Kelts & Hsü, 1978; Lowenstein *et al.*, 1985; Valero-Garcés & Kelts, 1995; Boyle, 2005; Birks & Birks, 2006; Morellón *et al.*, 2009; Juggins, 2013; Valero-Garcés *et al.*, 2014). Among such lacustrine systems, hypersaline lakes are particularly sensitive to climatic changes and anthropogenic pressures (Valero-Garcés *et al.*, 2000a). Aridity, hydrological restriction (Last, 2002), water table variations (Lowenstein & Hardie, 1985), strong physicochemical gradients, and low sedimentation rates generate highly irregular depositional conditions and in some cases, hiatuses (Jones *et al.*, 1998; Liu *et al.*, 2011). Consequently, the preservation of sedimentary deposits within these systems can be highly variable (Last & Schweyen, 1983, Comin & Alonso, 1988; Alonso, 1998).

There is however some uncertainty remaining when modelling depositional processes, facies distributions and sedimentological characteristics of hypersaline lakes (Brock & Hammer, 1987). Many such lakes contain spatially complex limnological and ecological sub-environments controlled by strong physicochemical gradients (Deocampo & Jones, 2013), including salinity (Zadereev *et al.*, 2020), temperature (Degermendzhy *et al.*, 2010), chemistry (Ohkouchi *et al.*, 2005) and biological niches. Extrinsic forcing factors such as climatic or anthropogenic shifts can additionally perturb internal thresholds (Diaz *et al.*, 1998; Williams, 2002), while erosional hiatuses induced by drawdown and subaerial exposure can further complicate the depositional sequence in non-permanent, ephemeral settings (Liu *et*

al., 2011). Thus, hypersaline lakes are complex depositional systems which require detailed investigations and adaptable environmental models generated from a wide variety of studies if they are to be fully represented and understood.

This study aimed to investigate spatio-temporal facies variations for the last 250 to 300 years within Laguna Salada de Chiprana, a hypersaline lake in the Ebro Basin of Northeast Spain. Previous studies of the site have focused upon a singular coring site (Davis, 1994; Valero-Garces *et al.*, 2000b), impeding the ability to investigate spatial variations within limnological and depositional processes. In this study, the interplay of climatic and anthropogenic factors occurring throughout the last 250-300 years and the effects of these fluctuations on both depositional processes and temporal and spatial facies variability were investigated. The findings from this study also contribute to our understanding of the complex and highly variable sedimentary sequences of hypersaline lakes and provides insights into key facies and sedimentological characteristics that may be relevant in other hypersaline lakes around the globe.

4.2 - Study Area

4.2.1 - Geology and geomorphology

Laguna Salada de Chiprana (abbreviated hereon to Lake Chiprana) (41°14'30"N, 0°10'50"W) is a permanent hypersaline lake with a surface area of approximately 0.25km², and is situated within the endorheic Ebro Basin in Northeast Spain (De Wit *et al.*, 2013)(Figure 4.1). It is the deepest and only permanent hypersaline lake in the Iberian Peninsula with a variable depth between 3.5 and 5m (Valero-Garcés *et al.*, 2000b) and is situated at an altitude of approximately 137m above sea level (Diaz *et al.*, 1998). The underlying geology of the area consists of Oligo-Miocene marls cross-cut by elongate Oligocene sandstone bodies formed by fluvial palaeochannels (IGME, 2003; Luzón, 2005). The geomorphology of the area is consequently defined by flat

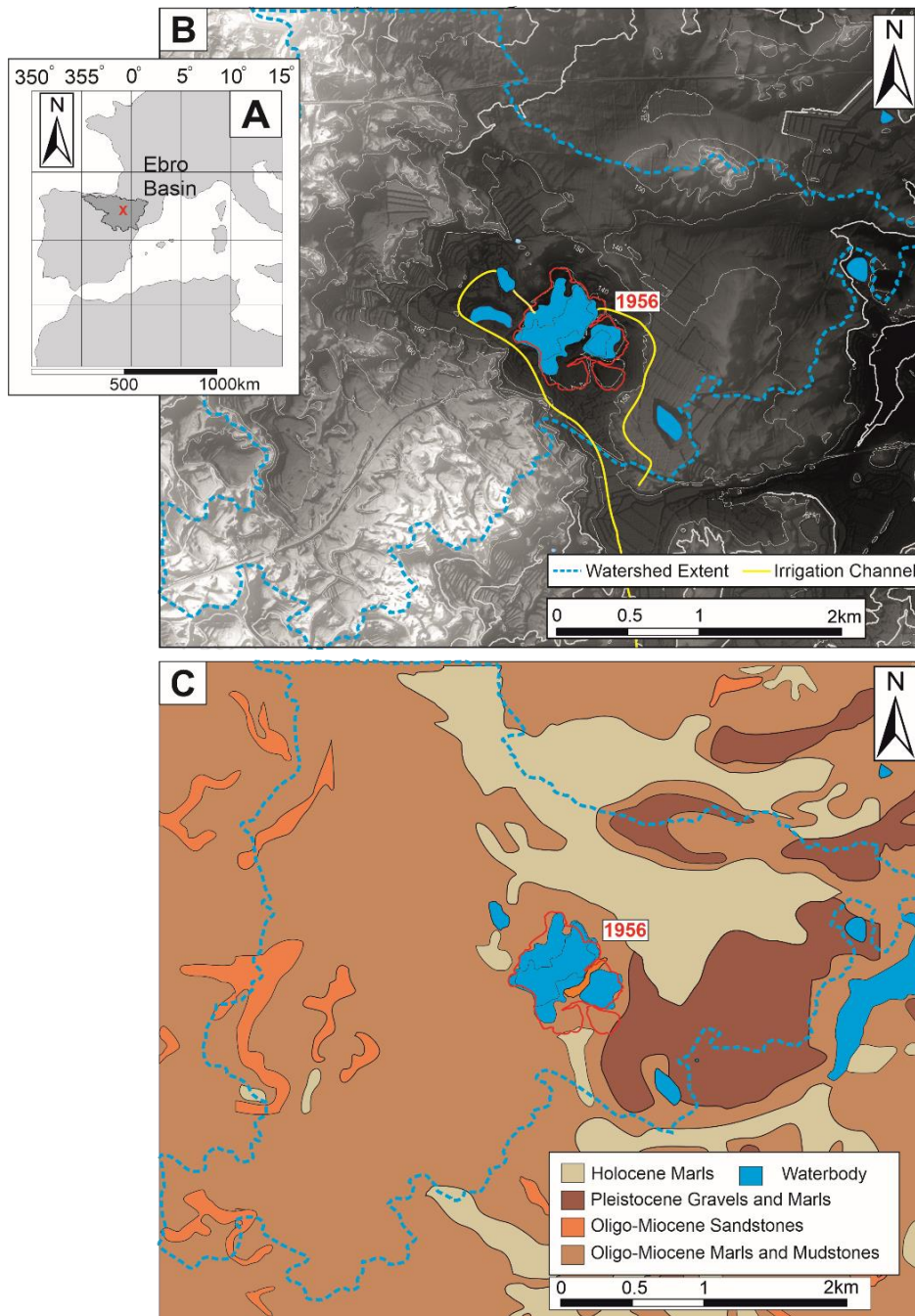


Figure 4.1 - Maps illustrating the location and morphology of Laguna Salada de Chiprana in the Ebro Basin, Northeast Spain. A) Overview map illustrating the location of Lake Chiprana within the Ebro Basin of Northeast Spain, B) 5m Digital elevation model (CNIG) of the area surrounding Laguna Salada de Chiprana generated using ArcMap 10.14.1 with the extent of the local watershed delineated by the red line, C) Local geology of the area surrounding Laguna Salada de Chiprana. The site is situated approximately 5km from the town of Chiprana, and is represented by a 0.25-3km² hypersaline water body with a singular freshwater inlet from a small pond to the Northwest, Laguna de Las Rocas, the flow of which is currently being monitored and managed by the Regional Government of Aragon. Data from IGME (2003) and CNIG.

terraces composed of the Oligo-Miocene marls, while sandstone palaeochannels form distinct ridges and topographic highs. In Lake Chiprana, many of these deposits occur as elongated sandstone ribbons that segment the lagoon (De Wit *et al.*, 2013). These sandstones are arenitic, highly permeable and porous, and are relatively soft and thus are a source of sediment to the lake during overland flow (IGME, 2003).

4.2.2 - Climatological setting

The climate governing Lake Chiprana is semi-arid and Mediterranean. The mean temperature is approximately 15.5°C with minima and maxima of 3°C and 34°C (Domínguez-Castro *et al.*, 2010). High evapotranspiration (~1500mm/yr) and groundwater output (~1000mm/yr) are the primary hydrological outputs, while inflow from irrigation is the primary hydrological input (~1700mm/yr) with relatively low rainfall (~300-400mm/yr) and moderate groundwater input (~300mm/yr) (Jódar *et al.*, 2020). Inflow from irrigation and overland flow is typically highest in spring, coinciding with the period of lowest salinity throughout the year. The average total surface area of Lake Chiprana was approximately 0.2km² in November 2019. This surface area varies on the order of ~10-50m² as a result of drawdown during the summer months and flooding and decreased evapotranspiration during the winter months (Vidondo *et al.*, 1993). Long-term drawdown of the lake and changing land management in the area since the 1980's (De Wit *et al.*, 2013) has led to a decrease in surface area from 0.3km² in 1991 (Vidondo *et al.*, 1993) to 0.15-0.2km² in the present day. Coupled with the outcrop of the Oligo-Miocene sandstone ribbons, compartmentalisation of the lake into several smaller side lagoons that frequently undergo desiccation during summer has become an increasingly common occurrence at the site for the last decade (De Wit *et al.*, 2013).

4.2.3 – Lake characteristics and anthropogenic management

Lake Chiprana is defined as a predominantly meromictic lake (Vidondo *et al.*, 1993), with lake waters consisting of, in descending order of concentration, ions of SO_4^{2-} > Mg^{2+} > Na^+ > Cl^- > Ca^{2+} . The lake displays high Mg/Ca ratios, and comprises an average total dissolved salinity value of approximately 80g/L (Vidondo *et al.*, 1993). Salinity does not generally vary significantly throughout an annual hydrological cycle, but has increased steadily from a mean value of 54g/L since the first limnological studies of the lake were undertaken in 1991 (Guerrero *et al.*, 1991). The results of a limnological survey undertaken in November 2019 are displayed in Table 1, and highlight, combined with a previous hydrological study undertaken in 2019-2020 by Jódar *et al.* (2020), that the lake is mostly homogeneous. However, during periods when there is a disconnection between these sub-basins due to lake drawdown, each sub-basin undergoes concentration along a distinct chemical gradient (Calder & Neal, 1984; Vidondo *et al.*, 1993).

Lake Chiprana demonstrates extensive development of gypsum-encrusted microbial mats and charophytic/macrophytic vegetation in the littoral areas (Valero-Garces *et al.*, 2000b), a strong halocline and chemocline (De Wit *et al.*, 2013) with a weak thermal stratification, and a pelagic setting characterised by meromixis and anoxia (Vidondo *et al.*, 1993). Both the halocline and chemocline remain constant throughout an annual hydrological cycle, but have gradually weakened over the past three decades (De Wit *et al.*, 2013). Conversely, temperature stratification is stronger within the lake in August where there is often a difference of up to 6°C, and typically it undergoes inverse stratification during midwinter (Vidondo *et al.*, 1993). The small size of the lake, compartmentalisation induced by sandstone ridges and its location in a semi-arid area where annual temperatures and hydrological input can fluctuate rapidly (Bridge *et al.*, 2012) are several key factors contributing to environmental variability. Drawdown of the lake occurring in the summer followed by rejuvenation of the water levels in the winter leads to cyclic annual and in some cases bi-annual exposure and re-submersion of shallow littoral environments (Vidondo *et al.*, 1993; De Wit *et al.*, 2013).

Table 4.1 – Limnological data of Laguna Salada de Chiprana at different sites at the lake surface during November 2019. Limnological data were collected with a YSI Exo1 Multiparameter multiprobe at multiple sampling sites throughout the lake to account for any variability and heterogeneity in water chemistry. Multiple probe analyses signified that the lake was largely chemically homogeneous, and the below readings are an average of these analyses.

Site	Water Depth	Temperature	Dissolved Oxygen	Conductivity	TDS	pH
	Metres	(°C)	(mg/L)	(uS/cm)	(mg/L)	
Chiprana - Southern Main Lagoon	0.5	11.42	8.65	46013	40388	9.22
Chiprana - Western Main Lagoon	0.2	12.12	8.30	47317	40796	10.05
Chiprana - Side Lagoon	0.3	12.09	8.55	47566	41035	9.68

In terms of anthropogenic impacts and controls on limnology and the local region, there are several key changes which must be stated that are likely to have played a significant role in the evolution of the Chiprana landscape and lake. According to Valero-Garcés *et al.* (2000b) an agrarian crisis occurred within the 18th century, followed by the expansion of farmland within the early 19th century. The introduction of farm machinery, and later a change in the dominant agriculture from olive trees to corn and alfalfa crops occurred in 1950 and 1970 respectively (Valero-Garcés *et al.*, 2000b). The latter of these changes is also postulated to be related to an increase in irrigation water consumption from the nearby Civan Canal (Valero-Garcés *et al.*, 2000b) and subsequently a higher magnitude of inflow to Lake Chiprana. Most recently, since 1994 until the present day, the lake has been under a Ramsar convention and is regularly monitored to sustain the unique ecological communities found there (De Wit *et al.*, 2013).

4.3 - Methods

In March 2019, seven short cores measuring 30-50cm were retrieved from Lake Chiprana using a UWITEC[®]-type gravity corer lowered from a pneumatic boat. Six cores were retrieved in a NE-SW transect across the primary waterbody (Figure 4.2), incorporating sediments from littoral and pelagic sub-environments. In addition, a single core was retrieved from the pelagic setting in the smaller side lagoon. The cores were transported to the Institute of Pyrenean Ecology (IPE-CSIC), Zaragoza, for temporary storage at 4°C. They were then express freighted to the Department of Earth and Environmental Sciences, University of Manchester for further analyses. An approach to describing and discussing the sedimentology of Lake Chiprana was undertaken following a similar approach taken by Morellón *et al.* (2009) for Lago de Estanya.

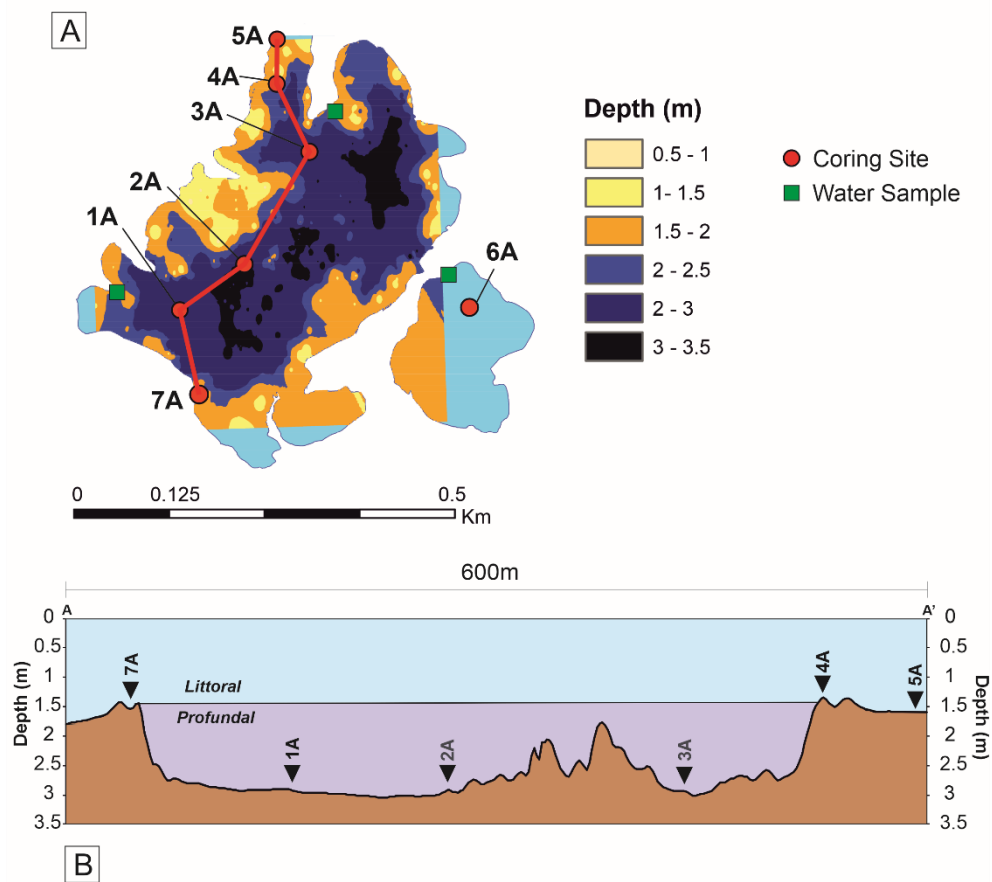


Figure 4.2 – Figure illustrating A) Bathymetric map of Lake Chiprana with the location of sediment cores and water samples retrieved from the lake during a field season in March 2019. B) Bathymetric cross-section following the line A-A' in section A, with the location of cores 1A-7A, with the exception of 6A, highlighted based on the availability of bathymetric data. Bathymetric data were collected by a previous survey undertaken by the Instituto Pirenaico de Ecología.

4.3.1 - Identification of Modern Environments

Depositional environments of Lake Chiprana (Figure 4.4) were investigated using satellite imagery and by retrieving sediments from multiple sampling points at various water depths throughout the site. Satellite images were sourced from the Organismo Autonomo Centro Nacional de Informacion Geografica, and included aerial photos taken as part of the Sentinel 2 and Landsat satellite platforms. These platforms provide ortho-image mosaics at varying degrees of pixel resolution at semi-annual periodicities. Images were retrieved from the Centro de Descargas of the Centro Nacional de Informacion Geografica for the years 2018, 2019 and 2020 to determine any large variations in lake environments during this timeframe. This satellite imagery was combined with onsite visual observations in order to determine ecological sub-environments associated with the site. In addition, samples were taken from littoral and pelagic environments, and variations in sedimentology, mineralogy and total associated with these samples allowed for key sub-environments to be identified as discussed in the results section.

4.3.2 - Facies Analysis

Facies in the cores were determined by core logging, including visual observation, measurement of visible sedimentary structures and analyses of sedimentary smear slides taken from the core sediments following the method of Schnurrenberger et al. (2003) and Morellón *et al.* (2009). Detailed observations of the smear slides and select thin sections created from resin-impregnated sediments were undertaken using a NIKON LV100ND optical microscope, a HITACHI TM3000 SEM (University of Liverpool) and a FEI QUANTA 650 SEM (University of Manchester), equipped with Bruker Instruments Quantax 70 and Bruker Xflash energy dispersive X-ray spectrometers respectively. Selected smear slides and sediment sections were analysed to produce backscattered electron images and energy dispersive X-ray maps.

4.3.2.1 - CT Scanning for Facies Identification

Sediment cores were subjected to high power X-ray computerised tomography scanning at the Henry Moseley X-ray Imaging Facility (HMXIF), School of Materials, University of Manchester using a Nikon High Flux XTEK Bay (Nikon Metrology Europe) specifically designed for time lapse X-ray Computed Tomography. Cores were placed into a cylindrical sample holder and mounted onto the rotating stage. Scanning was achieved by moving the manipulator to ensure that the sample remained in the field of view throughout a full rotation (Hickman-Lewis *et al.*, 2017). Sequential scans of 10cm x 12cm areas of each core were undertaken at regular intervals until scanned completely. A chromatic beam with an accelerating voltage of 210kV and a current of 210 μ A was used to acquire projections over a 360° rotation (Engelberg *et al.*, 2012). A 1mm thick copper filter was also placed over the tungsten X-ray source to reduce beam hardening. Raw data were processed and constructed using the ThermoFisher AVIZO® Lite software package, with data being compressed to reduce size and also being subjected to a 2-pass median filter to reduce noise.

4.3.3 - Bulk Mineralogy

Bulk mineralogy was determined by X-ray diffraction using a Bruker D8 Advance diffractometer (Bruker Corporation, Billerica, Massachusetts, United States) with a Göbel Mirror and Lynxeye detector (Department of Earth and Environmental Sciences, University of Manchester) according to standard operating procedures provided by Dr. John Waters. The X-ray tube contains a copper source and generates CuK α 1 X-rays with a wavelength of 1.5406Å. ~0.1g of sample was ground with a pestle and mortar and mixed with ~1 ml of amyl acetate. Powdered and mixed samples were transferred to glass microscope slides and air dried. Samples were scanned from 5-70°2 θ , with a step size of 0.02° and a count time of 0.2s per step. XRD diffractograms were analysed with the Bruker DIFFRAC.EVA software using standards from the International Centre for Diffraction Data Database. Quartz was used as an internal standard to correct peak shift that is typically on the order of 10s of millidegrees. The instrument is routinely calibrated using a Bruker corundum

standard. Quantitative analyses of XRD diffractograms was undertaken using DIFFRAC.TOPAS software in order to determine quantitative amounts of mineral phases. Error margins typically ranged from 0.1-2% according to wt% volume of each phase. Loss-on-ignition for determination of total organic carbon (TOC) and average carbonate content was undertaken on samples from the cores at 1cm intervals using the methods described by Vereş, (2002).

4.3.4 - XRF Scanning

Sediment cores were imaged at high-resolution using a Cox Analytical Systems ITRAX Core scanner (Cox Analytical Systems, Gothenburg, Sweden) at the School of Geography, University of Manchester. Cores were additionally scanned using X-ray fluorescence to produce measurements of the total intensity (counts per second, cps) of selected elements for correlation of key geochemical intervals between cores. Each core was scanned at 1mm spatial increments using a Mo-tube at a tube voltage of 30kv and tube current of 30mA. A wide range of elements were detected by the XRF scanner, but only Ca and Ti are considered in the scope of this study for sedimentological correlation.

4.3.5 - Chronological Model

The chronological model of the sedimentary sequence (Figure 4.3) was generated using two methods. The longest core (CHI19-1A) was correlated with the same sequence in a core retrieved from Lake Chiprana in 1997 (see Valero-Garcés *et al.*, 2000b) and 2007 (CHI97-1A and CHI07-1A) using sedimentological indicators such as distinct facies and sedimentary intervals, and geochemical indicators such as high resolution XRF data and mineralogical compositions. This provided a qualitative chronological constraint which was further complemented by radiometric dating of the older cores using ^{137}Cs and ^{14}C . Overall, the provided age model is the best possible outcome based on available data, and due to an absence of suitable woody and organic/carbonaceous material suitable for radiocarbon dating in the cores discussed in this study, remains, presently, the most suitable option for this study.

Naturally, uncertainties are thus present within this model, and these are considered in the palaeoenvironmental modelling of Lake Chiprana.

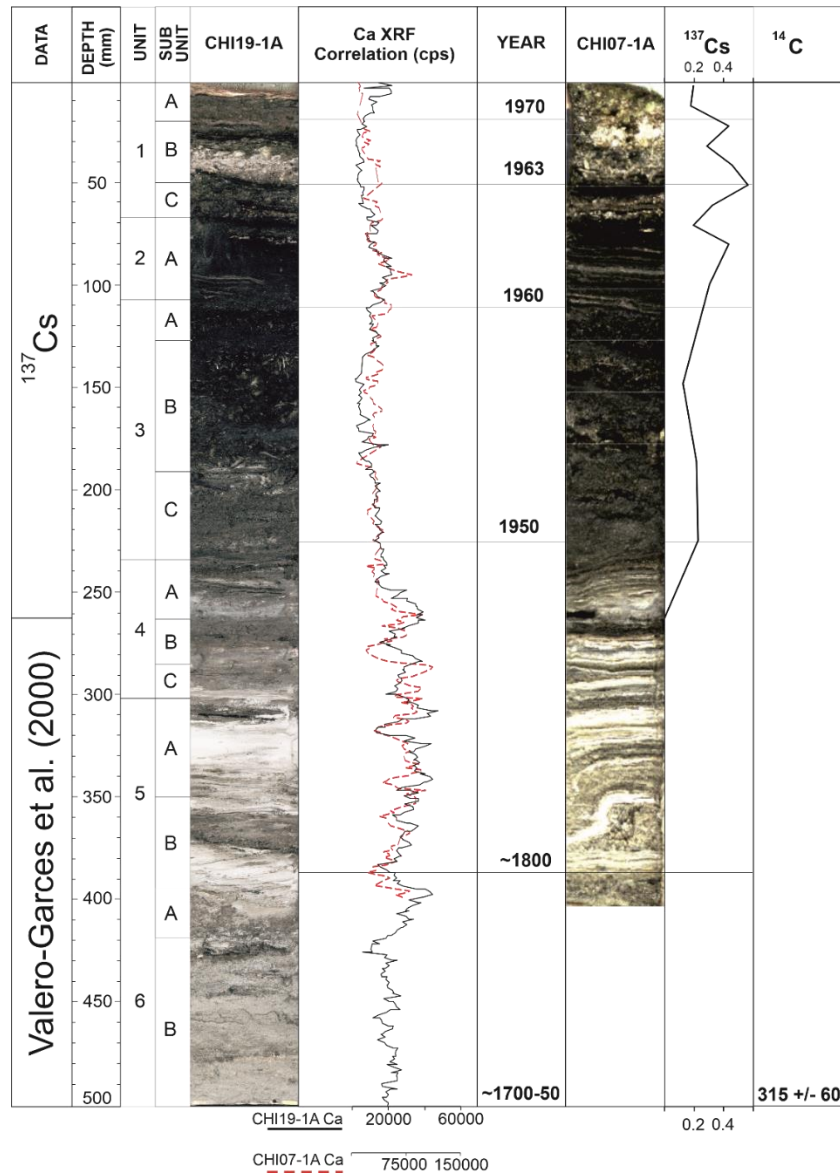


Figure 4.3 – Correlation between cores (CHI19-1A) retrieved for this study and a core (CHI07-1A) retrieved from the site in 2007. Correlation was achieved by means of facies analysis, downcore variations in sedimentology and by using qualitative measurements of Ca in both cores derived from an ITRAX XRF scanner. The chronological model of CHI07-1A was achieved using ¹³⁷Cs within the cores in relation to post WWII nuclear testing, sedimentological correlation to a core retrieved by Valero-Garces et al. (2000) and a single ¹⁴C AMS date at an approximate depth of ~50cm previously obtained by Davis et al. (1994). From left to right: Dating technique and/or correlation used for age-depth modelling, sedimentological units

and sub-units, CHI19-1A core photographs, calcium XRF profile for CHI-19-1A and CHI07-1A, approximate age based on age-depth modelling, CHI07-1A core photographs, ^{137}Cs measurements and ^{14}C dates. Horizontal core scale 5.4cm. Sedimentological features of the core are described further in Figure 6.

4.3.5.1 - Sedimentological Correlation and ^{14}C Dating

Based on initial correlation between all three sets of cores, and in particular between the 1997 and 2019 core, less than 0.5cm of sediment was deposited between their collection. Thus, the correlation can be considered largely reliable from the uppermost section. As a result, based on sedimentological correlation between cores CHI19-1A and CHI97-1A, a layer of microbial mats which appears at approximately ~25cm can be placed appearing downcore at approximately 1850A.D. In addition, assuming the low sedimentation rate between the collection of the cores, the sediments are primarily representative of the same cores for the timeframe between their collection.

4.3.5.2 - ^{137}Cs Profile – CHI-07

Core CHI07-1A was also chronologically dated using the activity of ^{137}Cs radioisotopes measured from 14 sediment samples (Valero-Garcés, 2010). The ^{137}Cs activity was measured with a photon detector Ortec-EGG (Oak Ridge TN) with an ultrapure germanium crystal well (well detector) associated with a digital gamma-ray spectrometer. The ^{137}Cs profile associated with the core taken from Lake Chiprana in 2007 (CHI07-1A) illustrates a peak at a depth of approximately 5cm. The ^{137}Cs peak relates to the accumulation of ^{137}Cs in the period between 1963-1964 (Walling and Qingping, 1992; Owens et al., 1997) owing to post World War Two nuclear testing. Furthermore, a peak at the depth range of 8.5 to 10.5cm likely corresponds to other ^{137}Cs increases during the 1950s associated with this testing. Based on the chronological model generated by the ^{137}Cs profile, unit 1 was deposited from approximately 1970 to the present day, unit 2 from ~1960 to 1970, and unit 3 from approximately 1950 onwards. A decrease in ^{137}Cs at a depth of

approximately 32cm suggests that the sediments of unit 4 were deposited prior to 1950.

4.4 - Results

4.4.1 – Modern Sedimentary Environments

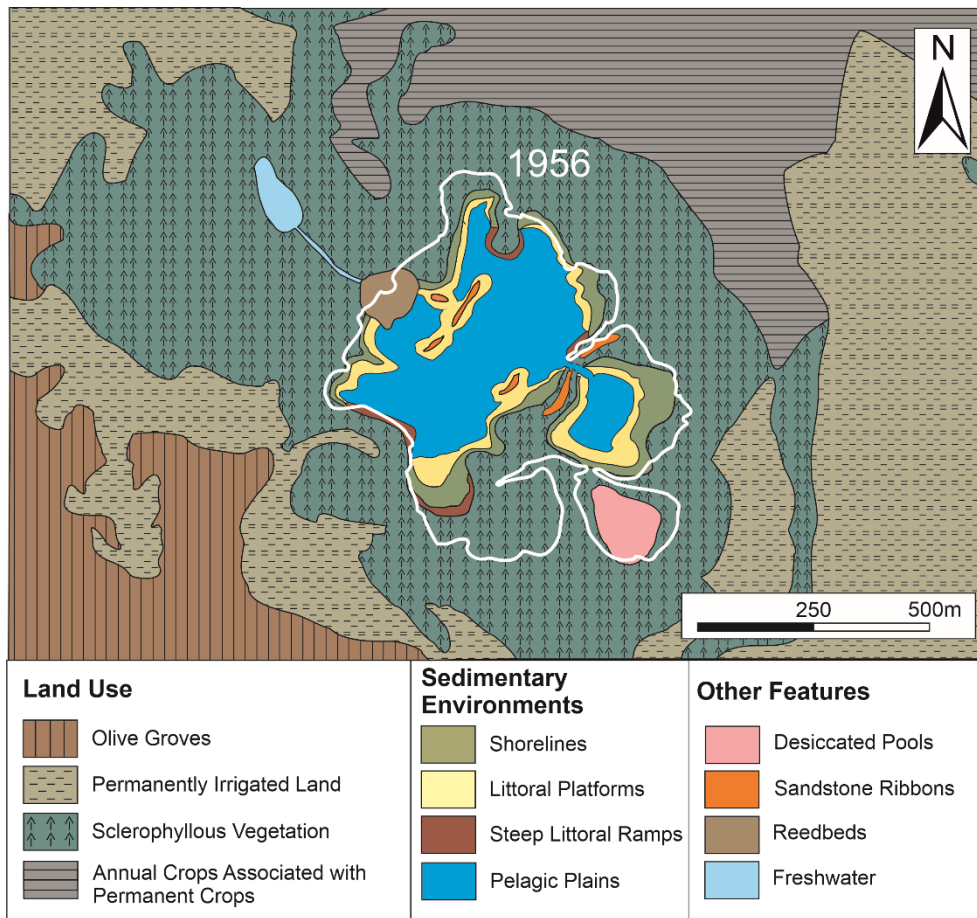


Figure 4.4 – Modern depositional sub-environments within and in proximity to Laguna Salada de Chiprana. Local land use and management mapped from CORINE land cover data in ArcMap, and palaeo-shorelines interpreted from satellite images obtained from the Centro Nacional de Información Geográfica (CNIG).

The analysis of satellite imagery sourced from the Organismo Autonomo Centro Nacional de Informacion Geografica coupled with sedimentological and visual analyses allowed for several key ecological and depositional sub-environments to be identified (Figure 4.4). These environments are placed into a classification scheme which considers visual variations identified in satellite images such as topographic relief, colour and extent, as well as the outcome of onsite investigations undertaken during fieldwork which revealed variations in ecology, sediment types and water depth, similar to examples described by Morellón *et al.* (2009). These classifications led to the development of a scheme which includes the following environments:






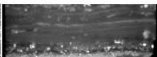





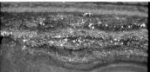
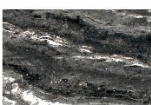
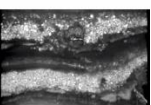







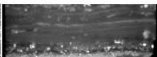





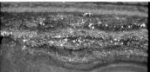
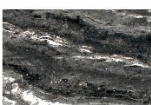
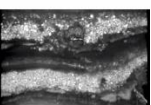







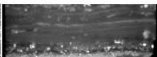





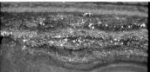
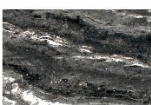
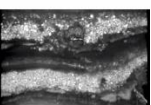


- Annually/bi-annually desiccated littoral shorelines dominated by cyanobacterial mats and large shrimp colonies of *Artemisia pathogenetica* with thick evaporitic crusts;
- Gently sloping littoral areas characterised by competition between cyanobacterial mats and charophytic and macrophytic halophilic vegetation, largely dominated by the benthic charophyte *Lamprothamnium papulosum* and beds of *Ruppia maritima* (De Wit, 2016);
- Steep-sided littoral ramps with sparse vegetation and decreased abundances of the aforementioned charophytes;
- Distal pelagic plains dominated by anoxia and the development of light-starved cyanobacterial communities intercalated with organic-rich muds.


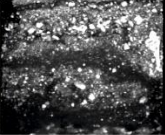



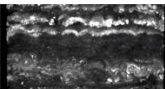
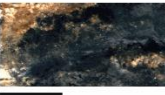

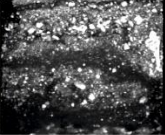



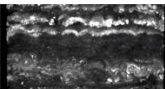
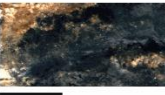

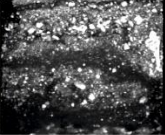



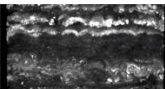
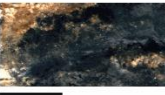
4.4.2 - Sedimentology and Stratigraphy

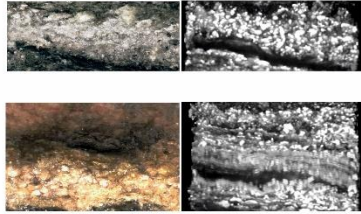
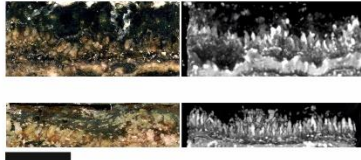
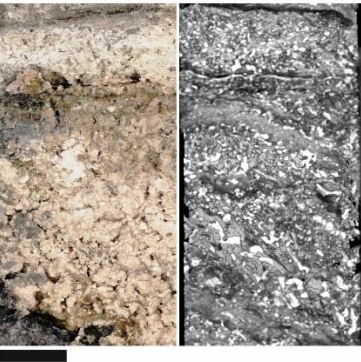
4.4.2.1 - Sedimentary Facies Analysis






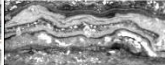



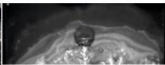









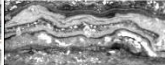



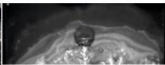









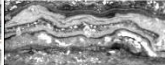



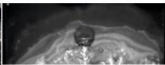




The sediment cores investigated in this study illustrate a range of facies (Figure 4.5, Table 4.2) and display variable sedimentological characteristics in different depositional sub-environments. Facies were defined from pelagic and littoral environments, with most facies being present in both settings. However, some facies were only present in either the littoral or pelagic setting as described in Table 4.2. In total, eight facies and one subfacies were identified and can be classified according


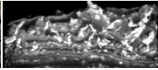

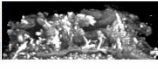




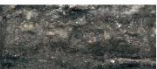




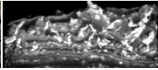

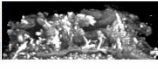




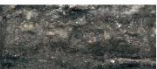




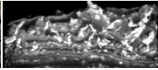

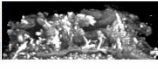




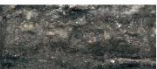



Table 4.2 - Table displaying sedimentological facies that were identified in both littoral and pelagic cores from Laguna Salada de Chiprana and both photographs and CT scans of each facies. Though many of these facies occur in varying abundance within each core, not all facies are present and in some cases are strictly limited to pelagic or littoral sedimentary environments. Mineralogical and sedimentological descriptions are also presented alongside an interpretation of the likely depositional environment that each facies formed in. Facies are represented at the same scale. Scale bars beneath each core photo represent 2cm, cores are 5.4cm in diameter. CT scan variations in grayscale represent variations in attenuation of the X-rays, corresponding to differences in composition and phase density in the samples.

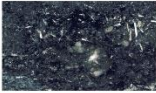
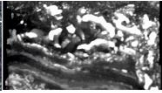

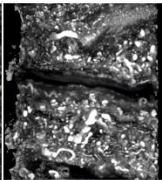

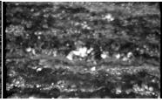

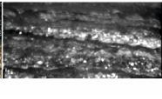
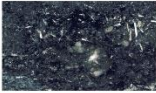
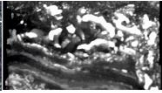

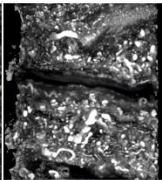

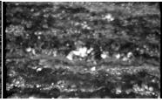

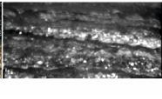
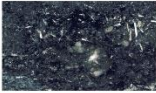
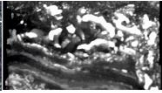

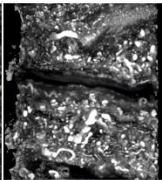

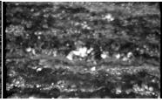

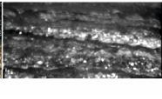
Facies	Sedimentary Characteristics		Depositional Environment																										
a	<p>Grey-yellow sandy mudstones (Detrital)</p> <p>a.1 Grey weakly bedded to massive heterolithic sandy siltstones, typically with heightened amounts of quartz and detrital aragonite and calcite. Low abundances of gypsum, halite and hexahydrate. Basal loading structures are present in some intervals.</p> <p>a.2 Massive sandy siltstones, typically illustrating a range of continuous and lenticular bed morphologies and in some cases displaying basal loading structures. Low abundances of gypsum and hexahydrate, high abundances of detrital calcite, phyllosilicates and quartz.</p>	<table border="0"> <thead> <tr> <th></th> <th>Photograph</th> <th>CT Scan</th> </tr> </thead> <tbody> <tr> <td rowspan="2">Pelagic</td> <td></td> <td></td> </tr> <tr> <td></td> <td></td> </tr> <tr> <td rowspan="2">Littoral</td> <td></td> <td></td> </tr> <tr> <td></td> <td></td> </tr> <tr> <td></td> <td>Photograph</td> <td>CT Scan</td> </tr> <tr> <td rowspan="2">Pelagic</td> <td></td> <td></td> </tr> <tr> <td></td> <td></td> </tr> <tr> <td rowspan="2">Littoral</td> <td></td> <td></td> </tr> <tr> <td></td> <td></td> </tr> </tbody> </table>		Photograph	CT Scan	Pelagic					Littoral						Photograph	CT Scan	Pelagic					Littoral					<p>Brackish to saline lake, increased terrigenous input and wet sediment deformation</p>
	Photograph	CT Scan																											
Pelagic																													
																													
Littoral																													
																													
	Photograph	CT Scan																											
Pelagic																													
																													
Littoral																													
																													




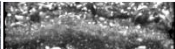

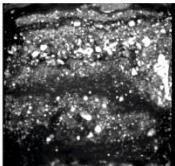

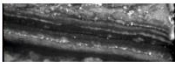





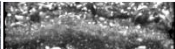

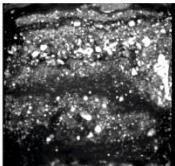

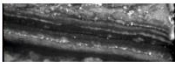





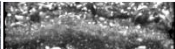

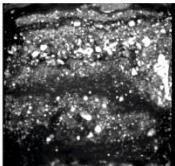

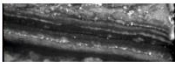


b	<p>Massive muds with gypsum Massive and poorly laminated dark coloured mudstones with abundant intergrowths of coarse gypsum as the primary mineralogical phase. Intercalated or interbedded with minor lenses of siliciclastic layers of various grain sizes or microbialite laminae. Magnesium sulphates and halite form secondary phases, carbonate and quartz absent.</p>	<table border="0" style="width: 100%; border-collapse: collapse;"> <thead> <tr> <th style="width: 10%;"></th> <th style="width: 45%; text-align: center;">Photograph</th> <th style="width: 45%; text-align: center;">CT Scan</th> </tr> </thead> <tbody> <tr> <td rowspan="2" style="vertical-align: middle; text-align: center;">Pelagic</td> <td></td> <td></td> </tr> <tr> <td></td> <td></td> </tr> <tr> <td rowspan="2" style="vertical-align: middle; text-align: center;">Littoral</td> <td></td> <td></td> </tr> <tr> <td></td> <td></td> </tr> </tbody> </table>		Photograph	CT Scan	Pelagic					Littoral					<p>Saline lake with moderate clastic input, gypsum crystals representing occasional drawdown and desiccation</p>
	Photograph	CT Scan														
Pelagic																
																
Littoral																
																

c	<p>Gypsum laminae White coloured beds and fine laminae of endogenic gypsum crystals and precipitates of highly variable grain sizes. The beds are often closely associated with Facies 1, typically overlying the upper surface of the latter facies. Minor amounts of hexahyrite and thenardite, absence of carbonates and quartz.</p>	<p style="text-align: center;">Photograph CT Scan</p> <div style="display: flex; flex-direction: column; align-items: center;"> <div style="display: flex; justify-content: space-around; width: 100%;"> <div style="text-align: center;"> <p>Pelagic</p>  </div> <div style="text-align: center;"> <p>Littoral</p>  </div> </div> </div>	<p>Hypersaline lake, likely forming during extreme periods of drought</p>
d	<p>Cemented charophytes Crystalline cemented masses of charophytes typically confined to littoral depositional environments. Predominantly composed of gypsum, with some minor amounts of aragonite, calcite and hexahyrite. Cemented charophytic and macrophytic intervals, typically massive and highly consolidated. Gypsum rich, with minor amounts of aragonite and thenardite throughout.</p>	<p style="text-align: center;">Photograph CT Scan</p> <div style="display: flex; flex-direction: column; align-items: center;"> <div style="text-align: center;"> <p>Littoral</p>  </div> </div>	<p>Littoral setting of brackish to saline lake, reduction in salinity and colonisation of littoral setting by charophytes</p>

e	<p>Laminated Microbial Mats with Mudstones Finely laminated (<1mm) cyanobacterial/microbial mats with strong red, green, and dark black staining of the sediment attributed to the presence of microbial pigments. Cyanobacterial sheaths can typically be found occurring alongside EPS, micrite matrices and densely packed microcrystalline carbonate and gypsum. Interstitial layers occurring between microbially-stained laminae consist primarily of aragonite/high-Mg calcite and gypsum/thenardite.</p>	<table border="0"> <thead> <tr> <th></th> <th>Photograph</th> <th>CT Scan</th> </tr> </thead> <tbody> <tr> <td rowspan="4">Pelagic</td> <td></td> <td></td> </tr> <tr> <td></td> <td></td> </tr> <tr> <td></td> <td></td> </tr> <tr> <td></td> <td></td> </tr> <tr> <td rowspan="3">Littoral</td> <td></td> <td></td> </tr> <tr> <td></td> <td></td> </tr> <tr> <td></td> <td></td> </tr> </tbody> </table>		Photograph	CT Scan	Pelagic									Littoral							<p>Hypersaline lake with actively forming microbial mats and small-scale precipitation of magnesium and calcium sulphates</p>
	Photograph	CT Scan																				
Pelagic																						
																						
																						
																						
Littoral																						
																						
																						

f	<p>Microbial mats with gypsum Very finely laminated dark brown and orange laminae (organic matter, diatoms) and white-yellow laminae (carbonate precipitates) interbedded with white crystalline phases (gypsum). Gypsum intergrowths form both as laminated/bedded intervals and as lenticular deposits between microbial laminae. Carbonates are primarily composed of aragonite and calcite, and other minor phases are constituted by hexahydrate and halite. Microbially-induced layering is strongly displaced by large (>0.5mm) gypsum crystals.</p>	<table border="0"> <thead> <tr> <th></th> <th>Photograph</th> <th>CT Scan</th> </tr> </thead> <tbody> <tr> <td rowspan="3">Pelagic</td> <td></td> <td></td> </tr> <tr> <td></td> <td></td> </tr> <tr> <td></td> <td></td> </tr> <tr> <td rowspan="3">Littoral</td> <td></td> <td></td> </tr> <tr> <td></td> <td></td> </tr> <tr> <td></td> <td></td> </tr> </tbody> </table>		Photograph	CT Scan	Pelagic							Littoral							<p>Hypersaline lake with actively forming microbial mats and <i>in situ</i> gypsum precipitation induced by drawdown and desiccation</p>
	Photograph	CT Scan																		
Pelagic																				
																				
																				
Littoral																				
																				
																				

g	<p>Charophytic muds Charophytic and macrophytic mudstones, typically massive, with an abundance of fragmented charophytes and macrophytes. These facies display predominantly clayey-silty grain sizes and contain moderate amounts of gypsum, hexahydrate and very small amounts of calcite, aragonite and halite. Organic content is typically high (4%-6%) and is composed of organic-rich biofilms, diatoms and charophytic remains.</p>	<table border="0"> <thead> <tr> <th></th> <th style="text-align: center;">Photograph</th> <th style="text-align: center;">CT Scan</th> </tr> </thead> <tbody> <tr> <td rowspan="2" style="vertical-align: middle; text-align: center;">Pelagic</td> <td></td> <td></td> </tr> <tr> <td></td> <td></td> </tr> <tr> <td rowspan="2" style="vertical-align: middle; text-align: center;">Littoral</td> <td></td> <td></td> </tr> <tr> <td></td> <td></td> </tr> </tbody> </table>		Photograph	CT Scan	Pelagic					Littoral					<p>Pelagial setting of brackish to saline lake, reduction in salinity and colonisation of littoral setting by charophytes</p>
	Photograph	CT Scan														
Pelagic																
																
Littoral																
																

h	<p>Black-grey laminated and organic-rich muds Very finely laminated black clayey muds with high amounts of organic carbon, moderate amounts of gypsum and halite and varying but relatively low amounts of quartz, calcite and aragonite. They are typically distinctive from adjacent facies due to their very dark black colour and strong degree of lamination.</p>	<table border="0"> <thead> <tr> <th></th> <th style="text-align: center;">Photograph</th> <th style="text-align: center;">CT Scan</th> </tr> </thead> <tbody> <tr> <td rowspan="3" style="vertical-align: middle; text-align: center;">Pelagic</td> <td></td> <td></td> </tr> <tr> <td></td> <td></td> </tr> <tr> <td></td> <td></td> </tr> <tr> <td rowspan="2" style="vertical-align: middle; text-align: center;">Littoral</td> <td></td> <td></td> </tr> <tr> <td></td> <td></td> </tr> </tbody> </table>		Photograph	CT Scan	Pelagic							Littoral					<p>Brackish to saline lake with suspension settling and little to no bioturbation</p>
	Photograph	CT Scan																
Pelagic																		
																		
																		
Littoral																		
																		

to their predominant composition including organic-rich, clastic, and gypsum-rich examples as similarly defined in the case of Lago Estanya by Morellon et al. (2009).

4.4.2.1.1 - Detrital Facies

Siliciclastic facies occur as massive to finely bedded/laminated and weakly heterolithic silt-rich beds (facies "a1") to massive to laminated clay-silt mudstone layers (facies "a2"). These facies are variably coloured, display changeable bed thicknesses, and display some basal loading and flaming. Predominant minerals include detrital calcite (30-60%), quartz (15-25%) and phyllosilicates (15-35%) (Figures 4.6-7). Moderate to small amounts of gypsum (~20%), hexahydrate (5-10%), and aragonite (15-40%) are also present in these facies.

4.4.2.1.2 - Gypsum-Rich Facies

Gypsum-rich facies consist of mudstones containing abundant microcrystalline gypsum (facies "b"), bedded intervals of endogenic gypsum crystals of varying grain size (facies "c"), and highly cemented charophytic and macrophytic vegetation (facies "d"). Gypsum crystals occurring in the mudstones are primarily between 0.05-0.1mm in size, generally being smaller than those within individual gypsum beds. Though gypsum is present in high quantities (~50%) alongside halite (~15%), thenardite (5-10%) and hexahydrate (25-40%), minor amounts of aragonite (primarily snail shells) (<5%) and calcite (~10%) occur within these facies (Figures 4.6-7).

4.4.2.1.3 - Organic-Rich Facies

Organic-rich facies include finely laminated and variably coloured microbial mats with varying amounts of gypsum (facies "e" and "f"), massive to moderately laminated clayey-silty sediments of variable thickness (facies "g"), and charophytic mudstones (facies "h"). All facies contain moderate amounts of calcite (5-15%), aragonite (~10%), quartz (5-10%), hexahydrate (20-30%), variable amounts of gypsum (20-70%) and halite (0-15%) and in some cases an abundance of fragmented charophytic and macrophytic material. In microbial mats, gypsum is present as

microcrystalline laminae and large (>0.5cm) lensoidal crystals that displace the layering of the mats. These facies display elevated loss-on-ignition (LOI) values (up to 5-6%), are predominantly black in colour, and occur in relative abundance within all cores as both bedded and massive deposits. These facies typically contain a wide range of minerals, but generally exhibit small increases in aragonite, calcite and gypsum relative to the rest of the sedimentary sequence (Figures 4.6-7).

4.4.2.2 - Sedimentological Sequence

Stratigraphical description of cores was undertaken using lithological variations, facies analysis and downcore fluctuations in bulk geochemistry, including Ti XRF counts per second values as a means to correlate sedimentological units based on geochemical characteristics. Considerable sedimentological variations were observed between cores from the pelagic (1A, 2A, 3A, 6A) and littoral (4A, 5A, 7A) sub-settings, and a generalised sequence for both sub-environments was generated (Figures 4.6-7). In the pelagic sedimentary sequence, 6 units can be identified which consist of 14 sub-units. In the littoral sedimentary sequence, 3 units can be identified which consist of 9 sub-units, and these units can be directly correlated to the 3 uppermost units of the pelagic sequence.

4.4.2.2.1 - Pelagic Sequence

The pelagic sequence of Lake Chiprana (Figure 4.6) is represented by cores 1A, 2A and 3A in the central basin and by core 6A from the smaller side basin. These cores represent the sedimentary sequence at or below an approximate mean water depth of 2-3.5 metres and are typically 40-50cm in length. Unit 6 consists of coarsening upwards mudstones and sandy siltstones of facies "a1" and "a2" respectively at its base and occasional gypsum and

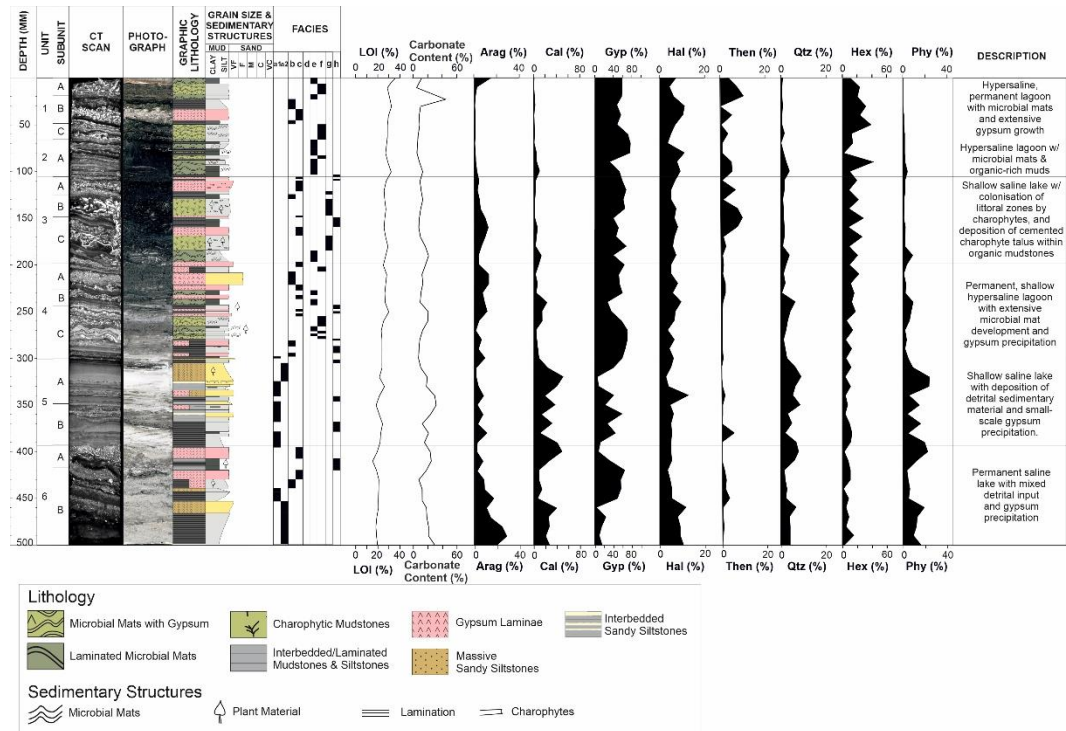


Figure 4.6 - Figure illustrating a typical sedimentary sequence of a pelagic core from Laguna Salada de Chiprana. Presented are the sedimentological units and sub-units, core photographs, graphic lithology and depositional structures, facies, loss-on ignition (%LOI), XRD results including aragonite (Arag %), calcite (Cal %), gypsum (Gyp %), halite (Hal %), thenardite (Then %) quartz (Qtz %), hexahydrite (Hex %), phyllosilicates (Phy %), and the palaeoenvironmental evolution of the lake throughout each sedimentological unit. CT scan variations in grayscale represent variations in attenuation of the X-rays, corresponding to differences in composition in the sample.

thin beds of facies “b” and “h” mudstones in the upper section. A bed of facies “c” gypsum is typically present at the top of the unit. **Unit 5** displays organic and clastic-rich facies “h” and “a2” mudstones which progress to several beds and laminae of facies “a1” heterolithic sandy siltstones, and finally to grey facies “h” mudstones. Grain size changes are common throughout this unit, and basal loading and flaming can be observed within sandy siltstone and mudstone lithologies respectively. **Unit 4** consists of finely interlaminated microbial mats with (facies “e”) and without (facies “f”) intergrown gypsum, facies “c” gypsum laminae and beds of facies “h” mudstone. The basal and middle sections of the unit are dominated by contorted microbial laminae with intergrowths of gypsum and organic-rich facies “h” mudstone. The unit progresses to an upper section dominated by facies “b” gypsum and thin beds of facies “h” microbial mats.

Unit 3 consists of a massive unit of facies “g” mudstone which contains significant volumes of charophyte and macrophyte-rich material. Several intercalated beds of facies “h” mudstones and facies “c” gypsum are present throughout the unit and are contorted where present. The unit contains several distinctive sub-units, with the upper of these containing an abundance of charophyte/macrophyte remains, and the lower sub-units containing scattered charophyte fragments and gypsum. **Unit 2** is a thin sequence that consists of very finely interbedded and laminated facies “e” microbial mats/microbialites that contain abundant microcrystalline gypsum. Microbial laminae are well-defined and relatively planar owing to the lack of distinctive gypsum crystals that often deform microbial laminae throughout the sedimentary sequence of Chiprana. **Unit 1** consists of laminated facies “f” microbial mats intercalated with facies “c” gypsum laminae and thin beds and laminae of facies “h” muds. Microbial laminae are commonly contorted, and facies “c” gypsum can be identified occurring within the microbial laminae in some cases. The unit displays an uppermost layer of laminated microbial mats directly underlain by a relatively thick layer of contorted microbial mats that are intercalated with dendritic gypsum precipitates. These layers are successively underlain by several cm-thick

intercalated beds of relatively coarse gypsum precipitates and microbial laminae, with many of the gypsum precipitates appearing to develop directly within the microbial laminae as small, rounded crystals.

4.4.2.2.2 - Littoral Sequence

The littoral sequence of Lake Chiprana is represented by cores 4A, 5A and 7A (Figure 4.7). These cores display an average length of 30-35cm, and 3 units can be identified with approximately 12-14 sub-units according to which core is observed.

Unit 3 consists of two distinctive subunits. The basal subunit contains multiple strongly laminated beds and laminae of dark black, organic-rich facies “g” charophytic mudstones with occasional thin laminae of massive facies “c” gypsum within the basal section. In the upper section, the sequence progresses to very finely laminated facies “b” mudstones and a relatively thick bed of facies “c” gypsum. The upper subunit consists of a thin interval of black laminated facies “h” mudstones and thin units of facies “g” charophytic mudstone with occasional thin gypsum beds in the basal section. In the upper section, the unit consists of partially slumped gypsum-rich facies “h” mudstones, thin microbial laminae and gypsum. Fragmented charophyte stems in this unit illustrate variable grain sizes, generally being coarsest within the orange-coloured slump features.

Unit 2 consists of a thin lower section of intercalated facies “d” gypsum and facies “b” microbial mats which progress to a thick sequence of highly cemented and highly consolidated facies “d” charophytes illustrating a dendritic morphology suggestive of the original morphology of the plants during growth. The cements are gypsum-rich with minor amounts of carbonate, and this unit is largely confined to the littoral areas of Lake Chiprana. In some cores, the very thin units of microbial mats are strongly associated with microbially-induced discolouration occurring within the subunit. **Unit 1** is comprised of thinly laminated facies “f” microbial mats with varying amounts of intergrown gypsum that are intercalated with distinct facies “c” gypsum laminae in the basal section. In its upper section, this unit consistently displays vertically

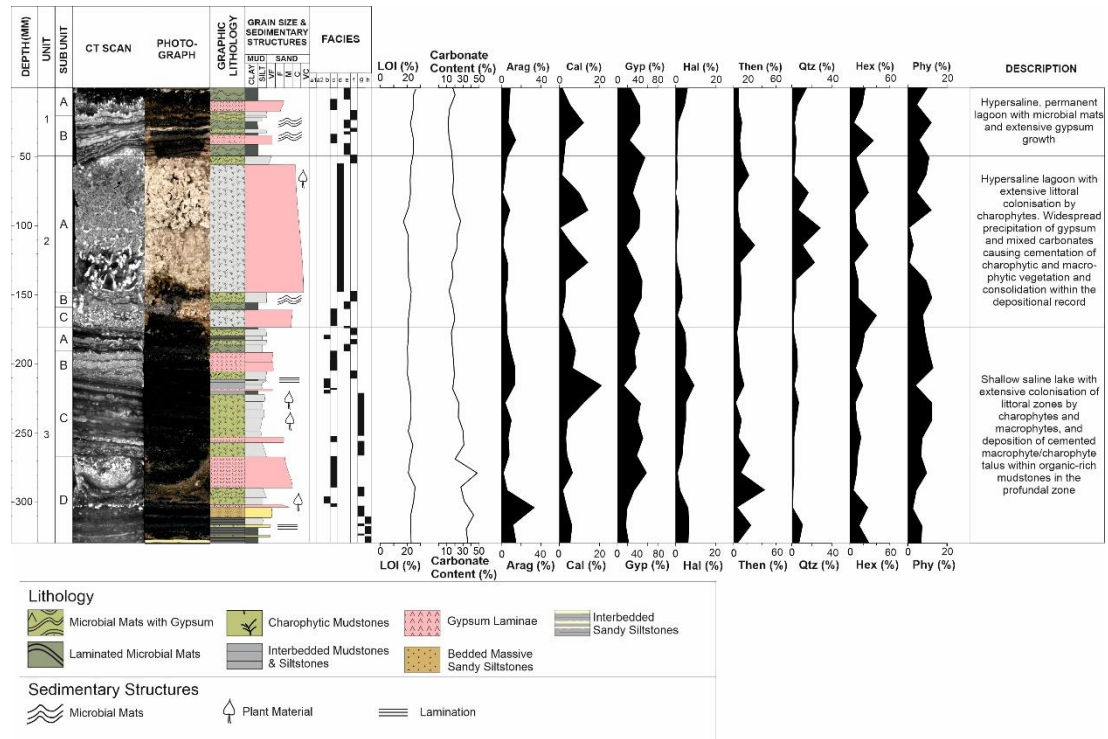


Figure 4.7 - Figure illustrating a standard sedimentary sequence of a littoral core from Laguna Salada de Chiprana. Presented are the sedimentological units and sub-units, core photographs, graphic lithology and depositional structures, facies, loss on ignition (%LOI), XRD results including aragonite (Arag %), calcite (Cal %), gypsum (Gyp %), halite (Hal %), thenardite (Then %) quartz (Qtz %), hexahydrite (Hex %), phyllosilicates (Phy %), and the palaeoenvironmental evolution of the lake throughout each sedimentological unit. CT scan variations in grayscale represent variations in attenuation of the X-rays, corresponding to differences in composition in the sample.

oriented pinnacles of gypsum that are both underlain and overlain by facies “f” microbial laminae containing varying amounts of intergrown gypsum. The lower section of the unit is characterised by thinly laminated and intercalated gypsum-rich microbial mats and gypsum laminae, with this intercalation being most pronounced in core 7A.

4.4.2.3 - Spatial Facies Variations

The sedimentary sequence of Chiprana reflects a spatially and temporally complex spectrum of depositional environments. Distinct disparities and comparisons can be observed between the pelagic and littoral depositional environments of the main lake and smaller side basin. Comparisons between facies distribution, mineralogy and geochemistry and prediction of spatial facies variability permit sedimentological correlation between cores from both sub-environments as illustrated in Figure 4.8.

Direct comparisons in depositional style can be made on a unit-by-unit basis. In the case of Unit 1, synchronous deposition of microbial mats within the modern day occurs within the pelagic and littoral sub-environments of Lake Chiprana. Those occurring more commonly within the pelagic setting (facies “e”) are strongly laminated, display poor microbial zonation and contain a mixture of non-displacive dendritic and lensoidal gypsum and smaller gypsum micro-crystals which cause little to no displacement of microbial lamination. In contrast, those occurring more commonly within the littoral setting (facies “f”) are often more poorly laminated and distorted, contain large, *in situ* gypsum crystals and cumulate gypsum, and display distinctive vertical zonation highlighted by variably coloured laminae throughout the mat (Jonkers *et al.*, 2003). Direct distinctions can also be made between the mineralogy of Unit 1 within the littoral and pelagic settings. Notably, cores from littoral environments typically contain much greater abundances of aragonite and moderately larger abundances of calcite and quartz, whilst cores from the pelagic setting typically display greater abundances of hexahydrite and halite.

Unit 2 displays significant variation between facies in the depositional environments of Lake Chiprana. In the deeper, pelagic setting, a relatively thin sequence of laminated facies "e" microbial mat intercalated with black, organic rich facies "h" laminated mudstones is present, characterised by abundant microcrystalline gypsum, moderate amounts of halite and hexahydrate, and a small amount of carbonate characterised predominantly by calcite. In contrast, cores retrieved from the littoral sedimentary environment are characterised by a variable thickness of highly cemented and consolidated facies "d" charophytes and macrophytes. This sequence is instead predominantly composed of a high abundance of gypsum cements and precipitates, with very small amounts of aragonite and thenardite as secondary phases. Correlation between these units can be made using comparisons made between unit 3 within both depositional settings as described below. Mineralogically, aragonite and calcite are in much greater abundance within the littoral cores, whilst halite and hexahydrate are typically in greater abundance within the pelagic cores.

Spatial sedimentological variations between the pelagic and littoral cores are least pronounced in unit 3. Here, all cores are characterised by a moderately thick unit of facies "g" mudstone with significant volumes of partially cemented charophyte and macrophyte fragments. The colour, thickness and overall appearance of this unit is comparable in both the pelagic and littoral cores. Lamination occurs much more frequently throughout this unit within the littoral cores than within the pelagic, and the abundance of different mineralogical phases varies between both environments. Cores from the littoral environment are also characterised by greater abundances of aragonite and quartz, whilst cores from the pelagic environment are typically characterised by greater abundances of hexahydrate. Though units 1, 2 and 3 can be correlated between cores from the pelagic and littoral sub-environments, the sedimentary sequence represented in the littoral cores does not allow for correlation to units 4, 5 and 6 within the pelagic cores. It is likely that the depocenter of Lake Chiprana has remained relatively static for the past 300 years, and thus erosion

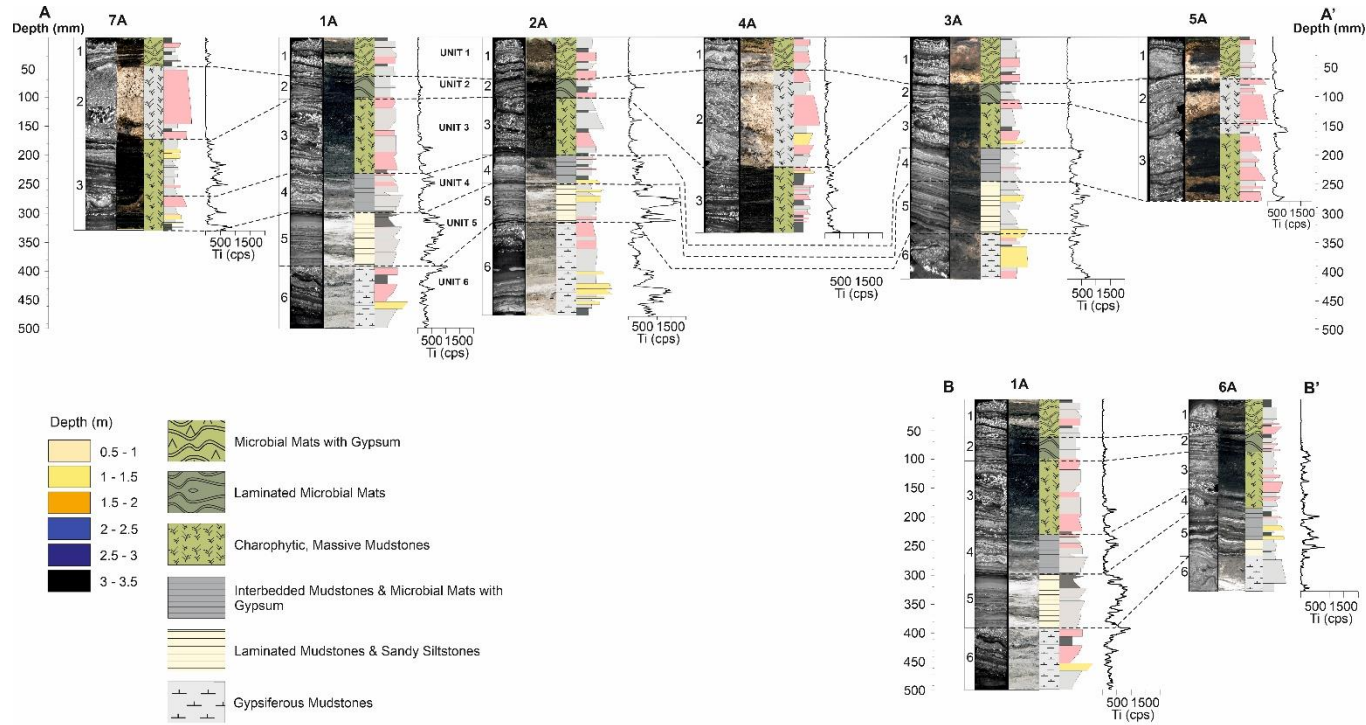


Figure 4.8 – Spatial variations in facies between cores from the pelagic and littoral settings of Laguna Salada de Chiprana. XRF data of element Ti, represented as counts per second (intensity), are included as a means of correlation between cores. Transect A-A' illustrates a sedimentological correlation between cores from the primary lake basin, whilst transect B-B' illustrates a sedimentological correlation between CHI-19-1A from the primary lake basin and CHI19-6A from the smaller side basin. Figure structure after Morellon et al. (2009).

associated with this desiccation has impacted the sequence represented within cores retrieved from the shallower depositional environments. As such, a suitable sedimentological correlation could not be carried out for the three lowermost units.

Such comparisons and distinctions can also be made between the pelagic sequences of the main basin and smaller side basin. Notably, little to no microbial mat development is observed in unit 4 in the side basin in contrast to that which occurs within the main basin. Unit 5 is characterised by thicker beds and laminae in the side basin, and in unit 6, the side basin is characterised by a sequence of highly slumped and deformed gypsum-rich sediments in contrast to the laminated detrital-gypsum rich sequence hosted within the main basin. Broadly, these disparities indicate that prior to the onset of the deposition of unit 3, significant environmental gradients were present between the two basins that led to the deposition of distinctive sedimentary sequences.

4.5 - Discussion

4.5.1 - Depositional evolution of Laguna Salada

4.5.1.1 Environmental Phase 1 (Pre-19th Century) – Shallow ephemeral lake with significant influxes of detrital sediments, moderate salinity and occasional carbonate/gypsum precipitation

The oldest sediments recovered from the profundal cores include unit 6 and indicate that Lake Chiprana was a relatively shallow, ephemeral lacustrine system (Valero-Garces *et al.*, 2000) receiving moderate amounts of detrital input from the surrounding carbonate-rich geology of the local catchment (IGME, 2003). The lake experienced variations in water volume and chemistry that likely led to the precipitation of gypsum and carbonate-rich precipitates within the detrital sediments.

In the basal section of the longest cores, silty, carbonate/gypsum-rich mudstones (facies “b” and “a1”/“a2”) indicate a period of detrital material delivered to the distal, pelagic areas of the lake with periods of small-scale lake drawdown. Such influxes of detrital material caused by input from local streams, irrigation and increased levels of runoff to the lake can be inferred by the appearance of coarsening upwards successions of massive (facies “a2”) and heterolithic bedded (facies “a1”) sandy siltstones. Prior to the deposition of sediments described here (Unit 6, Valero-Garcés et al., 2000b), Lake Chiprana was described as a shallow saline lake alike to other lakes in the modern Ebro Basin (Valero-Garcés *et al.*, 2000b). Deposition of massive fine muds (Unit 5, Valero-Garcés et al., 2000b) and erosional surfaces followed this and indicated an abrupt change in the depositional environment around 3.5 ka BP, with the lake transitioning to a dry mudflat around this time (Valero-Garcés *et al.*, 2000b).

The upper section of unit 6 and the onset of gypsum-rich mudstones (facies “b”), gypsum laminae (facies “c”), and laminated organic-rich mudstones (facies “h”) indicates several rapid environmental changes. Increases in water delivered to the system are also coherent with a “shallow ephemeral saline lake” setting (Valero-Garcés et al., 2000a) as indicated by increased detrital material and mixed evaporites in this study, while higher *Ruppia* and *Potamogeton* pollen identified by Valero-Garcés et al. (2000a) are coherent with the lake setting potentially becoming more permanent. Increases in gypsum content indicate that Lake Chiprana likely underwent drawdowns during the influx of detrital material to the lake, whilst short-term periods of anoxia within the pelagic setting and specifically within the sediment-water interface may have restricted biological activity in the pelagic zone. This succession was eventually succeeded by the input of a significant amount of coarse material to the lake, likely via a change in surface runoff that was being delivered to Lake Chiprana at the time.

4.5.1.2 - Environmental Phase 2 (1800-1900CE) – Permanent, shallow lake with extensive macrophyte development and detrital input

The shift from gypsum-rich muds (facies “b”) to finely interbedded detrital clays (facies “a2”), heterolithic laminated sandy siltstones (facies “a1”) and fine organic-rich mudstone laminae (facies “h”) associated with unit 5 reflects a clear environmental change within Lake Chiprana. The site underwent a transition from a semi-ephemeral to permanent lagoon (Valero-Garces *et al.*, 2000) with moderate detrital input to a shallow, permanent saline lake with heightened lake levels, increased detrital input, and brief periods of bottom-water anoxia. Detrital-rich (predominantly phyllosilicates, quartz and detrital calcite) material within the pelagic areas of the lake, and the punctuation of these sediments by black, organic-rich intervals (facies “h”) indicates the mobilisation and deposition of organic material during brief episodes of anoxia in the sediment-water interface (Valero-Garces *et al.*, 2000). Anoxia may have resulted from stratification of the lake-waters induced by a salinity gradient (Boehrer & Schultze, 2008; Morellón *et al.*, 2009), evidenced by increased proportions of gypsum relative to the increased amount of detrital material associated with sediments in this unit.

The periodic appearance of facies “a1” during this time also suggests that increased local input of detrital material sourced from the activity of nearby streams and increased runoff, likely from irrigation returns, occurred throughout this stage of the lake’s palaeoenvironmental history. Significant increases in the proportion of detrital calcite, quartz and phyllosilicates coupled with decreases in endogenic gypsum and aragonite within these facies are strong evidence for increased terrigenous input (Valero-Garces *et al.*, 2000), in this case being the Oligocene-Miocene carbonate-rich marls and sandstones that surround the lake (IGME, 2003).

4.5.1.3 - Environmental Phase 3 (~1900-1950CE) – Semi-permanent, shallow lagoon with high salinity and extensive microbial mat development, gypsum precipitation and reduced colonisation by macrophytes

During this phase, the lake underwent a transition to a shallow lagoon with high salinity, extensive colonisation by microbial mats (facies “e” and “f”) and the widespread development of gypsum (facies “c”) within the sediments and mats. Repeated occurrences of microbial mats (facies “e”) represents the onset of repeated periods of extensive colonisation of the lakebed by bacterial colonies (De Wit *et al.*, 2013). Small-scale variations in water chemistry were influenced by lake-level fluctuations, and seasonal desiccation of the lake led to the development of gypsum within the mats, which led to the occurrence of facies “f”. Stratification of the lake waters coupled with periods of anoxia and photosynthetic and sulphate-reducing activity likely also led to the concentration and precipitation of endogenic calcite and aragonite needles within the sediments (Morellón *et al.*, 2009; v. Knorre & Krumbein, 2013).

Comparisons of this stage with that of Lake Chiprana in the modern can be made due to the similarities and extensiveness of microbial mats that dominate the littoral and pelagic areas of the site at present. In this state, saline and hypersaline lacustrine systems are highly susceptible to small-scale variations in lake levels and lake water chemistry (Alonso, 1998), and are typically conducive to the formation of microbial mats due to the harsh environmental conditions which negate more complex cellular life (Bolhuis *et al.*, 2014). In the present, Lake Chiprana has illustrated both a long-term decrease in lake levels and seasonal desiccation and exposure of marginal and littoral areas (De Wit *et al.*, 2013). Similar conditions were likely prevalent throughout this period, with small-scale lake drawdown and flooding throughout annual hydrological cycles leading to cyclic development of microbial

mats and the precipitation of gypsum that deposited in the sequence represented here.

4.5.1.4 - Environmental Phase 4 (~1950CE) – Shallow lake with decreased salinity, extensive colonisation by macrophytes and charophytes in the littoral zone, and deposition of massive macro/charophytic remains in organic-rich mudstones in the lower littoral and pelagic zones

Based on ¹³⁷Cs dating, Lake Chiprana underwent a significant shift from a saline-hypersaline lagoon with extensive microbial mat development (Facies “e” and “f”) to a shallow, moderately saline lake with widespread growth of macrophytic and charophytic vegetation. In the littoral zones, the appearance of black, weakly to moderately laminated organic-rich facies with fragments of gypsum-cemented charophytes and macrophytes (facies “g”) are intercalated with thin organic-rich black mudstones (facies “h”). This suggests the lake was characterised by suspension settling of charophytic/macrophytic-rich mudstones within these areas, as evidenced by stronger lamination of the sediments within the cores retrieved from these areas. In contrast, the lack of such lamination and the appearance of the same sediments with more massive structures within the pelagic settings of the lake indicate mobilisation of these sediments was much more common in this zone, with much of the sedimentary material likely being transported to the deeper areas of the lake.

The onset of these facies suggest Lake Chiprana exhibited elevated water levels and experienced bottom water anoxia as evidenced by the dark black colour of the sediments associated with this timeframe and the lack of any distinct bioturbation. These increases in lake level, based on the widespread appearance of facies “g” in both pelagic and littoral cores, were clearly extensive. Moderate decreases in

aragonite and calcite formed from evaporation from the base to the top of the unit likely suggest a gradual increase in water volume throughout the deposition of this unit. Analogous examples of this facies and its associated depositional environment have been identified occurring in various other modern environments such as Lake Ganau within the Kurdistan region of Iraq (Khanaqa *et al.*, 2013), where both fossil and living macrophyte stems alike to those preserved in Lake Chiprana are found. Excellent examples of the calcified charophyte stems associated with this unit are also found in abundance in the geological past. This was highlighted by Soulié-Märsche *et al.* (2010) for the Late Pleistocene of “Trau au Natron”, where calcified charophyte stems alike to those found at Chiprana occur in abundance.

4.5.1.5 - Environmental Phase 5 (~1960s~90s) - Permanent, shallow lagoon with high salinity and extensive microbial mat development and formation of microcrystalline gypsums

The environmental transition during phase 5 led to the development of thinly laminated microbial mats (facies “e”) intercalated with thin organic-rich mudstones (facies “h”). These facies suggest that light penetration was sufficient to reach the bottom sediments of the lake, but anoxia was largely prevalent based on the absence of bioturbation, black colour and moderately high organic content of the sediments, particularly within the laminated black mudstones (facies “h”). It is likely that the mats developing in this environment were comprised of light-starved microbial communities (Jonkers *et al.*, 2003), with their development being sporadically interrupted by the deposition of the thinly laminated black mudstones (facies “h”) associated with this period.

In the littoral zone, high salinity and supersaturation with respect to gypsum induced the formation of microbial mats with large gypsum crystals (facies “f”). Strong gradients in salinity and water chemistry may have been induced by fluctuations in

nutrient loading (Diaz *et al.*, 1998) from the use of the lake as a reservoir, leading to variations in mat morphology and gypsum form. However, the initial development of microbial mats in the littoral zones was quickly diminished by the extensive colonisation of charophytic vegetation in these areas as evidenced by the presence of thick, cemented masses of these plants within the sequence (facies “d”). Precipitation of sulphate and carbonate within the lake waters led to much of this vegetation being coated by thick rinds of evaporitic and carbonate mineral phases (Apolinarska *et al.*, 2011). This process can be observed occurring in the modern day at the site, with littoral and sub-littoral vegetation and man-made objects being enclosed within thick, gypsum and carbonate-rich precipitates that form during drawdown of the lake during the annual summer desiccation period (De Wit *et al.*, 2013). Overall, this period of time indicates a slow yet progressive transition of the site to its current state in the modern day. Lake waters were slowly receding and salinity likewise increasing, microbial mats were developing throughout the lake, and intense competition between these mats and charophytes was occurring in both pelagic and littoral environments.

4.5.1.6 - Environmental Phase 6 (1990s-Present) - Permanent, shallow lagoon with high salinity and extensive microbial mat development and large-scale gypsum precipitation

A transition to gypsum- (facies “b”) and organic-rich mudstones (facies “h”) and facies “e” microbial mats in the pelagic sequence alongside lenticular gypsum (facies “d”), distorted microbial mats (facies “f”) and carbonate precipitates in the littoral sequence of Chiprana respectively represent the onset of increasing salinity, anoxia in the hypolimnion, and decreasing lake levels. Multiple sub-sequences of microbial mats overlain by microcrystalline to cm-scale gypsum suggest several cycles of lake drawdown and flooding, with drawdown being primarily reflected by gypsum beds and laminae and the onset of microbial mats by lake level increases. Intercalations

of thin laminae of gypsum-rich mudstones likely represent periods of reduced microbial mat growth, particularly within the pelagic setting where reduced light and strong anoxia may have limited the development of these communities (Jonkers *et al.*, 2003; Morellón *et al.*, 2009).

Broadly, the present-day sediments of Chiprana reflect an interplay between various processes occurring within the littoral and pelagic sub-settings of the lagoon. Extensive microbial mats colonise much of the littoral setting and extend into the pelagic setting, with morphological and mineralogical variations apparent between mats from both areas. Extensive precipitation of cumulate gypsum occurs within in the littoral zones and dendritic gypsum within the pelagic zones, and the distinctive variation in gypsum morphology likely reflects variations in saturation state (Morellón *et al.*, 2009) and the effects of lake level change between these zones.

4.5.2 - The Role of Climate and Anthropogenic Activities

When assessing the progression and evolution of anthropogenic activities and climatic change in the region, it is imperative these factors are fully understood in order to determine their effects upon processes of detrital influx, chemically induced deposition, ecological competition and biotically-induced deposition in Lake Chiprana.

4.5.2.1 - Phases 1-2 (Units 6 and 5): ~1700 to ~1800

The basal units of the sedimentary sequence identified in cores in this study broadly reflect the effects of an increase in lake level that occurred during the 18th century (Valero-Garcés *et al.*, 2000b). Palaeoclimatic reconstructions from other lakes in the region which were once saline (Valero-Garcés *et al.*, 2000a; Morellón *et al.*, 2008; Corella *et al.*, 2013) indicate an increase in the total annual precipitation within the Ebro Basin during this time, and other palaeoclimatic records also suggest increases in heavy rainfall events and flooding episodes throughout NE Spain during the mid-17th and 18th to mid 19th centuries (Llasat *et al.*, 2005; Barriendos & Rodrigo, 2006;

Corella *et al.*, 2014, 2016, 2019; Rodríguez-Lloveras *et al.*, 2017). Despite this, historical data, a recent hydrochemical modelling study by Jódar *et al.* (2020) and agricultural activity associated with the nearby Civan Canal (Valero-Garcés *et al.*, 2000b) throughout the last three centuries indicate that increasing lake levels during this time are more likely to be related to changes in anthropogenic activity within the region. The Civan canal, which is reported to have been constructed in the 12-13th centuries and has since been used to divert water from the Guadalupe River (Díaz *et al.*, 1998; Valero-Garcés *et al.*, 2000), with irrigation returns being diverted to

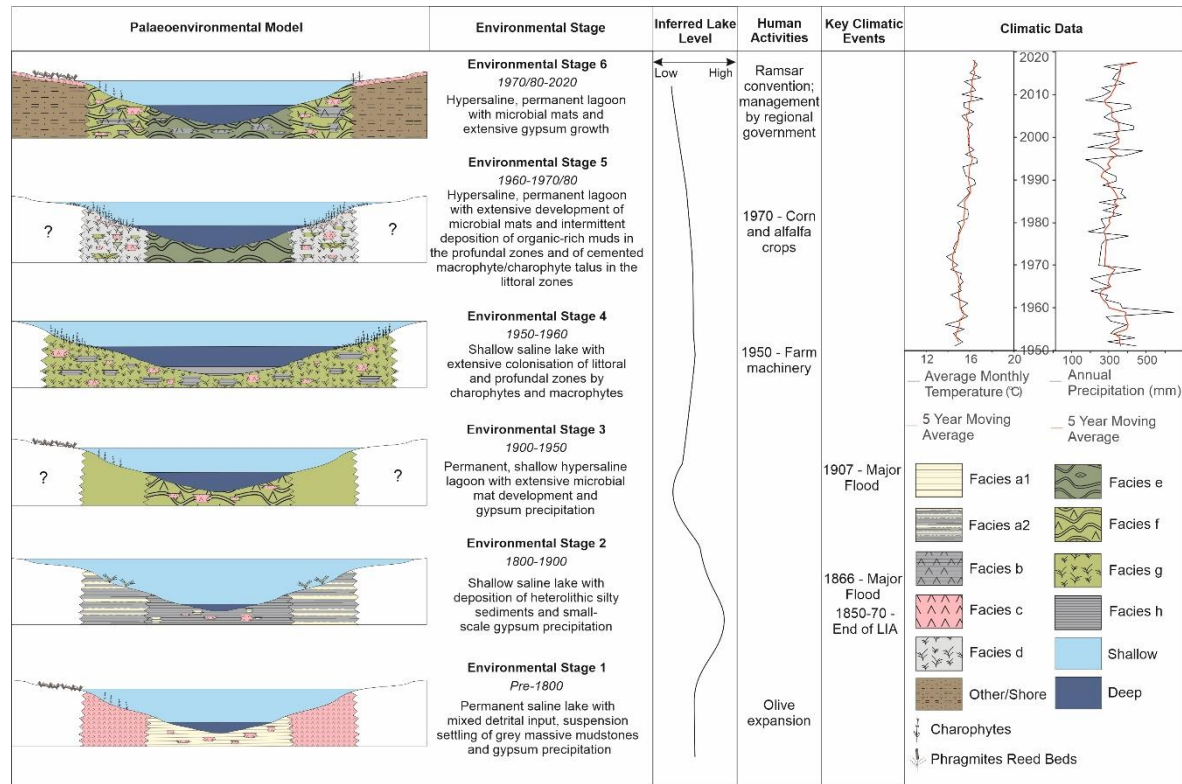


Figure 4.9 – Figure illustrating palaeoenvironmental models of Lake Chiprana for the last 250-300 years, inferred lake levels based on sedimentology and geochemistry, key climatic events and changes in anthropogenic activities, and climatic data for the region for the last ~70 years. Lake levels are inferred from broad sedimentological variations throughout the sequence and from mineralogical data of sediments. Climatic data are sourced from the KNMI Climate Explorer (<https://climexp.knmi.nl/start.cgi>).

Laguna de Las Rocas and then to Lake Chiprana (Valero-Garces *et al.*, 2000). Thus, the long-standing function of Lake Chiprana as a reservoir for excess discharge from nearby canals and drainage routes (Valero-Garces *et al.*, 2000; De Wit *et al.*, 2013), a factor that has allowed the lake to remain permanent due to the increased water surplus supplied from these inputs, clearly highlights the strong anthropogenic imprint already present upon the sedimentary sequence, and likely plays a key role in masking climatic and other environmental factors.

Previous investigations of Lake Chiprana and the local region have also revealed human impacts within the Ebro Basin that are coherent with the sequence described here (González-Sampériz *et al.*, 2008; López-Moreno *et al.*, 2011; Pérez-Lambán *et al.*, 2018). Such anthropogenic factors are also endorsed by pollen records (Valero-Garces *et al.*, 2000b) which place the onset of modern agriculture, increasing expansions of farmland, and the introduction and expansion of olive cultivation and irrigation occurring throughout the 16th-19th centuries. These developments are generally in time with increased lake levels in Chiprana associated with the increased detrital input present within units 5 and 6. Increased irrigation returns, most likely encapsulating a mixture of groundwater pumping and overland runoff from diversions of inflow water (Valero-Garcés *et al.*, 2000b; Jódar *et al.*, 2020), likely played a key role in the lake water levels during this time. Overall, it is likely that there is some interplay between climatic and anthropogenic factors within this section of the palaeoenvironmental reconstruction, but it is difficult to fully delineate their individual impacts due to the longstanding anthropogenic influences in the region of Chiprana.

4.5.2.2 - Phases 3-4 (Units 4 and 3): 1800-1950

The shift from detrital-rich claystones and sandy siltstones to laminated microbial mats with gypsum intergrowths marks a significant environmental change occurring within Lake Chiprana. Reduced precipitation during the early 20th century (Corella *et al.*, 2014, 2016, 2019) led to decreased lake levels, increased salinity, and the

development of an environment which promoted the formation of microbial mats and gypsum precipitation. Despite this period of long-term drawdown, the onset of organic-rich mudstones containing an abundance of calcified charophyte stems associated with unit 3 suggests that Lake Chiprana underwent lake level increases coinciding with the end of the 19th century (Valero-Garces *et al.*, 2000). It is well known that the end of the 19th century/early 20th century in the region largely coincides with increasing anthropogenic activity in the region, namely increasing agricultural practices (Valero-Garces *et al.*, 2000) which likely led to increased irrigation and inflow to the lake. Additionally, relatively high levels of gypsum within this unit and the development of distinctive gypsum laminae correspond with variations in water chemistry, potentially related to small-scale variations in lake level. Increasing irrigation returns may have caused lake level rises towards the upper section of unit 4 as indicated by increasing detrital minerals towards the upper sections of the unit. This likely coincides with increases in lake levels also associated with the base of unit 3 at approximately 1950. Such increases correlate directly to the introduction of farm machinery within the region of Chiprana (Valero-Garces *et al.*, 2000), again suggesting the role anthropogenic activity likely played in controlling lake levels.

4.5.2.3 - Phases 5-6 (Units 2 and 1): 1950-Present

The past 60 years of environmental change at Lake Chiprana have represented a period of high spatial variability throughout the lake, increasing and changing land use, and particularly within the last 2-3 decades, of increasing management of the site to preserve the unique biological communities it contains (De Wit *et al.*, 2013). Various studies and surveys of the region during this time show that increasing lake levels at Chiprana within the 1950s correlate strongly to the introduction of farm machinery in the area (Valero-Garces *et al.*, 2000; Valero-Garcés *et al.*, 2000a), and the abundance of organic-rich, black facies in the pelagic cores specifically highlights these increased lake levels. Additionally, shifting agricultural practices from the growth of olive trees to corn crops in the 1960s and 1970s have been correlated with

increasing water levels caused by increases in irrigation within the region (Valero-Garces *et al.*, 2000; Valero-Garcés *et al.*, 2000a). Direct comparisons of these increasing lake levels with climatic variations for the past 60 years also indicate a lack of climatic influences (Valero-Garces *et al.*, 2000). As is highlighted in Figure 4.9, meteorological data highlight increasing average temperatures from 1951-2018, no significant increases in precipitation, and only several humid years (annual rainfall > 350mm)(KNMI). It is plausible therefore that decreased inflow to the lake, potentially from reduced irrigation inflow, coupled with increasing temperatures, have led to the increasing salinity of the lake since the 1970s.

In the last three decades, the site has been managed by the Gobierno de Aragon, with a strong focus on the conservation of the microbial and ecological communities being undertaken following several decreases in salinity induced by irrigation inputs into the lake in the 1980s and 1990s (De Wit *et al.*, 2013). These management measures, emplaced in 1994, have included monthly measurements of water quality, lake levels, and inflow from Laguna de Las Rocas and has since allowed for a significant recovery and expansion of microbial mats throughout the lake (De Wit *et al.*, 2013). Despite this, there has since 2000 been a steady trend of increasing salinity within the lake as a result of decreasing lake levels (Diaz *et al.*, 1998). It is estimated that the lake surface area has decreased from 0.3km² to 0.2km² since the beginning of the 21st century which has drastically reduced the area of developing microbial mats while simultaneously inducing conditions that negate their formation.

4.5.3 - Further Applications

This study provides findings that are applicable to global saline lake research when considering the spatial variability of the sedimentary sequence of Lake Chiprana. Sedimentary sequences are often described temporally in such research, but very rarely are such sequences described with regards to their spatial variability. The seven cores retrieved from Lake Chiprana illustrate that the pelagic and littoral ecological sub-environments are governed by distinct rates and styles of

sedimentation. Understanding not only temporal but spatial variations within such settings is crucial for fully reconstructing past environments throughout the lake basin, particularly within larger basins such as Lake Van (Litt *et al.*, 2009) and Lake Mar Chiquita (Troin *et al.*, 2010) where such variability is significantly pronounced.

Additionally, the unique nature of many Spanish saline lakes (Valero-Garcés *et al.*, 2000a; Schröder *et al.*, 2018) such as Lake Chiprana lends itself to the reconstruction of similar analogues within the sedimentary record. Palaeolimnological studies such as that undertaken here and elsewhere (Hassani *et al.*, 2020) ultimately show that management efforts can be difficult, as they illustrate the complexities of saline lakes whilst also highlighting the anthropogenic impacts and controls upon many such settings (Finlayson, 2016). Thus, the management of these threatened ecosystems (Jellison *et al.*, 2008) must consider not only the climatic and environmental aspects, but also the history of anthropogenic impacts upon these ecosystems.

4.6 - Conclusions

The pelagic and littoral sub-environments of Lake Chiprana as represented by short sediment cores illustrate a spatially and temporally complex sedimentological sequence. Hypersaline lakes are often subject to rapid fluctuations due to changing water levels (Brock & Hammer, 1987; Schröder *et al.*, 2018), with primary controlling factors including climate, variations in hydrology, intrinsic variations in biogeochemistry, clastic input, and anthropogenic modification of the landscape. In Lake Chiprana, sub-decadal and potentially sub-annual fluctuations in these factors have led to the deposition of a convoluted sequence within the last three centuries. The results of the study highlight the ability of the lake to record environmental changes as represented by spatial and temporal variations in sedimentology and mineralogy. It additionally reveals how such settings may act as high-resolution palaeoenvironmental archives that allow for the reconstruction of environmental change over varying timescales. It is important that future work focuses on

delineating both intrinsic and extrinsic environmental processes and factors controlling these lakes if their full potential as palaeoenvironmental archives is to be recognised. Though anthropogenic activities have unquestionably contributed to the physicochemical attributes of Lake Chiprana for the last 300 years, the effect of climatic changes and their signal within the sedimentary record of the lake must be considered to determine the significance of such changes in influencing the environmental evolution of the lake for the last 300 years.

Acknowledgements

Financial support for this research was provided by the Natural Environment Research Council (NERC), grant no. NE/L002469/1 to C. Doyle, from the Spanish Ministry of Science and Technology, project MEDLANT to B. Valero-Garcés; and the European Union MSCA-IF-EF-ST funding scheme, project FLOODARC (796752) to J.P. Corella. We are grateful for assistance and guidance that was provided by technical staff and research associates at the Instituto Pirenaico de Ecología (IPE-CSIC) in Zaragoza. Additional thanks are given to Dr. John Waters at the University of Manchester for his extensive support in the collection and processing of X-ray diffraction data, and to Dr. Julia Behnsen at the Henry Moseley X-Ray Facility for assistance in the collection of computerised X-ray tomography data. Sincere thanks are also due to John Moore, Dr. Thomas Bishop and Dr. Jonathan Yarwood at the University of Manchester Geography laboratories for assistance in core preparation and storage. Sincere thanks are also due to Mario Morellon for personal communications regarding how the data could be presented.

Data Availability Statement

The data that support the findings of this study are openly available in the Environmental Information Data Centre.

References

- Alonso, M.** (1998) The lagoons of Peninsular Spain . *Limnetica*, **15**, 1–176.
- Apolinarska, K., Pelechaty, M. and Pukacz, A.** (2011) CaCO₃ sedimentation by modern charophytes (Characeae): can calcified remains and carbonate $\delta^{13}\text{C}$ and $\delta^{18}\text{O}$ record the ecological state of lakes? – a review. *Stud. Limnol. Telmatologica*, **5**, 55–66.
- Barriendos, M. and Rodrigo, F.S.** (2006) Study of historical flood events on Spanish rivers using documentary data. *Hydrol. Sci. J.*, **51**, 765–783.
- Birks, H.H. and Birks, H.J.B.** (2006) Multi-proxy studies in palaeolimnology. *Veg. Hist. Archaeobot.*, **15**, 235–251.
- Boehrer, B. and Schultze, M.** (2008) Stratification of lakes. *Rev. Geophys.*, **46**, 1–27.
- Bolhuis, H., Cretoiu, M.S. and Stal, L.J.** (2014) Molecular ecology of microbial mats. *FEMS Microbiol. Ecol.* 90:335–350.
- Boyle, J.F.** (2005) Inorganic Geochemical Methods in Palaeolimnology. In: *Tracking Environmental Change Using Lake Sediments*, 1st edn. (Ed. W.M. Last and J.P. Smol), *Springer*, Dordrecht, 83–141.
- Bridge, J., Demicco, R., Bridge, J. and Demicco, R.** (2012) Earth Surface Processes, Landforms and Sediment Deposits. *Cambridge University Press*, 563-594 pp.
- Brock, M.A. and Hammer, U.T.** (1987) Saline Lake Ecosystems of the World., 1st edn. *Springer*, Dordrecht, 580 pp.
- Calder, I.R. and Neal, C.** (1984) Evaporation from saline lakes: a combination equation approach. *Hydrol. Sci. Journal/Journal des Sci. Hydrol.*, **29**, 89–97.
- Comin, F.A. and Alonso, M.** (1988) Spanish salt lakes: Their chemistry and biota. *Hydrobiologia*, **158**, 237–245.
- Corella, J.P., Benito, G., Rodriguez-Lloveras, X., Brauer, A. and Valero-Garcés, B.L.** (2014) Annually-resolved lake record of extreme hydro-meteorological events since AD 1347 in NE Iberian Peninsula. *Quat. Sci. Rev.*, **93**, 77–90.
- Corella, J.P., Benito, G., Wilhelm, B., Montoya, E., Rull, V., Vegas-Vilarrúbia, T.**

- and **Valero-Garcés, B.L.** (2019) A millennium-long perspective of flood-related seasonal sediment yield in Mediterranean watersheds. *Glob. Planet. Change*, **177**, 127–140.
- Corella, J.P., Stefanova, V., El Anjoumi, A., Rico, E., Giralt, S., Moreno, A., Plata-Montero, A. and Valero-Garcés, B.L.** (2013) A 2500-year multi-proxy reconstruction of climate change and human activities in northern Spain: The Lake Arreo record. *Palaeogeogr. Palaeoclimatol. Palaeoecol.*, **386**, 555–568.
- Corella, J.P., Valero-Garcés, B.L., Vicente-Serrano, S.M., Brauer, A. and Benito, G.** (2016) Three millennia of heavy rainfalls in Western Mediterranean: Frequency, seasonality and atmospheric drivers. *Sci. Rep.*, **6**, 1–11.
- Davis, B.** (1994) Paleolimnology and Holocene Environmental Change from Endoreic Lakes in the Ebro Basin, North-east. University of Newcastle Upon Tyne
- De Wit, R.** (2016) Lake La Salada de Chiprana (NE Spain), an Example of an Athalassic Salt Lake in a Cultural Landscape. In: *Lake Sciences and Climate Change*, 1st edn. (Ed. M.N. Rashed), *IntechOpen*, Rijeka, 43–60.
- De Wit, R., Guerrero, M.C., Legaz, A., Jonkers, H.M., Blocier, L., Gumiaux, C. and Gautret, P.** (2013) Conservation of a permanent hypersaline lake: Management options evaluated from decadal variability of coleofasciculus chthonoplastes microbial mats. *Aquat. Conserv. Mar. Freshw. Ecosyst.*, **23**, 532–545.
- Degermendzhy, A.G., Zadereev, E.S., Rogozin, D.Y., Prokopkin, I.G., Barkhatov, Y. V., Tolomeev, A.P., Khromechek, E.B., Janse, J.H., Mooij, W.M. and Gulati, R.D.** (2010) Vertical stratification of physical, chemical and biological components in two saline lakes Shira and Shunet (South Siberia, Russia). *Aquat. Ecol.*, **44**, 619–632.
- Deocampo, D.M. and Jones, B.F.** (2013) Geochemistry of Saline Lakes. In: *Treatise on Geochemistry: Second Edition*, 2nd edn. (Ed. K. Turekian and H. Holland), *Elsevier*, **7**, 437–469.
- Diaz, P., Guerrero, M.C., Alcorlo, P., Baltanas, A., Florin, M. and Montes, C.**

- (1998) Anthropogenic perturbations to the trophic structure in a permanent hypersaline shallow lake: La Salada de Chiprana (north-eastern Spain). *Int. J. Salt Lake Res.*, **7**, 187–210.
- Domínguez-Castro, F., García-Herrera, R., Ribera, P. and Barriendos, M.** (2010) A shift in the spatial pattern of Iberian droughts during the 17th century. *Clim. Past*, **6**, 553–563.
- Engelberg, D.L., Patrick, R.A.D., Wilson, C., McCrae, R. and Withers, P.J.** (2012) Three-dimensional imaging of inhomogeneous lithologies using X-ray computed tomography: characterization of drill core from the Borrowdale Volcanic Group. *Mineral. Mag.*, **76**, 2931–2938.
- Finlayson, C.M.** (2016) Salt Lakes. In: *The Wetland Book* (Ed. C.M. Finlayson, G.R. Milton, R.C. Prentice, and N.C. Davidson), *Springer Netherlands*, Dordrecht, 1–12.
- González-Sampériz, P., Valero-Garcés, B.L., Moreno, A., Morellón, M., Navas, A., Machín, J. and Delgado-Huertas, A.** (2008) Vegetation changes and hydrological fluctuations in the Central Ebro Basin (NE Spain) since the Late Glacial period: Saline lake records. *Palaeogeogr. Palaeoclimatol. Palaeoecol.*, **259**, 157–181.
- Guerrero, M.C., Balsa, J., Pascual, M. and Martínez, B.** (1991) Caracterización limnológica de la Laguna Salada de Chiprana (Zaragoza, España) y sus comunidades de bacterias fototróficas. *Limnetica*, **7**, 83–96.
- Hassani, A., Azapagic, A., D’Odorico, P., Keshmiri, A. and Shokri, N.** (2020) Desiccation crisis of saline lakes: A new decision-support framework for building resilience to climate change. *Sci Total Environ.* doi: 10.1016/j.scitotenv.2019.134718
- Hickman-Lewis, K., Garwood, R.J., Withers, P.J. and Wacey, D.** (2017) X-ray microtomography as a tool for investigating the petrological context of Precambrian cellular remains. *Geol. Soc. Spec. Publ.*, **448**, 33–56.
- IGME** (2003) Mapa Geológico de España, 1:50000, (serie MAGNA). Hoja 988. Puente-Genil.

- Jellison, R., Williams, W.D., Timms, B., Alcocer, J. and Aladin, N. V.** (2008) Salt lakes: Values, threats and future. In: *Aquatic Ecosystems: Trends and Global Prospects*, 94–110.
- Jódar, J., Rubio, F.M., Custodio, E., Martos-Rosillo, S., Pey, J., Herrera, C., Turu, V., Pérez-Bielsa, C., Ibarra, P. and Lambán, L.J.** (2020) Hydrogeochemical, isotopic and geophysical characterization of saline lake systems in semiarid regions: The Salada de Chiprana Lake, Northeastern Spain. *Sci. Total Environ.*, **728**, 1–48.
- Jones, B.E., Grant, W.D., Duckworth, A.W. and Owenson, G.G.** (1998) Microbial diversity of soda lakes. *Extremophiles*, **2**, 191–200.
- Jonkers, H.M., Ludwig, R., De Wit, R., Pringault, O., Muyzer, G., Niemann, H., Finke, N. and De Beer, D.** (2003) Structural and functional analysis of a microbial mat ecosystem from a unique permanent hypersaline inland lake: “La Salada de Chiprana” (NE Spain). *FEMS Microbiol. Ecol.*, **44**, 175–189.
- Juggins, S.** (2013) Quantitative reconstructions in palaeolimnology: New paradigm or sick science? *Quat. Sci. Rev.*, **64**, 20–32.
- Kelts, K. and Hsü, K.J.** (1978) Freshwater Carbonate Sedimentation. In: *Lakes: Chemistry, Geology, Physics* (Ed. A. Lerman), Springer New York, New York, NY, 295–323.
- Khanaqa, P.A., Karim, K.H. and Thiel, V.** (2013) Characeae-derived carbonate deposits in Lake Ganau, Kurdistan Region, Iraq. *Facies*, **59**, 653–662.
- Last, W.M.** (2002) Geolimnology of salt lakes. *Geosci. J.*, **6**, 347–369.
- Last, W.M. and Schweyen, T.H.** (1983) Sedimentology and geochemistry of saline lakes of the Great Plains. *Hydrobiologia*, **105**, 245–263.
- Litt, T., Krastel, S., Sturm, M., Kipfer, R., Örcen, S., Heumann, G., Franz, S.O., Ülgen, U.B. and Niessen, F.** (2009) “PALEOVAN”, International Continental Scientific Drilling Program (ICDP): site survey results and perspectives. *Quat. Sci. Rev.*, **28**, 1555–1567.
- Liu, D., Abuduwaili, J., Lei, J., Wu, G. and Gui, D.** (2011) Wind erosion of saline playa sediments and its ecological effects in Ebinur Lake, Xinjiang, China.

Environ. Earth Sci., **63**, 241–250.

- Llasat, M.C., Barriados, M., Barrera, A. and Rigo, T.** (2005) Floods in Catalonia (NE Spain) since the 14th century. Climatological and meteorological aspects from historical documentary sources and old instrumental records. *J. Hydrol.*, **313**, 32–47.
- López-Moreno, J.I., Vicente-Serrano, S.M., Moran-Tejeda, E., Zabalza, J., Lorenzo-Lacruz, J. and García-Ruiz, J.M.** (2011) Impact of climate evolution and land use changes on water yield in the Ebro basin. *Hydrol. Earth Syst. Sci.*, **15**, 311–322.
- Lowenstein, T.K., Hadie, L.A. and Hardie, L.A.** (1985) Criteria for the recognition of salt-pan evaporites. *Sedimentology*, **32**, 627–644.
- Luzón, A.** (2005) Oligocene-Miocene alluvial sedimentation in the northern Ebro Basin, NE Spain: Tectonic control and palaeogeographical evolution. *Sediment. Geol.*, **177**, 19–39.
- Morellón, M., Valero-Garcés, B., Anselmetti, F., Ariztegui, D., Schnellmann, M., Moreno, A., Mata, P., Rico, M. and Corella, J.P.** (2009) Late quaternary deposition and facies model for karstic Lake Estanya (North-eastern Spain). *Sedimentology*, **56**, 1505–1534.
- Morellón, M., Valero-Garcés, B., Moreno, A., González-Sampériz, P., Mata, P., Romero, O., Maestro, M. and Navas, A.** (2008) Holocene palaeohydrology and climate variability in northeastern Spain: The sedimentary record of Lake Estanya (Pre-Pyrenean range). *Quat. Int.*, **181**, 15–31.
- Ohkouchi, N., Nakajima, Y., Okada, H., Ogawa, N.O., Suga, H., Oguri, K. and Kitazato, H.** (2005) Biogeochemical processes in the saline meromictic Lake Kaiike, Japan: Implications from molecular isotopic evidences of photosynthetic pigments. *Environ. Microbiol.*, **7**, 1009–1016.
- Owens, P.N., Walling, D.E., He, Q., Shanahan, J. and Foster, I.D.L.** (1997) Utilisation d'une technique de mesure par le césium-137 pour l'établissement du bilan sédimentaire du bassin versant "Start", dans le Devon (Royaume-Uni). *Hydrol. Sci. J.*, **42**, 405–423.

- Pérez-Lambán, F., Peña-Monné, J.L., Badía-Villas, D., Picazo Millán, J.V., Sampietro-Vattuone, M.M., Alcolea Gracia, M., Aranbarri, J., González-Sampériz, P. and Fanlo Loras, J.** (2018) Holocene environmental variability in the Central Ebro Basin (NE Spain) from geoarchaeological and pedological records. *Catena*, **163**, 147–164.
- Rodriguez-Lloveras, X., Corella, J.P. and Benito, G.** (2017) Modelling the Hydro-Sedimentary Dynamics of a Mediterranean Semiarid Ungauged Watershed Beyond the Instrumental Period. *L. Degrad. Dev.*, **28**, 1506–1518.
- Schnurrenberger, D., Russell, J. and Kelts, K.** (2003) Classification of lacustrine sediments based on sedimentary components. *J. Paleolimnol.*, **29**, 141–154.
- Schröder, T., van 't Hoff, J., Ortiz, J.E., de Torres Pèrez-Hidalgo, T.J., López-Sáez, J.A., Melles, M., Holzhausen, A., Wennrich, V., Viehberg, F. and Reicherter, K.** (2018) Shallow hypersaline lakes as paleoclimate archives: A case study from the Laguna Salada, Málaga province, southern Spain. *Quat. Int.*, **485**, 76–88.
- Soulié-Märsche, I., Bieda, S., Lafond, R., Maley, J., M'Baitoudji, Vincent, P.M. and Faure, H.** (2010) Charophytes as bio-indicators for lake level high stand at “Trou au Natron”, Tibesti, Chad, during the Late Pleistocene. *Glob. Planet. Change*, **72**, 334–340.
- Troin, M., Vallet-Coulomb, C., Sylvestre, F. and Piovano, E.** (2010) Hydrological modelling of a closed lake (Laguna Mar Chiquita, Argentina) in the context of 20th century climatic changes. *J. Hydrol.*, **393**, 233–244.
- v. Knorre, H. and Krumbein, W.E.** (2013) Bacterial Calcification. In: *Microbial Sediments*, 25–31.
- Valero-Garcés, B., Morellón, M., Moreno, A., Corella, J.P., Martín-Puertas, C., Barreiro, F., Pérez, A., Giralt, S. and Mata-Campo, M.P.** (2014) Lacustrine carbonates of Iberian Karst Lakes: Sources, processes and depositional environments. *Sediment. Geol.* 299:1–29.
- Valero-Garcés, B.L.** (2010) Radiometric dating by ¹³⁷Cs of the recent sediments of the Salt of Chiprana.

- Valero-Garcés, B.L., Delgado-Huertas, A., Navas, A., Machín, J., González-Sampériz, P. and Kelts, K.** (2000a) Quaternary palaeohydrological evolution of a playa lake: Salada Mediana, central Ebro Basin, Spain. *Sedimentology*, **47**, 1135–1156.
- Valero-Garcés, B.L. and Kelts, K.R.** (1995) A sedimentary facies model for perennial and meromictic saline lakes: Holocene Medicine Lake Basin, South Dakota, USA. *J. Paleolimnol.*, **14**, 123–149.
- Valero-Garcés, B.L., Navas, A., Machin, J., Stevenson, T. and Davis, B.** (2000) Responses of a saline lake ecosystem in a semiarid region to irrigation and climate variability: The history of Salada Chiprana, central Ebro basin, Spain. *Ambio*, **29**, 344–350.
- Vereş, D.** (2002) A Comparative Study Between Loss on Ignition and Total Carbon Analysis on Mineralogenic Sediments. *Stud. Univ. Babeş-Bolyai, Geol.*, **47**, 171–182.
- Vidondo, B., Martínez, B., Montes, C. and Guerrero, M.C.** (1993) Physico-chemical characteristics of a permanent Spanish hypersaline lake: La Salada de Chiprana (NE Spain). *Hydrobiologia*, **267**, 113–125.
- Walling, D.E. and Qingping, H.** (1992) Interpretation of caesium-137 profiles in lacustrine and other sediments: the role of catchment-derived inputs. *Hydrobiologia*, **235–236**, 219–230.
- Williams, W.D.** (2002) Environmental threats to salt lakes and the likely status of inland saline ecosystems in 2025. *Environ. Conserv.*, **29**, 154–167.
- Zadereev, E., Lipka, O., Karimov, B., Krylenko, M., Elias, V., Pinto, I.S., Alizade, V., Anker, Y., Feest, A., Kuznetsova, D., Mader, A., Salimov, R. and Fischer, M.** (2020) Overview of past, current, and future ecosystem and biodiversity trends of inland saline lakes of Europe and Central Asia. *Int. Waters*, **10**, 438–452.

Chapter 5 - Spatio-Temporal Variations in the Geochemistry of Laguna Salada de Chiprana, NE Spain

Connor Doyle^a, Stefan Schröder^a, Juan Pablo Corella Aznar^b, Blas Valero Garces^e

*a – Department of Earth and Environmental Sciences, University of Manchester,
Manchester, UK*

*b – CIEMAT – Environmental Department (DMA), Avenida Complutense 40, E-
28040 Madrid, Spain.*

*e – Instituto Pirenaico de Ecología, Consejo Superior de Investigaciones Científicas,
Zaragoza, Spain*

Abstract

Hypersaline lakes are sensitive and increasingly threatened ecological and depositional environments that are host to a diverse spectrum of industrial services, natural resources, and environmental processes. Furthermore, they are also important repositories of high-resolution palaeoenvironmental information and are potentially key archives in the reconstruction of environmental, climatic conditions and past human impact in areas where other such repositories may not be available. Many saline lakes are threatened by increased farming and irrigation practices and the effects of global warming. Geochemical XRF analyses of a transect of sediment cores from Laguna Salada de Chiprana, a permanent hypersaline lake in the Iberian Peninsula, provide insights into geochemical processes and palaeoenvironmental changes occurring at the site throughout the last 300-400 years. Key changes identified within the sequence are defined both from a spatial and temporal aspect and characterise the profundal and littoral sub-environments of the lake. Initially, the onset of a phase of widespread agriculture and irrigation in the region occurred in the late 16-17th century to ~1850AD and was associated with relative increases in lake levels. This was followed by decreasing lake levels between 1850-1950AD, likely associated with increasing evaporative processes and decreased irrigation returns to the lake, which also allowed for increased organic productivity in the profundal setting. This may have been associated with the transition of the site to a wetland-type setting where biological processes were able to flourish in the shallower central depocentres of the lake. In sequence, the introduction of farm machinery and changing irrigation patterns occurred around 1950 caused small increases in lake levels, colonization by charophytes as well as increased organic productivity in the littoral setting, likely due to the establishment of suitable environments for biological processes to occur in the shallower margins of the lake when water levels rose. Since this period to the present day, slow drawdown of the lake has occurred coupled with increasing management of the site by the regional government, leading to several phenomena. Evaporative processes are high throughout the lake, there are falling but highly variable water levels, and there is a

segmentation of organic productivity whereby falling lake levels permit increased organic productivity in the profundal setting but decrease productivity in the littoral setting due to the establishment of harsh evaporitic and erosive conditions in this area. The reconstruction reveals the high sensitivity of Lake Chiprana as an environmental archive, and illustrates the need to utilise multiple sediment cores for accurate palaeoenvironmental reconstructions of saline lakes due to the strong variability in depositional and geochemical sub-environments.

Keywords: lacustrine; sedimentology; geochemistry; anthropocene

5.1 - Introduction

Lacustrine basins are distributed worldwide and contain extensive and often detailed archives of palaeoenvironmental information essential to reconstructing the past and understanding the dynamics of such basins as well as global change (Dee *et al.*, 2018). Many studies have provided both numerous and detailed depositional, geochemical and palaeohydrological models for a wide range of these settings, including karstic (Martín-Puertas *et al.*, 2008; Morellón *et al.*, 2009a; Valero-Garcés *et al.*, 2014), freshwater (Sturm & Matter, 2009; Corella *et al.*, 2016), fluvio-lacustrine (Caran, 1998), tufaceous (Pellicer *et al.*, 2016) and volcanic (Sáez *et al.*, 2007) examples. Fewer studies have however considered the potential of hypersaline lacustrine systems (Schröder *et al.*, 2018) to act as valid repositories of environmental information. Many hypersaline lakes are highly complex systems with extreme environmental conditions which nullify the development of complex life (Jones *et al.*, 1998; Jellison *et al.*, 2008). Globally, they are generally concentrated in closed, endorheic basins with low rainfall and high rates of evapotranspiration (Hassani *et al.*, 2020). In many cases, saline-hypersaline lakes can effectively act as high-resolution archives of environmental information due to their high sensitivity to environmental and anthropogenic factors (Hardie *et al.*, 1978; Last, 2013).

Though many hypersaline lakes can indeed be considered excellent targets for the study of environmental change at high-resolution, this also lends premise to the need for detailed investigations of such sites if their sedimentology and geochemistry are to be fully understood (Brock & Hammer, 1987; Schröder *et al.*, 2018). Reliable environmental archives are often scarce in many arid to semi-arid areas of the globe (Schröder *et al.*, 2018), and subsequently hypersaline lakes can offer a potential source of critical palaeoenvironmental information if their sequences are characterised in similar detail to other studies focusing on lacustrine settings. This is however becoming progressively achievable with the increasing availability and ease of non-destructive techniques including microfacies description (Zhang *et al.*, 2020a;

Bonk *et al.*, 2021) and geochemical analyses, particularly (μ)X-ray fluorescence core scanning (Martín-Puertas *et al.*, 2011; Czymzik *et al.*, 2013; Chawchai *et al.*, 2016; Gebregiorgis *et al.*, 2020). Using such multidisciplinary approaches, many studies have effectively generated high-resolution palaeoenvironmental reconstructions of lacustrine sedimentary archives at varying temporal scales (Morellón *et al.*, 2008; Martín-Puertas *et al.*, 2011; Valero-Garcés *et al.*, 2014; Corella *et al.*, 2021), ranging from hundreds to tens of thousands of years. However, very few such studies have applied the same methods to hypersaline lake sediment records, and the global occurrence of such systems (Finlayson, 2016) coupled with their ability to respond to environmental change (Last, 2002; Martín-Puertas *et al.*, 2011) warrants further investigation of these environments in their consideration as palaeoenvironmental archives.

This study presents a multiproxy palaeoenvironmental reconstruction of the primary geochemical processes occurring in hypersaline Laguna Salada de Chiprana, Northern Spain, for the last ~350-400 years. This setting is a unique athalassic (non-sea originated) hypersaline permanent lake in Europe (De Wit, 2016), providing a natural laboratory to investigate environmental and anthropogenic processes occurring in the Ebro Basin (Valero-Garcés *et al.*, 2000). The study aimed to determine the primary intrinsic and extrinsic factors and processes represented within the sediment sequence comparatively to other Iberian lakes throughout the peninsula (Morellón *et al.*, 2009b; Martín-Puertas *et al.*, 2011; González-Sampériz *et al.*, 2017). To achieve this, the study describes and interprets various processes occurring in Lake Chiprana throughout the last three to four centuries, providing insights into the potential for hypersaline lacustrine systems to be used as palaeoenvironmental archives. Finally, the study aims to take a novel approach by adopting a multi-core approach to understanding both climatic and anthropogenic influences acting on the site, presenting novel ways to investigate these unique ecological and depositional systems. This study is also a continuation of previous work undertaken on Laguna Salada de Chiprana which considered the

sedimentological aspects of the different depositional sub-environments associated with the lake (Doyle *et al.*, 2022). Therein, nine facies, including one subfacies, were identified, including organic-, gypsum- and detrital-rich example as defined in Table S1. Integration of sedimentological and geochemical data was undertaken in order to further delineate palaeoenvironmental changes occurring within Lake Chiprana throughout the last three to four centuries.

5.2 - Study Area

5.2.1 - Geology and Geomorphology

Laguna Salada de Chiprana (41°14'30"N, 0°10'50"W) is situated in the endorheic Ebro Basin in Northeast Spain, 5km Southwest of the town of Chiprana on the Ebro River (Figure 5.1). The lake is approximately 5m deep and is the deepest, permanent hypersaline lake within the Iberian Peninsula (Valero-Garcés *et al.*, 2000). The regional geological setting is comprised of Oligocene-Miocene claystones and marls which are cross-cut by complexes of Oligocene sandstone palaeochannels (IGME, 2003a; Luzón, 2005). Primary geomorphological features include flat-topped terraces composed of the Oligo-Miocene marl and mudstone bodies and ridges and topographic highs composed of the Oligocene sandstone palaeochannels. In Lake Chiprana, these sandstone palaeochannels form a distinctive topographical feature known as "inverted topography" (De Wit *et al.*, 2013), whereby the ridges formed by the channels segment the lake into multiple sub-basins (Valero-Garcés *et al.*, 2000). This particular topographical feature has become increasingly more defined in recent years as a result of lake drawdown and segmentation (Gorny *et al.*, 2009).

5.2.2 - Climate and Hydrology

The region of Northeast Spain where Lake Chiprana is situated is defined by a semi-arid and Mediterranean climate (Vidondo *et al.*, 1993), with a strong summer drought and increased rainfall in winter. The mean temperature is 15.5°C (Domínguez-Castro *et al.*, 2010), with temperature minima and maxima of approximately 3°C and

34°C in winter and summer respectively. High rates of evapotranspiration act as the primary hydrological output (1000-1500mm/yr), whilst low rainfall (~400mm/yr), groundwater input (Jódar *et al.*, 2020) and an over-ground channel inlet from Laguna de las Roces, a nearby freshwater pond, are the main inputs. July is typically the driest month, while May and October are the wettest months. The surface area of the lake was approximately 0.2km² during November 2019, and had increased by approximately 0.01km² in December 2021 (Doyle *et al.*, 2022). This surface area has varied between 10-50m² throughout previous annual hydrological cycles due to the increased aridity during summer and flooding and increased rainfall that occurs in the winter. Increasing land management since the 1980's (De Wit *et al.*, 2013) has furthermore led to an overall fall in surface area of the lake from 0.3km² in 1991 (Vidondo *et al.*, 1993) to 0.2km² in 2019.

5.2.3 – Limnological characteristics

Na⁺, Mg²⁺, and Cl and SO₄²⁻ ions are the key chemical constituents of the lake water (De Wit *et al.*, 2013). Salinity values are reported as being around 70-80g/L (De Wit *et al.*, 2013), and observations from the Gobierno de Aragon (Aragon County Council) have shown it to be rising since the lake was first limnologically characterised in the early 1990's (Guerrero *et al.*, 1991). Two limnological surveys undertaken in November 2019 and in November 2021 are displayed in Table 5.1. The November 2019 survey shows that Lake Chiprana exhibits homogeneous chemistry in the primary waterbody and the Eastern side lagoon. During this survey, the lake exhibited an average temperature of 11.88°C, an average dissolved oxygen value of 8.5mg/L, an average conductivity of 46,965µs/cm, an average total dissolved solids (TDS) value of 40g/L, and an average pH of 9.65. The December 2021 survey illustrated an average surface temperature of approximately 8.85°C, an average dissolved oxygen value of 7.86mg/L, conductivity of 39767µs/cm, an average TDS of 37378mg/L and an average pH of 9.6. Furthermore, a survey of the entire water column illustrated a strong vertical gradient in all of these parameters, with significant increases in temperature, TDS and conductivity, and significant

Table 5.1 – Limnological characteristics of Laguna Salada de Chiprana at the lake surface during November 2019 and at both the lake surface and approximately 2m and 4m depth during December 2021. Limnological data are from a YSI Exo1 Multiparameter multiprobe.

Site	Water (m)	Depth	Temperature (C)	Dissolved Oxygen (mg/L)	Conductivity (uS/cm)	TDS (mg/L)	pH
	Metres		°C	mg/L	uS/cm	mg/L	
November 2019							
Chiprana - Southern Main Lagoon	0.5		11.42	8.65	46013	40388	9.22
Chiprana - Western Main Lagoon	0.2		12.12	8.30	47317	40796	10.05
Chiprana - Side Lagoon	0.3		12.09	8.55	47566	41035	9.68
December 2021							
Chiprana - Main Lagoon - Surface	0		8.85	7.86	39767.20	37378.00	9.60
Chiprana - Main Lagoon - 2m	2		8.798	7.38	39583.7	37260	10.1
Chiprana - Main Lagoon - 4m	4		24.404	1.76	113728.7	74775	3.23

decreases in dissolved oxygen and pH. Overall, the lake is largely meromictic but has been observed to show water mixing and non-stratification in the past due to changes in nutrient loading (Diaz *et al.*, 1998).

5.3 - Material and Methods

Seven short sediment cores measuring between ~30-50cm were retrieved from Lake Chiprana in March 2019 using a UWITEC®-type gravity corer lowered from a pneumatic boat across a 600m transect as defined earlier in Doyle *et al.* (2022). Six of the cores were retrieved in a NE-SW transect across the primary waterbody (Figure 5.1) to include a range of sediments from the different depositional sub-environments of the lake. A single sediment core measuring approximately 37cm was also retrieved from the smaller side lagoon. Cores were kept in a cool box and transported to the Institute of Pyrenean Ecology (IPE-CSIC), Zaragoza for temporary storage at 4°C. They were then transported to the School of Geography, the University of Manchester for analyses and permanent storage. Sediment cores were subjected to several methods of geochemical analysis, including ICP-MS and ICP-OES, μ -XRF scanning, X-ray diffraction and $\delta^{13}\text{C}_{\text{org}}$ measurements. Methods were undertaken and results carried out following a similar approach undertaken in Lake Zonar in 2011 due to the comparative similarity of the two settings (Martín-Puertas *et al.*, 2011).

5.3.1 - Bulk Geochemistry

5.3.1.1 - LOI & $\delta^{13}\text{C}_{\text{org}}$

Loss-on-ignition analyses also undertaken on samples from the cores at 1cm intervals using the methods described by Vereş (2002) in order to determine parameters such as organic and carbonate content. Samples were initially freeze-dried in bulk to remove water content and then heated in a furnace (CARBOLITE ELF11/14B). Samples were weighed before and after drying and after each stage of being subjected to the technique, with the determination of loss-on-ignition after

ignition at 550°C for 2 hours and carbonate content after ignition at 925°C for 4 hours (Vereş, 2002). For $\delta^{13}\text{C}_{\text{org}}$ measurements, organic carbon isotopes were measured on bulk rock samples via sealed tube combustion according to the methods of Froidl (2021). For this, between 7.5 and 35 mg of rock powder were decarbonated in a quartz tube using hydrochloric acid (25%). Subsequently, sample powder was rinsed with deionised water until neutrality and dried at 40 °C. Sample powder was homogeneously mixed with CuO wire. Carbon dioxide was liberated via sealed tube combustion at 850 °C for three hours, purified cryogenically in a vacuum distillation line, and collected in a Pyrex break-seal tube. Mass spectrometric measurements were performed on a ThermoScientific Delta V Advantage equipped with a dual inlet (Froidl, 2021).

5.3.1.2 - ICP-MS/OES

For ICP-MS and ICP-OES analyses, solid sediment samples were freeze-dried and weighed to ~0.2g. Digestion of a total of 381 samples was undertaken using an Aqua Regia (1 HNO₃ + 3N HCl) digestion method in a CEM MARS Xpress 6 Microwave digestion system. After digestion, samples were filtered and twice diluted to a dilution factor of 100. Sample aliquots were analysed according to standard operating procedure, as described by Dr. Jonathan Yarwood, using a Perkin Elmer Optima 8300 ICP-OES system and a PerkinElmer NexION 350D ICP-MS at the Department of Geography, School of Environment and Education, University of Manchester. The ICP-OES and ICP-MS methodology used a 5-point linear calibration with a 99.999% minimum regression, with an internal Yttrium standard made up in ~2% Nitric Acid, using 18M Ω Deionised Water and 70% Ultrapure Nitric Acid. To correct for instrument drift and matrix interferences, ICP-OES results were initially quantified against this curve in mg/L, or ppm, at a limit of detection of 0.005mg/L. ICP-MS results were quantified against an internal standard in $\mu\text{g/L}$, or ppb to a detection limit of 0.005 $\mu\text{g/L}$. Any figures below these detection limits were noted as being below the limit of detection (<LOD) including any quantities below zero, as the instrument cannot discern peaks from background noise below these levels.

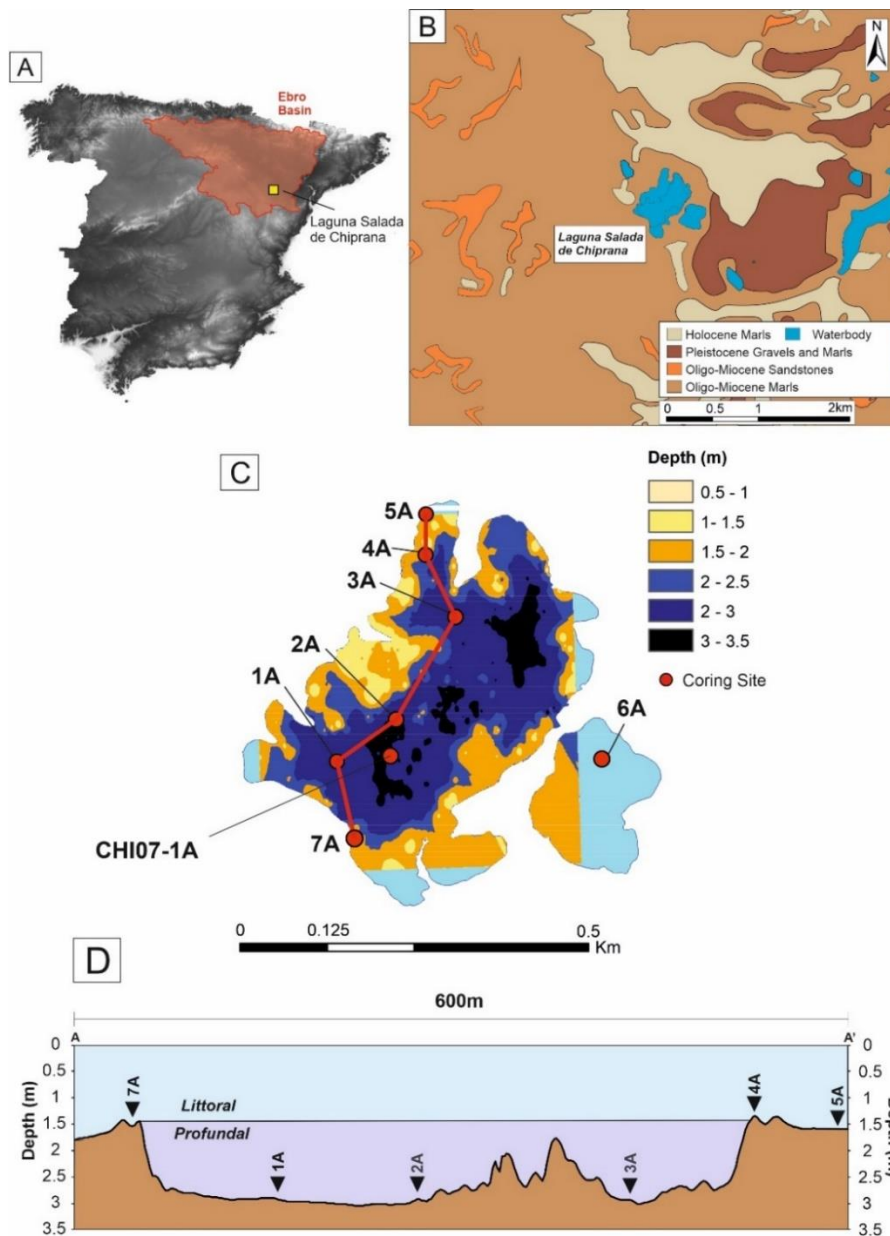


Figure 5.1 - Maps illustrating the location of Laguna Salada de Chiprana in Northeast Spain. A) Digital elevation model of the Iberian Peninsula generated using ArcMap 10.14.1 with the location of the Ebro Basin highlighted in red. The location of Laguna Salada de Chiprana is marked by a yellow square. B) Regional geology of the area of Laguna Salada de Chiprana. C) Bathymetric map of Laguna Salada de Chiprana with sediment cores collected from the lake during March 2019 highlighted. D) Bathymetrical cross-section, oriented NE-SW, of the main lakebody of Laguna Salada de Chiprana with all cores (with the exception of 6A, located in the side lagoon) marked on the section. Geological data sourced from (IGME, 2003a), DEM's from CNIG (Centro Nacional de Informacion Geografica), bathymetrical data provided by the Instituto Pirenaico de Ecologica. Figure partially modified from (Doyle *et al.*, 2022).

5.3.2 - XRF Scanning

Sediment cores were introduced to a Cox Analytical Systems Itrax XRF Core scanner in the School of Geography, University of Manchester. Photographs and radiographs were produced for subsequent sedimentological analyses (Croudace *et al.*, 2006; Doyle *et al.*, 2022). The cores were also scanned using a Molybdenum (Mo) X-ray source tube. The parameters for scanning included a tube voltage of 30kv, tube current of 30mA, and count time of 30 seconds, at a 1mm interval (Doyle *et al.*, 2022). Elemental data included a wide range of variables (approximately 30+ elements detected for each core) and were initially presented in the form of counts per second (cps). Processing and evaluation of X-ray spectra was undertaken with Qspec 6.5 software (Cox Analytical Systems) and plotted in the ItraxPLOT and ReDiCore software packages. For analysis of geochemical processes, logarithmic ratios of elements were utilised throughout.

5.3.3 - Analysis and transformation of geochemical data

Analyses of geochemical data were also undertaken to better define environmental processes occurring within Lake Chiprana. Despite this, in the case of the XRF data, there are a large number of elements detected by the Itrax XRF scanner, and not all elements can be used to interpret palaeoenvironmental variations (Gadd *et al.*, 2015). Thus, to reduce the number of elements considered for statistical analysis and palaeoenvironmental interpretation, several techniques were employed. This firstly involved the removal of elements that exhibited very low, exceedingly noisy, or high argon readings (signifying air in the cores)(Croudace *et al.*, 2006) and those with high mean standard errors. Secondly, basic statistical analysis was undertaken to determine possible relationships between geochemical characteristics of the sedimentary sequence, utilising Pearson's correlation coefficient tests, signified by r (Edelmann *et al.*, 2021). After elements were selected, XRF data was transformed via central log ratio calibration to account for the effects of factors such as grain size, water content and organic matter (Weltje & Tjallingii, 2008) using the ItraxR software package (Bishop, 2022). Grouping of elements according to their variability was

determined using both the former Pearson correlative coefficient tests and principal component analyses undertaken in the Past 4.0 software package (Hammer *et al.*, 2001). Elements which were quality-controlled to remove invalid data were then subjected to principal component analysis (PCA) also using the Past 4.0 software package.

5.3.4 - Chronological Model

The chronological model (Figure 5.2) was generated using sedimentological and geochemical indicators. The longest core (CHI19-1A) collected for this study was correlated with cores retrieved in 1997 and 2007 from Lake Chiprana (CHI97-1A and CHI07-1A, the former core being described and chronologically dated (Valero-Garces *et al.*, 2000) by using indicators such as facies variations and sedimentological units, in addition to using XRF data as described in an earlier study (Doyle *et al.*, 2022). This provides a qualitative chronological constraint, which is accompanied by radiometric dating techniques including ^{137}Cs and ^{14}C of the older cores, with the associated dates presented in Table 5.2. The model presented in the aforementioned study has however been revised and updated for this study following further statistical analysis, and the final model was generated from the dates in Table 2 using the R-based software Clam (Blaauw, 2010; Reimer *et al.*, 2020) via linear interpolation methods (Figure 2B).

Table 5.2 - ^{210}Pb , ^{137}Cs and ^{14}C dates for associated cores. The carbon-14 date is from Davis (1994) and Valero-Garcés *et al.* (2000), ^{210}Pb and ^{137}CS dates provided by the Instituto Pirenaico de Ecología.

Depth (cm)	Chronological Dating Method	Core	Dated Material	^{14}C Age (yr BP)	Age (yr BP)	Status
0	Modern	CHI19-1A	Sediment		2019	N/A
1	^{210}Pb	CHI97-1A	Sediment		1994.19	Accepted
2	^{137}Cs	CHI07-1A	Sediment		1970	Accepted
3	^{210}Pb	CHI97-1A	Sediment		1986.63	Rejected
5	^{137}Cs	CHI07-1A	Sediment		1963	Accepted
5	^{210}Pb	CHI97-1A	Sediment		1975.5	Rejected
9	^{210}Pb	CHI97-1A	Sediment		1956.32	Rejected
10.7	^{137}Cs	CHI07-1A	Sediment		1960	Accepted
23.5	^{137}Cs	CHI07-1A	Sediment		1950	Accepted
11	^{210}Pb	CHI97-1A	Sediment		1947.74	Rejected
13	^{210}Pb	CHI97-1A	Sediment		1929.49	Rejected
15	^{210}Pb	CHI97-1A	Sediment		1903.94	Rejected
17	^{210}Pb	CHI97-1A	Sediment		1872.6	Rejected
50	^{14}C	CHI97-1A	Carophyllaceae seeds	315 ± 60		Accepted

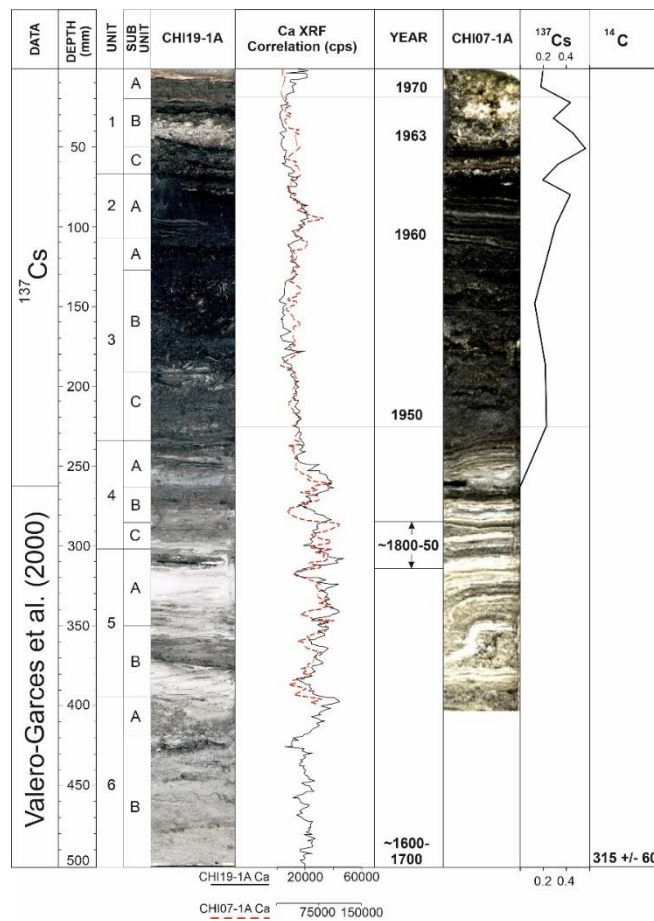
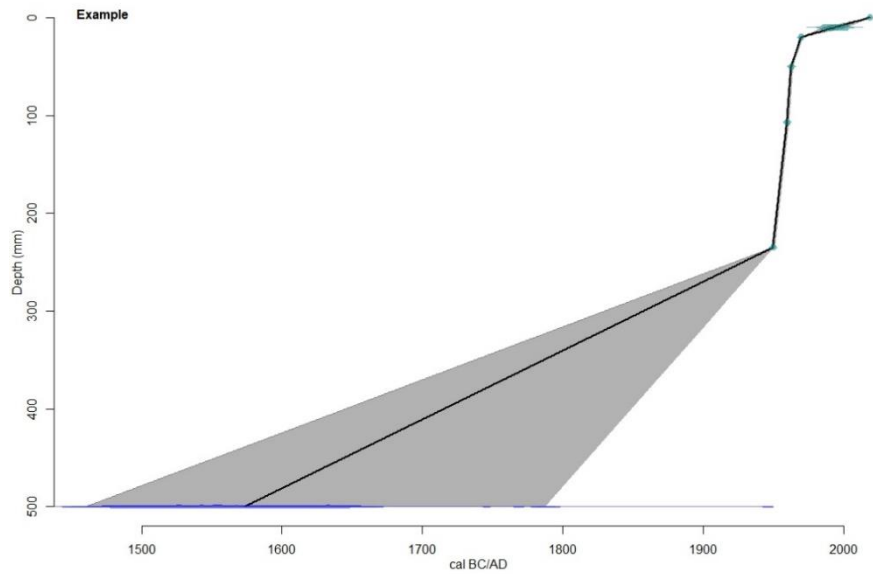


Figure 5.2 - A Clam (Blaauw, 2010) generated age-depth model portraying the last ~350-400 years of Lake Chiprana based on ^{210}Pb , ^{137}Cs and ^{14}C dates. Chronological model modified from (Doyle *et al.*, 2022). **B** Chronological correlation between core CHI19-1A and a core (CHI07-1A) retrieved from Lake Chiprana in 2007, provided by IPE. Adapted from (Doyle *et al.*, 2022), see this study for further details.

5.4 - Results

5.4.1 - Sedimentological Sequence

Sediment cores retrieved from Lake Chiprana illustrate multiple sedimentary facies (Table S1, (Doyle *et al.*, 2022)) and are associated with two distinctive depositional sub-environments – the profundal and littoral zones. Facies, sedimentary features and sedimentary structures associated with each of these zones are described and further interpreted in an earlier study (Doyle *et al.*, 2022). Nine facies in total were identified with one further sub-facies, and include a wide range of sedimentological and depositional characteristics.

5.4.2 - Geochemistry

5.4.2.1 - Overview

Variations in major elements associated with the profundal main basin, profundal side basin and littoral settings of Lake Chiprana are shown in Figures 5.4a, 5.4b and 5.6 respectively. The relationship between ICP-OES/MS and XRF data suggests that the qualitative XRF dataset is a valid and reliable indicator of downcore variations in geochemical composition (Martín-Puertas *et al.*, 2011; Zhang *et al.*, 2020b). Statistical analysis of XRF data associated with the profundal and littoral sequences led to the removal of several elements out of the 35 that were initially detected by the Itrax XRF scanner due to noisy, low counts or high mean standard errors associated with the data. These variables were not considered in subsequent data analyses.

5.4.2.2 - Profundal Setting

Table 5.3 displays Pearson correlative indices (r) for the raw (untransformed) element data associated with the profundal setting of Lake Chiprana. Principal component analysis includes elements which are considered suitable following data processing and transformation, and indicates the first four components associated with the profundal sequence account for 77.89% of the total variance of the dataset (Figure 3). The PCA biplot and Pearson correlative analyses also illustrate that four

groupings of the present variables can be made. Group P1a consists of elements Al, Si, Mn, Fe, Ti, K and Rb, which display moderate to strong correlation coefficients (r (significance) > 0.5) and are in proximity on the PCA biplot. Increases in detrital calcite, phyllosilicates and quartz are also characteristically related to an increase in the intensity of this group of elements (Doyle *et al.*, 2022). Group P1b consists solely of the element Ca. It displays moderate correlation with Group P1a, but also separation from this group within the PCA biplot. This group is associated with increases in both detrital calcite, phyllosilicates, quartz and gypsum in some intervals (Doyle *et al.*, 2022). Group P2 consists of elements S, Cl and Sr which are grouped due to their moderate correlation ($r > 0.35$) and proximity on the biplot. This group of elements is typically associated with increases in gypsum, aragonite, and non-detrital (i.e. precipitated) calcite. Group P3 is composed of elements Cu, Ni, Br, and the ratio of Inc/Coh (defined as the Incoherent/Coherent scattering ratio detected by the XRF scanner (Gadd *et al.*, 2015)).

Transformed XRF intensities of elemental variables from the profundal sedimentary sequence of Lake Chiprana are exhibited in Figures 5.4a and 5.4b with ICP-OES data. Elemental intensities are also consistent with the occurrence of different facies with varying mineralogy and sedimentological characteristics throughout the sequence (Table S1) (Doyle *et al.*, 2022). Elements from Group P1a (Al, Si, Zn, Mn, Fe, Ti, K and Rb) and Ca from Group P1b are both strongly associated with siliciclastic facies, and show moderate increases within units 5 and 6 which are dominated by these facies. Ca, which is strongly co-ordinated with these elements ($r > 0.75$, except in the case of Al), is however associated with multiple facies including gypsum, detrital-sourced carbonates and evaporitic carbonates as seen in other settings such as Lake Zonar (Martín-Puertas *et al.*, 2011). Higher intensities are for example recorded in facies “e” and “f” associated with Units 1 and 4, within gypsum facies “d”, and additionally within detrital facies “a.1”. Group P2, consisting

Table 5.3 - Table displaying Pearson correlation coefficients (r) between raw element cps data detected by the XRF scanner from profundal core CHI19-1A. Dark green shaded cells are indicative of variables which display a coefficient of $r > 0.5$, whilst light green shaded cells indicate variable with a correlation coefficient $0.25 < r < 0.5$. Orange shaded cells indicate a coefficient of $r < -0.5$, whilst light orange shaded cells indicate a correlation coefficient $-0.5 < r < -0.25$. LOI stands for loss on ignition.

	Al	Si	S	Cl	K	Ca	Ti	Mn	Fe	Sc	Ni	Cu	Zn	Br	Sr	Zr	Cr	Rb	Mo	Pb	Inc/Coh	
Al																						
Si	0.579																					
S	-0.127	-0.333																				
Cl	-0.202	-0.414	0.609																			
K	0.509	0.924	-0.418	-0.384																		
Ca	0.466	0.820	-0.030	-0.308	0.783																	
Ti	0.520	0.900	-0.443	-0.380	0.981	0.759																
Mn	0.450	0.777	-0.184	-0.222	0.815	0.800	0.839															
Fe	0.516	0.875	-0.426	-0.341	0.969	0.742	0.984	0.849														
Sc	-0.113	-0.200	0.353	0.175	-0.254	0.048	-0.282	-0.132	-0.262													
Ni	-0.073	-0.064	-0.048	0.105	-0.023	-0.171	-0.024	-0.061	-0.001	-0.153												
	-0.162	-0.292	0.047	0.417	-0.238	-0.476	-0.222	-0.256	-0.204	-0.168	0.399											
Zn	0.347	0.588	-0.259	-0.275	0.662	0.548	0.657	0.536	0.653	-0.140	0.044	-0.152										
Br	-0.299	-0.458	0.150	0.559	-0.405	-0.628	-0.389	-0.371	-0.359	-0.133	0.360	0.659	-0.337									
Sr	-0.121	-0.198	0.372	0.141	-0.297	0.076	-0.317	-0.145	-0.325	0.259	-0.039	-0.148	-0.172	-0.055								
Zr	-0.149	-0.207	0.281	0.176	-0.279	-0.052	-0.288	-0.156	-0.286	0.133	0.080	0.007	-0.177	0.208	0.835							
Cr	0.192	0.348	0.034	0.068	0.379	0.386	0.374	0.343	0.368	0.074	-0.131	-0.099	0.272	-0.223	-0.061	-0.132						
Rb	0.410	0.686	-0.418	-0.268	0.784	0.517	0.808	0.684	0.832	-0.268	0.036	-0.070	0.559	-0.190	-0.348	-0.263	0.271					
Mo	-0.017	-0.027	0.254	0.267	-0.113	0.089	-0.123	-0.017	-0.123	0.151	0.004	0.008	-0.076	0.074	0.238	0.249	-0.021	-0.147				
Pb	0.122	0.274	-0.307	-0.115	0.350	0.160	0.354	0.279	0.376	-0.178	0.129	0.073	0.242	0.081	-0.158	-0.082	0.033	0.394	-0.063			
Inc/Coh	-0.376	-0.566	0.032	0.334	-0.532	-0.771	-0.510	-0.518	-0.493	-0.160	0.374	0.611	-0.409	0.857	-0.033	0.202	-0.357	-0.299	0.003	0.010		

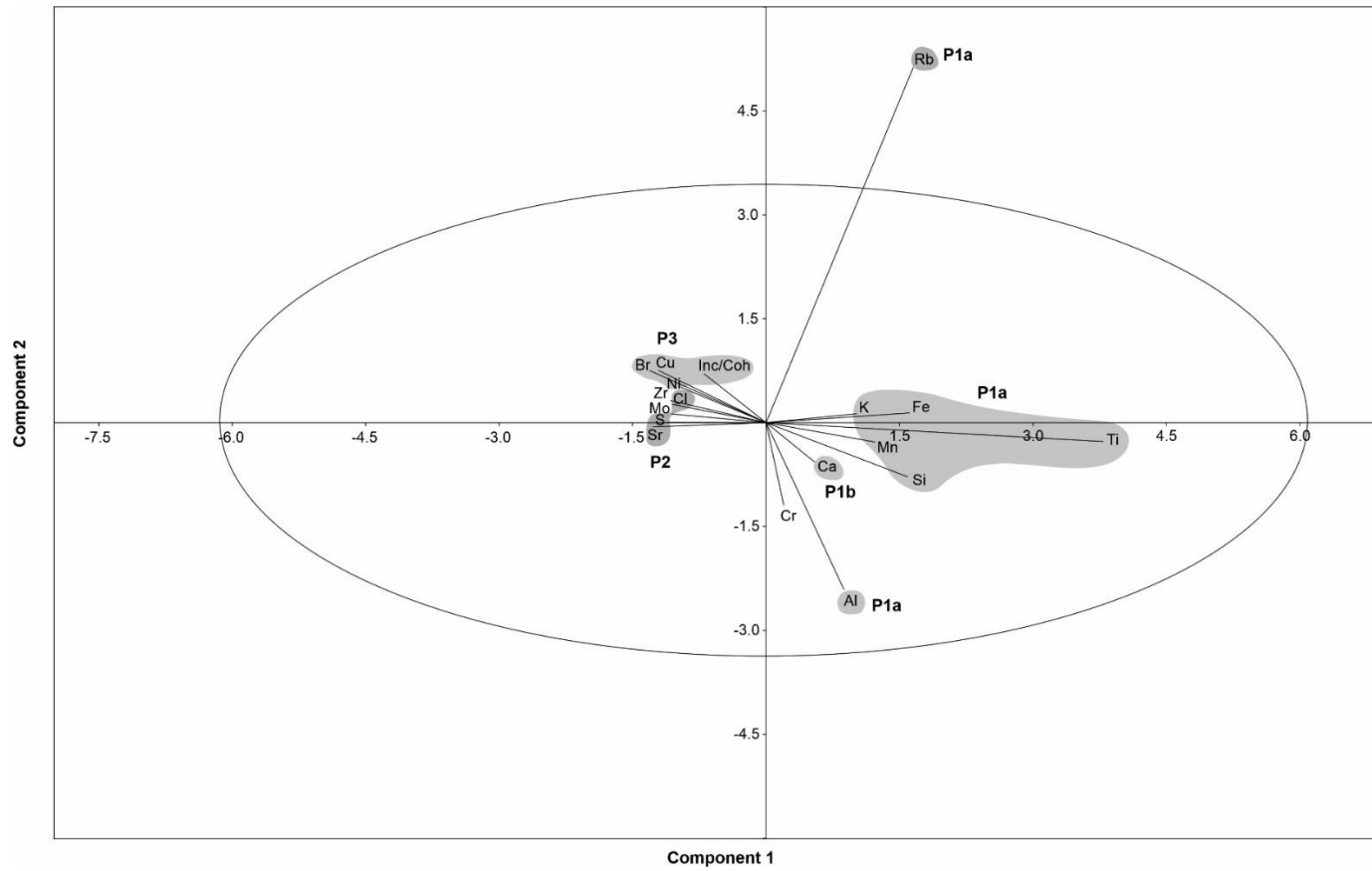


Figure 5.3 - PCA biplot illustrating groupings of the variables associated with the profundal cores (CHI19-1A) from Lake Chiprana. Rb and Al are included in Group P1a but are likely affected by noise causing the observed separation.

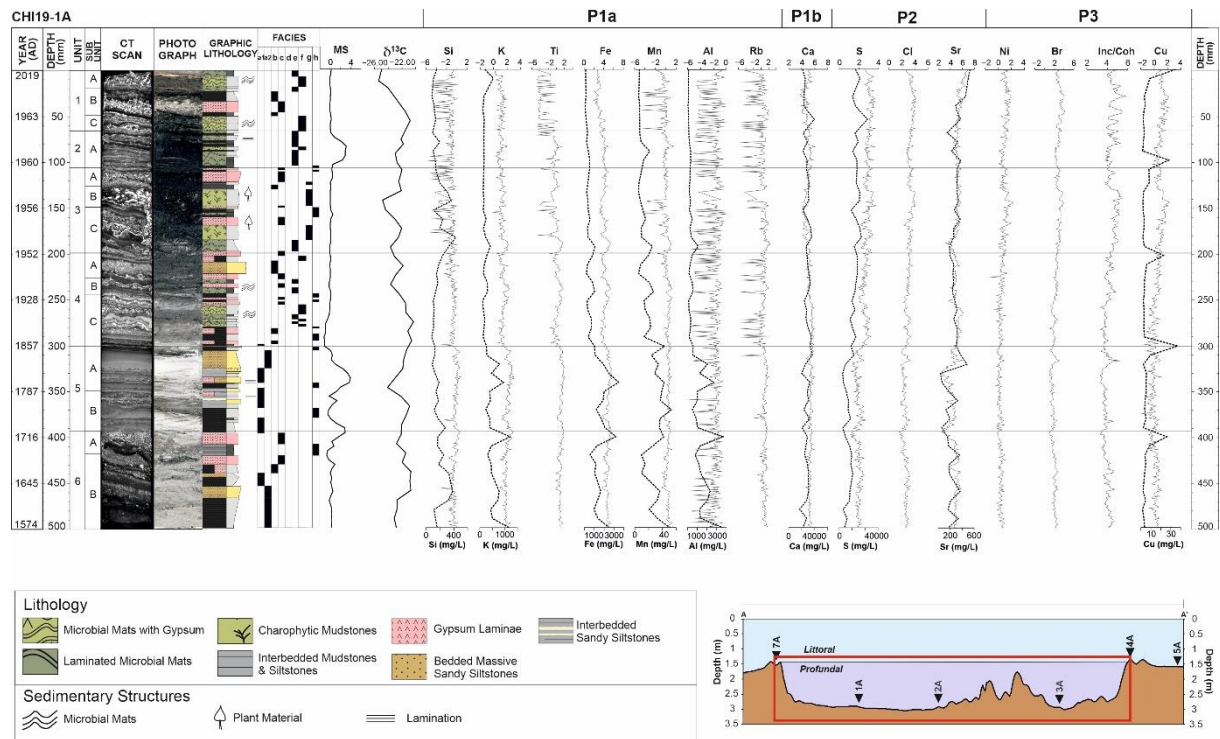


Figure 5.4a - Figure illustrating a geochemical sequence of the profundal depositional sub-environment of the main basin (CHI19-1A) of Lake Chiprana, with elemental XRF data, expressed as transformed counts per second, carbon-13 organic measurements, and magnetic susceptibility, expressed as SI, included. Elements are grouped according to the same groupings that are shown on the associated PCA biplot in Figure 3. Facies are described in Table S1. CT data, photographs, graphic lithology and facies are also defined in (Doyle *et al.*, 2022) and their collection methods described. Grey line = XRF, black line = ICP. Element ICP data expressed as mg/L.

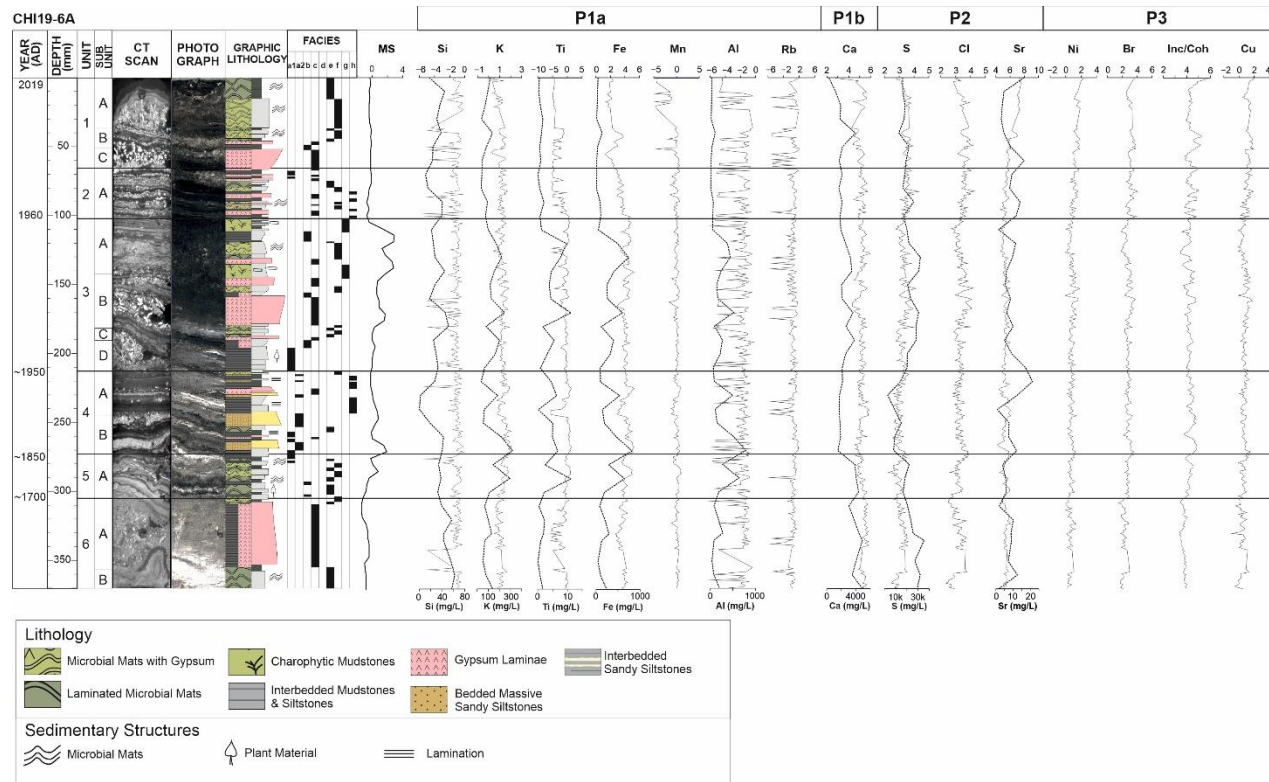


Figure 5.4b - Figure illustrating a geochemical sequence of the profundal depositional sub-environment of the side basin (CHI19-6A) of Lake Chiprana, with elemental XRF data, expressed as transformed cps, and magnetic susceptibility expressed as SI. Facies are described in Table S1. CT scans and high-resolution photographs are included alongside elemental data. CT data, photographs, graphic lithology and facies are also defined in [33]. Grey line = XRF, black line = ICP. Element ICP data expressed as mg/L.

of S, Cl and Sr, is largely associated with facies deposited during increased periods of evaporation (Martín-Puertas *et al.*, 2011), including facies “e” and “f” microbial mats, facies “c” gypsum and facies “b” mudstones. Both elements show increases in the uppermost sections of the core, throughout all of unit 2, with a marked increase initially occurring within the lower section of unit 4. Group P3, consisting of the variables Br, Inc/Coh, Cu and Ni, is associated with organic-rich and dark black facies throughout the sequence. Increases in variables from this group are apparent within charophytic facies “g” within unit 3, within some instances of facies “a.1” and “a.2” where organic material is distributed within the muds and silts, and additionally within facies “h” at the top of units 5 and 6. Typical increases observed in this group throughout are highlighted within unit 3 to the top of unit 1, and also at several small intervals of unit 5 and 6 where organic material is present.

5.4.2.3 - Littoral Setting

Table 5.4 displays the Pearson correlative indices for the elements associated with the littoral setting. Principal component analyses of XRF data from the littoral sequence are highlighted in Figure 5.5. The PCA shows that the first four components associated with the littoral sequence account for 83.9% of the total variance of the dataset. As with the profundal sequence, the PCA biplot and Pearson correlative analyses illustrate that 4 key groupings of the elements can be made. Group L1a is composed of elements Mn, Rb, Ti, Fe, K. The latter 3 of these elements are loosely grouped on the PCA biplot, whilst Mn illustrates lower eigenvectors on the PC1 axis and Rb higher values on the PC2 axis. This group of elements typically displays increases in intensity in association with similar increases in detrital calcite, quartz, and phyllosilicates (Doyle *et al.*, 2022). Group L1b consists of elements Al and Si which display a moderate correlation ($r = 0.515$) and are closely grouped on the PCA biplot. This group is considered a subgroup of group L1 due to the correlation of Si with elements from Group L1a. Al does not display a similar correlation, but the noisy signal displayed by this element may have contributed to the absence of any clear correlation. Group L2 consists of Ca, Cl, Sr and S, which

are closely grouped on the PCA biplot. In contrast to the profundal sequence, here Ca instead displays increases closely associated with increasing gypsum content as opposed to detrital calcite. Group L3 is associated with elements Cu, Ni, Br, and the ratio of Inc/Coh. As with the profundal cores, this group again is typically associated with organic-rich facies, and the association of proxies indicating organic content (Br, Inc/Coh).

Elemental fluctuations in the littoral setting of Lake Chiprana are depicted in Figure 5.6. Elements from Group L1a (Fe, K, Ti, Rb and Mn) again display increased intensities in detrital facies, those of which occur primarily within unit 3 of the littoral sequence. Overall, this group displays a downsequence increasing trend which is most pronounced throughout unit 3, with the exception of a small increase in K at the top of the sequence. Al and Si within Group L1b both display a relatively inconsistent trend, with increases primarily observed within the organic-rich charophyte mudstone laminae associated with unit 3 and within the gypsiferous microbial mats in the central section of unit 1. Group L2 represents elements S, Cl, Sr and Ca, those of which are typically correlated with gypsiferous facies (Doyle *et al.*, 2022) “b”, “c” and “d”. Increases can also be observed within the gypsum-rich microbial mats (facies “f”) associated with the upper section of unit 1, and within the cm-scale gypsum bed (facies “c”) that can be observed in the uppermost section of unit 3/base of unit 2. Group L3, pertaining to elements Br, Ni, Cu and the ratio of Inc/Coh, displays several significant changes throughout the sequence. Generally, the most significant increases within these variables can be observed within the organic-rich microbial mats within the uppermost section of unit 1, and within the charophytic, organic-rich black mudstones that are characteristic of unit 3. Heavy metals Cu and Ni again display specific covariance with Inc/Coh and Br, similar to that which occurred throughout the profundal sequence.

Table 5.4 - Table displaying Pearson correlation coefficients (r) between raw element cps data detected by the XRF scanner from littoral core CHI19-4A. Dark green shaded cells are indicative of variables which display a coefficient of $r > 0.5$, whilst light green shaded cells indicate variable with a correlation coefficient $0.25 < r < 0.5$. Orange shaded cells highlighted with red text indicative a coefficient of $r < -0.5$, whilst light yellow shaded cells indicate a correlation coefficient $-0.5 < r < -0.25$.

	Al	Si	S	Cl	K	Ca	Ti	Mn	Fe	Sc	Ni	Cu	Zn	Br	Sr	Zr	Rb	Cr	Mo	Pb	Inc/Coh	
Al																						
Si	0.515																					
S	0.176	0.310																				
Cl	0.233	0.332	-0.114																			
K	0.146	0.384	-0.370	0.644																		
Ca	0.268	0.511	0.792	0.062	-0.104																	
Ti	-0.059	0.011	-0.120	0.148	0.175	-0.101																
Mn	0.174	0.320	-0.115	0.326	0.467	0.106	0.018															
Fe	0.156	0.386	-0.353	0.617	0.874	-0.144	0.167	0.582														
Sc	0.079	0.280	0.414	0.169	-0.054	0.494	-0.117	-0.017	-0.057													
Ni	0.053	0.128	-0.164	0.419	0.307	-0.155	0.693	0.016	0.296	-0.073												
Cu	0.030	0.013	-0.363	0.570	0.438	-0.364	0.481	0.065	0.359	-0.177	0.632											
Zn	0.074	0.032	0.000	0.036	0.034	0.063	-0.019	0.102	0.098	0.074	-0.008	-0.030										
Br	0.046	0.087	-0.478	0.673	0.645	-0.319	0.126	0.278	0.636	-0.125	0.434	0.629	-0.026									
Sr	0.154	0.300	-0.056	0.427	0.280	0.285	0.025	0.184	0.331	0.269	0.215	0.083	0.059	0.377								
Zr	0.074	0.134	-0.354	0.492	0.475	-0.155	0.292	0.207	0.486	-0.040	0.512	0.461	0.026	0.619	0.724							
Rb	-0.032	0.133	-0.158	0.200	0.277	-0.100	0.048	0.198	0.320	-0.015	0.109	0.157	0.083	0.270	0.079	0.164						
Cr	0.047	0.182	0.208	0.290	0.074	0.189	0.119	0.035	0.114	0.267	0.161	0.161	0.149	0.063	0.166	0.065	0.021					
Mo	0.212	0.366	0.700	0.105	-0.171	0.679	-0.031	-0.061	-0.171	0.443	0.020	-0.171	-0.020	-0.241	0.074	-0.146	-0.052	0.148				
Pb	-0.029	0.118	-0.309	0.332	0.433	-0.176	0.036	0.177	0.458	0.058	0.159	0.235	0.015	0.431	0.203	0.271	0.269	0.003	-0.203			
Inc/Coh	-0.025	-0.039	-0.533	0.567	0.549	-0.511	0.439	0.120	0.492	-0.272	0.652	0.811	-0.052	0.802	0.182	0.622	0.232	0.023	-0.309	0.338		

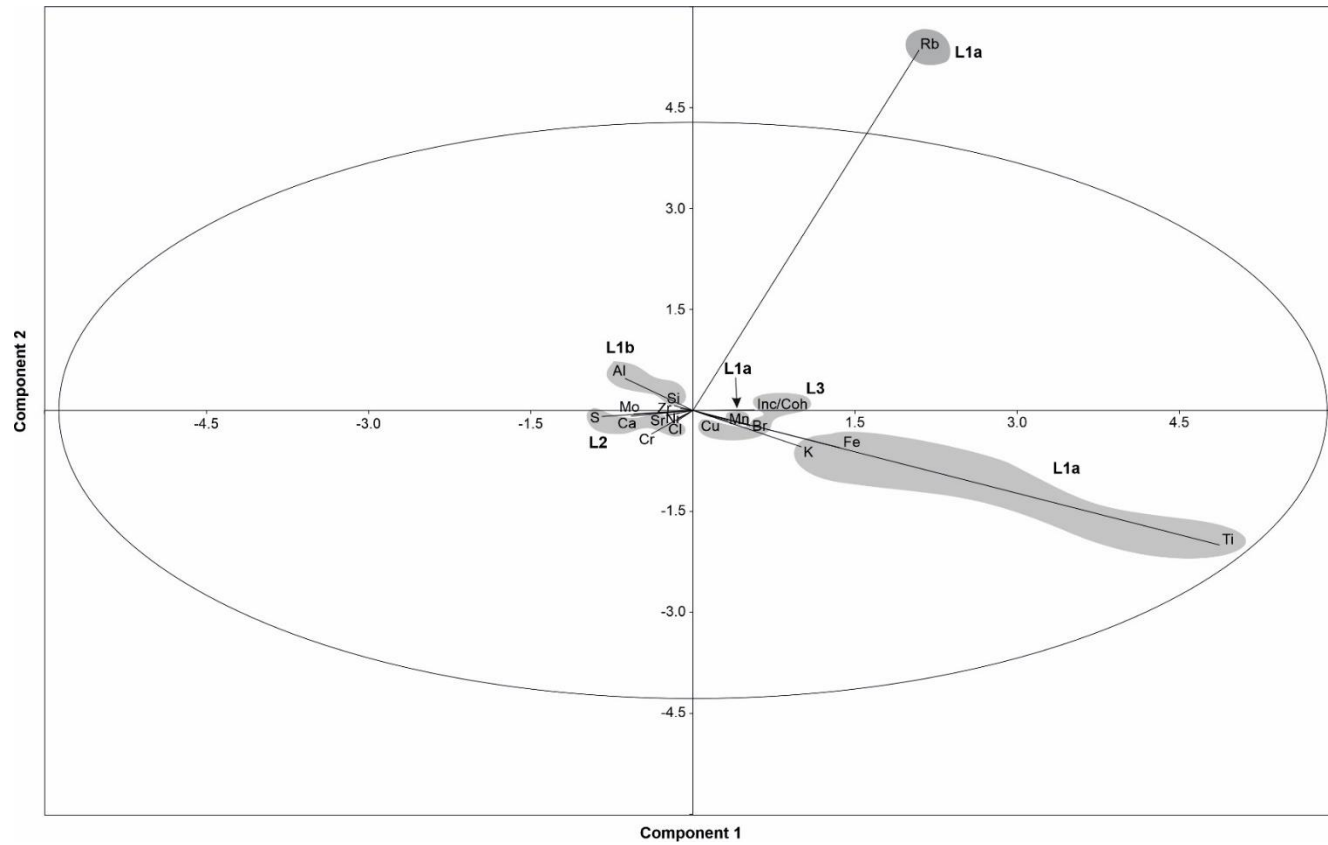


Figure 5.5 PCA biplot illustrating groupings of the variables associated with the littoral cores from Lake Chiprana.

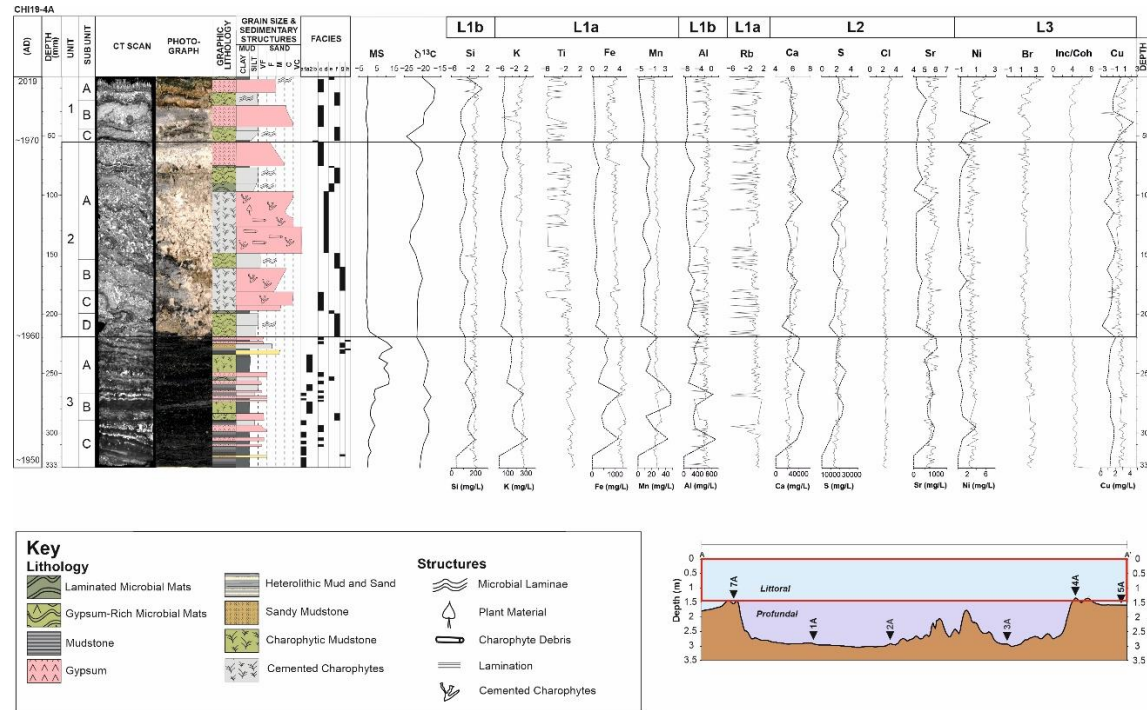


Figure 5.6 - Figure illustrating a geochemical sequence of the littoral depositional sub-environment of Lake Chiprana (CHI19-4A), with elemental XRF data, expressed as counts per second, and MS, expressed as SI, included. Elements are grouped according to the those shown on the associated PCA biplot in Figure 5.5. CT scans and high-resolution photographs are included alongside elemental data. CT data, photographs, lithology and facies are also defined in Doyle *et al.* (2022). Element ICP data expressed as mg/L. Grey line = XRF, black line = ICP.

5.5 – Discussion

A range of factors were identified in this study, comparable to many other lakes throughout the Iberian Peninsula such as Lake Arreo (Corella *et al.*, 2013), Estanya (Morellón *et al.*, 2009b), Montcortes (González-Sampériz *et al.*, 2017) and Zonar (Martín-Puertas *et al.*, 2011), and as such these processes are described in comparison with similar examples found in such settings.

5.5.1 - Intrinsic factors

5.5.1.1 - Oxygenation, meromixis and in-lake productivity

Correlation and interpretation of oxygenation and productivity in Lake Chiprana is attempted by using $(\log)\text{Fe}/(\log)\text{Mn}$ as an indicator of the intensity of reducing conditions occurring throughout the lake (Corella *et al.*, 2012; Vegas-Vilarrúbia *et al.*, 2018) and by using $(\log)\text{Mn}/(\log)\text{Fe}$ as an indicator of more oxic conditions (Figure 5.7). The use of raw or transformed elemental data as standalone indicators of oxygenation and reducing conditions is not feasible due to the effect of detrital and biological processes upon them (Martín-Puertas *et al.*, 2011), and thus the use of such ratios which effectively remove the effect of the denominating element are considered more reliable when interpreting redox and biological processes (Mackereth, 1966; Martín-Puertas *et al.*, 2011). In the profundal setting, periods of increased oxygenation occur at the base of unit 1 and within the basal sections of unit 4, corresponding to the deposition of microbial mats in the cores in the present day (Doyle *et al.*, 2022) and between ~1850-1950AD. Small increases are also observed in the lower half of unit 6. In the profundal setting of the smaller side basin, increased oxygenation occurs most prominently within the lowermost section of unit 1 and at the base of unit 6. In contrast, in the littoral setting, oxygenation is increased within unit 2, and appears to decrease within unit 3. In terms of $\log(\text{Fe})/\log(\text{Mn})$ and reducing conditions, small increases are apparent within the basal section of unit 5 and at the top of unit 6 within the profundal setting of the main basin, indicating that Lake Chiprana underwent more reducing conditions in the deeper sections of the lake between approximately 1600 and 1800AD. Furthermore, reducing conditions in

the profundal setting of Chiprana are often associated with increases in heavy metals Cu and Ni. It is likely that this coeval increase represents the adsorption of heavy metals to organic molecules (Lin & Chen, 1998; Marchand *et al.*, 2011) in more anoxic environments, and is not necessarily immediately indicative of increasing or decreasing levels of anthropogenic activity. Within the side basin, reducing conditions display small increases throughout unit 5, as well as at the base of unit 6. Reducing conditions within the littoral environments typically display a characteristic small to moderate increase in intensity towards the base of unit 3 which is first initiated at the base of unit 2.

Oxic conditions in Lake Chiprana can be related primarily to periods of microbial mat development (units 1 and 4) and also during the deposition of more massive units of white sandy siltstones (lower unit 6). Such oxic conditions and the presence of microbial mats are likely directly associated with decreasing lake levels (Figure 5.7), which lead to potential mixing of the lake water and subsequent increases in oxygenation at the base of the water column (Martín-Puertas *et al.*, 2011; Żarczyński *et al.*, 2019). In contrast, reducing conditions are closely associated with influxes of charophytic material embedded in dark black mudstones in the pelagial and littoral settings (unit 3) and with the sandy silts and small organic-rich layers within unit 5 of the pelagial setting, as well as throughout unit 6. This may correspond to periods of stronger stratification of the water column (Valero-Garces *et al.*, 2000; Martín-Puertas *et al.*, 2011; Seguin *et al.*, 2020), leading to stronger chemical gradients and harsh reducing conditions at the base of the column as identified throughout the profundal sedimentary sequence. Increases in anoxic conditions at the base of the column may also have occurred as a result of periods of higher inflow from nutrients and fertilisers associated with agricultural practices and subsequently increased eutrophication (Valero-Garces *et al.*, 2000; Corella *et al.*, 2012).

When considering the PCA in the profundal setting of Lake Chiprana in terms of redox and productivity, decreases in the first eigenvector associated with the biplot

(Figure 5.4) for the profundal setting are interpreted to represent the increasing intensity of organic and biological processes (Morellón *et al.*, 2009b; Martín-Puertas *et al.*, 2011) in confluence with evaporitic processes. Negative eigenvector values are associated with increased organic productivity and also evaporation (see section 5.2.1) whilst positive values are instead associated with increases in the detrital signature throughout the sediments of Lake Chiprana (Morellón *et al.*, 2009b; Martín-Puertas *et al.*, 2011; Corella *et al.*, 2013). This may reflect the transition of Lake Chiprana to a wetland-based environment where organic productivity increases when lake levels fall, with more extensive organic processes occurring throughout the deeper areas of the lake under a shallower water depth (Corella *et al.*, 2021). However, in the case of the littoral setting, the grouping of variables indicative of increased biological productivity (Figure 5.5) with those associated with increased detrital input means that the intensity of such productivity is difficult to reliably constrain within this setting. This phenomenon may instead relate to stronger evaporation within the littoral setting negating organic productivity and preservation due to harsh environmental conditions and erosion, whereby increases in the significance of both of these processes are achieved when lake levels rise in confluence with increasing detrital input (Arthur & Sageman, 2005).

5.5.1.2 – Evaporation and lake drawdown

Elemental and environmental proxies which indicate increased mineral precipitation and evaporation within Lake Chiprana can be inferred from raw elemental data of S and Sr, from the normalisation of Sr to Ti as $\log(\text{Sr})/\log(\text{Ti})$ (Martín-Puertas *et al.*, 2011), and from the normalisation of Ca via $\log(\text{Ca})/\log((\sum(\text{S}+\text{Ti}+\text{Fe}+\text{Al})))$ (Figure 5.8) (Mueller *et al.*, 2009; Kylander *et al.*, 2011). These ratios, according to the study on Lake Zonar in Southern Spain (Martín-Puertas *et al.*, 2011), provide indicators for drier conditions and subsequently increased mineral precipitation. Increasing values associated with these proxies in units 1, 3 and at the base of unit 4 broadly coincides with the increased formation of evaporitic carbonate and gypsum and reflects decreasing lake levels and increasing salinity in the modern-day and in the period of

approximately 1850-1950AD, respectively. Correlation of elemental proxies between sediment cores additionally highlights the spatio-temporal variability of evaporitic processes throughout Lake Chiprana. The greatest degree of variability can be identified between sediments from the profundal and littoral sub-environments of the primary lake basin, and between the profundal sediments of the primary lake basin and the smaller side basin (Figure 5.8). In the profundal setting of the primary lake basin, there are more evaporative facies within units 1, 3 and 4 and within the upper sub-unit of unit 6 (Figure 5.8) and correspondingly an increase in Sr/Ti. Contrastingly, within the profundal setting of the side lagoon such processes are generally only heightened in unit 4, and in the littoral settings, within unit 3.

The negative values of the first eigenvector in the profundal PCA (Figure 5.4) correlate with evaporitic processes occurring within the profundal setting of the lake as also identified in Lake Zonar (Martín-Puertas *et al.*, 2011), Lake Estanya (Morellón *et al.*, 2009b) and Lake Arreo (Corella *et al.*, 2013), indicated by the grouping of elements S, Cl and Sr on the biplot. In the littoral setting, the second eigenvector is also represented by evaporitic processes (Figure 5.5), as highlighted by the strong association of elements S, Cl, Sr, and in the case of this setting, Ca, towards the negative end of PC2. In both cases, the negative values of eigenvector 1 are generally representative of periods of decreased lake level, detrital input, and the increased precipitation of evaporitic mineralogical assemblages (Martín-Puertas *et al.*, 2011). Such variation in the contribution of different elements to the PCA is furthermore indicative of a shift in the importance and nature of different environmental processes between the profundal and littoral settings. For example, the inclusion of Ca within the evaporitic grouping in the littoral setting indicates that the Ca signal is more influenced here by evaporation and instead by detrital carbonates delivered from the geology of the catchment (IGME, 2003b) in the lower units of the profundal setting.

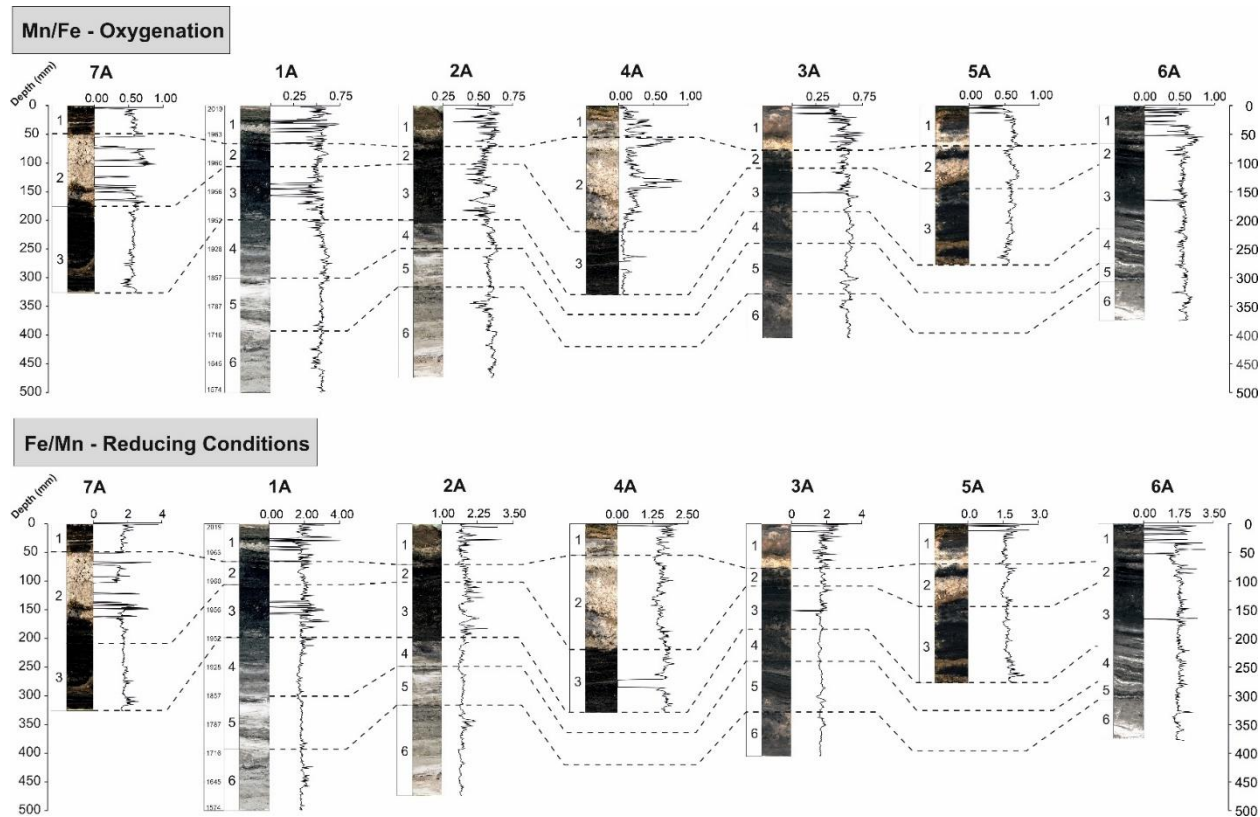


Figure 5.7 - Figure illustrating spatio-temporal variations in geochemical proxies typically used for determination of oxygenation (Naeher *et al.*, 2013) and anoxia and lowered oxygen levels (Makri *et al.*, 2021).

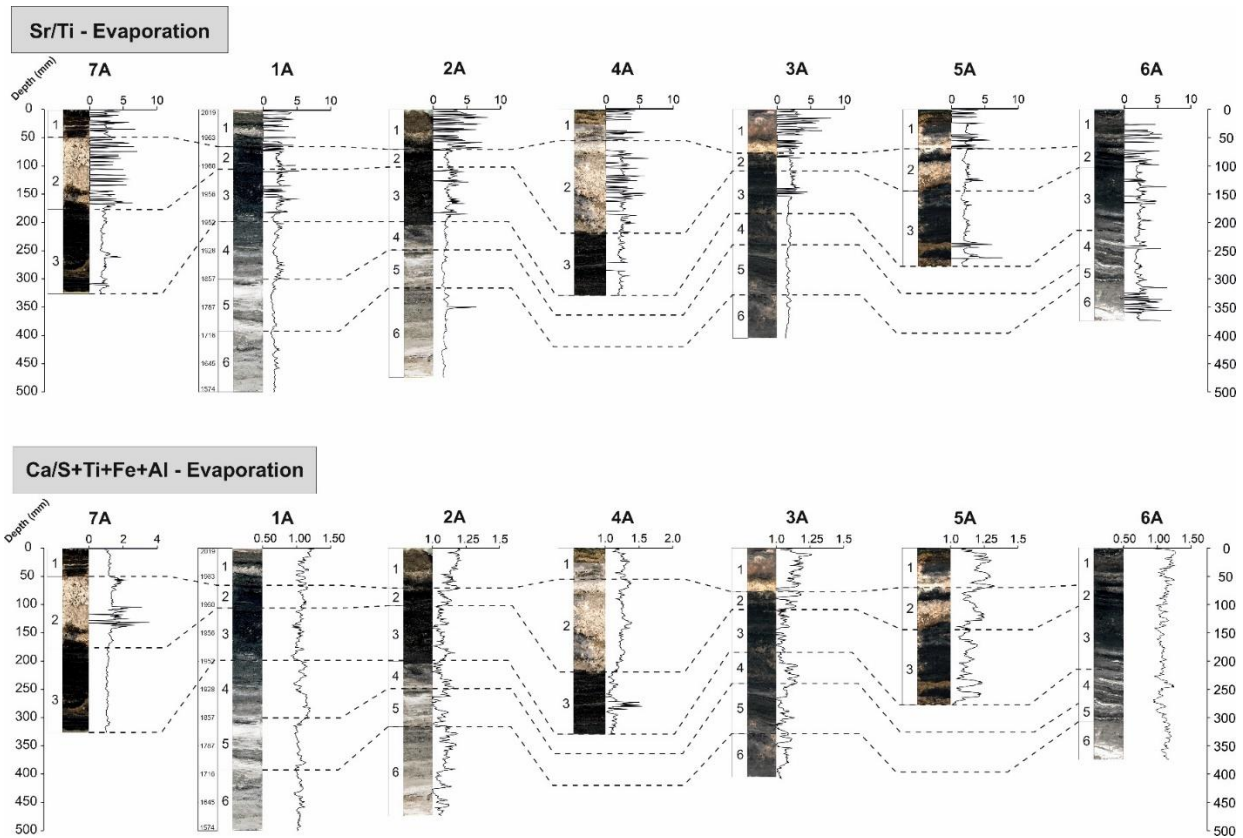


Figure 5.8 - Figure illustrating spatio-temporal variations in geochemical proxies typically used for determination of the intensity of evaporation (Martín-Puertas *et al.*, 2011).

5.5.2 - Extrinsic factors

5.5.2.1 - Delivery of detrital material

There is a relatively significant influx of detrital material delivered to Lake Chiprana from surface runoff, small ephemeral streams, and irrigation channels installed during periods of changing land management (Valero-Garces *et al.*, 2000) throughout the cores. The ratio $\log(\text{Ti})/\log(\text{Ca})$ (Figure 5.9), which provides insights into processes of runoff and sediment delivery into the lake (Litt *et al.*, 2009), was used as the primary indicator for the degree of detrital influx throughout the sedimentary sequences of Chiprana (Figure 5.9). This ratio also removes the mixed signal of Ca which is influenced by multiple environmental processes (Martín-Puertas *et al.*, 2011; Scholz *et al.*, 2011). For example, in many lacustrine environments, external Ca can be delivered to the lake from the catchment, particularly where marls or other carbonate-rich lithologies are present as is the case for Lake Chiprana (Kylander *et al.*, 2011), or can increase as a result of *in situ* evaporative concentration of the lake-waters leading to carbonate and sulphate precipitation (Brown, 2011). In the profundal sequence of the main basin, detrital input is typically highest in units 5 and 6 corresponding to approximately 1600-1850AD, but also shows marked increases in the lower subunits of unit 3 around 1950AD. Contrastingly, in the profundal setting of the smaller side basin, detrital input moderately increases in unit 3 and 4, significantly increases in unit 5, but is relatively low within unit 6. Within the littoral setting, detrital input is relatively low in unit 1 in all cores, but generally increases moderately in units 2 and continues to increase throughout unit 3.

In the case of the principal component analyses, the detrital signal of Lake Chiprana can also be discussed when considering the first eigenvector of the PCA results in both the profundal and littoral settings. As shown in other Iberian lakes (Lake Zonar (Martín-Puertas *et al.*, 2011), Lake Sanabria (Giralt *et al.*, 2008); Lake Arreo (Corella *et al.*, 2011a); Lake Montcortès (Corella *et al.*, 2011b); Lake Taravilla (Moreno *et al.*, 2008)), this eigenvector illustrates variance between the input of detrital material to

the lake and the degree at which evaporative processes and thus mineral precipitation occurs. In the case of the profundal setting, positive values represent an increasing amount of detrital material being delivered to the lake and characterise the lower intervals of the sedimentary sequence (units 5 and 6) where detrital facies are more prevalent. In contrast, negative eigenvector 1 values suggest decreased detrital input, and are associated with evaporitic facies such as those associated with microbial mat and gypsum development in units 1 and 4. However, in the littoral setting, positive values are also associated with increasing organic matter as highlighted by the correlation of Br and Inc/Coh to detrital elements and the close association of these elements on the PCA biplot. This may relate to an input of mixed organic and detrital material to the littoral environments of the lake during runoff, a process which likely did not distribute the same organic material to the profundal zone. Alternatively, this may also reflect the establishment of increased biological processes in the shallower margins of the lake when water levels rise and subsequently the intensity of evaporation is lower and erosion is reduced allowing for organic preservation (Arthur & Sageman, 2005).

Ti/Ca - Detrital Input

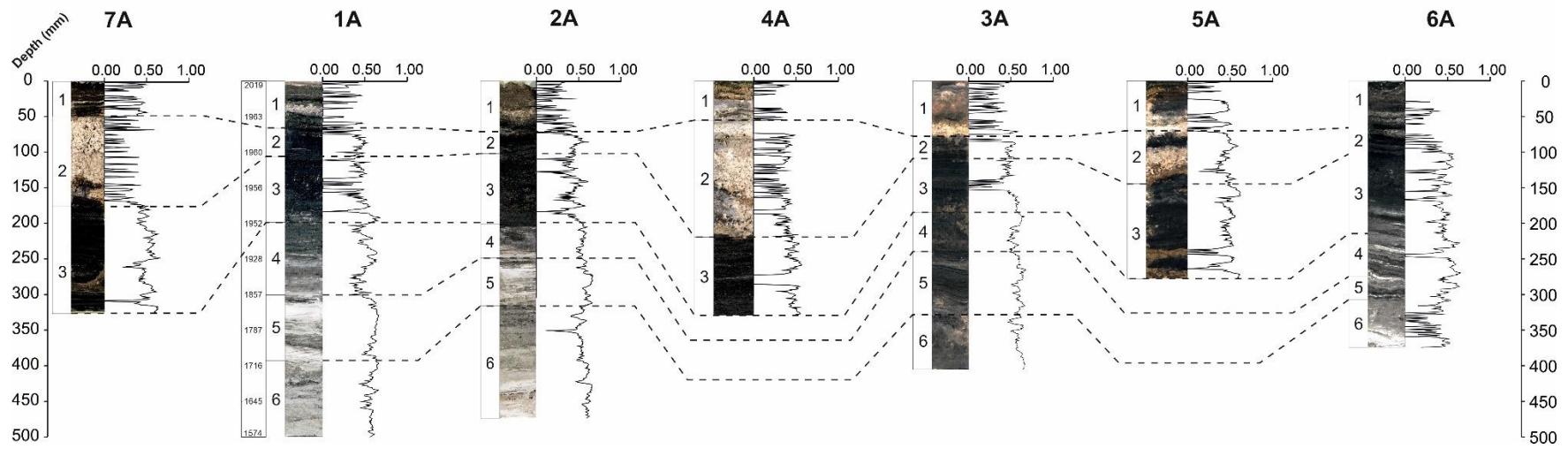


Figure 5.9 - Figure illustrating spatio-temporal variations in geochemical proxies typically used for determination the degree of detrital input (Kylander *et al.*, 2011).

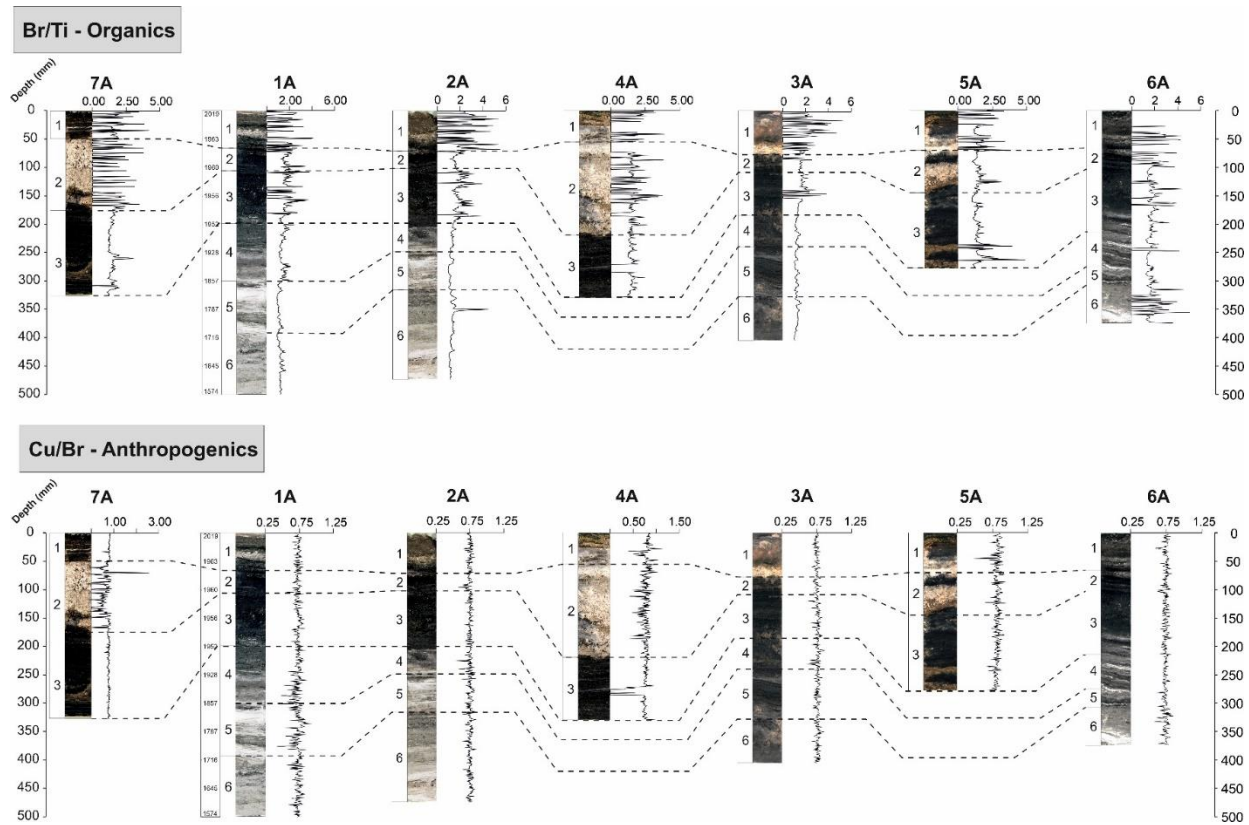


Figure 5.10 Figure illustrating spatio-temporal variations in geochemical proxies typically used for determination of the degree of organics/bioproductivity (Fedotov *et al.*, 2012) and anthropogenic input (Guyard *et al.*, 2007). Cu/Br is used here due to the strong association of organics with Cu and Ni (see discussion).

5.5.2.2 - Anthropogenic water management

A significant portion of Lake Chiprana's late Holocene history has involved management from local regional authorities and from evolving farming practices (Valero-Garcés *et al.*, 2000; De Wit *et al.*, 2013). In the present day and for the last three decades in particular, the lake has been under the designation of a Ramsar convention which aims to preserve unique mammalian and reptilian biological communities (De Wit *et al.*, 2013), vegetation and the unique microbial mat assemblages found here. Thus, in the present, lake water levels are continuously monitored and regulated by inflow via an inlet channel connecting to the nearby freshwater to brackish Laguna de Las Rocas (Díaz *et al.*, 1998; Jódar *et al.*, 2020), highlighting the strong anthropogenic factor in the lake's present day environmental signatures. In the long-term past, the lake has primarily been used as a reservoir for output from irrigation associated with the use of water from the nearby Civan Canal (Valero-Garcés *et al.*, 2000). Varying agricultural activities and the intensity of such activities throughout the last four centuries as discussed throughout this study and other studies (Valero-Garcés *et al.*, 2000; Jódar *et al.*, 2020; Doyle *et al.*, 2022) have led to varying amounts of irrigation water delivered via inlet channels to Lake Chiprana, likely strongly associated with the degree of detrital material (highlighted by detrital elements and the ratio of $\log(\text{Ti})/\log(\text{Ca})$) being delivered to the lake. The lake has thus maintained a relatively long-standing history of anthropogenic impact throughout the Late Holocene, a factor that has undoubtedly contributed to the sedimentological and geochemical processes that are discussed throughout this study.

5.5.3 - Spatial variations

In both the profundal and littoral settings of Lake Chiprana, alike to the case of Lake Zonar in Southern Spain (Martín-Puertas *et al.*, 2011), increasing lake levels are associated with the most positive values of eigenvector 1, whereas more saline conditions and decreasing lake levels are associated with the most negative values of the same eigenvector. However, in the profundal setting, negative values of the

first eigenvector are typically associated with increased biological productivity and subsequently evaporation and lower lake levels. The intensity of biological productivity is potentially obscured within the first eigenvector due to increased detrital input (see Figure 5.4), a characteristic that potentially relates to the strong stratification of Lake Chiprana and the heterogeneity of biological processes between the littoral and profundal settings (Jódar *et al.*, 2020). The lack of strong anoxic conditions alike to those of the profundal setting may explain why these values are not grouped with indicators of organic productivity in the littoral setting, as Cu and Ni adsorption to these organic compounds would be reduced in a more oxic environment (Yang *et al.*, 2010). In general, a plausible scenario is the development of a wetland when Lake Chiprana undergoes drawdown, leading to increased organic productivity in the now shallower profundal basin. In confluence, such drawdown may lead to harsh environmental conditions in the littoral settings, where high salinity and erosion in small pools and brines may negate any complex productivity and reduce preservation.

5.5.4 - Environmental and human impacts in the semi-arid Central Ebro Basin

Fluctuations in the significance of geochemical proxies within Lake Chiprana reflect the responses of the lake to the effects of various external and intrinsic impacts during the last few centuries in the semi-arid Central Ebro Basin. Periods of increased lake level were recognised between ~1600 and ~1800AD. In contrast, periods of reduced lake level occur primarily in the modern day to approximately 1960AD, and between ~1850-1950AD. Increases in elements such as Ti, Fe, and K and minerals including quartz and phyllosilicates are often interpreted as being reflective of increased bottom water anoxia due to their association with increased lake levels and subsequently water stratification (Kylander *et al.*, 2011). Increases in lake levels in Lake Chiprana are however contrastingly result in decreased organic productivity in the profundal settings of the lake, and are instead more prominent when lake levels decreased, indicating the prominence of biological processes

occurring under shallower conditions. The reverse effect is true for the littoral setting, whereby increases in lake levels likely promote organic productivity as a result of more suitable conditions occurring for biological processes to take place. In tandem, increases in variables such as $\log(\text{Sr})/\log(\text{Ti})$, S, and minerals such as gypsum, halite and hexahydrate (Doyle *et al.*, 2022) are instead indicative of decreases in lakewater levels and thus increasing salinity and evaporation (Martín-Puertas *et al.*, 2011).

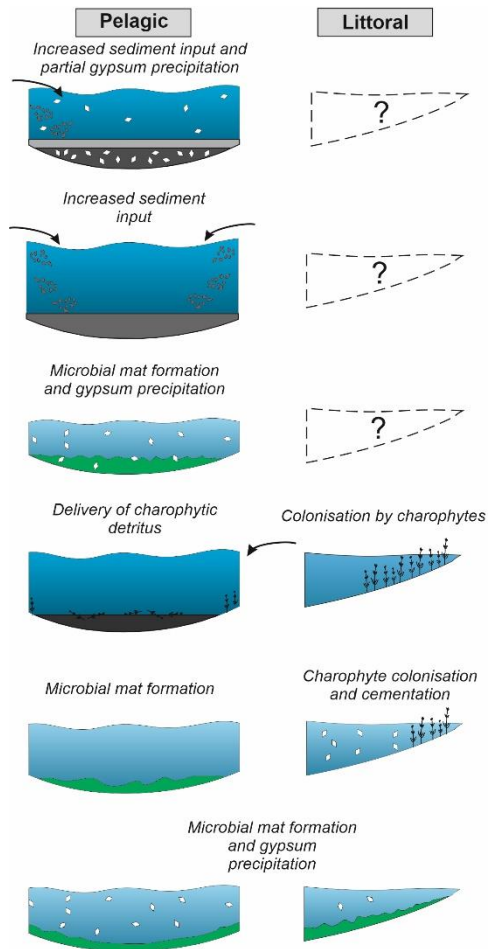
A range of climatic, environmental and biological factors must be considered in the environmental reconstruction of Lake Chiprana (Figure 5.11). Despite this, the anthropogenic factor must also be considered as in any palaeoenvironmental investigation focusing upon lake sediments (Martínez-Cortizas *et al.*, 2009), and previous investigations of the site have revealed strong human impacts within the region of Chiprana and the Ebro Basin that are also reflected by the geochemical data presented here (Valero-Garces *et al.*, 2000). At the base of the sequence (~1600_{AD}) where increasing lake levels are apparent, studies have shown that areas of Northeast Spain experienced moderate increases in rainfall associated with the Late Maunder Minimum (1675-1715_{AD}) as recorded in historical archives (Barriendos, 1997) and Pre-Pyrenean lake sediments (Vegas-Vilarrúbia *et al.*, 2022). Flood events have for example been identified in the North-western Ebro Basin around the beginning of the 17th and 18th centuries in Lake Arreo (Corella *et al.*, 2021), while periods of higher lake levels in Lake Estanya (González-Sampéris *et al.*, 2008; Morellón *et al.*, 2008) also occurred during some phases of the Little Ice Age. However, the onset of modern agricultural practices in the 15th century and their later expansion in the 17th century (Valero-Garcés *et al.*, 2000) are coeval with increased lake levels occurring throughout the basal units of Lake Chiprana, indicating that increased irrigation returns may have represented a strong component of the hydrological input to the lake (Valero-Garces *et al.*, 2000; Doyle *et al.*, 2022).

The onset of microbial mats within the lower section unit 4 and the subsequent lake level decreases associated with Lake Chiprana throughout 1850-1950AD represents a transition to more saline conditions. This timeframe is associated with the end of the Little Ice Age, coinciding with a decrease in flood variability in the northern Ebro basin and generally lower autumn precipitation in the Pre-Pyrenees (Corella *et al.*, 2021; Vegas-Vilarrúbia *et al.*, 2022). This timeframe also correlates with an agrarian crisis throughout Spain (Valero-Garces *et al.*, 2000), and it is likely that relatively stable, non-anthropogenic conditions occurred throughout the early 19th century, allowing lake levels to fall and microbial mats to develop. However, the effects of increased water delivery to Lake Chiprana from anthropogenic activities may have caused lake level rises occurring at the base of unit 3 around approximately 1950 (Doyle *et al.*, 2022) based on the changes in PC1, likely in response to increasing irrigation returns again influenced by expanding agricultural activities (Valero-Garcés *et al.*, 2000; Doyle *et al.*, 2022). Finally, in the modern-day, hydrological management and the designation of the site under a Ramsar convention (De Wit *et al.*, 2013) have led to significant anthropogenic involvement in order to preserve the unique ecological reserves the lake is associated with.

Thus, it is clear that for the past three to four centuries, the responses of lake Chiprana to multiple anthropogenic perturbations have been significant, and changing lake levels must be interpreted with regards to the impact of both human and environmental factors. Additionally, the presence of facies such as microbial mats occurring throughout the history of Lake Chiprana points to unique environmental conditions that may have promoted processes such as mineral formation, dissolution and complex biological productivity which can further skew the geochemical record (Visscher & Stolz, 2005; Dupraz *et al.*, 2009). Microbial mats in the modern-day setting of Chiprana are associated with heightened carbonate and sulphate precipitation as a result of metabolic activities such as photosynthesis and sulphate reduction, both of which induce increases in pH and the liberation of Ca²⁺ ions (Camacho & De Wit, 2003; Jonkers *et al.*, 2003). Caution must therefore be

exercised and distinctions made between abiotic processes (e.g. evaporation, lake drawdown) and biotic processes (photosynthesis, sulphate reduction) leading to mineral precipitation in cases such as Lake Chiprana where both processes are prevalent (De Wit *et al.*, 2013).

Overall, the results of the study have not only shed light on the depositional changes in lake Chiprana during the last centuries and their relationship with human disturbance and climate change, but have also shown several key findings for the palaeolimnological community. Firstly, the geochemical sequence of Lake Chiprana has highlighted the reliability of saline-hypersaline lakes as potential palaeoenvironmental archives. In areas such as the Ebro Basin where saline lakes are characteristic features (Alonso, 1998; Vegas-Vilarrúbia *et al.*, 2013), the occurrence of a permanent lake such as Chiprana and the subsequent preservation potential of sediments within the site illustrate its critical role as an archive of environmental information. Additionally, the study has also revealed the large geochemical and sedimentological variability associated with saline lake depositional environments, both from a temporal and a spatial perspective. This ultimately emphasises the need for a multi-core strategy to better understand its past dynamics and past processes.



Description
<p><i>Pre-1700</i> Permanent saline lake with mixed detrital input and intermittent phases of increased evaporation and higher organic productivity</p>
<p><i>1700-1850</i> Permanent saline lake with increased detrital input, decreased organic productivity and higher lake levels</p>
<p><i>~1850-1950</i> Shallow hypersaline lagoon-wetland with development of microbial mats from increased evaporation and increased organic productivity with shallower lake levels</p>
<p><i>1950-1960</i> Shallow saline lake with small amounts of detrital input and colonisation of littoral and profundal zones by charophytes and macrophytes</p>
<p><i>1960-1970/80</i> Hypersaline, permanent lagoon with deposition of microbial mats and organic-rich muds, with increased evaporation throughout and increased organic productivity in the profundal setting</p>
<p><i>1970/80-2020</i> Hypersaline, permanent lagoon with microbial mats, high evaporation and increased organic productivity in the profundal setting</p>

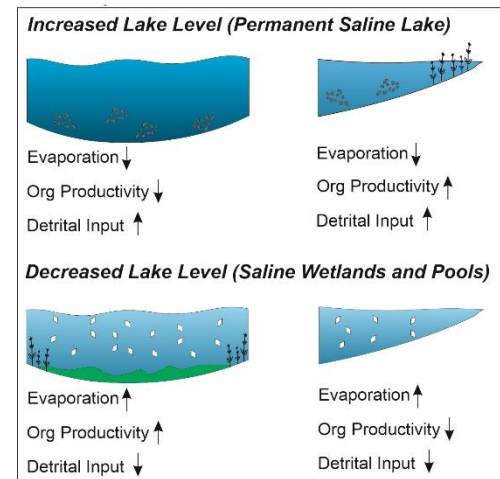
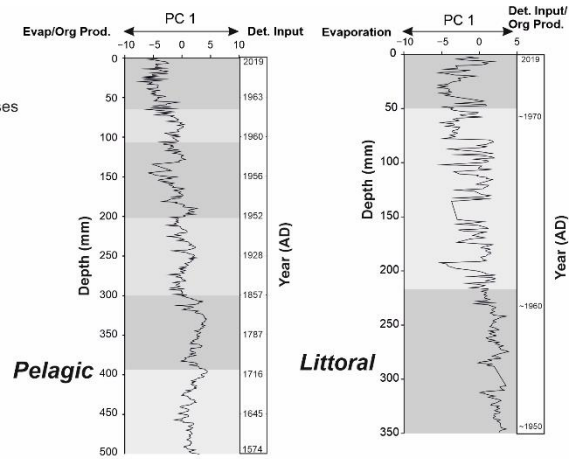


Figure 5.11 - Palaeoenvironmental models constructed from the sedimentary and geochemical sequence from Lake Chiprana. The sequence has been subdivided into six primary phases. Each phase represents largely different environmental conditions leading to the highly variable sedimentary and geochemical characteristics associated with the sequence. In addition, principal components associated with the profundal and littoral settings are presented. These components highlight the degree of key environmental processes occurring within Lake Chiprana and additionally illustrate the variability and intensity of such processes in the spatial domain. The effects of increasing and decreasing on lake-levels upon the different environments are also presented.

5.6 - Conclusions

Intrinsic and extrinsic processes in Lake Chiprana are interpreted from a multi-parameter dataset and highlight a complex interaction between various environmental and anthropogenic factors, while also displaying good comparison with geochemical processes occurring in other lakes in the Iberian peninsula such as Lake Zonar (Martín-Puertas *et al.*, 2011), Lake Estanya (Morellón *et al.*, 2008), Lake Montcortes (González-Sampériz *et al.*, 2017), and further afield (Brock & Hammer, 1987). Firstly, organic productivity is complex, and increases are typically associated with lake level decreases when oxic conditions prevail in the profundal setting of the lake. In contrast, lake level increases in the shallower settings likely allowed for the establishment of greater biological activity in this zone of the lake. Increases in organic matter are also strongly correlated with increases in heavy metal content (Ci and Nu) as a result of heavy metal adsorption to organic compounds. Contrastingly, increases in the concentration of S, Cl, Sr and the ratio of $\log(\text{Sr})/\log(\text{Ti})$ indicate increased evaporation and the precipitation of mineralogical phases (Martín-Puertas *et al.*, 2011). Increases in these proxies essentially reflect intermittent periods of lake drawdown and the development of microbial mats throughout the lakebed, and are likely reflective of periods of stable saline conditions induced by decreasing anthropogenic input. Finally, increased flow of water to the lake is highlighted by increases in the volume of clastic material as a result of increased runoff from agricultural land use and increased flooding during higher intensity rainfall. Overall, the sequence and geochemistry of Lake Chiprana illustrates the strong variability of these unique ecosystems that should be considered in any study focusing upon saline lakes. Significant variations in sedimentology and geochemistry between the profundal and littoral settings also portray a widely heterogeneous ecological system that highlights both the temporal and spatial sensitivity of these settings.

Supplementary Material

Table S1 - Table displaying sedimentological facies that were identified in both littoral and profundal cores from Laguna Salada de Chiprana (see (Doyle *et al.*, 2022)). Though many of these facies occur in varying abundance within each core, not all facies are present and in some cases are strictly limited to profundal or littoral sedimentary environments. Mineralogical and sedimentological descriptions and values of LOI (loss-on-ignition) are also presented alongside an interpretation of the likely depositional environment that each facies formed in.

Facies	Characteristics
a	<p>Grey-yellow sandy mudstones</p> <p>a.1 Grey weakly bedded to massive heterolithic sandy siltstones, typically with heightened amounts of quartz and detrital aragonite and calcite. Low abundances of gypsum, halite and hexahydrite. Basal loading structures are present in some intervals.</p> <p>a.2 Massive sandy siltstones, typically illustrating a range of continuous and lenticular bed morphologies and in some cases displaying basal loading structures. Low abundances of gypsum and hexahydrite, high abundances of detrital calcite, phyllosilicates and quartz.</p>
b	<p>Massive muds with gypsum Massive and poorly laminated dark coloured mudstones with abundant intergrowths of coarse gypsum as the primary mineralogical phase. Intercalated or interbedded with minor lenses of siliciclastic layers of various grain sizes or microbialite laminae. Magnesium sulphates and halite form secondary phases, carbonate and quartz absent.</p>
c	<p>Gypsum laminae White coloured beds and fine laminae of endogenic gypsum crystals and precipitates of highly variable grain sizes. The beds are often closely associated with Facies 1, typically overlying the upper surface of the latter facies. Minor amounts of hexahydrite and thenardite, absence of carbonates and quartz.</p>
d	<p>Cemented charophytes Crystalline cemented masses of charophytes typically confined to littoral depositional environments. Predominantly composed of gypsum, with some minor amounts of aragonite, calcite and hexahydrite. Cemented charophytic and macrophytic intervals, typically massive and highly consolidated. Gypsum rich, with minor amounts of aragonite and thenardite throughout.</p>
e	<p>Laminated Microbial Mats with Mudstones Finely laminated (<1mm) cyanobacterial/microbial mats with strong red, green, and dark black staining of the sediment attributed to the presence of microbial pigments. Cyanobacterial sheaths can typically be found occurring alongside EPS, micrite matrices and densely packed microcrystalline carbonate and gypsum. Interstitial layers occurring between microbially-stained laminae consist primarily of aragonite/high-Mg calcite and gypsum/thenardite.</p>

f	<p>Microbial mats with gypsum Very finely laminated dark brown and orange laminae (organic matter, diatoms) and white-yellow laminae (carbonate precipitates) interbedded with white crystalline phases (gypsum). Gypsum intergrowths form both as laminated/bedded intervals and as lenticular deposits between microbial laminae. Carbonates are primarily composed of aragonite and calcite, and other minor phases are constituted by hexahydrate and halite. Microbially-induced layering is strongly displaced by large (>0.5mm) gypsum crystals.</p>
g	<p>Charophytic muds Charophytic and macrophytic mudstones, typically massive, with an abundance of fragmented charophytes and macrophytes. These facies display predominantly clayey-silty grain sizes and contain moderate amounts of gypsum, hexahydrate and very small amounts of calcite, aragonite and halite. Organic content is typically high (4%-6%) and is composed of organic-rich biofilms, diatoms and charophytic remains.</p>
h	<p>Black-grey laminated and organic-rich muds Very finely laminated black clayey muds with high amounts of organic carbon, moderate amounts of gypsum and halite and varying but relatively low amounts of quartz, calcite and aragonite. They are typically distinctive from adjacent facies due to their very dark black colour and strong degree of lamination.</p>

Table S2 - Table displaying the output of the principal component analyses for the profundal and littoral settings.

		Profundal										Littoral							
		1		2		3		4		1		2		3		4			
Eigenvalue		6.18		1.92		1.69		1.37		43.13		13.38		11.81		9.58			
Variance (%)		43.13		13.38		11.81		9.58		42.61		22.69		11.89		6.70			
Cumul. (%)		43.13		56.51		68.31		77.89		42.61		65.31		77.20		83.90			
		Al	Si	S	Cl	K	Ca	Ti	Cr	Mn	Fe	Ni	Cu	Br	Rb	Sr	Zr	Mo	Inc/Coh
Profundal	Eigenvector 1	0.14	0.26	-0.18	-0.17	0.17	0.09	0.63	0.03	0.20	0.27	-0.16	-0.20	-0.22	0.27	-0.21	-0.18	-0.18	-0.11
	Eigenvector 2	-0.40	-0.13	0.00	0.04	0.02	-0.09	-0.05	-0.20	-0.05	0.02	0.08	0.12	0.12	0.85	-0.01	0.05	0.02	0.12
	Eigenvector 3	0.85	0.12	-0.01	-0.01	-0.04	-0.07	-0.33	-0.06	-0.07	-0.08	0.01	0.04	0.02	0.36	-0.05	0.00	-0.04	0.03
	Eigenvector 4	-0.06	-0.02	0.02	0.04	0.00	0.00	-0.12	0.97	-0.01	-0.02	-0.03	0.02	-0.01	0.19	-0.03	-0.02	-0.03	-0.02
Littoral	Eigenvector 1	-0.11	-0.03	-0.15	-0.03	0.17	-0.10	0.84	-0.07	0.06	0.24	-0.02	0.03	0.09	0.36	-0.04	-0.02	-0.09	0.10
	Eigenvector 2	0.08	0.01	-0.02	-0.03	-0.09	-0.01	-0.34	-0.06	-0.03	-0.10	-0.02	-0.02	-0.04	0.92	-0.01	0.01	-0.01	0.00
	Eigenvector 3	0.97	0.13	-0.03	-0.04	-0.01	-0.01	0.14	-0.06	0.07	0.01	-0.03	-0.05	-0.06	-0.05	-0.05	-0.06	-0.01	-0.02
	Eigenvector 4	0.14	-0.15	-0.15	0.17	0.31	-0.17	-0.23	-0.04	-0.16	0.16	0.22	0.46	0.46	-0.02	0.09	0.19	-0.07	0.40

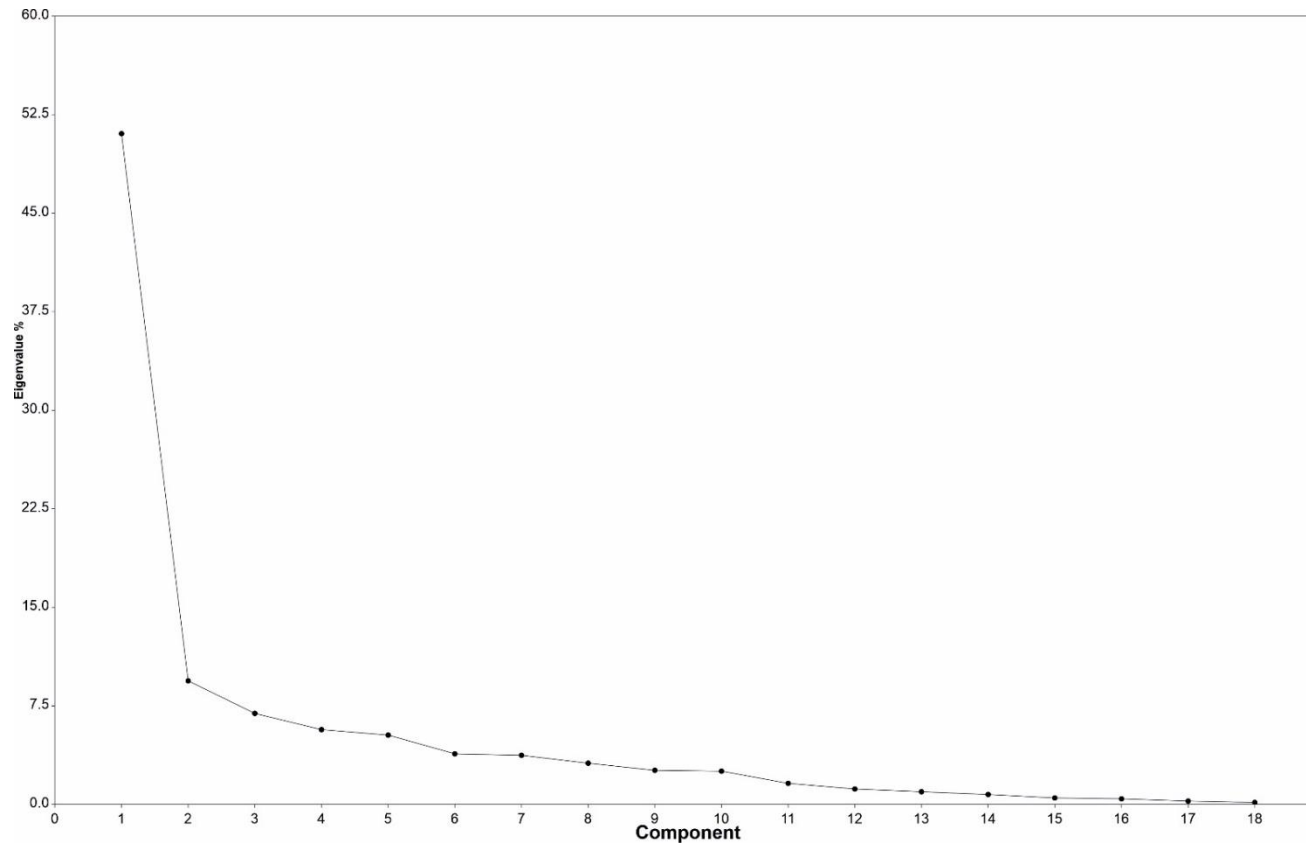


Figure S1 - Scree plot from elements from core CHI19-1A (profundal setting).

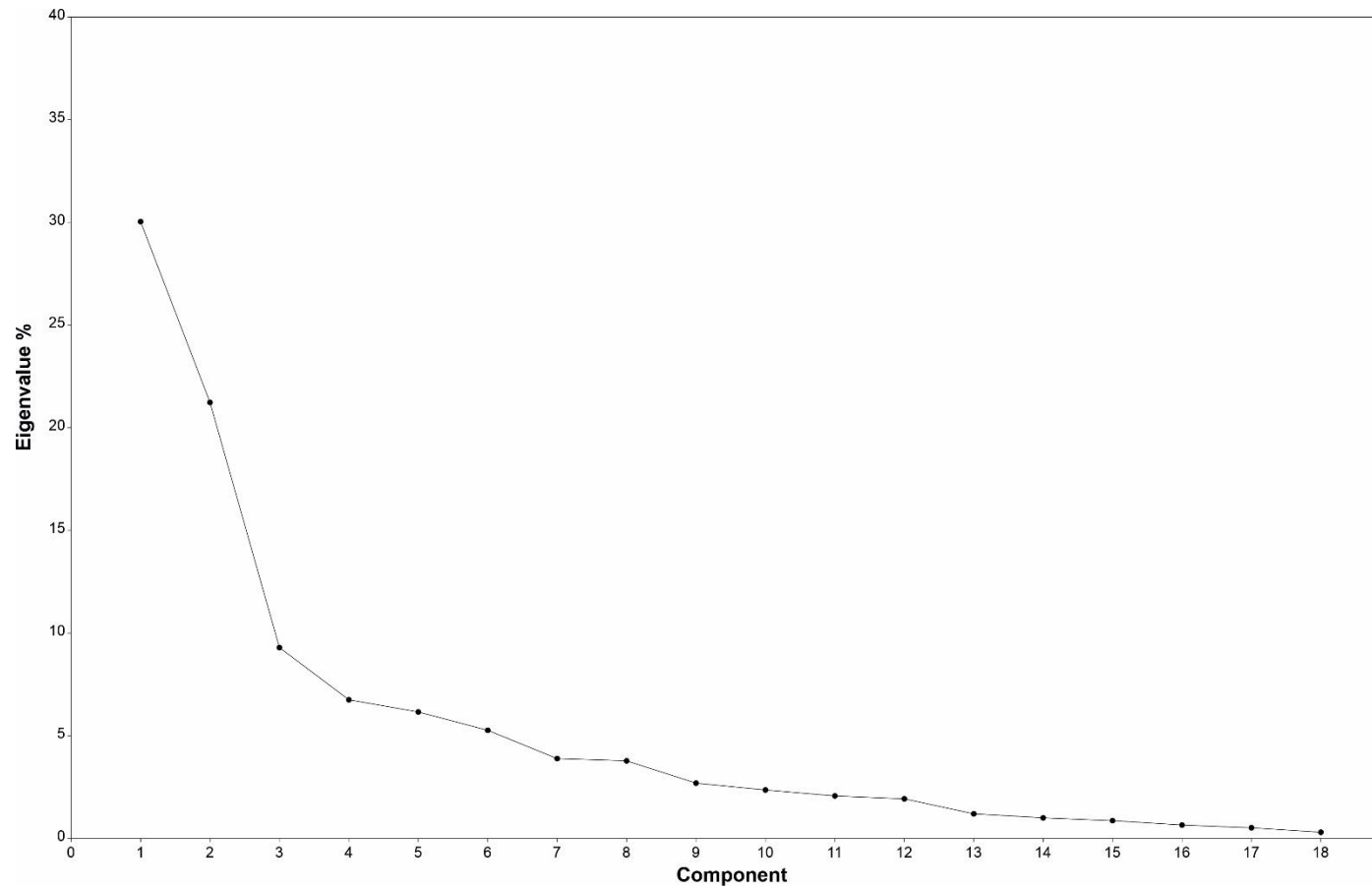


Figure S2 - Scree plot from elements from core CHI19-4A (littoral setting).

Chronological Acceptance

Dates for the chronological model were assessed based on their agreement with the clam generated model. The output of the model determined that the majority of the ^{210}Pb dates were in disagreement with the model, and were within significant error margins such that they could not be considered viable for the model.

References

- Alonso, M.** (1998) The lagoons of Peninsular Spain . *Limnetica*, **15**, 1–176.
- Arthur, M.A. and Sageman, B.B.** (2005) The deposition of organic-carbon-rich sediments : models, mechanisms, and consequences. *Depos. Org. Sediments Model. Mech. Consequences*, **1**, 35–59.
- Barriendos, M.** (1997) Climatic variations in the Iberian Peninsula during the late Maunder minimum (AD 1675-1715): An analysis of data from rogation ceremonies. *Holocene*, **7**, 105–111.
- Bishop, T.** (2022) Using Itrax Data in R. <https://tombishop1.github.io/itraxBook/>. Accessed 26 Aug 2022
- Blaauw, M.** (2010) Methods and code for “classical” age-modelling of radiocarbon sequences. *Quat Geochronol.* doi: 10.1016/j.quageo.2010.01.002
- Bonk, A., Müller, D., Ramisch, A., Kramkowski, M.A., Noryśkiewicz, A.M., Sekudewicz, I., Gąsiorowski, M., Luberd-Durnaś, K., Słowiński, M., Schwab, M., Tjallingii, R., Brauer, A. and Błaszkiwicz, M.** (2021) Varve microfacies and chronology from a new sediment record of Lake Gościąż (Poland). *Quat Sci Rev.* doi: 10.1016/j.quascirev.2020.106715
- Brock, M.A. and Hammer, U.T.** (1987) *Saline Lake Ecosystems of the World.*, 1st edn. *Springer*, Dordrecht, 580 pp.
- Brown, E.T.** (2011) Lake Malawi’s response to “megadrought” terminations: Sedimentary records of flooding, weathering and erosion. *Palaeogeogr Palaeoclimatol Palaeoecol.* doi: 10.1016/j.palaeo.2010.01.038
- Camacho, A. and De Wit, R.** (2003) Effect of nitrogen and phosphorus additions on a benthic microbial mat from a hypersaline lake. *Aquat. Microb. Ecol.*, **32**, 261–273.
- Caran, S.C.** (1998) Quaternary paleoenvironmental and paleoclimatic reconstruction: A discussion and critique, with examples from the southern high plains. *Plains Anthropol.*, **43**, 111–124.
- Chawchai, S., Kylander, M.E., Chabangborn, A., Löwemark, L. and Wohlfarth, B.** (2016) Testing commonly used X-ray fluorescence core scanning-based proxies for organic-rich lake sediments and peat. *Boreas*, **45**, 180–189.
- Corella, J.P., Amrani, A. El, Sigró, J., Morellón, M., Rico, E. and Valero-**

- Garcés, B.L.** (2011a) Recent evolution of Lake Arreo, northern Spain: Influences of land use change and climate. *J. Paleolimnol.*, **46**, 469–485.
- Corella, J.P., Benito, G., Monteoliva, A.P., Sigro, J., Calle, M., Valero-Garcés, B.L., Stefanova, V., Rico, E., Favre, A.C. and Wilhelm, B.** (2021) A 1400-years flood frequency reconstruction for the Basque country (N Spain): Integrating geological, historical and instrumental datasets. *Quat. Sci. Rev.*, **262**, 1–15.
- Corella, J.P., Brauer, A., Mangili, C., Rull, V., Vegas-Vilarrúbia, T., Morellón, M. and Valero-Garcés, B.L.** (2012) The 1.5-ka varved record of Lake Montcortès (southern Pyrenees, NE Spain). *Quat. Res. (United States)*, **78**, 323–332.
- Corella, J.P., Loizeau, J.L., le Dantec, N., Hilbe, M., Gerard, J., le Dantec, N., Stark, N., González-Quijano, M. and Girardclos, S.** (2016) The role of mass-transport deposits and turbidites in shaping modern lacustrine deepwater channels. *Mar. Pet. Geol.*, **77**, 515–525.
- Corella, J.P., Moreno, A., Morellón, M., Rull, V., Giralt, S., Rico, M.T., Pérez-Sanz, A. and Valero-Garcés, B.L.** (2011b) Climate and human impact on a meromictic lake during the last 6,000 years (Montcortès Lake, Central Pyrenees, Spain). *J. Paleolimnol.*, **46**, 351–367.
- Corella, J.P., Stefanova, V., El Anjoumi, A., Rico, E., Giralt, S., Moreno, A., Plata-Montero, A. and Valero-Garcés, B.L.** (2013) A 2500-year multi-proxy reconstruction of climate change and human activities in northern Spain: The Lake Arreo record. *Palaeogeogr. Palaeoclimatol. Palaeoecol.*, **386**, 555–568.
- Croudace, I.W., Rindby, A. and Rothwell, R.G.** (2006) ITRAX: Description and evaluation of a new multi-function X-ray core scanner. *Geol. Soc. Spec. Publ.*, **267**, 51–63.
- Czymzik, M., Brauer, A., Dulski, P., Plessen, B., Naumann, R., von Grafenstein, U. and Scheffler, R.** (2013) Orbital and solar forcing of shifts in Mid- to Late Holocene flood intensity from varved sediments of pre-alpine Lake Ammersee (southern Germany). *Quat. Sci. Rev.*, **61**, 96–110.
- Davis, B.** (1994) Paleolimnology and Holocene Environmental Change from Endoreic Lakes in the Ebro Basin, North-east. University of Newcastle Upon Tyne
- De Wit, R.** (2016) Lake La Salada de Chiprana (NE Spain), an Example of an Athalassic Salt Lake in a Cultural Landscape. In: *Lake Sciences and Climate Change*, 1st edn. (Ed. M.N. Rashed), *IntechOpen*, Rijeka, 43–60.
- De Wit, R., Guerrero, M.C., Legaz, A., Jonkers, H.M., Blocier, L., Gumiaux, C. and Gautret, P.** (2013) Conservation of a permanent hypersaline lake: Management options evaluated from decadal variability of coleofasciculus chthonoplastes microbial mats. *Aquat. Conserv. Mar. Freshw. Ecosyst.*, **23**,

532–545.

- Dee, S.G., Russell, J.M., Morrill, C., Chen, Z. and Neary, A.** (2018) PRYSM v2.0: A Proxy System Model for Lacustrine Archives. *Paleoceanogr. Paleoclimatology*, **33**, 1250–1269.
- Diaz, P., Guerrero, M.C., Alcorlo, P., Baltanas, A., Florin, M. and Montes, C.** (1998) Anthropogenic perturbations to the trophic structure in a permanent hypersaline shallow lake: La Salada de Chiprana (north-eastern Spain). *Int. J. Salt Lake Res.*, **7**, 187–210.
- Domínguez-Castro, F., García-Herrera, R., Ribera, P. and Barriendos, M.** (2010) A shift in the spatial pattern of Iberian droughts during the 17th century. *Clim. Past*, **6**, 553–563.
- Doyle, C., Schröder, S., Corella, J.P. and Valero Garces, B.** (2022) Facies variability and depositional settings of Laguna Salada de Chiprana, an Iberian hypersaline lake. *Sedimentology*, **69**, 2615–2641.
- Dupraz, C., Reid, R.P., Braissant, O., Decho, A.W., Norman, R.S. and Visscher, P.T.** (2009) Processes of carbonate precipitation in modern microbial mats. *Earth-Science Rev.*, **96**, 141–162.
- Edelmann, D., Móri, T.F. and Székely, G.J.** (2021) On relationships between the Pearson and the distance correlation coefficients. *Stat Probab Lett.* doi: 10.1016/j.spl.2020.108960
- Fedotov, A.P., Phedorin, M.A., Enushchenko, I. V., Vershinin, K.E., Melgunov, M.S. and Khodzher, T. V.** (2012) A reconstruction of the thawing of the permafrost during the last 170years on the Taimyr Peninsula (East Siberia, Russia). *Glob. Planet. Change*, **98–99**, 139–152.
- Finlayson, C.M.** (2016) Salt Lakes. In: *The Wetland Book*, 1–12.
- Froidl, F.** (2021) Kinetics of petroleum generation from terrestrial organic matter: The examples of the lacustrine Berriasian Wealden Shales and Pennsylvanian hard coals, western Germany. Rheinisch -Westfälischen Technischen Hochschule Aachen
- Gadd, P., Heijnis, H., Chagué-Goff, C., Zawadzki, A., Fierro, D., Atahan, P., Croudace, I.W. and Goralewski, J.** (2015) ITRAX Core Scanner Capabilities Combined with Other Geochemical and Radiochemical Techniques to Evaluate Environmental Changes in a Local Catchment, South Sydney, NSW, Australia. 443–455.
- Gebregiorgis, D., Giosan, L., Hathorne, E.C., Anand, P., Nilsson-Kerr, K., Plass, A., Lückge, A., Clemens, S.C. and Frank, M.** (2020) What Can We Learn From X-Ray Fluorescence Core Scanning Data? A Paleomonsoon Case Study. *Geochemistry, Geophys Geosystems.* doi: 10.1029/2019GC008414
- Giralt, S., Moreno, A., Bao, R., Sáez, A., Prego, R., Valero-Garcés, B.L., Pueyo,**

- J.J., González-Sampérez, P. and Taberner, C.** (2008) A statistical approach to disentangle environmental forcings in a lacustrine record: The Lago Chungará case (Chilean Altiplano). *J. Paleolimnol.*, **40**, 195–215.
- González-Sampérez, P., Aranbarri, J., Pérez-Sanz, A., Gil-Romera, G., Moreno, A., Leunda, M., Sevilla-Callejo, M., Corella, J.P., Morellón, M., Oliva, B. and Valero-Garcés, B.** (2017) Environmental and climate change in the southern Central Pyrenees since the Last Glacial Maximum: A view from the lake records. *Catena*, **149**, 668–688.
- González-Sampérez, P., Valero-Garcés, B.L., Moreno, A., Morellón, M., Navas, A., Machín, J. and Delgado-Huertas, A.** (2008) Vegetation changes and hydrological fluctuations in the Central Ebro Basin (NE Spain) since the Late Glacial period: Saline lake records. *Palaeogeogr. Palaeoclimatol. Palaeoecol.*, **259**, 157–181.
- Gorny, C., Busby, C., Pluhar, C.J., Hagan, J. and Putirka, K.** (2009) An in-depth look at distal Sierra Nevada palaeochannel fill: Drill cores through the Table Mountain Latite near Knights Ferry. *Int Geol Rev.* doi: 10.1080/00206810902944960
- Guerrero, M.C., Balsa, J., Pascual, M. and Martínez, B.** (1991) Caracterización limnológica de la Laguna Salada de Chiprana (Zaragoza, España) y sus comunidades de bacterias fototróficas. *Limnetica*, **7**, 83–96.
- Guyard, H., Chapron, E., St-Onge, G., Anselmetti, F.S., Arnaud, F., Magand, O., Francus, P. and Mélières, M.A.** (2007) High-altitude varve records of abrupt environmental changes and mining activity over the last 4000 years in the Western French Alps (Lake Bramant, Grandes Rousses Massif). *Quat. Sci. Rev.*, **26**, 2644–2660.
- Hammer, Ø., Harper, D.A.T. and Ryan, P.D.** (2001) PAST: Paleontological statistics software package for education and data analysis. *Palaeontologia electronica*.
- Hardie, L.A., Smoot, J.P. and Eugster, H.P.** (1978) Saline Lakes and their Deposits: A Sedimentological Approach. In: *Modern and Ancient Lake Sediments*, 7–41.
- Hassani, A., Azapagic, A., D’Odorico, P., Keshmiri, A. and Shokri, N.** (2020) Desiccation crisis of saline lakes: A new decision-support framework for building resilience to climate change. *Sci Total Environ.* doi: 10.1016/j.scitotenv.2019.134718
- IGME** (2003a) Mapa Geologico de Espana, 1:50000, (serie MAGNA). Hoja 988. Puente-Genil.
- IGME** (2003b) Mapa Geologico de Espana, 1:50000, (serie MAGNA). Hoja 137. Miranda de Ebro.
- Jellison, R., Williams, W.D., Timms, B., Alcocer, J. and Aladin, N. V.** (2008) Salt

lakes: Values, threats and future. In: *Aquatic Ecosystems: Trends and Global Prospects*, 94–110.

- Jódar, J., Rubio, F.M., Custodio, E., Martos-Rosillo, S., Pey, J., Herrera, C., Turu, V., Pérez-Bielsa, C., Ibarra, P. and Lambán, L.J.** (2020) Hydrogeochemical, isotopic and geophysical characterization of saline lake systems in semiarid regions: The Salada de Chiprana Lake, Northeastern Spain. *Sci. Total Environ.*, **728**, 1–48.
- Jones, B.E., Grant, W.D., Duckworth, A.W. and Owenson, G.G.** (1998) Microbial diversity of soda lakes. *Extremophiles*, **2**, 191–200.
- Jonkers, H.M., Ludwig, R., De Wit, R., Pringault, O., Muyzer, G., Niemann, H., Finke, N. and De Beer, D.** (2003) Structural and functional analysis of a microbial mat ecosystem from a unique permanent hypersaline inland lake: “La Salada de Chiprana” (NE Spain). *FEMS Microbiol. Ecol.*, **44**, 175–189.
- Kylander, M.E., Ampel, L., Wohlfarth, B. and Veres, D.** (2011) High-resolution X-ray fluorescence core scanning analysis of Les Echets (France) sedimentary sequence: New insights from chemical proxies. *J. Quat. Sci.*, **26**, 109–117.
- Last, F.M.** (2013) Carbonate microbialite formation in a prairie saline lake in Saskatchewan, Canada: paleohydrologic and paleoenvironmental implications. University of Manitoba
- Last, W.M.** (2002) Geolimnology of salt lakes. *Geosci. J.*, **6**, 347–369.
- Lin, J.G. and Chen, S.Y.** (1998) The relationship between adsorption of heavy metal and organic matter in river sediments. *Environ. Int.*, **24**, 345–352.
- Litt, T., Krastel, S., Sturm, M., Kipfer, R., Örcen, S., Heumann, G., Franz, S.O., Ülgen, U.B. and Niessen, F.** (2009) “PALEOVAN”, International Continental Scientific Drilling Program (ICDP): site survey results and perspectives. *Quat. Sci. Rev.*, **28**, 1555–1567.
- Luzón, A.** (2005) Oligocene-Miocene alluvial sedimentation in the northern Ebro Basin, NE Spain: Tectonic control and palaeogeographical evolution. *Sediment. Geol.*, **177**, 19–39.
- Mackereth, F.J.H.** (1966) Some chemical observations on post-glacial lake sediments. *Philos. Trans. R. Soc. Lond. B. Biol. Sci.*, **250**, 165–213.
- Makri, S., Wienhues, G., Bigalke, M., Gilli, A., Rey, F., Tinner, W., Vogel, H. and Grosjean, M.** (2021) Variations of sedimentary Fe and Mn fractions under changing lake mixing regimes, oxygenation and land surface processes during Late-glacial and Holocene times. *Sci Total Environ.* doi: 10.1016/j.scitotenv.2020.143418
- Marchand, C., Allenbach, M. and Lallier-Vergès, E.** (2011) Relationships between heavy metals distribution and organic matter cycling in mangrove sediments (Conception Bay, New Caledonia). *Geoderma*, **160**, 444–456.
- Martín-Puertas, C., Valero-Garcés, B.L., Mata, M.P., González-Sampériz, P.,**

- Bao, R., Moreno, A. and Stefanova, V.** (2008) Arid and humid phases in southern Spain during the last 4000 years: The Zoñar Lake record, Córdoba. *Holocene*, **18**, 907–921.
- Martín-Puertas, C., Valero-Garcés, B.L., Mata, M.P., Moreno, A., Giralt, S., Martínez-Ruiz, F. and Jiménez-Espejo, F.** (2011) Geochemical processes in a Mediterranean Lake: A high-resolution study of the last 4,000 years in Zoñar Lake, southern Spain. *J. Paleolimnol.*, **46**, 405–421.
- Martínez-Cortizas, A., Costa-Casais, M. and López-Sáez, J.A.** (2009) Environmental change in NW Iberia between 7000 and 500 cal BC. *Quat. Int.*, **200**, 77–89.
- Morellón, M., Valero-Garcés, B., Anselmetti, F., Ariztegui, D., Schnellmann, M., Moreno, A., Mata, P., Rico, M. and Corella, J.P.** (2009a) Late quaternary deposition and facies model for karstic Lake Estanya (North-eastern Spain). *Sedimentology*, **56**, 1505–1534.
- Morellón, M., Valero-Garcés, B., Moreno, A., González-Sampériz, P., Mata, P., Romero, O., Maestro, M. and Navas, A.** (2008) Holocene palaeohydrology and climate variability in northeastern Spain: The sedimentary record of Lake Estanya (Pre-Pyrenean range). *Quat. Int.*, **181**, 15–31.
- Morellón, M., Valero-Garcés, B., Vegas-Vilarrúbia, T., González-Sampériz, P., Romero, Ó., Delgado-Huertas, A., Mata, P., Moreno, A., Rico, M. and Corella, J.P.** (2009b) Lateglacial and Holocene palaeohydrology in the western Mediterranean region: The Lake Estanya record (NE Spain). *Quat. Sci. Rev.*, **28**, 2582–2599.
- Moreno, A., Valero-Garcés, B.L., González-Sampériz, P. and Rico, M.** (2008) Flood response to rainfall variability during the last 2000 years inferred from the Taravilla Lake record (Central Iberian Range, Spain). *J. Paleolimnol.*, **40**, 943–961.
- Mueller, A.D., Islebe, G.A., Hillesheim, M.B., Grzesik, D.A., Anselmetti, F.S., Ariztegui, D., Brenner, M., Curtis, J.H., Hodell, D.A. and Venz, K.A.** (2009) Climate drying and associated forest decline in the lowlands of northern Guatemala during the late Holocene. *Quat. Res.*
- Naeher, S., Gilli, A., North, R.P., Hamann, Y. and Schubert, C.J.** (2013) Tracing bottom water oxygenation with sedimentary Mn/Fe ratios in Lake Zurich, Switzerland. *Chem. Geol.*, **352**, 125–133.
- Pellicer, X.M., Corella, J.P., Gutiérrez, F., Roqué, C., Linares, R., Carbonel, D., Zarroca, M., Guerrero, J. and Comas, X.** (2016) Sedimentological and palaeohydrological characterization of Late Pleistocene and Holocene tufa mound palaeolakes using trenching methods in the Spanish Pyrenees. *Sedimentology*, **63**, 1789–1819.
- Reimer, P.J., Austin, W.E.N., Bard, E., Bayliss, A., Blackwell, P.G., Bronk**

- Ramsey, C., Butzin, M., Cheng, H., Edwards, R.L., Friedrich, M., Grootes, P.M., Guilderson, T.P., Hajdas, I., Heaton, T.J., Hogg, A.G., Hughen, K.A., Kromer, B., Manning, S.W., Muscheler, R., Palmer, J.G., Pearson, C., Van Der Plicht, J., Reimer, R.W., Richards, D.A., Scott, E.M., Southon, J.R., Turney, C.S.M., Wacker, L., Adolphi, F., Büntgen, U., Capano, M., Fahrni, S.M., Fogtmann-Schulz, A., Friedrich, R., Köhler, P., Kudsk, S., Miyake, F., Olsen, J., Reinig, F., Sakamoto, M., Sookdeo, A. and Talamo, S. (2020) The IntCal20 Northern Hemisphere Radiocarbon Age Calibration Curve (0-55 cal kBP). *Radiocarbon*, **62**, 725–757.
- Sáez, A., Valero-Garcés, B.L., Moreno, A., Bao, R., Pueyo, J.J., González-Sampériz, P., Giralt, S., Taberner, C., Herrera, C. and Gibert, R.O. (2007) Lacustrine sedimentation in active volcanic settings: The Late Quaternary depositional evolution of Lake Chungará (northern Chile). *Sedimentology*, **54**, 1191–1222.
- Scholz, C.A., Cohen, A.S., Johnson, T.C., King, J., Talbot, M.R. and Brown, E.T. (2011) Scientific drilling in the Great Rift Valley: The 2005 Lake Malawi Scientific Drilling Project - An overview of the past 145,000 years of climate variability in Southern Hemisphere East Africa. *Palaeogeogr. Palaeoclimatol. Palaeoecol.*, **303**, 3–19.
- Schröder, T., van 't Hoff, J., Ortiz, J.E., de Torres Pèrez-Hidalgo, T.J., López-Sáez, J.A., Melles, M., Holzhausen, A., Wennrich, V., Viehberg, F. and Reicherter, K. (2018) Shallow hypersaline lakes as paleoclimate archives: A case study from the Laguna Salada, Málaga province, southern Spain. *Quat. Int.*, **485**, 76–88.
- Seguin, J., Avramidis, P., Haug, A., Kessler, T., Schimmelmann, A. and Unkel, I. (2020) Reconstruction of palaeoenvironmental variability based on an inter-comparison of four lacustrine archives on the Peloponnese (Greece) for the last 5000 years. *E&G Quat. Sci. J.*, **69**, 165–186.
- Sturm, M. and Matter, A. (2009) Turbidites and Varves in Lake Brienz (Switzerland): Deposition of Clastic Detritus by Density Currents. In: *Modern and Ancient Lake Sediments*, 147–168.
- Valero-Garcés, B., Morellón, M., Moreno, A., Corella, J.P., Martín-Puertas, C., Barreiro, F., Pérez, A., Giralt, S. and Mata-Campo, M.P. (2014) Lacustrine carbonates of Iberian Karst Lakes: Sources, processes and depositional environments. *Sediment. Geol.* 299:1–29.
- Valero-Garcés, B.L., Navas, A., Machin, J., Stevenson, T. and Davis, B. (2000) Responses of a saline lake ecosystem in a semiarid region to irrigation and climate variability: The history of Salada Chiprana, central Ebro basin, Spain. *Ambio*, **29**, 344–350.
- Valero-Garcés, B.L., Navas, A., Machin, J., Stevenson, T., Davis, B., Valero-

- Garcés, B.L., Navas, A., Machin, J., Stevenson, T., Davis, B., Valero-Garcés, B.L., Navas, A., Machin, J., Stevenson, T. and Davis, B.** (2000) Responses of a Saline Lake Ecosystem in a Semiarid Region to Irrigation and Climate Variability. *AMBIO A J. Hum. Environ.*, **29**, 344–350.
- Vegas-Vilarrúbia, T., Corella, J.P., Pérez-Zanón, N., Buchaca, T., Trapote, M.C., López, P., Sigró, J. and Rull, V.** (2018) Historical shifts in oxygenation regime as recorded in the laminated sediments of lake Montcortès (Central Pyrenees) support hypoxia as a continental-scale phenomenon. *Sci. Total Environ.*, **612**, 1577–1592.
- Vegas-Vilarrúbia, T., Corella, J.P., Sigró, J., Rull, V., Dorado-Liñan, I., Valero-Garcés, B. and Gutiérrez-Merino, E.** (2022) Regional precipitation trends since 1500 CE reconstructed from calcite sublayers of a varved Mediterranean lake record (Central Pyrenees). *Sci. Total Environ.*, **826**, 1537–73.
- Vegas-Vilarrúbia, T., González-Sampériz, P., Morellón, M., Gil-Romera, G., Pérez-Sanz, A. and Valero-Garcés, B.** (2013) Diatom and vegetation responses to late glacial and early holocene climate changes at lake estanya (southern pyrenees, NE Spain). *Palaeogeogr. Palaeoclimatol. Palaeoecol.*, **392**, 335–349.
- Vereş, D.** (2002) A Comparative Study Between Loss on Ignition and Total Carbon Analysis on Mineralogenic Sediments. *Stud. Univ. Babeş-Bolyai, Geol.*, **47**, 171–182.
- Vidondo, B., Martínez, B., Montes, C. and Guerrero, M.C.** (1993) Physico-chemical characteristics of a permanent Spanish hypersaline lake: La Salada de Chiprana (NE Spain). *Hydrobiologia*, **267**, 113–125.
- Visscher, P.T. and Stolz, J.F.** (2005) Microbial mats as bioreactors: Populations, processes, and products. *Palaeogeogr. Palaeoclimatol. Palaeoecol.*, **219**, 87–100.
- Weltje, G.J. and Tjallingii, R.** (2008) Calibration of XRF core scanners for quantitative geochemical logging of sediment cores: Theory and application. *Earth Planet. Sci. Lett.*, **274**, 423–438.
- Yang, X., Xiong, B. and Yang, M.** (2010) Relationships among heavy metals and organic matter in sediment cores from lake nanhu, an urban lake in wuhan, China. *J. Freshw. Ecol.*, **25**, 243–249.
- Żarczyński, M., Wacnik, A. and Tylmann, W.** (2019) Tracing lake mixing and oxygenation regime using the Fe/Mn ratio in varved sediments: 2000 year-long record of human-induced changes from Lake Żabińskie (NE Poland). *Sci. Total Environ.*, **657**, 585–596.
- Zhang, C., Scholz, C.A. and Harris, A.D.** (2020a) Sedimentary fills and sensitivity analysis of deep lacustrine facies in multi-segment rift basins: Insights from

3D forward modeling. *Sediment Geol.* doi: 10.1016/j.sedgeo.2020.105753

Zhang, X., Zhang, H., Chang, F., Ashraf, U., Peng, W., Wu, H., Liu, Q., Liu, F., Zhang, Y. and Duan, L. (2020b) Application of corrected methods for high-resolution xrf core scanning elements in lake sediments. *Appl. Sci.* 10:1–17.

Chapter 6 - Mineralogical Assemblages and Hydrochemical Modelling of Laguna Salada de Chiprana, Northeast Spain

Connor Doyle^a, Fernando Gázquez^b, Stefan Schröder^a, Blas Valero Garces^c, Ana Moreno^c, Juan Pablo Corella Aznar^d,

a - Department of Earth and Environmental Sciences, University of Manchester, Manchester, UK

b - Water Resources and Environmental Geology Research Group, Department of Biology and Geology. University of Almería, Almería, Spain/Andalusian Centre for the Monitoring and Assessment of Global Change (CAESCG), University of Almería, Spain

c - Instituto Pirenaico de Ecología, Consejo Superior de Investigaciones Científicas, Zaragoza, Spain

d - CIEMAT - Environmental Department (DMA), Avenida Complutense 40, E-28040 Madrid, Spain

connor.doyle@postgrad.manchester.ac.uk

Abstract

Lake Chiprana, a hypersaline lake situated in the Ebro Basin of Spain, contains a complex sedimentological and geochemical sequence representing the evolution of a saline-hypersaline lacustrine environment throughout the Late Holocene. Saline lakes such as Lake Chiprana are important from both industrial and scientific perspectives, and can offer significant information in the advancement of our understanding of mineralogical and hydrochemical processes. Many saline lakes are often able to record minute environmental and anthropogenic perturbations within their limnological and mineralogical characteristics. This study describes such characteristics using X-ray diffraction (XRD) of sediment cores retrieved from the site. Increasing abundances of quartz, detrital carbonate and various phyllosilicate and clay minerals suggest increasing detrital input derived from marl and sandstone lithologies within the local catchment. Changing abundances of gypsum, halite, hexahydrate and thenardite alongside authigenic aragonite and calcite indicate variations in lake water level and the intensity of evaporation. Furthermore, hydrochemical modelling of the lake waters coupled with isotopes of gypsum hydration water both illustrate the hypothetical mineral precipitation sequence of the Lake associated with increasing evaporation, and adds further insights into the potential hydrological evolution of Lake Chiprana throughout the last three to four centuries. The model illustrates initial precipitation of calcite and gypsum, followed by later halite, thenardite and hexahydrate with increasing evaporation. Secondly, $\delta^{18}\text{O}$ and δD isotopes illustrate reduced values at a depth of 300-350mm in CHI19-1A, reflecting increased detrital input to the lake, and likely higher lake levels and inflow. The coupling of detailed mineralogical analyses with a simple hydrochemical model and novel application of gypsum hydration water isotopes lend insights into the complex sequence represented in the sedimentary archives of Lake Chiprana, and allow for potential decoupling of anthropogenic and climatic signals preserved within the lacustrine record throughout the last three to four centuries.

6.1 - Introduction

In the Iberian Peninsula, hundreds of studies have constructed detailed palaeoenvironmental models of Quaternary environmental variability and anthropogenic influences using the sedimentary sequences of lacustrine systems (Comin & Alonso, 1988; Alonso, 1998; Martín-Puertas *et al.*, 2008; Morellón *et al.*, 2009; Valero-Garcés *et al.*, 2014; Schröder *et al.*, 2018). Karstic lacustrine settings have for example established a strong basis for understanding the succession of climatic, environmental and anthropogenic factors that have occurred throughout many regions of Spain (Morellón *et al.*, 2011; Valero-Garcés *et al.*, 2014; Camacho *et al.*, 2017). Nonetheless, there is still much to be learned when considering the impacts of climate and anthropogenic activities upon saline lacustrine systems, as many such systems are highly sensitive to extrinsic perturbations and can act as high-resolution archives of palaeoenvironmental information. Several saline lacustrine systems located throughout the Iberian peninsula have in fact more recently been identified as a viable source of environmental information, as well as many others around the globe (Garber *et al.*, 1987; Alcocer & Hammer, 1998; Alonso, 1998; Schröder *et al.*, 2018; Baxter & Butler, 2020).

The sediments and minerals of many lacustrine settings are influenced by both environmental and anthropogenic processes (Valero-Garcés *et al.*, 2014; McHenry *et al.*, 2020; Seguin *et al.*, 2020). Increases in precipitation (López-Blanco & Romero-Viana, 2019), catchment run-off and excess water from agricultural activities (Morellón *et al.*, 2018) and changing climatic conditions (Valero-Garcés *et al.*, 2000; Valero-Garcés & Moreno, 2011) may increase the abundance of quartz, feldspars, clays and other detrital material delivered to the system (Ontiveros-Cuadras *et al.*, 2018). In contrast, increased evaporation or the use of lakewaters for agriculture may contribute to lake drawdown (Martín-Puertas *et al.*, 2011), which in turn leads to the increased precipitation of endogenic minerals (Martín-Puertas *et al.*, 2008). Thus, variations in mineral assemblages within these unique settings can potentially

act as high-resolution repositories of information concerning climatic and environmental shifts (Last, 2013; Schröder *et al.*, 2018).

In this study, spatio-temporal variations in mineral assemblages as well as the isotopic composition of structurally-bound hydration water of gypsum ($\text{CaSO}_4 \cdot 2\text{H}_2\text{O}$), also known as gypsum hydration water (GHW) (Gázquez *et al.*, 2018) throughout the sediments of Laguna Salada de Chiprana within the Ebro Basin of Northeast Spain were investigated, to be composited with previous studies focusing upon the sedimentology (Doyle *et al.*, 2022b) and geochemistry (Doyle *et al.*, 2022a) of the lake. The study further considers the effects of hydrochemistry upon these assemblages by utilising hydrochemical modelling of lake water geochemistry. By interpreting variations in mineral content and hydrochemistry, this study aims to further contribute to the understanding of palaeohydrological and mineralogical changes occurring in Lake Chiprana throughout the last 3-4 centuries, and to improve the understanding of how different environmental processes and potentially anthropogenic activities can be reflected by changing mineralogical assemblages and the isotopic composition of gypsum hydration water. This study also aimed to characterize and better understand the present-day physicochemical characteristics and evaporation-driven mineralogical precipitation sequence of Lake Chiprana by incorporating hydrochemical modelling and an evaporation model using the PhreeqC software package. These observations and the output of the hydrochemical evaporation model will permit increased understanding of modern limnological and geochemical processes occurring at the site which may be extrapolated to the sedimentary sequence, allow for a further appreciation of the mineralogical precipitation sequence, and also allow for the anticipation of the potential future evolution of the lake, a Ramsar-designated site, in response to both anthropogenic and climatic factors.

6.2 - Study Area

Laguna Salada de Chiprana (41°14'30"N, 0°10'50"W) is a hypersaline lake located in the semi-arid Ebro Basin of Northeast Spain, approximately 12km from the nearby town of Caspe, and approximately 5km from the Ebro River and nearby village of Chiprana. The region of Northeast Spain where Lake Chiprana is situated is governed by a Mediterranean climate typified by low rainfall and high temperatures (average 24.4°C, maximum 34°C in July, (Domínguez-Castro *et al.*, 2010)) in the summer months and increased humidity and reduced temperatures (average 7°C, minimum 3°C in January (Domínguez-Castro *et al.*, 2010)) in the winter months.

The lake's salinity and geochemical characteristics are maintained by a closed hydrological system governed by high rates of evaporation (1000-1500mmyr⁻¹) and groundwater outflow (1000mmyr⁻¹) as the main outputs, and rainfall (~400mmyr⁻¹), groundwater input (~300 mmyr⁻¹) and flow from irrigation channels (~600mmyr⁻¹), irrigation returns (~1300mmyr⁻¹) and a nearby inlet channel connecting Lake Chiprana to a freshwater reservoir named Laguna de Las Rocas (Vidondo *et al.*, 1993; De Wit *et al.*, 2013; Jódar *et al.*, 2020) as the main inputs. The surface area of Lake Chiprana also varies between approximately 0.15-0.2km², and the maximum depth of the lake has been shown to vary to around 4-5m (De Wit, 2016). The lake is primarily meromictic, being defined by a strong thermocline and halocline (Diaz *et al.*, 1998), and there are significant chemical gradients from the surficial waters to the profundal parts of the lake basin (Guerrero *et al.*, 1991; Vidondo *et al.*, 1993; De Wit, 2016). The waters are defined as saline to hypersaline, being characterised by an abundance of Na⁺, Mg²⁺, Cl⁻ and SO₄²⁻ ions, and with salinity values varying around 40—80g L⁻¹ (Vidondo *et al.*, 1993; Jódar *et al.*, 2020).

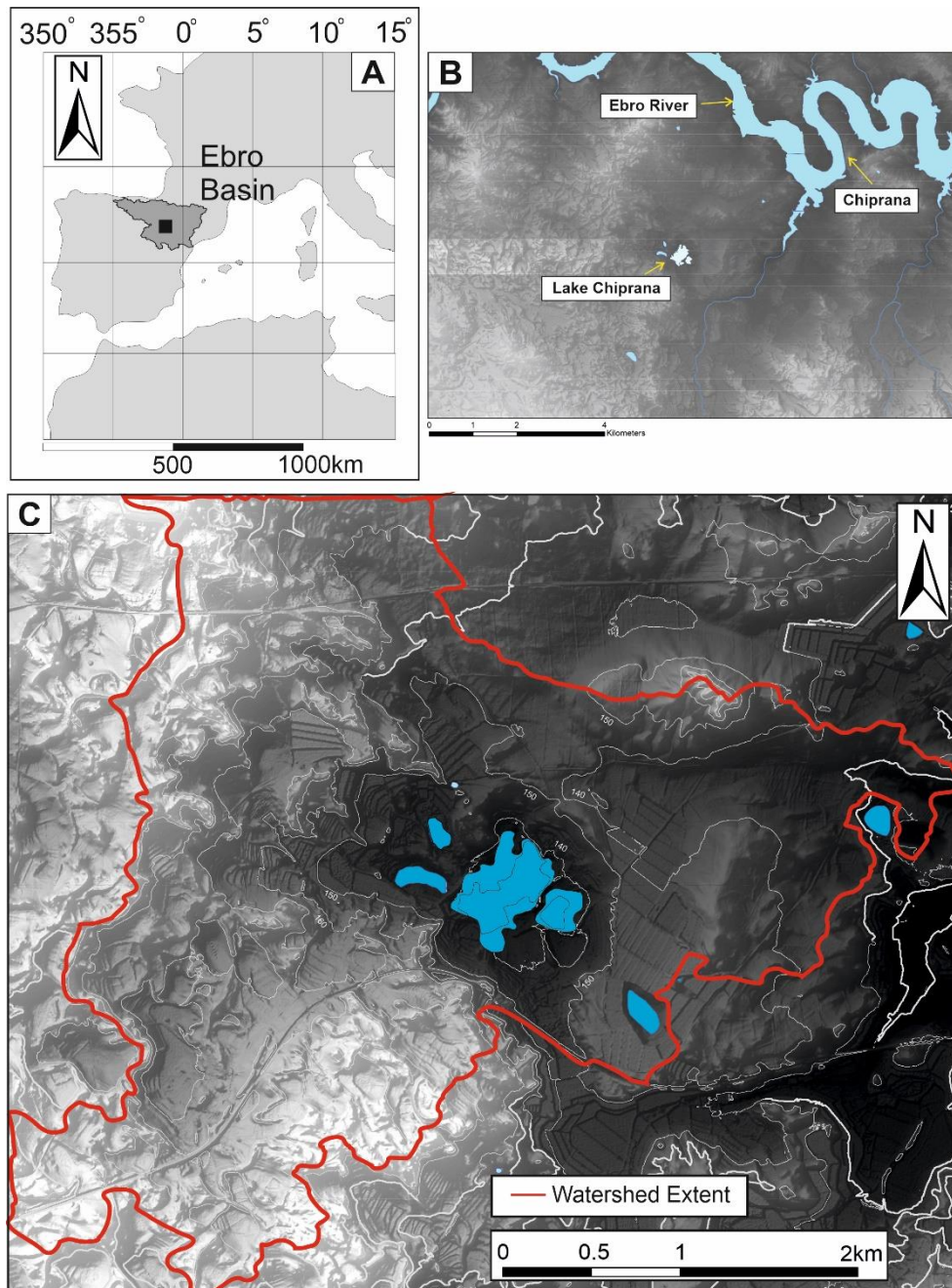


Figure 6.1 - Maps illustrating the location of Laguna Salada de Chiprana. A) Overview of Western Europe and the location of the Ebro Basin, with the locality of Chiprana marked by the black box. B) Digital elevation model highlighting the region surrounding Lake Chiprana, with the nearby Ebro River and town of Chiprana highlighted. C) Digital elevation model of the local watershed of Lake Chiprana, with the extent of this watershed marked and the nearby waterbodies marked. Data modelled from CNIG. Partially adapted from Doyle *et al.* (2022).

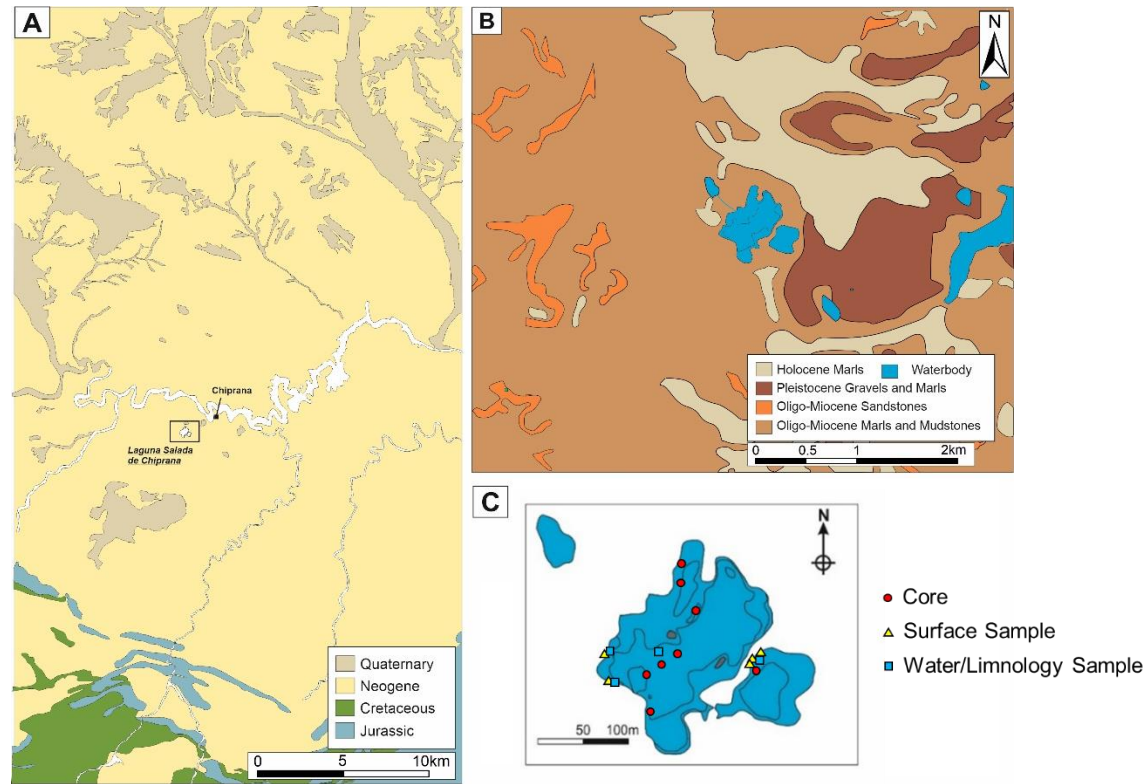


Figure 6.2 – Geological setting of Lake Chiprana and the location of the cores and waters sampled for this study. A) Overview of the primary geological formations associated with the Caspe region of the Ebro Basin, highlighting Quaternary to Jurassic formations. B) Local geological map (also produced in Doyle *et al.* (2022)) illustrating the detailed geology of the area surrounding Lake Chiprana. C) Map of Lake Chiprana with the location of cores and water samples collected for this study. Geological data from IGME (2003), bathymetrical data provided by IPE.

The geological setting of Lake Chiprana is represented by a combination of Oligo-Miocene marls, claystones and other mudstones interbedded with muddy limestones and gypsum formations (IGME, 2003; De Wit *et al.*, 2013) which form flat-topped eroding terrace features (Valero-Garcés *et al.*, 2000a). These mudstones and marls are however cross-cut by Oligocene age sandstone ribbons formed by fluvial palaeochannels (Luzón, 2005), with the ribbons forming distinctive elongated topographical ridges up to 1-2m high throughout the lake and the area surrounding it. Where they outcrop, they cause segmentation of the lake into several smaller sub-basins that are often partially to fully separated from the primary waterbody during extreme periods of lake drawdown (Valero-Garcés *et al.*, 2000a). In some cases, they have been termed an “inverted topography” due to the distinctive topographical features that they produce (De Wit *et al.*, 2013).

6.3 - Material & Methods

6.3.1 – Sampling and Limnological Measurements

Modern samples of sediment and associated microbial mats were taken from Lake Chiprana during field visits in November 2019 and December 2021. Samples were transported in sterile universal 30ml tubes and initially stored at 4°C before being freeze-dried for later geochemical and petrographic analyses. Samples were also taken using a scalpel at 0.5cm intervals from Lake Chiprana cores 1A, 2A, 3A, 4A, 5A, 6A and 7A. At this 0.5cm interval, 105 samples were collected from core 1A (0-500mm), 97 from core 2A (0-485mm), 85 from core 3A (0-410mm), 68 from core 4A (0-330mm), 68 from core 5A (0-300mm), 80 from core 6A (0-400mm), and 67 from core 7A (0-333mm) Several samples from core 7A were not included due to poor scan quality. In each core, samples selected for XRD were analysed at 1cm intervals, amounting to half of these sample numbers previously given for a total of 277 samples. Samples were classified in a previous study (Doyle *et al.*, 2022b) according to the dominant sedimentary facies they were taken from, with facies being determined by microscopic analyses of smear slides, observations of grain size

changes, colour and sedimentary structures (Schnurrenberger *et al.*, 2003; Morellón *et al.*, 2009).

Lake Chiprana displays variable geochemical and limnological characteristics throughout the different sub-domains of the lake, the water column, and also on a temporal basis. Several field trips were conducted to the site over the course of 2018-2021, with visits in October 2018, March 2019, November 2019, and November 2021. The limnological parameters of the lake are summarised in Tables 6.1-6.2 and Figure 6.3. Strong chemical gradients associated with the water column were discovered in the December 2021 survey and are highlighted in Figure 6.3. In the case of all variables, a significant shift is observed at a depth of approximately 2.5m, with temperature, TDS, salinity and conductivity increasing, while decreases occur in pH and dissolved oxygen. The chemical composition of the water as measured using titration and ion chromatography illustrated the key ionic constituents of the water was characterised by Mg^{2+} , SO_4^{2-} , Cl^- , and Na^+ ions, a characteristic type IV brine as defined by Hardie & Eugster (1970).

6.3.2 – Thin Section Analyses

Thin sections were generated by sampling both modern sediments from the contemporary lake-bed and by using rectangular plastic slabs to remove intervals of sediment from the cores collected for the study. Samples were stored at 4°C to prevent desiccation before being freeze-dried. Following complete drying, samples were resin impregnated (Epo-Flo resin and hardener) and the resin allowed to cure over the course of 1-2 days under ultraviolet light in order to solidify the sample such that thin sections could be generated. Sections were analysed using a Nikon Eclipse LV100NPOL with CoolLED UV source microscope for initial characterisation, and were subsequently carbon coated using a Cressington 208 carbon coater for scanning electron microscope analyses. Samples were analysed using both a Hitachi TM3000 SEM and a FEI QUANTA 650 operating at high vacuum at 15kV. The SEM instruments were equipped with Bruker Instruments Quantax 70 and

Bruker Xflash energy dispersive X-ray spectrometers respectively, and these instruments were used in generating EDS-maps of mineralogical phases distributed throughout the samples.

6.3.3 - X-Ray Diffraction

Bulk mineralogy was evaluated by the method of X-ray diffraction using a Bruker D8 Advance diffractometer (Bruker Corporation, Billerica, Massachusetts, United States) equipped with a Göbel Mirror and Lynxeye detector (Department of Earth and Environmental Sciences, University of Manchester) following standard procedure as provided by Dr. John Waters. The X-ray tube had a copper source, providing CuK α 1 X-rays with a wavelength of 1.54 06Å. Samples taken from core cuts were freeze-dried in plastic zip lock bags for several days prior to analysis. Dry sample material (0.1g) was ground and mixed with ~1 ml of amyl acetate. The resultant sediment slurries were transferred to glass microscope slides and air dried. Samples were scanned from 5-70°2 θ , with a step size of 0.02° and a count time of 0.2s per step. XRD diffractograms were evaluated using Bruker DIFFRAC.EVA version 5. Diffractograms were initially smoothed to minimise potential noise and background readings were subtracted. Mineralogical phases were identified using standards provided by the International Centre for Diffraction Data Powder Diffraction Files (ICDD PDF) database. Qualitative relative abundances of different mineral phases were estimated by comparing peak heights, and absolute estimates of abundance were undertaken using the TOPAS software. Error margins typically ranged from 0.1-2% according to wt% volume of each phase.

6.3.4 - $\delta^{18}\text{O}$ and δD of Gypsum Hydration Water

Methods presented here are following the standard operating procedure presented by Gázquez et al. (2022), and were undertaken at the University of Almeria. 1 gram of powdered sediment was ground initially and separated using a 0.45mm sieve and distilled water to remove the clay fraction from the samples. The remaining sample powder was dried overnight in an oven at 40°C, subsequently being ground down

and reheated again overnight at 40°C to remove adsorbed water. The isotopic analyses were undertaken using a Heat Induction Module (IM-CRDS, Picarro©) coupled to a Cavity Ring-Down Spectrometer (CRDS, Picarro© L2140i) at the University of Almeria. Powdered samples were heated to a final temperature of 250°C within the IM-CRDS, and the resultant water vapor was transferred to the CRDS analyser. This allowed for the measurement of $\delta^{18}\text{O}$ and $\delta^2\text{H}$ within the water vapor. Results are standardised to the Vienna Standard Mean Ocean Water (V-SMOW), Standard Light Antarctic Precipitation (SLAP) and Greenland Ice Sheet Precipitation (GISP). Standardisation was achieved by analysing four gypsum standards prior to analysis of the samples, and these standards were calibrated against liquid water using the cryogenic extraction method defined by Gázquez et al. (2015). To account for instrument drift and repeatability, each sample was analysed 3–4 times consecutively. The mean analytical precision of the 3–4 repetitions was 0.2‰ for $\delta^{18}\text{O}$ and 1‰ for $\delta^2\text{H}$. The drift of the CRDS instrument was monitored by measuring one of the gypsum standards for every 10–12 samples (Gázquez et al., 2015).

6.3.5 – Hydrochemistry and Modelling with PhreeqC

6.3.5.1 - Geochemical and Hydrochemical Measurements

Hydrochemical modelling was undertaken on water samples obtained and analysed from the surface and bottom of the primary basin of Lake Chiprana. Samples were collected in sterile 1L bottles and transported to the Instituto Pirenaico de Ecología, and were kept in a refrigerator at 4°C. Analyses for major anions and cations were undertaken at the Laboratorio de Aguas Instituto Pirenaico de Ecología according to standard operating procedures described here. Concentrations of major and trace ions within the lakewaters were measured using ion chromatography and alkalinity titration. Analyses for major anions and cations were undertaken at the Instituto Pirenaico de Ecología, and are defined here according to their standard operating procedure and as defined by Lambán et al. (2015). Samples were stored at 4°C in a dark cold-room and analysed within a week of being stored. The samples were first

filtered through GF/F Whatman filters to remove particulate material, and were subsequently aliquoted into 4 x 12ml plastic tubes, each washed prior with 10% HCl. Eluents for cations and anions were comprised of 4.0 mmol/l tartaric acid + 0.75 mmol/l dipicolinic acid, and 3.2 mmol/l sodium carbonate + 1mmol/l sodium bicarbonate, respectively. Analysis of both cation and anion concentrations were undertaken using Chemical Suppressed Ion Chromatography (APHA, 2018a) within a Metrohm 861 Advanced Compact IC. In the case of cations, analyses were undertaken in a Metrosep A Sup 2 polystyrene- divinylbenzene polymer column, while analyses were undertaken using a Metrosep C 2-250 silica gel with carboxyl groups column.

In addition, samples were also analysed for alkalinity as defined by IPE standard operating procedures. 100 mL of the sample was initially measured in a beaker, followed by adding 3 drops of phenolphthalein and stirring. This solution was then titrated in a Metrohm 798 MPT Titrino using Potentiometric Titration (APHA, 2018b), with 0.02N of sulfuric acid being added until the colour of the solution disappeared. Following this, 3 drops of mixed indicator were added to the sample. The sample was then titrated again with sulphuric acid until a pink tint was visible. The volume of acid remaining was then used for the calculation of total alkalinity.

6.3.5.2 - Modelling of evaporation and mineral precipitation

The geochemical characteristics of the lake waters were also inputted to the PHREEQC Interactive Software Package (Parkhurst, 1995). This software undertakes geochemical calculations for the hydrochemical modelling of aqueous solutions. In this study, geochemical modelling of evaporative concentration and mineralogical saturation indices was undertaken using code supplied by the provided software manual (Parkhurst & Appelo, 2013) and from the PhreeqC forums (<https://phreeqcusers.org/index.php>). This allowed for insights into the effect evaporation had upon the saturation and subsequently precipitation and/or dissolution of different mineralogical phases. The application of these modelling

methods was hypothesised to provide further insights into the hydrodynamics of Lake Chiprana, particularly for investigating the mineralogical precipitation sequence and potentially allowing for the anticipation of the future evolution of the lake in response to both anthropogenic and climatic factors.

Modelling of the effects of evaporation on the concentration and saturation indices of specific elements and phases was undertaken using the geochemical and limnological analyses of lake water. Evaporation was modelled at a constant temperature of 25°C following guidelines from Parkhurst & Appelo (2013), and in the case of this study, the progression of increasing evaporation was measured within the limits of the PHREEQC software package (Parkhurst, 1995). Evaporation was undertaken by removing a set amount of moles of H₂O in the program in defined steps, and several mineral phases identified from X-Ray diffraction were assumed to be in equilibrium with the solution within the code. For the evaporation sequence, it is assumed that there are approximately 55.55 moles of H₂O in one litre of water, and thus this value was used as a guideline for the percentage of moles removed in each evaporation step. Analytes and variables used in the initial solution reactions included anions Cl⁻, Br⁻, SO₄²⁻ and cations Na⁺, K⁺, Ca²⁺, Mg²⁺ in addition to alkalinity and pH.

6.4 – Results

6.4.1 - Key Mineral Phases and Deposits

In the modern lakebed, deposits include microbial mats consisting of *Coleofasciculus (Microcoleus) chthonoplastes* (Jonkers *et al.*, 2003), evaporitic crusts comprised of gypsum, halite, hexahydrite and minor amounts of epsomite and bloedite, silty-sandy lenses and wedges of detrital material, and cemented and mineral-coated vegetation such as foxtail stonewort (*Lamprothamnium papulosum*), *Phragmites australis*, and *Salicornia* spp. (Vidondo *et al.*, 1993; De Wit *et al.*, 2013) that occur within littoral platforms, ramps, and the profundal areas of the lake (Doyle *et al.*, 2022b). The

extent and character of such deposits varied between field visits, with a significant portion of the microbial mat communities and mineral-coated vegetation being exposed during the October 2019, March 2019 and November 2019 visits. In December 2021, lake levels had risen by approximately 0.5m, leading to submersion of many of the evaporitic crusts and microbial mat communities. In all cases, mineral crusts persisted during both low and high lake levels, but microbial mats had more stratiform morphologies at high water levels and more pinnacled morphologies at low water levels.

Figures 6.5a-b, 6.6a-g and 6.7a-d illustrate, respectively, photomicrographs of key minerals associated with the Lake Chiprana sequence, from each unit and the approximate percentages of minerals throughout each core. The major minerals are silicates (clays and quartz [SiO₂]), calcium sulphates (gypsum [CaSO₄·2H₂O]) and (hexahydrate [MgSO₄·6H₂O], thenardite [Na₂SO₄]), carbonates (calcite [CaCO₃], aragonite [CaCO₃]) and halides (halite [NaCl]). Other minerals which are not included in the bathymetrical cross-sections due to their low abundance or sporadic occurrence throughout the sequence include epsomite [MgSO₄·7H₂O], bloedite [Na₂Mg(SO₄)₂·4H₂O] and anhydrite [CaSO₄]. Aragonite occurs throughout the sediments as small (50-100µm) blades and needles. Calcite is also found as small (10-25µm) precipitates within microbial laminae, and is also strongly associated with charophyte oogonium which are often strongly calcite-cemented.

Clays and other silicates are distributed throughout the sediments, with some silty and sandy laminae displaying high abundances of these phases. Quartz typically occurs as very fine grains (<50µm), whereas phyllosilicates, typically muscovite, occurs as small grains throughout the matrices of the sediments. In contrast, gypsum occurs both as distinctive, prismatic euhedral crystals of variable size (100-1000µm) (Figure 6.4a) subset within the samples and within laminae of variable thickness (typically 0.2-10mm), and a lack of rounded edges upon the gypsum crystals suggests they are not reworked.

Table 6.1 – Limnological characteristics of Laguna Salada de Chiprana measured using a YSI Exo1 multiparameter multiprobe at different sites at the lake surface during November 2019 and November 2021. These data are used in the hydrochemical model. DO: Dissolved oxygen, TDS: Total dissolved solids.

Site	Depth	Temperature	DO	Conductivity	TDS	pH	Salinity
	m	°C	mg/L	Us/cm	mg/L		PSU
November 2019							
Chiprana - Southern Main Lagoon	0.5	11.42	8.65	46013	40388	9.22	41.61
Chiprana - Western Main Lagoon	0.2	12.12	8.30	47317	40796	10.05	42.13
Chiprana - Side Lagoon	0.3	12.09	8.55	47566	41035	9.68	42.41
December 2021							
Chiprana - Main Lagoon - Surface	0	8.85	7.86	39767	37378	9.60	37.93
Chiprana - Main Lagoon - 2m	2	8.79	7.38	39583	37260	10.10	37.79
Chiprana - Main Lagoon – 3.4m	3.4	23.13	4.43	104856	70670	6.03	80.33

Table 6.2 – Geochemical characteristics and major cations and anions of water samples collected from Lake Chiprana between December 2021 and May 2022.

Site	Depth	TDS	pH	Total Alk.	F	Cl-	Br-	SO42-	Na+	NH4+	K+	Ca2+	Mg2+
	m	ppm		ppm	ppm	ppm	ppm	ppm	ppm	ppm	ppm	ppm	ppm
Lake Chiprana - Surface Water	0.1	37378.000	9.600	572.860	21.224	8231.781	36.959	25679.449	9618.669	2.653	192.057	585.604	8233.564
Lake Chiprana - Profundal Water	3.4	70670.600	3.230	457.000	20.499	5755.479	27.058	18778.617	5316.303	1.951	99.902	13.750	4670.639

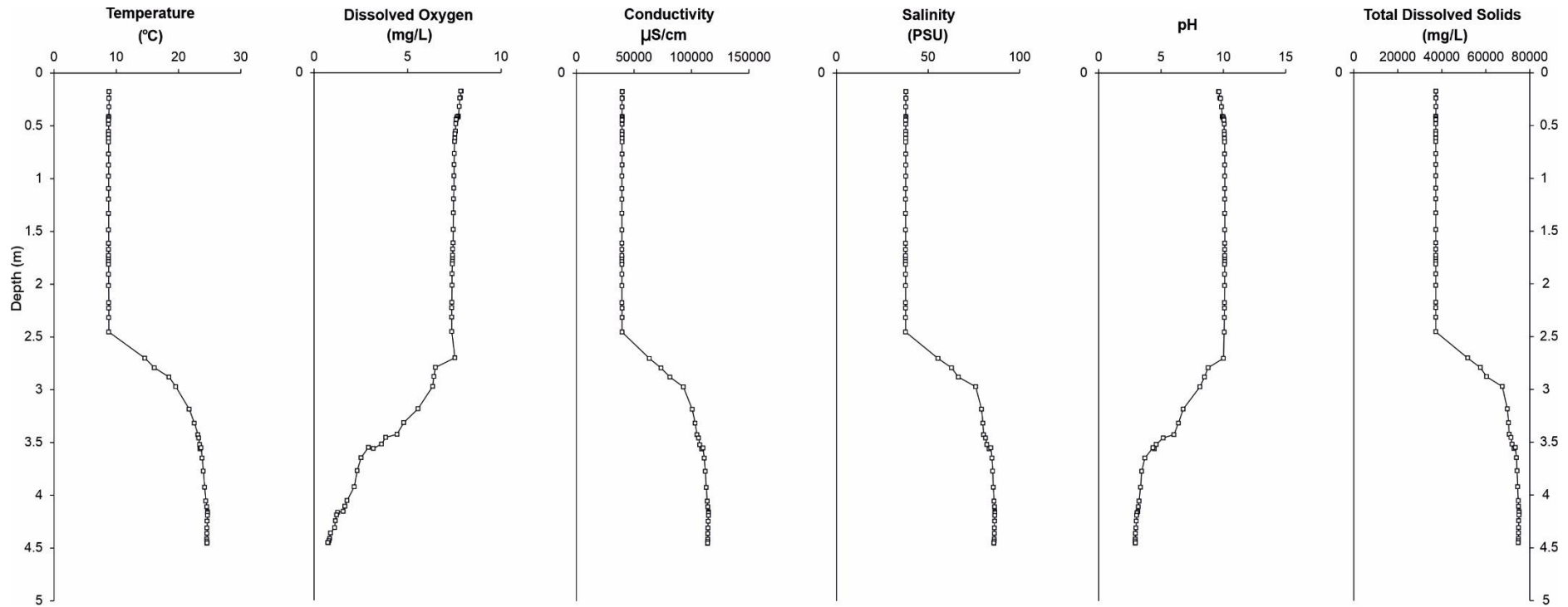


Figure 6.3 – Depth-based limnological characteristics of Lake Chiprana obtained by lowering a YSI Exo1 multiparameter multiprobe from a pneumatic boat into the lake waters. A clear gradient can be observed in the profiles occurring at approximately 2.5m, with visible shifts in all variables representing the stratification of the water column at this depth

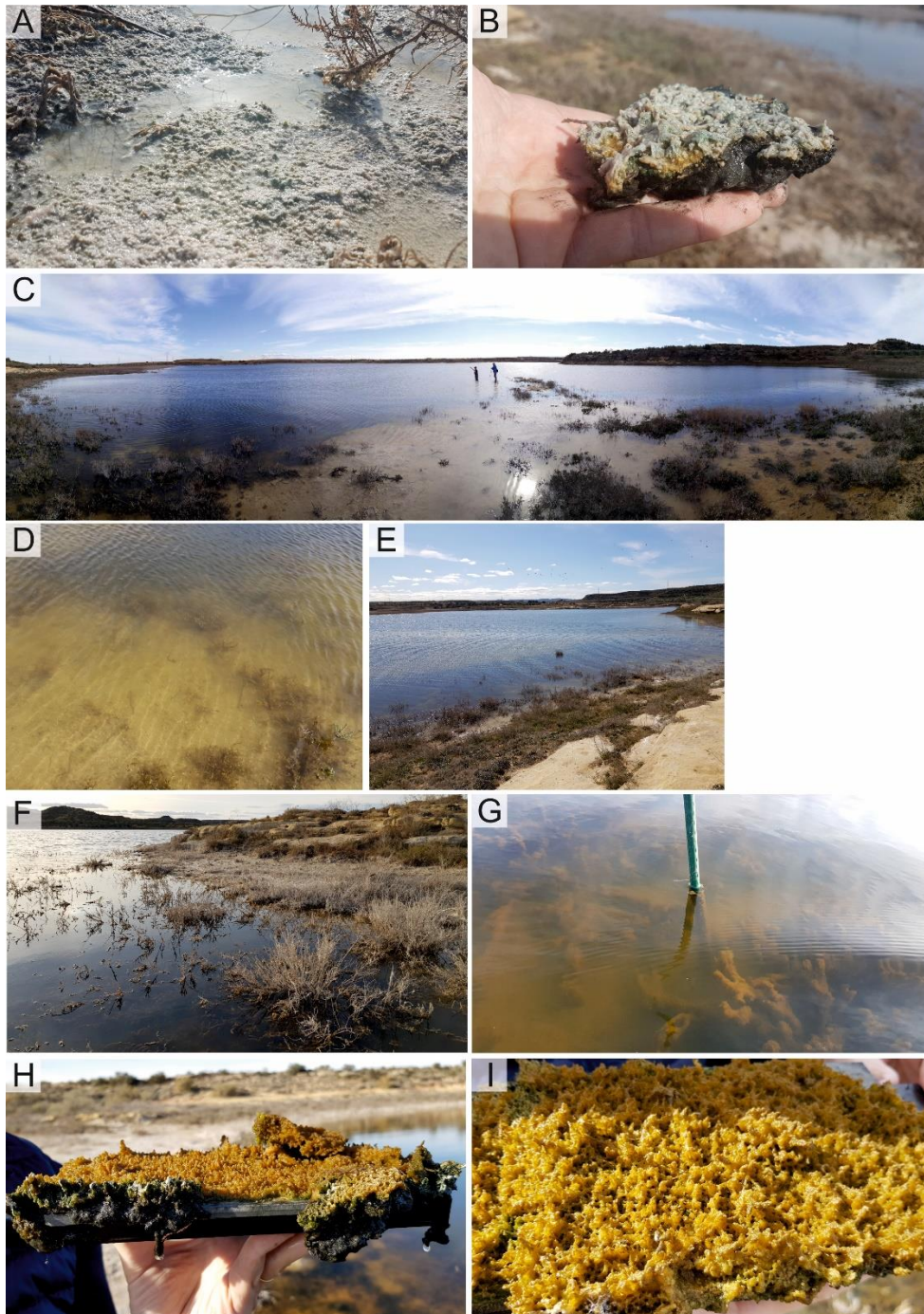
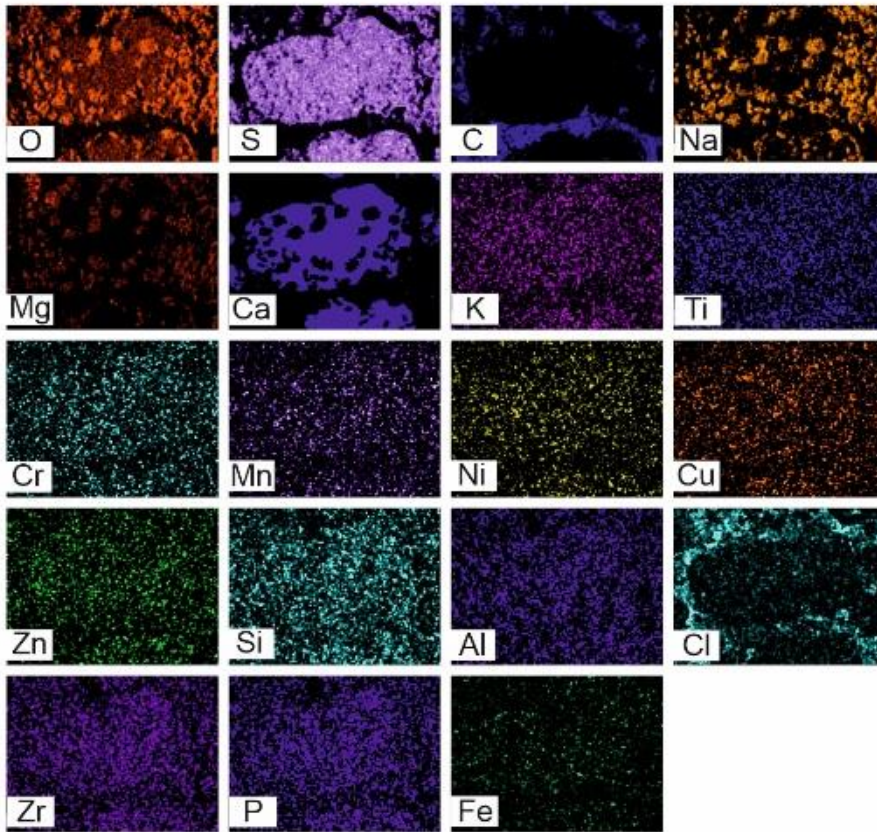
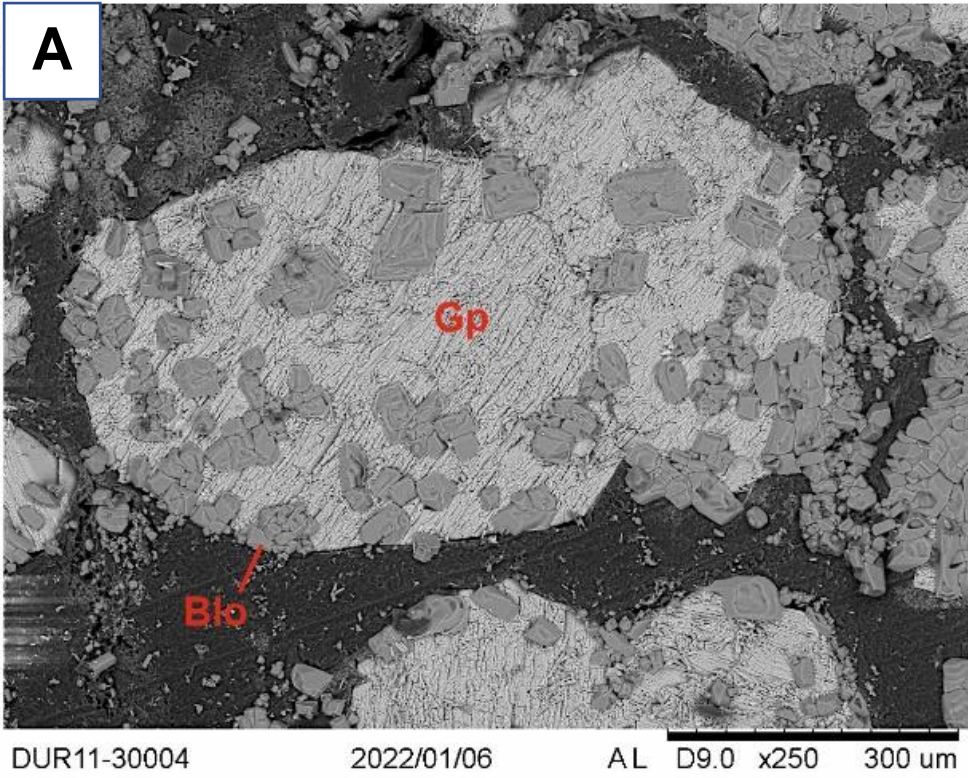
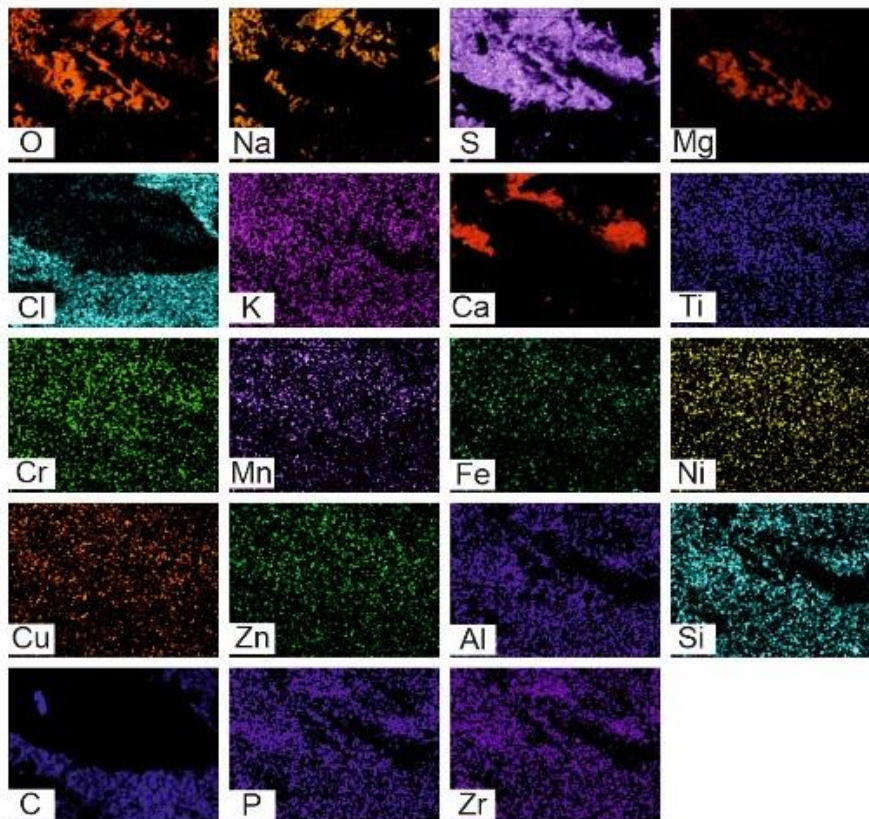
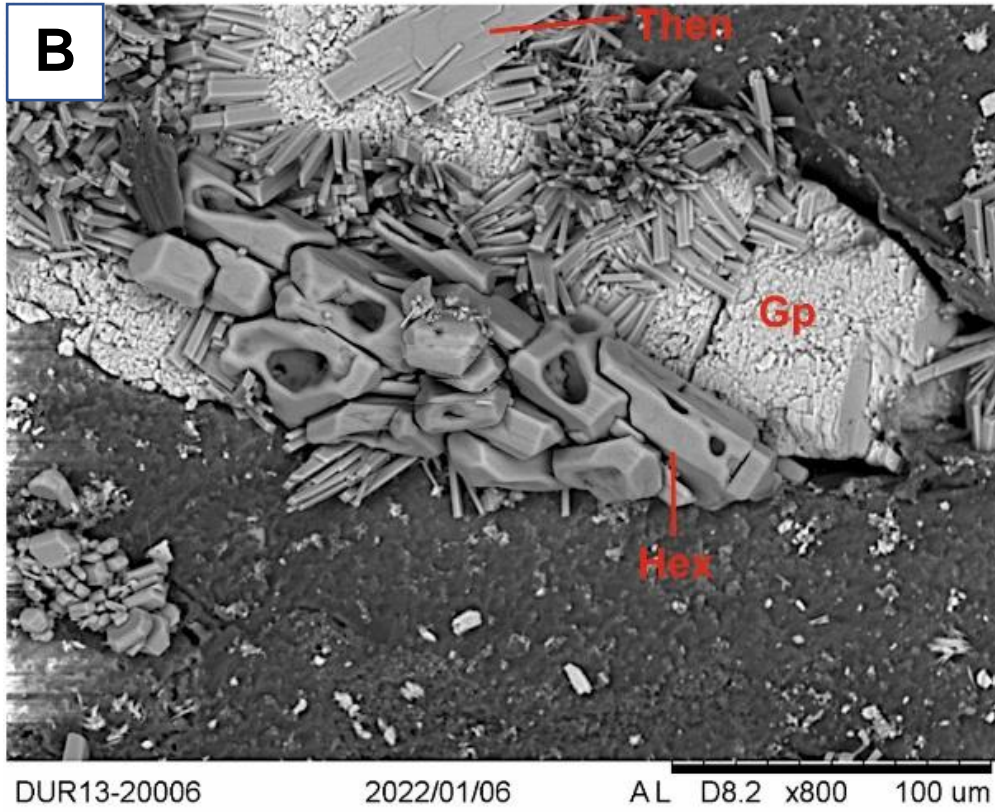


Figure 6.4 – Photographs illustrating the characteristics of Lake Chiprana during several field visits between 2018-2021. A) Mineral crust in October 2018 composed of mixed gypsum, halite, hexahydrite and minor phases such as thenardite, bloedite and epsomite with surrounding vegetation, B) Cross-section of a microbial mat structure developing in the lake in October 2018, C) Panoramic view of the lake and an underlying sandstone ribbon taken in March 2019 during low lake levels, D) Overview of the mineral crust in March 2019, E) Overview of the vegetated shorelines and sandstone palaeochannel bodies segmenting the lake in March 2019,

F) Overview of vegetative communities and exposed mineral crusts and microbial mats in November 2019, G) Photograph from November 2019 exhibiting the mixed mineralogy evaporitic crust nucleating on vegetation submerged below the water surface and mineralisation upon a measurement pole emplaced within the lake in March 2019, H) Photograph of microbial mats grown on a Solnhofen limestone plate with an extensive overlying mixed gypsum and halite crust, I) Photograph of the pinnacled and interconnected mineral crust atop the microbial mat structures.





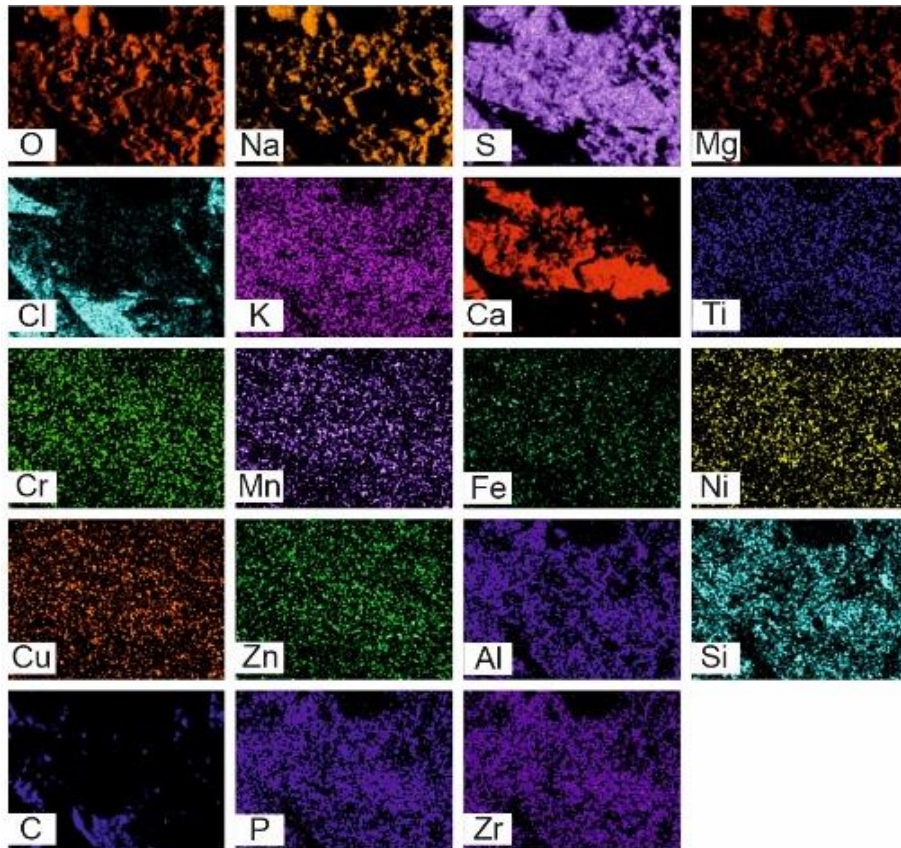
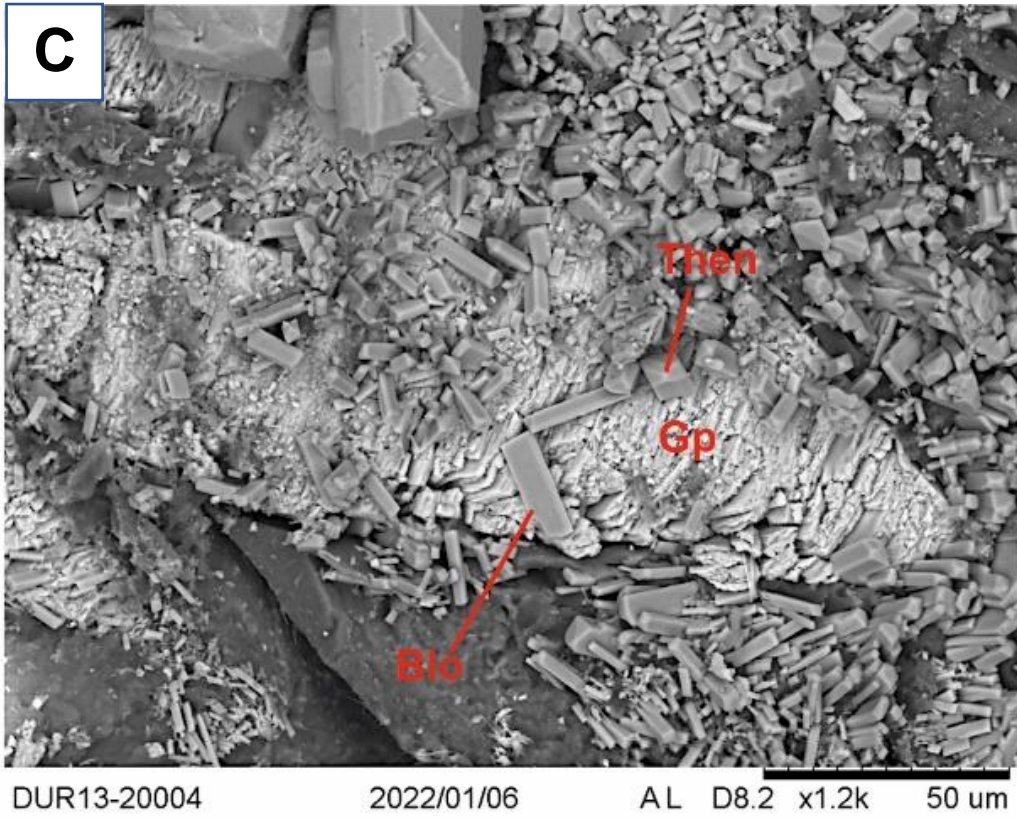


Figure 6.5 – SEM photomicrographs and SEM-EDX spectral maps illustrating the characteristics of key minerals associated with the sedimentary sequence of Lake Chiprana. A) Euhedral gypsum with nucleations of bloedite on the upper surface of the crystal. B) Examples of blocky, partly dissolved hexahydrite with adjacent thenardite and euhedral gypsum. C) Euhedral gypsum with overgrowths of tabular bloedite and prismatic thenardite, Hex: Hexahydrite, Hal: Halite. Gp: Gypsum, Blo: Bloedite. Increasing intensity of colour = greater intensity of the element.

Hexahydrate is commonly found occurring as a tabular to blocky phase within the sediments, often displaying some small dissolution features (Figure 6.5b). In some cases, hexahydrate also nucleates upon the surfaces of gypsum crystals. Halite is found occurring as distinctive white blocky masses that are often replaced by minor phases such as bloedite and thenardite. Thenardite, where present, occurs as elongated to blocky prisms with sizes varying around 10-30µm. Bloedite occurs as approximately 50-100µm blocky to bladed crystals that often nucleate on the surface of euhedral gypsum or within the existing structures of previously precipitated halite crystals (Figure 6.4b).

6.4.2 - Spatio-Temporal Mineralogy

6.4.2.1 - Unit 6 (Profundal Cores only)

Unit 6 (39.2-50cm depth) is a predominantly detrital sequence (Doyle *et al.*, 2022b) present only in cores 1A, 2A, 3A and 6A. The unit contains heterolithic siltstones and sandstones that display grain size variations between very fine to medium sand alongside interfingers of organic-rich mudstones and gypsum lenses. XRD results indicate that in core 1A, aragonite decreases from approximately 25-30% at the base of the unit to ~5% at the top. It is absent in the lower half of unit 6 within core 2A, and displays a decreasing trend from ~25% to 10% in the upper section of the unit. Cores 3A and 6A display much lower abundances with a small upwards increasing trend (<1% to 12%) in core 3A and a decreasing trend in core 6A. In cores 1A, 2A and 3A, calcite displays high abundances throughout unit 6 (~25-50%) with the exception of a calcite-poor interval between 410-450mm in core 1A (<10%) and a decreasing trend in cores 2A and 3A (~40% → ~10%). Calcite is also generally less abundant throughout core 6A (<10%).

Quartz and phyllosilicates display abundances of 5-15% and 10-25% respectively, and are primarily characterised by decreasing trends from the base to the top of the unit. Gypsum is variable throughout unit 6, ranging between ~10% and 60%+. This high variability is pronounced within cores 1A, 2A and 3A, with gypsum typically

illustrating a moderate increasing trend from the base to the top of the unit and a large decrease in abundance in the centre of the unit. In contrast, gypsum remains high (~70%) throughout unit 6 in core 6A. Hexahydrate exhibits a moderate abundance throughout, typically maintaining values between 10-25%. Finally, halite and thenardite display low abundances (<2% to 10% and <1%-3% respectively), with halite exhibiting upwards increasing trends in core 2A, 3A and 6A and a upwards decreasing trend in core 1A. In contrast, thenardite illustrates several small peaks throughout each core (~3%).

6.4.2.2 - Unit 5 (Profundal Cores only)

Unit 5 (30.2-39.7cm depth) is composed of mixed composition mudstones which progress to heterolithic sandy siltstones, and grey-yellow sandy mudstones (Doyle *et al.*, 2022b). Aragonite is variable within cores 1A, 2A and 3A, typically fluctuating between <5 to 10%, but is abundant (15-20%) within core 6A. Calcite is abundant in cores 1A, 2A and 3A (20-50%) and generally displays a small upwards increasing trend, but is highly reduced in abundance in core 6A (<5%). Quartz illustrates higher abundances in cores 1A, 2A and 3A (5-10%) but is mostly absent within core 6A (<2%). Phyllosilicates typically vary between 5~25% in core 1A and 2A, but are significantly less abundant in cores 3A (<10%) and core 6A (<1%). Gypsum is highly variable in cores 1A, 2A and 3A, varying between ~10% and 70% in unit 5 and generally displays a moderate upwards increasing trend. However, it is consistently abundant throughout core 6A (~50%). Hexahydrate fluctuates between 10-15% in cores 1A and 2A, but between 10-25% in core 3A. Halite displays fluctuations between 4-6% in all cores and a peak of ~10% in the mid-section of core 1A, while thenardite is typically reduced to less than 2% in the same interval.

6.4.2.3 - Unit 4 (Profundal Cores only)

Unit 4 (19.8-30.2cm depth) consists of microbial mats with intergrown gypsum, gypsum laminae and thin beds and laminae of organic mudstones (Doyle *et al.*, 2022b). Aragonite generally displays a trend of increasing, albeit variable abundance

from the base of the unit to the top in all cores, but is generally more abundant in core 6A (~10-25%) than cores 1A, 2A and 3A (~5-10%). Calcite displays lower abundances in comparison to the underlying unit 5 throughout all cores and generally becomes less abundant from the base (~10-25%) to the top (~5-10%) of the unit. Quartz is typically a minor phase in all cores (~5%), whilst phyllosilicates are furthermore reduced in abundance, typically being no greater than 10% in abundance and displaying a small upwards decreasing trend. Gypsum remains abundant in cores 1A, 2A and 3A, typically between 30-70%, but displays a significant decrease in abundance in core 6A to approximately 5-20% throughout. Hexahydrate is again a common phase throughout this unit, maintaining abundances between 10-25%, and generally displays an upwards increasing trend from ~10% to ~25%. Halite increases in abundance in cores 1A and 2A from approximately 5 to 7%, whereas it displays an upwards decreasing trend from 7 to 5% in core 3A and from 15 to 5% in core 6A. Thenardite is generally very minor (<1%) in cores 1A, 2A and 3A, but displays small increases in abundance in core 6A (~3-4%).

6.4.2.4 - Unit 3 (All Cores)

Unit 3 is present in all cores and occurs as a massive unit of charophytic mudstone with a base defined by intercalated gypsum laminae and thin beds. Several intercalated beds of organic mudstones are also present throughout the unit. Mineralogically, aragonite generally decreases in abundance throughout the unit (~10% → <5%) in all cores but is marked by several moderate to high peaks (30-60%) in the lower section of unit 3 within the littoral cores. Calcite is typically low in abundance in all cores (~5-15%) and is typified by a small upwards decreasing trend. Quartz and phyllosilicates are either significantly reduced in abundance in all cores throughout unit 3, with abundances fluctuating between 1-5% for quartz and between 1-10% for phyllosilicates. Gypsum is abundant throughout unit 3 in all cores, with abundances between 50-80%, typically being higher in abundance in the littoral cores (60-80%) with the exception of a trough (10%) at the base of core 7A and the mid-section of core 4A (5%). Hexahydrate abundances vary between 15-25% in all

cores with the exception of core 5A, where abundances are reduced to between 5-10%. Halite displays decreasing abundances up-unit in the littoral cores from approximately 7-10% to 3-5%, and is stable between 5-10% in the profundal cores. Thenardite occurs in increased abundances (5-10%) within cores 1A, 3A and 6A, but is generally absent in all other cores (<2%).

6.4.2.5 - Unit 2 (All Cores)

Unit 2 occurs as two distinctive sedimentary sequences within the profundal and littoral settings of Lake Chiprana. Finely interbedded and interlaminated microbial mats are strongly intercalated with fine organic mudstones in the profundal cores, while cemented charophyte masses are present in the littoral cores (Doyle *et al.*, 2022b). Mineralogically, unit 2 is complex. Aragonite is typically low in abundance (<5%) within cores from the profundal setting, but is typified by increased abundances in the littoral cores (>10%) in addition to several moderate peaks in cores 4A and 5A (20-35%). Calcite on the other hand is lower in abundance throughout all cores (~5%) with the exception of 4A and 5A, where several peaks of up to 15-25% occur. Quartz and phyllosilicates are generally trace throughout the unit, with abundances no greater than 5% in both cases. Gypsum displays very high abundances in unit 2 in all cores, with values between 50-85% in all cores with the exception of two troughs in core 5A (~35%). Hexahydrite is lower within cores 7A, 1A and 2A, with average abundances of ~5-10% with the exception of a peak to ~40% in the lower section of core 1A. The phase remains around an average abundance of 25% in all other cores. Halite illustrates increased abundances within cores 1A and 6A (~10-12%), but is reduced in cores 2A and 3A (~5-7%) and typically trace within the littoral cores (<5%). Thenardite exhibits small increases in abundance in cores 1A (~5%) and 6A (~3%), but is generally absent in all other cores (<2%).

6.4.3.6 - Unit 1 (All Cores)

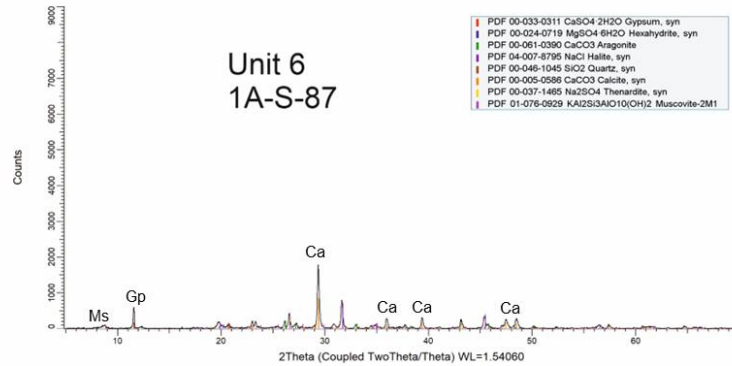
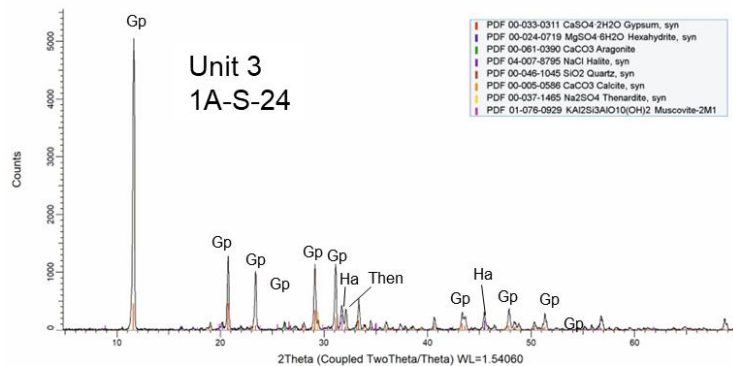
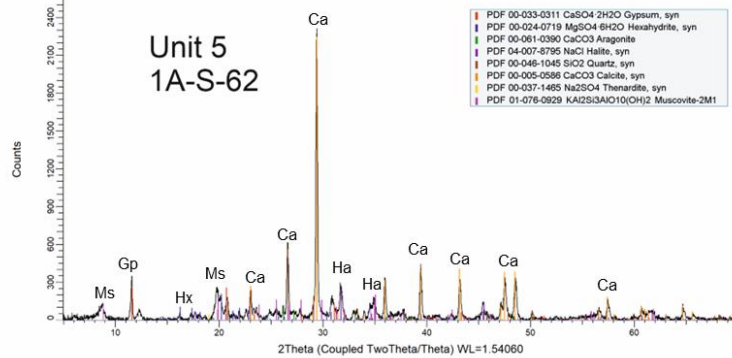
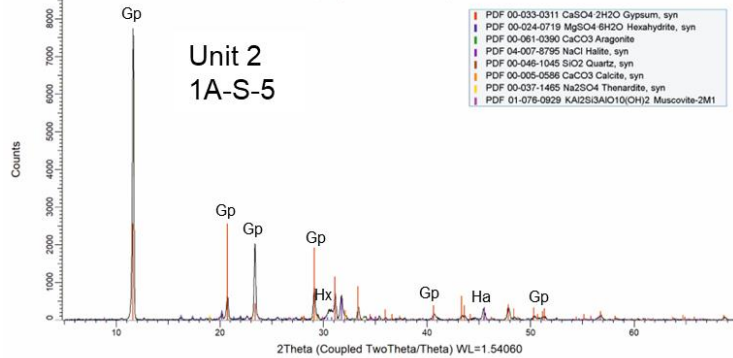
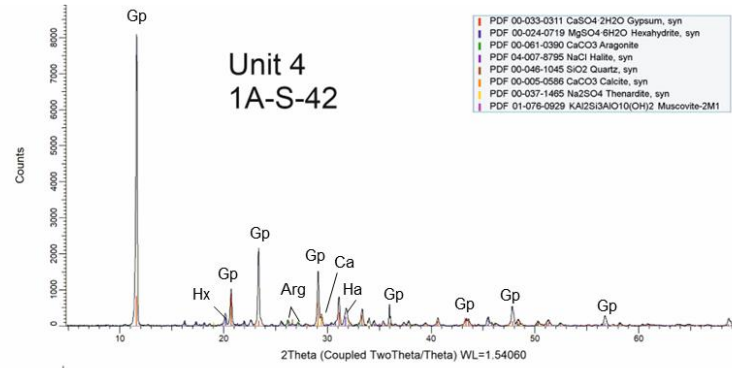
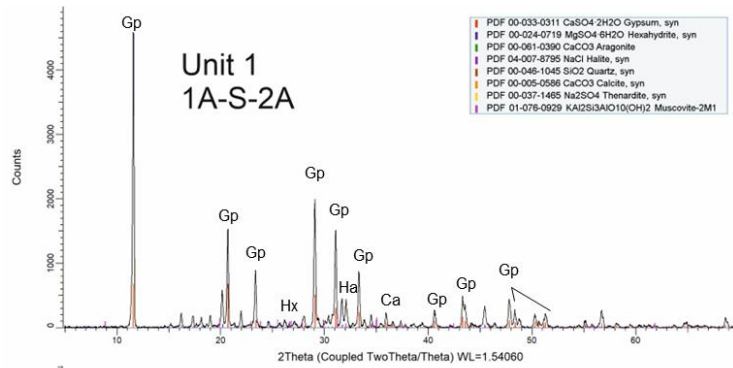
In the profundal section, unit 1 is comprised of microbial mats with intergrown gypsum, while the littoral section displays vertically oriented cumulate gypsum underlain and overlain by microbial laminae (Doyle *et al.*, 2022b). Mineralogically, aragonite has a trace abundance at the bottom of the unit in all cores (~5%) but increases to a common phase towards the top (10-30%) with the exception of core 6A. Calcite is a minor mineral in all cores, with abundances generally below 5%. Quartz and phyllosilicates are again mostly trace throughout the unit, with abundances no greater than 5% in both cases, but with some small increases for both phases at the top of the littoral cores to approximately 5-7%. Gypsum is abundant but variable in abundance throughout unit 1, generally illustrating the highest abundances (50-75%) in core 6A and the littoral cores, but slightly reduced (50-60%) abundances in the profundal cores. Hexahydrite displays variation between 10-25% in all cores, with the exception of core 6A where a large peak (~60%) is identified at the top of the unit. Halite illustrates variability between 3-10% in most cores but displays a synchronous increase at the top of the littoral cores (~7-12%) and core 6A (~20%). Thenardite is primarily a trace phase in most cores but illustrates a large increase in abundance at the top of cores 1A (10%) and 6A (~40%).

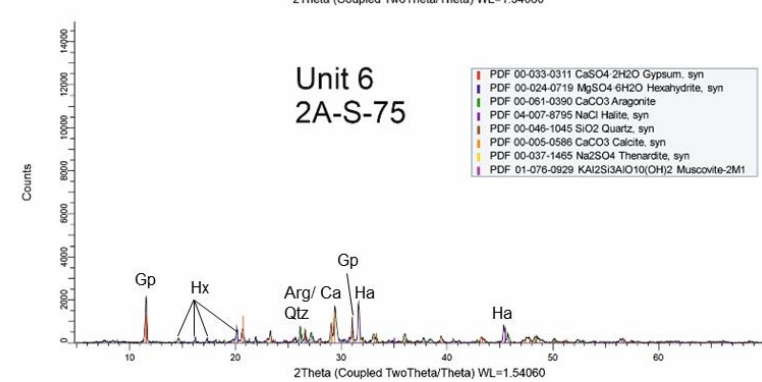
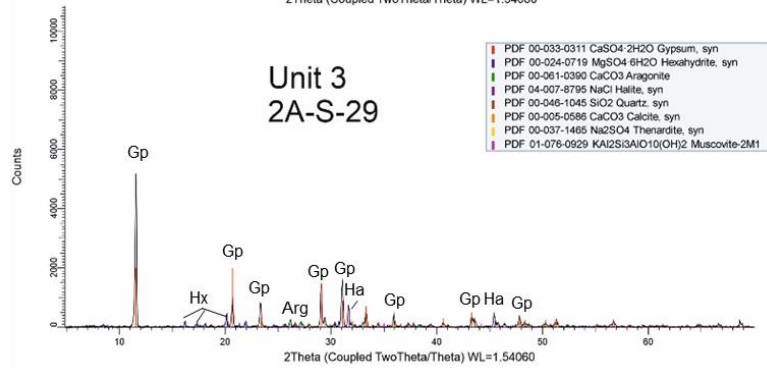
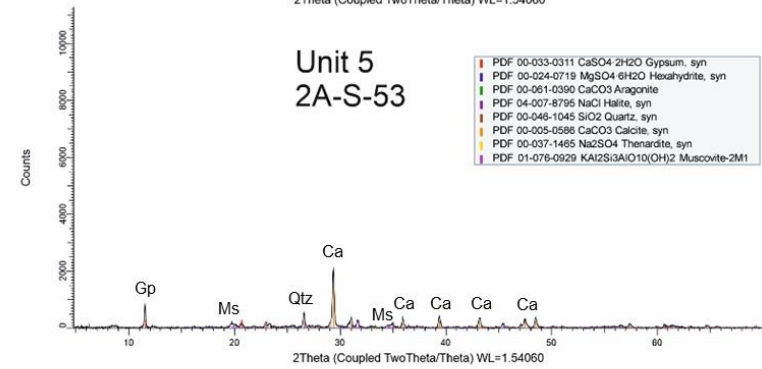
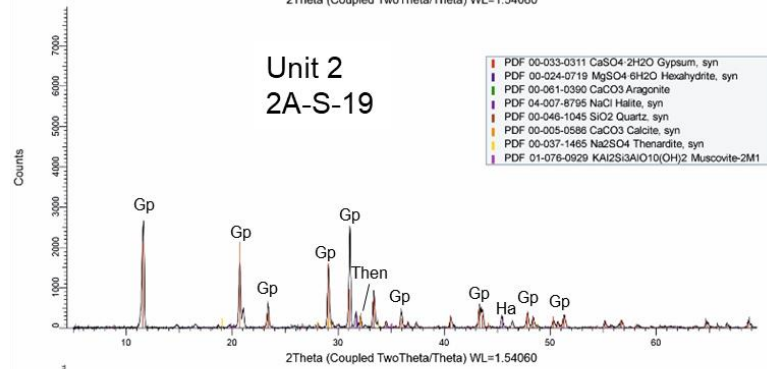
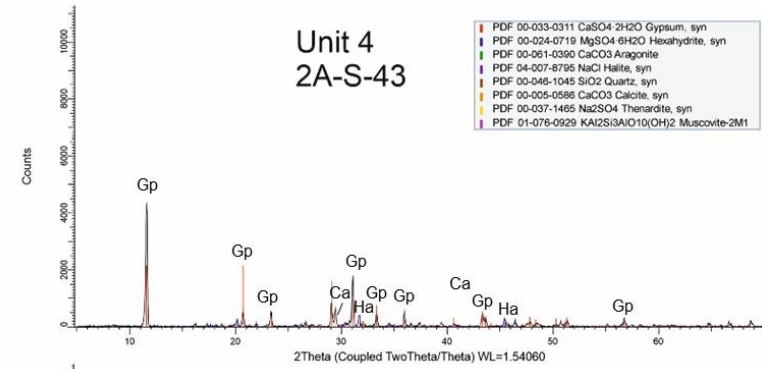
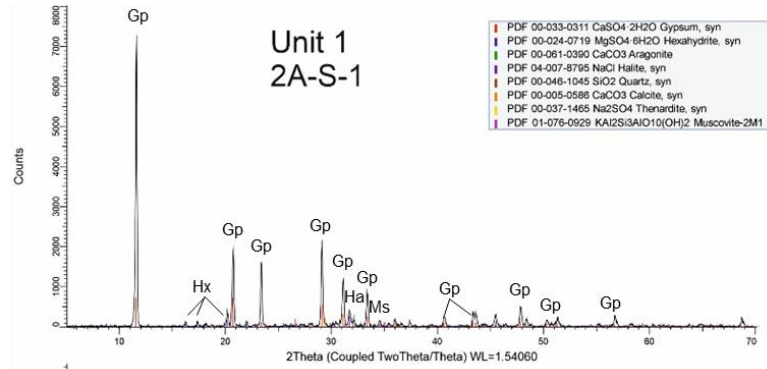
6.4.3 - PhreeqC Modelling

This section details the outcome of hydrochemical modelling undertaken using the PhreeqC Interactive software package (Parkhurst, 1995; Parkhurst & Appelo, 2013). In this study, modelling to determine the effect of evaporative concentration on the molality of key anions and cations within the lake and the saturation indices of key mineralogical phases was undertaken. Anions included within the model include Cl⁻, Br⁻, and SO₄²⁻, while cations included Na⁺, K⁺, Ca²⁺ and Mg²⁺. The concentration of both the anions and cations was modelled with increasing degrees of evaporation of a 1 litre solution, and was coupled with the assessment of the saturation indices of key phases associated with the sequence.

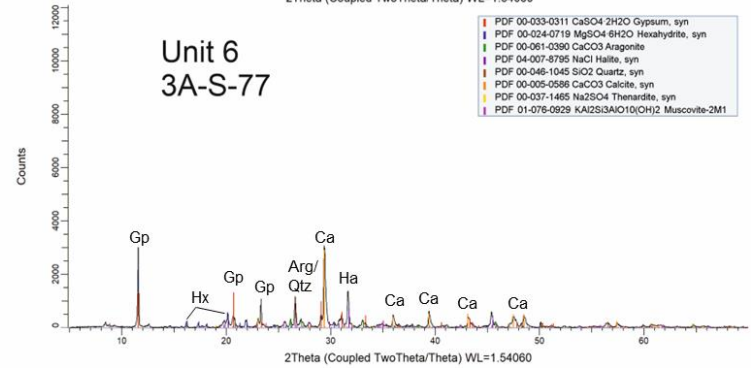
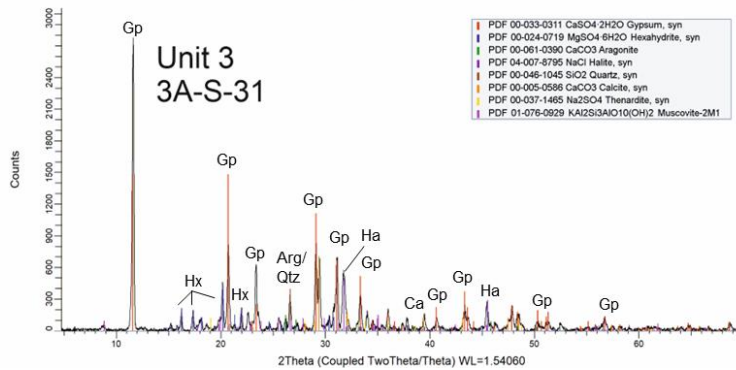
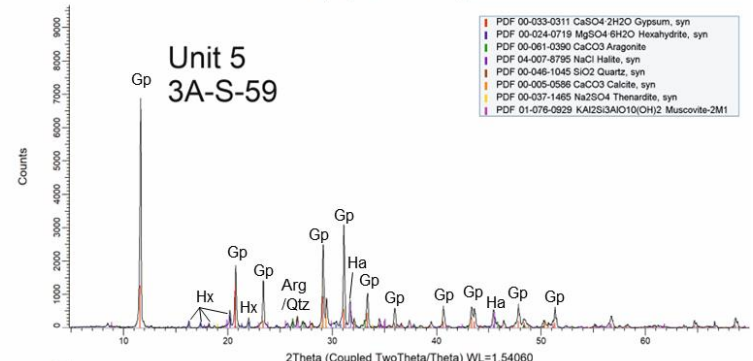
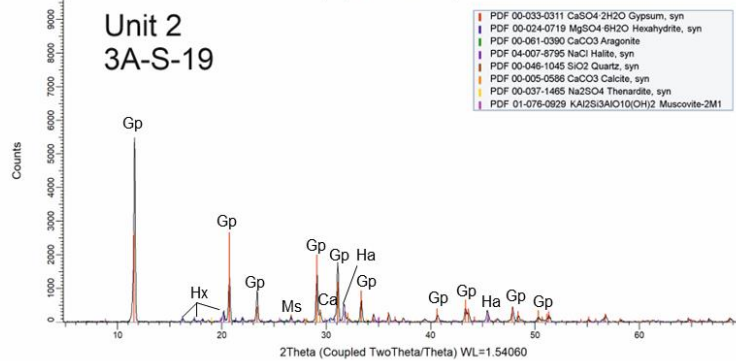
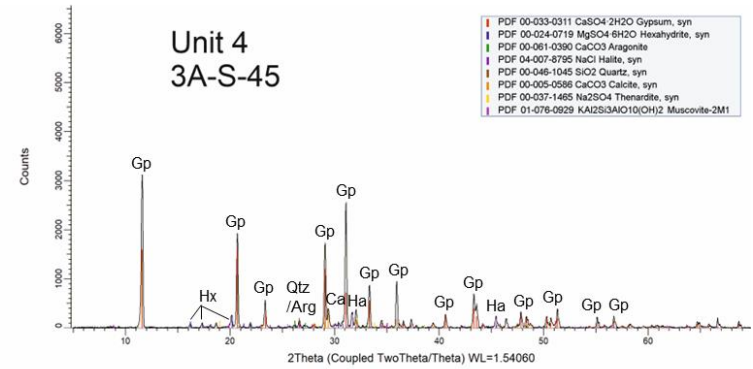
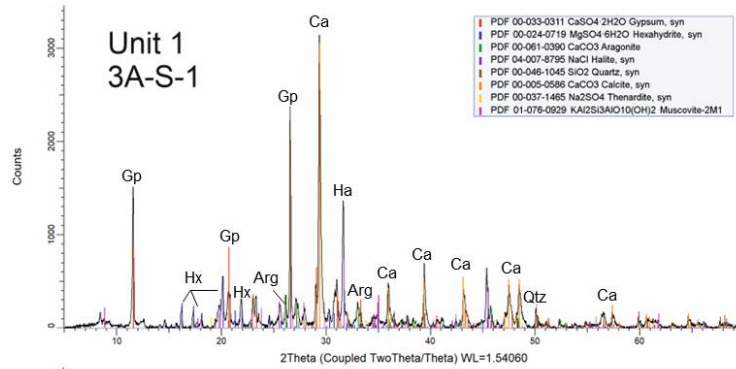
6.4.3.1 - Anion-Cation Concentrations and Saturation Indices

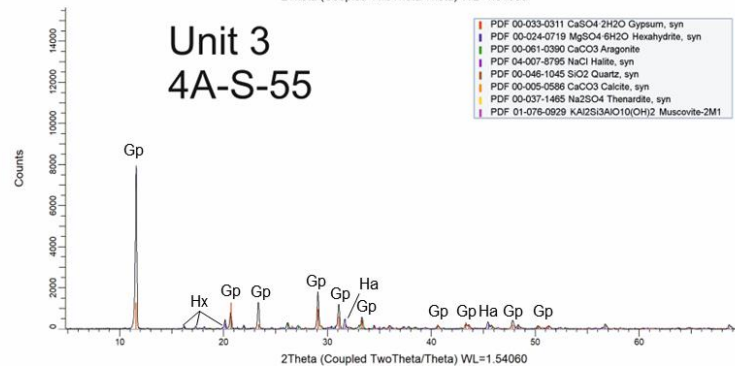
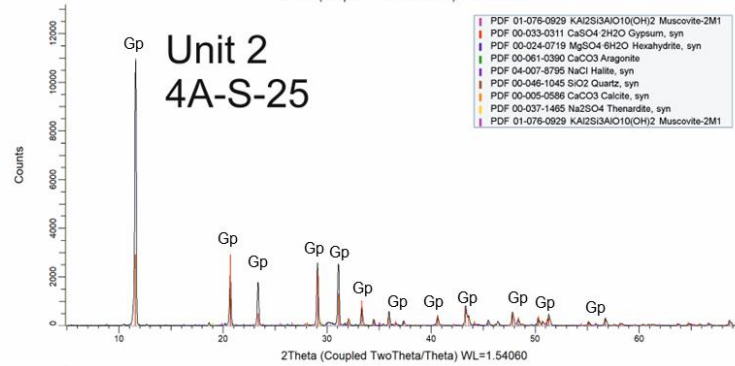
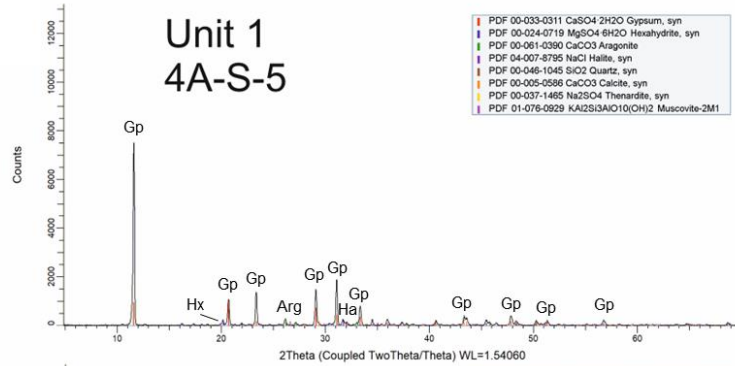
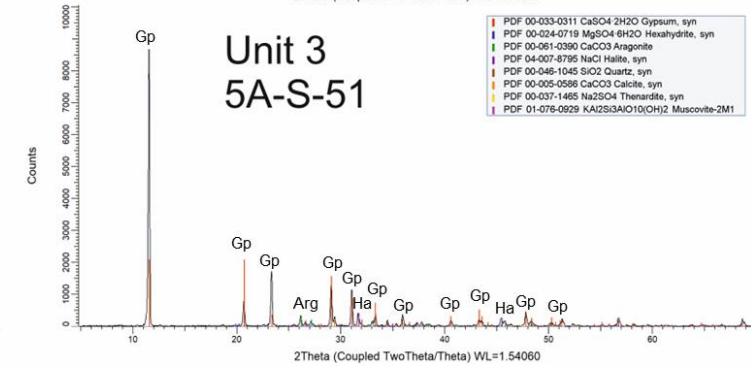
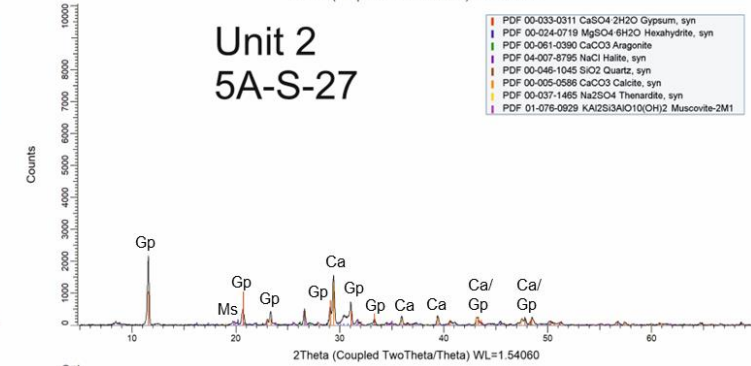
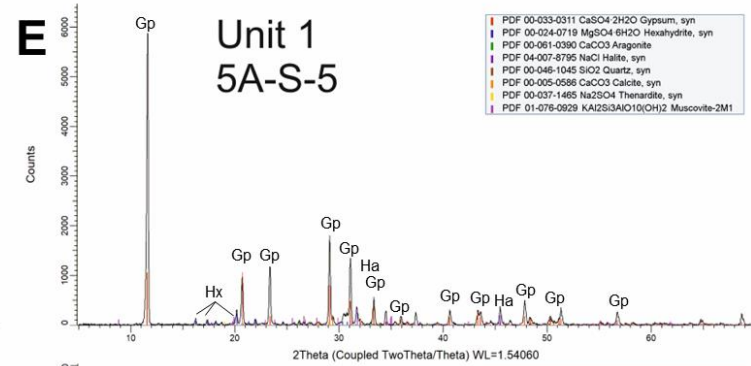
The geochemical data utilised in PHREEQC Interactive are defined in Table 6.2. All models of evaporation were undertaken at a theoretical temperature of 25°C according to the PHREEQC manual (Parkhurst, 1995) utilising the pitzer.dat database, and increasing degrees of evaporation were modelled by removing a specific amount of moles from a 1 litre solution of water containing the geochemical data. For the surficial lake waters, modelling was undertaken via the removal of 95% of water in 95 steps such that 1% of water or 0.5555 moles was removed in each step, with the upper bounds of this modelling being restricted by the limits of the program. In all cases, the concentration of the analytes is reported in (log) molality due to the large degree of variation between their concentrations. In the surface waters of Lake Chiprana, anions and cations typically displayed an exponential increase in concentration (log molality) with increasing concentration (% water removed) with the exception of Ca^{2+} , which displayed an overall trend of decreasing concentration, albeit with a small increase at approximately 92% water removed. Furthermore, SO_4^{2-} , Na^+ , and Cl^- exhibit a sharp decrease in concentration at approximately 88% water removed.



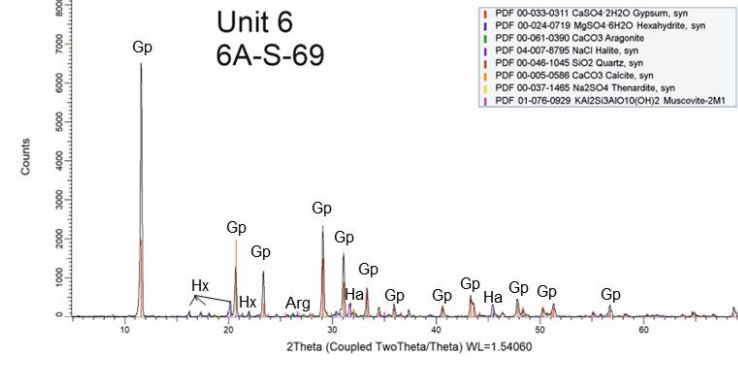
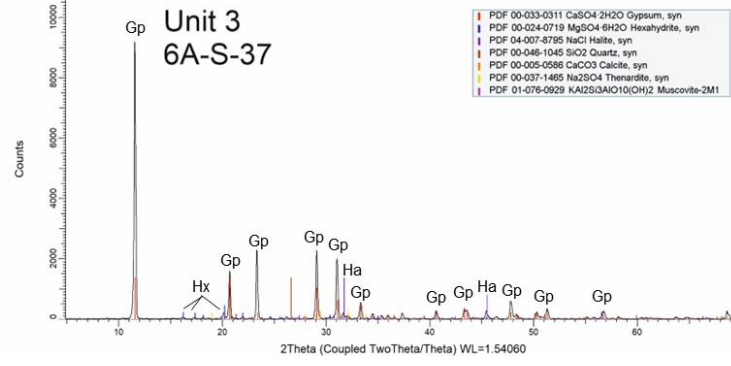
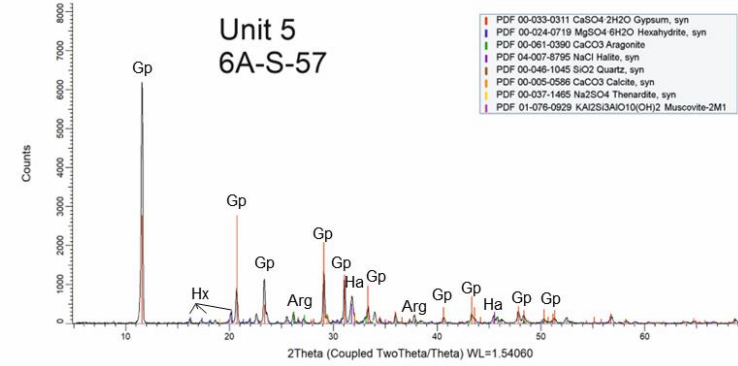
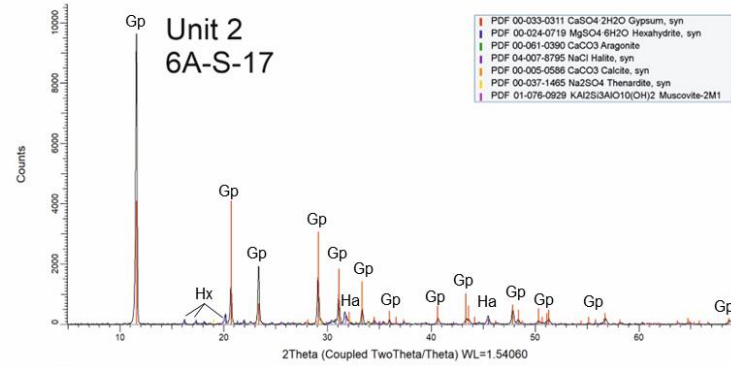
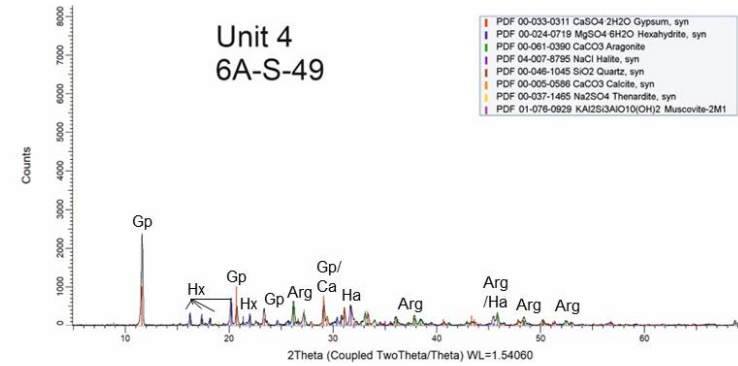
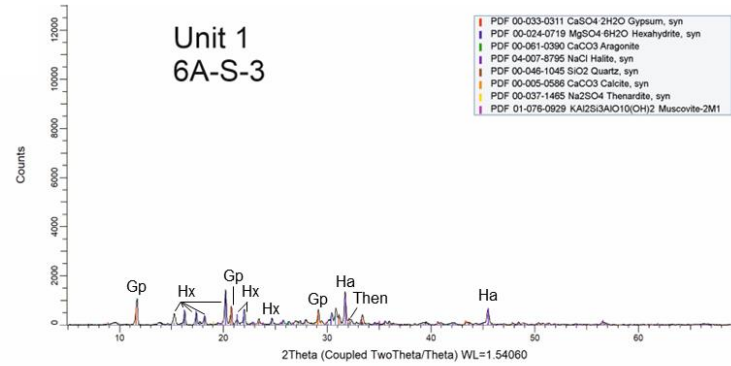
B

C



D**E**

F



G

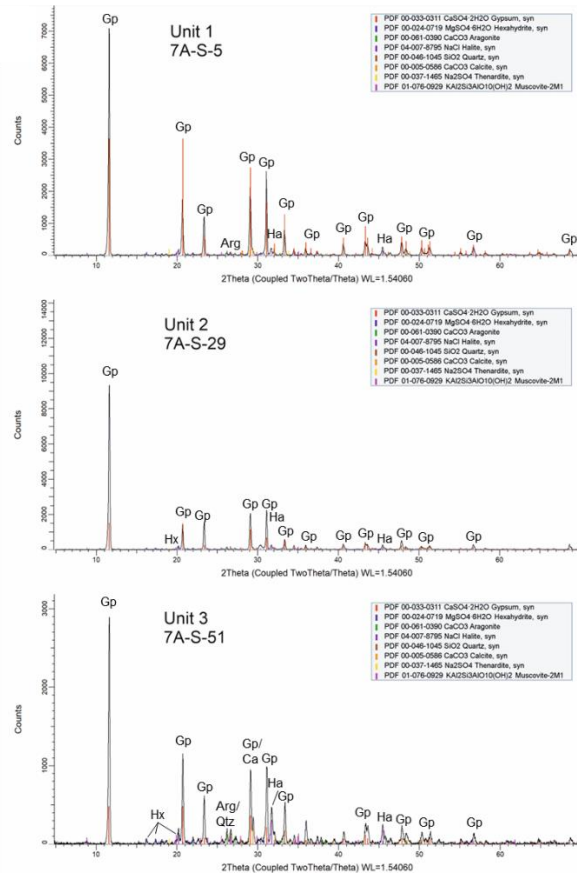


Figure 6.6 – XRD diffractograms displaying the typical mineralogy of units 1 to 6, from cores A) 1A, B) 2A, C) 3A, D) 4A, E) 5A, F) 6A, G) 7A. Data shown were smoothed and background noise subtracted in order to increase the readability of the charts and align the mineral diffractogram patterns more accurately. Minerals detected in significant abundances included aragonite, calcite, gypsum hexahydrate, halite, thenardite, quartz, and phyllosilicates (typically muscovite 2m1). Other minerals detected include epsomite and anhydrite.

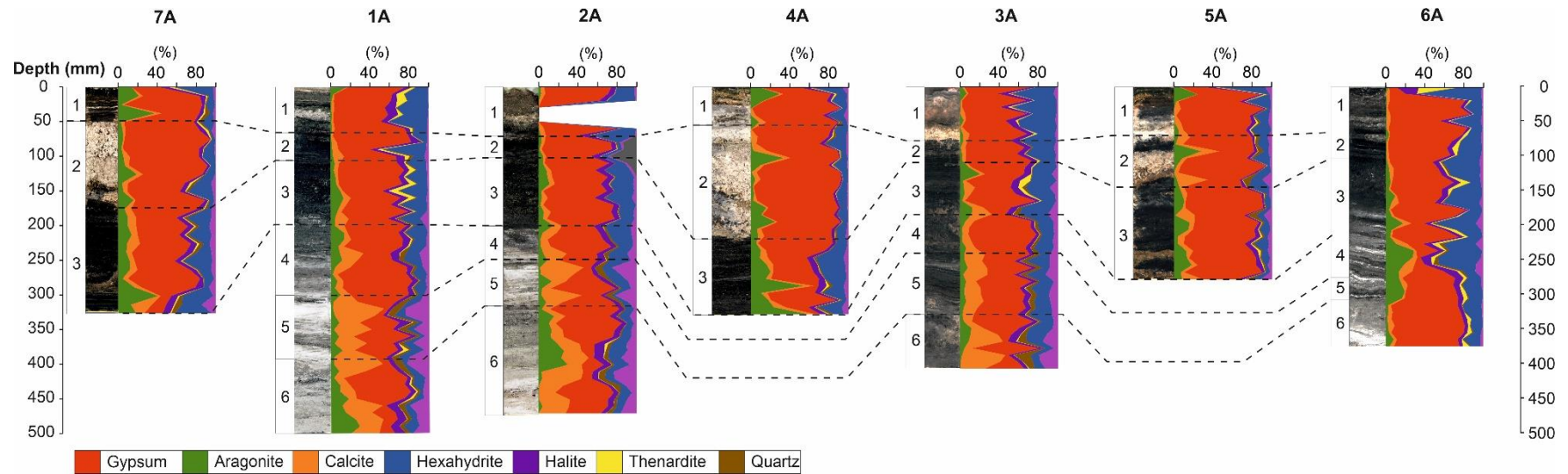


Figure 6.7 – Sedimentological cross-section of cores retrieved from Lake Chiprana with mineralogical data illustrating the abundance various mineralogical phases throughout each throughout the lake.

Figure 6.9 displays saturation indices modelling of different phases for the surface waters. Generally, a saturation index (SI) < 0 is stipulated to refer to undersaturated waters, while a SI > 0 indicates supersaturation. In the surface waters, modelling indicates that the water from Lake Chiprana is initially supersaturated with respect to calcite and gypsum, with both displaying a saturation index of 0 at the first modelling step and subsequently precipitating at each step throughout the model, with the exception of calcite precipitation ceasing at a concentration factor of 9.194 (89% water removed) (see Figure 6.9) and overall precipitating 0.072 moles. Gypsum displays continuous precipitation throughout, with a weak logarithmic trend of precipitation with increasing concentration, precipitating 0.664 moles in total.

Furthermore, the analysis shows that at the initial modelling step the lakewaters are undersaturated with respect to halite, hexahydrite, thenardite and aragonite (first modelling step, no evaporation, Figure 6.9), but that the former three phases typically exhibit an exponential increase in saturation with increasing evaporative concentration, all reaching supersaturation at different steps. In this case, halite reaches supersaturation at 92% water removed, precipitating 0.547 moles, hexahydrite at 92%, precipitating 0.302 moles, and thenardite at 89%, precipitating 0.586 moles. Aragonite however remains at a constant saturation index of -0.19 throughout the model and thus does not reach supersaturation.

Table 6.3 - Outputs of the PHREEQC hydrochemical model, illustrating the concentration of cations and anions and saturation indices of key phases in the initial solution in the profundal and littoral settings.

Littoral Hydrochemical Characteristics									
Profundal	Anions/Cations	C	Cl	Br	S(6)	Na	K	Ca	Mg
		0.005	0.170	0.000	0.205	0.242	0.003	0.000	0.201
	Saturation Indices	Aragonite	Calcite	Gypsum	Halite	Hexahydrite	Thenardite		
		-3.275	-3.088	-1.548	-3.363	-1.761	-3.100		
Littoral	Anions/Cations	C	Cl	Br	S(6)	Na	K	Ca	Mg
		0.000	0.248	0.000	0.285	0.446	0.005	0.015	0.361
	Saturation Indices	Aragonite	Calcite	Gypsum	Halite	Hexahydrite	Thenardite		
		-0.186	0.000	-0.011	-2.935	-1.591	-2.586		

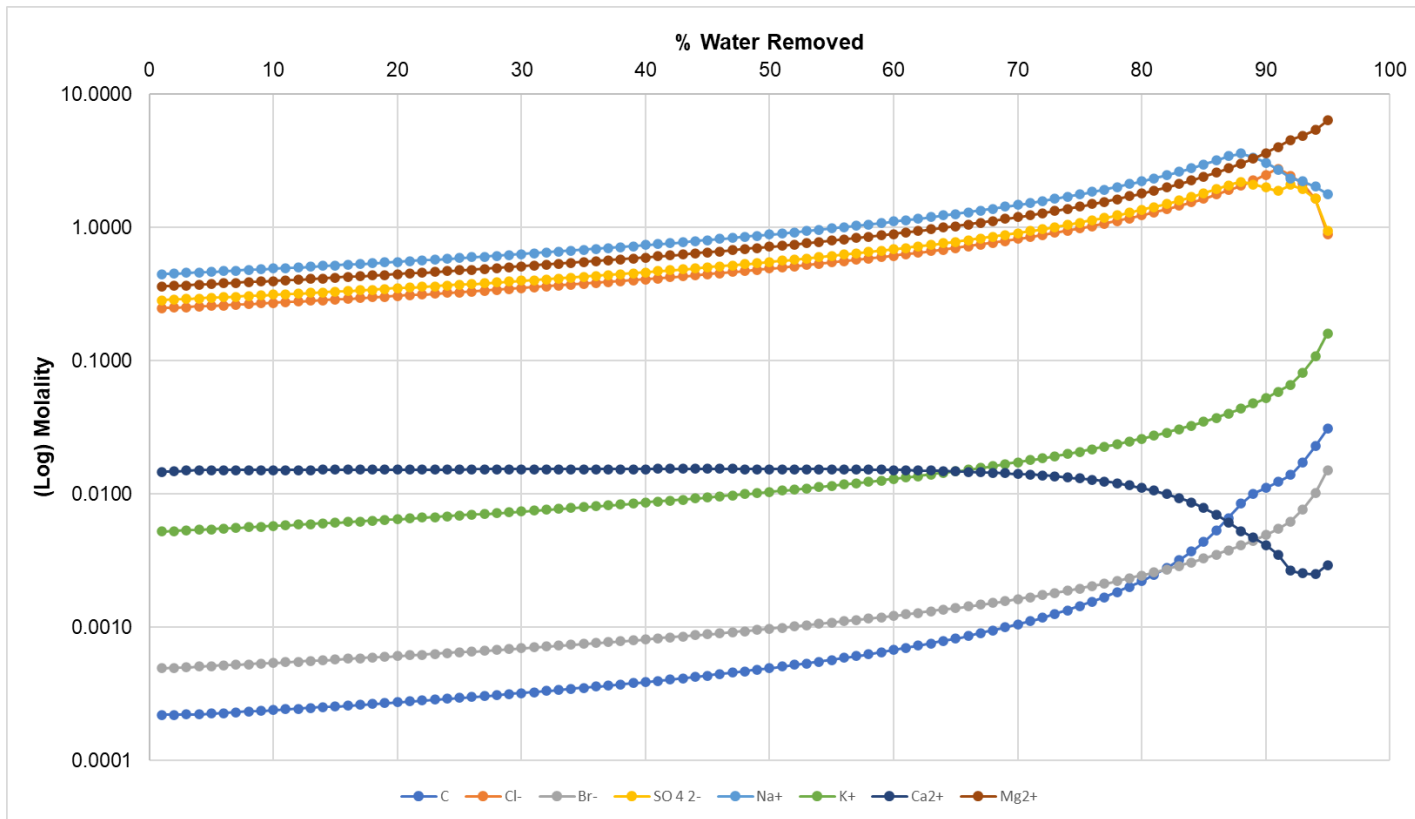


Figure 6.8 - PHREEQC-modelled increases in key anions and cations associated with Lake Chiprana in relation to increasing moles of water removed from a theoretical 1 litre solution. Each step represents 1% of water removed from the solution and subsequently represents the effect of increasing evaporation for each modelled step.

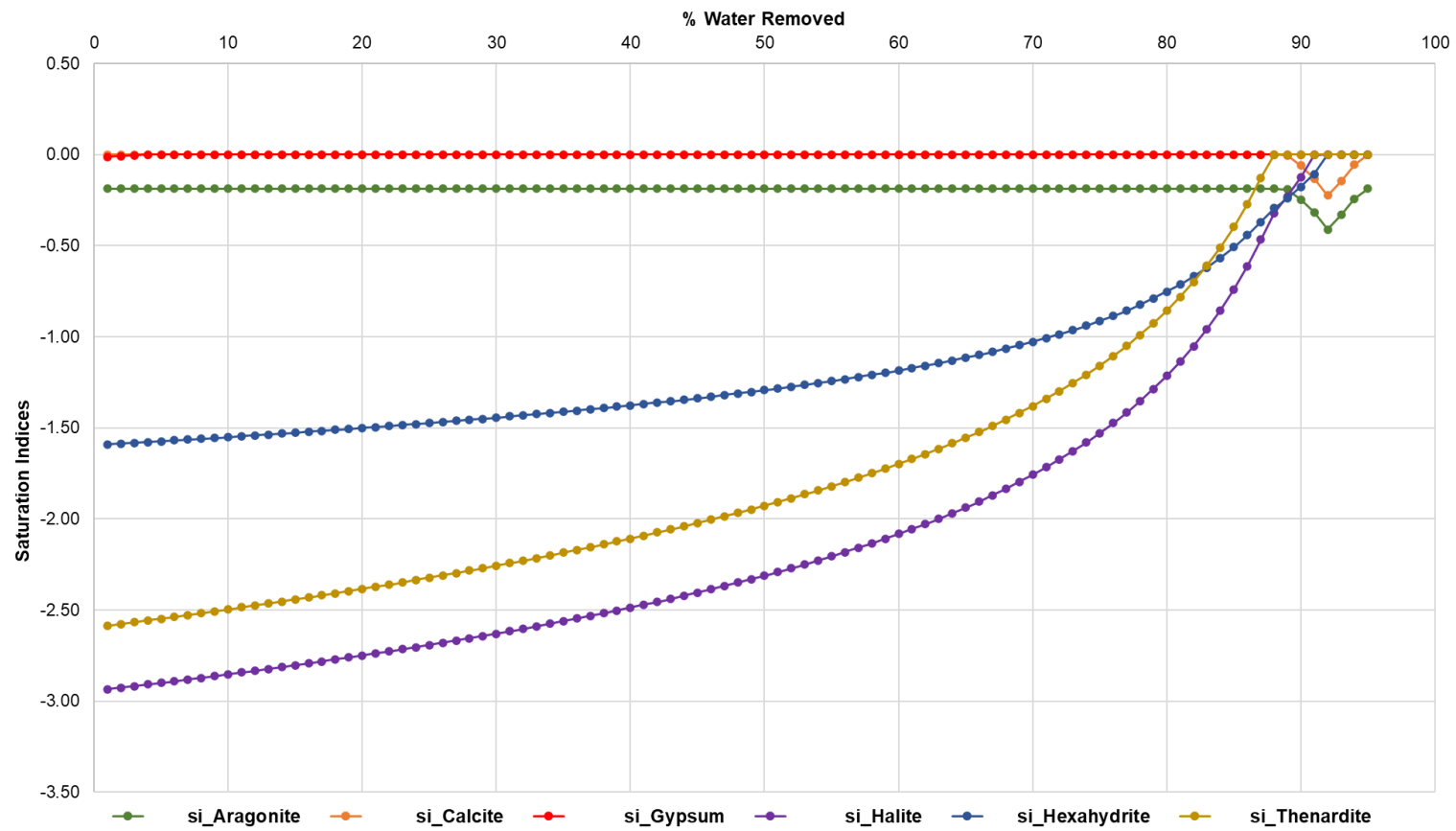


Figure 6.9 - Graph illustrating the saturation indices of key minerals in the surface waters of Lake Chiprana as modelled using PHREEQC Interactive.

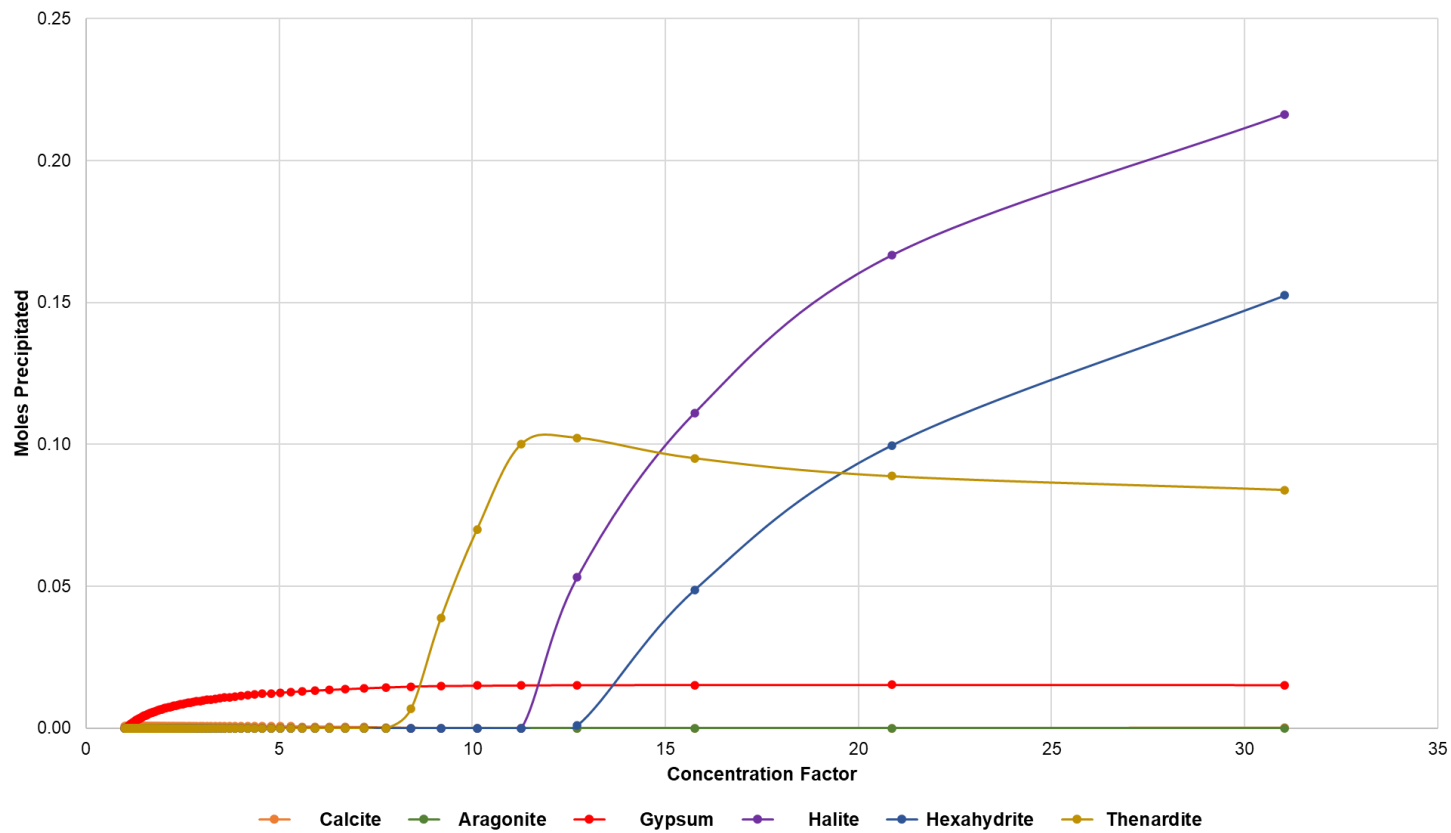


Figure 6.10 - Graph illustrating the amount of moles precipitated at each step of the PHREEQC simulation with increasing concentration and % water removed. Calcite precipitates initially, followed by gypsum, thenardite, halite and hexahydrate.

6.4.4 – Isotopic Data

Figure 6.10, 6.11 and Table 6.4 illustrate $\delta^{18}\text{O}$ and δD (both pre and post-fractionation correction) values obtained from gypsum hydration water for this study, and the same parameters from modern lakewaters, wells and piezometers and nearby rivers, canals and irrigation channels provided by the Instituto Pirenaico de Ecología, and from a recent hydrogeochemical study focusing on the lake by Jódar *et al.* (2020). In total, 33 samples ranging from ages of between approximately 0 to 0.3ka were analysed, and illustrated pre-fractionation (uncorrected) $\delta^{18}\text{O}$ values ranging between 4.3 and 10.1‰ and δD values ranging between -29.7 and -2.6‰. The isotopic compositions are however corrected using fractionation factors defined by Gázquez *et al.* (2017, 2018). These factors are defined here as $\alpha^{18}\text{O}_{\text{gypsum-water}}$ of 1.0035 and $\alpha\text{D}_{\text{gypsum-water}}$ of 0.981 corresponding to a temperature of 15°C, which is similar to the current average temperature of the lake in the winter months at 10-12°C. Furthermore, according to Gázquez *et al.* (2022), the oxygen and hydrogen isotope fractionations between the host fluid and the gypsum hydration water are insignificantly affected by different temperatures and salinities during precipitation of gypsum, with temperatures in the range of 10-35°C typically having no effect on this fractionation (Gázquez *et al.*, 2018).

Post-fractionation (corrected) isotopic data illustrate $\delta^{18}\text{O}_{\text{VSMOW}}$ values ranging between 0.8 and 6.6‰ and δD values ranging between -10.9 and 16.7‰. The cross-plot presented in Figure 6.10 illustrates that the evaporative line associated with the data has an equation of: $\delta\text{D}_{\text{VSMOW}} = 4.436\delta^{18}\text{O}_{\text{VSMOW}} - 15.262$, with an R^2 value of 0.857. Further values depicted on the chart include data provided by the Instituto Pirenaico de Ecología for the lake and nearby wells, piezometers and channels in 2004, and the aforementioned isotopic data from the study by Jódar *et al.* (2020) which also depicts data from these sources. The local meteoric water line (LMWL) is defined as $\delta\text{D} = 7.194 * \delta^{18}\text{O} + 0.967$ by Négrel *et al.* (2016), which largely fits with the trend of the dataset presented here.

Table 6.4 - $\delta^{18}\text{O}$ and δD values obtained from gypsum hydration water with data presented both prior to and following the correction for fractionation of the isotope during assimilation of water into the gypsum crystal structure.

Depth (mm)	Pre-Fractionation Correction				Post-Fractionation Correction			
	d18O _{gyp}	1SD	dD _{gyp}	1SD	d18O _{paleo}	1SD	dD _{paleo}	1SD
5	8.29	0.07	-14.85	1.51	4.77	0.07	4.23	1.51
15	9.01	0.32	-10.52	1.72	5.49	0.32	8.65	1.72
25	10.09	0.21	-2.60	1.12	6.56	0.21	16.71	1.12
45	8.70	0.14	-9.05	0.21	5.18	0.14	10.15	0.21
55	8.76	0.08	-8.27	0.23	5.24	0.08	10.93	0.23
65	9.82	0.09	-10.71	0.93	6.30	0.09	8.45	0.93
75	9.35	0.10	-13.39	1.38	5.83	0.10	5.71	1.38
125	7.74	0.22	-17.28	1.11	4.23	0.22	1.75	1.11
135	8.32	0.19	-14.04	1.42	4.80	0.19	5.05	1.42
145	7.75	0.13	-17.67	0.59	4.24	0.13	1.36	0.59
155	7.26	0.18	-16.86	0.50	3.75	0.18	2.18	0.50
165	7.66	0.05	-19.29	0.54	4.14	0.05	-0.30	0.54
175	8.50	0.08	-13.78	0.68	4.98	0.08	5.32	0.68
185	7.24	0.11	-16.40	0.76	3.73	0.11	2.65	0.76
195	7.31	0.08	-17.88	0.88	3.80	0.08	1.15	0.88
205	7.32	0.16	-17.58	0.51	3.81	0.16	1.45	0.51
215	7.73	0.14	-18.56	0.81	4.21	0.14	0.45	0.81
225	8.22	0.08	-15.27	0.54	4.70	0.08	3.80	0.54
235	9.17	0.09	-6.31	0.43	5.65	0.09	12.94	0.43
245	8.95	0.15	-10.28	1.29	5.43	0.15	8.89	1.29
255	8.56	0.21	-12.47	1.18	5.04	0.21	6.65	1.18
265	9.40	0.05	-7.92	0.16	5.88	0.05	11.30	0.16
275	9.40	0.13	-7.14	0.41	5.87	0.13	12.09	0.41
285	9.44	0.13	-9.27	1.54	5.92	0.13	9.91	1.54
295	9.72	0.10	-7.14	1.20	6.20	0.10	12.09	1.20
305	9.55	0.12	-7.42	0.87	6.03	0.12	11.80	0.87
315	6.13	0.10	-19.62	0.89	2.62	0.10	-0.63	0.89
325	7.71	0.15	-14.78	1.28	4.19	0.15	4.30	1.28
335	4.33	0.83	-29.68	3.89	0.83	0.83	-10.88	3.89
365	7.94	0.36	-13.57	1.56	4.42	0.36	5.54	1.56
385	9.22	0.23	-5.33	1.28	5.70	0.23	13.93	1.28
425	9.91	0.13	-4.31	0.45	6.39	0.13	14.97	0.45
465	8.84	0.09	-10.07	0.43	5.33	0.09	9.10	0.43

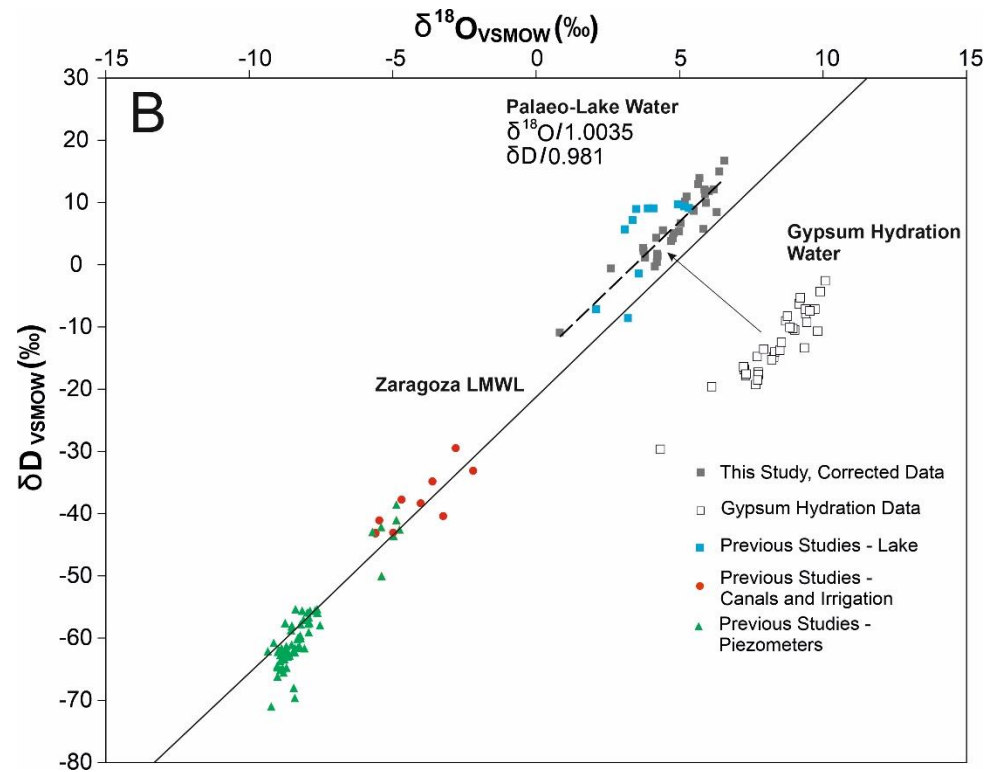


Figure 6.10 - $\delta^{18}\text{O}$ and δD values in a cross-plot with comparative isotopic data of lakewater, wells, piezometers and nearby canals and irrigation from 2004 as provided by IPE and from the recent study by Jódar *et al.* (2020). Translation of the isotopic data account for fractionation of water into the gypsum crystal lattice using a factor of 1.0035 for $\alpha^{18}\text{O}_{\text{gypsum-water}}$ of 1.0035 and 0.981 for $\alpha^{\text{D}}_{\text{gypsum-water}}$ of corresponding to a temperature of 15°C. Local meteoric water line from Zaragoza (Négrel *et al.*, 2016).

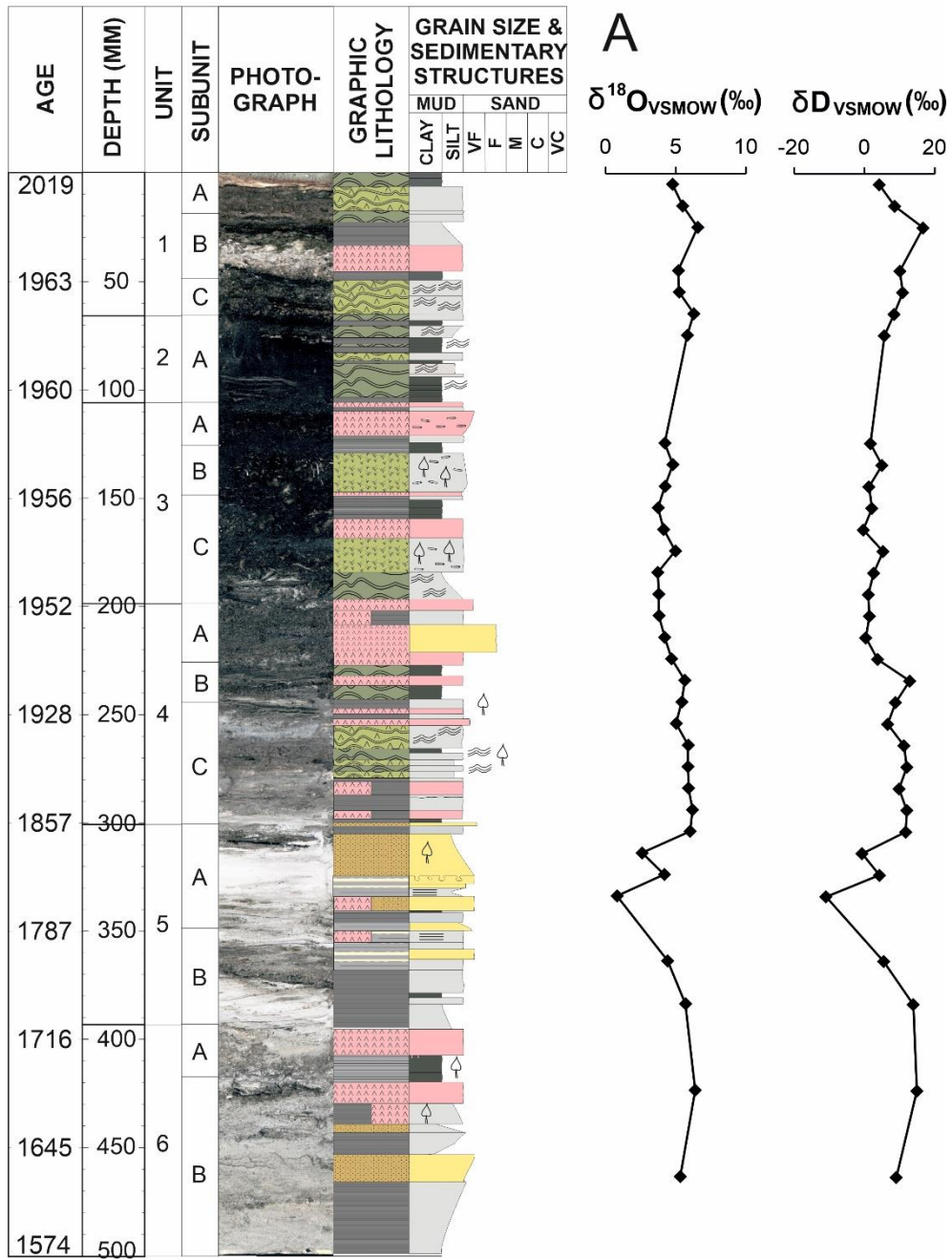


Figure 6.11 - Figure illustrating: A) the downcore evolution of $\delta^{18}\text{O}$ and δD values throughout core CHI19-1A with associated ages from previous age models generated for Lake Chiprana (see Doyle *et al.*, (2022a)).

The cross-plots clearly illustrate the increase of $\delta^{18}\text{O}$ and δD values within the lake, both in the case of the values corresponding to the modern lake-waters (Jóðar *et al.*, 2020) and from gypsum hydration water throughout the sedimentary sequence. These values are also enriched relative to meteoric waters associated with rainfall, groundwater and the moderately enriched values associated with water from irrigation channels and the Civan Canal (Jóðar *et al.*, 2020).

The temporal trends of the isotopic data illustrate higher $\delta^{18}\text{O}$ (5.3-6.4‰) and δD (9.1-15‰) values within the upper section of unit 6 (388-465mm, approximately 1700-1750_{AD}), coeval with the occurrence of several gypsum layers and increased gypsum and calcium-magnesium sulphate precipitation occurring at the top of the unit. In contrast, $\delta^{18}\text{O}$ and δD are lower throughout unit 5 (300-388mm, approximately 1750-1850), exhibiting the lowest values throughout the sequence (0.8‰ and -10.9‰ respectively) at the top of the unit in confluence with a detrital unit identified within chapter 4. This is again contrasted by an increase to some of the higher $\delta^{18}\text{O}$ and δD values (5.0-6.2‰ and 6.7-12.9‰ for $\delta^{18}\text{O}$ and δD respectively) in the lower to mid-section of unit 4 (~230-300mm, approximately 1850-1930 to 1940) which coincide with the development of microbial mats throughout the unit. This is followed by an decrease of approximately 1-3‰ for $\delta^{18}\text{O}$ and 5-7‰ for δD respectively throughout much of unit 2 and 3 (~65-200mm), but increases are again observed in unit 1 by magnitudes of 1-2‰ and 4-7‰ for $\delta^{18}\text{O}$ and δD respectively.

6.5 - Discussion

6.5.1 - Detrital Inputs

Units 5 and 6 (approx. ~1600 to ~1850_{AD}) associated with cores 1A, 2A, 3A and 6A provide insights into the provenance of detrital material that is delivered to Lake Chiprana from the local catchment via surface run-off, irrigation input and various other hydrological inputs due to the increased abundance of such detrital material throughout these units (McHenry *et al.*, 2020; Doyle *et al.*, 2022b). Samples from

these units in all cores contain high amounts of quartz, phyllosilicates and detrital calcite (Doyle *et al.*, 2022b). These likely derive from several geological formations present in the catchment area. Pleistocene-age gravels and sandstones occurring to the Southeast of Lake Chiprana and Oligo-Miocene sandstone ribbon palaeochannels present throughout the lake likely act as a source of phyllosilicates and quartz, while Pleistocene to Holocene marls encapsulating much of the remaining catchment area (Vidondo *et al.*, 1993; IGME, 2003) are the most plausible source of detrital calcite. Increasing overland flow and water delivery to the lake via streams, canals and channels from irrigation returns during this timeframe delivered detrital materials to the lakewaters (Valero-Garcés & Kelts, 1995; Valero-Garcés *et al.*, 2000; Jódar *et al.*, 2020; Doyle *et al.*, 2022b). The increased abundances of quartz and phyllosilicates in the profundal and littoral sediments of Lake Chiprana are thus likely to be an indicator for more intense periods of runoff and inflow into the lake (Doyle *et al.*, 2022b).

6.5.2 - Geochemistry and Evaporite Precipitation

Lake Chiprana is currently a meromictic saline lake defined by an average salinity value of approximately 40psu in the surficial waters and approximately 80-85psu in the deeper profundal waters (Table 6.1), and contains Na⁺, Mg²⁺, SO₄²⁻ and Cl⁻ as the major ions (De Wit *et al.*, 2013). Evaporitic minerals identified in this study include gypsum, thenardite, halite, hexahydrate and very minor amounts of epsomite, which are characteristic of such brine types according to Hardie & Eugster (1970) and Cabestrero *et al.* (2018). Lake Chiprana however, lacks mirabilite, perhaps due to a reduced Na⁺/Mg²⁺ ratio (Cabestrero *et al.*, 2018), and also has a low, often trace abundance of bloedite and epsomite in the majority of samples. This may be due to a lack of the required geochemical conditions for these phases to precipitate. The permanent nature of the lake may have inhibited the supersaturation of these specific minerals or due to inflow from the regulation of the lake by the local government (De Wit *et al.*, 2013). In addition, the potential dehydration of epsomite to hexahydrate may have caused the higher abundances of hexahydrate throughout

the sequence (Chipera *et al.*, 2006). Many other saline lakes throughout Spain such as Altillo Chica and Altillo Grande in La Mancha, Central Spain (Cabestrero *et al.*, 2018), and Salada Mediana in the Ebro Basin upstream from Lake Chiprana (Mees *et al.*, 2011) have contrastingly been associated with more significant amounts of bloedite and mirabilite, which may have been due to surface brines being more supersaturated with respect to these phases (Hardie & Eugster, 1970) due to the ephemeral nature of these sites.

Within many saline lacustrine environments, there is often reduced inflow, and outflow is reduced over long periods of time (Logan, 1987; Deocampo & Jones, 2013). Fluctuations in saline lake water levels are well documented to be able to lead to significant shifts in the geochemistry and mineralogy of the sedimentary deposits associated with their lakebeds (Renaut & Last, 1994; Yechieli & Wood, 2002). In Lake Chiprana, during lake drawdown, endogenic phases including gypsum, calcite, hexahydrate, halite and thenardite increase in saturation (Figure 6.10). These minerals subsequently precipitate in greater abundances, particularly within units 1 and 2 (modern~1960_{AD}), unit 4 (1850-1950_{AD}) and in several small intervals throughout unit 6 (1600-1700_{AD}). It is probable that in the marginal areas of the lake and within partially desiccated pools, greater abundances of bloedite may occur where saturation indices increase (Cabestrero *et al.*, 2018).

Such endogenic phases (Figure 6.12) can ultimately provide insights into the geochemical composition of the waters of Lake Chiprana, and potentially also the level of the lake waters throughout the site over geological time (McHenry *et al.*, 2020). Increases in the abundance of such phases likely reflect increases in evaporation, while retrospective decreases are indicative of increases in lake level as compensated by increasing abundances of detrital phases. Such increases are identified occurring in unit 4 (~1850-1950_{AD}), coeval with the occurrence of microbial mats that are typically indicative of lower lake levels (Valero-Garcés *et al.*, 2000a; Doyle *et al.*, 2022b), and also within units 2 (~1960-1962_{AD}) and 1 (~1962_{AD}-present)

in both the profundal and littoral areas of the lake, likely suggesting periods of increased evaporative concentration during these intervals.

6.5.3 – Hydrochemical Analyses & Model Output

The outputs of hydrochemical modelling generated by PhreeqC provide further insights into the hydrological evolution of Lake Chiprana. The lake is ultimately a complex hydrochemical system with multiple environmental and biological factors (Vidondo *et al.*, 1993; Jonkers *et al.*, 2003; De Wit *et al.*, 2013) that are known to cause fluctuations in the geochemical composition of the waters and subsequently the saturation indices of key mineralogical phases. The hydrochemical model indicates that with progressive removal of 95% of water, all major anions and cations typically increase in saturation, in this case by a factor of 20. Furthermore, the model indicates that the surficial lakewaters of Chiprana as measured in samples taken during December 2021 were initially undersaturated with respect to thenardite, halite and hexahydrite, but are supersaturated with respect to aragonite, calcite and gypsum. With increasing evaporative concentration, all phases with the exception of calcite, aragonite, epsomite and hexahydrite illustrated exponential increases in saturation, with the aforementioned phases displaying relative decreases in saturation at high percentages of water removal.

The model illustrates that the paragenetic sequence of minerals proceeds with initial precipitation of calcite, followed by gypsum, thenardite, halite and hexahydrite. Based on the chemical composition of the waters (Mg^{2+} , SO_4^{2-} , Cl^- , and Na^+). and the identified mineral sequence, Lake Chiprana is classified as a Type IV brine (Hardie & Eugster, 1970). Despite this, there are a wide range of sub-environments and geochemical characteristics associated with Lake Chiprana, and limnological analyses in this study illustrate a clear thermocline, halocline and chemocline from the littoral to profundal waters (see Figure 6.3), For example, salinity, temperature and TDS are typically around ~40PSU, ~12°C and ~40000mg/L in the littoral areas of the lake respectively, while values are generally much higher at 80PSU, ~23°C

and 70000mg/L in the profundal areas of the lake (Figure 6.3, Table 6.1). The saturation index of minerals thus also varies throughout the lake in response to these factors (see Table 6.3), and likely contributes to the varied mineralogical sequences and textures identified in this study.

Despite this, other minerals associated with Type IV brines such as epsomite and bloedite are scarce in the Lake Chiprana sediments, while other typical mineral phases such as bischofite and mirabilite are almost entirely absent. This contrasts to other saline lakes in the region and in other areas of Spain, where such minerals are typically present (Cabestrero *et al.*, 2018; Sanz-Montero *et al.*, 2019). In the case of Lake Chiprana, it is likely that a wide range of factors have a role to play in the precipitation and/or dissolution of mineralogical phases within the sediments. Biological processes are well-known to affect mineral precipitation and dissolution in a wide range of settings (Dupraz *et al.*, 2009; Mercedes-Martín *et al.*, 2022). For example, Dupraz *et al.* (2009) have shown that the effects of photosynthetic activity and sulphate reduction can lead to an increase in carbonate saturation and precipitation as a by-product of these processes, leading to the development of carbonate crusts within mat structures (Dupraz *et al.*, 2004). Dupraz *et al.* (2009) and other studies have shown that microbial biota can also play a role in the dissolution of mineral phases, with processes such as sulphide oxidation (Leprich *et al.*, 2021) and fermentation (Cutts *et al.*, 2022) often leading to the reduction in the saturation of carbonate and its subsequent dissolution. In cases such as Lakes Altillo Chica and Altillo Grande in

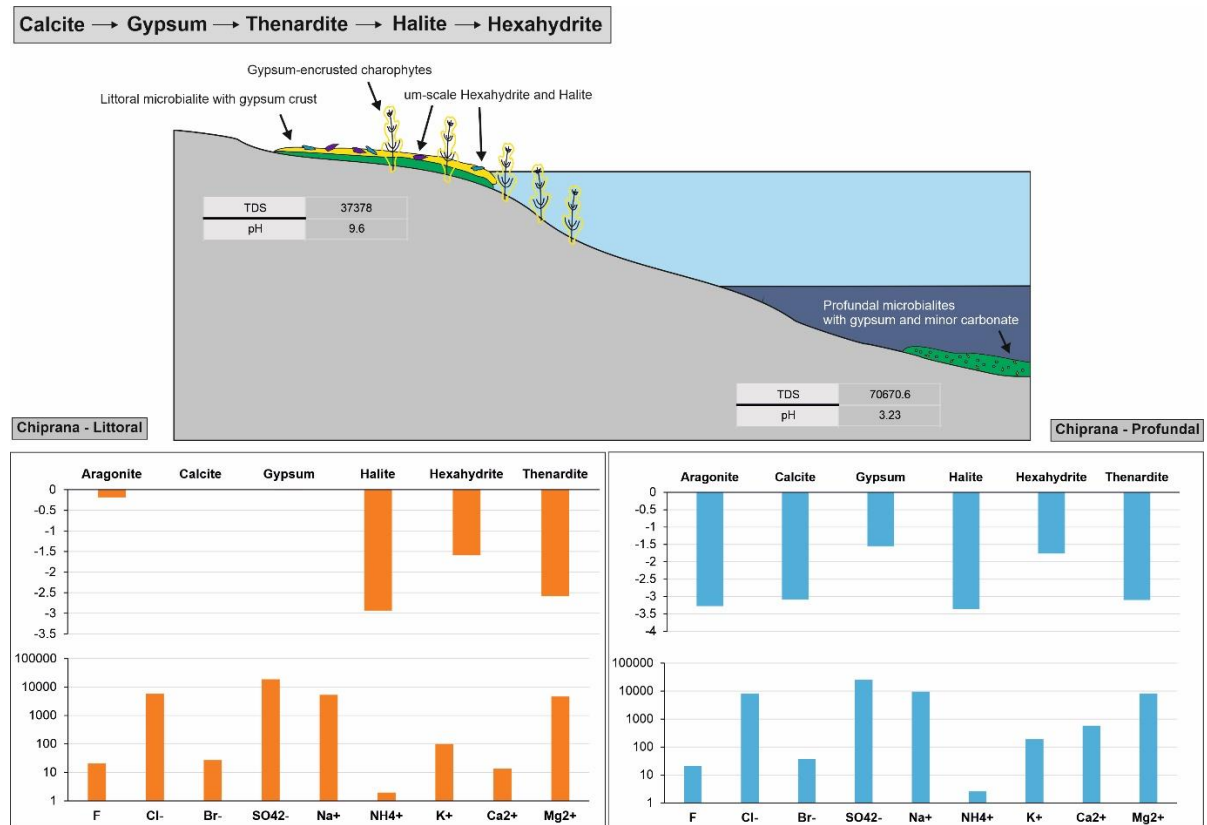


Figure 6.12 – Summary model of Lake Chiprana highlighting the interplay of key minerals and hydrochemical characteristics occurring throughout the lake. Specifically, the saturation indices and key anions and cations are displayed in relation to the nature of the waters they were sampled from.

Central Spain, Cabestrero *et al.* (2018) for example illustrated a clear influence of biotic activity upon mineralisation, with organic matrices generated by microbialites facilitating the precipitation of bloedite, epsomite and mirabilite by providing templates for the generation and organisation of the minerals. Furthermore, aragonite is not seen to precipitate within the hydrochemical model (Figure 6.10), yet can be observed to display small increases in abundance in association with the onset of microbial mat development. Microbialite-induced precipitation of carbonates has previously been identified at Lake Chiprana (De Wit, 2016), and thus it is plausible that biotic processes, such as the localised liberation of Ca^{2+} ions from EPS degradation, or the use of EPS as a template for mineralisation, may have occurred here (Cabestrero *et al.*, 2018).

However, as the PhreeqC Interactive software package cannot model such biotic factors, their role in the mineralogical characteristics of the sediments of Lake Chiprana requires further clarification in future studies. Though some previous work has been undertaken in the past on mats from Lake Chiprana (Jonkers *et al.*, 2003), such future works may aim to clarify the effect of individual metabolic activities upon mineral saturation states throughout the mat and the water in proximity to the mat structure. It is probable that the biotic factors associated with the microbial mats have some significance in both the precipitation or negation of precipitation of mineral products, in this case potentially being negation of the precipitation of abundant epsomite, mirabilite and bloedite throughout the sediments of Lake Chiprana.

6.5.4 – Isotopic Indicators

6.5.4.1 – Data Significance

The use of $\delta^{18}\text{O}$ and δD isotopic compositions of gypsum hydration water allow for further insights into the hydrological evolution of Lake Chiprana throughout the last three to four centuries. Though the method is novel in its application (Gázquez *et al.*, 2017), many studies have illustrated that higher $\delta^{18}\text{O}$ and δD values can signify more evaporated water, drier climate and higher evaporation/inflow ratios, while less evaporated water, more humid conditions, and lower evaporation/inflow ratios when values are lower (Gázquez *et al.*, 2018). Results presented here correlate well with other sedimentological and geochemical work undertaken on the sediment cores (Valero-Garcés *et al.*, 2000a; Doyle *et al.*, 2022b), illustrating decreases in evaporation/inflow ratios between approximately associated with reduced $\delta^{18}\text{O}$ and δD at approximately ~300-350yrs BP, synchronous with increased irrigation returns to the lake identified previously by Doyle *et al.* (2022b). Furthermore, according to Gázquez *et al.* (2018) though caution must be taken due to the effects of diagenesis upon isotopic compositions, it is likely that, in the case of Lake Chiprana, as also identified by Gázquez *et al.* (2018) in the case of Lake Estanya, that the original and primary isotopic values are preserved. The fractionation-corrected data presented here match isotopic values of the lake water provided elsewhere from other sources and studies, but state also that shallow burial may affect isotopic gradients due to diffusion and advection with overlying lake-water.

Such isotopic data can be utilised as supporting evidence in the interpretation of environmental and anthropogenic perturbations acting upon Lake Chiprana for the last few centuries (Gázquez *et al.*, 2018). In the local region and around Zaragoza, the 2-year weighted average $\delta^{18}\text{O}$ and δD of meteoric water are -5.86‰ and -39.37‰ respectively, with a local meteoric water line (LMWL) of $\delta\text{D} = 5.66 \cdot \delta^{18}\text{O} - 4.86$. (see Figure 6.10). Fractionation-corrected gypsum hydration data illustrates significantly higher values for Lake Chiprana lakewaters, with average $\delta^{18}\text{O}$ and δD throughout the core sequence being 4.9‰ and 6.42‰ respectively. The evaporation

line for the fractionation-corrected gypsum hydration water $\delta^{18}\text{O}$ and δD isotopic values is defined as $\delta\text{D} = 4.4357 * \delta^{18}\text{O} - 15.262$.

6.5.4.2 – Downcore Evolution of Isotopic Data

Between approximately ~1600-1750_{AD} (unit 6), there are moderate to high $\delta^{18}\text{O}$ and δD values which may be reflective of intermediate evaporation to input ratios and/or potentially moderate decreases in humidity during this timeframe that were synchronous with some increased input of detrital material to the lake. Comparison to regional climatic records and historical land-use records signify that this is most closely synchronous with increasing regional agricultural practices and the expansion of modern irrigation practices (Valero-Garcés *et al.*, 2000b; Doyle *et al.*, 2022b). Following this, the lowest $\delta^{18}\text{O}$ and δD values identified throughout the sequence correspond to approximately ~1800-1850_{AD} (unit 5), and are congruent with both the increased deposition of detrital material during this timeframe (chapter 4) and the XRF data discussed in chapter 5 which also indicated increased detrital inflow to the lake based on increasing concentrations of Ti, Al and K (Valero-Garcés *et al.*, 2000). This suggests that the composition of the water during this time reflected decreased evaporation to inflow ratios, a process that is also apparent from elemental X-ray fluorescence analysis of the same core in a previous study which suggest decreased salinity and increased delivery of detrital material to the system (Doyle *et al.*, 2022a). This likely represents the greatest increase in inflow to the lake throughout the timeframe represented in the core, and correlates with the expansion of olive farming and most likely increased input of irrigation water to the lake from farming activities (Valero-Garcés *et al.*, 2000a).

The increase to moderate and high $\delta^{18}\text{O}$ and δD values associated with the time period of approximately ~1850-1950_{AD} (unit 4) are associated with the formation of microbial mats and increased evaporation (Doyle *et al.*, 2022b), and thus reflect increased evaporative concentration of the isotopic values induced by lower lake levels (Valero-Garcés *et al.*, 2000a; Gázquez *et al.*, 2018). Though it is probable that

climatic factors are responsible for this, it may also be assigned to a reduction in anthropogenic activities and subsequently a reduction in the degree of inflow delivered to the lake via irrigation returns (Doyle *et al.*, 2022a). Following this, the period between approximately 1950~1960_{AD} (unit 3) is characterised by a return to $\delta^{18}\text{O}$ and δD values, again being consistent with sedimentological, geochemical and mineralogical data (Doyle *et al.*, 2022b; a) that indicate a small increase in water level during this time as indicated by extensive organic-rich charophytic muds throughout the lake. Finally, the increase in $\delta^{18}\text{O}$ and δD values throughout the period from ~1960_{AD} to the present day are congruous with the evolution of the lake to its present state (Doyle *et al.*, 2022a), with relative decreases in lake level and evaporitic conditions becoming dominant. Overall, the isotopic data provide excellent supporting evidence in delineating the palaeohydrology of Lake Chiprana throughout the last three centuries. The data furthermore allow for a deeper insight into the composition of the waters of Lake Chiprana throughout this same timeframe, with no effect of temperature upon the fractionated isotopic data (Gázquez *et al.*, 2018). The data additionally provide a framework for future modelling work to be carried out which may be used as a local environmental proxy to be integrated into other regional palaeoclimate and anthropogenic perturbation records.

6.6 - Conclusions

The analysis of mineralogical assemblages by X-ray diffraction techniques, analyses of the isotopic composition of $\delta^{18}\text{O}$ and δD associated with gypsum hydration water and basic hydrochemical modelling of lake waters associated with Lake Chiprana illustrated a complex hydrogeochemical environment whilst also further highlighting the potential applications of such environments as reliable archives of palaeoenvironmental and palaeoclimatic information. The fluctuating abundance of detrital minerals provides an understanding of the provenance of detrital input and subsequently inflow to the lake as induced by changing climatic or anthropogenic perturbations (McHenry *et al.*, 2020). Much of the detrital material appears to be

sourced from the carbonate-rich marls and quartzitic sandstones associated with the catchment drainage basin throughout the 17th to 19th centuries. In tandem, evaporitic minerals and their abundances provide insights into fluctuations in lake levels and the geochemistry of the lakewaters. However, due to the nature of saline Lake Chiprana, such minerals remain high in abundance throughout the sequence, but relative increases identified during the period of ~1850-1950_{AD} and from ~1965_{AD} to the present day are indicative of increasing evaporative concentration and perhaps reduced irrigation returns and precipitation during these timeframes.

Basic hydrochemical modelling of the sequence provides insights into the hydrochemistry of the lakewaters and the effects evaporative processes have upon mineral precipitation and dissolution. The data highlighted supersaturation of the surficial lakewaters with respect to gypsum, aragonite and calcite. Modelled evaporative concentration of the lakewaters indicates that sulphatic and halitic minerals are typically the dominant evaporitic phase, while carbonates become increasingly less significant with greater intensities of evaporation. The hydrochemical model furthermore illustrates a typical precipitation sequence associated with Type IV brines, albeit with an absence of consistent bloedite, epsomite or mirabilite precipitation. It is probable that biotic factors may have inhibited the nucleation and precipitation of these minerals, though further work is required to determine the causes of this specific characteristic.

Furthermore, analyses of the isotopic composition of gypsum hydration water ($\delta^{18}\text{O}$ and δ) were applied in this study, and allow for further understanding of the palaeohydrological evolution of Lake Chiprana throughout the last three to four centuries. $\delta^{18}\text{O}$ and δD compositions provide insights into lake water composition and conditions throughout this timeframe, with heightened values potentially reflecting increased evaporation/inflow ratios and/or lower relative humidity, and vice versa. The data are consistent with the local meteoric water line for Zaragoza, provide a framework for future modelling of the lake, acting as a proxy for variations

in relative humidity and changes in evaporation and inflow. Specifically, the data here suggest decreases in the evaporation/inflow ratio between 1650-1800_{AD}, followed by subsequent increases between 1800-1850_{AD} which largely persist to the present day.

Overall, further modelling should attempt to relate long-term variations in mineral abundances to evaporitic concentration, shedding light onto the degree of lake water evaporation occurring throughout the last three to four centuries, while also considering the potential for biotic processes to influence mineral precipitation and/or dissolution throughout the lake.

References

- Alcocer, J. and Hammer, U.T.** (1998) Saline lake ecosystems of Mexico. *Aquat. Ecosyst. Heal. Manag.*, **1**, 291–315.
- Alonso, M.** (1998) The lagoons of Peninsular Spain. *Limnetica*, **15**, 1–176.
- Baxter, B.K. and Butler, J.K.** (2020) Climate Change and Great Salt Lake. In: *Great Salt Lake Biology*, 23–52.
- Brock, M.A. and Hammer, U.T.** (1987) Saline Lake Ecosystems of the World., 1st edn. *Springer*, Dordrecht, 580 pp.
- Cabestrero, Ó., del Buey, P. and Sanz-Montero, M.E.** (2018) Biosedimentary and geochemical constraints on the precipitation of mineral crusts in shallow sulphate lakes. *Sediment. Geol.*, **366**, 32–46.
- Camacho, A., Miracle, M.R., Romero-Viana, L., Picazo, A. and Vicente, E.** (2017) Lake La Cruz, an Iron-Rich Karstic Meromictic Lake in Central Spain. 187–233.
- Chipera, S.J.S., Vaniman, D.T.D. and Carey, J.W.** (2006) Water Content and Dehydration Behavior of Mg-Sulfate Hydrates.
- Comin, F.A. and Alonso, M.** (1988) Spanish salt lakes: Their chemistry and biota. *Hydrobiologia*, **158**, 237–245.
- Cutts, E.M., Baldes, M.J., Skoog, E.J., Hall, J., Gong, J., Moore, K.R. and Bosak, T.** (2022) Using Molecular Tools to Understand Microbial Carbonates. *Geosci.*

doi: 10.3390/geosciences12050185

- De Wit, R.** (2016) Lake La Salada de Chiprana (NE Spain), an Example of an Athalassic Salt Lake in a Cultural Landscape. In: *Lake Sciences and Climate Change*, 1st edn. (Ed. M.N. Rashed), *IntechOpen*, Rijeka, 43–60.
- De Wit, R., Guerrero, M.C., Legaz, A., Jonkers, H.M., Blocier, L., Gumiaux, C. and Gautret, P.** (2013) Conservation of a permanent hypersaline lake: Management options evaluated from decadal variability of coleofasciculus chthonoplastes microbial mats. *Aquat. Conserv. Mar. Freshw. Ecosyst.*, **23**, 532–545.
- Deocampo, D.M. and Jones, B.F.** (2013) Geochemistry of Saline Lakes. In: *Treatise on Geochemistry: Second Edition*, 2nd edn. (Ed. K. Turekian and H. Holland), *Elsevier*, 7, 437–469.
- Diaz, P., Guerrero, M.C., Alcorlo, P., Baltanas, A., Florin, M. and Montes, C.** (1998) Anthropogenic perturbations to the trophic structure in a permanent hypersaline shallow lake: La Salada de Chiprana (north-eastern Spain). *Int. J. Salt Lake Res.*, **7**, 187–210.
- Domínguez-Castro, F., García-Herrera, R., Ribera, P. and Barriendos, M.** (2010) A shift in the spatial pattern of Iberian droughts during the 17th century. *Clim. Past*, **6**, 553–563.
- Doyle, C., Corella, J.P., Schröder, S., Strauss, H., Bishop, T., Yarwood, J. and Valero-Garcés, B.** (2022a) Spatio-Temporal Variations in the Geochemistry of Laguna Salada de Chiprana, NE Spain. *Geosci.* **12**:
- Doyle, C., Schröder, S., Corella, J.P. and Valero Garces, B.** (2022b) Facies variability and depositional settings of Laguna Salada de Chiprana, an Iberian hypersaline lake. *Sedimentology*, **69**, 2615–2641.
- Dupraz, C., Reid, R.P., Braissant, O., Decho, A.W., Norman, R.S. and Visscher, P.T.** (2009) Processes of carbonate precipitation in modern microbial mats. *Earth-Science Rev.*, **96**, 141–162.
- Dupraz, C., Visscher, P.T., Baumgartner, L.K. and Reid, R.P.** (2004) Microbe-mineral interactions: Early carbonate precipitation in a hypersaline lake

- (Eleuthera Island, Bahamas). *Sedimentology*, **51**, 745–765.
- Garber, R.A., Levy, Y. and Friedman, G.M.** (1987) The sedimentology of the Dead Sea. *Carbonates and Evaporites*, **2**, 43–57.
- Gázquez, F., Evans, N.P. and Hodell, D.A.** (2017) Precise and accurate isotope fractionation factors ($\alpha^{17}\text{O}$, $\alpha^{18}\text{O}$ and αD) for water and $\text{CaSO}_4 \cdot 2\text{H}_2\text{O}$ (gypsum). *Geochim. Cosmochim. Acta*, **198**, 259–270.
- Gázquez, F., Monteserín, A., Obert, C., Fernández-Cortés, Á. and Calaforra, J.M.** (2022) The Absolute Age and Origin of the Giant Gypsum Geode of Pulpí (Almería, SE Spain). *Geosci.* doi: 10.3390/geosciences12040144
- Gázquez, F., Morellón, M., Bauska, T., Herwartz, D., Surma, J., Moreno, A., Staubwasser, M., Valero-Garcés, B., Delgado-Huertas, A. and Hodell, D.A.** (2018) Triple oxygen and hydrogen isotopes of gypsum hydration water for quantitative paleo-humidity reconstruction. *Earth Planet. Sci. Lett.*, **481**, 177–188.
- Guerrero, M.C., Balsa, J., Pascual, M. and Martínez, B.** (1991) Caracterización limnológica de la Laguna Salada de Chiprana (Zaragoza, España) y sus comunidades de bacterias fototróficas. *Limnetica*, **7**, 83–96.
- Hardie, L. and Eugster, H.** (1970) Evolution of closed-basin brines. *Miner. Soc. Amer. Spec.*, **3**, 273–290.
- IGME** (2003) Mapa Geológico de España, 1:50000, (serie MAGNA). Hoja 988. Puente-Genil.
- Jódar, J., Rubio, F.M., Custodio, E., Martos-Rosillo, S., Pey, J., Herrera, C., Turu, V., Pérez-Bielsa, C., Ibarra, P. and Lambán, L.J.** (2020) Hydrogeochemical, isotopic and geophysical characterization of saline lake systems in semiarid regions: The Salada de Chiprana Lake, Northeastern Spain. *Sci. Total Environ.*, **728**, 1–48.
- Jonkers, H.M., Ludwig, R., De Wit, R., Pringault, O., Muyzer, G., Niemann, H., Finke, N. and De Beer, D.** (2003) Structural and functional analysis of a microbial mat ecosystem from a unique permanent hypersaline inland lake: “La Salada de Chiprana” (NE Spain). *FEMS Microbiol. Ecol.*, **44**, 175–189.

- Last, F.M.** (2013) Carbonate microbialite formation in a prairie saline lake in Saskatchewan, Canada: paleohydrologic and paleoenvironmental implications. University of Manitoba
- Leprich, D.J., Flood, B.E., Schroedi, P.R., Ricci, E., Marlow, J.J., Girguis, P.R. and Bailey, J. V.** (2021) Sulfur bacteria promote dissolution of authigenic carbonates at marine methane seeps. *ISME J.* doi: 10.1038/s41396-021-00903-3
- Logan, B.W.** (1987) The MacLeod Evaporite Basin, Western Australia_{title>Holocene Environments, Sediments and Geological Evolution}.
- López-Blanco, C. and Romero-Viana, L.** (2019) Dry and wet periods over the last millennium in central-eastern Spain a paleolimnological perspective. *Limnetica.* doi: 10.23818/limn.38.03
- Luzón, A.** (2005) Oligocene-Miocene alluvial sedimentation in the northern Ebro Basin, NE Spain: Tectonic control and palaeogeographical evolution. *Sediment. Geol.*, **177**, 19–39.
- Martín-Puertas, C., Valero-Garcés, B.L., Mata, M.P., González-Sampériz, P., Bao, R., Moreno, A. and Stefanova, V.** (2008) Arid and humid phases in southern Spain during the last 4000 years: The Zoñar Lake record, Córdoba. *Holocene*, **18**, 907–921.
- Martín-Puertas, C., Valero-Garcés, B.L., Mata, M.P., Moreno, A., Giral, S., Martínez-Ruiz, F. and Jiménez-Espejo, F.** (2011) Geochemical processes in a Mediterranean Lake: A high-resolution study of the last 4,000 years in Zoñar Lake, southern Spain. *J. Paleolimnol.*, **46**, 405–421.
- McHenry, L.J., Kodikara, G.R.L., Stanistreet, I.G., Stollhofen, H., Njau, J.K., Schick, K. and Toth, N.** (2020) Lake conditions and detrital sources of Paleolake Olduvai, Tanzania, reconstructed using X-ray Diffraction analysis of cores. *Palaeogeogr. Palaeoclimatol. Palaeoecol.*, **556**, 1–24.
- Mees, F., Castañeda, C., Herrero, J. and Van Ranst, E.** (2011) Bloedite sedimentation in a seasonally dry saline lake (Salada Mediana, Spain).

- Mercedes-Martín, R., Rao, A., Rogerson, M. and Sánchez-Román, M. (2022)** Effects of salinity, organic acids and alkalinity on the growth of calcite spherulites: Implications for evaporitic lacustrine sedimentation. *Depos Rec.* doi: 10.1002/dep2.136
- Morellón, M., Aranbarri, J., Moreno, A., González-Sampériz, P. and Valero-Garcés, B.L. (2018)** Early Holocene humidity patterns in the Iberian Peninsula reconstructed from lake, pollen and speleothem records. *Quat. Sci. Rev.*
- Morellón, M., Valero-Garcés, B., Anselmetti, F., Ariztegui, D., Schnellmann, M., Moreno, A., Mata, P., Rico, M. and Corella, J.P. (2009)** Late quaternary deposition and facies model for karstic Lake Estanya (North-eastern Spain). *Sedimentology*, **56**, 1505–1534.
- Morellón, M., Valero-Garcés, B., González-Sampériz, P., Vegas-Vilarrúbia, T., Rubio, E., Rieradevall, M., Delgado-Huertas, A., Mata, P., Romero, Ó., Engstrom, D.R., López-Vicente, M., Navas, A. and Soto, J. (2011)** Climate changes and human activities recorded in the sediments of Lake Estanya (NE Spain) during the Medieval Warm Period and Little Ice Age. *J. Paleolimnol.*, **46**, 423–452.
- Négrel, P., Petelet-Giraud, E. and Millot, R. (2016)** Tracing water cycle in regulated basin using stable $\delta^{18}\text{O}$ - $\delta^2\text{H}$ isotopes: The Ebro river basin (Spain). *Chem. Geol.*, **422**, 71–81.
- Ontiveros-Cuadras, J.F., Ruiz-Fernández, A.C., Sanchez-Cabeza, J.A., Pérez-Bernal, L.H., Preda, M. and Páez-Osuna, F. (2018)** Mineralogical signatures and sources of recent sediment in a large tropical lake. *Int. J. Sediment Res.*, **33**, 183–190.
- Parkhurst, D.L. (2021)** PhreeqC Forums. <https://phreeqcusers.org/index.php?topic=1890.0>.
- Parkhurst, D.L. (1995)** User's guide to PHREEQC: a computer program for speciation, reaction-path, advective-transport, and inverse geochemical calculations. *Lakewood, Colo.: U.S. Dept. of the Interior, U.S. Geological*

Survey; Denver, CO: Earth Science Information Center, Open-File Reports Section [distributor], 1995.

- Parkhurst, D.L. and Appelo, C.A.J.** (2013) Description of input and examples for PHREEQC Version 3 — A computer program for speciation, batch-reaction, one-dimensional transport, and inverse geochemical calculations.
- Renaut, R.W. and Last, W.M.** (1994) Sedimentology and geochemistry of modern and ancient saline lakes. *Sedimentol geochemistry Mod Anc saline lakes*. doi: 10.2110/pec.94.50
- Sanz-Montero, M.E., Cabestrero, Ó. and Sánchez-Román, M.** (2019) Microbial Mg-rich carbonates in an extreme alkaline lake (Las Eras, Central Spain). *Front. Microbiol.*, **10**, 1–15.
- Schnurrenberger, D., Russell, J. and Kelts, K.** (2003) Classification of lacustrine sediments based on sedimentary components. *J. Paleolimnol.*, **29**, 141–154.
- Schröder, T., van 't Hoff, J., Ortiz, J.E., de Torres Pérez-Hidalgo, T.J., López-Sáez, J.A., Melles, M., Holzhausen, A., Wennrich, V., Viehberg, F. and Reicherter, K.** (2018) Shallow hypersaline lakes as paleoclimate archives: A case study from the Laguna Salada, Málaga province, southern Spain. *Quat. Int.*, **485**, 76–88.
- Seguin, J., Avramidis, P., Haug, A., Kessler, T., Schimmelmann, A. and Unkel, I.** (2020) Reconstruction of palaeoenvironmental variability based on an inter-comparison of four lacustrine archives on the Peloponnese (Greece) for the last 5000 years. *E&G Quat. Sci. J.*, **69**, 165–186.
- Valero-Garcés, B., Morellón, M., Moreno, A., Corella, J.P., Martín-Puertas, C., Barreiro, F., Pérez, A., Giralt, S. and Mata-Campo, M.P.** (2014) Lacustrine carbonates of Iberian Karst Lakes: Sources, processes and depositional environments. *Sediment. Geol.* 299:1–29.
- Valero-Garcés, B.L. and Kelts, K.R.** (1995) A sedimentary facies model for perennial and meromictic saline lakes: Holocene Medicine Lake Basin, South Dakota, USA. *J. Paleolimnol.*, **14**, 123–149.
- Valero-Garcés, B.L. and Moreno, A.** (2011) Iberian lacustrine sediment records:

Responses to past and recent global changes in the Mediterranean region. *J. Paleolimnol.*

Valero-Garces, B.L., Navas, A., Machin, J., Stevenson, T. and Davis, B. (2000)

Responses of a saline lake ecosystem in a semiarid region to irrigation and climate variability: The history of Salada Chiprana, central Ebro basin, Spain. *Ambio*, **29**, 344–350.

Valero-Garcés, B.L., Navas, A., Machin, J., Stevenson, T., Davis, B., Valero-

Garcés, B.L., Navas, A., Machin, J., Stevenson, T., Davis, B., Valero-Garcés, B.L., Navas, A., Machin, J., Stevenson, T. and Davis, B. (2000a)
Responses of a Saline Lake Ecosystem in a Semiarid Region to Irrigation and Climate Variability. *AMBIO A J. Hum. Environ.*, **29**, 344–350.

Valero-Garcés, B.L., Navas, A., Machin, J., Stevenson, T., Davis, B., Valero-

Garcés, B.L., Navas, A., Machin, J., Stevenson, T., Davis, B., Valero-Garcés, B.L., Navas, A., Machin, J., Stevenson, T. and Davis, B. (2000b)
Responses of a saline lake ecosystem in a semiarid region to irrigation and climate variability: The history of Salada Chiprana, central Ebro basin, Spain. *Ambio*, **29**, 344–350.

Vidondo, B., Martínez, B., Montes, C. and Guerrero, M.C. (1993)

Physico-chemical characteristics of a permanent Spanish hypersaline lake: La Salada de Chiprana (NE Spain). *Hydrobiologia*, **267**, 113–125.

Yechieli, Y. and Wood, W.W. (2002)

Hydrogeologic processes in saline systems: Playas, sabkhas, and saline lakes. *Earth-Science Rev.* doi: 10.1016/S0012-8252(02)00067-3

Supplementary Material

PhreeqC Code (Parkhurst, 2021)

```
SOLUTION 1
units      ppm
      Alkalinity 130 as CaCO3
      pe          0
```

```

        redox      pe
        temp      25
        pH        9.60
        Cl        8231.781
        Br        36.959
        S(6)      25679.449
        Na        9618.6691
        K         192.057
        Ca        585.604
        Mg        8233.564
        density 1
        -water 1 # kg
END
USE solution 1
EQUILIBRIUM_PHASES 1
Calcite 0 0
Aragonite 0 0
Gypsum 0 0
Halite 0 0
Hexahydrite 0 0
Thenardite 0 0

REACTION
H2O -1
52.7725 moles in 95 steps
USER_GRAPH 1
    -headings          Factor Calcite Aragonite Gypsum
    Halite Hexahydrite Thenardite
    -axis_titles       "Concentration factor"
    "Precipitation, moles" ""
    -initial_solutions true
    -connect_simulations true
    -plot_concentration_vs x
    -start
10 GRAPH_X 1 / TOT("water")
20 GRAPH_Y EQUI("Calcite"), EQUI("Aragonite"),
EQUI("Gypsum"), EQUI("Halite"), EQUI("Hexahydrite"),
EQUI("Thenardite")
    -end
    -active            true

PRINT
SELECTED_OUTPUT 1
-file          output.xls
-high_precision true
-reset         true
-simulation    true
-state         true
-solution      true
-distance      true
-time          true
-step          true
-pH            true
-pe            true
-reaction      true
-temperature   true
-alkalinity    true
-ionic_strength true
-water         true
-charge_balance true
-percent_error  true

```

-totals	C	Cl	Br	S(6)	Na	K	Ca	Mg			
-molalities	OH-		H+		H2O	Br	Br-		C(4)	MgCO3	CO3-2
	HCO3-	CO2	Ca	Ca+2	Cl	Cl-			K	K+	Mg
	Mg+2	MgCO3	MgOH+	Na	Na+	S(6)			SO4-2	HSO4-	
-saturation_indices			Anhydrite		Aragonite				Arcanite		
	Artinite		Bischofite		Bloedite				Brucite		
	Burkeite		Calcite		Carnallite				CO2(g)		
	Dolomite		Epsomite		Gaylussite				Glaserite		
	Glauberite		Goergeyite		Gypsum				H2O(g)		Halite
	Hexahydrate		Huntite		Kainite				Kalicynite		
	Kieserite		Labile_S		Leonhardite				Leonite		
	Magnesite		MgCl2_2H2O		MgCl2_4H2O				Mirabilite		
	Misenite		Nahcolite		Natron				Nesquehonite		
	Pentahydrate		Pirssonite		Polyhalite				Portlandite		
	Schoenite		Sylvite		Syngenite				Thenardite		Trona

END

Chapter 7 - Development of modern and sub-recent lacustrine microbialites in southwestern Europe: Insights into environmental and depositional controls using X-Ray CT and petrography

Connor Doyle^a, Juan Pablo Corella^b, Stefan Schroeder^a, Julia Behnsen^c, Mario Morellon^d, Celia Martin-Puertas^e, Blas Valero Garces^f

a - Department of Earth and Environmental Sciences, University of Manchester, Manchester, UK

b - CIEMAT - Environmental Department (DMA), Avenida Complutense 40, E-28040 Madrid, Spain

c – Henry Moseley X-Ray Imaging Facility, Royce Hub Building, University of Manchester, Manchester, UK

d – Departamento de Geodinámica, Estratigrafía y Paleontología, Facultad de Ciencias Geológicas, Universidad Complutense de Madrid, Calle José Antonio Nováis 12, E-28040 Madrid, Spain

e – Department of Geography, Royal Holloway University of London, Egham Hill, Egham, TW20 0EX, Surrey (UK)

f - Instituto Pirenaico de Ecología, Consejo Superior de Investigaciones Científicas, Zaragoza, Spain

Corresponding Author Email: connor.doyle@manchester.ac.uk

Abstract

Microbial mats and microbialites are described in both modern and ancient saline lacustrine environments, and they are highly responsive to a variety of intrinsic and extrinsic factors. Their distribution spans from the Archaean to the modern day, and as such, they are considered important sources of high-resolution environmental data across a wide range of geological time. Nonetheless, they have been somewhat overlooked as such repositories due to many factors such as diagenetic modification, preservation, and complex characteristics. In this study, X-ray computed tomographical (CT) scans were undertaken in tandem with high resolution morphological and petrographic analyses of modern and sub-recent microbial mats from several sites in the Iberian Peninsula in order to determine relationships between microbialite morphology, texture, and environmental controls. The peninsula is host to many saline lakes which contain microbial mats throughout their sedimentary sequences. Modern microbial mats were sampled from Laguna Salada de Chiprana, a permanent hypersaline lake in Northeast Spain, while sub-recent (0.1-10ka) mats were sampled from sediment cores also from Lake Chiprana and from previously retrieved cores from Lago de Arreo, a saline lake in Northern Spain, Laguna Zonar, a saline lake in southern Spain, and Lago de Estanya, a brackish-saline lake in North-eastern Spain. Variations in microbialite (micro-)morphology, composition and texture provide insights into environmental factors occurring in the different settings, and allow for an opportunity to understand how microbialites developed in distinctive sedimentological and geochemical environments of varying age. The increased abundance of grains within microbialites such as those from Lake Arreo and Lake Estanya suggest an increase in trapping and binding, while mineralogical phases such as gypsum generate proliferate mat structures and generate domal structures within mats from Lake Chiprana and Zonar. Understanding the controls on these unique deposits in a range of settings and timescales and how such controls produce varying microbialite characteristics will allow for a clearer understanding of how microbialites can be effectively used in palaeoenvironmental reconstruction.

7.1 Introduction

Microbialites are described by Burne and Moore (1987) as 'organosedimentary deposits that have accreted as a result of a benthic microbial community trapping and binding detrital sediment and/or forming the locus of mineral precipitation'. They are unique sedimentary deposits that have been discovered in a wide range of marine to terrestrial settings (Schieber, 2007; Franks & Stolz, 2009; Bourillot *et al.*, 2020), and their formation has been documented from the early Precambrian to the present day, with the oldest examples from Western Australia and southwest Greenland up to 3.4-3.7 billion years old (Nutman *et al.*, 2016; Suosaari *et al.*, 2016). Many microbialites are restricted to environments where conditions are extreme as a result of high salinity or complex geochemical characteristics (White, 2020). Key examples include parts of the marine realm (Stal *et al.*, 1985; Dupraz & Visscher, 2005; Ginsburg & Planavsky, 2008; Suosaari *et al.*, 2018), alkaline lakes (Sanz-Montero *et al.*, 2013), and in the case of this study, saline lakes (Guerrero, 1992; De Wit *et al.*, 2013). Thus, microbial mats are increasingly being recognised as archives with which palaeoenvironmental and palaeobiological change can be reconstructed (Dupraz *et al.*, 2009; Hickman-Lewis *et al.*, 2019), and due to their broad geological range (Chen & Lee, 2014), are considered excellent indicators of long-term geological and environmental change.

A range of microbialite studies have provided insights into the factors controlling the characteristics of these deposits (Stal *et al.*, 1985; Bowlin *et al.*, 2012; Pace *et al.*, 2016; Cardoso *et al.* 2019). In many settings throughout geological time, environmental conditions are well known to cause variations in the form, chemical composition and structure of microbialites as well as the microbial community (Dupraz *et al.*, 2004; Verleyen *et al.*, 2010). In tandem, many studies have also shown that microbes can exhibit a wide range of biological processes which may lead to subsequent changes in their local environment (Baumgartner *et al.*, 2009; Dupraz *et al.*, 2009). Examples of factors which may affect mat development include the microbes present in the mat (Dupraz *et al.*, 2004; Prieto-Barajas *et al.*, 2018),

the types of chemical cycling (Canfield & Des Marais, 1993; Wong *et al.*, 2018), the degree of both biotic and abiotic mineral precipitation and trapping of detritus (Dupraz & Visscher, 2005; Riding, 2011), and the geochemical composition of the mat itself (Wingender *et al.*, 1999; Braissant *et al.*, 2007). In contrast, environmental factors leading to variations in mat morphology may include the amount of available accommodation space (Riding, 2011; Bouton *et al.*, 2016b), rates of deposition (Johnson & Grotzinger, 2006; Mackey *et al.*, 2017b), the availability of light (Nishida *et al.*, 2018), and the geochemistry of the environment they develop within (Grotzinger & Rothman, 1996; Bowlin *et al.*, 2012). In turn, microbialites are associated with a wide range of sedimentary features and petrographic characteristics, and as such, a significant issue that is still present when studying these deposits is the comparison of modern and ancient microbialite features and subsequently what information they can hold when reconstructing palaeoenvironmental conditions (Tan *et al.*, 2018; Bourillot *et al.*, 2020). Thus, further investigations are needed if the relationships between environmental and biological factors and microbialite development in both the modern and the geological past are to be understood.

In this study, samples of modern and sub-recent (Holocene) microbial mats from multiple lacustrine sites were characterised both by computerised tomographical (CT) scanning and detailed petrography. This was carried out to determine the variety of morphological and textural characteristics associated with them, while shedding light on what controls may influence these characteristics, and how such texture may be related to environment. The studied examples are sourced from the modern lakebeds and Holocene sedimentary sequences of several saline-hypersaline lacustrine systems located in the Iberian Peninsula (Guerrero, 1992) governed by a range of physicochemical conditions. At the mesoscale (>1cm), microbialites throughout this study are described using tomographical scans, which provide greater three-dimensional detail into mat structure, texture and morphology than standard naked-eye observations and core description. This description is

presented according to the classification scheme defined by Grey & Awramik (2020). Key characteristics described include the margins of the microbialites and their relationship to surrounding sediment and bedding planes, their plan view morphology, overall shape and morphology in cross-section, height to width, the variability of the growth of each microbialite structure, and the attitude (e.g. angles of growth) of the mat structure. This scheme provides context as to the descriptive terms used in this study and their application to the microbialite deposits from each of the lacustrine settings. At the sub-meso to micro-scale, microbialite texture and fabric are assessed using light and scanning electron microscopy following the nomenclature of the same scheme. By providing insights into the morphological, petrographic and textural characteristics of these deposits, the goal of the study is to understand how key textures and fabrics can provide clearer insights into the environment of deposition that microbialites formed within. Understanding the texture, fabric and morphology of microbialites is ultimately critical for the interpretation of palaeoenvironmental processes, application to the fossil record, and linkage of modern processes to ancient products.

7.2 Site Background & Methods

7.2.1 Study Settings

Figure 7.1 illustrates the four sites chosen for this study. Each contains evidence of microbial mat development occurring either within their modern lakebeds or Quaternary sedimentary sequences and were selected due to the presence of these deposits and also due to the large amount of work previously undertaken upon their sedimentary sequences (González-Sampérez *et al.*, 2008; Martín-Puertas *et al.*, 2008, 2011; Morellón *et al.*, 2009b; Corella *et al.*, 2013). Both modern and sub-recent (~0.1-0.2ka) mats were studied in Laguna Salada de Chiprana, while sub-recent (<0.5ka) and Late to Early Holocene (0.8-9.4ka) age mats were sampled from three other lakes: Lago de Estanya, Laguna Zonar and Lago de Arreo, situated in the Northeast, South, and North of Spain, respectively. Lake Chiprana has been described by several studies recently (Valero-Garcés *et al.*, 2000; Doyle *et al.*,

2022b), while lakes Arreo (Corella *et al.*, 2011, 2013, 2021), Estanya (Morellón *et al.*, 2008, 2009a, 2011) and Zonar (Martín-Puertas *et al.*, 2008, 2009, 2011) have been described in the recent past and their sedimentary sequences characterised.

7.2.1.1 Laguna Salada de Chiprana

Laguna Salada de Chiprana (Lake Chiprana, 41°14'30"N, 0°10'50"W) is represented by a 0.18km², 4-5m deep waterbody situated approximately 140m above sea level in the Northeastern region of the Iberian Peninsula. The regional climate is Mediterranean (De Wit *et al.*, 2013), with an average temperature of 15.5°C (Domínguez-Castro *et al.*, 2010). There is high evapotranspiration (~1500mm/yr) and moderate groundwater output (~1000mm/yr), while inflow from irrigation is the primary input to the lake (~1700mm/yr). Rainfall (~300-400mm/yr) and groundwater input (~300mm/yr) are both low (Jódar *et al.*, 2020). July is the driest month of the year, whilst the most humid months are May and October. The geological setting of the lake is represented by Oligo-Miocene marls, siltstones and sandstones (IGME, 2003a).

7.2.1.2 Lago de Estanya

Lago de Estanya (42°01'44.2"N 0°31'44.2"E) is located 670m above sea level near the small town of Estaña in North-eastern Spain (Morellón *et al.*, 2009a). The 2.45km², brackish lake has a closed hydrological system which receives influxes of groundwater input and drainage from nearby streams, and evapotranspiration is the primary outflow (Morellón *et al.*, 2009a). The underlying geology of the lake and the surrounding region is characterised by Triassic Muschelkalk and Keuper facies which formed the lake basin following dissolution and karstification processes (Morellón *et al.*, 2009a; Valero-Garcés *et al.*, 2014), while overlying Cretaceous sandstones, mudstones and carbonates followed occur to the Southwest of the basin (IGME, 2003b; Morellón *et al.*, 2009a). Various quaternary age gravels, sandstones

and calcareous muds are also distributed throughout the catchment area (IGME, 2003b).

7.2.1.3 Laguna Zonar

Laguna Zonar (37°29'00"N, 4°41'22"W) is situated 300 metres a.s.l, and is represented by a 0.37km², 15m deep saline waterbody in the Córdoba province of Southern Spain (Martín-Puertas *et al.*, 2008). The lake's hydrological balance is governed by input from several springs that drain to the lake and output by evaporation (Martín-Puertas *et al.*, 2011). The geological setting is defined by Triassic age mixed calcareous mudstones, evaporites and carbonates (IGME, 2003b; Martín-Puertas *et al.*, 2008), as well as large formations of Neogene to Miocene age calcareous mudstones and clays (IGME, 2003b). Several formations of Pleistocene to Holocene age conglomerates, sandstones and claystone-mudstones are also present in the area and directly surrounding the lake basin (IGME, 2003b).

7.2.1.4 Lago de Arreo

Lago de Arreo (42° 46' N, 2° 59' W; 655 m a.s.l.) is located approximately 650m a.s.l in the Basque Country in Northeast Spain (Corella *et al.*, 2011). The lake is represented by a 0.0657km², 24-metre deep waterbody, and is currently hydrologically open with two small inlets to the west and east providing input and output to and from the lake, respectively. The site is governed by an Atlantic-Mediterranean climate (Corella *et al.*, 2011), with an average temperature of 13°C and an average annual calculated rainfall of 670mm (Corella *et al.*, 2021). It is brackish to saline and characterised by an abundance of Ca, Mg, Na, SO₄ and HCO₃⁻ ions. The lake's geological setting is defined by Triassic claystones and mudstones, and volcanic rocks termed "ophites" appear in small outcrops throughout the catchment (IGME, 2003a; Corella *et al.*, 2011).

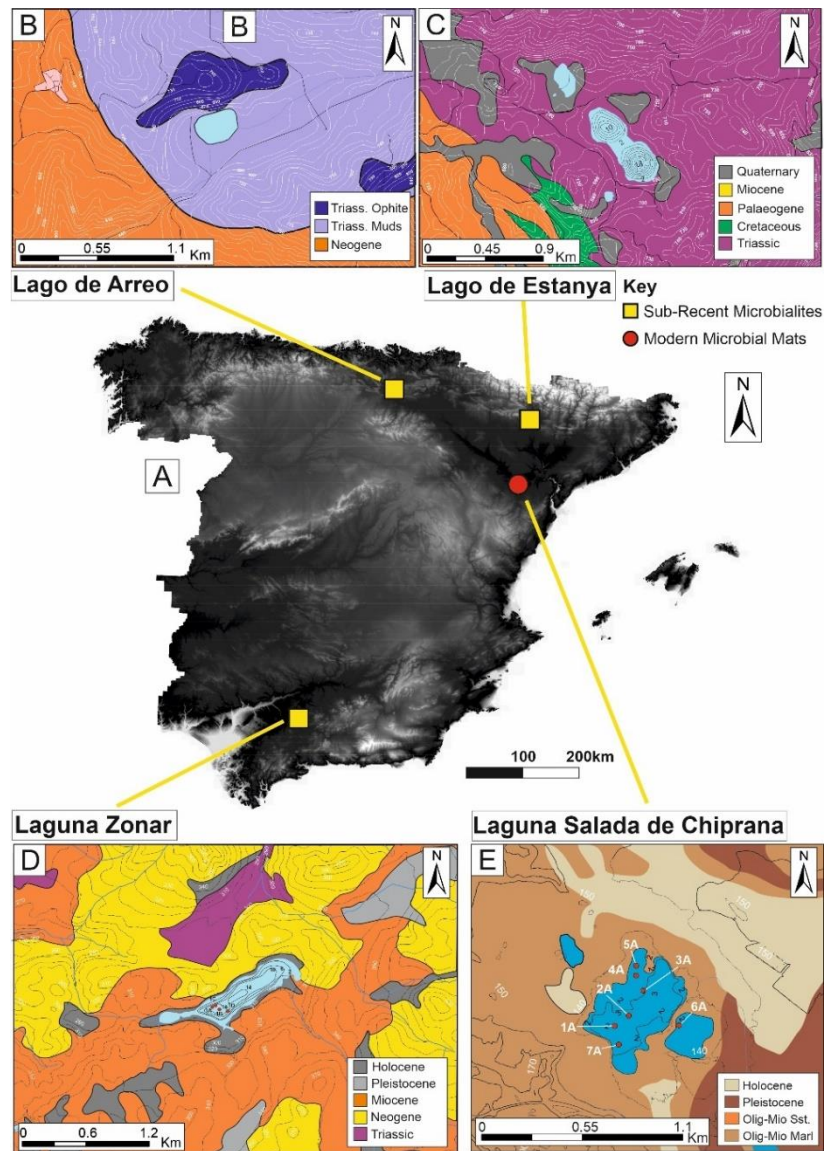


Figure 7.1 – Site location maps illustrating A) Digital elevation model of the Iberian Peninsula with the sites under investigation marked by corresponding markers. The red circle indicates the site contains modern mats, while the yellow squares indicate that the site contains sub-recent mats preserved in the sedimentary record. B) Topographical map/digital elevation model of Lago de Arreo within the Basque country. The pink area is the village of Villambrosa, and two rivers flowing into the lake occur to the East and Southwest. C) Topographical map/digital elevation model of karstic Lago de Estanya within the Benabarre region of the Pre-Pyrenees, D) Topographical map/digital elevation model of Laguna Zonar within the Cordoba region of Southern Spain, with the location of sediment cores marked, E) Topographical map/digital elevation model of Laguna Salada de Chiprana within the Caspe region of Northeastern Spain, with the location of sediment cores marked. Geological data from IGME (2003a; b; c; d), DEM data from CNIG.

7.2.2 Sampling

Modern microbial mats were sampled from the littoral and profundal environments of Lake Chiprana using a sterilised trowel and a UWITEC gravity corer operated from a boat. Fresh microbial mat samples were immediately frozen and stored at -20°C at the Instituto Pirenaico de Ecología. Sub-recent samples of microbialites were collected from sediment cores previously retrieved from Lago de Arreo (Corella *et al.*, 2013), Laguna Zonar (Martín-Puertas *et al.*, 2009, 2011) and Lago de Estanya (Morellón *et al.*, 2009b; a) in 2004, and from seven short sediment cores that were collected in a Northeast-Southwest transect (Figure 7.2) from Lake Chiprana in 2019 (Doyle *et al.*, 2022b). The sampled cores from Lakes Arreo, Estanya and Zonar are stored at the Instituto Pirenaico de Ecología in Zaragoza and Jaca, Spain, while the cores collected from Lake Chiprana are stored at the University of Manchester Geography Laboratories. Microbialites from each core were sampled by collecting sediment blocks between 10-25cm in length from areas of interest following sedimentological descriptions and analyses (Figure 8.2). 98 thin sections were generated from the samples for this study.

7.2.3 Computerised Tomographical Scanning

Morphological characteristics of microbial mats and associated sediments were initially described and interpreted using naked-eye observations (Stolz, 1994). However, techniques such as computerised tomographical (CT) scanning, which have become more commonplace in recent decades (Hickman-Lewis *et al.*, 2017; Emmanouilidis *et al.*, 2020), were utilised in this study to gain detailed insights into the morphological and compositional characteristics of the microbialite deposits. In this study, samples were subjected to computerised tomographical scanning at the Henry Moseley X-ray Imaging Facility (HMxIF), School of Materials, the University of Manchester, using a Nikon High Flux XTEK Bay. Sediment cores were placed into a cylindrical sample holder and mounted onto the rotating stage, whilst smaller rectangular sediment blocks were secured in a small plastic container on the same stage. In both cases, the scans were undertaken by utilising a chromatic

X-ray beam with parameters set at an accelerating voltage of 210kV and a current of 210 μ A (Engelberg *et al.*, 2012). Sequential scans of 10cm x 12cm areas of larger samples were undertaken at regular intervals and stitched together. A 1mm thick copper filter was also placed over the tungsten X-ray source to reduce beam hardening (Engelberg *et al.*, 2012). The X-ray projections produced by the instrument were initially constructed in a 16-bit filetype in the AVIZO® Lite software package, and reduced to an 8-bit filetype in order to reduce the size of the dataset for workability. The dataset was also passed through a 2-step median filter to reduce noise. Voxel size and resolution typically ranged between 0.075 and 0.1mm.

7.2.4 Petrography

Thin sections were generated parallel to microbialite and sediment structures. Samples extracted from cores and lakebed sediments were initially saturated with water on extraction and were shock-frozen with liquid nitrogen and freeze-dried for several days. Dried samples were impregnated with EpoFlo resin and cured prior to sectioning at the University of Durham Thin Section Laboratory. Thin section analyses were performed at the University of Manchester Department of Earth and Environmental Sciences, and observations of sections were undertaken under transmitted light using a NIKON LV100 petrographic microscope. Images were additionally compiled using the Petrog 4.0 Software in both singular image and image stitching modes to generate entire-section scans. SEM-EDS (energy dispersive spectroscopy) analyses were also conducted in order to determine mineralogical compositions and the micro-scale textures and fabric associated with the mats. Analyses were performed using two instruments at the University of Manchester Department of Earth and Environmental Sciences: a Philips XL30 environmental SEM, and a FEI QUANTA 650 SEM with Bruker Instruments Quantax 70 EDX. In addition, a select number of samples were also analysed at the University of Liverpool using a Hitachi TM3000 Environmental SEM at 15kV with Bruker Quantax70 software. For all instruments, samples were carbon-coated using a

Cressington 208 Carbon Coater. Elemental maps were also generated using the EDS-mapping feature of the FEI 650 QUANTA SEM.

7.2.5 Microbialite Description

Microbialites throughout this study are described according to the classification scheme defined by Grey & Awramik (2020) which considers a wide range of characteristics of microbialites. Key characteristics described throughout include the margins of the microbialites and their relationship to surrounding sediment and bedding planes, their plan view morphology, overall shape and morphology in cross-section view, height to width classifications, the variability of the growth of each microbialite structure, and the attitude (e.g. angles of growth) of the mat structure (see Table 7.2). This scheme provides context as to the descriptive terms used in this study and their application to the microbialite deposits from each of the lacustrine settings, and forms the framework for description of structures at both the mesoscale (>1cm) and microscale (<1cm) throughout this study.

7.3 Results

The cores and sediment slabs investigated in this study revealed a range of features associated with microbial mats in addition to a range of facies associated with each of the lakes (Martín-Puertas *et al.*, 2009; Morellón *et al.*, 2009a; Corella *et al.*, 2013; Doyle *et al.*, 2022b). Integrated computerised tomographical scans and petrographic whole-section scans in addition to photomicrographs and SEM analyses of key textures of microbialites from each setting are presented in Figures 7.4-7.12. CT images are presented in the XY (axial), XZ and YZ (longitudinal) planes, while petrographic analyses are presented both as whole thin-section scans and individual photomicrographs. Varying textures, fabrics and components were observed in both modern and sub-recent samples at both the meso and micro scale.

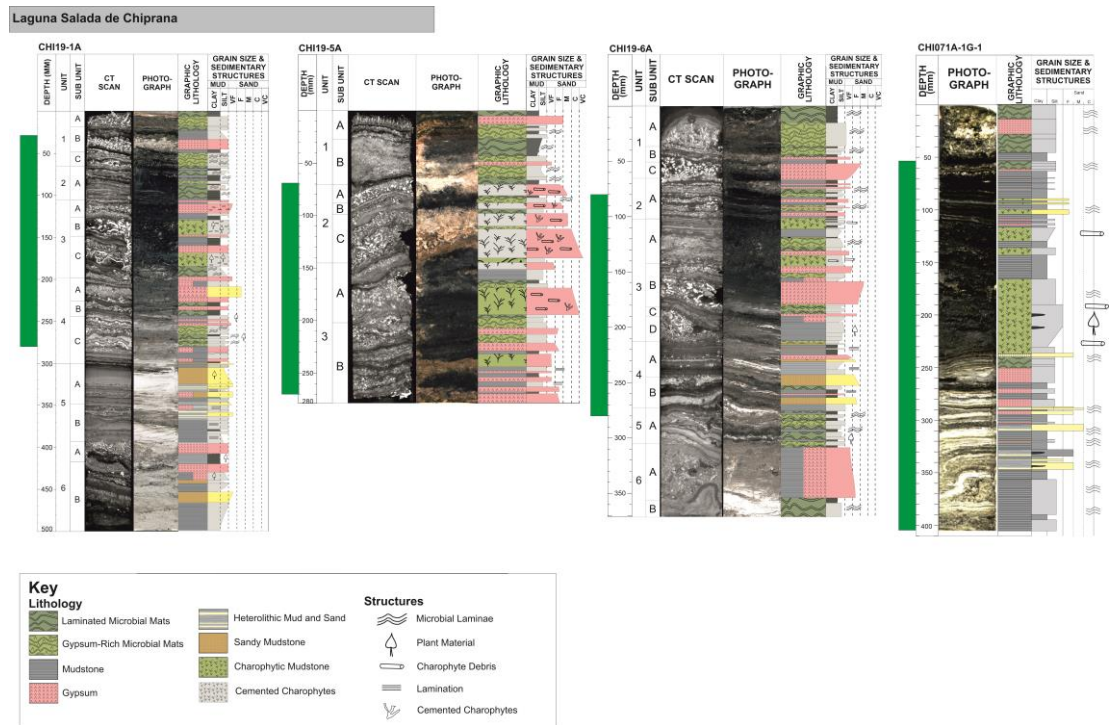


Figure 7.2a – Core logs of Laguna Salada de Chiprana with associated high-resolution photographs, lithology and approximate grain size. Cores CHI19-1A, 5A, 6A (2019) and CHI07-1A (2007) were sampled from Lake Chiprana. The locations of microbial mats sampled for this study are highlighted by green boxes with associated sample identifiers. Sample identifier prefixes relate to the depositional environment from which mats were taken. P = Profundal, L = Littoral. Suffixes a, b, c, etc. indicate samples taken from the same interval of microbial mats,

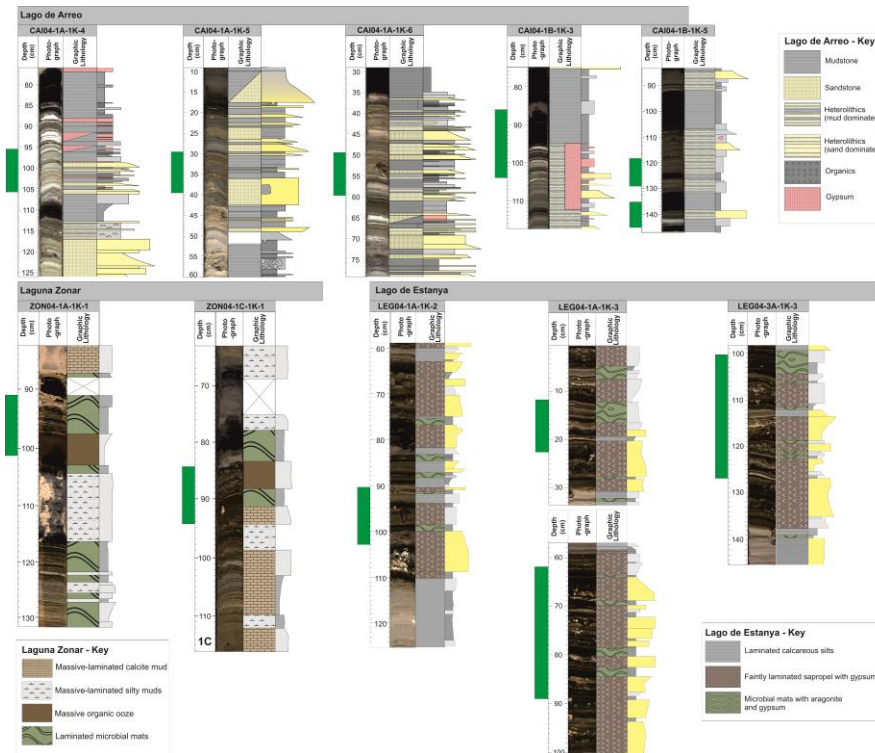


Figure 7.2b – Core logs of Lago de Arreo (Corella *et al.*, 2011, 2013), Laguna Zonar (Martín-Puertas *et al.*, 2008, 2009, 2011) and Lago de Estanya (Morellón *et al.*, 2009a; b, 2011) with associated photographs, lithology and approximate grain size. Green boxes highlight the locations at which samples were taken from the cores, with prefix A indicating a sample from Lago de Arreo, prefix Z indicating a sample from Laguna Zonar, and prefix E indicating a sample from Lago de Estanya.

7.3.1 Overview

Microbialite morphology and texture, defined using the scheme of Grey & Awramik (2020), include a range of characteristics in both plan view and cross-section as depicted throughout Figures 7.3-7.7. Morphological characteristics include varying contortion of laminae, distinctive morphological features such as pinnacles and tufts, compositional characteristics; including the presence of detrital, calcitic and gypsiferous material and the degree of interconnectivity between laminae. The key features identified at this scale are summarised in Table 7.1 with key examples from CT scans. At the micro-scale, petrographic analyses highlighted eleven textures and fabrics (Table 7.2) occurring throughout samples from Lakes Arreo, Chiprana, Estanya and Zonar based on the application of the same scheme by Grey & Awramik (2020) used for mesoscale characteristics. Planar stratiform laminations (PLa) are typically associated with non-undulating microbial structures of varying thickness (<0.1mm to 1mm), and contain a mixture of micritic material, Ca-rich precipitates and other trapped and bound detrital material. Wavy/undulatory laminations (WLa) are typically composed of similar phases, but display more crinkly and undulating structures. Horizontal interconnecting laminae (HLa) as termed “Lh-laminae” are described here in addition to the Awramik and Grey scheme (Grey & Awramik, 2020) and also by Gerdes et al. (2000), and consist of micrometer to sub-millimetre scale disparate and interlinked laminae. A further laminated fabric is domal laminations (DLa), which typically appear as strongly up-domed/columnar (0.1-5mm) laminae with variable composition. Finally, an uncommon, laminated fabric identified in the samples is a stratiform laminated microbial mat with inclusions of centric and pennate diatoms (DaLa). In contrast, non-laminated fabrics include pinnacle and tuft (Grotzinger & Rothman, 1996) structures (Pin), which occur as variably sized (0.01-0.1mm) erect structures occurring at the tops of microbial laminae. Finally, the last fabric associated with microbialites is a clotted (Clo) fabric of non-laminated, mm-scale aggregates of microbial material and micrite with cross-cutting by later precipitated gypsum and/or carbonate precipitates.

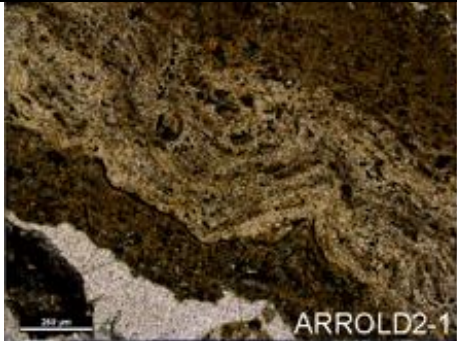
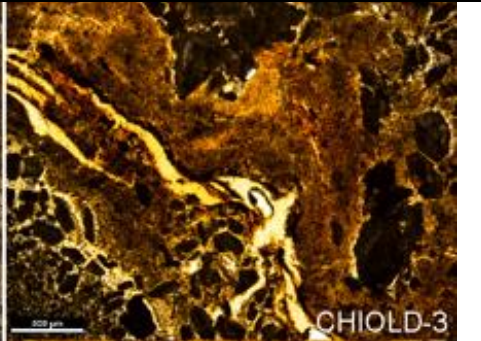
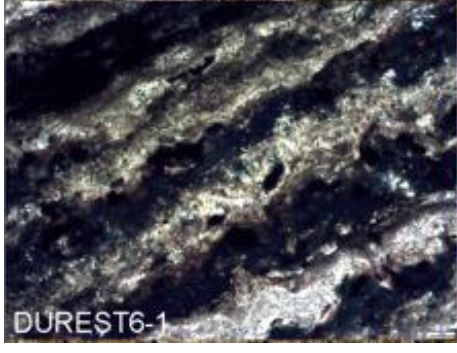
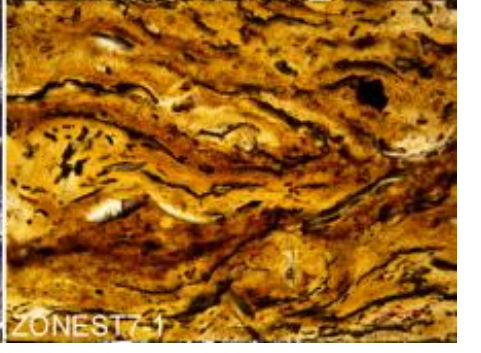
Table 7.1 – Summary of morphological characteristics identified using CT scanning throughout the study.

Site/Mat	Margins	Plan View Structure	Microbialite Shape	Height to Width Description	Variability of Growth	Attitude
Lake Chiprana – Profundal Upper Section – Upper Interval	Smooth/Wrinkled	Labyrinthine	Undulatory Layered /Branching to Stratiform	Crustose	Ragged	Inclined (<45 to bedding)
Lake Chiprana – Profundal Upper Section – Lower Interval	Smooth/Wrinkled	Linear	Stratiform to Undulatory Layered	Crustose	Uniform	Erect (perpendicular to bedding)
Lake Chiprana – Profundal Lower Section	Smooth	Labyrinthine to Linear	Undulatory Layered	Crustose	Uniform	Inclined (<45 to bedding)

Lake Chiprana – Littoral	Smooth/Wrinkled	Labyrinthine to Linear	Stratiform to Undulatory Layered	Crustose	Uniform	Inclined (<45 to bedding)
Lake Arreo	Smooth	Linear	Stratiform to Undulatory Layered	Crustose	Uniform to Ragged	Inclined (<45 to bedding) to erect (perpendicular to bedding)
Lake Zonar	Smooth	Linear	Stratiform to Undulatory Layered	Crustose	Uniform to Ragged	Inclined (<45 to bedding) to erect (perpendicular to bedding)
Lake Estanya	Smooth	Linear	Stratiform to Undulatory Layered	Crustose	Uniform to Ragged	Inclined (<45 to bedding) to erect (perpendicular to bedding)

Table 7.2 – Summary of micro-scale fabrics and textures identified throughout the study.

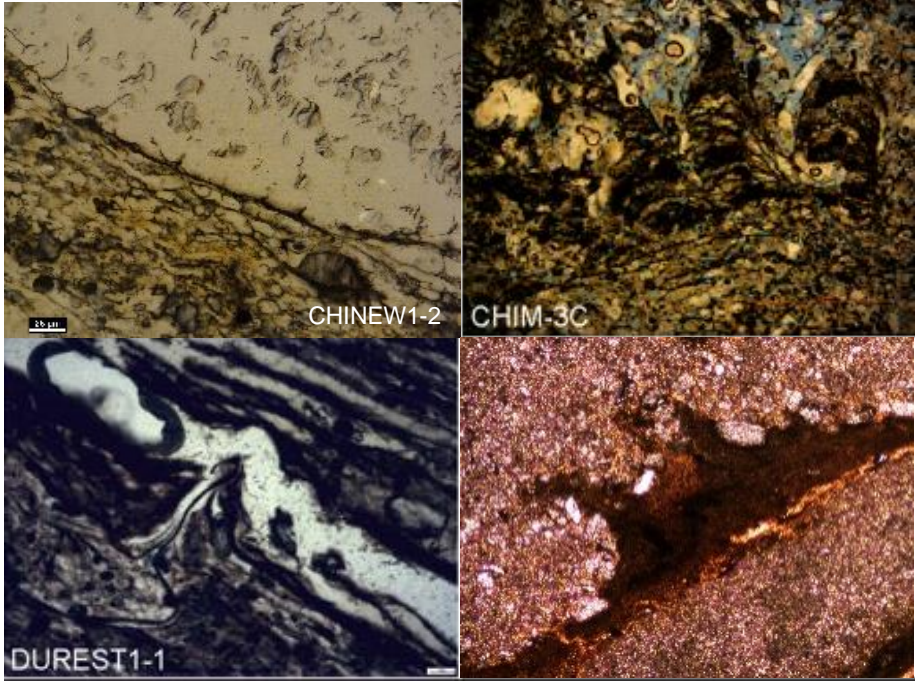
Group	Fabric/Grey & Awramik Classification	Abbreviation	Petrographic Characteristics	Reference Photomicrograph
Microbialite-Laminated	Planar/stratiform laminated	PLa	Planar laminated microbial laminae with various phases intercalated throughout laminae.	

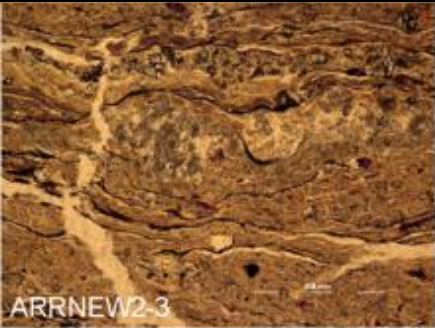
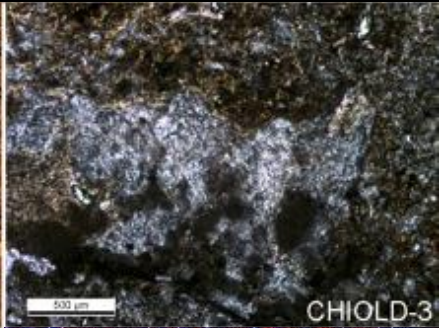
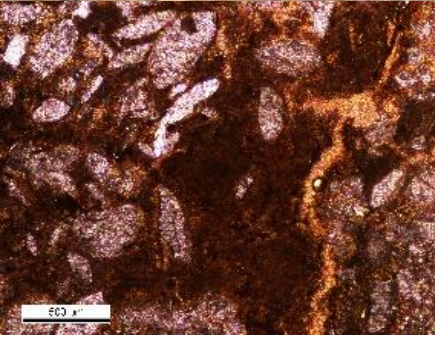
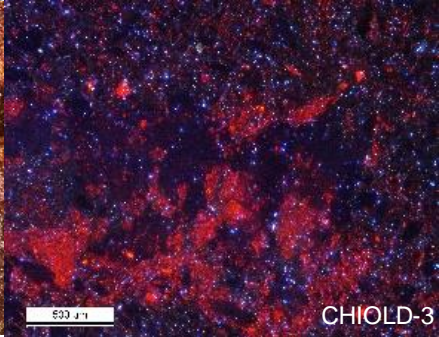
<p>Wavy/undulatory laminated</p>	<p>WLa</p>	<p>Wavy laminated microbial laminae with significant undulations and phases.</p>	 <p>ARROLD2-1</p>	 <p>CHIOLD-3</p>  <p>DUREŞT6-1</p>  <p>ZONEST7-1</p>
----------------------------------	------------	--	--	---

<p>Domal columnar laminated</p>	<p>DLa</p>	<p>Domed microbial laminae with significant growth of laminae above bed and laminae surface.</p>	<p>ARROLD2-1 200 µm</p> <p>CHIOLD-1 1000 µm</p> <p>DUREST4-3</p> <p>ZONEST6-1</p>
---------------------------------	------------	--	---


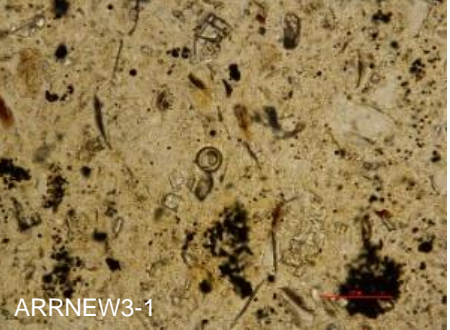
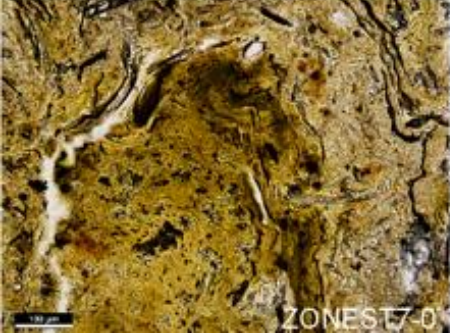

<p>Horizontal interconnected laminae – New definition</p>	<p>HLa</p>	<p>Highly interconnected microbial laminae of μm to mm scale.</p>	
---	------------	---	--

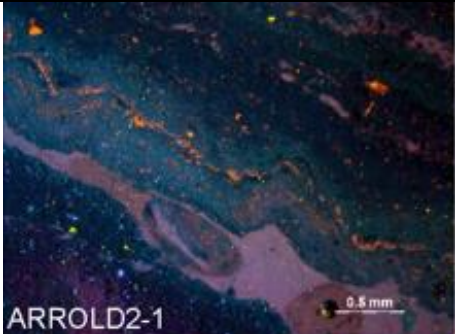
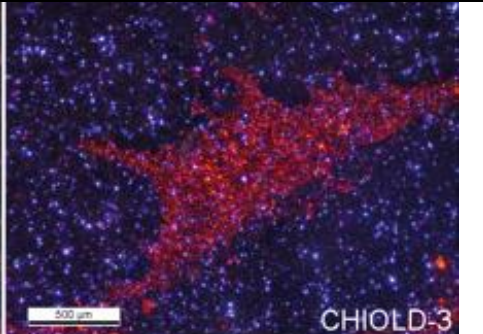
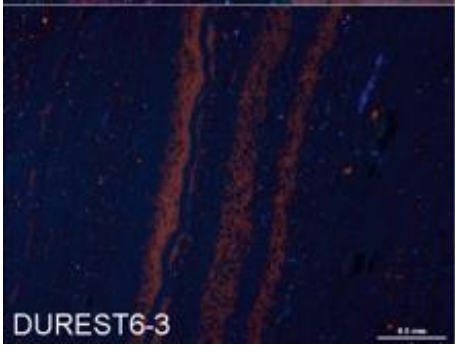

<p>Diatom stratiform laminated</p>	<p>DaLa</p>	<p>Intercalated microbial and diatom-rich laminae.</p>	
------------------------------------	-------------	--	--


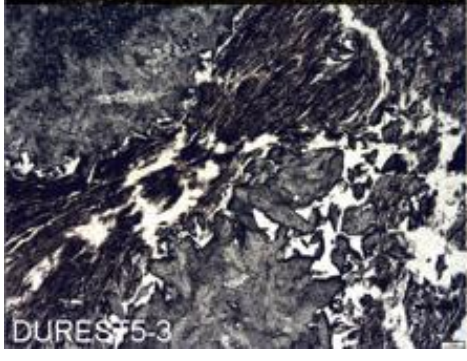
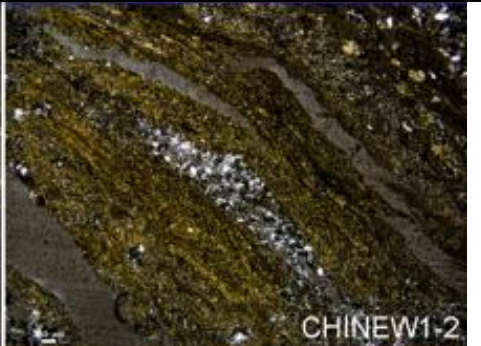

<p style="writing-mode: vertical-rl; transform: rotate(180deg);">Microbialite-Non Laminated</p>	<p>Pinnacles</p>	<p>Pin</p>	<p>Microbially-produced erect pinnacle structures atop microbial laminae.</p>	 <p>The figure consists of four micrographs arranged in a 2x2 grid. The top-left image, labeled CHINEW1-2, shows a cross-section of a microbialite with a distinct layered structure and a small white scale bar. The top-right image, labeled CHIM-3C, shows a dense, textured microbialite surface with some circular features. The bottom-left image, labeled DUREST1-1, shows a dark, layered microbialite structure with a prominent, light-colored, curved feature. The bottom-right image, also labeled CHIM-3C, shows a reddish-brown microbialite surface with a dark, linear feature.</p>
---	------------------	------------	---	---

Clotted fabrics	Clo	"Thrombotic"-like structures consisting of biogenic material.		
				

<p style="writing-mode: vertical-rl; transform: rotate(180deg);">Non-Microbialites</p>	<p>Siliciclastic material</p>	<p>SiL</p>	<p>Detrital-rich laminae and lenticular pockets.</p>	
--	-------------------------------	------------	--	--

<p>Diatom laminae</p>	<p>DiL</p>	<p>Diatom-rich laminae and intervals.</p>	 <p>ARROLD4-1</p>	 <p>ARRNEW3-1</p>  <p>ZONEST7-0</p>  <p>DURZON8-1</p>
-----------------------	------------	---	--	--

<p>Calcium precipitates</p>	<p>CaP</p>	<p>μm to mm sized calcium-rich precipitates.</p>	 <p>ARROLD2-1</p>	 <p>CHIOLD-3</p>
			 <p>DUREST6-3</p>	 <p>DURZON9-2</p>

Gypsum	GpL	Laminae and lenticular pockets of euhedral endogenic gypsum.	 <p>ARROLD4-1</p>  <p>DURES75-3</p>	 <p>CHINEW1-2</p>  <p>ZONEST7-1</p>
--------	-----	--	--	--

7.3.2 Modern to Sub-Recent Microbialites

7.3.2.1 Lake Chiprana – Profundal Setting

7.3.2.1.1 Morphology and Mesoscale Characteristics

In the upper section of cores from the profundal setting of Lake Chiprana (Figure 7.3a), there are two intervals of microbial mats separated by a bed of 2-5cm bed of gypsum. The margins of microbialites from both intervals display smooth to wrinkled margins, and in plan view are labyrinthine/maceriate. In cross-section, mats display stratiform to undulatory lamination of varying thickness (<0.1 to 2cm) as well as development of pinnacles, and are occasionally domical to branching, being cross-cut and deformed by vertically oriented gypsum growths (Grey & Awramik, 2020). The microbialites are crustose due to their low height to width ratio, and have a ragged mode of growth with an inclined attitude of growth (<45°). The lower interval of microbial mats displays planar lamination with no apparent distortion of laminae by gypsum growth as well as a reduction in the number of pinnacles associated with the mats. However, gypsum and other detrital material is present throughout the mats as small, unintrusive deposits. Such microbialites are stratiform layered types that display no positive relief (Grey & Awramik, 2020), have height to width ratios that can be defined as crustose, and generally have erect attitudes.

In the lower section of cores CHI19-1A, 2A and 3A, one interval of microbial mats is present, and the thickness of this interval varies on the order of several centimetres between each core. These mats display variable morphological characteristics in both the XZ and YZ orientations. In all cases, they display smooth contacts with surrounding bedding, and often have an erect attitude. The most common structures include moderately contorted and domed laminae, with laminae displaying varying thicknesses and attenuation throughout suggesting compositional changes throughout the mats between various carbonates and sulphates (XRD analyses, see chapter 6). Small pinnacles are also observed in several of these laminae similar to those identified in the upper core sections. In many cases, these pinnacles and domed structures are also associated with intrusive deposits of gypsum that occupy the individual domes and pinnacles. The mats also display smooth margins with

surrounding sediment and have a labyrinthine/maceriated structure in plan view. In cross-section, mats are undulatory and layered, crustose, and are slightly inclined to overlying and underlying bedding planes (Grey & Awramik, 2020).

7.3.2.1.2 Texture and Microfabric

In section, mats from both sections of the profundal sediments of Chiprana include pinnacles (Pin), laminae (PLa) (including Lh laminae (HLa), see below), and clotted textures (Clo). Interconnected laminated textures (HLa) are also visible throughout some laminated horizons and correspond to Lh laminae as described by Gerdes *et al.* (2000). Such intervals are often disrupted by gypsum crystals of varying sizes. In addition to the laminae, microbial mats also occur in a clotted morphology (Clo). This feature is characterised by strong concentrations of Ca-rich material associated with microbial organic laminae that are cross-cut and disrupted by euhedral gypsum, leading to the microfabrics observed in Figure 7.3b. Clotted carbonates high in Mn are also common in the mats in these structures and occur as a mixture of in situ growths and trapped carbonate grains. The final structure exhibited by mats in section from the profundal setting of Lake Chiprana are pinnacles (Pin) alike to those identified in mats from the modern-day mats of Chiprana. These pinnacles are sparse throughout the mats, are enriched in Mg and Ca and have bright luminescence, being underlain by a 0.5-1mm thick interval of organic-rich material likely related to the initial laminae generated by the microbial community.

SEM-EDS analyses of mats from Chiprana illustrate needle-like magnesium sulphate clusters throughout which display varying sizes and formative habits throughout the mats. Other primary phases include blocky halite crystals that are commonly found nucleating upon existing euhedral gypsum, and blocky bloedite and possible eugsterite that also exhibit nucleation upon euhedral gypsum. Mat structures typically exhibit enrichment of Mg, Ca, and S, indicating a concentration of sulphates (primarily gypsum) and carbonates within their structural framework.

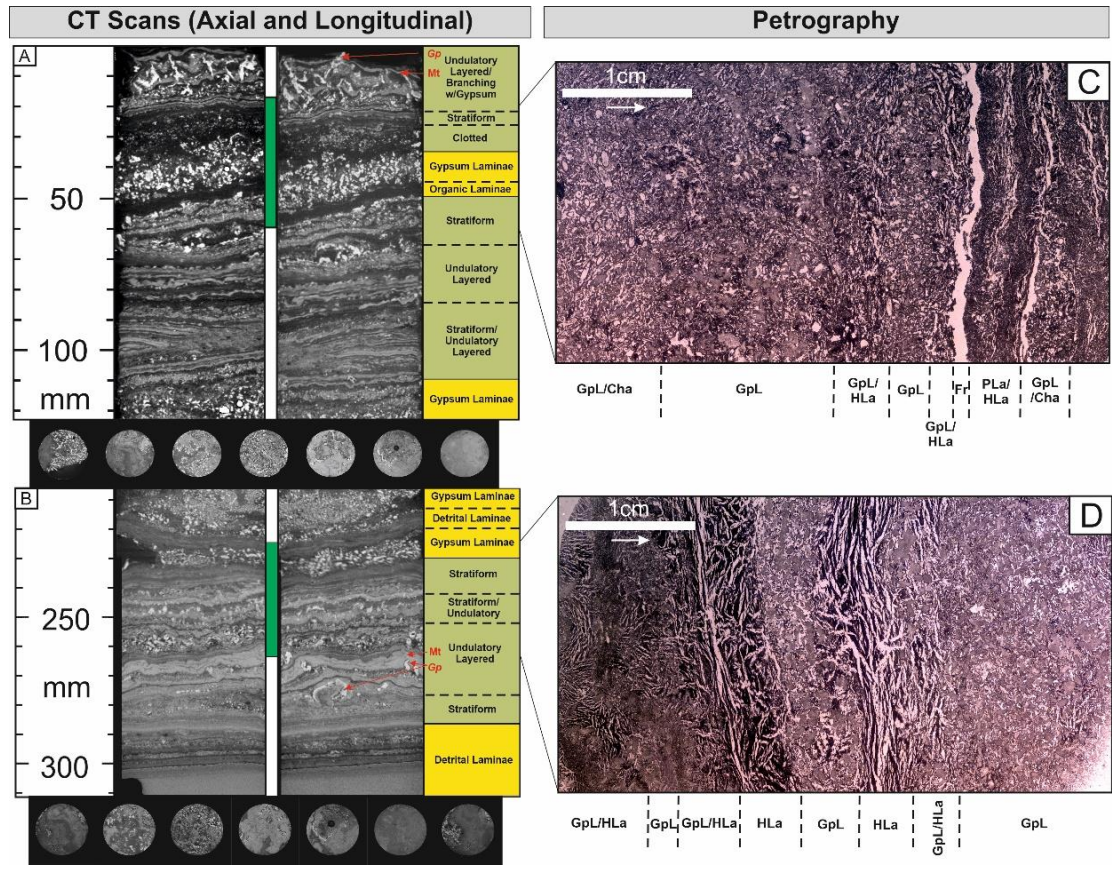


Figure 7.3a – Combined CT and full-thin-section petrographic scans of microbialites from the profundal setting of Lake Chiprana. Scans A-B are both of core CHI19-1A, while scans C and D are of thin section samples DUR13-1 and DUR13-6. Green = mat, yellow = non-mat. Gp: Gypsum, Mt: Microbialite.

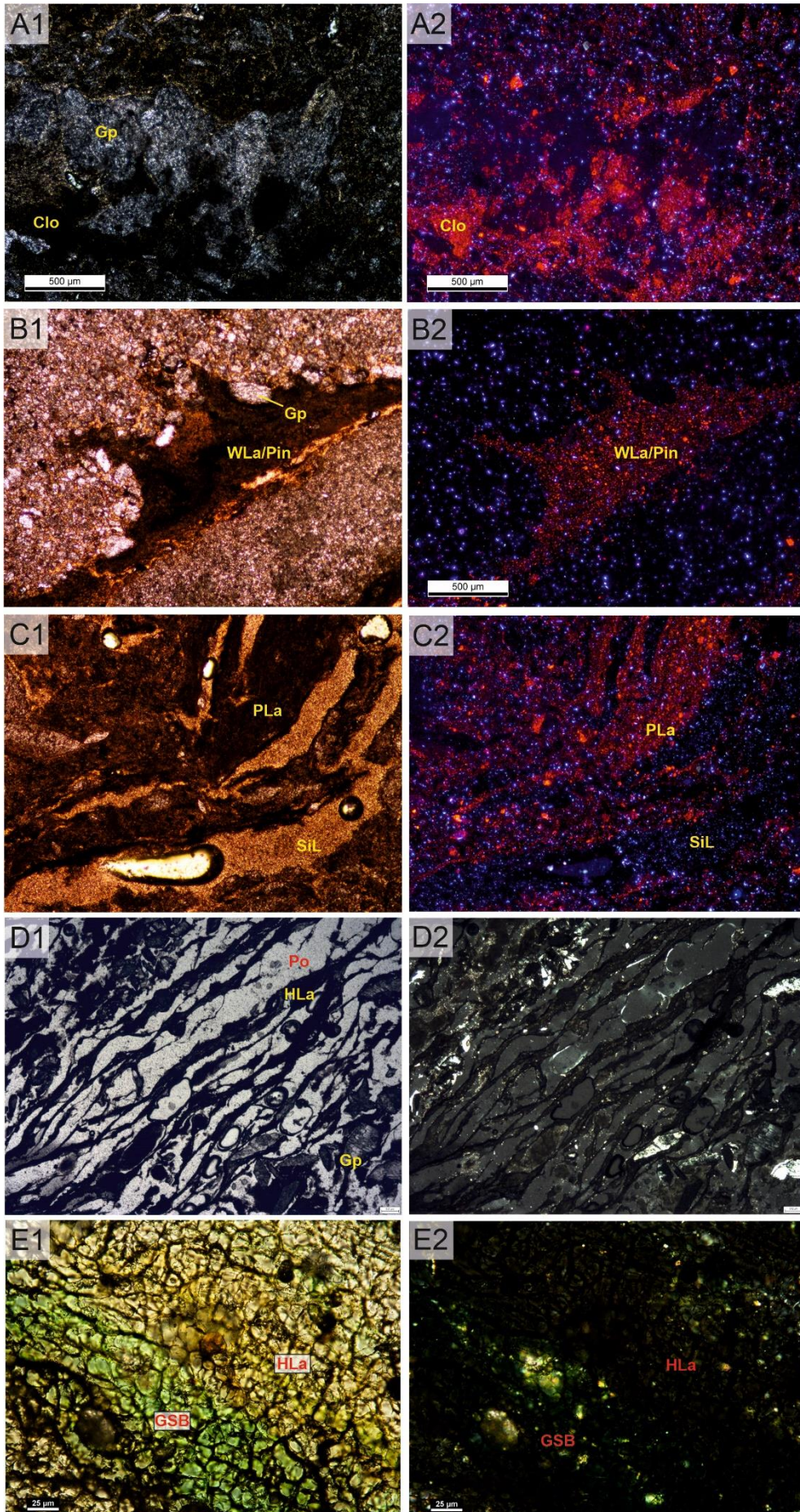


Figure 7.3b – Photomicrographs of microbial structures from the sub-recent sediments (~100-200yrs BP) of Laguna Salada de Chiprana. A1-A2) Gypsum and clotted microbial laminae (Clo), with gypsum precipitates distorting microbial textures. Microbial clotted textures are identifiable by the red luminescent phases under CL, with gypsum crystals forming the secondary interstitial material. B1-B2) Pinnacled structures (Pin) common of microbial mats from Chiprana. The pinnacles are clearly highlighted by bright luminescence in contrast to the surrounding detrital and organic matrix. C1-C2) Laminated/stratiform microbial structures (PLa/WLa) with interstitial detrital material (SiL). D1-D2) Photomicrographs displaying highly interconnected microbial laminae with various detrital material and gypsum crystals distributed throughout and distorting laminae. E1-E2) Photomicrographs displaying interconnected microbial structures (HLa) and strong green staining induced by the presence and metabolic activities of green sulphur bacteria. Gp: Isolated gypsum, Po: Porosity and fractures, GSB: Distribution of green sulphur bacteria within microbial mats illustrated by green staining.

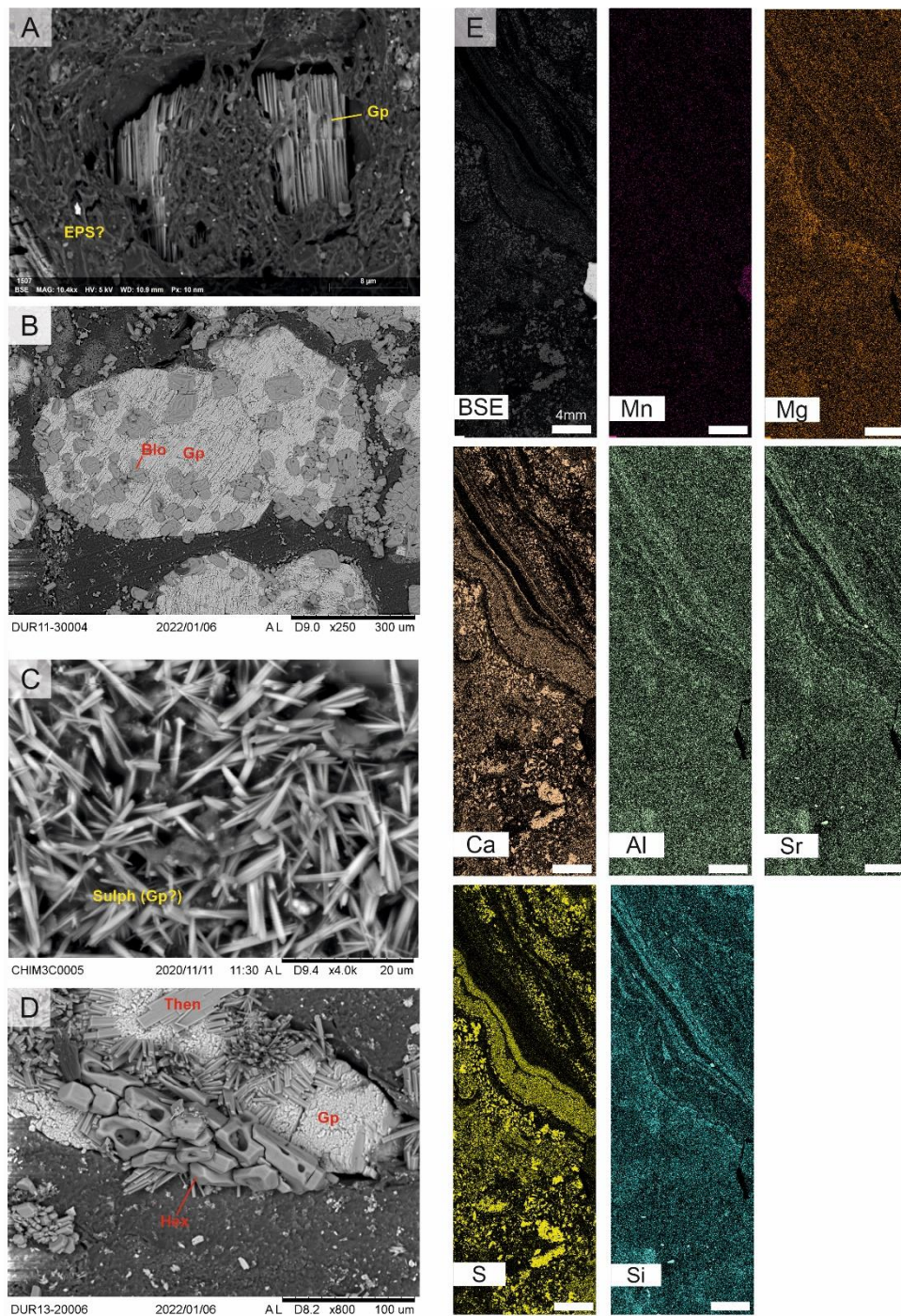


Figure 7.3c – SEM microphotographs of microbial structures from Lake Chiprana. A) Microbial laminae with encapsulated gypsum grain, and clay minerals distributed within matrix throughout sample. B) Blocky and fine acicular/fibrous phases of gypsum and aragonite respectively. They are subset in a gypsum-rich and partially detrital matrix. C) Acicular and fibrous sulphate (likely gypsum) crystals within microbial laminae. D) Blocky hexahydrite with dissolution features, prismatic thenardite and euhedral gypsum. Gp: Euhedral, variably sized gypsum grains. Sulph: Sulphatic crystals, Hex: Hexahdrite, Blo: Bloedite, Then: Thenardite. E) ESEM-XRF maps displaying the intensity of different elemental phases throughout a typical profundal microbial mat from Lake Chiprana.

7.3.2.2 Lake Chiprana – Littoral Setting

7.3.2.2.2 – Morphology and Mesoscale Characteristics

Microbial mats are identified within the upper section of each core and are typically divided into three intervals, with the exception of core CHI19-7A. The uppermost interval of microbial mats are undulatory and overlain by cumulate, vertically oriented gypsum crystals, and these crystals often displace the mats and create pockets of porosity. The second interval of mats are fragmented and strongly interlaminated with gypsum and organic-rich muds. Mats are stratiform to undulatory and display some doming and distortion of laminae throughout, particularly in the upper portion of the mats. Finally, the lowest interval of mats are present as a singular interval of microbial laminae at the base of the core. These mats are thinly laminated, illustrate no distortion or apparent doming, and are compacted between dendritic, gypsum-encrusted charophytes. According to the classification scheme of Grey & Awramik (2020), the mats have smooth to wrinkled margins with the surrounding sediment, display labyrinthine to linear plan view morphologies, and are stratiform to undulatory layered in cross section. They are also crustose and have an inclined attitude relative to bedding structures.

7.3.2.2.2 – Texture and Microfabric

Microscale characteristics of mats from the littoral areas of Lake Chiprana display strong interconnected textures (HLa) that are interspersed by euhedral prismatic gypsum. The uppermost sections of the mats are strongly associated with the development of pinnacles (Pin) typically no more than 10mm in height and are overlain by a thin white gypsum-halite crust. These pinnacle structures display interstitial laminae (HLa) throughout their internal structure, and typically contain silt-sized euhedral gypsum grains towards their base. Subsurface sediments directly beneath the layer of pinnacles and white gypsum-halite crust typically comprise a laminated microbial community, composed of green cyanobacteria, purple sulphur-reducing bacteria and a dark black sulphate-rich layer containing sulphate-reducing organisms. The most abundant minerals occurring within the modern mats are typically gypsum, hexahydrite, halite and in some cases, thenardite. Other common

minerals include calcite, aragonite, and detrital phases such as quartz and mixed phyllosilicates.

SEM-EDS analyses further illustrate the habit of mineral phases associated with the mats and the dominant geochemical signals associated with the mat structures. Bladed bloedite, cubic halite and fibrous aragonitic phases, all occurring as micrometer scale crystals, are all abundant throughout the mat laminae, and are commonly associated with euhedral lenticular gypsum of varying size. EDS analyses highlight a dominant Ca and Mg signal throughout the mats at low magnification, suggesting that calcite occurs throughout each mat structure. Mg in particular is strongly concentrated within the pinnacle structures, and also shows a uniform distribution throughout laminated structures. The occurrence of carbonates within the mats is also confirmed by XRD analyses (see chapter 6). Al, Fe, Si and K are typically associated with detrital material throughout the samples, and this is commonly observed where such material is concentrated within microbial laminae. Increased concentrations of Si are however also related to the distribution of diatoms occurring throughout the samples.

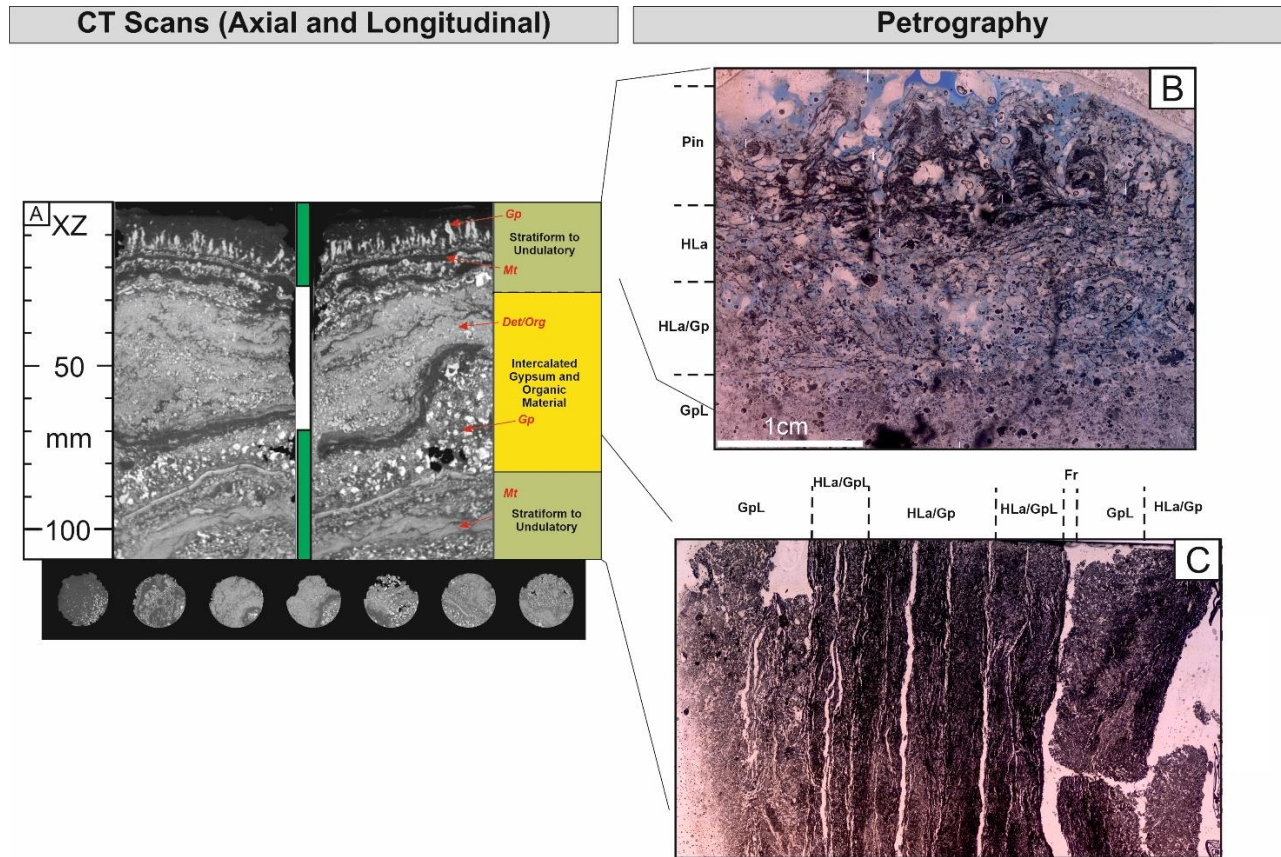


Figure 7.4a – Combined CT and petrographic scans of microbialites from the littoral setting of Lake Chiprana. Scan A is from core CHI19-5A, while scans B and C are of thin section samples CHIM-3C and DUR11-1. Green = mat, yellow = non-mat. Gp: Gypsum, Mt: Microbialites, Det/Org = Detrital/organics.

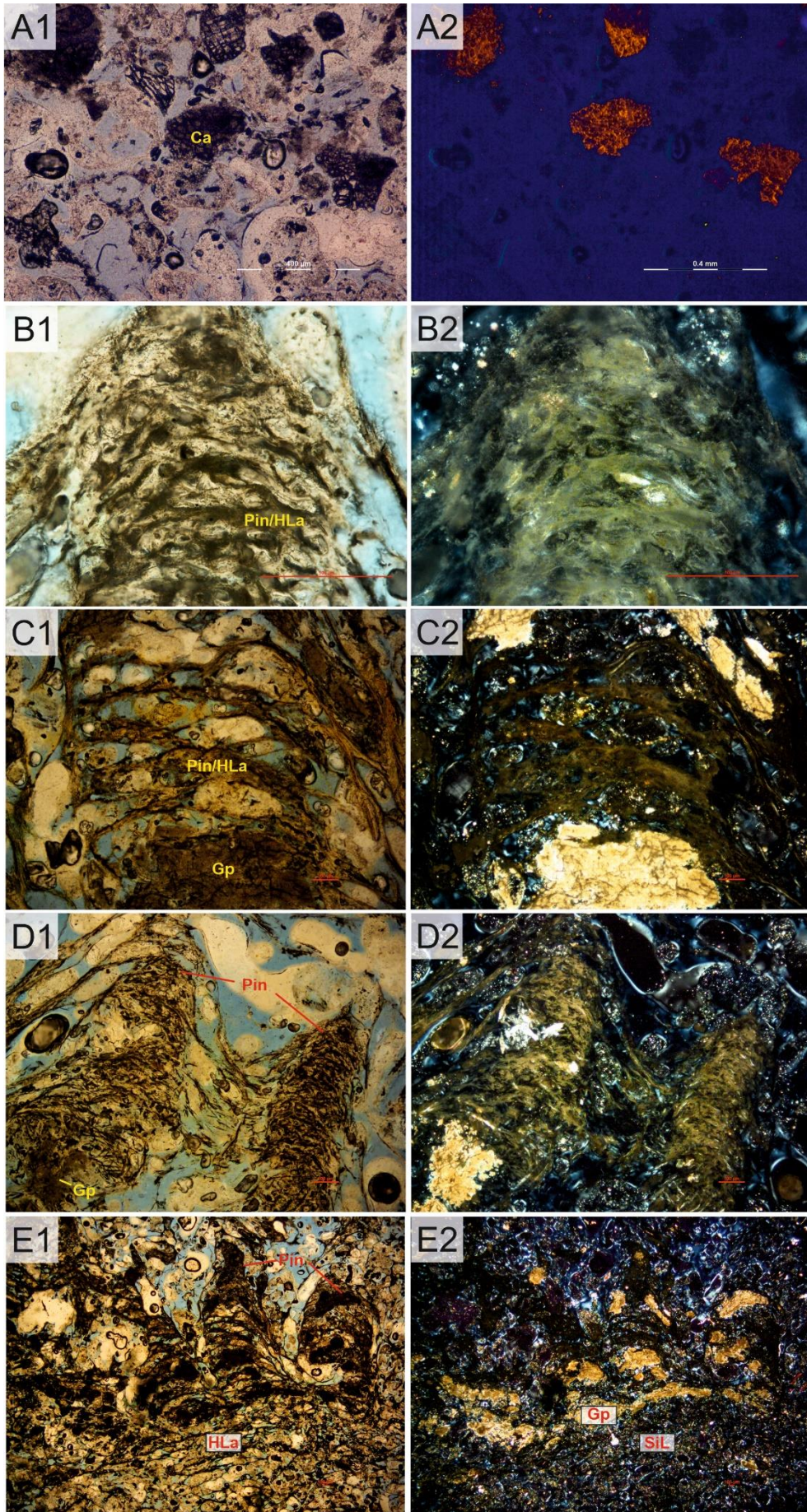


Figure 7.4b – Photomicrographs of modern microbial structures from Laguna Salada de Chiprana. A1-E1: Optical, A2-E2 Cathodoluminescence. A1-A2) Optical and cathodoluminescence photomicrographs of Ca-rich detrital grains, fragmented and deposited within the gelatinous matrix of the mats. B1-B2) High-magnification photomicrograph of the internal structure of a mat pinnacle, highlighting a clotted interior and HLa fabrics with detrital and gypsiferous material distributed throughout. C1-C2) High-magnification photomicrograph of a separate pinnacle developed by microbial processes, illustrating a strongly interconnected matrix throughout the pinnacle developed by successive inter-lamination, deposition of precipitates and trapping of detrital material induced by the microbial community. D1-D2) Overview of pinnacle structures generated by microbial communities. The pinnacles are variable in size, orientation and thickness, and are typically interconnected by thin strands of organic material. E1-E2) Overview of pinnacle structures with extensive development of calcitic and gypsiferous material at their base, providing a nucleation site for pinnacle formation and subsequent development.

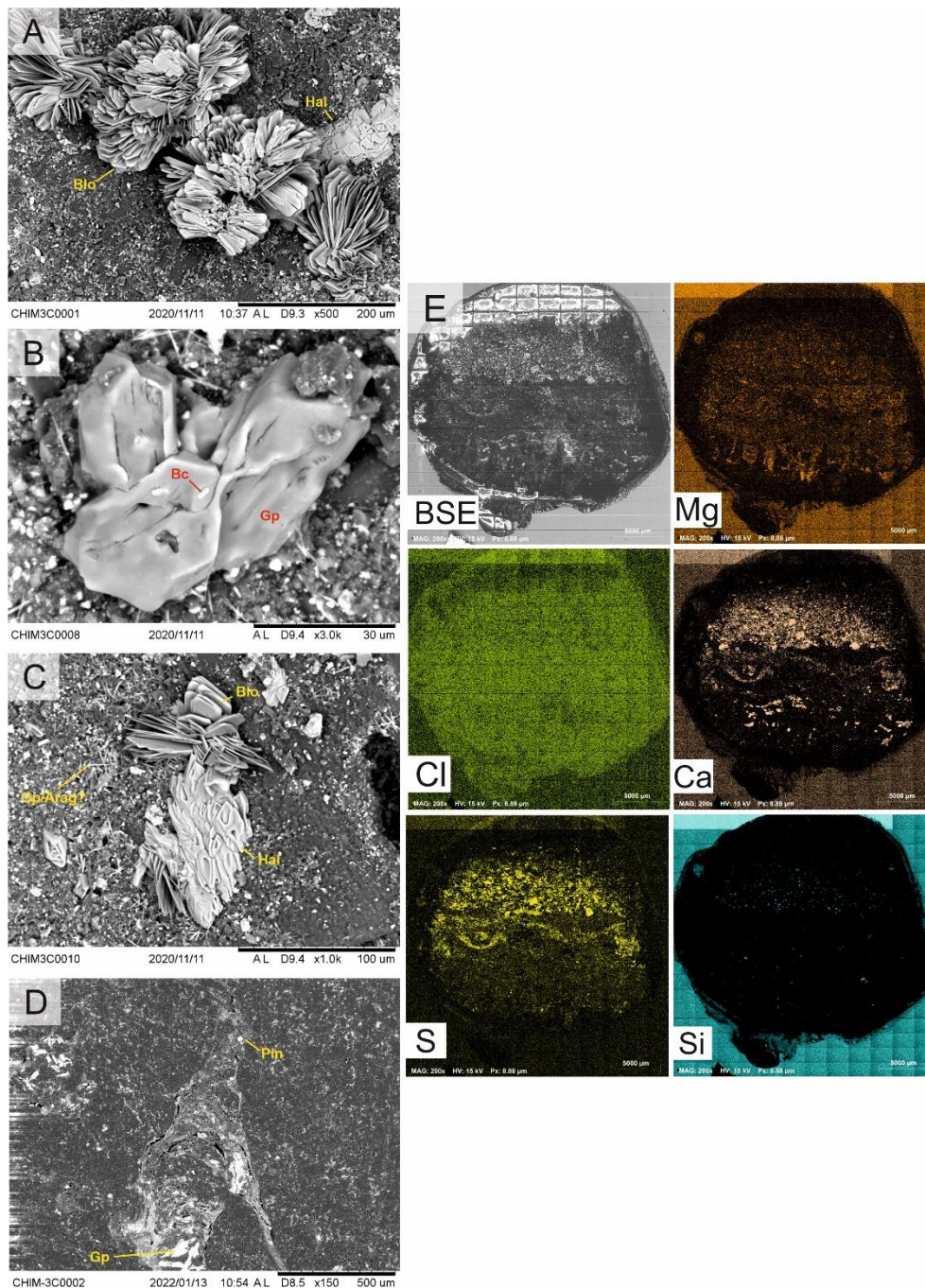


Figure 7.4c – SEM photomicrographs from littoral Lake Chiprana. A) Radial, fibrous and bladed bloedite crystals developing within a mixed siliciclastic and sulphatic matrix. They are directly subset adjacent to cubic halite grains. B) Gypsum crystals with indications of dissolution induced by bacterial activity. C) Further examples of bloedite crystals and cubic halite, with halite displaying extensive pitting throughout. D) SEM microphotograph illustrating the structure of a pinnacle generated by the microbial community. Extensive deposition/precipitation of gypsiferous and calcitic material can again be identified at the base of the pinnacle. E) ESEM-XRF maps displaying the intensity of different elemental phases throughout a typical modern microbial mat from Lake Chiprana.

7.3.2.3 Lake Zonar

7.3.2.3.1 Morphology and Mesoscale Characteristics

CT scans of microbial mats from Laguna Zonar are presented in Figures 7.5. The cores the mats were taken from are previously described in studies by Martín-Puertas *et al.* (2008, 2009, 2011) and correspond to the period 1950-1800_{AD} based on sedimentological and chronological analyses. Therein, they are described as organic ooze laminated sediments with authigenic calcite laminae and reflect an overall decrease in both lake levels and sediment delivery occurring within a brackish to saline lake (Martín-Puertas *et al.*, 2011).

Microbial mats within cores ZON04-1A, 1B, 1C and 1D from Laguna Zonar are primarily confined to a small interval within the uppermost section of the cores. In the case of this study, core ZON04-1A and ZON04-1C are used to represent mat morphology. Mats occur within two ~10cm thick intervals between 84cm and 94cm and 91cm and 101cm. The defining feature of microbial mats from Laguna Zonar is a thin stratiform to crinkly/undulatory lamination. This lamination varies in thickness (1-20 mm) and composition throughout each interval and between samples. Morphologically, the laminae are complex and display variations in their attitude and angle to bedding, typically no greater than 45° in inclination. In the upper interval of core ZON04-1C (76-86cm), mats display sub-mm scale contrasting light and dark laminae throughout, with density contrasts typically distinct between individual laminae. They display complex structures with significant doming of laminae throughout. Similar density contrasts are observed in the lower interval (88-98cm) between microbial mats and gypsum-rich laminae. However, microbial laminae display less doming in this interval and are generally flatter in habit. With regards to the classification scheme of Grey & Awramik (2020), the mats have smooth margins with the surrounding sediment, and display a linear morphology in plan view. In cross-section the mats are stratiform to undulatory layered, with very small examples of small columns. The height-to-width ratio is crustose, and the mats display erect to inclined attitudes.

7.3.2.3.2 Texture and Microfabric

At the micro-scale, Laguna Zonar mats illustrate a mixture of textures and structures superimposed upon the stratiform to undulatory fabrics identified at the mesoscale in the CT scans. Stratiform planar laminae (PLa), interconnected horizontally laminae (HLa) and strongly domed columnar structures (DLa) are present, and in all cases, they contain an abundance of crystalline material incorporated into the microbial layers (partial CaP). The domed structures are particularly well developed in several cases and form isolated, linked columnar structures according to Grey & Awramik (2020). Individual, sand-sized gypsum crystals also occur and are infrequent within microbial laminae, whilst microcrystalline calcite grains are often concentrated within the micritic up-domed layers. Laminae include a very fine, micritic type, and a fine, crystalline type containing the Ca-rich precipitates (CaP). Diatoms are also common at the tops of microbial laminae (DaLa), and the tops of many microbial laminae are sometimes distorted by pinnacle structures (Pin). Microbial Lh-laminae (HLa) are also sporadic throughout the Zonar microbial mats, with these structures displaying strong interconnected fabrics indicative of microbial activity (Brehm *et al.*, 2002). In many cases, both the Lh laminae and other microbially-induced structures display weak to moderate staining by green sulphur-reducing bacteria (Martínez-Alonso *et al.*, 2005).

SEM and high-magnification optical analyses show that Zonar samples exhibit a wide variety of microscopic crystalline phases associated with mat structures and laminae. Needle-like aragonite fibres, cubic halite and micrometer-scale gypsum are particularly abundant (Figure 7.5c), and occur in globular clusters throughout mat-related structures. SEM-EDS analyses indicate high concentrations of Ca, Mg, and Si throughout microbial laminae, with the presence of Si indicating the concentration of diatoms throughout these laminae. There is also a minor distribution of some detrital elements such as Fe and Al throughout the mats, likely corresponding to trapped and bound detrital material within the laminae.

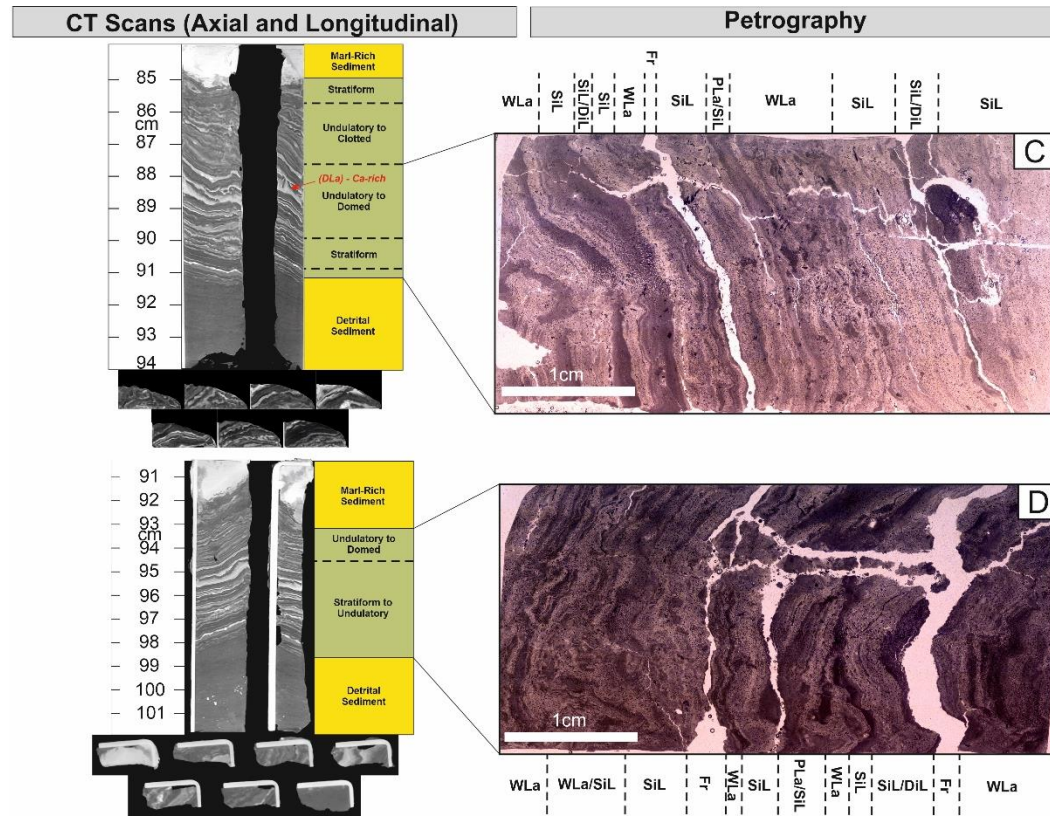


Figure 7.5a – Combined CT and full-thin-section petrographic scans of microbialites from the Lake Zonar. Scans A-B are both of core CHI19-1A, while scans C and D are of thin section samples DUR13-1 and DUR13-6. Green = mat, yellow = non-mat. Gp: Gypsum, Mt: Microbialite.

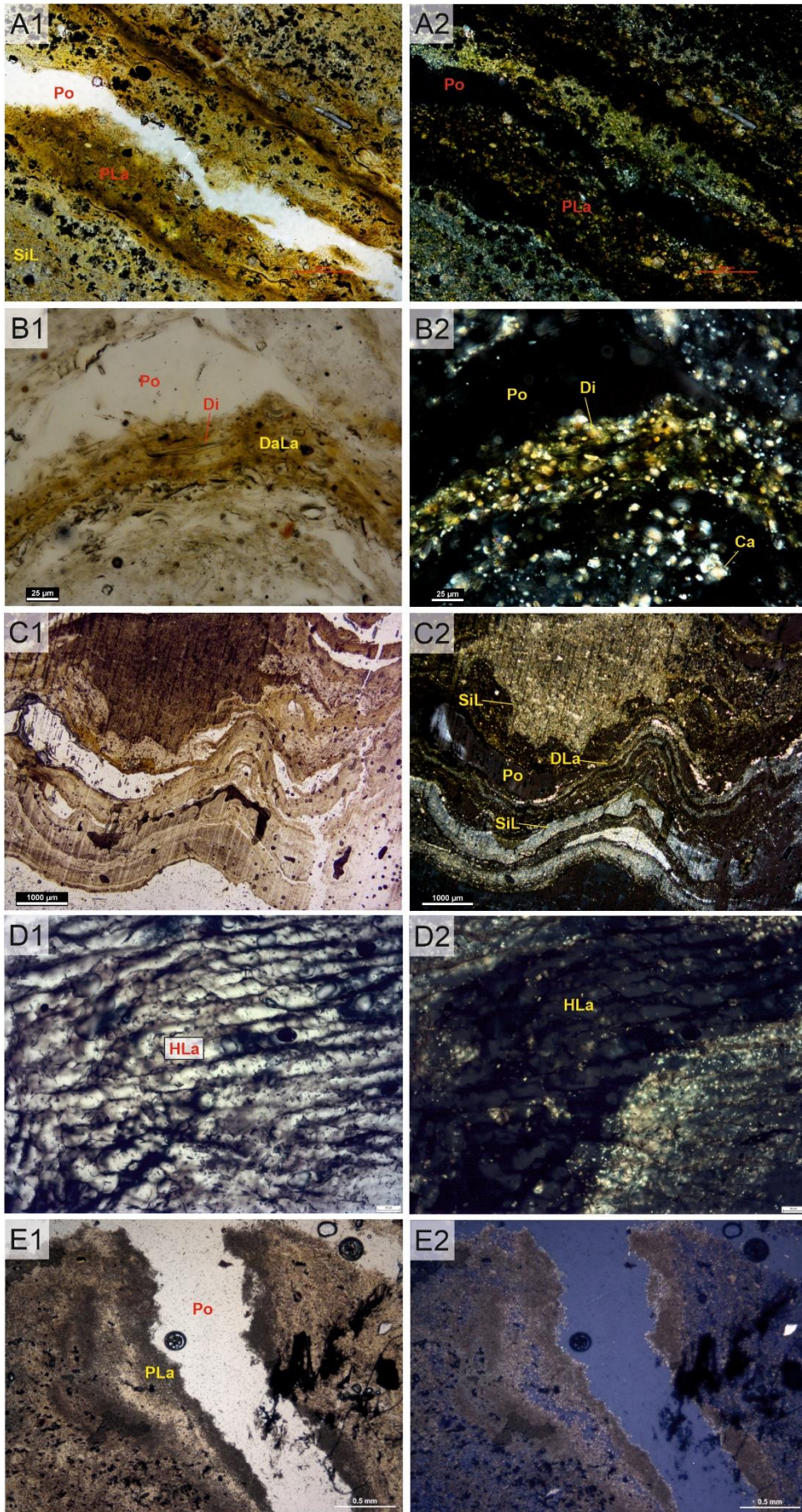


Figure 7.5b – Photomicrographs of microbial structures from Laguna Zonar. A1-A2) Planar/stratiform laminated (PLa) microbial laminae with highlighted microbial layering, interstitial siliciclastic layering and porosity. Diatoms are common at the topmost section of the layers, and the thickness of individual laminae varies throughout. B1-B2) High magnification view of microbial laminae with diatoms visible (DaLa). Diatoms are often fragmented and situated in an organic-rich matrix. C1-C2) Overview illustrating photomicrographs of strongly domed microbial structures (DLa) distributed throughout the sample. Detrital matrix is observed above the domal microbialites with variable laminae composition, including detrital, gypsum and organic-rich variants. D1-D2) Interconnected microbial textures and laminae (HLa) associated with Zonar microbial mats. Various detrital material and gypsum crystals are also present within the matrix. E1-E2) Photomicrographs illustrating mud-rich stratiform laminated microbial mats (PLa) with microcrystalline gypsum and detrital material.

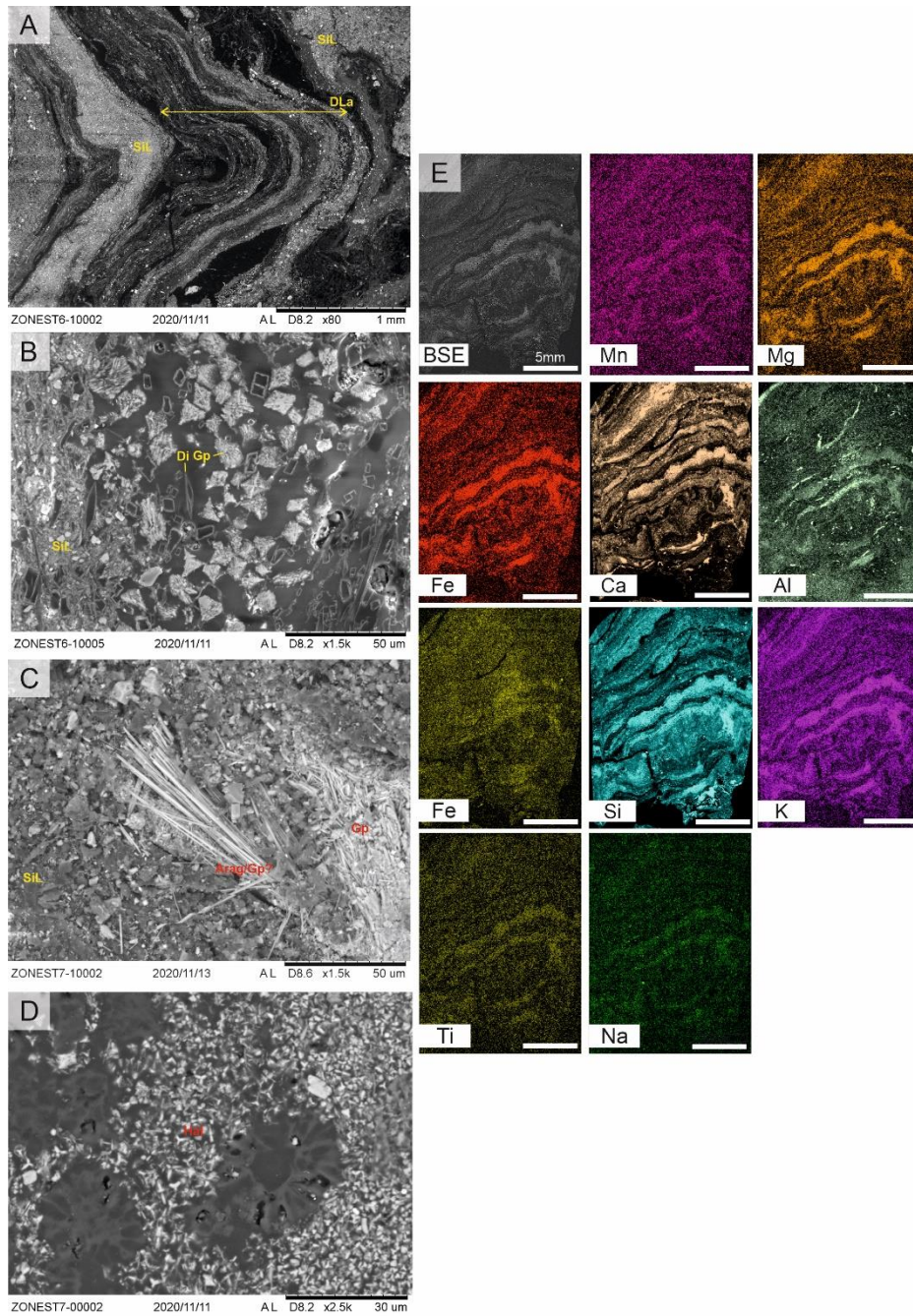


Figure 7.5c – SEM photomicrographs of phases and fabrics from Laguna Zonar. A) Strongly domed microbial laminae with highlighted microbial layering (DLa), interstitial siliciclastic layering and porosity. Diatoms are common at topmost layers, and the thickness of individual laminae varies throughout. B) Nature of sample micro-matrix. Clay minerals are dominant, while other phases include pyrite framboids, diatom frustules, and microcrystalline gypsum. C) Acicular, micrometre-scale aragonite distributed throughout the sample. D1-D2) Overview of microbial laminae characteristic of sediments from Lake Zonar. Strong doming of the laminae is apparent throughout. E) ESEM-XRF maps illustrating the abundance of various element phases within Laguna Zonar microbialites.

7.3.3 Non-Recent (Holocene) Microbialites

7.3.3.1 Lake Estanya

7.3.3.1.1 Morphology and Mesoscale Characteristics

Microbial mats from Lago de Estanya are distributed throughout the sedimentary sequence of the lake in several intervals, and in this study, mats from core LEG04-1A-1K were investigated. Mats from the 62-72cm interval display strongly laminated and stratiform characteristics with some distortion induced by gypsum growth leading to undulatory structures. The mats are very thinly laminated and separated by equally thin laminae of gypsum, and compositional variations can be identified based on the variance in attenuation throughout the laminae. Mats from the 78-88cm interval (E2) display very similar characteristics, with thinly (<0.2mm) laminated microbial mats being interlaminated with gypsum deposits that cause moderate displacement of the mats, as well as several thin laminae of gypsum occurring concordantly between microbial laminae. With regards to the classification scheme of Grey & Awramik (2020), the mats from Lake Estanya generally display wrinkled to smooth margins with the surrounding sediment, and have a linear plan view morphology. In cross-section, the mats display stratiform to undulatory layered morphological characteristics, are crustose with regards to their height to width ratio, and typically have erect to inclined attitudes.

7.3.3.1.2 Texture and Microfabric

Microbial mats from Lago de Estanya display primarily stratiform planar lamination (PLa) in addition to rare undulatory laminae and interconnected fabrics (HLa). The mats are very thinly laminated, and characteristically display “network” fabrics generated by interconnecting laminae has been previously termed and described as “Lh” laminae by Gerdes et al. (2000). The intensity and thickness of these “Lh” laminae varies throughout each sample, and green staining of microbial laminae is common (GSB, see figure 7.6b). Unambiguous pinnacles and small tufts as well as doming (DLa) and crinkly laminae are common within the upper surfaces of some mats. The mats are often displaced by large grains of euhedral gypsum and other detrital material (SiL), while gypsum-rich laminae often overlie microbial laminae

(GpL). Pyrite framboids are also distributed throughout the mats in abundance. Porosity is often extensive within the microbial mat matrices, particularly between interconnected microbial Lh laminae (HLa) and larger gypsum grains.

SEM analyses reveal common pyrite framboids and diatoms throughout the sample matrices, and varying gypsum morphologies associated with microbial laminae. Pyrite framboids occur both as individual solitary grains and within distinctive laminae associated with mat structures. In both cases, they occur both in rounded and cubic habits, and are between 2 and 5 microns in size. SEM-EDS mapping of Estanya mats and samples further exhibits a strong distribution of Mg and Ca (CaP) within individual mat laminae, and a minor distribution of some detrital elements such as Al and Si.

7.3.3.2 Lago de Arreo

7.3.3.2.1 Morphology and Mesoscale Characteristics

Microbial mats from Lago de Arreo occur throughout the sedimentary sequence of the lake in several intervals, and in this study, mats from core CAI04-1B-1K were investigated. Mats from all intervals illustrate strongly stratiform morphologies, with small undulations induced by gypsum crystals that nucleate and develop throughout the microbialite laminae. Much like mats from Lake Estanya, The mats are also very thinly laminated, being separated by laminae of gypsum and other detrital material, while compositional variations can again be identified based on the variance in attenuation throughout the laminae. Small euhedral gypsum crystals can also be identified nucleating throughout the mats. The mats generally have smooth margins and are laminated in plan-view, and exhibit a crustose height-to-width ratio with an erect attitude.

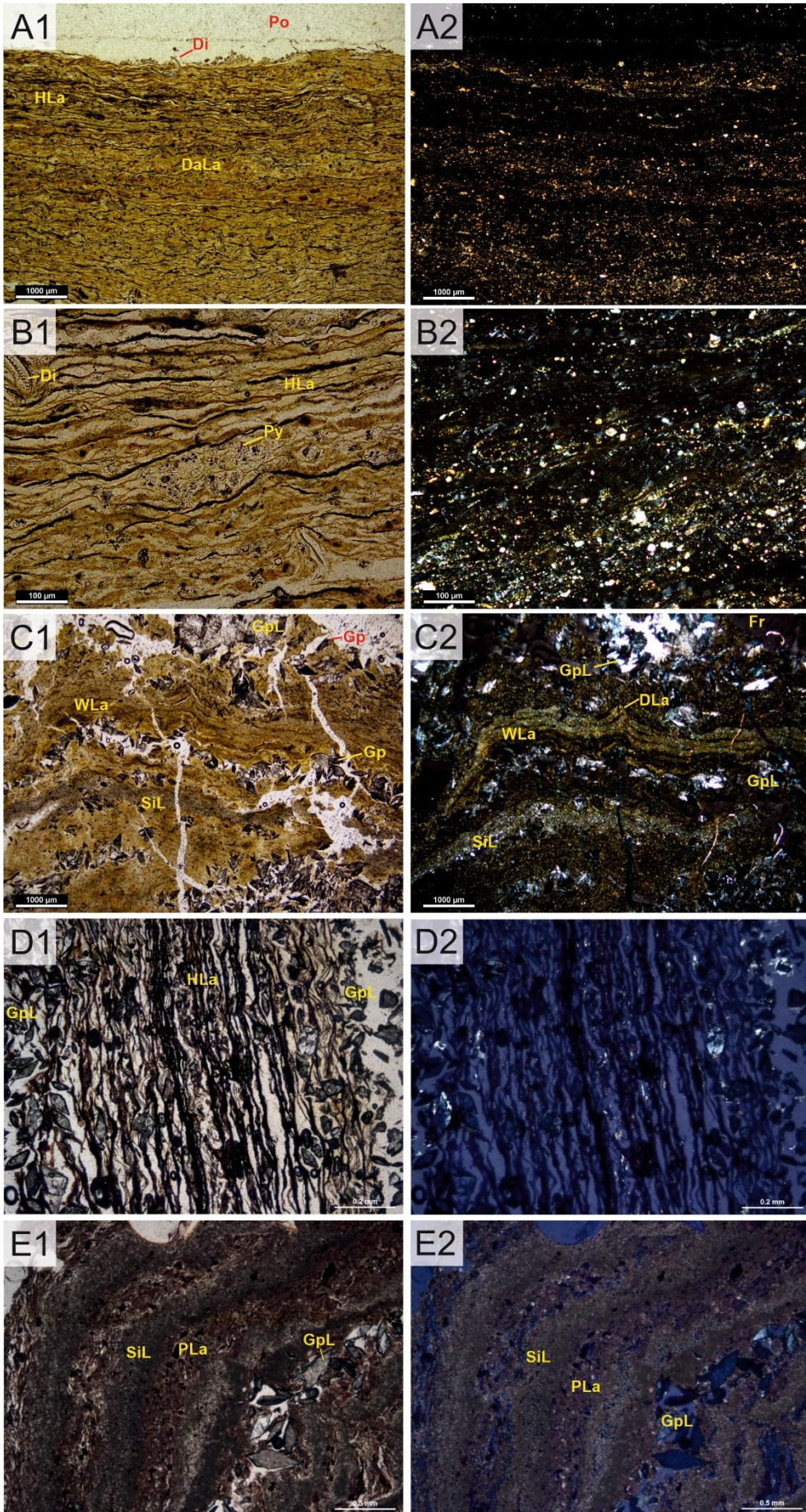


Figure 7.6b – Photomicrographs of microbial structures from Lago de Estanya in PPL and XPL view. A1-A2) Overview of fine microbial laminae (HLa) distributed throughout the sample. Organic material is abundant within and between microbial laminae, and diatoms are commonly found throughout (DaLa/Di). Small, rounded precipitates and pyrite framboids are also present. B1-B2) Increased magnification view of pyrite framboids, interconnected microbial laminae (HLa) and diatoms within an organic-rich layer, C1-C2) Overview of undulatory microbial mats (WLa) and isolated domal structures (DLa) which are distributed throughout the sample. The domal structures are commonly distorted by enveloping gypsum crystals (GpL), and are composed of compositionally variable material within each individual lamina. D1-D2) Photomicrographs displaying highly interconnected microbial laminae (HLa) with various detrital material (SiL) and gypsum crystals (GpL) distributed throughout and distorting laminae. E1-E2) Mud-rich microbial laminae common within Arreo sediments. Gypsum crystals (GpL) develop between laminae and cause moderate distortion of the layers. Various other detrital material is also present within and between the layers (SiL). Di: Singular diatoms distributed throughout microbial and other detrital laminae. Py: Potential pyrite framboids distributed within microbial laminae and detrital matrices. Gp: Euhedral individual (non-laminated or conglomerated) gypsum crystals of varying size, Po: Porosity or gaps between sediment.

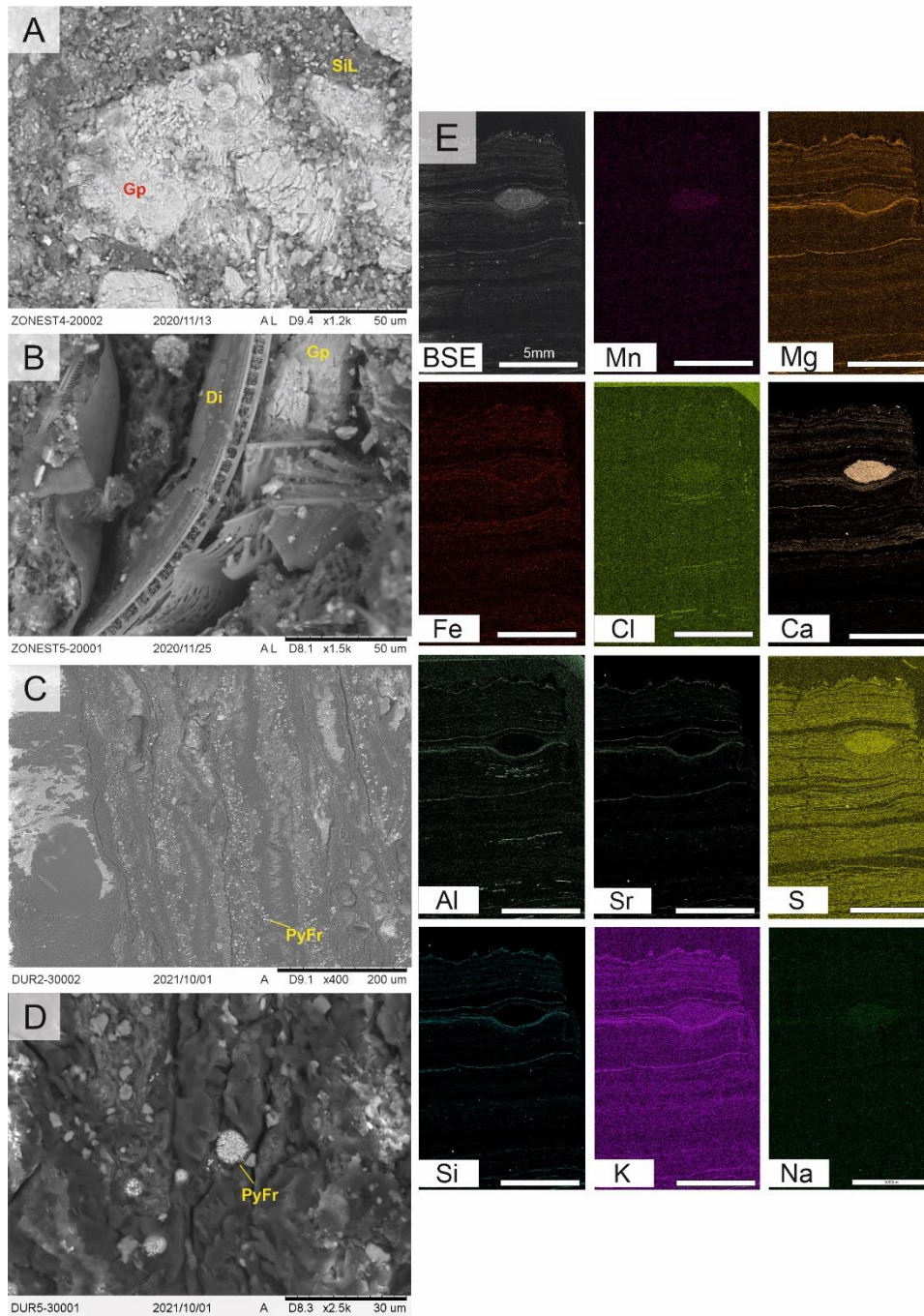


Figure 7.6c – SEM photomicrographs of phases and fabrics from Lago de Estanya. A) Gypsum precipitates within microbial laminae, illustrating euhedral crystal forms and surrounding organic-clay matrix. B) Diatom frustule associated with microbial laminae, partially fragmented and surrounded by clay. C) SEM photomicrograph displaying micrometre-scale spherical Fe-rich precipitates distributed throughout the matrix. D) SEM photomicrograph displaying examples of spherical and sub-spherical pyrite framboids present throughout the sediments of Lake Estanya. E) ESEM XRF map illustrating distribution of different selected elements. Di: Diatoms and diatom frustules, Cl: Clay minerals. PyFr: Pyrite framboids distributed within microbial laminae and detrital matrices.

7.3.3.2.2 Texture and Microfabric

Primary structures associated with microbial mats from Lago de Arreo (see Figures 7.7a-b) include a fine, stratiform microbialite type consisting of either micritic or calcitic spar (PLa), grain size variations (typically fining upwards) and banding of heterogeneous wavy/undulatory microbial laminae (WLa) due to deformation by larger gypsum crystals and clastic grains. Microbial mats are typically strongly laminated throughout sediments from Lago de Arreo, with laminae varying in thickness from the sub-micrometre to millimetre scale. Many of these microbial laminae also display some degree of contortion and undulatory laminae (WLa/DLa). Many of these distorted microbial laminae additionally display strong concentrations of calcium carbonate (likely related to calcite cementation) as illustrated by SEM-EDS analyses. Distorted and domed crystalline layers rich in calcium (CaP) are also widespread throughout the sample, with the Ca-rich crystals presenting as sub-micrometre-sized euhedral crystals arranged within the layers.

High-resolution optical and SEM analyses further reveal common diatoms (DiL), pyrite framboids and the habit of the Ca-rich (CaP) precipitates occurring within the microbial mats. Diatom frustules, both intact and fragmented, are often distributed directly adjacent to or throughout microbial laminae (DaLa). On the other hand, pyrite framboids are typically rounded in nature, no larger than 5 microns in size and are generally randomly distributed throughout mat laminae. The Ca-rich precipitates are euhedral and typically between 1-5 microns in size. SEM-EDS mapping commonly illustrates the infrequent distribution of these Ca-rich precipitates throughout the samples under examination, and they are typically cross-cut by lenticular growths of euhedral gypsum (GpL).

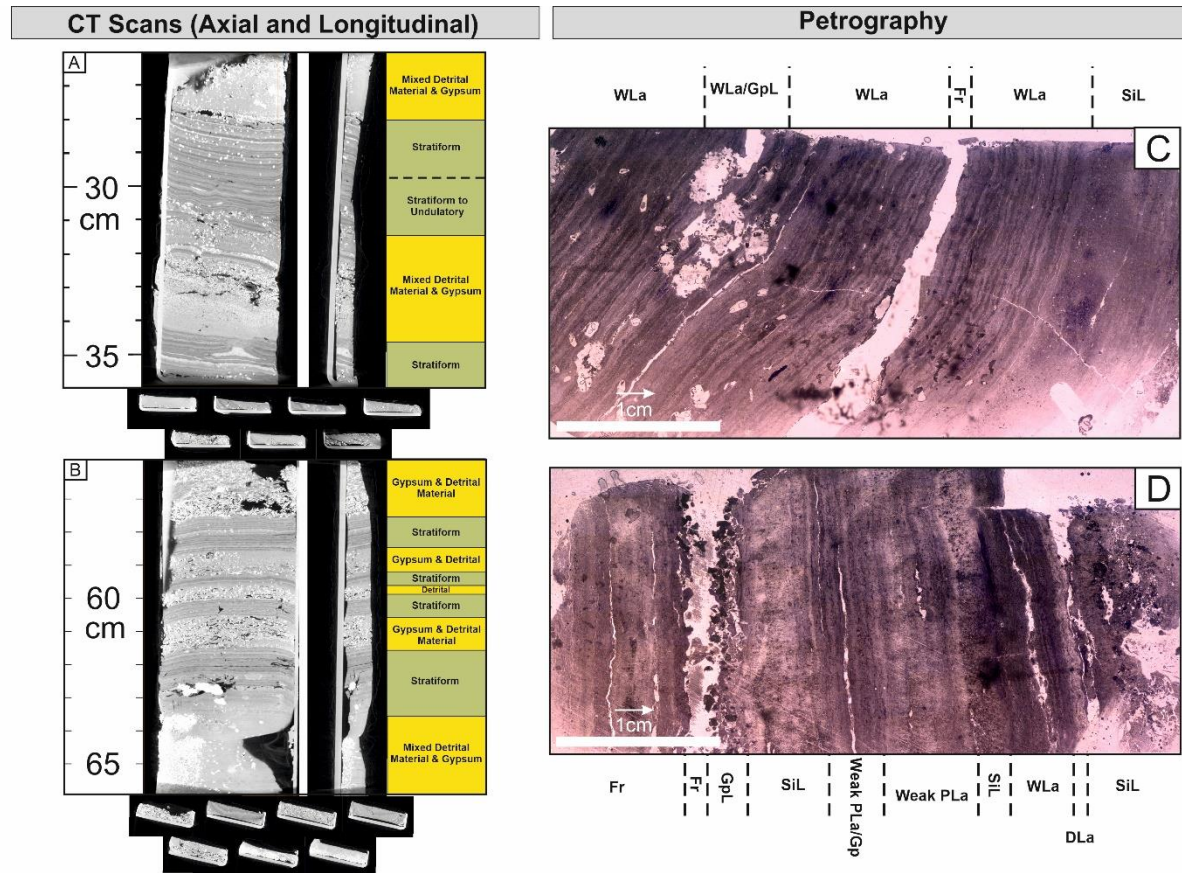


Figure 7.7a – Combined CT and full-thin-section petrographic scans of microbialites from Lake Arreo. Scans A-B are of core CAO04-1B-1K-4 while scans C and D are of samples ARROLD2-1 and ARROLD4-1. Green = mat, yellow = non-mat. Gp: Gypsum, Mt: Microbialite.

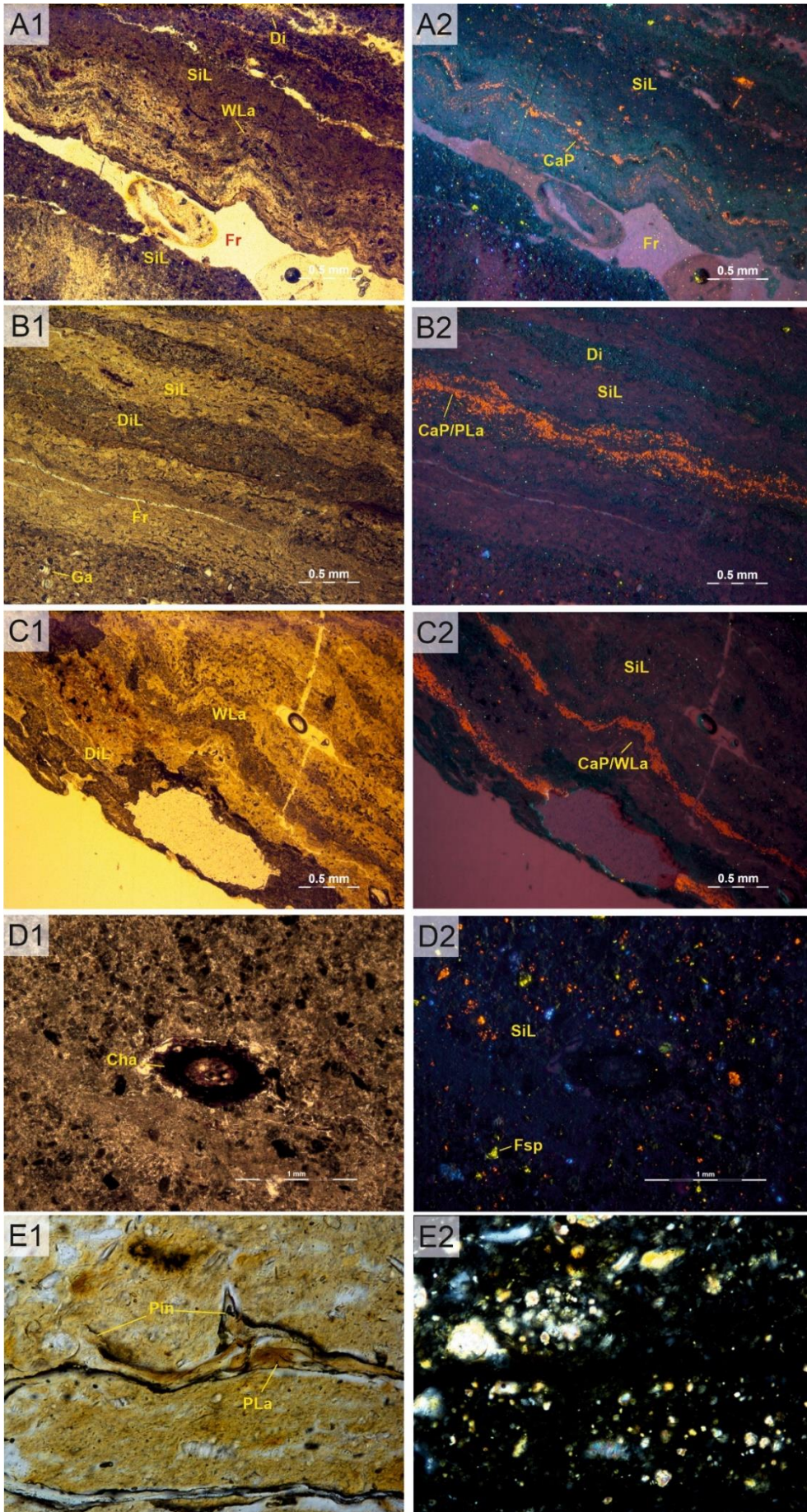


Figure 7.7b – Photomicrographs in optical and cathodoluminescence of microbial mat textures and fabrics from Lago de Arreo. A1-E1: Optical, A2-E2: Cathodoluminescence/XPL. A1-A2: Photomicrographs illustrating domal microbial mat layering (DLa) with concentration of Ca (CaP) and Mn within domal layers. Moderate amounts of other Ca/Mn-rich material is distributed throughout the matrix. Blue bright luminescent grains represent feldspars, while green luminescent grains also likely represent feldspars but of different chemical composition. B1-B2: Moderately laminated section (PLa/WLa) with inclusions of diatoms and distinctive layers of rounded, micrometre-scale Ca/Mn-rich precipitates (CaP). C1-C2: Photomicrographs illustrating wavy microbial mat layering (WLa) with concentration of Ca (CaP) and Mn within domal layers. Moderate amounts of other Ca/Mn-rich material is distributed throughout the matrix. D1-D2: Photomicrographs displaying an example of charophyte oogonium typical of Lago de Arreo sediments. Bright red and green grains in CL illustrate a mixed matrix surrounding the grain consisting of calcitic, feldspathic and other material (SiL). E1-E2: Photomicrographs displaying an example of weakly to moderately developed pinnacles (Pin) associated with the microbial mats distributed in Lago de Arreo core sediments, overlying a planar laminated microbial mat. Di: Diatoms, Fr: Fracture, Ga: Gastropods, Cha: Charophyte oogonium, Fsp: Feldspars of mixed origin.

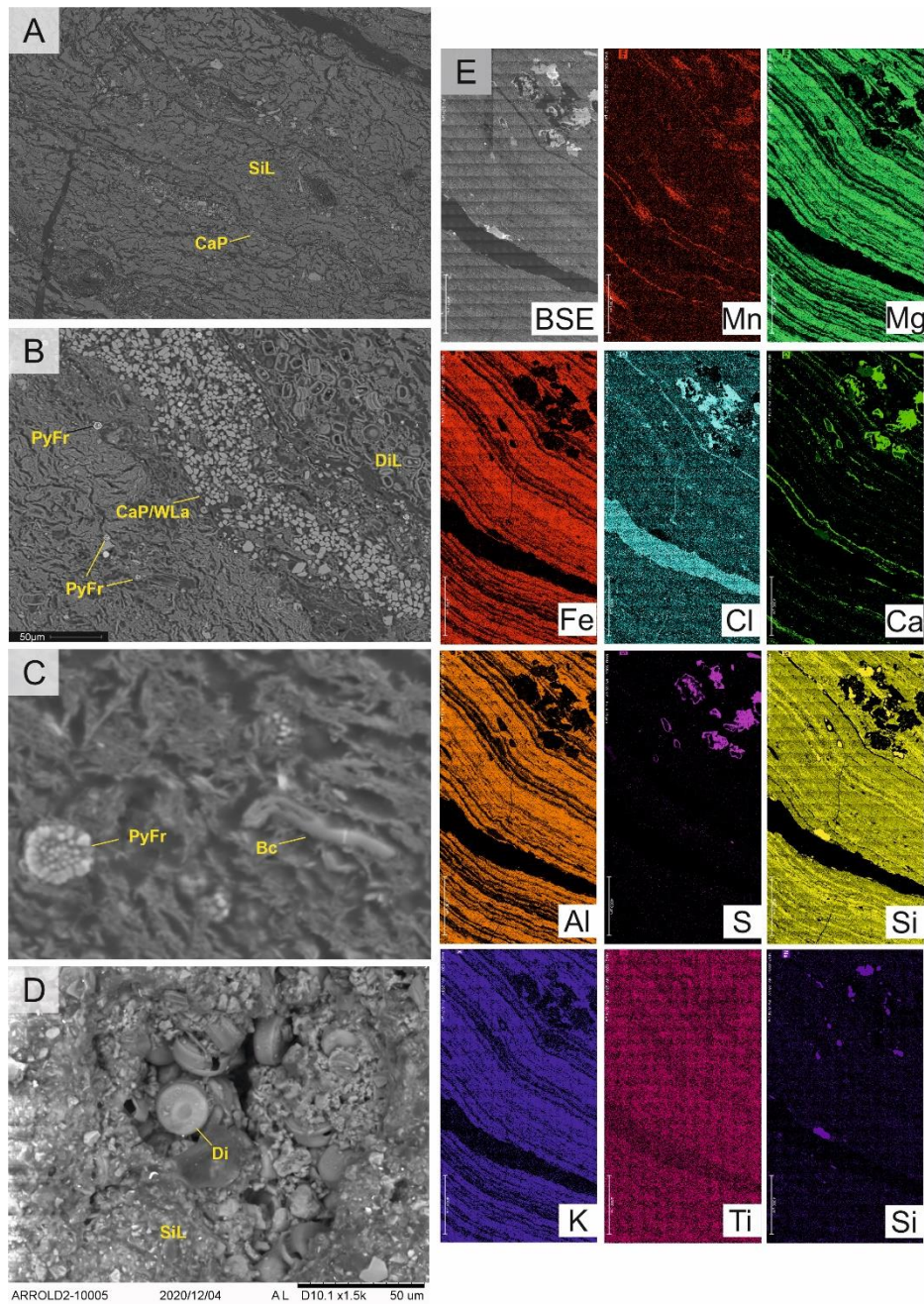


Figure 7.7c – SEM photomicrographs and EDS-maps of microbial mats from Lago de Arreo. A) Overview of desiccation structures (most likely induced during sample preparation) and laminae within microbialite sample. B) μm -scale Ca precipitates (CaP) and diatom frustules and relicts. C) High magnification view of pyrite framboid and bacterial fragment. D) Concentric diatoms present within matrices. They are strongly concentrated within specific laminae throughout each sample. E) ESEM-XRF map of sample illustrating distribution of different selected elements. SiL: Siliciclastic layering. CaP: Calcium deposits and precipitates, typically occurring as μm -scale euhedral crystals. PyFr: μm -scale pyrite framboids, of varying size, distributed throughout the sample. Di: Diatom relicts, both concentric and pennate, distributed within distinctive laminae. Bc: Remnants of bacterial sheaths.

7.4 Discussion

7.4.1 Overview

The results of the study have highlighted that microbial mats from Lakes Chiprana, Arreo, Estanya and Zonar exhibit a wide variety of morphological characteristics as well as distinctive fabrics and textures associated with mat development across varying timescales. These timescales are defined in Chiprana as ranging from the modern to ~300yrs BP, in Lake Arreo from ~400 to 500yrs BP, in Lake Estanya from 800-9400 yrs BP, and in Lake Zonar from ~50-200yrs BP. These fabrics, textures and morphological characteristics are discussed further here in terms of the environmental factors leading to their formation and development, and how key textures at varying scales may be indicative of specific environmental conditions and/or biological-environmental interactions.

7.4.2 Morphology and mesoscale characteristics as insights into environmental and depositional controls

Microbialites and microbial mats are affected by a wide range of biological (Visscher & Stolz, 2005), anthropogenic (De Wit *et al.*, 2013) and environmental factors (Casillas-Martinez *et al.*, 2005; Prieto-Barajas *et al.*, 2018; Bourillot *et al.*, 2020), the latter of which have been proven by many studies to have significant effects on their characteristics (Riding, 2011). According to Dodd *et al.* (2021), the seminal study by Walter (1976) broadly delineates the primary abiotic or abiotically-influenced processes which define microbialite morphology and geochemistry. These processes include the input of detritus and organic matter to the mats and the precipitation of minerals, the latter of which are often controlled by geochemical biological variations (Dodd *et al.*, 2021). Detrital input has been shown to lead to the development of coarse and sandy microbialite structures (Riding, 2011), while the predominance of mineral precipitation generally leads to more fine-grained and crystalline types (Riding, 2008, 2011). In the case of microbialites identified in this

study, there is a clear interplay of such processes, and both biotic and abiotic precipitation, based on the textures and fabrics discovered.

In lakes Chiprana, Zonar and Estanya, a combination of the aforementioned factors are at play, leading to the diverse characteristics of mats described in this study. All four lakes have been subjected to variable climatic, environmental and anthropogenic factors throughout the Holocene to the present day (Morellón *et al.*, 2008; Martín-Puertas *et al.*, 2009; Corella *et al.*, 2021; Doyle *et al.*, 2022b; a), and microbial mats and sediments associated with these lakes ultimately represent a combination of different timescales of formation and environmental controls. Though the effects of such controls on microbial mat formation are perhaps more readily available to interpret in the case of modern examples within Lake Chiprana, it is widely agreed in the case of Lakes Estanya (Morellón *et al.*, 2009a) and Zonar (Martín-Puertas *et al.*, 2008, 2011) that microbialites generally formed during times of decreased lake levels and subsequently increased salinity.

7.4.2.1 Lake Chiprana

Microbialite mesoscale characteristics in Lake Chiprana appear to be partly linked to environmental variations associated with the profundal and littoral ecological and depositional sub-environments. Mats identified within the profundal setting are primarily characterised by planar/stratiform lamination, dendritic morphologies, an abundance of crystalline gypsum distributed throughout the laminae (Figure 7.3a), and impeded (or entirely absent) photosynthetic, green and red sulphur communities with extensive development black sulphate-rich laminae. Morphological complexity of the mats is variable in the form of both weakly domed to undulatory laminae to significant updoming induced by dendritic gypsum deposits throughout the mat structure which furthermore lead to the development of maceriated and dendritic structures. Contrastingly, mats developing within the littoral settings are characterised by pinnacle formation, underlying cumulate gypsum, and flourishing photosynthetic, green and red sulphur bacterial communities, comparative to those

identified previously by Jonkers *et al.* (2003). Pinnacle formation in this shallow setting appears relatively uniform throughout the lake, but it is likely that external factors such as sedimentation rate, geochemistry and even bioturbation by brine shrimp may impact pinnacle morphology and development (Pinckney *et al.*, 1995; Hickman-Lewis *et al.*, 2019).

The strong limnological gradients associated with Lake Chiprana (Doyle *et al.*, 2022a) likely also play a role in establishing distinctive morphological characteristics in the profundal and littoral settings (Casillas-Martinez *et al.*, 2005). These gradients, coupled with decreasing light intensity throughout the water column, generate unique environments in which the mats develop (Kirillin & Shatwell, 2016; Woolway *et al.*, 2021). Stratification of the water column further allows for the depletion of oxygen within the monimolimnion (Foley *et al.*, 2012), represented by a decrease in dissolved oxygen from ~8mg/L within the mixolimnion to <1mg/L within the monimolimnion (see Doyle *et al.* (2022a)). This likely causes a significant change in the microbial community from the littoral to the pelagic setting, with visible shifts from an abundance of photosynthetic, green and red sulphur bacteria in the littoral setting mats (see also Jonkers *et al.*, 2003) to an increased visual abundance of purple sulphur and sulphate-reducing bacteria occurring in the profundal setting being observed. In this study, progression from the littoral to profundal setting is associated with a decrease in doming, pinnacled and tufting, illustrating decreasing morphological complexity of the mats as has been documented in other settings such as Lake Vanda (Mackey *et al.*, 2017a). The decreased availability of light and increased temperature may have resulted in a shift from primarily phototrophic to heterotrophic communities, causing the microbial community to undergo a nulled response to light due to reduced abundances of photosynthetic organisms (Nishida *et al.*, 2018).

Shifts in microbialite morphology associated with Lake Chiprana are likely also driven by changing lake levels. Variations in lake levels have been documented at

the site for the past several decades and throughout the Late Holocene by Valero-Garcés et al. (2000) and Doyle *et al.* (2022b). Previous observations from De Wit et al. (2013) have also illustrated that Lake Chiprana mats underwent significant erosion and disappeared during a water level fall in the early 1990s. During a period of reduced lake level (approximately 3.5m total depth) identified in this study in November 2019 (Doyle *et al.*, 2022b), mats displayed an extensive network of pinnacling, were overlain by a thin (3mm) mixed gypsum-halite coating, and were subject to bioturbation from active *Artemia pathogenetica* within the sediment-water interface (see chapter 6). In contrast, during a period of high lake level (~0.5m increase from November 2019) in December 2021, microbial mats exhibited a more domed, stratiform morphology in the littoral setting. Such examples of increased doming of microbial mats associated with increasing water levels has also been identified in many other lacustrine and marine settings. Andres and Reid (2006) observed increasing doming and height growth of stromatolites in Highborne Cay associated with increased water depth, while Hawes et al. (2013) identified increased laminae deposition and heightened microbialite growth in Lake Vanda over a two-decade period of lake level increase. Furthermore, the pinnacling of mats associated with decreased lake levels or shallower areas has also been described by Greco et al. (2020) in the case of lake Untersee.

In any case, understanding the characteristics of microbial mats occurring within the present is crucial if microbial mats preserved within the geological record are to be correctly interpreted (Suosaari *et al.*, 2018). This can be attempted directly in this study due to microbial mats occurring within the sedimentary sequence of the same lake between approximately 1850-1950_{AD}. Mats found in this interval illustrate comparable morphological characteristics to those observed within the modern-day profundal setting. Here, they display low morphological complexity with moderate doming and pinnacling (Figure 7.3) as well as modification of laminae by the growth of endogenic minerals such as gypsum (e.g. Figure 7.3c). As with many microbialites preserved in the geological record, interpreting biotic processes is often difficult due

to the low preservation of biological material (PARK, 1977; Riding, 2000), but the similar morphological characteristics of both modern and sub-recent mats from the same depocenter indicate that environmental conditions and potentially mat community structure may have been comparable (Jonkers et al., 2003; Riding, 2011). These distinctive sub-environments in Lake Chiprana have likely maintained a strong effect on the characteristics of microbial mats developing here. Other examples of the effects of in-lake variations in mat morphology which may be applicable to Lake Chiprana have also been discussed in the cases of Lake Clifton by Warden et al. (2016), and by Bouton et al. (2016b) for the case of Great Salt Lake. In such studies and also this work, the identification and categorisation of variations in microbialite morphology has proven critical for understanding the effect of environmental factors upon microbialite characteristics (Vennin *et al.*, 2021).

7.4.2.2 Lake Zonar

Previous studies of Lake Zonar (Martín-Puertas *et al.*, 2008, 2011) place the development of microbial mats investigated in this study between the time period of approximately 0.2-0.15ka BP. The deposits are described as a “benthic bacterial-algal mat” and are postulated to have developed within a shallow saline lake system with anoxic bottom waters as indicated by Valero-Garcés et al. (2006) and Martín-Puertas et al. (2008). The development of microbialites throughout Lake Zonar is further described by Martín-Puertas et al. (2011) as being primarily related to the degree of detrital input to the lake. In particular, they correlate the onset of extensive microbial mat development between 1800-1950AD, during which the intensity of sediment delivery to the lake decreased and biological activity increased (Martín-Puertas *et al.*, 2008, 2011). Prior to this, it is speculated that higher sediment delivery associated with changing land use and climatic conditions restricted the development of the mats throughout the lake (Valero-Garcés *et al.*, 2006).

The tomographical scans of Lake Zonar microbialites indicate that they are primarily laminated and moderately morphologically complex, illustrating weak doming and

moderate variations in dome orientation and scale throughout with some examples of updoming and potential pinnacle formation superimposed on the macrostructure of the mats (see Figure 7.5). The low to moderate morphological complexity and strong interlamination with calcitic muds and diatomaceous deposits (Valero-Garcés *et al.*, 2006; Martín-Puertas *et al.*, 2008) may be representative of reduced mineral precipitation occurring directly within the mats. For example, extensive precipitation of gypsum within Lake Chiprana microbialites, both modern and sub-recent, caused deformation of the mats leading to a “dendritic” morphology (Figure 7.3), a feature not characteristic of Lake Zonar microbialites. Changes in environmental factors as discussed previously in this study likely also led to morphological and biological variations (Bowlin *et al.*, 2012).

7.4.2.3 Lakes Arreo and Estanya

In Lakes Arreo and Estanya, based on previous studies by Corella *et al.* (2013, 2021) and Morellón *et al.* (2008, 2009a) respectively, microbial mats developed intermittently between 0.4-1ka BP in Lake Arreo and between approximately 9.4-0.8ka BP in Lake Estanya. In Lake Arreo, mats are postulated to have developed initially during the onset of an arid period beginning around 1000_{AD}, and subsequently developed until approximately 1600_{AD} during which climatic conditions became more humid, lake levels rose, and mats were not able to develop.

In Lake Estanya, increasing lake levels allowed for the development of a deep saline lake, allowing for the development of microbial mats and microbialites throughout the majority of the lakebed (Morellón *et al.*, 2009b). The environment of deposition during most of this period is described as a shallow saline lake system with abundant microbial mats. During this time, Morellón *et al.* (2009b) state that anoxic conditions and saline stratification allowed for the precipitation of calcite, aragonite and gypsum in addition to the development of microbial mats as distal facies which suggest periods of higher organic productivity. (Morellón *et al.*, 2009a)

The tomographical and petrographical analyses of Lake Arreo and Lake Estanya mats indicate that both sets of microbialites are highly comparable, being strongly laminated and generally displaying the least degree of morphological complexity of all mats described in this study. This may again be related to the relative absence of any significant mineral formation occurring directly within the mats, with much of the material within the mats primarily being composed of allogenic detritus. Distal deposits with microbial mats are predominant in Lake Estanya during most of the Holocene, but absent or limited during episodes of increased runoff and sediment delivery and characterised by the deposition of clastic facies and centred at 8.6, 6.2 and 4.8 cal kyrs BP (Morellón *et al.*, 2009a). In Lake Arreo, mats are instead concentrated between approximately 0.5-1.0ka in coincidence with an increase in aridity (Corella *et al.*, 2013). Furthermore, no microbial mats are found throughout the last 800 years in Lake Estanya and from the last 400-500 years in Lake Arreo, coinciding with significant increases of sedimentation rate from the previous rate (from 0.30 to 2.11 mm/yr) under significantly higher lake levels. This environmental change is attributed by the onset of farming activities in the area and associated higher sediment delivery in the lake catchment (Morellón *et al.*, 2009a). Therefore, it is probable that the interplay of sediment delivery and lake level fluctuations played a key role on the development of microbial mats in these lakes. Specifically, periods of increased sedimentation may have impacted the growth of the microbial mats, with the increased turbidity causing reductions in microbialite complexity and the degree of updoming of the mats (Suosaari *et al.*, 2018).

7.4.3 Using microscale texture and fabric as deeper insights into environmental and depositional factors

7.4.3.1 Lamination and Doming

Throughout this study, the shape and form of microbialite laminae are variable between stratiform, undulatory domal, and interconnected, and reflect varying processes of formation and subsequently both extrinsic and intrinsic controls (Casillas-Martinez *et al.*, 2005; Bourillot *et al.*, 2020). Perhaps the most common

lamination fabric identified is that of the interconnected horizontal laminae (HLa). Similar structures have been previously described by Gerdes *et al.* (2000), and are postulated therein to form as a result of the activities of *Coleofasiculus (Microcoleus) chthonoplastes*, whereby microbes are recognised to create continual overgrowths on the surfaces of underlying mat structures in response to the effects of environmental factors such as light and chemistry (Gerdes *et al.*, 2000; Brehm *et al.*, 2002; Prieto-Barajas *et al.*, 2018). Thus, according to Gerdes *et al.* (2000) this structure as identified in this study is likely indicative of diurnal cycling of chemical gradients, and of a longer-term seasonal effect whereby the mat structure shifts between a dominance of *Coleofasiculus (Microcoleus)* in the winter months and a dominance of coccoid cyanobacteria in the summer months. Fluctuations in such community composition have been previously identified in the case of Lake Chiprana by Jonkers *et al.* (2003), whereby changes in lake level lead to an oscillation between red sulphur bacteria appearing in the winter but not within the summer.

In the case of stratiform planar (PLa) and (WLa) lamination, the initial development of microbial mats in this study occurs as a result of the segmentation of specific functional groups throughout the mat (Visscher & Stolz, 2005; Prieto-Barajas *et al.*, 2018). Variations in the morphology of the mat are subsequently related to the nature of the underlying substrate (Hawes *et al.*, 2013), the gliding of bacteria throughout the mat in response to environmental and chemical factors (Gerdes *et al.*, 2000; Suosaari *et al.*, 2018), and potential dewatering processes when lake levels fall (De Wit *et al.*, 2013). Subsequent variations in the degree of detrital material delivered to the mats, as well as precipitation of endogenic minerals such as carbonates, calcium and magnesium sulphates identified in mats throughout this study allow for the development of distinctive intervals of organic-rich microbial laminae with interspersed allogenic and endogenic laminae (e.g. Figure 7.6a). For example, mats from Lakes Estanya and Arreo display increased abundances of detrital material within the mats and also as interlaminae between mats, a characteristic that suggests the increased detrital material led to the negation of complex morphologies

by stunting microbialite growth and causing increased interlamination of detrital and microbial facies.

The precipitation of specific minerals is also responsible for some microscale morphological variations associated with microbialites in this study. Extensive post-depositional gypsum precipitation throughout the profundal mats of Lake Chiprana causes significant updoming and a characteristic “dendritic” morphology, a characteristic that has also been identified elsewhere as in the case of microbial mats from the Canary Islands (Gerdes *et al.*, 2000). SEM analyses highlight the distribution of gypsiferous needle-like phases, cubic halite, and rose-like magnesium sulphates often found in close association with the mat structures from each of the lakes. These minerals cause minor disruptions of the mat surfaces, suggesting they likely nucleated and precipitated within the mat surface as a result of supersaturation following lake drawdown. It is also conceivable that microbial activity has an influence on the precipitation of minerals. For example, in the case of Bahamian microbialites in Big Pond, Eleuthera, Dupraz *et al.* (2004) noted the effects of microbial sulphate reduction on carbonate precipitation within the upper crusts of stratiform microbial mats. Though thick carbonate-rich crusts are not apparent in any of the microbialites identified in this study, the influence of microbial activities such as photosynthesis, sulphate reduction and the potential role of EPS (Dupraz *et al.*, 2009) on mineral precipitation cannot be discounted in any case. It is plausible that, as has previously been identified in the case of Lake Chiprana by Jonkers *et al.* (2003), processes of photosynthesis and sulphate reduction (Dupraz *et al.*, 2009) may have led to the precipitation of mineral phases such as carbonate throughout the mats identified in this study all four lakes, generating very thin laminae or pockets of these minerals throughout their structure.

Furthermore, in all of the studied microbialites, one must also consider the varying abundances of detrital material and the effect this has on mat structure, microscale

morphology and laminar characteristics. It is generally well-accepted that microbial mats can trap detrital material due to their production of sticky extracellular polymeric substances (Riding, 1991; Davies *et al.*, 2016; Suarez-Gonzalez *et al.*, 2019). Many studies have shown that the EPS can effectively glue grains in place within biofilms and microbial mats (Riding, 1991; Tosti & Riding, 2017), leading to the development of coarser and more sandy microbial textures as is common in the case of most mats identified in this study, particularly those from Lago de Estanya and Lago de Arreo. This influx of detrital material may have also directly impacted the morphology of the mats analysed throughout this study. In sub-recent mats from Lake Chiprana and Zonar microbialites for example, little detrital material is apparent (see Figures 7.3 and 7.5), and they exhibit highly domed and typically more complex structures. In contrast, microbialites from Lake Arreo and Estanya are stratiform and contain increased abundances of detrital material (see Figure 7.6 and 7.7). This may indicate that increased sediment input to the mats may have inhibited mat formation (Casillas-Martinez *et al.*, 2005), with increased sediment input potentially negating complex formation in more stratiform and non-domed mats.

7.4.3.2 Pinnacles and Clot Structures

Pinnacles are typically described as “bundles of vertically oriented filamentous microbial communities, typically cyanobacteria, that contribute to the structure of the microbial mats” (Sumner *et al.*, 2016; Hickman-Lewis *et al.*, 2019). Examples of such structures are identified in this study occurring extensively in modern and sub-recent microbial mats from Lake Chiprana and ambiguously within Holocene mats from Lake Estanya. Their development has been attributed to a wide range of factors in various studies. Studies have observed that pinnacle formation occurs as a result of microbes being affected by changes in factors such as chemistry, light intensity and geochemical parameters such as salinity (Sumner *et al.*, 2016; Hickman-Lewis *et al.*, 2019). Browne *et al.* (2000) for example illustrated that reduced water depth is generally responsible for the initiation of bundles of microbial filaments arranging into pinnacle morphologies occurring above the basal laminae of the mat. Furthermore,

according to Gerdes & Krumbein (1994) and Gerdes *et al.* (2000), pinnacle structure is postulated to occur as a result of filaments and bacteria “gliding” across the substrate and becoming entangled to reach areas of greater light intensity. In many cases, such pinnacles are primarily associated with cyanobacterial photosynthetic communities, as has been established in the case of many Antarctic settings such as Lake Vanda (Sumner *et al.*, 2016) and Lake Untersee (Greco *et al.*, 2020).

In the case of Lake Chiprana, mats developing during periods of increased lake level exhibited more stratiform morphologies and reduced pinnacled compared to mats that developed when lake levels were recessing. This may highlight the potential effect of water depth and factors such as salinity and chemistry upon the community and mat morphology. During low lake levels, when pinnacles were observed, increased light intensity reaching the mats may have induced microbes to glide across the substrate towards the light source, or increased salinity may have caused a shift in the microbial community to a predominance of organisms that preferentially develop pinnacle structures to grow towards the light source (Bosak *et al.*, 2013; Sumner *et al.*, 2016).

Finally, rare clotted fabrics consisting of clumped organic material and micrite associated with mats in Chiprana and Zonar were also identified and are akin to thrombolitic structures as discussed in detail by Riding (2011). The formation of thrombolitic microbialites has been stipulated therein and in other studies (Riding, 1991) to arise from microbially-induced precipitation and calcification involving coccoidal cyanobacteria (Mei *et al.*, 2020), in the case of this study being characterised by carbonate-rich material and micrite forming in interstitial voids between gypsum grains. Microbially-induced precipitation of carbonate initially took place and was associated with minor trapping of other detritus such as organic matter and detrital material (Riding, 2011), followed by nucleation and precipitation of gypsum throughout the clot structures, destroying some of the original fabric.

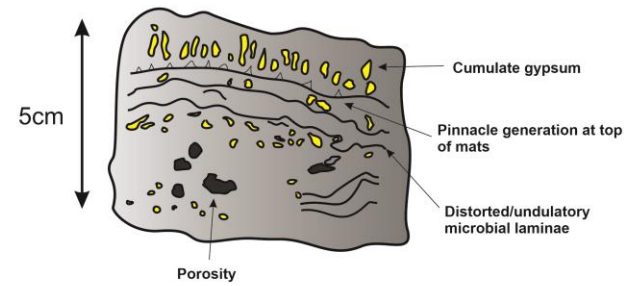
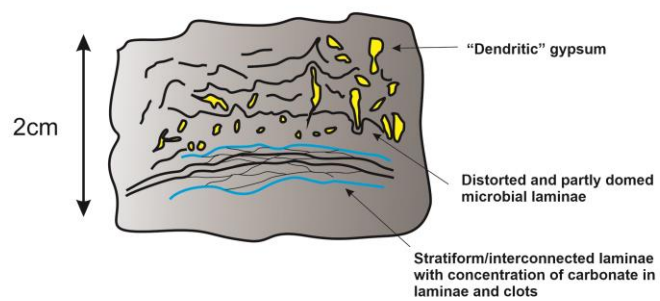
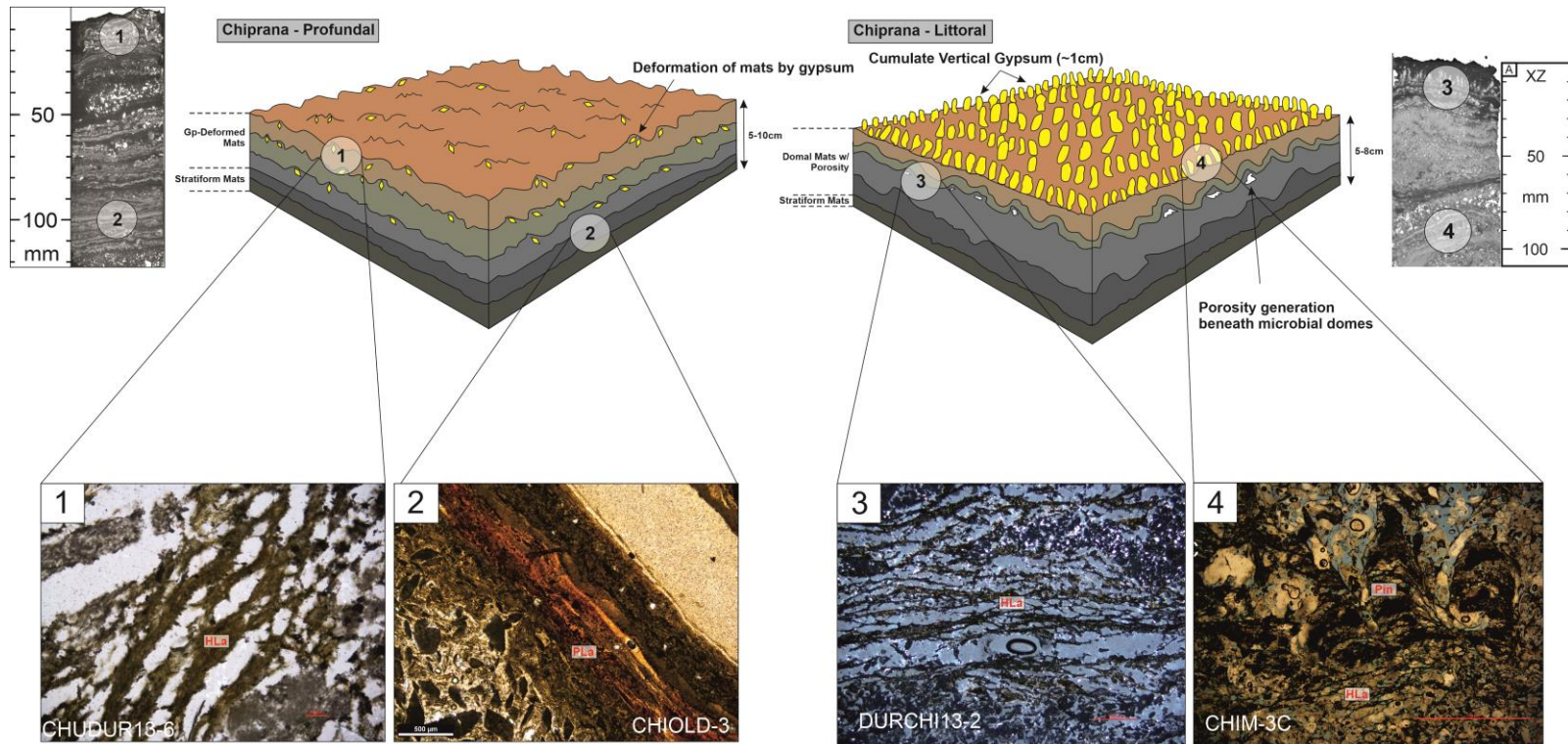


Figure 7.12a - Figure summarising the key characteristics of microbial mats from A) The profundal setting of Lake Chiprana, and B) The littoral setting of Lake Chiprana. The mesoscale morphology of the mats is presented with insights into microscale characteristics and key microfabrics identified using petrography.

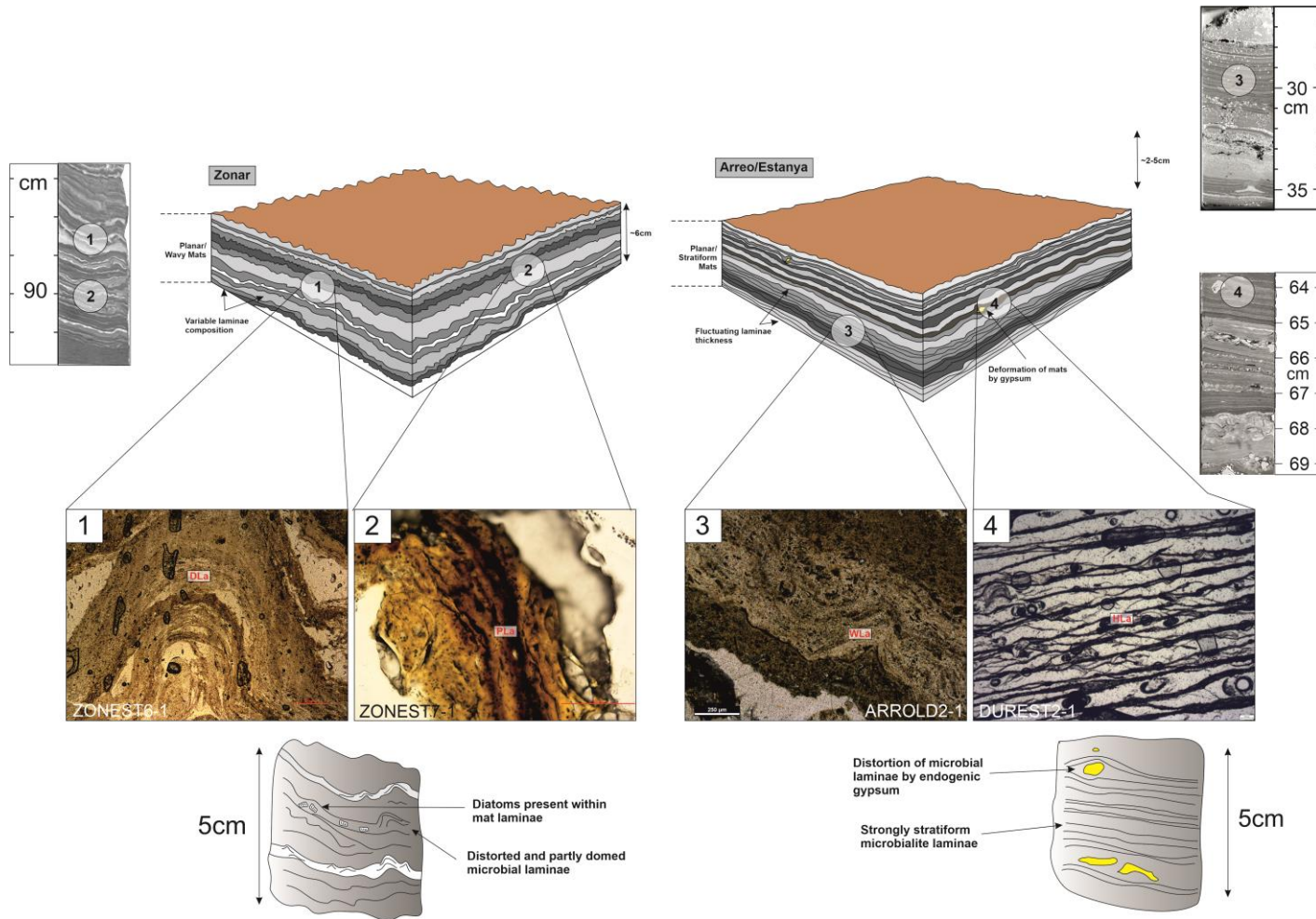
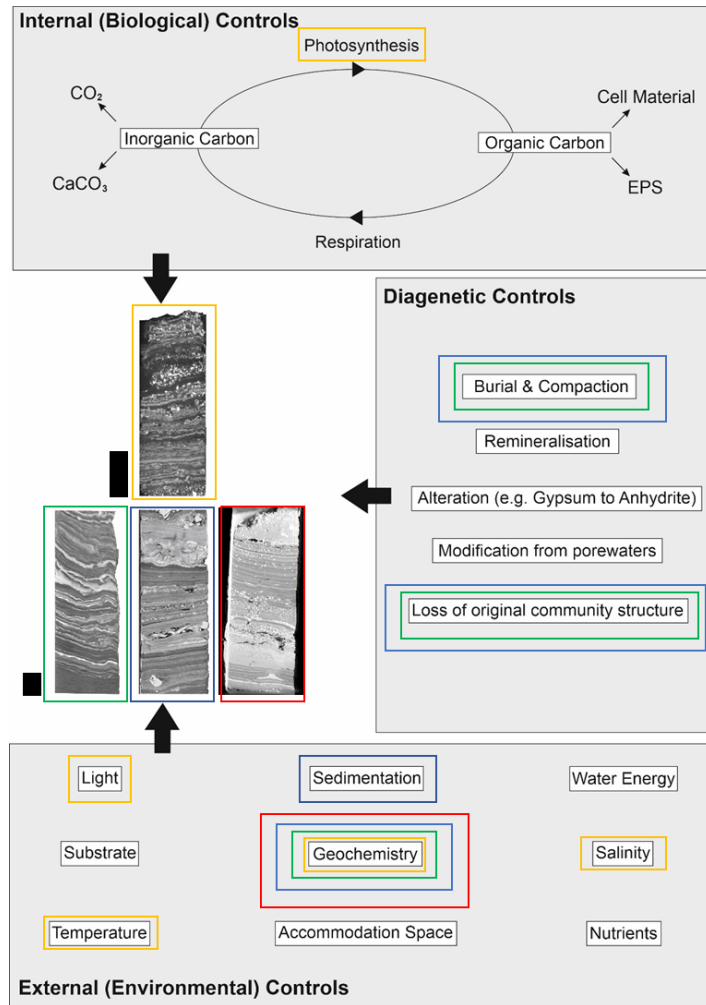


Figure 7.12b - Figure summarising the key characteristics of microbial mats from A) Lake Zonar, and B) Lakes Arreo and Estanya. The mesoscale morphology of the mats is presented with insights into microscale characteristics and key microfabrics identified using petrography.



- Lago de Arreo
- Laguna Salada de Chiprana
- Lago de Estanya
- Laguna Zonar

Figure 7.13 – Synthesis of the primary internal and external factors acting upon the development of microbial mats postulated from results in this study, as well as the potential diagenetic effects involved. The importance of such factors can vary significantly between different sites, and it is often difficult to disentangle the individual effects of each factor. Diagenetic effects may also vary significantly depending on the timescale of sedimentation and burial that has impacted the mats. Modified from Dupraz et al. (2006). Black scale bars = 1

7.5 Conclusions

Computerised tomographical scanning and petrographic analyses of microbialites throughout saline-hypersaline lakes and sedimentary sequences in the Iberian Peninsula provide deep insights into the mesoscale and microscale characteristics of these unique deposits. The high-resolution CT scanning sheds new light on within-mat morphological variations from the four lakes, while whole thin-sections scans, high resolution photomicrographs and SEM bridge the gap between morphology and fabric in attempting to understand how these deposits form. In all cases of microbial mat formation within Laguna Salada de Chiprana, Laguna Zonar, Lago de Estanya and Lago de Arreo, development of microbial mats occurred primarily during periods of lower lake levels occurring at each site (Valero-Garces *et al.*, 2000; Morellón *et al.*, 2009b; Martín-Puertas *et al.*, 2011; Lindsay *et al.*, 2019). Subsequent variations in mat morphology at the mesoscale and microscale are related to changing environmental conditions in the settings in which they are found, but intrinsic biological factors must also be investigated when considering these complex deposits. In Lake Chiprana, microbialite morphologies are related primarily to varying geochemical conditions and mineralogical phases developing throughout the mats in the profundal and littoral settings. Specifically, mats from the profundal setting display characteristics that are strongly influenced by the precipitation of gypsum throughout the mat structure, leading to dendritic and slightly updomed morphologies at the mesoscale. Superimposed upon these mats is a strongly interconnected fabric termed “Lh” laminae which formed as a result of bacteria gliding throughout the mat structure. In contrast, mats from the littoral setting display stratiform to undulatory morphologies at the mesoscale, yet display complex pinnacled and interlaminated fabrics at the microscale which are suggestive of complex geochemical stressor and biotic-abiotic interactions. In Lakes Arreo and Estanya, mats display highly stratiform morphologies with low morphological complexity, though similar deformation of the mats by endogenic gypsum is identified in some cases. These mats are postulated to have been affected by detrital input due to the interlamination and presence of increased detritus associated with these mats, though it is plausible that diagenetic

processes, burial and compaction may have led to further reduction of microbialite complexity due to the older age of these mats.

Overall, discussions and interpretations of microbialite macrostructures must account for the biological factors associated with the mats themselves as well as external factors that act upon the mats (Riding, 2011; Bourillot *et al.*, 2020). Ultimately, the relationships between these factors generate a wide spectrum of characteristics in microbialites, and it is the wide variability of this spectrum that has remained a point of investigation in many studies focusing upon these unique deposits (Camoin *et al.*, 2006; Mata & Bottjer, 2012; Chagas *et al.*, 2016).

References

- Andres, M.S. and Reid, R.P.** (2006) Growth morphologies of modern marine stromatolites: A case study from Highborne Cay, Bahamas. *Sediment. Geol.*, **185**, 319–328.
- Baumgartner, L.K., Dupraz, C., Buckley, D.H., Spear, J.R., Pace, N.R. and Visscher, P.T.** (2009) Microbial species richness and metabolic activities in hypersaline microbial mats: Insight into biosignature formation through lithification. *Astrobiology*, **9**, 861–874.
- Bosak, T., Knoll, A.H. and Petroff, A.P.** (2013) The meaning of stromatolites. *Annu. Rev. Earth Planet. Sci.*, **41**, 21–44.
- Bourillot, R., Vennin, E., Dupraz, C., Pace, A., Foubert, A., Rouchy, J.M., Patrier, P., Blanc, P., Bernard, D., Lesseur, J. and Visscher, P.T.** (2020) The record of environmental and microbial signatures in ancient microbialites: The terminal carbonate complex from the neogene basins of southeastern Spain. *Minerals*, **10**, 1–50.
- Bouton, A., Vennin, E., Boule, J., Pace, A., Bourillot, R., Thomazo, C., Brayard, A., Désaubliaux, G., Goslar, T., Yokoyama, Y., Dupraz, C. and Visscher, P.T.** (2016a) Linking the distribution of microbial deposits from the Great Salt Lake (Utah, USA) to tectonic and climatic processes. *Biogeosciences*, **13**, 5511–5526.
- Bouton, A., Vennin, E., Pace, A., Bourillot, R., Dupraz, C., Thomazo, C., Brayard, A., Désaubliaux, G. and Visscher, P.T.** (2016b) External controls on the distribution, fabrics and mineralization of modern microbial mats in a coastal hypersaline lagoon, Cayo Coco (Cuba). *Sedimentology*, **63**, 972–1016.
- Bowlin, E.M., Klaus, J.S., Foster, J.S., Andres, M.S., Custals, L. and Reid, R.P.** (2012) Environmental controls on microbial community cycling in modern marine stromatolites. *Sediment. Geol.*, **263–264**, 45–55.
- Braissant, O., Decho, A.W., Dupraz, C., Glunk, C., Przekop, K.M. and Visscher, P.T.** (2007) Exopolymeric substances of sulfate-reducing bacteria: Interactions with calcium at alkaline pH and implication for formation of carbonate minerals. *Geobiology*, **5**, 401–411.
- Brehm, U., Gasiewicz, A., Gerdes, G. and Krumbein, W.E.** (2002) Biolaminoid facies in a peritidal sabkha: Permian platy dolomite of Northern Poland. *Int J Earth Sci.* doi: 10.1007/s005310100207
- Browne, K.M., Golubic, S. and Seong-Joo, L.** (2000) Shallow Marine Microbial Carbonate Deposits. In: *Microbial Sediments*,

- Camoin, G., Cabioch, G., Eisenhauer, A., Braga, J.C., Hamelin, B. and Lericolais, G.** (2006) Environmental significance of microbialites in reef environments during the last deglaciation. *Sediment. Geol.*, **185**, 277–295.
- Canfield, D.E. and Des Marais, D.J.** (1993) Biogeochemical cycles of carbon, sulfur, and free oxygen in a microbial mat. *Geochim. Cosmochim. Acta*, **57**, 3971–3984.
- Cardoso, D.C., Cretoiu, M.S., Stal, L.J. and Bolhuis, H.** (2019) Seasonal development of a coastal microbial mat. *Sci Rep.* doi: 10.1038/s41598-019-45490-8
- Casillas-Martinez, L., Gonzalez, M.L., Fuentes-Figueroa, Z., Castro, C.M., Nieves-Mendez, D., Hernandez, C., Ramirez, W., Sytsma, R.E., Perez-Jimenez, J. and Visscher, P.T.** (2005) Community structure, geochemical characteristics and mineralogy of a hypersaline microbial mat, Cabo Rojo, PR. *Geomicrobiol. J.*, **22**, 269–281.
- Chagas, A.A.P., Webb, G.E., Burne, R. V. and Southam, G.** (2016) Modern lacustrine microbialites: Towards a synthesis of aqueous and carbonate geochemistry and mineralogy. *Earth-Science Rev.*, **162**, 338–363.
- Chen, J. and Lee, J.H.** (2014) Current progress on the geological record of microbialites and microbial carbonates. *Acta Geol. Sin.*, **88**, 260–275.
- Corella, J.P., Amrani, A. El, Sigró, J., Morellón, M., Rico, E. and Valero-Garcés, B.L.** (2011) Recent evolution of Lake Arreo, northern Spain: Influences of land use change and climate. *J. Paleolimnol.*, **46**, 469–485.
- Corella, J.P., Benito, G., Monteoliva, A.P., Sigro, J., Calle, M., Valero-Garcés, B.L., Stefanova, V., Rico, E., Favre, A.C. and Wilhelm, B.** (2021) A 1400-years flood frequency reconstruction for the Basque country (N Spain): Integrating geological, historical and instrumental datasets. *Quat. Sci. Rev.*, **262**, 1–15.
- Corella, J.P., Stefanova, V., El Anjoumi, A., Rico, E., Giralt, S., Moreno, A., Plata-Montero, A. and Valero-Garcés, B.L.** (2013) A 2500-year multi-proxy reconstruction of climate change and human activities in northern Spain: The Lake Arreo record. *Palaeogeogr. Palaeoclimatol. Palaeoecol.*, **386**, 555–568.
- Davies, N.S., Liu, A.G., Gibling, M.R. and Miller, R.F.** (2016) Resolving MISS conceptions and misconceptions: A geological approach to sedimentary surface textures generated by microbial and abiotic processes. *Earth-Science Rev.*, **154**, 210–246.
- De Wit, R., Guerrero, M.C., Legaz, A., Jonkers, H.M., Blocier, L., Gumiaux, C.**

and **Gautret, P.** (2013) Conservation of a permanent hypersaline lake: Management options evaluated from decadal variability of coleofasciculus chthonoplastes microbial mats. *Aquat. Conserv. Mar. Freshw. Ecosyst.*, **23**, 532–545.

Dodd, C., Anderson, C.R., Rishworth, G.M., Perissinotto, R. and van Niekerk, X. (2021) Metazoan activity facilitates passive sediment trapping in modern supratidal microbialites: Revealed using μ -CT-scanning and microscopy. *Geobiology*, **19**, 585–600.

Doyle, C., Corella, J.P., Schröder, S., Strauss, H., Bishop, T., Yarwood, J. and Valero-Garcés, B. (2022a) Spatio-Temporal Variations in the Geochemistry of Laguna Salada de Chiprana, NE Spain. *Geosci.* **12**:

Doyle, C., Schröder, S., Corella, J.P. and Valero Garces, B. (2022b) Facies variability and depositional settings of Laguna Salada de Chiprana, an Iberian hypersaline lake. *Sedimentology*, **69**, 2615–2641.

Dupraz, C., Pattisina, R. and Verrecchia, E.P. (2006) Translation of energy into morphology: Simulation of stromatolite morphospace using a stochastic model. *Sediment. Geol.*, **185**, 185–203.

Dupraz, C., Reid, R.P., Braissant, O., Decho, A.W., Norman, R.S. and Visscher, P.T. (2009) Processes of carbonate precipitation in modern microbial mats. *Earth-Science Rev.*, **96**, 141–162.

Dupraz, C. and Visscher, P.T. (2005) Microbial lithification in marine stromatolites and hypersaline mats. *Trends Microbiol.*, **13**, 429–438.

Dupraz, C., Visscher, P.T., Baumgartner, L.K. and Reid, R.P. (2004) Microbe-mineral interactions: Early carbonate precipitation in a hypersaline lake (Eleuthera Island, Bahamas). *Sedimentology*, **51**, 745–765.

Emmanouilidis, A., Messaris, G., Ntzanis, E., Zampakis, P., Prevedouros, I., Bassukas, D.A. and Avramidis, P. (2020) CT scanning, X-ray fluorescence: Non-destructive techniques for the identification of sedimentary facies and structures. *Rev. Micropaleontol.*, **67**, 1–15.

Engelberg, D.L., Pattrick, R.A.D., Wilson, C., McCrae, R. and Withers, P.J. (2012) Three-dimensional imaging of inhomogeneous lithologies using X-ray computed tomography: characterization of drill core from the Borrowdale Volcanic Group. *Mineral. Mag.*, **76**, 2931–2938.

Foley, B., Jones, I.D., Maberly, S.C. and Rippey, B. (2012) Long-term changes in oxygen depletion in a small temperate lake: Effects of climate change and eutrophication. *Freshw. Biol.*, **57**, 278–289.

- Franks, J. and Stolz, J.F.** (2009) Flat laminated microbial mat communities. *Earth-Science Rev.*, **96**, 163–172.
- Gerdes, G. and Krumbein, W.E.** (1994) Peritidal Potential Stromatolites — A Synopsis. In: *Phanerozoic Stromatolites II*,
- Gerdes, G., Krumbein, W.E. and Noffke, N.** (2000) Evaporite Microbial Sediments. In: *Microbial Sediments*, 196–208.
- Ginsburg, R.N. and Planavsky, N.J.** (2008) Diversity of bahamian microbialite substrates. In: *Modern Approaches in Solid Earth Sciences*, 4, 177–195.
- González-Sampériz, P., Valero-Garcés, B.L., Moreno, A., Morellón, M., Navas, A., Machín, J. and Delgado-Huertas, A.** (2008) Vegetation changes and hydrological fluctuations in the Central Ebro Basin (NE Spain) since the Late Glacial period: Saline lake records. *Palaeogeogr. Palaeoclimatol. Palaeoecol.*, **259**, 157–181.
- Greco, C., Andersen, D.T., Hawes, I., Bowles, A.M.C., Yallop, M.L., Barker, G. and Jungblut, A.D.** (2020) Microbial Diversity of Pinnacle and Conical Microbial Mats in the Perennially Ice-Covered Lake Untersee, East Antarctica. *Front. Microbiol.*, **11**, 1–15.
- Grey, K. and Awramik, S.M.** (2020) Handbook for the study and description of microbialites, Bulletin 1. *Geological Survey of Western Australia*, 1-278 pp.
- Grotzinger, J.P. and Rothman, D.H.** (1996) An abiotic model for stromatolite morphogenesis. *Nature*, **383**, 423–425.
- Guerrero, M.C.** (1992) Microbial mats in the inland saline lakes of Spain. *Limnetica*, **8**, 197–204.
- Hawes, I., Sumner, D.Y., Andersen, D.T., Jungblut, A.D. and Mackey, T.J.** (2013) Timescales of growth response of microbial mats to environmental change in an ice-covered Antarctic lake. *Biology (Basel)*, **2**, 151–176.
- Hickman-Lewis, K., Garwood, R.J., Withers, P.J. and Wacey, D.** (2017) X-ray microtomography as a tool for investigating the petrological context of Precambrian cellular remains. *Geol. Soc. Spec. Publ.*, **448**, 33–56.
- Hickman-Lewis, K., Gautret, P., Arbaret, L., Sorieul, S., De Wit, R., Foucher, F., Cavalazzi, B. and Westall, F.** (2019) Mechanistic morphogenesis of organo-sedimentary structures growing under geochemically stressed conditions: Keystone to proving the biogenicity of some Archaean stromatolites? *Geosci.*, **9**, 1–31.
- IGME** (2003a) Mapa Geológico de España, 1:50000, (serie MAGNA). Hoja 137.

Miranda de Ebro.

IGME (2003b) Mapa Geologico de Espana, 1:50000, (serie MAGNA). Hoja 988. Puente-Genil.

Jódar, J., Rubio, F.M., Custodio, E., Martos-Rosillo, S., Pey, J., Herrera, C., Turu, V., Pérez-Bielsa, C., Ibarra, P. and Lambán, L.J. (2020) Hydrogeochemical, isotopic and geophysical characterization of saline lake systems in semiarid regions: The Salada de Chiprana Lake, Northeastern Spain. *Sci. Total Environ.*, **728**, 1–48.

Johnson, J. and Grotzinger, J.P. (2006) Affect of sedimentation on stromatolite reef growth and morphology, Ediacaran Omkyk Member (Nama Group), Namibia. *South African J. Geol.*, **109**, 87–96.

Jonkers, H.M., Ludwig, R., De Wit, R., Pringault, O., Muyzer, G., Niemann, H., Finke, N. and De Beer, D. (2003) Structural and functional analysis of a microbial mat ecosystem from a unique permanent hypersaline inland lake: “La Salada de Chiprana” (NE Spain). *FEMS Microbiol. Ecol.*, **44**, 175–189.

Kirillin, G. and Shatwell, T. (2016) Generalized scaling of seasonal thermal stratification in lakes. *Earth-Science Rev.* 161:179–190.

Lindsay, M.R., Johnston, R.E., Baxter, B.K. and Boyd, E.S. (2019) Effects of salinity on microbialite-associated production in Great Salt Lake, Utah. *Ecology*, **100**, 1–15.

Mackey, T.J., Sumner, D.Y., Hawes, I. and Jungblut, A.D. (2017a) Morphological signatures of microbial activity across sediment and light microenvironments of Lake Vanda, Antarctica. *Sediment. Geol.*, **361**, 82–92.

Mackey, T.J., Sumner, D.Y., Hawes, I., Jungblut, A.D., Lawrence, J., Leidman, S. and Allen, B. (2017b) Increased mud deposition reduces stromatolite complexity. *Geology*, **45**, 663–666.

Martín-Puertas, C., Valero-Garcés, B.L., Brauer, A., Mata, M.P., Delgado-Huertas, A. and Dulski, P. (2009) The Iberian-Roman Humid Period (2600–1600 cal yr BP) in the Zoñar Lake varve record (Andalucía, southern Spain). *Quat. Res.*, **71**, 108–120.

Martín-Puertas, C., Valero-Garcés, B.L., Mata, M.P., González-Sampériz, P., Bao, R., Moreno, A. and Stefanova, V. (2008) Arid and humid phases in southern Spain during the last 4000 years: The Zoñar Lake record, Córdoba. *Holocene*, **18**, 907–921.

Martín-Puertas, C., Valero-Garcés, B.L., Mata, M.P., Moreno, A., Giral, S.,

- Martínez-Ruiz, F. and Jiménez-Espejo, F.** (2011) Geochemical processes in a Mediterranean Lake: A high-resolution study of the last 4,000 years in Zoñar Lake, southern Spain. *J. Paleolimnol.*, **46**, 405–421.
- Martínez-Alonso, M., Van Bleijswijk, J., Gaju, N. and Muyzer, G.** (2005) Diversity of anoxygenic phototrophic sulfur bacteria in the microbial mats of the Ebro Delta: A combined morphological and molecular approach. *FEMS Microbiol. Ecol.*, **52**, 339–350.
- Mata, S.A. and Bottjer, D.J.** (2012) Microbes and mass extinctions: Paleoenvironmental distribution of microbialites during times of biotic crisis. *Geobiology*, **10**, 3–24.
- Mei, M., Latif, K., Mei, C., Gao, J. and Meng, Q.** (2020) Thrombolitic clots dominated by filamentous cyanobacteria and crusts of radio-fibrous calcite in the Furongian Changshan Formation, North China. *Sediment. Geol.*, **395**, 1–15.
- Morellón, M., Valero-Garcés, B., Anselmetti, F., Ariztegui, D., Schnellmann, M., Moreno, A., Mata, P., Rico, M. and Corella, J.P.** (2009a) Late quaternary deposition and facies model for karstic Lake Estanya (North-eastern Spain). *Sedimentology*, **56**, 1505–1534.
- Morellón, M., Valero-Garcés, B., González-Sampériz, P., Vegas-Vilarrúbia, T., Rubio, E., Rieradevall, M., Delgado-Huertas, A., Mata, P., Romero, Ó., Engstrom, D.R., López-Vicente, M., Navas, A. and Soto, J.** (2011) Climate changes and human activities recorded in the sediments of Lake Estanya (NE Spain) during the Medieval Warm Period and Little Ice Age. *J. Paleolimnol.*, **46**, 423–452.
- Morellón, M., Valero-Garcés, B., Moreno, A., González-Sampériz, P., Mata, P., Romero, O., Maestro, M. and Navas, A.** (2008) Holocene palaeohydrology and climate variability in northeastern Spain: The sedimentary record of Lake Estanya (Pre-Pyrenean range). *Quat. Int.*, **181**, 15–31.
- Morellón, M., Valero-Garcés, B., Vegas-Vilarrúbia, T., González-Sampériz, P., Romero, Ó., Delgado-Huertas, A., Mata, P., Moreno, A., Rico, M. and Corella, J.P.** (2009b) Lateglacial and Holocene palaeohydrology in the western Mediterranean region: The Lake Estanya record (NE Spain). *Quat. Sci. Rev.*, **28**, 2582–2599.
- Nishida, A., Thiel, V., Nakagawa, M., Ayukawa, S. and Yamamura, M.** (2018) Effect of light wavelength on hot spring microbial mat biodiversity. *PLoS One*, **13**, 1–17.

- Nutman, A.P., Bennett, V.C., Friend, C.R.L., Van Kranendonk, M.J. and Chivas, A.R.** (2016) Rapid emergence of life shown by discovery of 3,700-million-year-old microbial structures. *Nature*, **537**, 535–538.
- Pace, A., Bourillot, R., Bouton, A., Vennin, E., Galaup, S., Bundeleva, I., Patrier, P., Dupraz, C., Thomazo, C., Sansjofre, P., Yokoyama, Y., Franceschi, M., Anguy, Y., Pigot, L., Virgone, A. and Visscher, P.T.** (2016) Microbial and diagenetic steps leading to the mineralisation of Great Salt Lake microbialites. *Sci. Rep.*, **6**, 1–12.
- PARK, R.K.** (1977) The preservation potential of some recent stromatolites. *Sedimentology*, **24**, 485–506.
- Pinckney, J., Paerl, H.W. and Fitzpatrick, M.** (1995) Impacts of seasonality and nutrients on microbial mat community structure and function. *Mar. Ecol. Prog. Ser.*, **123**, 207–216.
- Prieto-Barajas, C.M., Valencia-Cantero, E. and Santoyo, G.** (2018) Microbial mat ecosystems: Structure types, functional diversity, and biotechnological application. *Electron. J. Biotechnol.* 31:48–56.
- Riding, R.** (1991) Classification of Microbial Carbonates. In: *Calcareous Algae and Stromatolites* (Ed. R. Riding), *Springer Berlin Heidelberg*, Berlin, Heidelberg, 21–51.
- Riding, R.** (2011) Microbialites, stromatolites, and thrombolites. In: *Encyclopedia of Earth Sciences Series*, 635–654.
- Riding, R.** (2008) Abiogenic, microbial and hybrid authigenic carbonate crusts: Components of Precambrian stromatolites. *Geol. Croat.*, **61**, 73–103.
- Riding, R.** (2000) Microbial carbonates: The geological record of calcified bacterial-algal mats and biofilms. *Sedimentology*, **47**, 179–214.
- Sanz-Montero, M., Cabestrero Aranda, O. and P. Rodríguez Aranda, J.** (2013) Hydromagnesite precipitation in microbial mats from a highly alkaline lake, Central Spain.
- Schieber, J.** (2007) Atlas of microbial mat features preserved within the siliciclastic rock record.
- Stal, L.J., van Gernerden, H. and Krumbein, W.E.** (1985) Structure and development of a benthic marine microbial mat. *FEMS Microbiol. Lett.*, **31**, 111–125.
- Stolz, J.F.** (1994) Light and electron microscopy in microbial mat research: An overview. In: *Microbial Mats*, 173–182.

- Suarez-Gonzalez, P., Benito, M.I., Quijada, I.E., Mas, R. and Campos-Soto, S.** (2019) 'Trapping and binding': A review of the factors controlling the development of fossil agglutinated microbialites and their distribution in space and time. *Earth-Science Rev.* 194:182–215.
- Sumner, D.Y., Jungblut, A.D., Hawes, I., Andersen, D.T., Mackey, T.J. and Wall, K.** (2016) Growth of elaborate microbial pinnacles in Lake Vanda, Antarctica. *Geobiology*, 14, 556–574.
- Suosaari, E.P., Awramik, S.M., Reid, R.P., Stolz, J.F. and Grey, K.** (2018) Living dendrolitic microbial mats in hamelin pool, Shark Bay, Western Australia. *Geosci.*, 8, 1–17.
- Suosaari, E.P., Reid, R.P., Playford, P.E., Foster, J.S., Stolz, J.F., Casaburi, G., Hagan, P.D., Chirayath, V., Macintyre, I.G., Planavsky, N.J. and Eberli, G.P.** (2016) New multi-scale perspectives on the stromatolites of Shark Bay, Western Australia. *Sci. Rep.*, 6, 1–15.
- Tan, Q., Shi, Z., Hu, X.Q., Wang, Y., Tian, Y.M. and Wang, C.C.** (2018) Diagenesis of microbialites in the lower Cambrian Qingxudong Formation, South China: Implications for the origin of porosity in deep microbial carbonates. *J. Nat. Gas Sci. Eng.*, 51, 166–182.
- Tosti, F. and Riding, R.** (2017) Fine-grained agglutinated elongate columnar stromatolites: Tieling Formation, ca 1420 Ma, North China. *Sedimentology*, 64, 871–902.
- Valero-Garcés, B., Morellón, M., Moreno, A., Corella, J.P., Martín-Puertas, C., Barreiro, F., Pérez, A., Giral, S. and Mata-Campo, M.P.** (2014) Lacustrine carbonates of Iberian Karst Lakes: Sources, processes and depositional environments. *Sediment. Geol.* 299:1–29.
- Valero-Garcés, B.L., González-Sampériz, P., Navas, A., Machín, J., Mata, P., Delgado-Huertas, A., Bao, R., Moreno, A., Carrión, J.S., Schwab, A. and González-Barrios, A.** (2006) Human impact since medieval times and recent ecological restoration in a Mediterranean lake: The Laguna Zoñar, southern Spain. *J. Paleolimnol.*, 35, 441–465.
- Valero-Garcés, B.L., Navas, A., Machin, J., Stevenson, T. and Davis, B.** (2000) Responses of a saline lake ecosystem in a semiarid region to irrigation and climate variability: The history of Salada Chiprana, central Ebro basin, Spain. *Ambio*, 29, 344–350.
- Valero-Garcés, B.L., Navas, A., Machin, J., Stevenson, T., Davis, B., Valero-Garcés, B.L., Navas, A., Machin, J., Stevenson, T., Davis, B., Valero-**

- Garcés, B.L., Navas, A., Machin, J., Stevenson, T. and Davis, B.** (2000) Responses of a Saline Lake Ecosystem in a Semiarid Region to Irrigation and Climate Variability. *AMBIO A J. Hum. Environ.*, **29**, 344–350.
- Vennin, E., Bouton, A., Roche, A., Gérard, E., Bundeleva, I., Boussagol, P., Wattinne, A., Kolodka, C., Gaucher, E., Virgone, A. and Visscher, P.T.** (2021) The Limagne Basin: A journey through modern and fossil microbial deposits. *BSGF - Earth Sci. Bull.*, **192**, 1–17.
- Verleyen, E., Sabbe, K., Hodgson, D.A., Grubisic, S., Taton, A., Cousin, S., Wilmotte, A., De Wever, A., Van Der Gucht, K. and Vyverman, W.** (2010) Structuring effects of climate-related environmental factors on Antarctic microbial mat communities. *Aquat. Microb. Ecol.*, **59**, 11–24.
- Visscher, P.T. and Stolz, J.F.** (2005) Microbial mats as bioreactors: Populations, processes, and products. *Palaeogeogr. Palaeoclimatol. Palaeoecol.*, **219**, 87–100.
- Walter, M..** (1976) *Stromatolites* / edited by M. R. Walter. *Elsevier Scientific Pub. Co*, Amsterdam ; New York.
- Warden, J.G., Casaburi, G., Omelon, C.R., Bennett, P.C., Breecker, D.O. and Foster, J.S.** (2016) Characterization of microbial mat microbiomes in the modern thrombolite ecosystem of lake clifton, western australia using shotgun metagenomics. *Front. Microbiol.*, **7**, 1–16.
- White, R.A.** (2020) The Global Distribution of Modern Microbialites: Not So Uncommon After All. 107–134.
- Wingender, J., Neu, T.R. and Flemming, H.-C.** (1999) What are Bacterial Extracellular Polymeric Substances? In: *Microbial Extracellular Polymeric Substances*, 1–19.
- Wong, H.L., White, R.A., Visscher, P.T., Charlesworth, J.C., Vázquez-Campos, X. and Burns, B.P.** (2018) Disentangling the drivers of functional complexity at the metagenomic level in Shark Bay microbial mat microbiomes. *ISME J.*, **12**, 2619–2639.
- Woolway, R.I., Sharma, S., Weyhenmeyer, G.A., Debolskiy, A., Golub, M., Mercado-Bettín, D., Perroud, M., Stepanenko, V., Tan, Z., Grant, L., Ladwig, R., Mesman, J., Moore, T.N., Shatwell, T., Vanderkelen, I., Austin, J.A., DeGasperi, C.L., Dokulil, M., La Fuente, S., Mackay, E.B., Schladow, S.G., Watanabe, S., Marcé, R., Pierson, D.C., Thiery, W. and Jennings, E.** (2021) Phenological shifts in lake stratification under climate change. *Nat. Commun.*, **12**, 1–16.

BLANK PAGE

Chapter 8 – Conclusions & Synthesis

As discussed in Chapter 1, there are a number of key questions and issues that remain unresolved with regards to our understanding of how saline lakes can act as valid repositories of environmental information, and how microbial mats can be used specifically to add a deeper understanding of paleoenvironmental processes occurring within these settings. The several key questions approached throughout the thesis included:

- ***Problem 1 - What information can be extracted from saline lakes to determine (palaeo)environmental processes both spatially and temporally, and subsequently:***
 - ***Can saline lacustrine sedimentary sequences be reliably utilised for high-resolution palaeoenvironmental reconstructions?***
- ***Problem 2 - How do microbialite morphological and geochemical characteristics vary through space and time in different saline lacustrine settings?***
- ***Problem 3 - What are the effects of environmental and geochemical conditions on microbial mats in the present and the recent past?***

Subsequently, the aims as stated below and in chapter 1 were developed with a subsidiary set of specific objectives in order to investigate the above questions and understand how both saline lakes and microbialites can be used in the reconstruction of palaeoenvironmental conditions.

- ***Aim 1 - Assess spatio-temporal variability and subsequently palaeoenvironmental characteristics reflected in the sedimentology, geochemistry and hydrochemistry of Lake Chiprana, a hypersaline lake in Northeast Spain.***
- ***Aim 2 - Integrate a detailed assessment of variations in the petrography and morphology of modern and sub-recent microbial mats from the same setting and from comparable lacustrine settings in the Iberian***

peninsula to provide further detail into potential environmental signatures associated with saline lakes in the Iberian Peninsula.

These aims were designed to provide a better understanding of the use of saline lakes as palaeoenvironmental archives by adopting a multidisciplinary and multi-faceted approach, while also evaluating the characteristics of microbial mats and their use as unique indicators of palaeoenvironmental conditions. Saline lakes globally are relatively understudied and their role as such archives has only very recently been recognised in greater detail. Very rarely have studies considered the use of microbial mat deposits within their sedimentary sequences to act as distinctive intervals of high-resolution environmental information.

8.1 Saline lakes as palaeoenvironmental archives

8.1.1 Conclusion of results

This topic was primarily addressed throughout chapters 4, 5 and 6, and directly addresses the first aim of this thesis. Sedimentological (chapter 4), geochemical (chapter 5) and mixed mineralogical and hydrochemical (chapter 6) analyses of Laguna Salada de Chiprana, a saline-hypersaline lake situated in Northeast Spain, were undertaken in order to determine the key fluctuations in depositional, geochemical and where possible biological processes associated with the lake. The selection of the lake was justified based on the permanence of the lake and the extensive studies that have characterised hydrological and biological processes operating here in the present day (Guerrero *et al.*, 1991; Vidondo *et al.*, 1993; Diaz *et al.*, 1998; Valero-Garcés *et al.*, 2000; Jonkers *et al.*, 2003; De Wit *et al.*, 2013).

A sedimentological and depositional framework was generated for the lake following the production of an age-depth model from ¹³⁷Cs dating and correlation with previous cores collected from the lake in 1997 and 2007 (see Valero-Garcés *et al.* (2000)). This age depth model initially defined the age of the base of the longest core (~50cm

depth) to correspond to approximately ~1700AD, but a revised age model was presented in chapter 5 which correlated the base to approximately ~1600AD. The sedimentary analyses delineated nine facies and subfacies including, but not limited to, detrital silts and muddy sands, gypsiferous mudstones and individual gypsum and evaporite layers, organic-rich mudstones and charophytes, and microbial mats with unique morphological characteristics. Facies were comparable to and subsequently defined in a similar manner to other lakes studied around the Iberian peninsula (Martín-Puertas *et al.*, 2008; Morellón *et al.*, 2009a).

The findings of this chapter ultimately highlight that the sequence illustrated a transition from a semi-permanent saline lagoon defined by detrital mudstones and sandy siltstones (units 5 and 6) with varying degrees of evaporite precipitation between approximately ~1600/50-1850_{AD}, to a receding saline lake complex established in approximately ~1960_{AD} that persists to the present day. This sequence also provided evidence of the onset of several fluctuations in lake level as reflected by the varying characteristics of sediments throughout the profundal and littoral areas of the lake. In the profundal setting, the development of microbial mats reflected the effects of lake drawdown between approximately 1850-1950_{AD} (unit 4), while moderate increases in lake level around approximately ~1950-1960_{AD} led to the widespread deposition of organic-rich charophytic mudstones in both the profundal and littoral settings. Spatial contrasts are however drawn in particular for the period of deposition between approximately ~1960-1965_{AD}, whereby extensive deposits of gypsum-encrusted charophytes were found in the littoral setting, forming synchronous with laminated microbial mats occurring in the profundal setting. In summary, the sedimentological and facies analysis illustrated a complex array of depositional environments that are both temporally and spatially dynamic over short timescales, and yielded detailed insights into how saline lakes can act as high-resolution repositories of environmental change due to the complex nature of the sediments at such small scales (Valero-Garcés *et al.*, 2000).

In confluence with the sedimentological findings, chapter 5 addressed geochemical processes occurring in the lake throughout the last three to four centuries. XRF measurements coupled with ICP were employed alongside uni- and multi-variate statistical analyses, and were effective in delineating the key geochemical processes associated with the lake and their spatio-temporal complexity. The findings of the chapter highlight complex geochemical signatures preserved in the cores comparable to other examples throughout the Iberian Peninsula such as Lake Zonar (Martín-Puertas *et al.*, 2011), Lake Estanya (Morellón *et al.*, 2009b), Lake Montcortes (González-Sampéris *et al.*, 2017) and Laguna Salada in the Malaga province (Schröder *et al.*, 2018). Processes included: inputs of detrital material from the catchment via irrigation channels and overland flow as highlighted by increases in clastic elements (e.g. Ti, K, Fe, Mn and Al) and proxies (e.g. $\log(\text{Ca})/\log(\text{Ti})$) (Litt *et al.*, 2009; Morellón *et al.*, 2009b), evaporation of the lakewaters and brines in confluence with the deposition of evaporitic phases depicted by elements S, Cl and Sr and proxies such as $\log(\text{Sr})/\log(\text{Ti})$ (Kylander *et al.*, 2011; Martín-Puertas *et al.*, 2011), fluctuations in organic productivity, redox and oxygenation indicated by proxies of $\log(\text{Fe})/\log(\text{Mn})$ (Corella *et al.*, 2012) and $\log(\text{Mn})/\log(\text{Fe})$ (Burn & Palmer, 2014), and the varying degree of anthropogenic activities leading to the influx of detrital material from irrigation returns and heavy metals associated with agricultural activities (Valero-Garcés *et al.*, 2000).

This data was again analysed from both a temporal and spatial aspect, and the findings illustrated a significant degree of variability in the intensity of geochemical processes occurring in both the littoral and profundal settings of Lake Chiprana. For example, evaporative processes were found to be consistent with the expected outcomes in that they were more intense and significant in the littoral settings comparatively to the profundal setting, while organic productivity and preservation (highlighted by $\log(\text{Br})/\log(\text{Ti})$) and Inc/Coh ratios) were significantly more complex. It was theorised that increased lake levels led to decreased organic productivity in the profundal areas of the lake, while promoting increased organic productivity in the

littoral zone with increased colonisation of the shallower zones of the lake by vegetation (Valero-Garces *et al.*, 2000). Detrital inputs were also clear from increases in proxies of typical allogenic elements, with such signals being more apparent throughout units 5 and 6 (approx. ~1600-1850_{AD}) in confluence with the allogenic facies identified here, and with small rises identified in unit 3 (approx. ~1950-1960_{AD}) in both the profundal and littoral settings.

Finally, chapter 6 addressed hydrochemical and mineralogical aspects of the lake by utilising XRD and PHREEQC-based hydrochemical modelling to determine downcore and spatial variations in the abundance of allogenic, endogenic and authigenic mineral phases associated with Lake Chiprana. This chapter provided insights into the provenance of sediments being delivered to the lake from the local catchment, as well as allowing for an interpretation of key periods of lake-level fluctuations as recorded by the variability of endogenic mineral assemblages (Martín-Puertas *et al.*, 2011). The analyses illustrated that quartz, phyllosilicates, calcite and aragonite were sourced from the siliciclastic and carbonate-rich rocks of the catchment of the lake (IGME, 2003), and that evaporitic, endogenic and authigenic phases also included calcite and aragonite, gypsum, halite, hexahydrite, thenardite, as well as minor amounts of epsomite, bloedite and anhydrite. The application of the hydrochemical model distinguished a clear sequence of mineralisation occurring within the littoral area of the lake, and furthermore exhibited that microbial controls may have acted upon the inhibition of key mineral phases such as bloedite and mirabilite. These findings ultimately provide further evidence of the complexity of Lake Chiprana, highlighting specific mineralogical assemblages throughout the lake controlled by an equally complex set of environmental parameters throughout the profundal and littoral areas.

These findings were also coupled with modelling of evaporation/inflow variations as evidenced by the isotopic enrichment of $\delta^{18}\text{O}$ and δD within gypsum hydration water, a novel technique that has been recently applied in several other Iberian lakes

(Gázquez *et al.*, 2017, 2018). This technique allowed for deeper insights into the palaeohydrology of Lake Chiprana, with relatively enriched $\delta^{18}\text{O}$ and δD in gypsum hydration water in saline intervals identified in units 4, 2 and 1, and reduced enrichment of these variables particularly in unit 5 that were associated with influxes of fresh water to the lake.

8.1.2 Synthesis and contributions to research

Broadly, the findings from chapters 4, 5 and 6 focused primarily upon the first aim of this study, and each chapter provided a deeper insight into the complex internal and external processes associated with saline lakes and how these processes are represented within their sedimentary records. Each chapter was in good agreement, and overall illustrated that saline lake sedimentary archives such as those from Lake Chiprana can provide exceptional insights into palaeoenvironmental change. Specifically, the sediments of Lake Chiprana indicated relative increases in allogenic phases and overall lake levels between ~1600-1850_{AD} in congruence with the onset of detrital facies and detrital-dominated geochemical signatures. Evaporitic phases and lower lake levels contrastingly occurred between ~1850-1950_{AD} and from approximately 1960_{AD} to the present day. Overall, the integrated sedimentological, geochemical and hydrochemical dataset illustrated that saline lakes such as Lake Chiprana can act as a reliable archive of environmental information. The data were instrumental in delineating the character and extent of unique depositional sub-environments associated with saline lakes, the record and fluctuating intensity of geochemical processes, and the mineralogical aspects of the lake sediments. Thus, the first aim of this study and its associated objectives were able to provide a significant contribution to knowledge of saline lake processes not only a high resolution temporal scale, but also on a significantly intricate spatial scale throughout Lake Chiprana.

Furthermore, this thesis contributes to how saline lakes, and other lake sediments can be more effectively studied and the spatio-temporal characteristics of these systems better understood. Generally, the use of a single or composite sedimentary sequence of a specific depocenter of a lacustrine setting is typically undertaken when analysing palaeoenvironmental change (Valero-Garcés *et al.*, 2000; Martín-Puertas *et al.*, 2008; Morellón *et al.*, 2009a). In this thesis, a different approach was undertaken by (as detailed in chapters 4-6) assessing the sedimentological characteristics of multiple depositional sub-environments. The classification of sedimentary structures, facies, mineralogy and geochemical processes from both settings was augmented with high-resolution photographs and a novel method of using computerised tomographical scans of the entire cores. This approach allowed for the identification of spatial and temporal variations in facies at high-resolution, in some cases at the sub-millimetre scale as a result of the high fidelity of sedimentary structures provided by the tomographical scans. Though discussed further in chapter 7, it is the recommendation that many future studies should consider investing into the opportunities that computerised tomographical scanning can offer when undertaking sedimentary facies analysis of lacustrine sediment cores (Hickman-Lewis *et al.*, 2017).

Finally, this thesis applies a newly-emerging technique in the form of the analysis of the isotopic composition of gypsum hydration water to Lake Chiprana, not only further assessing the validity of this technique but also providing deeper insights into the original composition of the lakewater during gypsum formation. The results of the analyses show that lake water composition varied significantly throughout the last three to four centuries, and was potentially governed by a rapidly shifting evaporation/inflow ratio that itself was controlled by rapid expansion and shifting of agricultural practices and use of the lake as a reservoir for runoff irrigation. Further modelling of these data, coupled with measurements of $\delta^{17}\text{O}$, will be able to provide increased resolution and delineation of anthropogenic and climatic processes affecting lake levels, and will likely be instrumental in assessing further small scale

variations in climate that may ultimately be applicable to the modelling of future climatic scenarios.

8.2 Microbialite morphological and geochemical characteristics

8.2.1 Conclusion of results

This question was addressed partly by the sedimentological and geochemical framework established in chapters 4, 5 and 6 and primarily throughout chapter 7. Analyses of Lake Chiprana as detailed in chapters 4 and 5 were coupled with further sedimentological and depositional analyses of cores from Lake Arreo, Lake Estanya and Lake Zonar (also see appendix 2). Extensive work has already been undertaken on each lake to define the key environmental and geochemical processes occurring throughout the Holocene (0~11.7ka) depositional sequences associated with each site. In each series of studies focusing upon each lake, microbial mats were defined occurring at specific intervals throughout their sedimentary sequences. The justification of the selection of these sites was therefore based firstly on the previously extensive work undertaken upon them (Arreo - Corella *et al.* (2011, 2013, 2021), Estanya - Morellón *et al.* (2008, 2009b; a, 2011), Zonar (Martín-Puertas *et al.*, 2008, 2009, 2011)) which provided a framework for the analysis of microbial mats occurring within the depositional record of each site.

In each case, a review and later detailed analysis of sedimentological and geochemical data provided by the aforementioned studies was instrumental in assessing the distribution and sedimentological characteristics of microbial mats associated with the four lakes. The use of CT scanning of whole sediment cores proved to be particularly effective for the initial assessment of the distribution of microbial mats and later in chapter 7 for morphological analyses of mats in each sedimentary sequence as has been shown in many other studies (Hickman-Lewis *et al.*, 2017, 2019). CT scanning of mats from the four sites allowed for the identification

and definition of a wide variety of meso-fabrics at the mat scale, and provided insights into morphological variations that could not otherwise be identified with routine core description techniques. Mats exhibited planar/stratiform laminated, domal and wavy/undulatory structures which illustrated varying conditions of formation as well as a range of biotic and abiotic processes acting upon them. The study furthermore highlighted the clear variability of microbialites occurring throughout Iberian lacustrine settings which incorporate these unique deposits across a spectrum of timeframes throughout the Late Holocene. Utilising a recently developed classification scheme proposed by Grey & Awramik (2020) also allowed for refined categorisations of the mats in question, a method that should hopefully be implemented more widely in studies undertaking work upon microbialites in the near future.

Though difficult to ascribe specific biotic and abiotic processes to the development of the macro- and mesostructures of the mats in this study, the findings highlighted that morphological characteristics of the mats could be related to site-specific environmental factors such as rates of sedimentation, the degree of endogenic mineral precipitation and trapping of detritus throughout the mats, and the water depth and subsequently geochemical characteristics of the water in which the mats were developing. For example, comparative analysis of mats from the modern and sub-recent profundal setting of Lake Chiprana revealed relatively similar morphological characteristics, suggesting similar environmental conditions and microbial communities occurring during mat development (Jonkers *et al.*, 2003). In contrast, varying amounts of detrital input to the lakes likely led to varying mat structures, with relatively simplistic structures in Lake Estanya likely being related to increased rates of sedimentation (Morellón *et al.*, 2009b) compared to Lake Zonar (Martín-Puertas *et al.*, 2008) and Chiprana, where more wavy and domal structures were identified. It is probable that site-specific variations in such factors also led to contrasts in microbialite characteristics (Bourillot *et al.*, 2020), as could be identified

by the variable laminae thickness, macrostructure (e.g. heights and intensity of doming within the mats from all of the settings).

Petrographic characterisation of the mats was achieved by utilising optical, cathodoluminescence and scanning electron microscopy techniques, and allowed for the determination of the meso- and micromorphological variations associated with mats from the different lakes. A range of fabrics were broadly categorised into laminated and non-laminated microbialitic fabrics, and non-microbialitic fabrics. Laminated fabrics included stratiform/planar laminated, domal laminated, wavy/undulatory laminated, horizontally interconnected laminae, and intercalated microbial and diatom laminae. The non-laminated fabrics included pinnacles, often with superimposed lamination occurring inside the pinnacle structure, and clotted fabrics. Each structure and its composition provided insights into environmental controls acting upon the mats, with variations in laminae composition and morphology relating to varying degrees of detrital input, endogenic and biogenic mineral precipitation within the mats, as well as the varying biological composition of the mats. Pinnacle and clot structures comparatively point to microbial communities responding to environmental stressors such as variations in salinity, light intensity and geochemistry respectively.

8.2.2 Synthesis and contributions to research

The composition of high-resolution computerised tomographical and petrographic data with a detailed sedimentological and geochemical model generated for Lake Chiprana as presented in chapters 4, 5 and 6, and the large degree of previous work undertaken on Lakes Arreo (Corella *et al.*, 2011, 2013, 2021), Estanya (Morellón *et al.*, 2008, 2009a; b, 2018) and Zonar were instrumental in providing insights into the dynamics of these unique deposits. Fascinating relationships could be established between the effect of environmental conditions and the variation in microbial morphological and geochemical characteristics. For example, stratiform/planar and undulatory/wavy laminae are attributed to periods of alternating intervals of microbial

laminae formation and the precipitation of biogenic and endogenic minerals between the mats, while the amount of detrital material trapped within the mats provides an indication of periods of increased detrital input to the lacustrine systems. Domal and undulatory morphologies produced by microbialites point to increased rates of microbial mat accretion, potentially due to decreased sediment rates, particularly in the case of Lakes Chiprana and Zonar. Finally, the development of characteristic “Lh” laminae suggest seasonally fluctuating microbial communities (Gerdes *et al.*, 2000), leading to interconnected, network like fabrics, while the development of pinnacles throughout mats from Estanya and Chiprana may indicate periods of changing lake levels and subsequently geochemical stressors which induce the gliding of bacteria vertically throughout the mat structure (Gerdes *et al.*, 2000; Sumner *et al.*, 2016). The fluctuations in microbialite meso- and micromorphology could be related to variations in palaeoenvironmental conditions occurring in each of the studied settings. Lamination and pinnaciling occurring throughout each microbial mat can however be attributed to a wide variety of abiotic and biotic factors, and as such it is often difficult to ascribe a specific process or set of processes to a particular morphological feature.

The findings overall illustrated the clear diversity of microbialite structures occurring within both modern and sub-recent lacustrine settings throughout the Iberian Peninsula, and provide insights into the formative processes and potential environmental conditions occurring during their development. The work ultimately utilises and furthermore builds upon the identification and description scheme of Grey & Awramik (2020), adding further understanding as to how both mesoscale (>1cm) and micro-scale (<1cm) characteristics of microbial mats can be used to infer palaeoenvironment. Furthermore, the findings from this chapter not only highlight the clear variability of microbialite structure, texture and fabric in unique lacustrine environments, but also how microbialite morphology can display significant variations throughout the sub-environments of a single lacustrine setting. In particular, this chapter overall contributes to providing an increased understanding

of microbialite mesoscale and microscale both within distinctive saline lacustrine environments and throughout the Holocene in the Iberian Peninsula. These findings have allowed for a further insight into small-scale environmental and anthropogenic perturbations, and how their onset can affect the various sub-domains of a saline lake by using the varying characteristics of microbialites from these specific sub-domains. Though the initial onset of microbialites in all of these lakes is generally related to the onset of more saline conditions, their varying morphology, texture and fabric have here provided a framework with which to understand temporally minute changes in both extrinsic and intrinsic processes acting upon saline lakes. Namely, key findings here include the identification of dendritic and updomed morphologies associated with increased salinity and gypsum formation, the development of pinnacles in response to chemical, light and salinity gradients, and the negation of complex morphology as a result of increased detrital input and likely increased lake levels during microbialite formation.

8.3 Recommendations and Future Work

The findings presented in this thesis provide extensive insights into the unique sedimentological, geochemical and mineralogical characteristics of a saline lake in Northeast Spain, providing a model for understanding how such unique settings can be reliably and effectively utilised as high-resolution palaeoenvironmental archives. Furthermore, long-standing, established techniques such as petrographical analyses, coupled with techniques such as computerised tomographical scanning, provided further answers to the complex phenomena that is the development of microbialites through geological time. Despite this broad spectrum of findings and detailed insights into these areas, there are undoubtedly further avenues of study which must be undertaken if these environments and the unique deposits of microbial mats found within them are to be better understood.

Further studies of not only saline lakes but lacustrine settings in general should aim to incorporate a variety of depositional environments, in particular considering and

encapsulating the spatial extent of the profundal and littoral settings. This would undoubtedly provide further insights into many such environments not only from a temporal but also from a spatial perspective, and would understanding of how environmental factors can impact different domains of lakes in varying ways. Due to time constraints and the difficulties of increased fieldwork during this project as a result of the COVID-19 pandemic, it should be a priority for further studies of saline lakes to incorporate a wide range of depositional environments, perhaps with deeper sediment cores (Valero-Garcés *et al.*, 2014), in order to fully appreciate the clear spatio-temporal sensitivity of many of these settings.

Microbial mats are also, in addition to being complex sedimentological and geochemical ecosystems, biologically and organically intricate deposits (Prieto-Barajas *et al.*, 2018). Though sedimentological, mineralogical and geochemical data were utilised throughout this thesis to provide insights into the record of environmental change associated with the development of distinctive intervals and examples of microbial mats, further work should undoubtedly aim to integrate organic geochemical methods such as total lipid extractions (Słowakiewicz *et al.*, 2016) in order to fully understand the geochemical and biological signatures preserved in the mats. In turn, this will permit an increased understanding of the contribution of biotic processes, and when coupled with inorganic geochemical methods utilised in this thesis, allow for insights into the interplay of both biotic and abiotic processes occurring in these unique deposits throughout saline lake sequences.

References

Bourillot, R., Vennin, E., Dupraz, C., Pace, A., Foubert, A., Rouchy, J.M.,

Patrier, P., Blanc, P., Bernard, D., Lesseur, J. and Visscher, P.T. (2020)

The record of environmental and microbial signatures in ancient microbialites:

The terminal carbonate complex from the neogene basins of southeastern

Spain. *Minerals*, **10**, 1–50.

- Burn, M.J. and Palmer, S.E.** (2014) Solar forcing of Caribbean drought events during the last millennium. *J. Quat. Sci.*, **29**, 827–836.
- Corella, J.P., Amrani, A. El, Sigró, J., Morellón, M., Rico, E. and Valero-Garcés, B.L.** (2011) Recent evolution of Lake Arreo, northern Spain: Influences of land use change and climate. *J. Paleolimnol.*, **46**, 469–485.
- Corella, J.P., Benito, G., Monteoliva, A.P., Sigro, J., Calle, M., Valero-Garcés, B.L., Stefanova, V., Rico, E., Favre, A.C. and Wilhelm, B.** (2021) A 1400-years flood frequency reconstruction for the Basque country (N Spain): Integrating geological, historical and instrumental datasets. *Quat. Sci. Rev.*, **262**, 1–15.
- Corella, J.P., Brauer, A., Mangili, C., Rull, V., Vegas-Vilarrúbia, T., Morellón, M. and Valero-Garcés, B.L.** (2012) The 1.5-ka varved record of Lake Montcortès (southern Pyrenees, NE Spain). *Quat. Res. (United States)*, **78**, 323–332.
- Corella, J.P., Stefanova, V., El Anjoumi, A., Rico, E., Giral, S., Moreno, A., Plata-Montero, A. and Valero-Garcés, B.L.** (2013) A 2500-year multi-proxy reconstruction of climate change and human activities in northern Spain: The Lake Arreo record. *Palaeogeogr. Palaeoclimatol. Palaeoecol.*, **386**, 555–568.
- De Wit, R., Guerrero, M.C., Legaz, A., Jonkers, H.M., Blocier, L., Gumiaux, C. and Gautret, P.** (2013) Conservation of a permanent hypersaline lake: Management options evaluated from decadal variability of coleofasciculus chthonoplastes microbial mats. *Aquat. Conserv. Mar. Freshw. Ecosyst.*, **23**, 532–545.
- Diaz, P., Guerrero, M.C., Alcorlo, P., Baltanas, A., Florin, M. and Montes, C.** (1998) Anthropogenic perturbations to the trophic structure in a permanent hypersaline shallow lake: La Salada de Chiprana (north-eastern Spain). *Int. J. Salt Lake Res.*, **7**, 187–210.
- Gázquez, F., Evans, N.P. and Hodell, D.A.** (2017) Precise and accurate isotope fractionation factors ($\alpha^{17}\text{O}$, $\alpha^{18}\text{O}$ and α^{D}) for water and $\text{CaSO}_4 \cdot 2\text{H}_2\text{O}$ (gypsum). *Geochim. Cosmochim. Acta*, **198**, 259–270.

- Gázquez, F., Morellón, M., Bauska, T., Herwartz, D., Surma, J., Moreno, A., Staubwasser, M., Valero-Garcés, B., Delgado-Huertas, A. and Hodell, D.A.** (2018) Triple oxygen and hydrogen isotopes of gypsum hydration water for quantitative paleo-humidity reconstruction. *Earth Planet. Sci. Lett.*, **481**, 177–188.
- Gerdes, G., Krumbein, W.E. and Noffke, N.** (2000) Evaporite Microbial Sediments. In: *Microbial Sediments*, 196–208.
- González-Sampériz, P., Aranbarri, J., Pérez-Sanz, A., Gil-Romera, G., Moreno, A., Leunda, M., Sevilla-Callejo, M., Corella, J.P., Morellón, M., Oliva, B. and Valero-Garcés, B.** (2017) Environmental and climate change in the southern Central Pyrenees since the Last Glacial Maximum: A view from the lake records. *Catena*, **149**, 668–688.
- Grey, K. and Awramik, S.M.** (2020) Handbook for the study and description of microbialites, Bulletin 1. *Geological Survey of Western Australia*, 1-278 pp.
- Guerrero, M.C., Balsa, J., Pascual, M. and Martínez, B.** (1991) Caracterización limnológica de la Laguna Salada de Chiprana (Zaragoza, España) y sus comunidades de bacterias fototróficas. *Limnetica*, **7**, 83–96.
- Hickman-Lewis, K., Garwood, R.J., Withers, P.J. and Wacey, D.** (2017) X-ray microtomography as a tool for investigating the petrological context of Precambrian cellular remains. *Geol. Soc. Spec. Publ.*, **448**, 33–56.
- Hickman-Lewis, K., Gautret, P., Arbaret, L., Sorieul, S., De Wit, R., Foucher, F., Cavalazzi, B. and Westall, F.** (2019) Mechanistic morphogenesis of organo-sedimentary structures growing under geochemically stressed conditions: Keystone to proving the biogenicity of some Archaean stromatolites? *Geosci.*, **9**, 1–31.
- IGME** (2003) Mapa Geológico de España, 1:50000, (serie MAGNA). Hoja 137. Miranda de Ebro.
- Jonkers, H.M., Ludwig, R., De Wit, R., Pringault, O., Muyzer, G., Niemann, H., Finke, N. and De Beer, D.** (2003) Structural and functional analysis of a microbial mat ecosystem from a unique permanent hypersaline inland lake:

- “La Salada de Chiprana” (NE Spain). *FEMS Microbiol. Ecol.*, **44**, 175–189.
- Kylander, M.E., Ampel, L., Wohlfarth, B. and Veres, D.** (2011) High-resolution X-ray fluorescence core scanning analysis of Les Echets (France) sedimentary sequence: New insights from chemical proxies. *J. Quat. Sci.*, **26**, 109–117.
- Litt, T., Krastel, S., Sturm, M., Kipfer, R., Örcen, S., Heumann, G., Franz, S.O., Ülgen, U.B. and Niessen, F.** (2009) “PALEOVAN”, International Continental Scientific Drilling Program (ICDP): site survey results and perspectives. *Quat. Sci. Rev.*, **28**, 1555–1567.
- Martín-Puertas, C., Valero-Garcés, B.L., Brauer, A., Mata, M.P., Delgado-Huertas, A. and Dulski, P.** (2009) The Iberian-Roman Humid Period (2600–1600 cal yr BP) in the Zoñar Lake varve record (Andalucía, southern Spain). *Quat. Res.*, **71**, 108–120.
- Martín-Puertas, C., Valero-Garcés, B.L., Mata, M.P., González-Sampériz, P., Bao, R., Moreno, A. and Stefanova, V.** (2008) Arid and humid phases in southern Spain during the last 4000 years: The Zoñar Lake record, Córdoba. *Holocene*, **18**, 907–921.
- Martín-Puertas, C., Valero-Garcés, B.L., Mata, M.P., Moreno, A., Giralt, S., Martínez-Ruiz, F. and Jiménez-Espejo, F.** (2011) Geochemical processes in a Mediterranean Lake: A high-resolution study of the last 4,000 years in Zoñar Lake, southern Spain. *J. Paleolimnol.*, **46**, 405–421.
- Morellón, M., Aranbarri, J., Moreno, A., González-Sampériz, P. and Valero-Garcés, B.L.** (2018) Early Holocene humidity patterns in the Iberian Peninsula reconstructed from lake, pollen and speleothem records. *Quat. Sci. Rev.*
- Morellón, M., Valero-Garcés, B., Anselmetti, F., Ariztegui, D., Schnellmann, M., Moreno, A., Mata, P., Rico, M. and Corella, J.P.** (2009a) Late quaternary deposition and facies model for karstic Lake Estanya (North-eastern Spain). *Sedimentology*, **56**, 1505–1534.
- Morellón, M., Valero-Garcés, B., González-Sampériz, P., Vegas-Vilarrúbia, T., Rubio, E., Rieradevall, M., Delgado-Huertas, A., Mata, P., Romero, Ó.,**

- Engstrom, D.R., López-Vicente, M., Navas, A. and Soto, J.** (2011) Climate changes and human activities recorded in the sediments of Lake Estanya (NE Spain) during the Medieval Warm Period and Little Ice Age. *J. Paleolimnol.*, **46**, 423–452.
- Morellón, M., Valero-Garcés, B., Moreno, A., González-Sampériz, P., Mata, P., Romero, O., Maestro, M. and Navas, A.** (2008) Holocene palaeohydrology and climate variability in northeastern Spain: The sedimentary record of Lake Estanya (Pre-Pyrenean range). *Quat. Int.*, **181**, 15–31.
- Morellón, M., Valero-Garcés, B., Vegas-Vilarrúbia, T., González-Sampériz, P., Romero, Ó., Delgado-Huertas, A., Mata, P., Moreno, A., Rico, M. and Corella, J.P.** (2009b) Lateglacial and Holocene palaeohydrology in the western Mediterranean region: The Lake Estanya record (NE Spain). *Quat. Sci. Rev.*, **28**, 2582–2599.
- Prieto-Barajas, C.M., Valencia-Cantero, E. and Santoyo, G.** (2018) Microbial mat ecosystems: Structure types, functional diversity, and biotechnological application. *Electron. J. Biotechnol.* 31:48–56.
- Schnurrenberger, D., Russell, J. and Kelts, K.** (2003) Classification of lacustrine sediments based on sedimentary components. *J. Paleolimnol.*, **29**, 141–154.
- Schröder, T., van 't Hoff, J., Ortiz, J.E., de Torres Pèrez-Hidalgo, T.J., López-Sáez, J.A., Melles, M., Holzhausen, A., Wennrich, V., Viehberg, F. and Reicherter, K.** (2018) Shallow hypersaline lakes as paleoclimate archives: A case study from the Laguna Salada, Málaga province, southern Spain. *Quat. Int.*, **485**, 76–88.
- Słowakiewicz, M., Whitaker, F., Thomas, L., Tucker, M.E., Zheng, Y., Gedl, P. and Pancost, R.D.** (2016) Biogeochemistry of intertidal microbial mats from Qatar: New insights from organic matter characterisation. *Org Geochem.* doi: 10.1016/j.orggeochem.2016.09.006
- Sumner, D.Y., Jungblut, A.D., Hawes, I., Andersen, D.T., Mackey, T.J. and Wall, K.** (2016) Growth of elaborate microbial pinnacles in Lake Vanda, Antarctica. *Geobiology*, **14**, 556–574.

- Valero-Garcés, B., Morellón, M., Moreno, A., Corella, J.P., Martín-Puertas, C., Barreiro, F., Pérez, A., Giralt, S. and Mata-Campo, M.P.** (2014) Lacustrine carbonates of Iberian Karst Lakes: Sources, processes and depositional environments. *Sediment. Geol.* **299**:1–29.
- Valero-Garces, B.L., Navas, A., Machin, J., Stevenson, T. and Davis, B.** (2000) Responses of a saline lake ecosystem in a semiarid region to irrigation and climate variability: The history of Salada Chiprana, central Ebro basin, Spain. *Ambio*, **29**, 344–350.
- Valero-Garcés, B.L., Navas, A., Machin, J., Stevenson, T., Davis, B., Valero-Garces, B.L., Navas, A., Machin, J., Stevenson, T., Davis, B., Valero-Garcés, B.L., Navas, A., Machin, J., Stevenson, T. and Davis, B.** (2000) Responses of a Saline Lake Ecosystem in a Semiarid Region to Irrigation and Climate Variability. *AMBIO A J. Hum. Environ.*, **29**, 344–350.
- Vidondo, B., Martínez, B., Montes, C. and Guerrero, M.C.** (1993) Physico-chemical characteristics of a permanent Spanish hypersaline lake: La Salada de Chiprana (NE Spain). *Hydrobiologia*, **267**, 113–125.

Appendix 1 – Sample Lists

Table A1.1 – Samples and core cuts taken from each of the cores from Lake Chiprana.

1A		2A		3A		4A	
Sample	Depth (mm)	Sample	Depth (mm)	Sample	Depth (mm)	Sample	Depth (mm)
1	0-10	1	0-10	1	0-5	1	0-5
1A	0-5	2	10-15	2	5-10	2	5-10
1B	5-10	3	15-20	3	10-15	3	10-15
2	10-20	4	20-30	4	15-20	4	15-20
2A	10-15	5	20-25	5	20-25	5	20-25
2B	15-20	6	25-30	6	25-30	6	25-30
3	20-30	7	30-35	7	30-35	7	30-35
3A	20-25	8	35-40	8	35-40	8	35-40
3B	25-30	9	40-45	9	40-45	9	40-45
4	30-40	10	45-50	10	45-50	10	45-50
4A	30-35	11	50-55	11	50-55	11	50-55
4B	35-40	12	55-60	12	55-60	12	55-60
5	40-45	13	60-70	13	60-65	13	60-65
6	45-50	14	70-75	14	65-70	14	65-70
7	50-55	15	75-80	15	70-75	15	70-75
8	55-60	16	80-85	16	75-80	16	75-80
9	60-70	17	85-90	17	80-85	17	80-85
10	70-75	18	90-95	18	85-90	18	85-90
11	70-75	19	95-100	19	90-95	19	90-95
12	75-80	20	100-105	20	95-100	20	95-100
13	80-85	21	105-110	21	100-105	21	100-105
14	85-90	22	110-115	22	105-110	22	105-110
15	90-95	23	115-120	23	110-115	23	110-115
16	95-100	24	120-125	24	115-120	24	115-120
17	100-105	25	125-130	25	120-125	25	120-125
17b	105-110	26	130-135	26	125-130	26	125-130
18	110-115	27	135-140	27	130-135	27	130-135
19	115-120	28	140-145	28	135-140	28	135-140
20	120-125	29	145-150	29	140-145	29	140-145
21	125-130	30	150-155	30	145-150	30	145-150
22	130-135	31	155-160	31	150-155	31	150-155
23	135-140	32	160-165	32	155-160	32	155-160
24	140-145	33	165-170	33	160-165	33	160-165
25	145-150	34	170-175	34	165-170	34	165-170
26	150-155	35	175-180	35	170-175	35	170-175
27	155-160	36	180-185	36	175-180	36	175-180
28	160-165	37	185-190	37	180-185	37	180-185
29	165-170	38	190-195	38	185-190	38	185-190
30	170-175	39	195-200	39	190-195	39	190-195
31	175-180	40	200-210	40	195-200	40	195-200
32	180-185	41	210-220	41	200-205	41	200-205
33	185-190	42	220-225	42	205-210	42	205-210
34	190-195	43	225-230	43	210-215	43	210-215
35	195-200	44	230-235	44	215-220	44	215-220
36	200-205	45	235-240	45	220-225	45	220-225
37	205-210	46	240-245	46	225-230	46	225-230
38	210-215	47	245-250	47	230-235	47	230-235
39	215-220	48	250-255	48	235-240	48	235-240
40	220-225	49	255-260	49	240-245	49	240-245
41	225-230	50	260-265	50	245-250	50	245-250
42	230-235	51	265-270	51	250-255	51	250-255
43	235-240	52	270-275	52	255-260	52	255-260
44	240-245	53	275-280	53	260-265	53	260-265
45	245-250	54	280-285	54	265-270	54	265-270
46	250-255	55	285-290	55	270-275	55	270-275
47	255-260	56	290-295	56	275-280	56	275-280
48	260-265	57	295-300	57	280-285	57	280-285
49	265-270	58	300-305	58	285-290	58	285-290
50	270-275	59	305-310	59	290-295	59	290-295
51	275-280	60	310-315	60	295-300	60	295-300
52	280-285	61	315-320	61	300-305	61	300-305
53	285-290	62	320-325	62	305-310	62	305-310
54	290-295	63	325-330	63	310-315	63	310-315
55	295-300	64	330-335	64	315-320	64	315-320
56	300-305	65	335-340	65	320-325	65	320-325
57	305-310	66	340-345	66	325-330	66	325-330
58	310-315	67	345-350	67	330-335	67	330-335
59	315-320	68	350-355	68	335-340	68	335-340
60	320-325	69	355-360	69	340-345		
61	325-330	70	360-365	70	345-350		

62	330-335	71	365-370	71	350-355		
63	335-340	72	370-375	72	355-360		
64	340-345	73	375-380	73	360-365		
65	345-350	74	380-385	74	365-370		
66	350-355	75	385-390	75	370-375		
67	355-360	76	390-395	76	375-380		
68	360-365	77	395-400	77	380-385		
69	365-370	78	400-405	78	385-390		
70	370-375	79	405-410	79	390-395		
71	375-380	80	410-415	80	395-400		
72	380-385	81	415-420	81	400-405		
73	385-390	82	420-425	82	405-410		
74	390-395	83	425-430	83	410-415		
75	395-400	84	430-435	84	415-420		
76	400-405	85	435-440	85	420-425		
77	405-410	86	440-445				
78	410-415	87	445-450				
79	415-420	88	450-460				
80	420-425	89	460-465				
81	425-430	90	465-470				
82	430-435	91	470-475				
83	435-440	92	475-480				
84	440-445	93	480-485				
85	445-450	94	485-490				
86	450-460	95	490-495				
87	460-465	96	495-500				
88	465-470	97	500-505				
89	470-475						
90	475-480						
91	480-485						
92	485-490						
93	490-495						
94	495-500						
95	500-505						
96	505-510						

5A		6A		7A	
Sample	Depth (mm)	Sample	Depth (mm)	Sample	Depth (mm)
1	0-5	1	0-5	1	0-5
2	5-10	2	5-10	2	5-10
3	10-15	3	10-15	3	10-15
4	15-20	4	15-20	4	15-20
5	20-25	5	20-25	5	20-25
6	25-30	6	25-30	6	25-30
7	30-35	7	30-35	7	30-35
8	35-40	8	35-40	8	35-40
9	40-45	9	40-45	9	40-45
10	45-50	10	45-50	10	45-50
11	50-55	11	50-55	11	50-55
12	55-60	12	55-60	12	55-60
13	60-65	13	60-65	13	60-65
14	65-70	14	65-70	14	65-70
15	70-75	15	70-75	15	70-75
16	75-80	16	75-80	16	75-80
17	80-85	17	80-85	17	80-85
18	85-90	18	85-90	18	85-90
19	90-95	19	90-95	19	90-95
20	95-100	20	95-100	20	95-100
21	100-105	21	100-105	21	100-105
22	105-110	22	105-110	22	105-110
23	110-115	23	110-115	23	110-115
24	115-120	24	115-120	24	115-120
25	120-125	25	120-125	25	120-125
26	125-130	26	125-130	26	125-130
27	130-135	27	130-135	27	130-135
28	135-140	28	135-140	28	135-140
29	140-145	29	140-145	29	140-145
30	145-150	30	145-150	30	145-150
31	150-155	31	150-155	31	150-155
32	155-160	32	155-160	32	155-160
33	160-165	33	160-165	33	160-165
34	165-170	34	165-170	34	165-170
35	170-175	35	170-175	35	170-175
36	175-180	36	175-180	36	175-180
37	180-185	37	180-185	37	180-185
38	185-190	38	185-190	38	185-190
39	190-195	39	190-195	39	190-195
40	195-200	40	195-200	40	195-200
41	200-205	41	200-205	41	200-205
42	205-210	42	205-210	42	205-210

43	210-215	43	210-215	43	210-215
44	215-220	44	215-220	44	215-220
45	220-225	45	220-225	45	220-225
46	225-230	46	225-230	46	225-230
47	230-235	47	230-235	47	230-235
48	235-240	48	235-240	48	235-240
49	240-245	49	240-245	49	240-245
50	245-250	50	245-250	50	245-250
51	250-255	51	250-255	51	250-255
52	255-260	52	255-260	52	255-260
53	260-265	53	260-265	53	260-265
54	265-270	54	265-270	54	265-270
55	270-275	55	270-275	55	270-275
56	275-280	56	275-280	56	275-280
57	280-285	57	280-285	57	280-285
58	285-290	58	285-290	58	285-290
59	290-295	59	290-295	59	290-295
		60	295-300	60	295-300
		61	300-305	61	300-305
		62	305-310	62	305-310
		63	310-315	63	310-315
		64	315-320	64	315-320
		65	320-325	65	320-325
		66	325-330	66	325-330
		67	330-335	67	330-335
		68	335-340	68	335-340
		69	340-345		
		70	345-350		
		71	350-355		
		72	355-360		
		73	360-365		
		74	365-370		
		75	375-380		
		76	380-385		
		77	385-390		
		78	390-395		
		79	395-400		
		80	400-405		

Table A1.2 – Thin sections generated from sediments from Lago de Arreo.

File Name	Site	Core ID	Depth (cm)
ARRNEW1-1	Lago de Arreo	ESP-CAI04-1B-1K-5	119-129
ARRNEW1-2	Lago de Arreo	ESP-CAI04-1B-1K-5	119-129
ARRNEW1-3	Lago de Arreo	ESP-CAI04-1B-1K-5	119-129
ARRNEW2-1	Lago de Arreo	ESP-CAI04-1B-1K-5	135-145
ARRNEW2-2	Lago de Arreo	ESP-CAI04-1B-1K-5	135-145
ARRNEW2-3	Lago de Arreo	ESP-CAI04-1B-1K-5	135-145
ARRNEW3-1	Lago de Arreo	ESP-CAI04-1B-1K-3	94-104
ARRNEW3-2	Lago de Arreo	ESP-CAI04-1B-1K-3	94-104
ARRNEW3-3	Lago de Arreo	ESP-CAI04-1B-1K-3	94-104
ARRNEW4-1	Lago de Arreo	ESP-CAI04-1B-1K-3	86-96
ARRNEW4-2	Lago de Arreo	ESP-CAI04-1B-1K-3	86-96
ARRNEW4-3	Lago de Arreo	ESP-CAI04-1B-1K-3	86-96
ARROLD1-1	Lago de Arreo	ESP-CAI04-1A-1K-4	96-106
ARROLD1-2	Lago de Arreo	ESP-CAI04-1A-1K-4	96-106
ARROLD2-1	Lago de Arreo	ESP-CAI04-1A-1K-5	29-39
ARROLD2-1S	Lago de Arreo	ESP-CAI04-1A-1K-5	29-39
ARROLD2-2	Lago de Arreo	ESP-CAI04-1A-1K-5	29-39
ARROLD2-3	Lago de Arreo	ESP-CAI04-1A-1K-5	29-39
ARROLD2-3S	Lago de Arreo	ESP-CAI04-1A-1K-5	29-39
ARROLD3-0	Lago de Arreo	ESP-CAI04-1A-1K-6	49-59
ARROLD3-1	Lago de Arreo	ESP-CAI04-1A-1K-6	49-59
ARROLD4-1	Lago de Arreo	ESP-CAI04-1A-1K-6	59-69
ARROLD4-1S	Lago de Arreo	ESP-CAI04-1A-1K-6	59-69
ARROLD4-2	Lago de Arreo	ESP-CAI04-1A-1K-6	59-69

Table A1.3 – Thin sections generated from sediments from Laguna Salada de Chiprana.

CHIPRANA

File Name	Site	Core ID	Depth (cm)
CHIOLD1	Laguna Salada de Chiprana	CHI07-1A	25-35
CHIOLD2	Laguna Salada de Chiprana	CHI07-1A	25-35
CHIOLD3	Laguna Salada de Chiprana	CHI07-1A	33-43
CHIOLD4	Laguna Salada de Chiprana	CHI07-1A	15-25
CHIOLD5	Laguna Salada de Chiprana	CHI07-1A	15-25
CHIOLD6	Laguna Salada de Chiprana	CHI07-1A	15-35
CHINEW1-1	Laguna Salada de Chiprana	CHI-07-1A	6-24
CHINEW1-2	Laguna Salada de Chiprana	CHI-07-1A	6-24
CHINEW1-3	Laguna Salada de Chiprana	CHI-07-1A	6-24
CHINEW1-4	Laguna Salada de Chiprana	CHI-07-1A	6-24
DUR11-1	Laguna Salada de Chiprana	CHI19-5A	12-37
DUR11-2	Laguna Salada de Chiprana	CHI19-5A	12-37
DUR11-3	Laguna Salada de Chiprana	CHI19-5A	12-37
DUR11-4	Laguna Salada de Chiprana	CHI19-5A	12-37
DUR11-5	Laguna Salada de Chiprana	CHI19-5A	12-37
DUR11-6	Laguna Salada de Chiprana	CHI19-5A	12-37
DUR11-7	Laguna Salada de Chiprana	CHI19-5A	12-37
DUR12-1	Laguna Salada de Chiprana	CHI19-6A	3-28
DUR12-2	Laguna Salada de Chiprana	CHI19-6A	3-28
DUR12-3	Laguna Salada de Chiprana	CHI19-6A	3-28
DUR12-4	Laguna Salada de Chiprana	CHI19-6A	3-28
DUR12-5	Laguna Salada de Chiprana	CHI19-6A	3-28
DUR12-6	Laguna Salada de Chiprana	CHI19-6A	3-28
DUR13-1	Laguna Salada de Chiprana	CHI19-1A	2-27
DUR13-2	Laguna Salada de Chiprana	CHI19-1A	2-27
DUR13-3	Laguna Salada de Chiprana	CHI19-1A	2-27
DUR13-4	Laguna Salada de Chiprana	CHI19-1A	2-27
DUR13-5	Laguna Salada de Chiprana	CHI19-1A	2-27
DUR13-6	Laguna Salada de Chiprana	CHI19-1A	2-27
CHIM-2A	Laguna Salada de Chiprana	Modern	N/A
CHIM-3C-1	Laguna Salada de Chiprana	Modern	N/A

Table A1.4 – Thin sections generated from sediments from Lago de Estanya.

File Name	Site	Core ID	Depth (cm)
EST4-0	Lago de Estanya	LEG04-1A-1K-2	119-142
EST4-1	Lago de Estanya	LEG04-1A-1K-2	119-142
EST4-2	Lago de Estanya	LEG04-1A-1K-2	119-142
EST5-0	Lago de Estanya	LEG04-1A-1K-2	119-142
EST5-1	Lago de Estanya	LEG04-1A-1K-2	119-142
EST5-2	Lago de Estanya	LEG04-1A-1K-2	119-142
DUR1-1	Lago de Estanya	LEG04-1A-1K-3	62-72
DUR1-2	Lago de Estanya	LEG04-1A-1K-3	62-72
DUR1-3	Lago de Estanya	LEG04-1A-1K-3	62-72
DUR2-1	Lago de Estanya	LEG04-1A-1K-3	12-22
DUR2-2	Lago de Estanya	LEG04-1A-1K-3	12-22
DUR2-3	Lago de Estanya	LEG04-1A-1K-3	12-22
DUR3-1	Lago de Estanya	LEG04-3A-1K-3	100-127
DUR3-2	Lago de Estanya	LEG04-3A-1K-3	100-127
DUR3-3	Lago de Estanya	LEG04-3A-1K-3	100-127
DUR4-1	Lago de Estanya	LEG04-3A-1K-3	100-127
DUR4-2	Lago de Estanya	LEG04-3A-1K-3	100-127
DUR4-3	Lago de Estanya	LEG04-3A-1K-3	100-127
DUR4-4	Lago de Estanya	LEG04-3A-1K-3	100-127
DUR5-1	Lago de Estanya	LEG04-1A-1K-3	78-88
DUR5-2	Lago de Estanya	LEG04-1A-1K-3	78-88
DUR5-3	Lago de Estanya	LEG04-1A-1K-3	78-88
DUR6-1	Lago de Estanya	LEG04-1A-1K-3	71-81
DUR6-2	Lago de Estanya	LEG04-1A-1K-3	71-81
DUR6-3	Lago de Estanya	LEG04-1A-1K-3	71-81
DUR7-1	Lago de Estanya	LEG04-1A-1K-2	90-100
DUR7-2	Lago de Estanya	LEG04-1A-1K-2	90-100
DUR7-3	Lago de Estanya	LEG04-1A-1K-2	90-100
DUR10-1	Lago de Estanya	LEG04-4A-1K-2	68-80
DUR10-2	Lago de Estanya	LEG04-4A-1K-2	68-80
DUR10-3	Lago de Estanya	LEG04-4A-1K-2	68-80

Table A1.5 – Thin sections generated from sediments from Laguna Zonar.

File Name	Site	Core ID	Depth (cm)
DUR8-1	Laguna Zonar	ZON04-1A-1K-1	91-101
DUR8-2	Laguna Zonar	ZON04-1A-1K-1	91-101
DUR8-3	Laguna Zonar	ZON04-1A-1K-1	91-101
DUR9-1	Laguna Zonar	ZON04-1C-1K-1	85-95
DUR9-2	Laguna Zonar	ZON04-1C-1K-1	85-95
DUR9-3	Laguna Zonar	ZON04-1C-1K-1	85-95
ZON6-0	Laguna Zonar	ZON04-1C-1K-1	87-94
ZON6-1	Laguna Zonar	ZON04-1C-1K-1	87-94
EST7-0	Laguna Zonar	ZON04-1A-1K-1	36-46
EST7-1	Laguna Zonar	ZON04-1A-1K-1	36-46
EST7-2	Laguna Zonar	ZON04-1A-1K-1	36-46

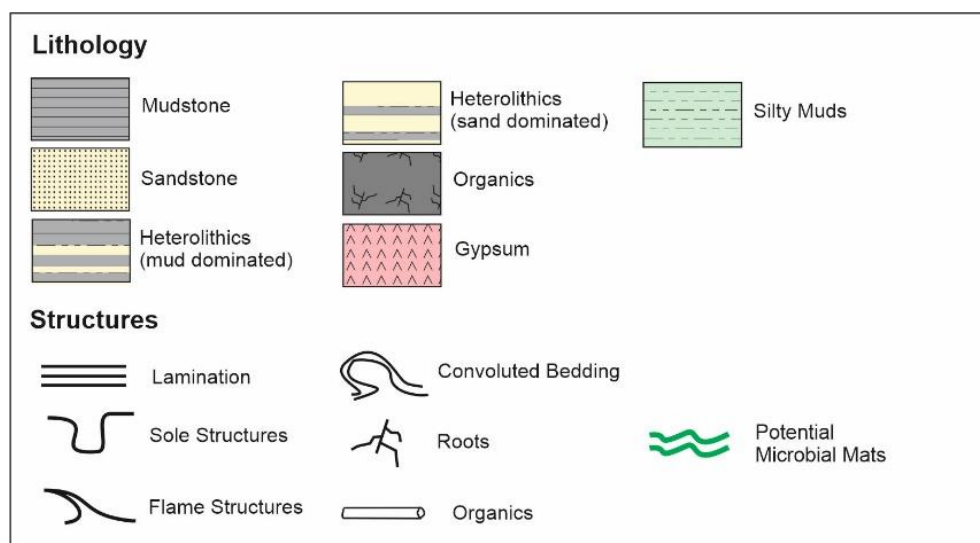
Appendix 2 - Sedimentological Data

Lago de Arreo

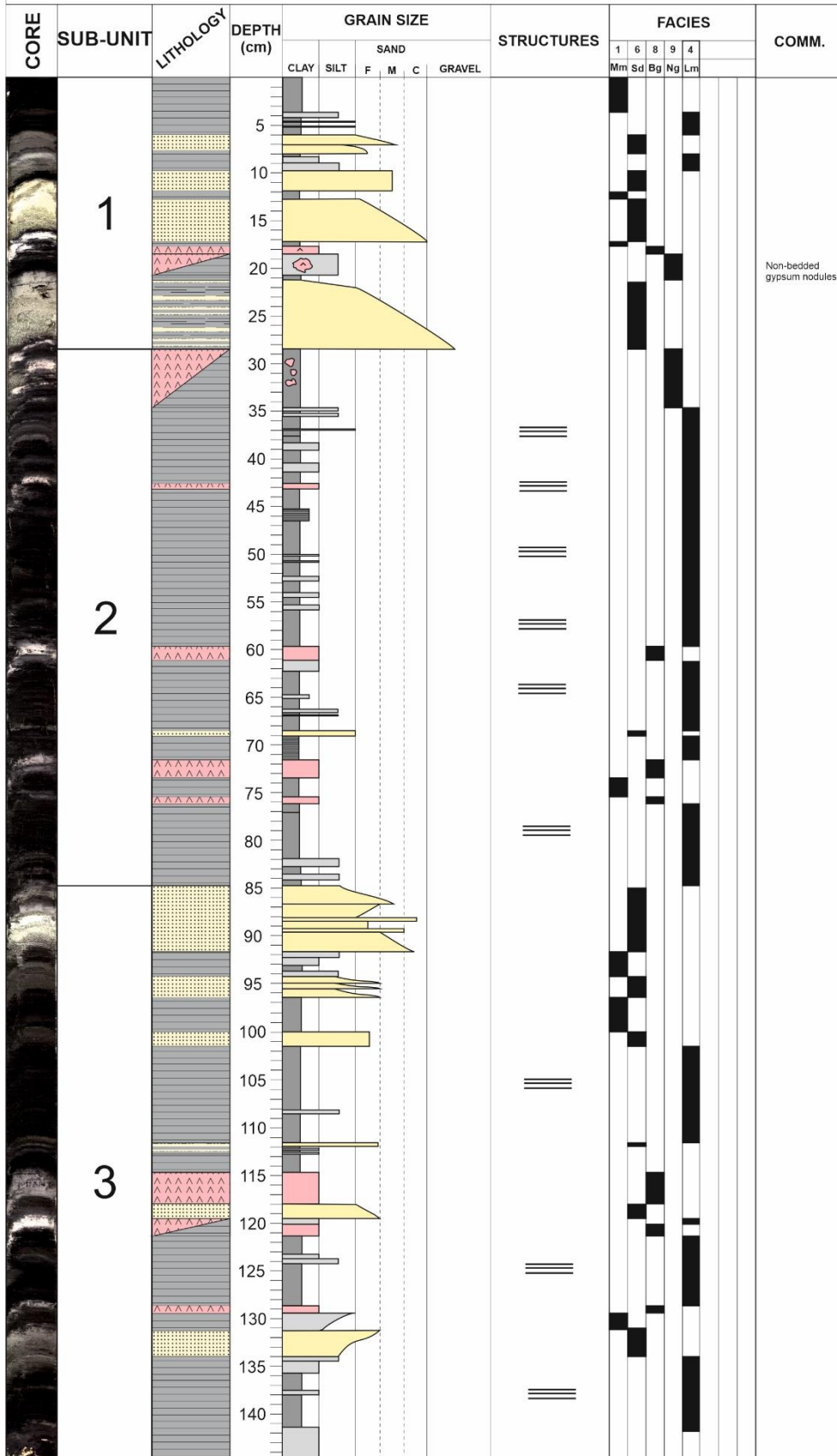
Facies and Key

Logs and facies described after Corella *et al.* (2013).

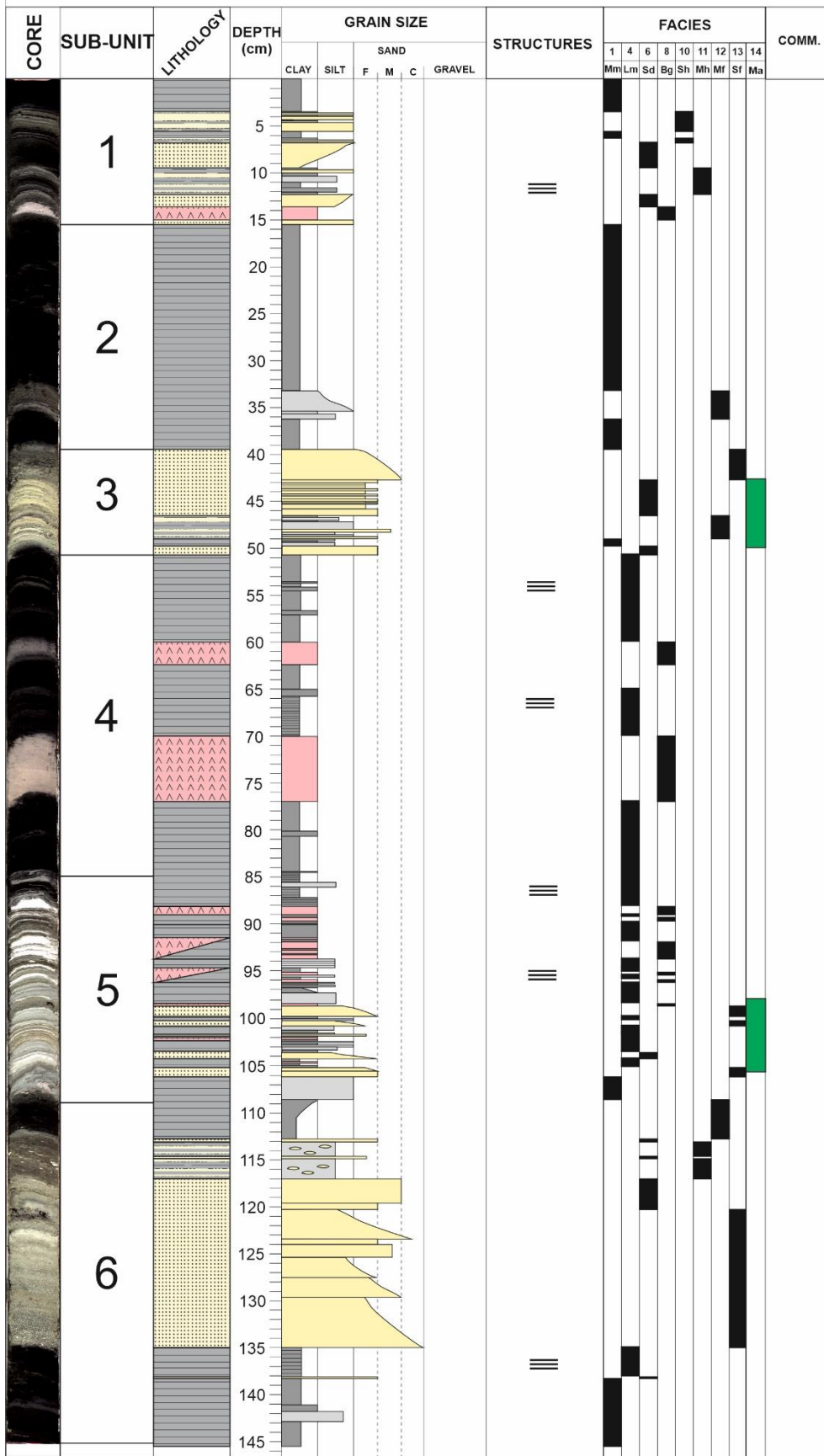
- 1 – Massive mudstones with grain size variations (Mm)
- 2 – Interbedded/interlaminated mudstones and sandstones (Sm)
- 3 – Massive sandstones (Ms)
- 4 – Laminated mudstones (Lm)
- 5 – Massive woody deposits (Wd)
- 6 – Bedded sandstones (Sd)
- 7 - Interbedded/interlaminated sandstones and mudstones (Ss)
- 8 – Bedded gypsum (Bg)
- 9 – Mudstones with nodular/interlaminated gypsum (Ng)
- 10 – Sand-dominated heterolithics (Sh)
- 11 – Mud-dominated heterolithics (Mh)
- 12 – Fining upwards mudstones (Mf)
- 13 – Fining upwards sandstones (Sf)
- 14 – Potential microbial mats (Ma)



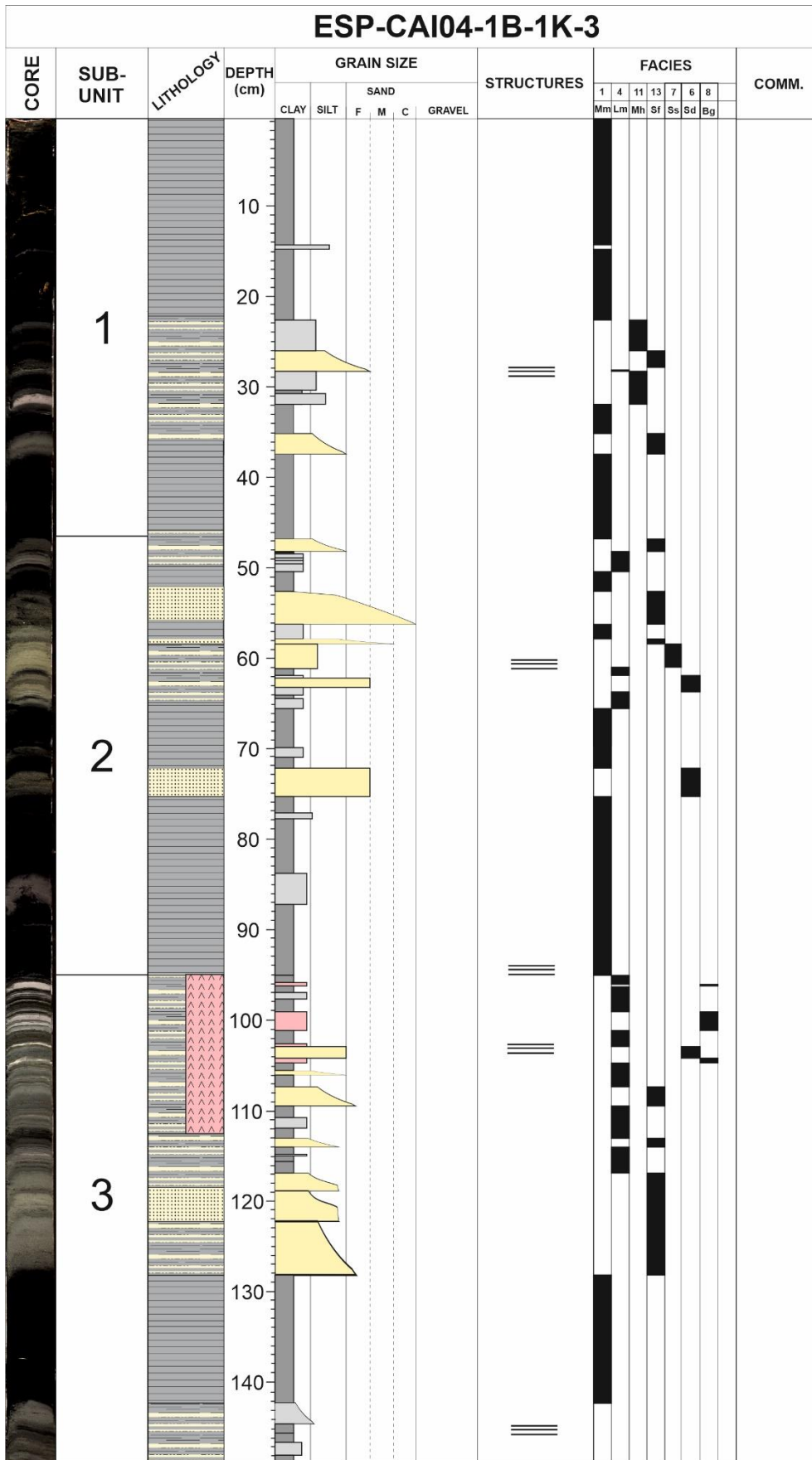
ESP-CAI04-1A-1K-3



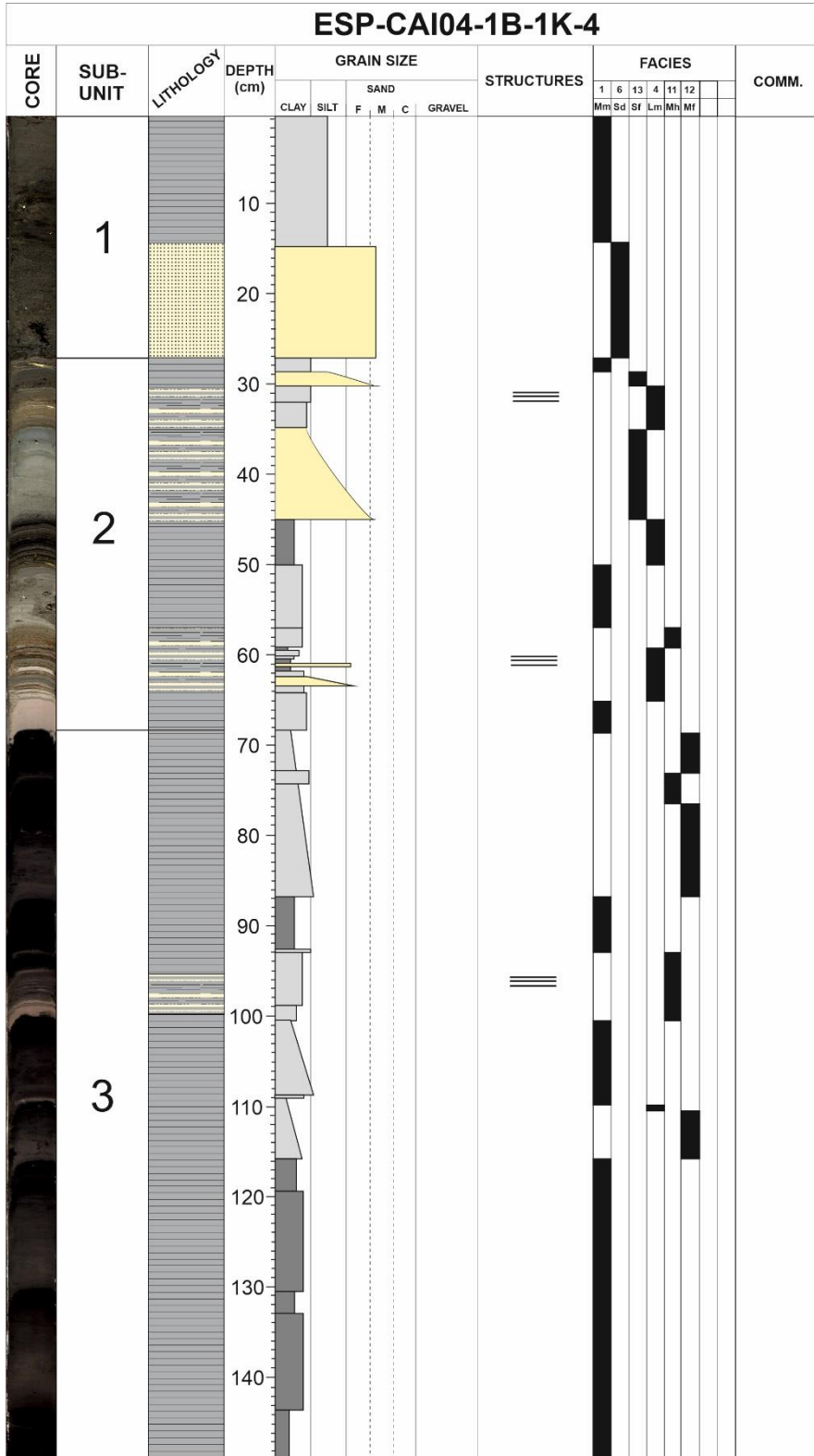
ESP-CAI04-1A-1K-4



ESP-CAI04-1B-1K-3



ESP-CAI04-1B-1K-4



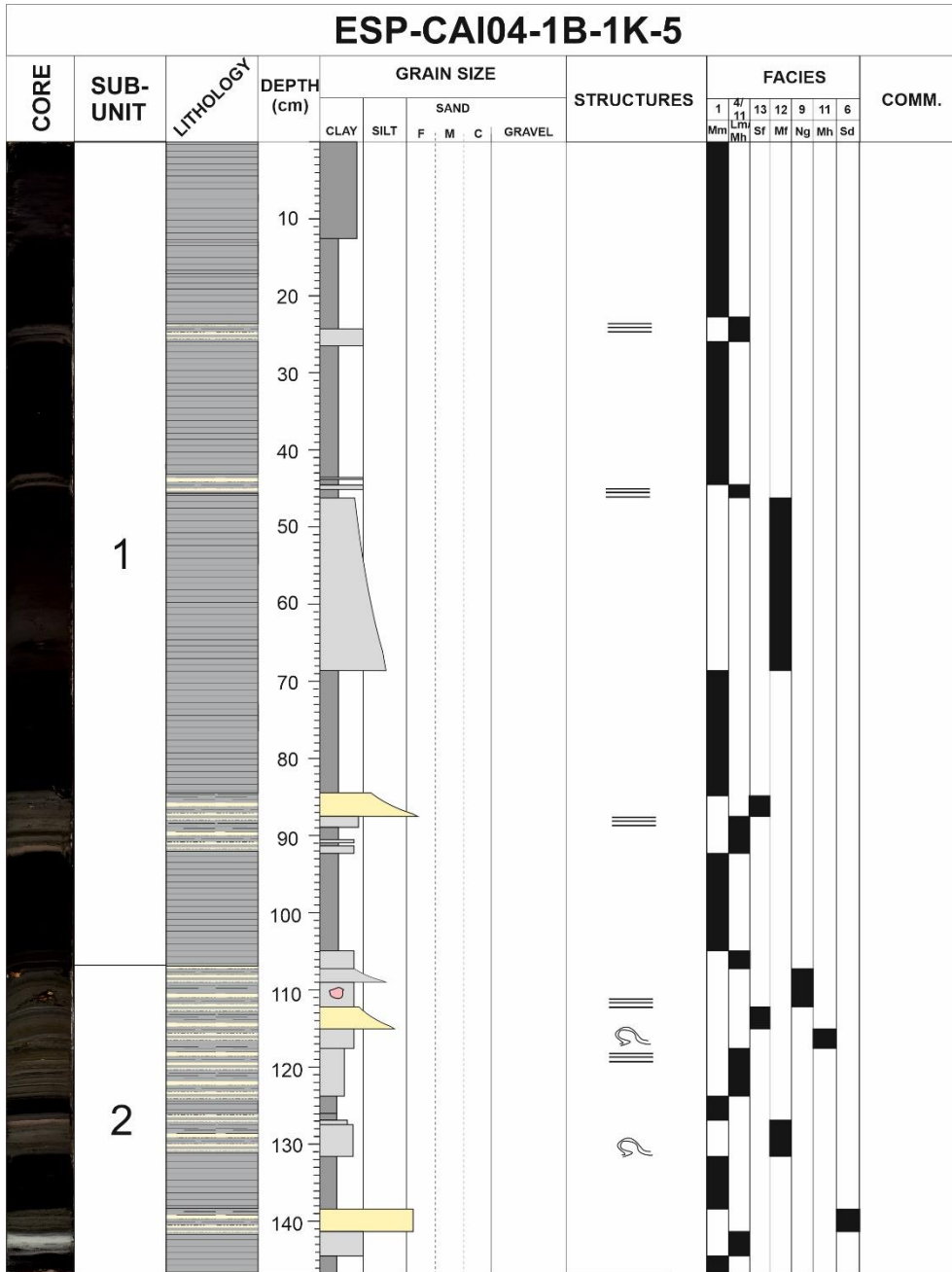


Figure A2.2 – Sedimentary logs illustrating facies, structures, lithology and intervals of microbial mats from core CAI04-1B-1K from Lago de Arreo.

Lago de Estanya

Facies and Key

Logs and facies described after Morellón *et al.* (2009).

Facies 1 - Blackish, banded carbonate clayey silts



Facies 2 - Grey, banded to laminated calcareous silts



Facies 3 - Black, massive to faintly laminated silty clay



Facies 4 - Brown, massive to faintly laminated sapropel with gypsum



Facies 5 - Variegated finely laminated microbial mats with aragonite and gypsum



Facies 6 - Grey and mottled massive carbonate silt with plant remains and gypsum



Facies 7 - Grey, banded to laminated carbonate-rich silts



Facies 8 - Variegated, finely laminated gypsum, carbonates and clay



Facies 9 - Variegated, banded gypsum, carbonates and clay



Facies 10 - Yellowish, massive, coarse-grained gypsum



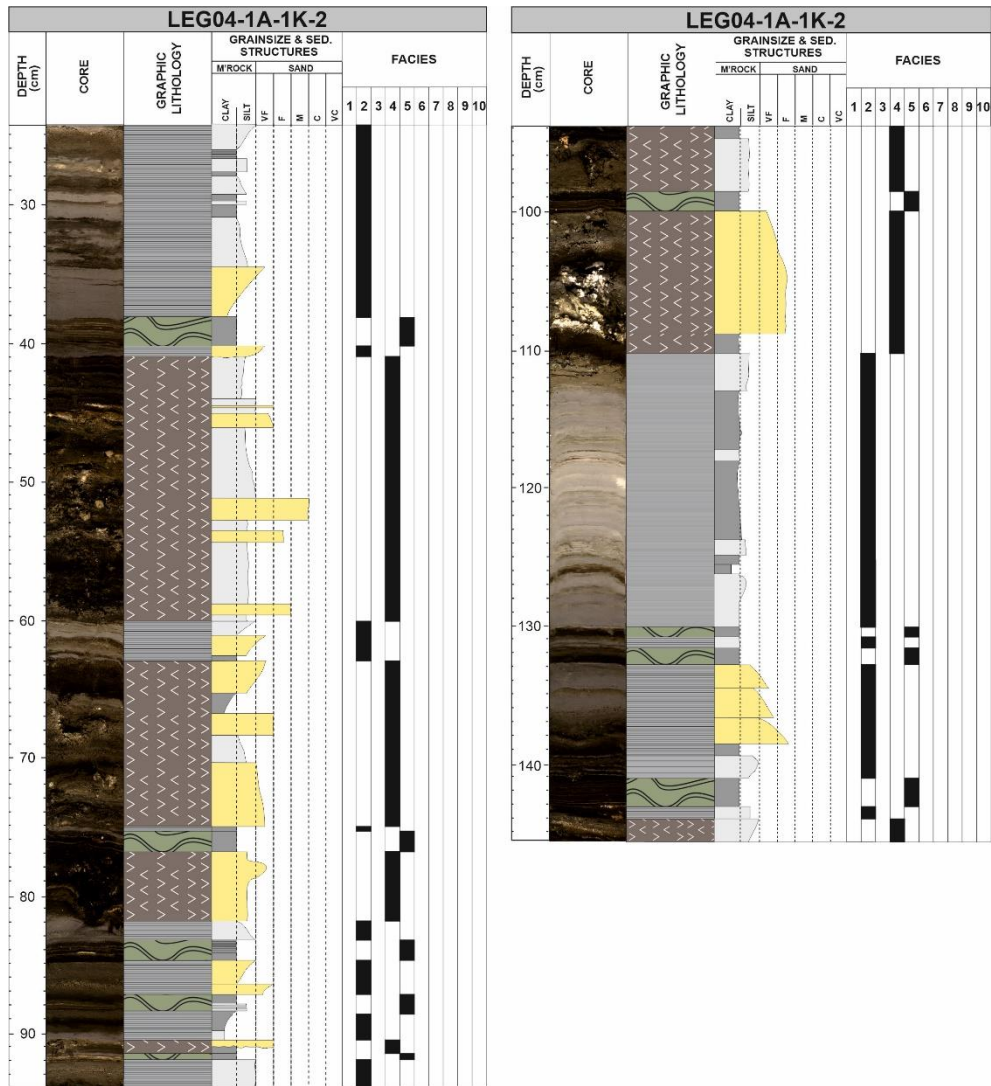


Figure A2.3 – Sedimentary logs illustrating facies, structures, lithology and intervals of microbial mats from core LEG04-1A-1K-2 from Lago de Estanya.

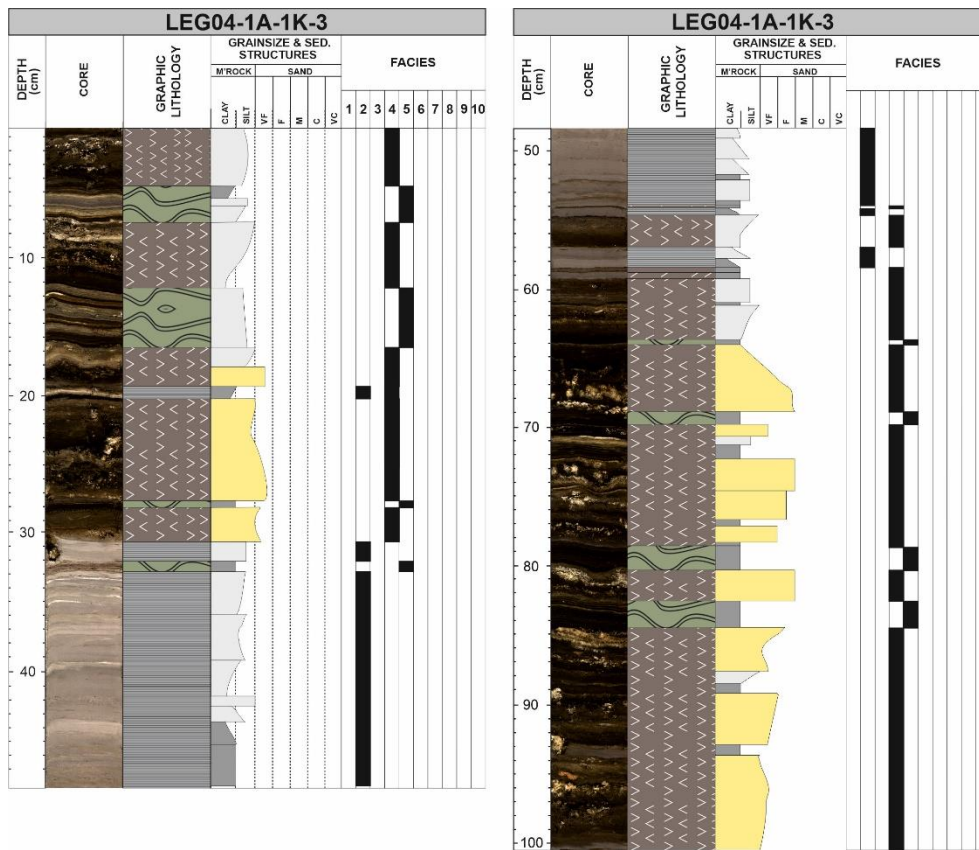


Figure A2.4 – Sedimentary logs illustrating facies, structures, lithology and intervals of microbial mats from core LEG04-1A-1K-3 from Lago de Estanya.

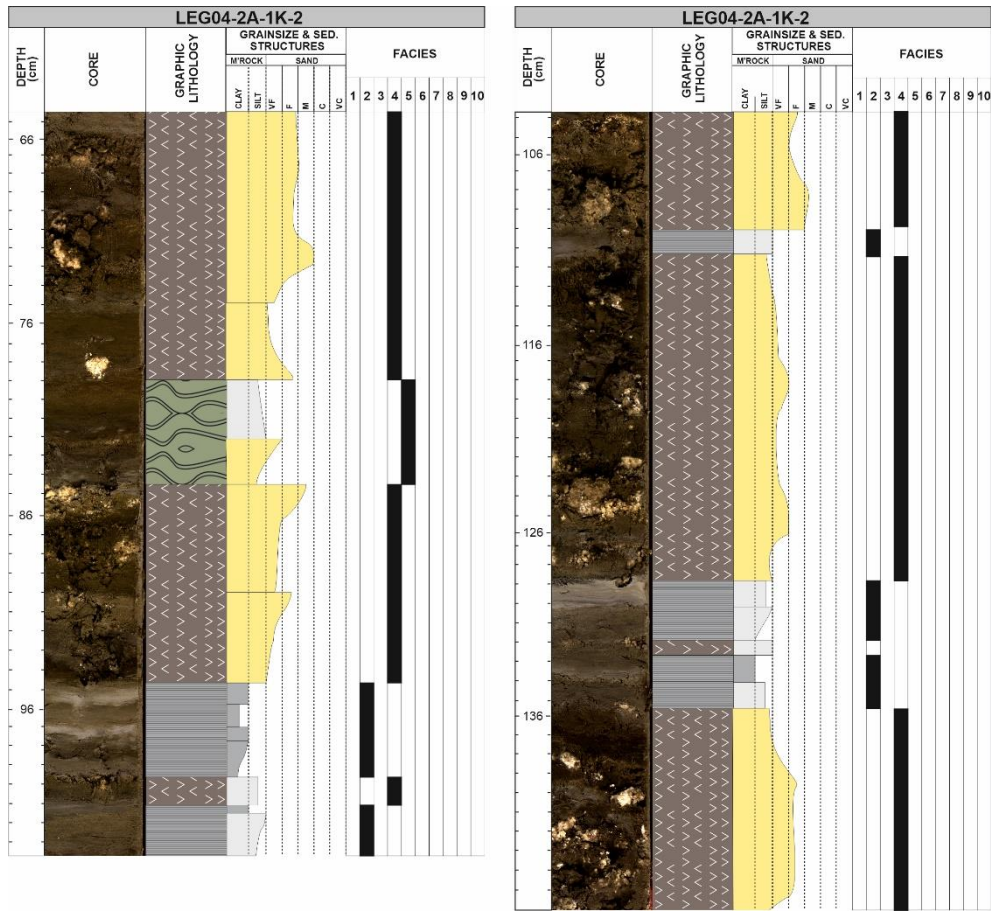


Figure A2.5 – Sedimentary logs illustrating facies, structures, lithology and intervals of microbial mats from core LEG04-2A-1K-2 from Lago de Estanya.

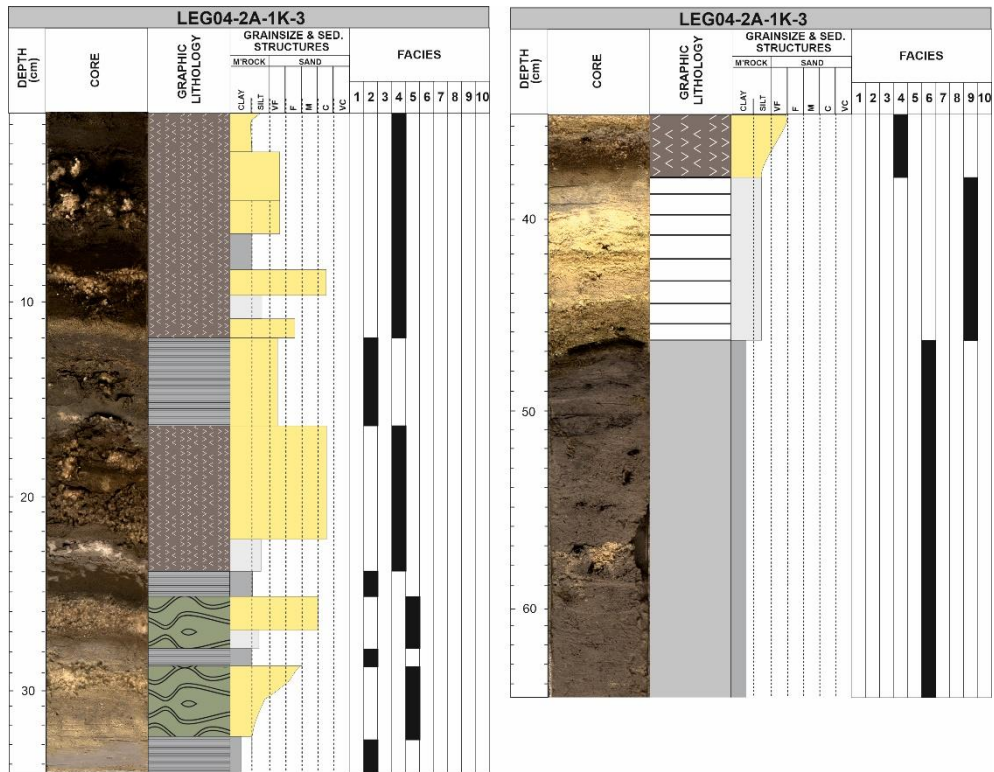


Figure A2.6 – Sedimentary logs illustrating facies, structures, lithology and intervals of microbial mats from core LEG04-2A-1K-3 from Lago de Estanya.

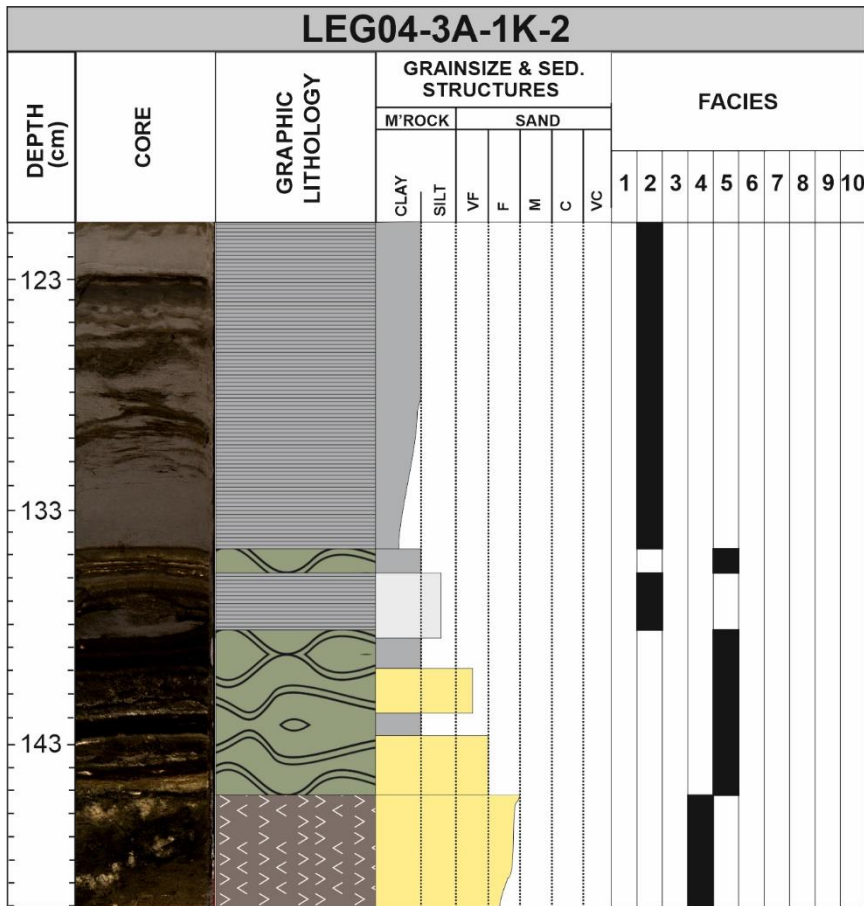


Figure A2.7 – Sedimentary logs illustrating facies, structures, lithology and intervals of microbial mats from core LEG04-3A-1K-2 from Lago de Estanya.

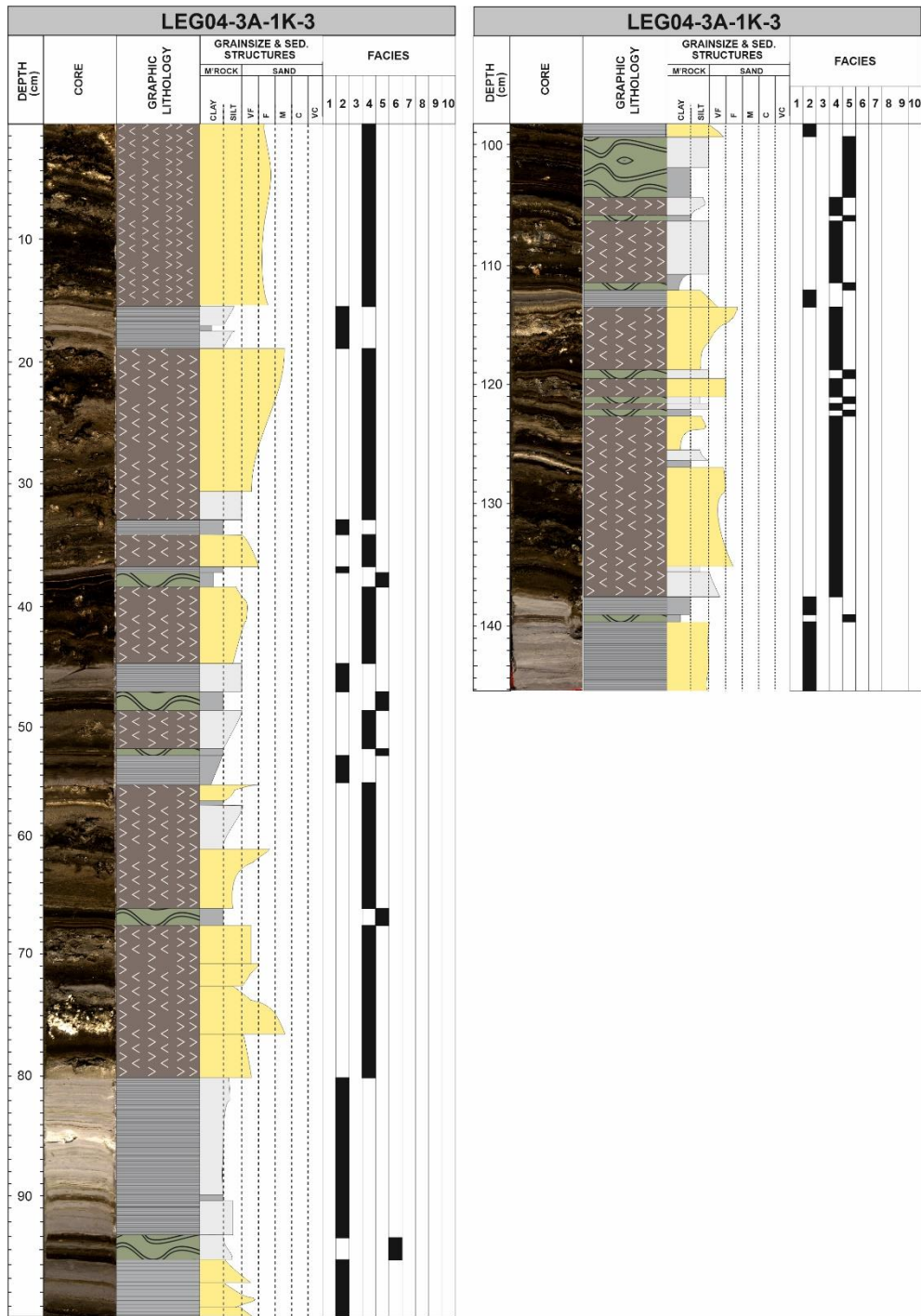


Figure A2.8 – Sedimentary logs illustrating facies, structures, lithology and intervals of microbial mats from core LEG04-3A-1K-3 from Lago de Estanya.

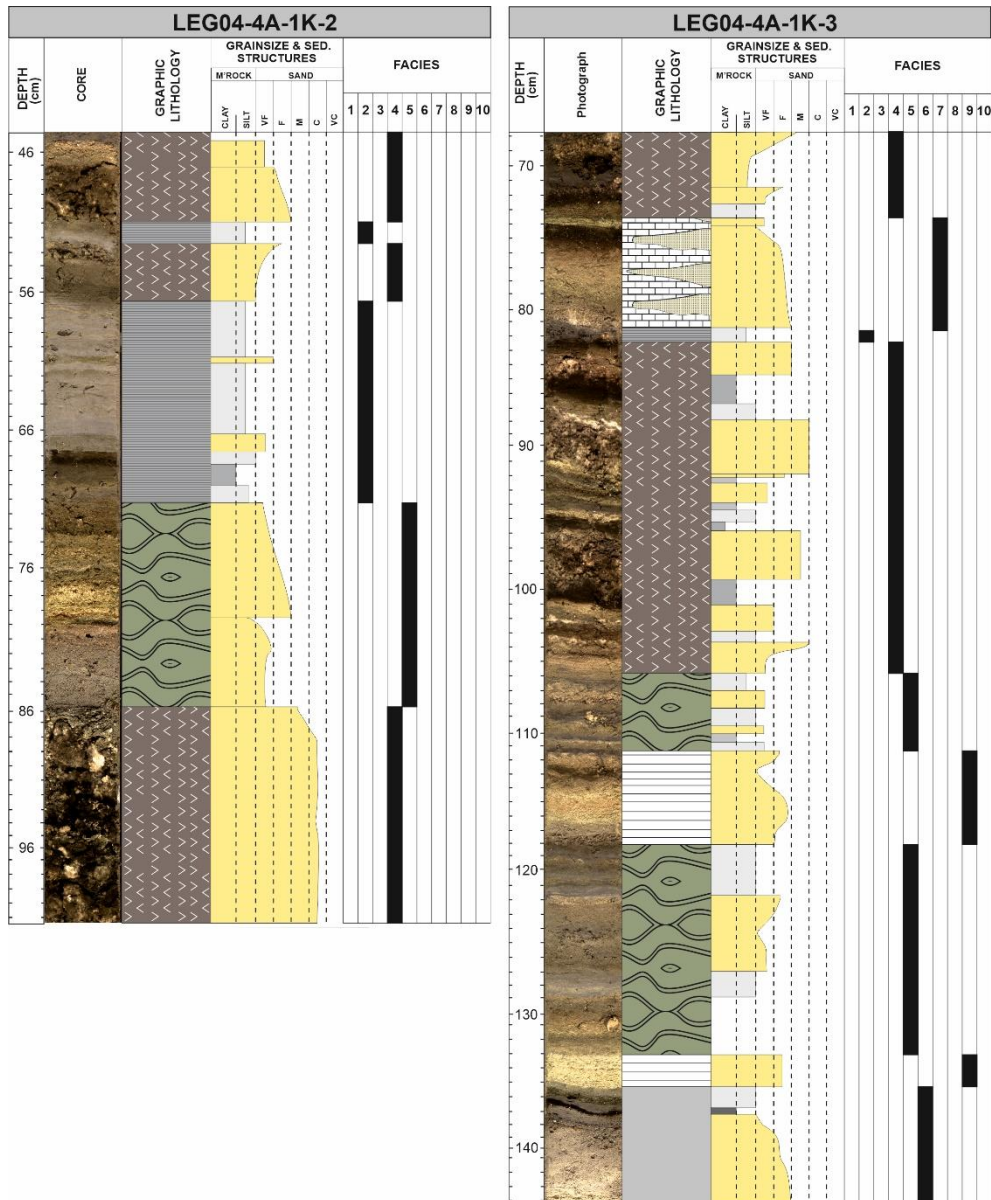


Figure A2.10 – Sedimentary logs illustrating facies, structures, lithology and intervals of microbial mats from core LEG04-4A-1K-2 from Lago de Estanya.

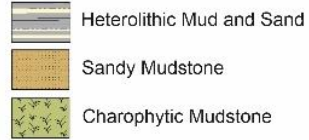
Laguna Salada de Chiprana

Facies and Key

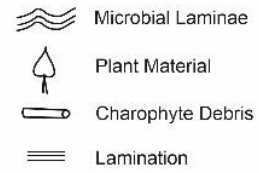
See chapter 4 for facies descriptions.

Key

Lithology



Structures



CHI19-1A

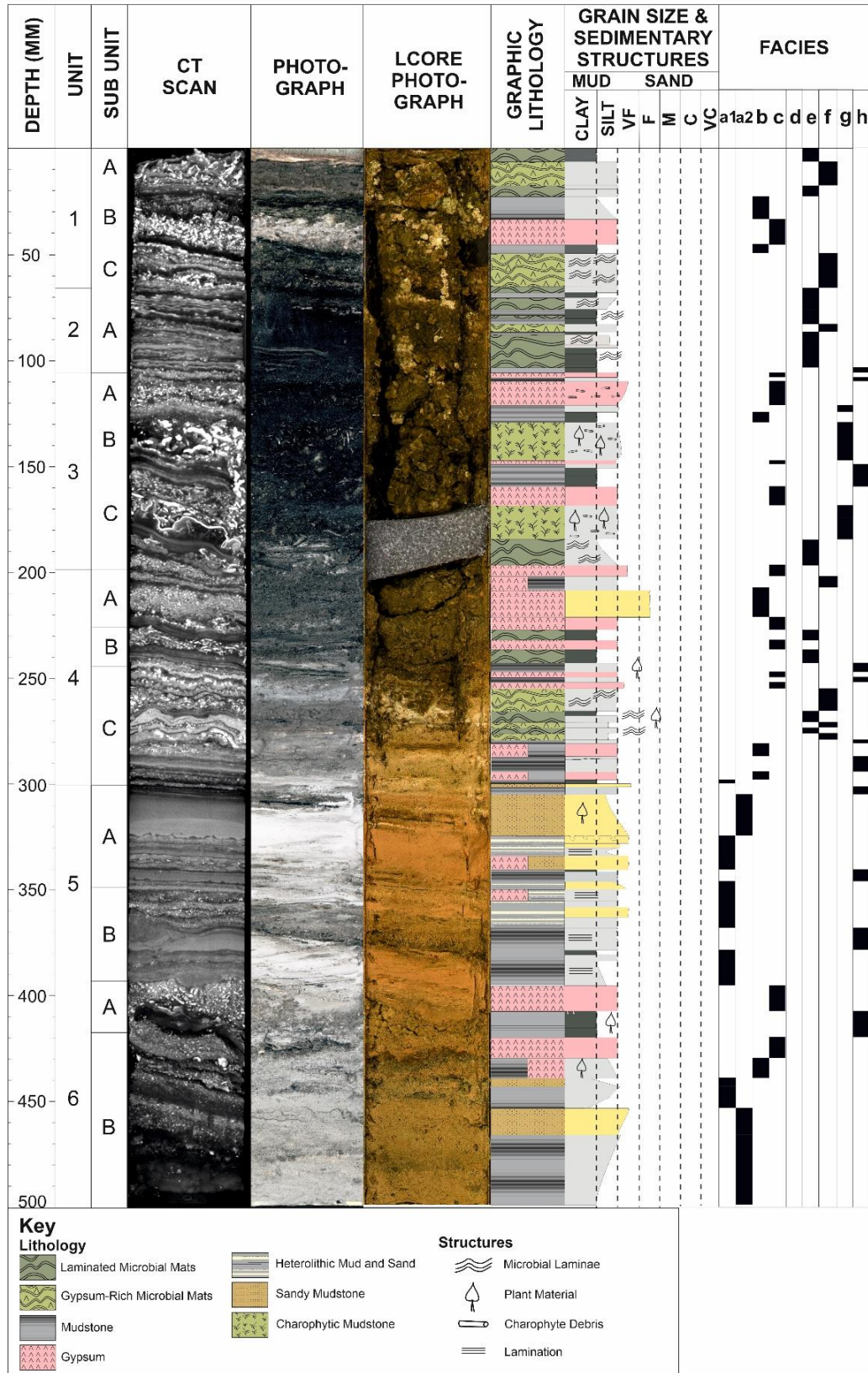


Figure A2.11 – Sedimentary logs illustrating facies, structures, lithology and intervals of microbial mats from core CHI19-1A from Lake Chiprana.

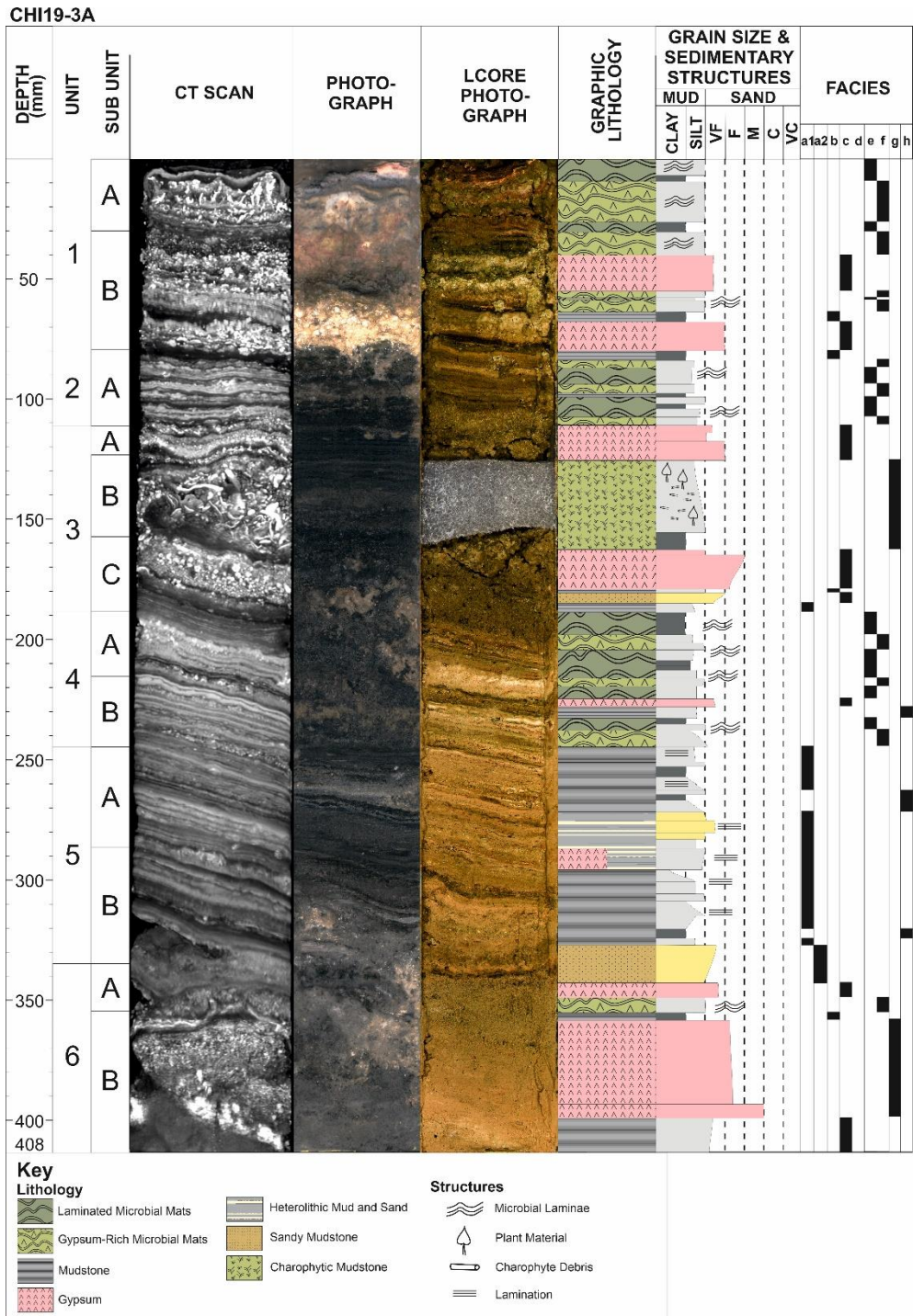


Figure A2.13 – Sedimentary logs illustrating facies, structures, lithology and intervals of microbial mats from core CHI19-3A from Lake Chiprana.

CHI19-5A

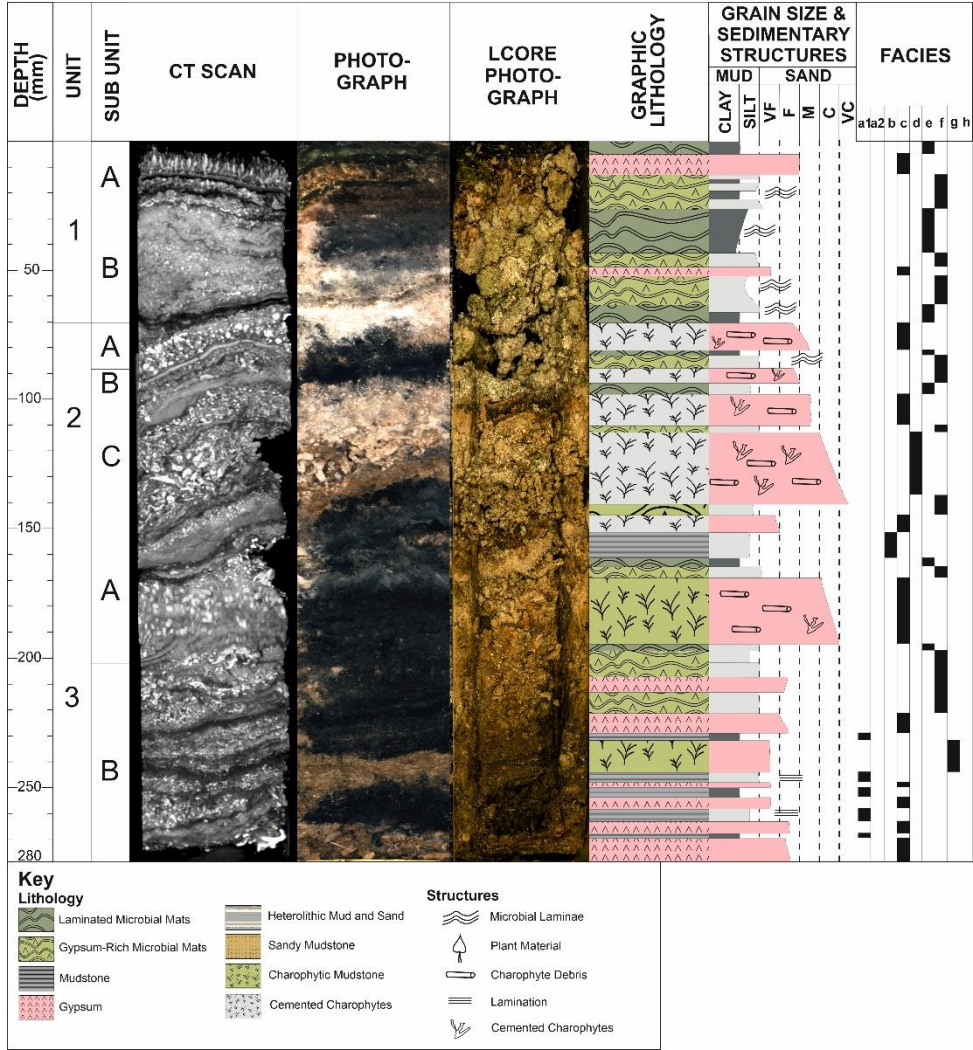


Figure A2.15 – Sedimentary logs illustrating facies, structures, lithology and intervals of microbial mats from core CHI19-5A from Lake Chiprana.

CHI19-6A

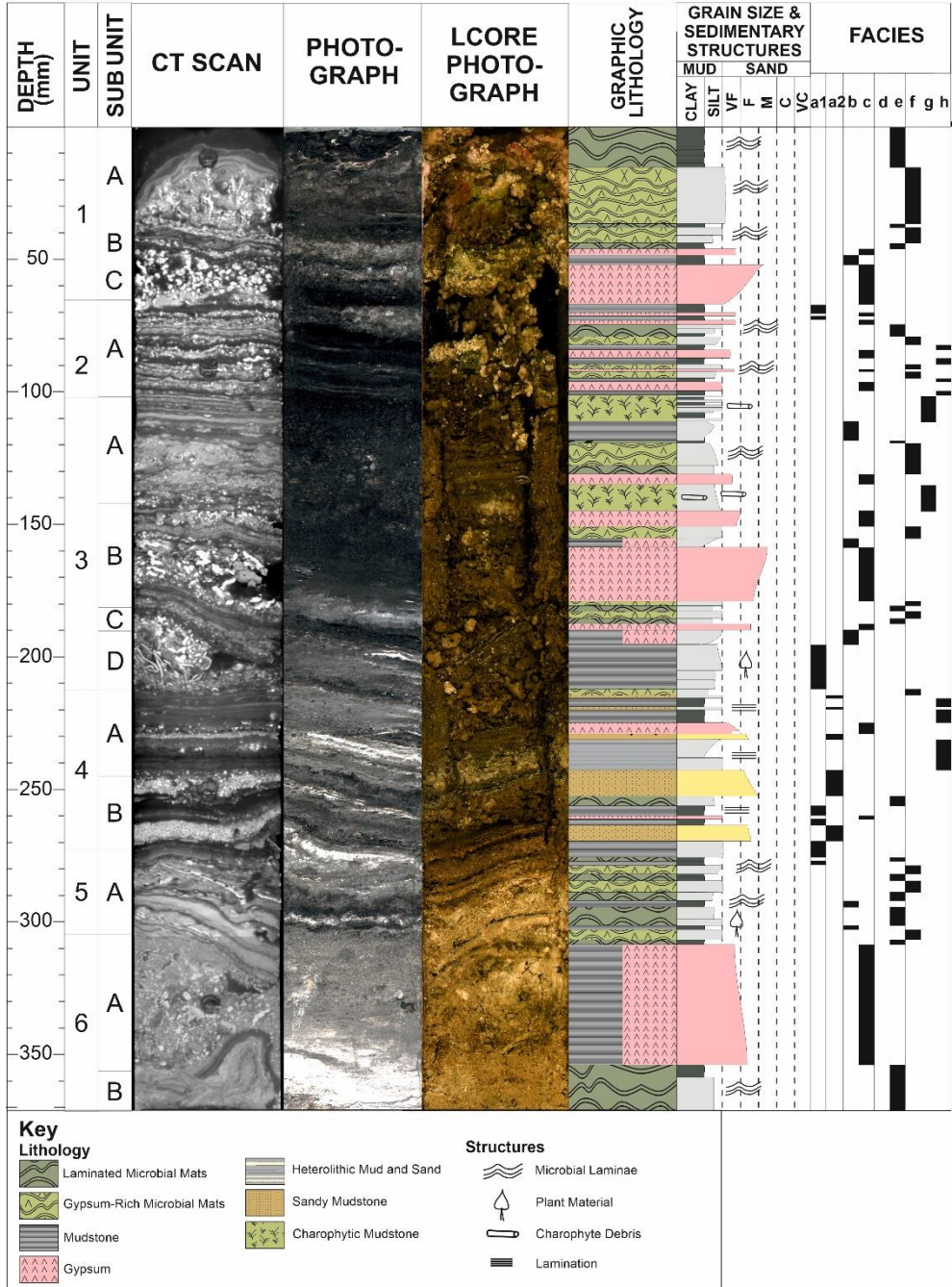


Figure A2.16 – Sedimentary logs illustrating facies, structures, lithology and intervals of microbial mats from core CHI19-6A from Lake Chiprana.

Laguna Zonar

Facies and Key

Logs and facies described after Martín-Puertas *et al.* (2008).

Facies 1 - Massive to faintly laminated brownish calcite mud



Facies 2 - Massive to faintly laminated gray calcite silty mud



Facies 3 - Cm-thick, massive, dark brown organic ooze



Facies 4 - Organic-rich, finely laminated and variegated (Microbial mats)



Facies 5 - Irregularly laminated and variegated



Facies 6 - Gypsum laminae



Facies 7 - Varves



Facies 8 - Massive, aragonite-bearing mud with edaphic and pedogenic textures



Facies 9 - Massive, quartz and clay-rich carbonate mud with edaphic and pedogenic textures



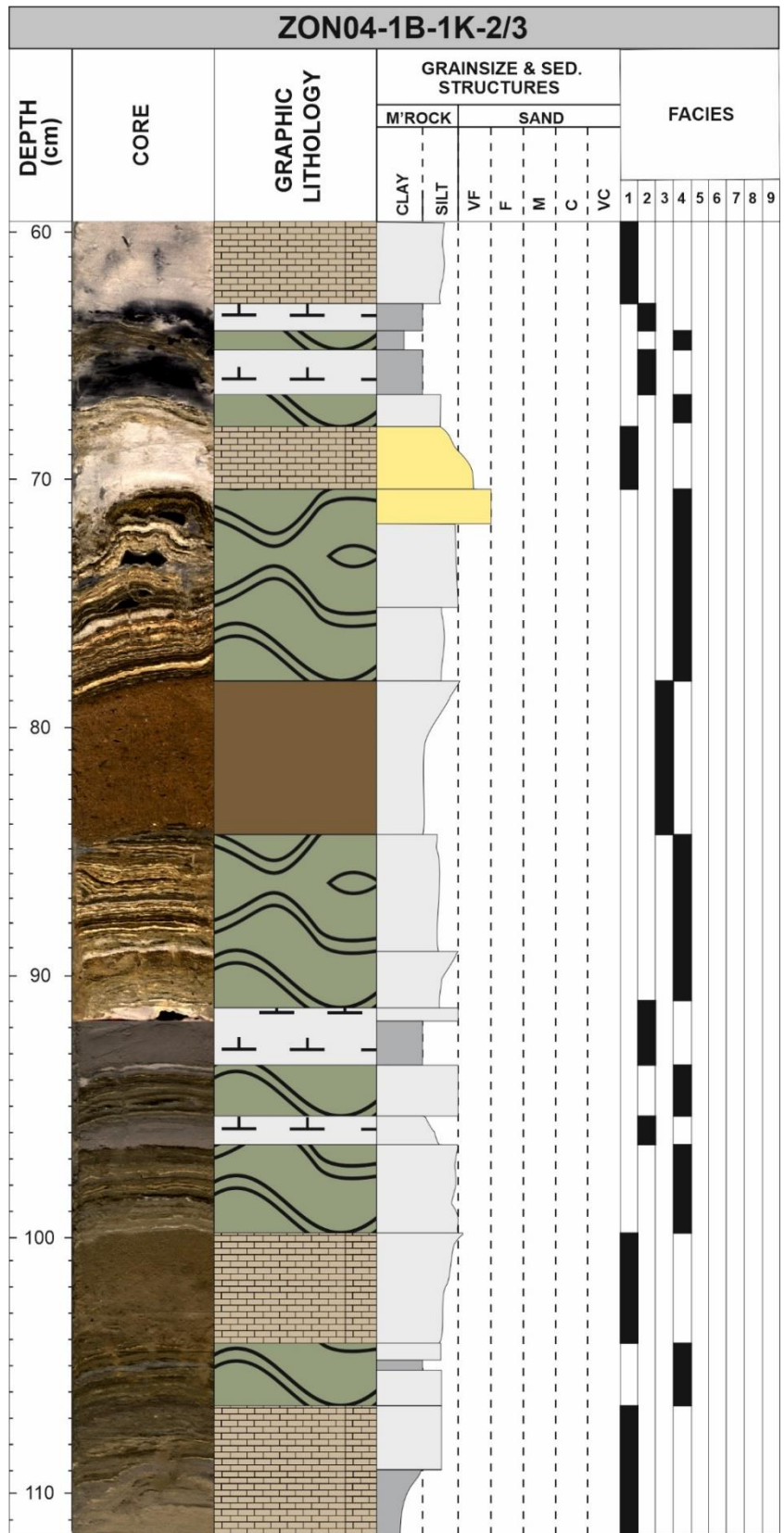


Figure A2.19 – Sedimentary logs illustrating facies, structures, lithology and intervals of microbial mats from core ZON04-1B-1K-2/3 from Lake Zonar.

Appendix 3 – Other Material

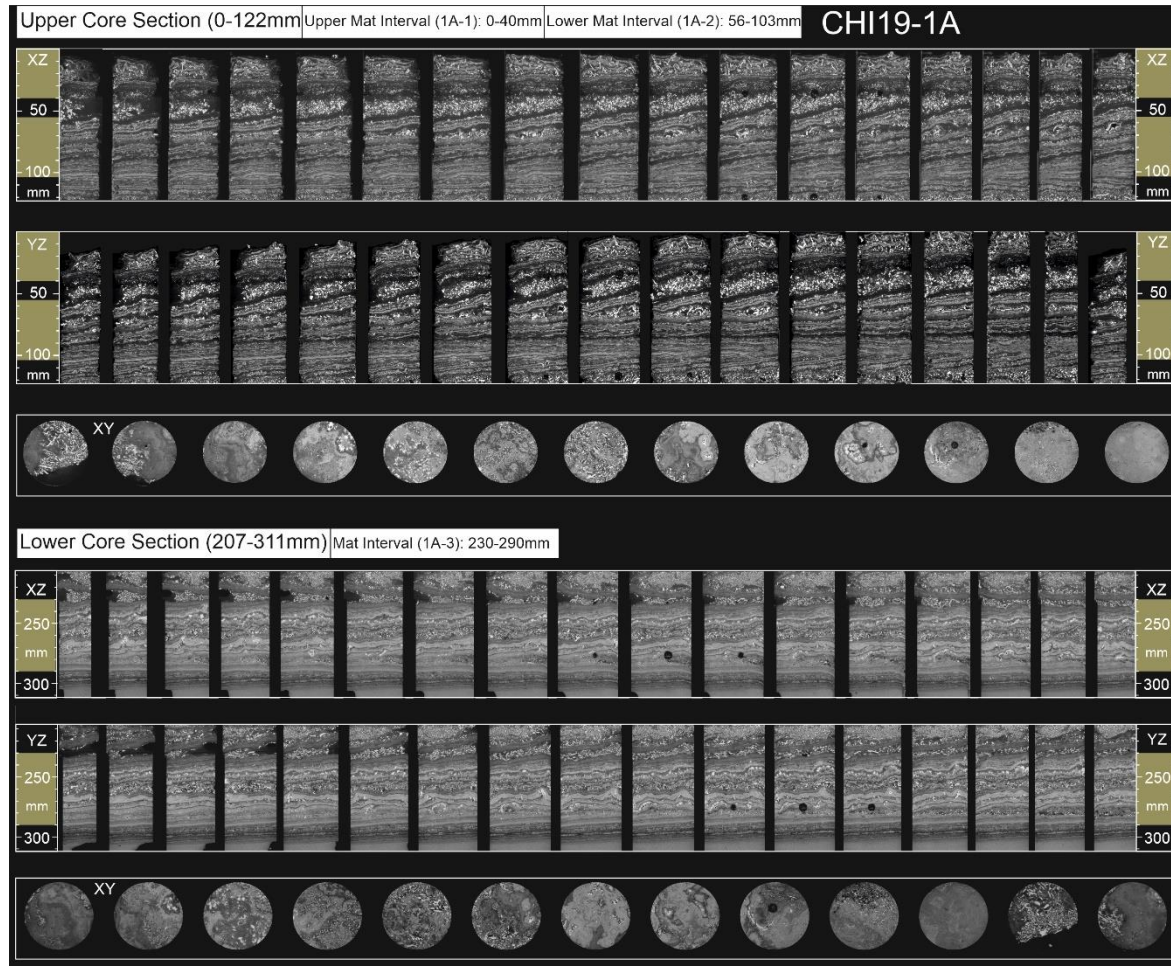


Figure A3.1 – Ortho slices of microbial mats in core CHI19-1A from Lake Chiprana. The upper interval of microbial mats is present between 0-122mm, while the lower interval is present between 207-311mm. The morphology of the mats is displayed in XZ, YZ and XY orientations. In the XZ and YZ intervals, ortho slice intervals represent approximately 0.3cm shifts throughout the core, while the XY intervals represent ~1cm intervals.



Figure A3.2 – Ortho slices of microbial mats in core CHI19-2A from Lake Chiprana. The upper interval of microbial mats is present between 0-142mm, while the lower interval is present between 163-312mm. The morphology of the mats is displayed in XZ, YZ and XY orientations. In the XZ and YZ intervals, ortho slice intervals represent approximately 0.3cm shifts throughout the core, while the XY intervals represent ~1cm intervals.



Figure A3.3 – Ortho slices of microbial mats in core CHI19-3A from Lake Chiprana. The upper interval of microbial mats is present between 0-110mm, while the lower interval is present between 181-342mm. The morphology of the mats is displayed in XZ, YZ and XY orientations. In the XZ and YZ intervals, ortho slice intervals represent approximately 0.1cm shifts throughout the core, while the XY intervals represent ~1cm intervals.

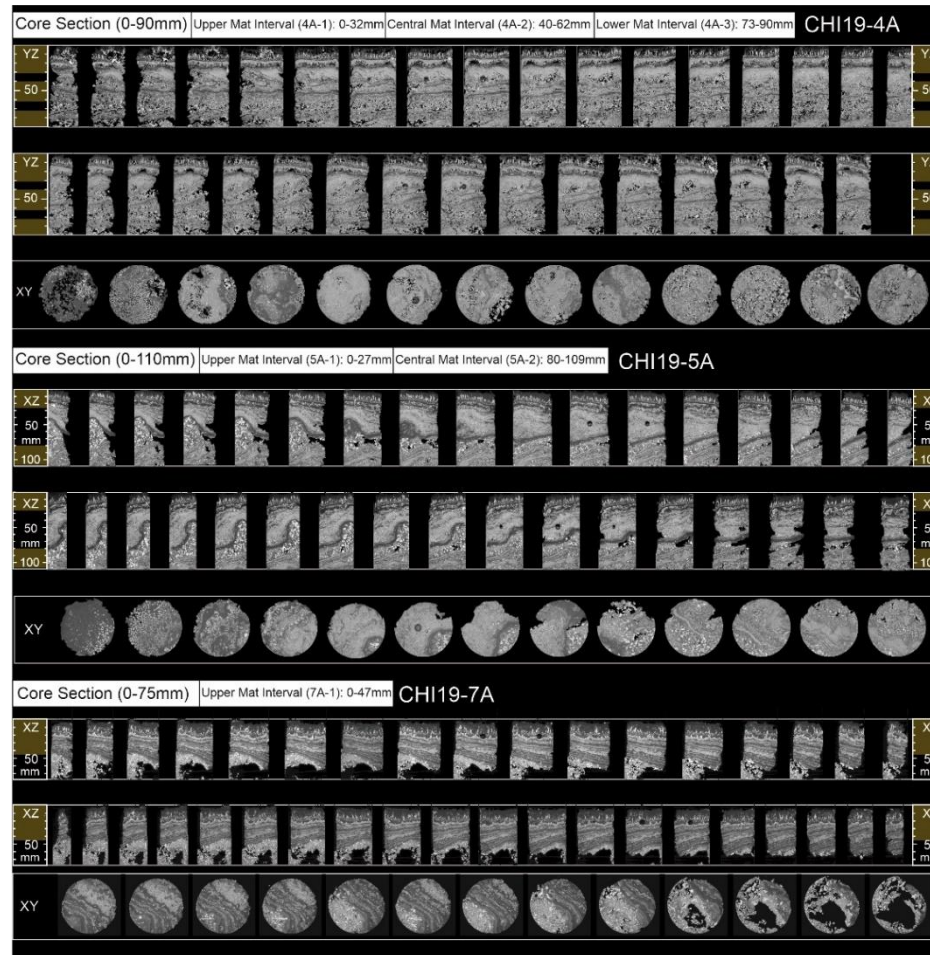


Figure A3.4 – Ortho slices of microbial mats in littoral cores CHI19-4A, CHI19-5A and CHI19-7A from Lake Chiprana. The upper section of microbial mats in core 4A is present between 0-90mm, between 0-110mm in core 5A, and between 0-75mm. The morphology of the mats is displayed in XZ, YZ and XY

orientations. In the XZ and YZ intervals, ortho slice intervals represent approximately 0.1cm shifts throughout the core, while the XY intervals represent 0.2cm intervals.

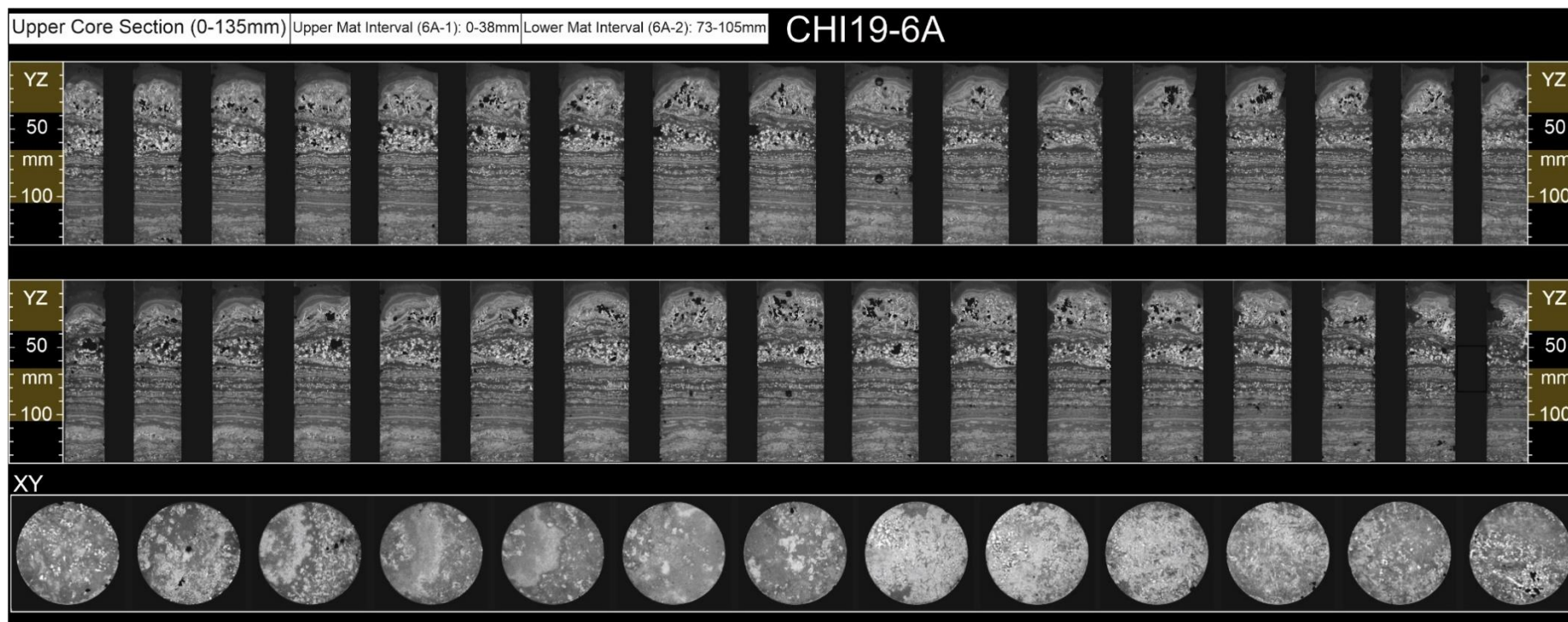


Figure A3.5 - Ortho slices of microbial mats in core CHI19-6A from Lake Chiprana. This interval of microbial mats is present between 0-135mm. The morphology of the mats is displayed in XZ, YZ and XY orientations. In the XZ and YZ intervals, ortho slice intervals represent approximately 0.1cm shifts throughout the core, while the XY intervals represent ~1cm intervals.

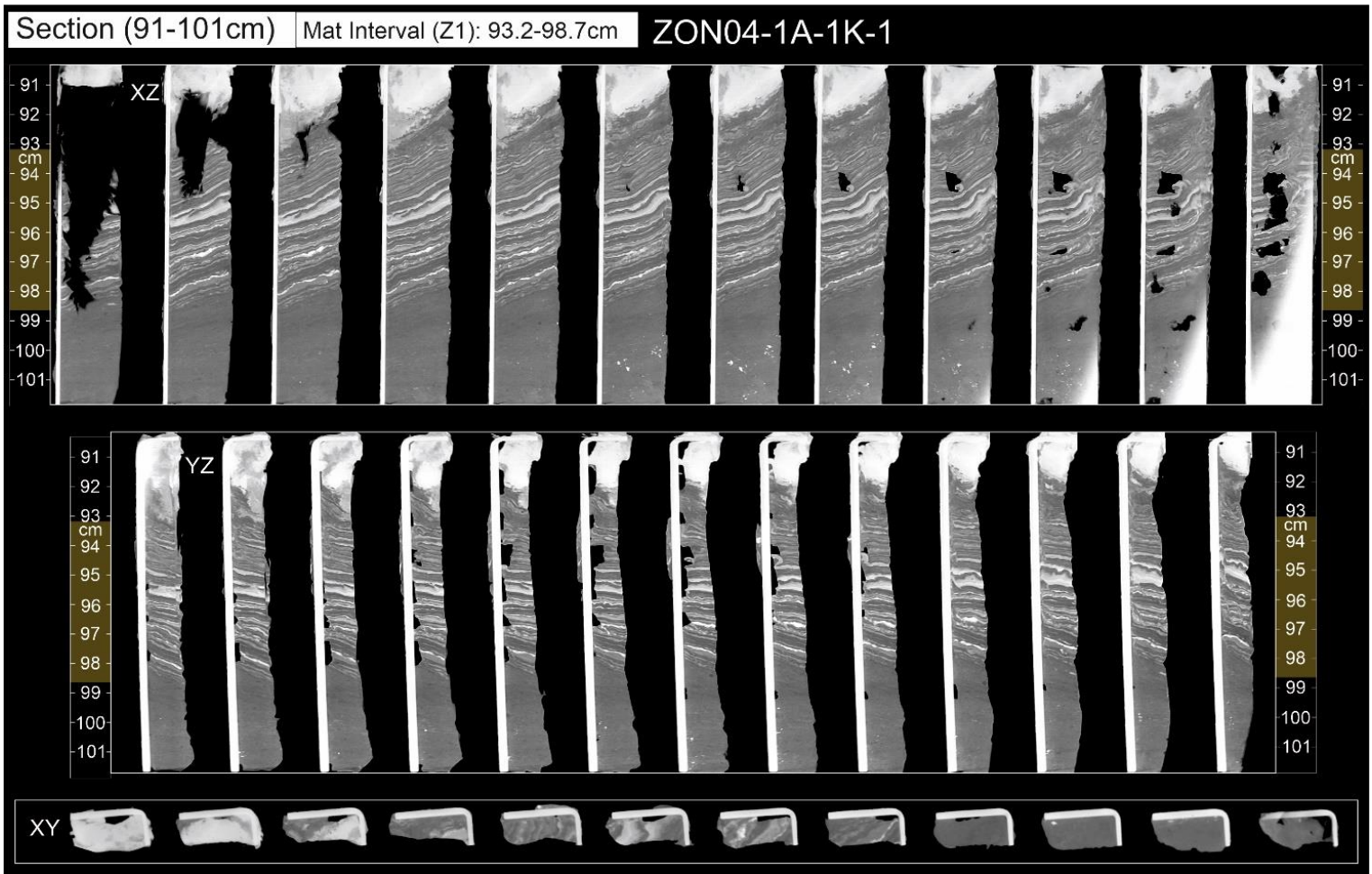


Figure A3.6 – Ortho slices of microbial mats from the 92-102cm interval from core 1A from Lake Zonar (Martín-Puertas et al., 2008). The morphology of the mats is displayed in XZ, YZ and XY orientations. In the XZ and YZ intervals, ortho slice intervals represent approximately 0.1cm shifts throughout the core, while the XY intervals represent ~0.5cm intervals.

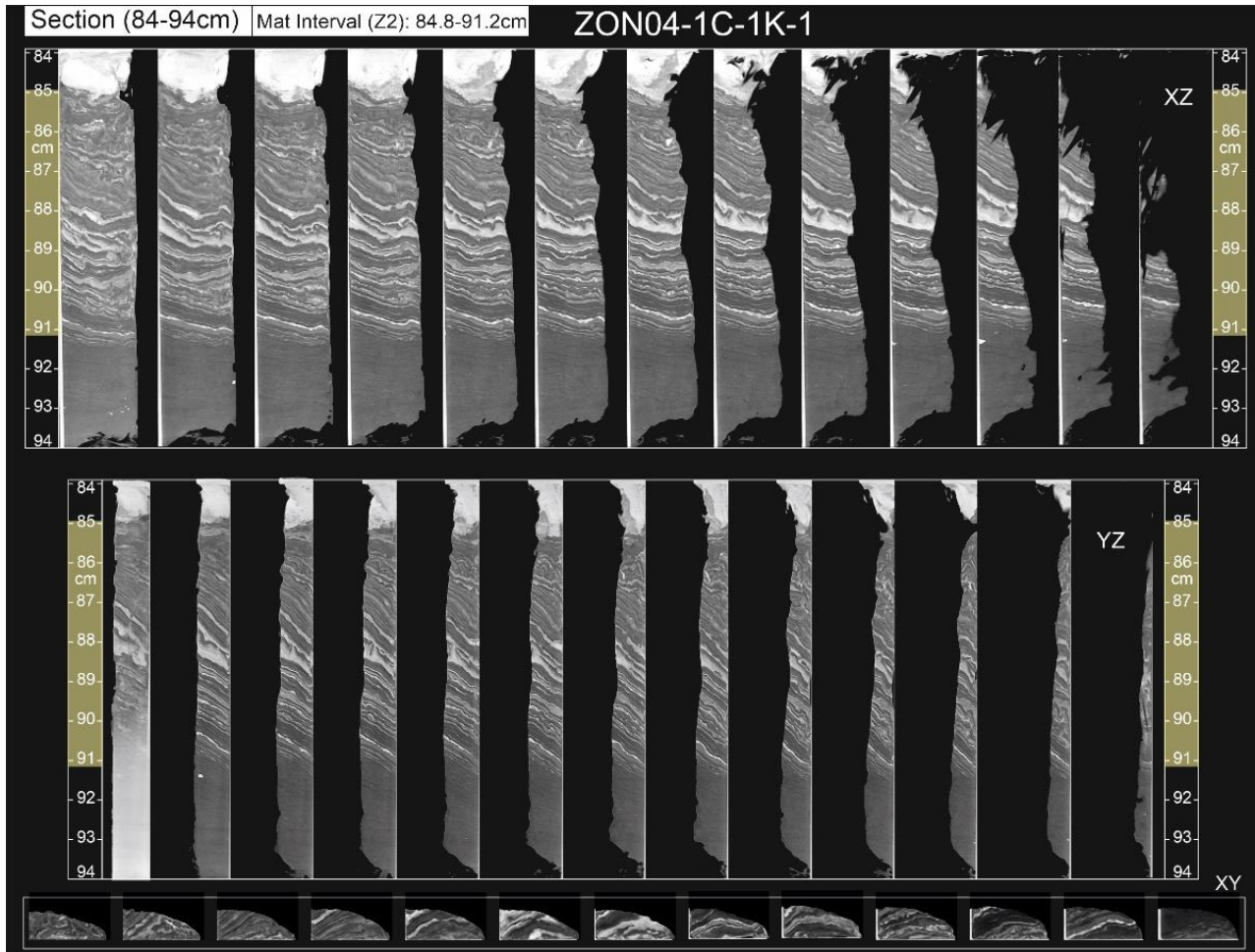


Figure A3.7 – Ortho slices of microbial mats from the 84-94cm interval from core 1C from Lake Zonar (Martín-Puertas et al., 2008). The morphology of the mats is displayed in XZ, YZ and XY orientations. In the XZ and YZ intervals, ortho slice intervals represent approximately 0.1cm shifts throughout the core, while the XY intervals represent ~0.5cm intervals.

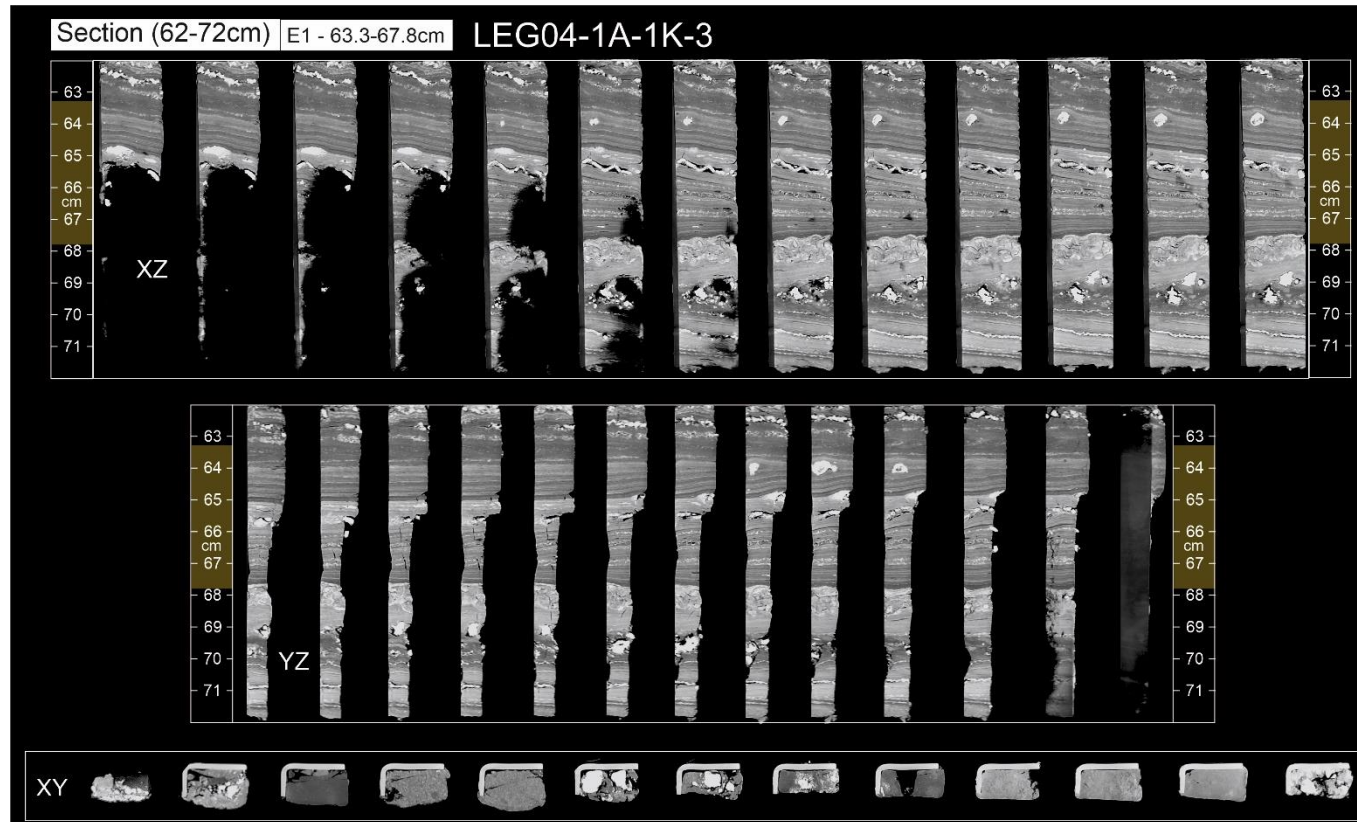


Figure A3.8 – Ortho slice intervals of microbial mats from the 62-72cm interval from core LEG04-1A-1K-3 from Lake Estanya. The morphology of the mats is displayed in XZ, YZ and XY orientations. In the XZ and YZ intervals, ortho slice intervals represent approximately 0.1cm shifts throughout the core, while the XY intervals represent ~1cm intervals.

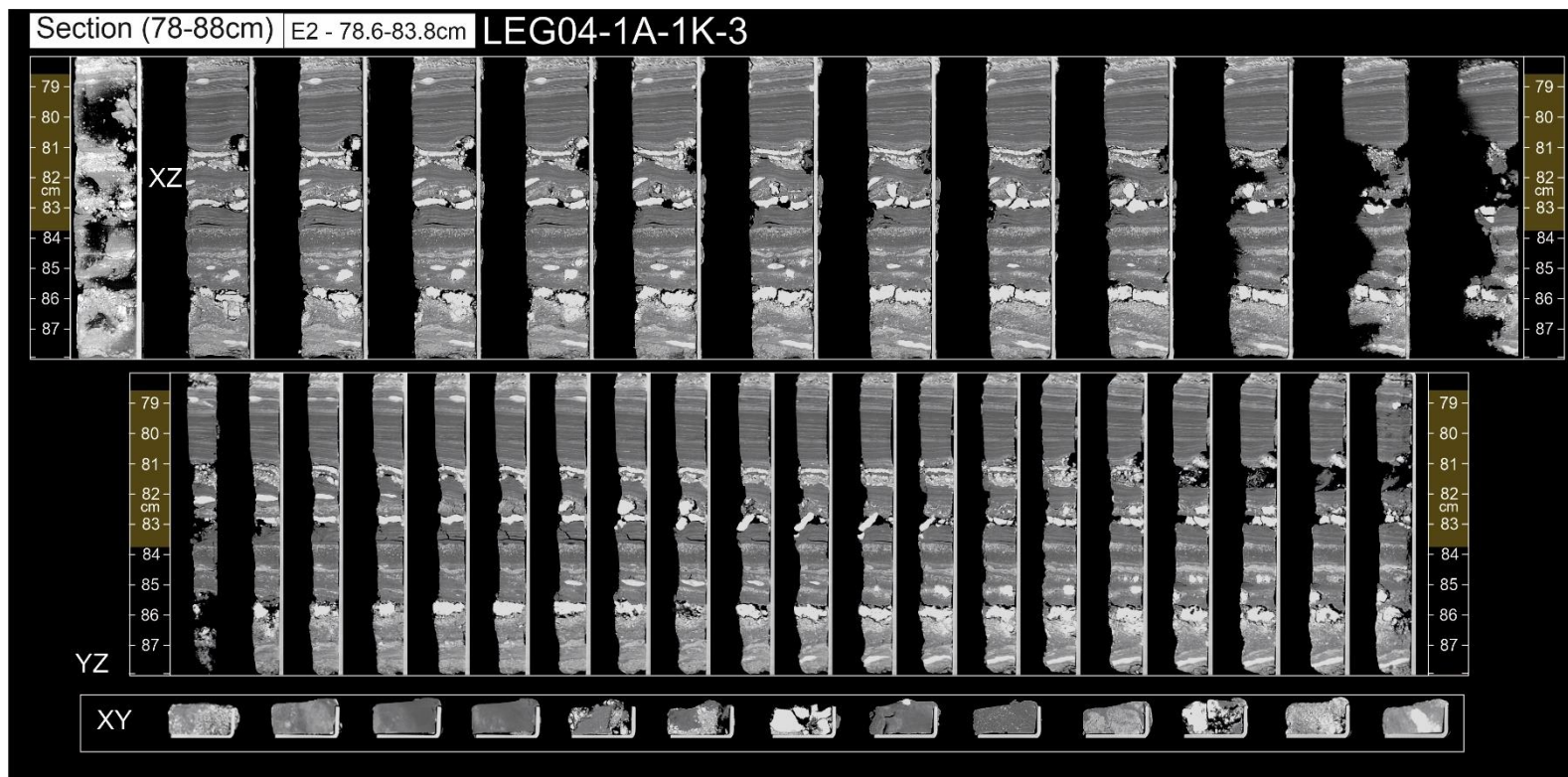


Figure A3.9 – Ortho slice intervals of microbial mats from the 78-88cm interval from core LEG04-1A-1K-3. The morphology of the mats is displayed in XZ, YZ and XY orientations, while the geochemistry is overlain in the XZ morphology. In the XZ and YZ intervals, ortho slice intervals represent approximately 0.1cm shifts throughout the core, while the XY intervals represent ~1cm intervals.

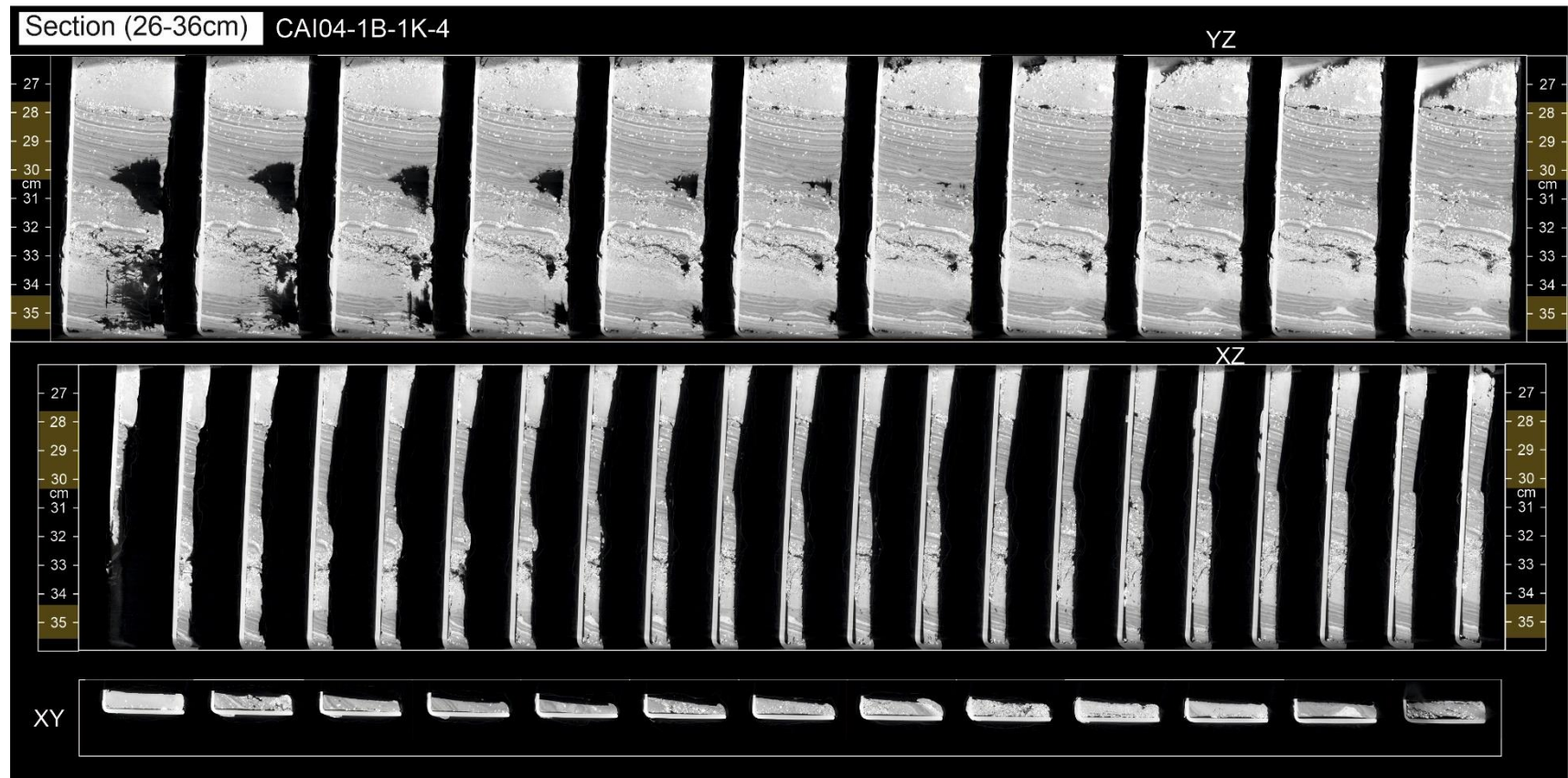


Figure A3.10 – Ortho slices generated by computerised tomographical scanning of unambiguous microbial mats from Lago de Arreo core CAI04-1B-1K-4, interval 26-36cm.

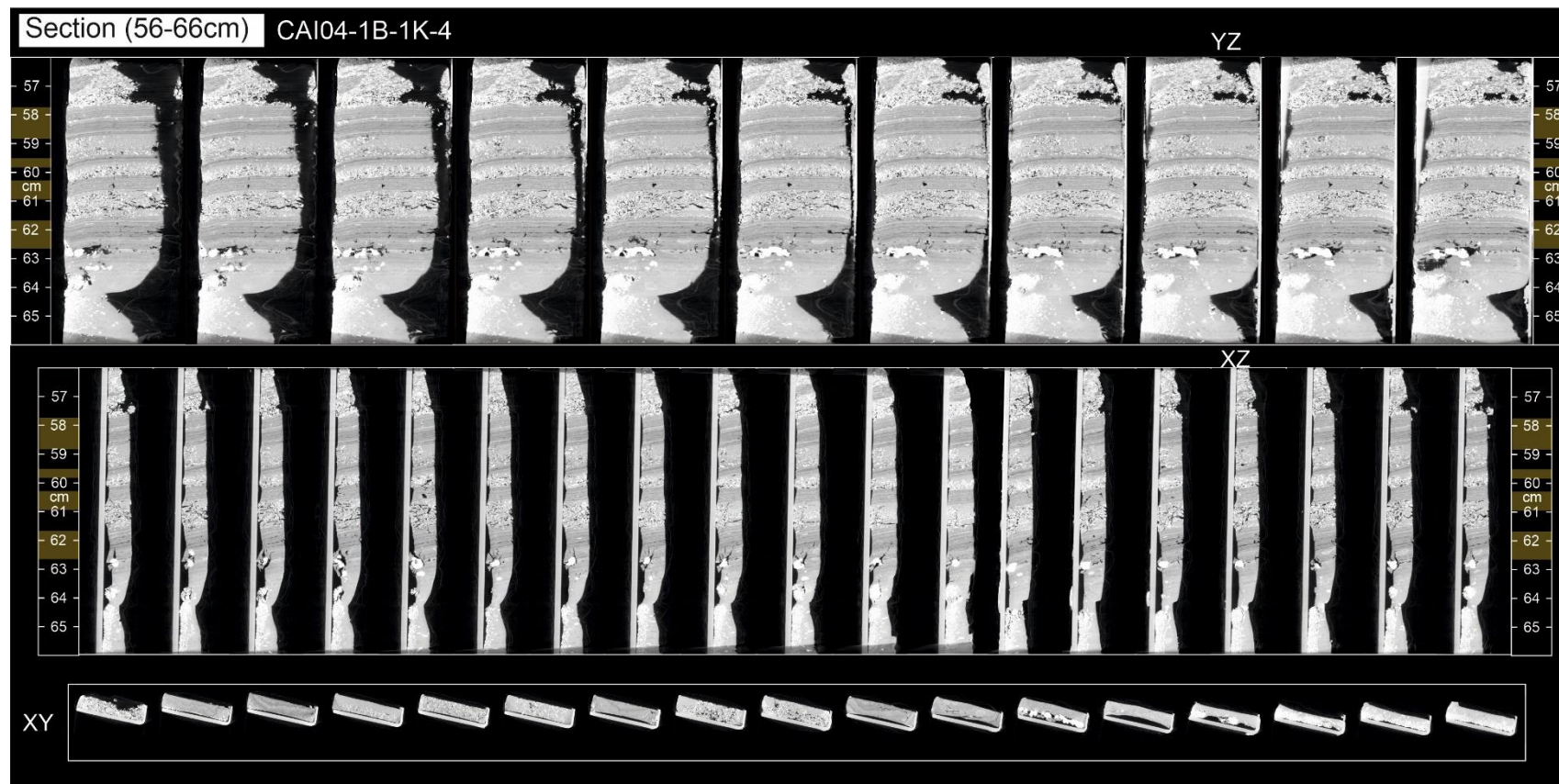


Figure A3.11 – Ortho slices generated by computerised tomographical scanning of unambiguous microbial mats from Lago de Arreo core CAI04-1B-1K-4, interval 56-66cm.

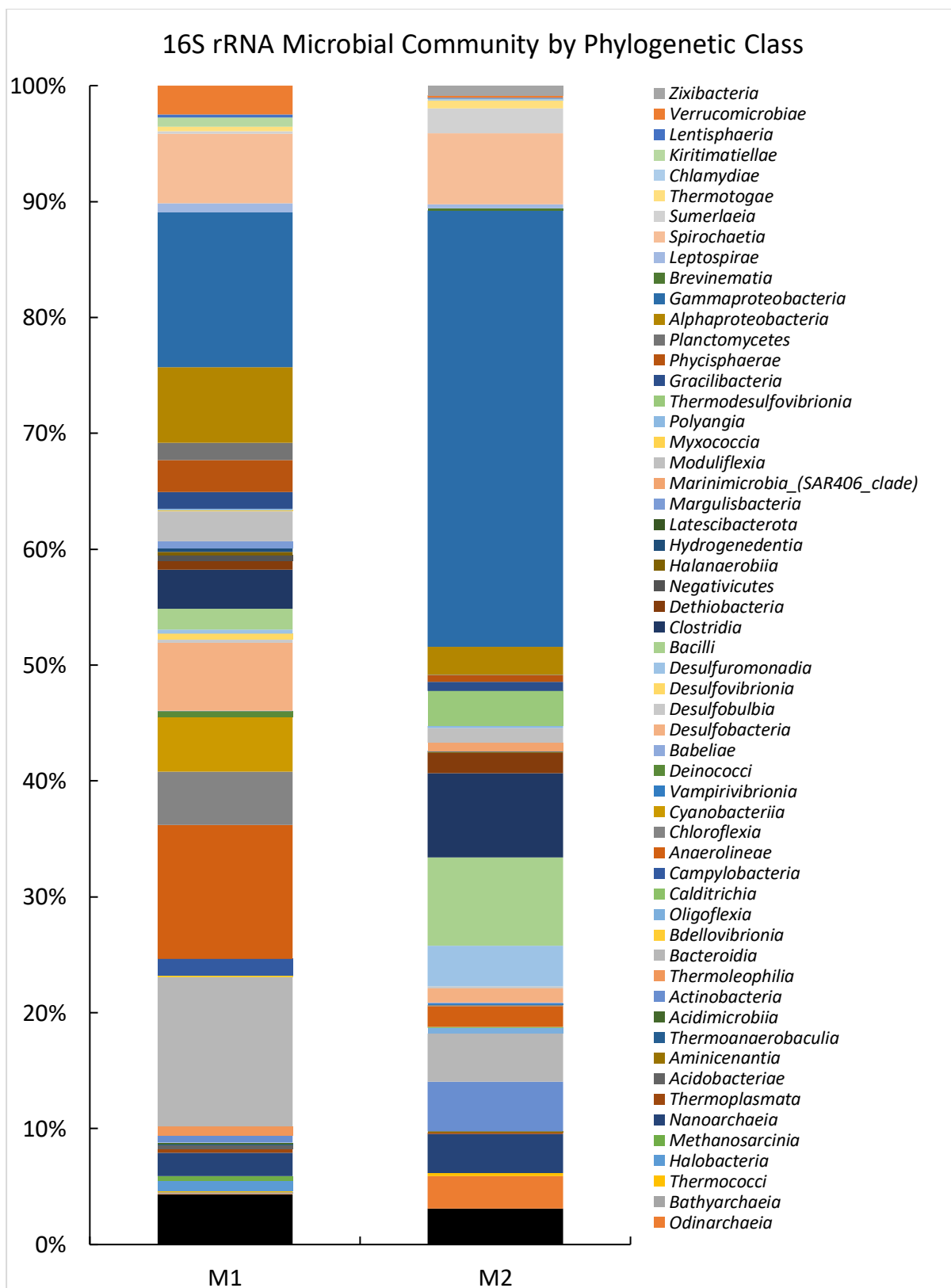


Figure A3.12 – Microbial community composition of modern, littoral mats from Lake Chiprana.

Lake Chiprana – Profundal Mat Geochemistry

In core CHI19-1A, CHI19-1A-1 mats display increases in Sr and Zr at the uppermost section of the mat (0-10mm), and there is also significant variability in Ca, S and Cl throughout. In addition, a detrital-rich layer between 18-22mm can also be observed based on increases in Si, K, Ti and Fe. 1A-2 mats exhibit variability in Si, K, Ti, Fe and Mn, with a moderate increase in these elements between 70-90mm. Ca, S, Cl and Inc/Coh display minimal downcore increases. In the lower section of core CHI19-1A, 1A-3 mats exhibit a moderate increase in Si, K, Ti, Fe, Ca, S, Sr and Zr throughout, particularly between 270-.mb,+290mm. Small decreases in Br and Inc/Coh occur in the same interval. In the upper interval of Core CHI19-2A, 2A-1 mats (0-31mm) illustrate a slight increase in Si, a moderate increase in Ca and S, and a considerable increase in Sr and Zr in the topmost section of the mats (0-15mm). There is also a relatively small increase in Cl towards the base of the mats (20-30mm). 2A-2 mats (56-103mm) display moderate increases in Si, K, Ti, Fe and Mn and relatively significant increases in Ca and S throughout. Moderate increases in Br and Inc/Coh can also be observed in the upper half of the mats. In the lower interval, 2A-3 mats (199-248mm) small downcore increases in Si, K, Ti, Fe, Mn, Br and Inc/Coh. A moderate increase in Ca, S and Sr can also be identified in the central section of the mats (220-235mm).

In the upper section of core CHI19-3A, 3A-1 mats (0-35mm), there is a moderate to significant increase in Ca, S, Sr and Zr in the upper to middle section of the mats (10-30mm), and a moderate increase in Ni, Cu, Br and Inc/Coh in the uppermost section of the mats (0-20mm). Downsequence, 3A-2 mats (79-106mm) exhibit moderate to relatively large increases in Si, K, Ti, Fe, Ca, and S. In tandem, small increases can be observed in Sr, Zr, Br and Inc/Coh. In the lower section of core CHI19-3A, 3A-3 mats (188-236mm) a significant increase in Si, K, Ti, Fe and Al can be observed in the uppermost section of the mats (188-210mm), while similarly large increases in the form of a solitary peak can be observed in Sr and Zr at a depth of

approximately 210-215mm). Furthermore, increases in Ca, S and Cl occur in the middle section to the base of the mats (210-230mm). Finally, significant decreases in Br and Inc/Coh can be observed from the topmost section of the mats to the middle section (188-210mm). Finally, in core CHI19-6A, 6A-1 mats (0-38mm) in the upper interval of the cores display small downsequence increases in Si, K, Al, Ca and S, and substantial increases in Sr and Zr within the uppermost and middle sections of the mats (0-25mm). Minimal increases in Cu, Ni, Br and Inc/Coh in the uppermost section of the mats. Downsequence, 6A-2 mats (73-111mm), moderate increases in Si, K, Ti, Fe and Mn occur in the lower half of the mats (95-111mm), while all other elements remain relatively unchanged throughout.

Lake Chiprana – Littoral Mat Geochemistry

In core CHI19-4A, 4A-1 mats in the uppermost section (0-32mm) exhibit moderate downsequence increases in Si, Ca, S and Sr, and moderate decreases in Br and Inc/Coh. 4A-2 mats (40-63mm) illustrate a small increase in Si, K, Ti, Fe, Mn, Ca, Br and Inc/Coh within the uppermost section (40-48mm). A moderate increase in Ca and S can also be observed in the lower section of the mats (55-62mm). 4A-3 mats, finally, display relatively unchanged elemental compositions throughout, with small variability only observed in Cl. In 4A-3 mats (73-90mm), small downsequence increases are observed in Si, K, Ti, Mn, and Cl, while there is a particularly large increase in Zr throughout the entire microbial mat sequence.

In core CHI19-5A, 5A-1 mats (0-26mm) exhibit moderate increases in Si, K, Mn, Ca, S, Br and Inc/Coh in the uppermost section of the mat (0-12mm). In the lower section

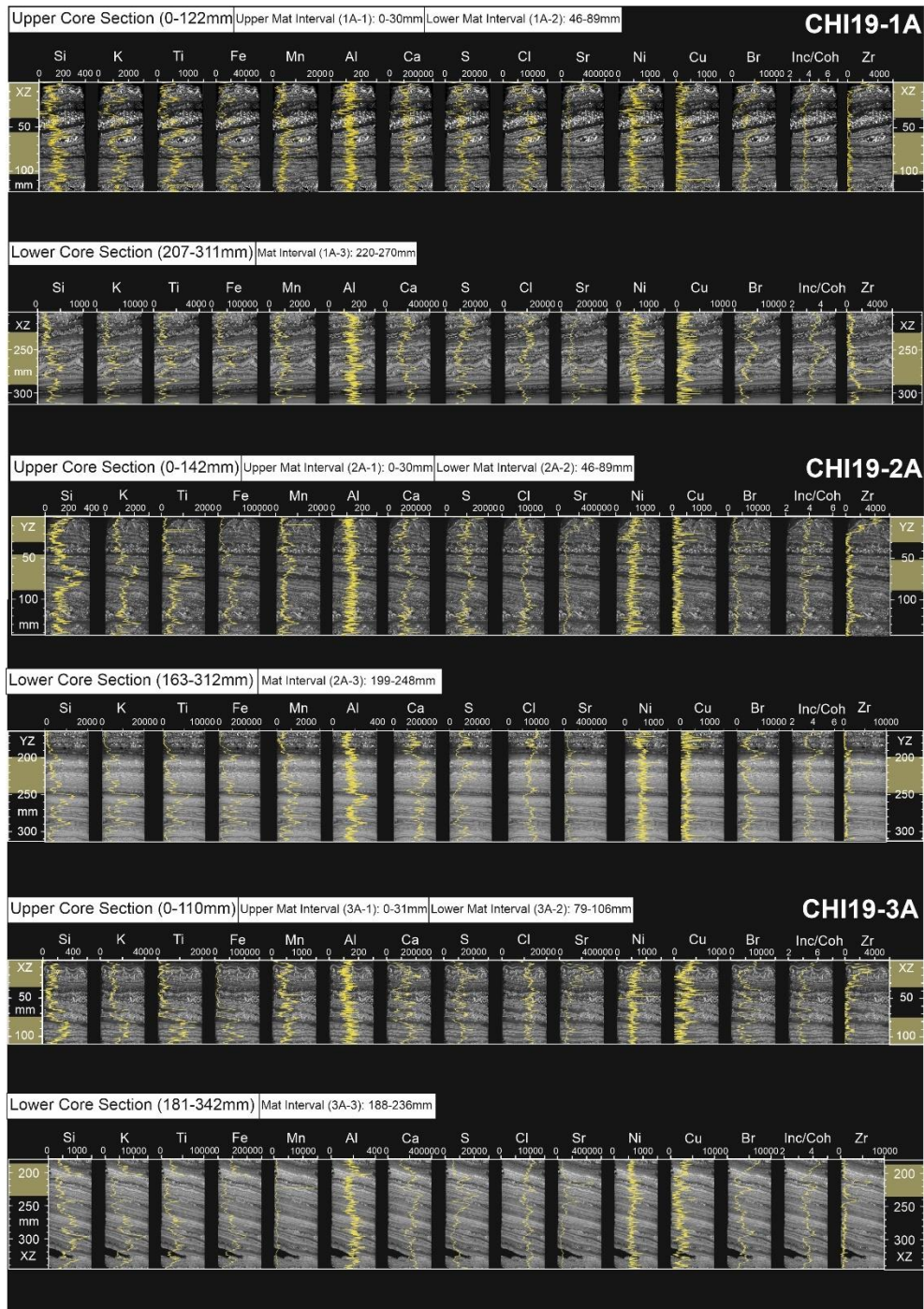


Figure A3.13 – Elemental XRF data of microbial mats in sediment cores CHI19-1A, 2A, 3A and 4A in Lake Chiprana.

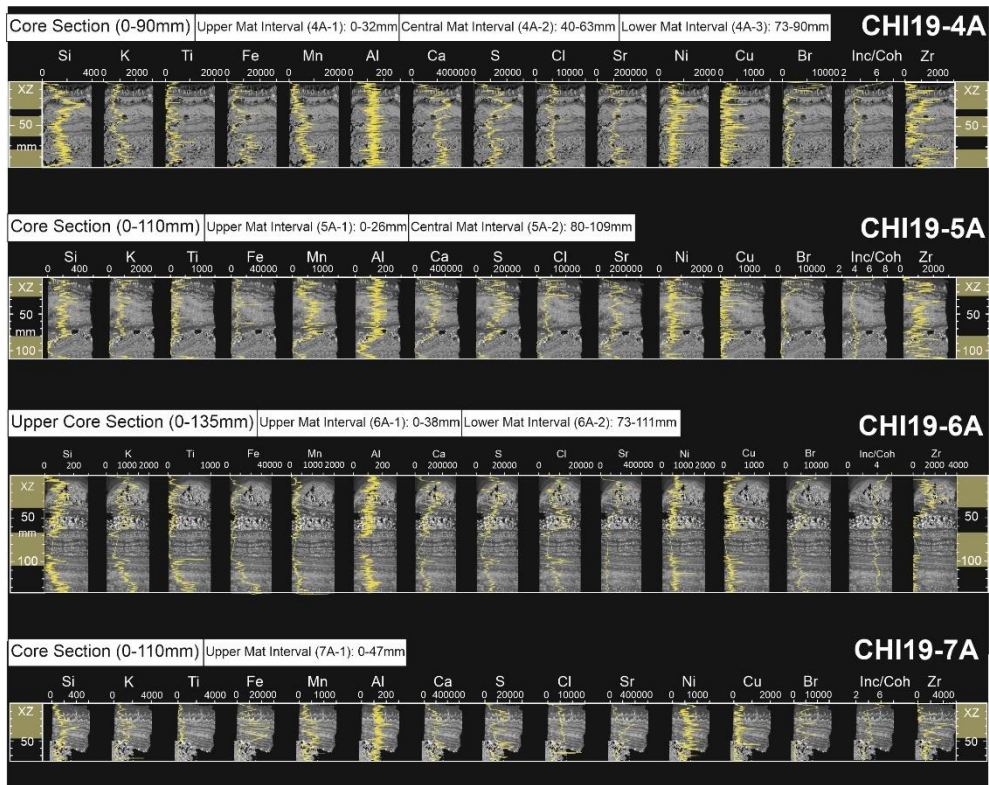


Figure A3.14 – Elemental XRF data of microbial mats in sediment cores CHI19-5A, 6A, and 7A in Lake Chiprana.

of the mat, further increases in Ca and S can be observed, an overall increase in Sr occurs, and several moderate peaks in Cl occur throughout. In 5A-2 mats (80-109mm), all elements display significant decreases to near 0 counts per second with the exception of Zr, Ni and Sr. Finally, in core CHI19-7A, the singular interval of microbial mats, 7A-1 (0-47mm), exhibits downsequence increases in Si, K, Ti, Fe, Mn, Ca, S, Sr, and Zr. In particular, Fe displays significant variability in the central section of the mats (20-45mm), while all other aforementioned elements display a large peak in the 30-35mm interval. Finally, Br and Inc/Coh display a large increase at the topmost section of the mat (0-15mm) and moderate variability throughout the rest of the mat sequence.

Lake Zonar – Mat Geochemistry

XRF data for Lake Zonar were following a field study of Lake Zonar in 2004, and these data are described and interpreted in full by Martín-Puertas *et al.* (2008, 2009, 2011). In Z1 mats from Core ZON04-1C, Ca, Mn and Fe display minor increases in intensity within mat laminae, while Ti displays a relative decrease. All other elements do not display any significant change. There is also typically a relative decrease in all elements relative to the underlying sediment beneath the mats.

Lake Estanya – Mat Geochemistry

XRF data were previously obtained following a field study of Lake Estanya in 2004, and these data are described and interpreted in full by Morellón *et al.* (2008, 2009a; b). In summary, E1 mats display increases in Ca, Al and S, decreases in Fe and Ti, while all other elements remain relatively constant. E2 mats display moderate increases in Ca, S, and as small increase Al, while all other elements display moderate decreases. E3 mats display a small increase in Si, Al and K, while all other elements are relatively stable. E4 mats display moderate increases in Ca, S and Fe, and small decreases in all other elements. Finally, E5 mats display small increases in all elements.

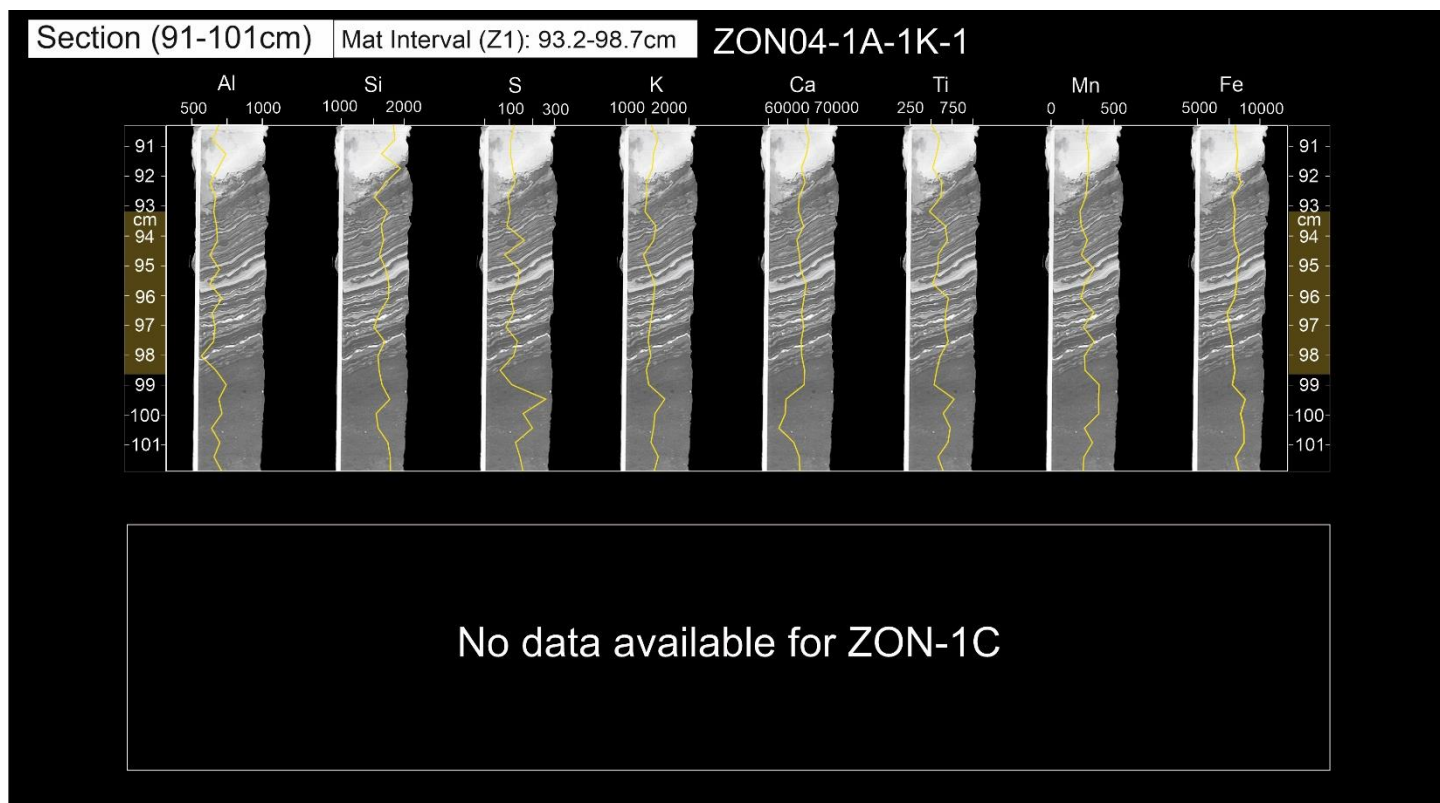


Figure A3.15 – Elemental XRF data of microbial mats in sediment core ZON04-1A in Lake Zonar.

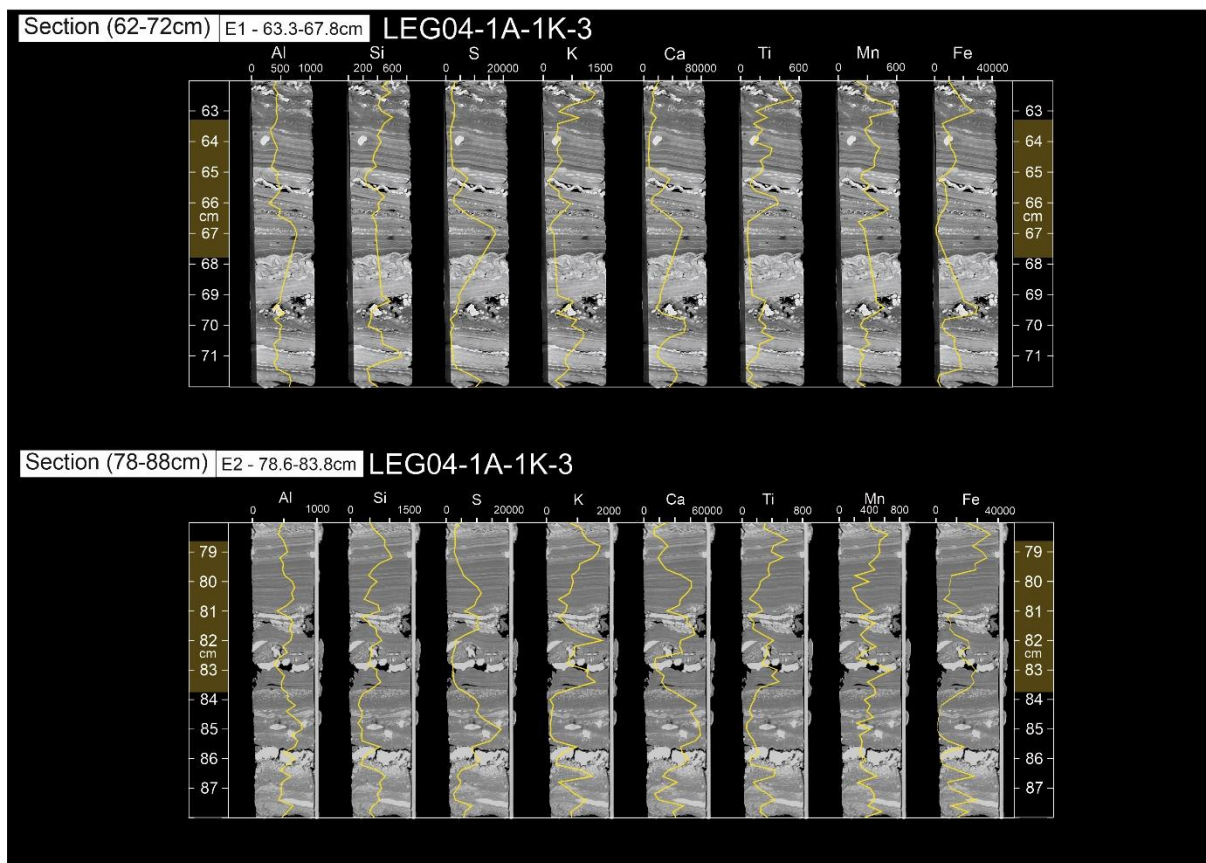


Figure A3.16 – Elemental XRF data of microbial mats in sediment core LEG04-1A-1K-3 in Lake Estanya.

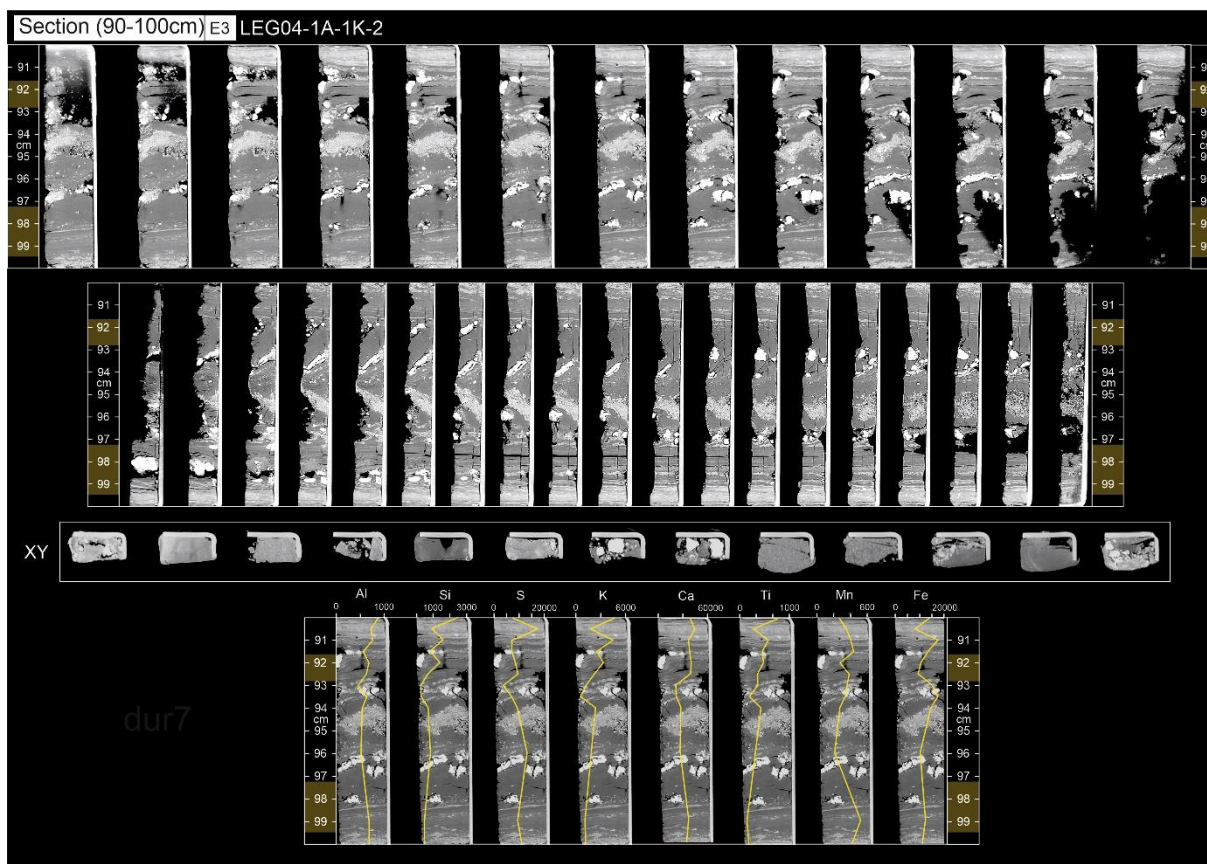


Figure A3.17 – Elemental XRF data and CT scans of microbial mats in sediment core LEG04-1A-1K-2 in Lake Estanya.



Figure A3.18 – Elemental XRF data and CT scans of microbial mats in sediment core LEG04-1A-1K-3 in Lake Estanya.

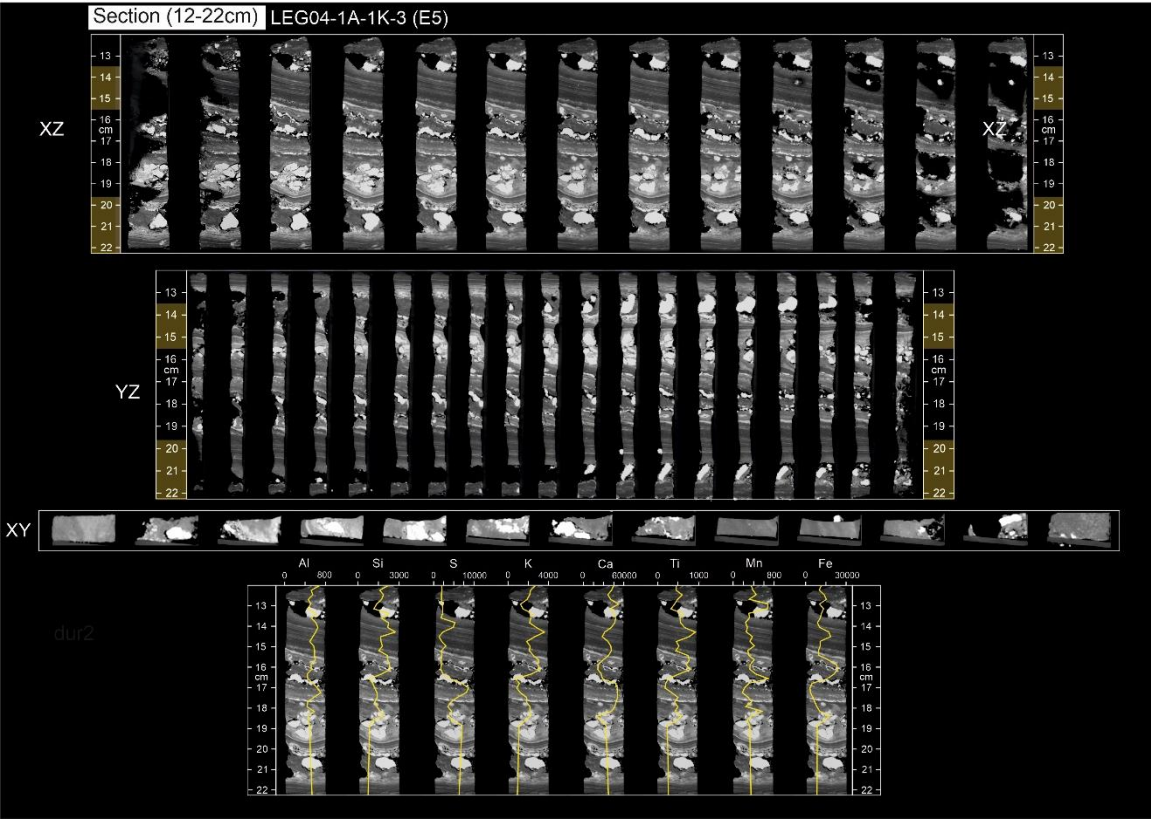


Figure A3.19 – Elemental XRF data and CT scans of microbial mats in sediment core LEG04-1A-1K-3 in Lake Estanya.